Studies of VHMS-related alteration: geochemical and mineralogical vectors to ore

AMIRA/ARC project P439

Volume 2, Final Report
May 1998

CODES SRC

Centre for Ore Deposit Research,
School of Earth Sciences,
University of Tasmania,
GPO Box 252-79,
Hobart, Tasmania,
Australia 7001

http://www.geol.utas.edu.au/codes

another Pongratz, Hlaing & Blake Production 1998

Contents

cont.

Introduction

Project objectives P439

The five project objectives of P439 as outlined in the original research proposal are:

- To characterise the mineralogy and geochemistry for the various styles of hydrothermal alteration throughout the Mount Read Volcanics (MRV) and the Mount Windsor Volcanics (MWV). This will be based on mapping supported by whole-rock and trace element geochemistry, mineral chemistry, REE and stable isotope geochemistry.

- To determine the relationship between geochemical alteration patterns and sub-volcanic intrusions that are coeval with VHMS formation.

- To undertake case studies of alteration halos related to specific VHMS deposits with particular emphasis on hangingwall alteration, and the relationship between alteration patterns and volcanic facies.

- To develop a set of vectors towards ore based on the regional studies and ore deposit specific studies that can be applied in the exploration for VHMS deposits in submarine volcanic sequences throughout Australia. The vector matrix will include whole-rock, trace element, mineral chemistry, REE, isotope and volcanic facies factors.

- To produce a book on "Alteration mineralogy, geochemistry and textures in volcanics related to VHMS deposits" as a follow-up to the successful publication by CODES of "Volcanic Textures".

At the first progress meeting (April 1995), and in subsequent meetings, a number of sponsors emphasised the importance of including studies on mineral chemistry in both the regional and deposit case studies. In response to this request the work on mineral chemistry was expanded in the latter part of the project at the expense of some of the planned isotopic and REE research.

Research framework

This project involved a multidisciplinary approach utilising studies in volcanic facies analysis, volcanic petrology and geochemistry, with alteration and mineralisation to develop models for the composition, style and extent of alteration throughout submarine volcanic environment hosting VHMS deposits. The venn diagram below outlines the relationships between the different modules of the project.

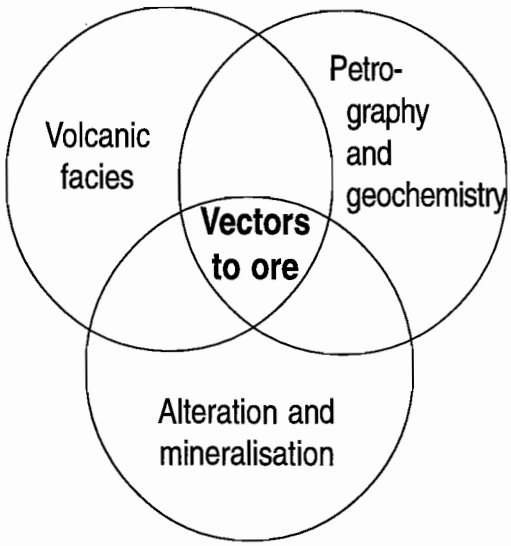

The research was undertaken at the regional scale and the deposit scale in order to develop criteria useful for both regional exploration and mine scale exploration. The regional studies concentrated in the Mt Read Volcanics with lesser work in the Mt Windsor Volcanics. The emphasis was (a) to determine the relationship between volcanic facies and alteration, and (b) to develop criteria to distinguish amongst diagenetic alteration, metamorphic-related alteration and hydrothermal alteration (VHMS related). The deposit case studies included research at Mt Lyell, Hellyer, Rosebery and Henty in the Mt Read Volcanics; Thalanga and Highway Reward in the Mt Windsor Volcanics and Gossan Hill in the Murchison Volcanics (WA). The emphasis in the deposit studies was (a) to map out alteration assemblages and zonation, (b) relate alteration mineralogy and geochemistry, (c) investigate trace element halos, and (d) to study variations in mineral chemistry and their relationship to alteration zonation. Because considerable research has been published about VHMS footwall alteration, then the focus of the P439 deposit studies was on hangingwall alteration. Our ultimate objective was to combine the regional and deposit scale studies to characterise hydrothermal alteration and develop vectors to ore.

Achievements of project

This project has made a major advance in our understanding and interpretation of alteration in submarine volcanics related to VHMS hydrothermal systems. The principle achievements listed in the order that they appear in this final report are given below.

1. Detailed halo alteration models have been developed for the following seven VHMS deposits; Hellyer, Rosebery, Henty, Western Tharsis, Thalanga, Highway-Reward and Gossan Hill.

   Each model includes a set of criteria and vectors that are useful for regional and mine scale exploration. This is the first time that a set of VHMS alteration models has been presented which include volcanic facies, chemostratigraphy, lithogeochemistry, alteration zonation, halo geochemistry, mineral chemistry and vectors to ore.

2. The deposit case study reports (Volume 2) include a series of Alteration Data Sheets which combine geological, geochemical, textural and mineralogical information, including photos on the one page, to allow comparison of the main characteristics of alteration. This format was developed during the project and emphasises the advantages of a multidisciplinary approach in the study of alteration.

3. An in-depth evaluation of the application of PIMA to alteration studies around VHMS deposits has been completed with emphasis on the spectral characteristics of muscovite and their relationship to VHMS deposits (Western Tharsis, Rosebery and Highway-Reward). This work combines PIMA spectral data, with micro-probe mineral chemistry, whole-rock chemistry and thin section petrography. No study of this type has been previously completed for VHMS deposits.

4. A set of criteria have been developed to distinguish diagenetic alteration, metamorphic alteration and hydrothermal (VHMS-related) alteration in submarine volcanics. The criteria combine studies on volcanic facies, volcanic textures, petrology and lithogeochemistry.

5. An alteration box plot has been developed and tested, which enables comparison of alteration mineralogy with geochemistry to provide a classification of alteration facies related to VHMS systems.

6. A Pearce element ratio analysis of altered and unaltered rock compositions within the andesitic footwall to the Hellyer VHMS deposit was revealed several new concepts regarding the hydrothermal alteration. In addition, new innovative exploration vectors have been developed.

7. Preliminary thermodynamic modelling of low temperature seawater-volcanic rock interaction has been completed, and demonstrates the value of this approach in determining the temperature and fluid chemical controls on diagenetic and hydrothermal alteration.

8. A data base of whole rock and trace element geochemistry for samples from the Mt Read Volcanics, Mt Windsor Volcanics and the seven ore deposit case studies has been compiled. The data base includes 1730 rock analyses (this project), 2845 MRV rock analyses from other sources (Tas Uni, MRT and Pasminco), and 1020 microprobe mineral analyses from the deposit studies. The data base is provided to all sponsors on a compact disc located in the back envelope of this report (Volume 1).

9. A study of ironstone geochemistry, including REE and isotopes has shown the application of this approach to exploration in the Mt Windsor Volcanics.

10. Controls on both diagenetic alteration and hydrothermal alteration by volcanic facies and volcanic textures has been evaluated and shown to be critically important, especially at the diagenetic stage. This work includes regional studies especially the Mt Black Volcanics, and focussed research at Rosebery and Highway-Reward.

This report

The final Report for P439 is divided into four volumes:

Vol. 1: Executive Summary
Vol. 2: Ore deposit case studies and related research
Vol. 3: Regional studies and volcanic facies controls
Vol. 4: Field meeting guide, Mt Windsor Volcanic Belt.

Acknowledgements

This project has been supported by the following companies and organisations:

Aberfoyle Resources Limited
Copper Mines of Tasmania
Denehurst Limited
Mineral Resources Tasmania
Normandy Exploration
Pasminco Exploration
Queensland Metals Corporation Ltd
RGC Exploration
Rio Tinto Exploration

On behalf of the research team I would like to thank all the company representatives, collaborators and AMIRA for their support and scientific interaction throughout this three year program. In particular we are indebted to those companies that provided access to their deposits for the case studies: RGC, Pasminco, Murchison Zinc, Copper Mines of Tasmania and Aberfoyle.

This project would not have been possible without the very significant contributions by a number of dedicated and hardworking postgraduate students: Catherine Gifkins, Robina Sharpe, Mark Doyle, Holger Paulick, Bill Wyman and Russell Fulton. Thanks also for the tireless work of Mike Blake in organising the alteration data sheets, and to Nilar Hlaing for printing and collating the papers. As usual June Pongratz has done a great job in coordinating and producing this final report.

We hope that the final outcome of this project is the discovery of a new VHMS deposit in the near future.

Ross R. Large
Director
Centre for Ore Deposit Research.

Alteration halo model for the Rosebery VHMS deposit, western Tasmania

Ross Large, Rod Allen, Mike Blake and Walter Herrmann
Centre for Ore Deposit Research

Summary

A detailed study of alteration mineralogy, mineral chemistry and lithogeochemistry in the host rocks surrounding the A-B and K lenses at the north-end of the Rosebery mine has revealed a series of overlapping alteration halos with characteristic mineralogy and geochemistry.

The study involved logging and sampling (255 samples) from nine drill holes spaced at varying distances from the A-B and K lenses. The stratiform Zn-Pb-Cu ore lenses, have a sheet-like attitude and are hosted by medium grained feldspar-phyric pumice and/or crystal-rich rhyolitic to dacitic volcaniclastics, overlying a thick homogenous sequence of rhyolitic pumiceous breccia mass flows.

Chemostratigraphic studies using immobile element geochemistry have revealed that the immediate host unit and overlying quartz-feldspar-biotite porphyry have a distinct Ti/Zr ratio (12–14) which is consistently different from the ratio in the footwall pumiceous mass flows (7–9), and the hangingwall volcanogenic sandstones (10–30). This result emphasises the value of chemostratigraphic studies, in parallel with conventional drill core logging, to aid identification of favourable units for mineralisation.

The major alteration minerals at Rosebery are arranged in a complex series of zones passing away from the deposit; quartz-sericite zone, Mn-carbonate zone, chlorite zone and outer sericite zone. The outermost visible sericitic alteration extends about 60 to 100 m into the footwall, 10–20 m into the hangingwall and over 500 m along the upper contact of the rhyolitic pumiceous mass flows (Ti/Zr = 7 to 9).

A series of lithogeochemical halos with associated vectors have been developed which are critical in exploration either at the mine scale or in regional exploration:

- Proximal vectors — Zn, Pb, MnO, Ba are $\delta^{18}O$ carbonate; may predict ore lenses at 200–500 m along strike and 3–50 m across strike.
- Medial vectors — S/Na_2O, Ba/Sr, K_2O, Na_2O depletion, Ishikawa AI, CCPI and Mn content of carbonate; may predict presence of ore at 500–1000 m along strike, 10–80 m into hangingwall and 60–120 m into footwall.
- Distal vectors — Tl and Sb may predict presence of ore at greater than 1000 m along strike, 200–300 m into hangingwall and 60–100 m into the footwall.

Detailed studies of alteration mineral chemistry at Rosebery have revealed some important chemical relationships that may assist with exploration. The Mn content of alteration carbonate increases toward ore both along strike and across strike. Close to ore, alteration carbonates contain >20 mole % $MnCO_3$ (kutnahorite, rhodochrosite, siderite and ankerite) while at distances of 40–60 m across strike the mole % $MnCO_3$ in carbonate drops to below 10%. At greater than 80 m the carbonates are Mn poor calcites, and commonly located in syn-metamorphic structures.

Muscovite chemistry changes with stratigraphy and alteration assemblages and may be related to the mineralising event, although this has not been convincingly demonstrated. Proximal muscovite contains minor Ba substituting for K in the structure, and are phengetic with 0.5 to 1.0 (Fe + Mg) cations

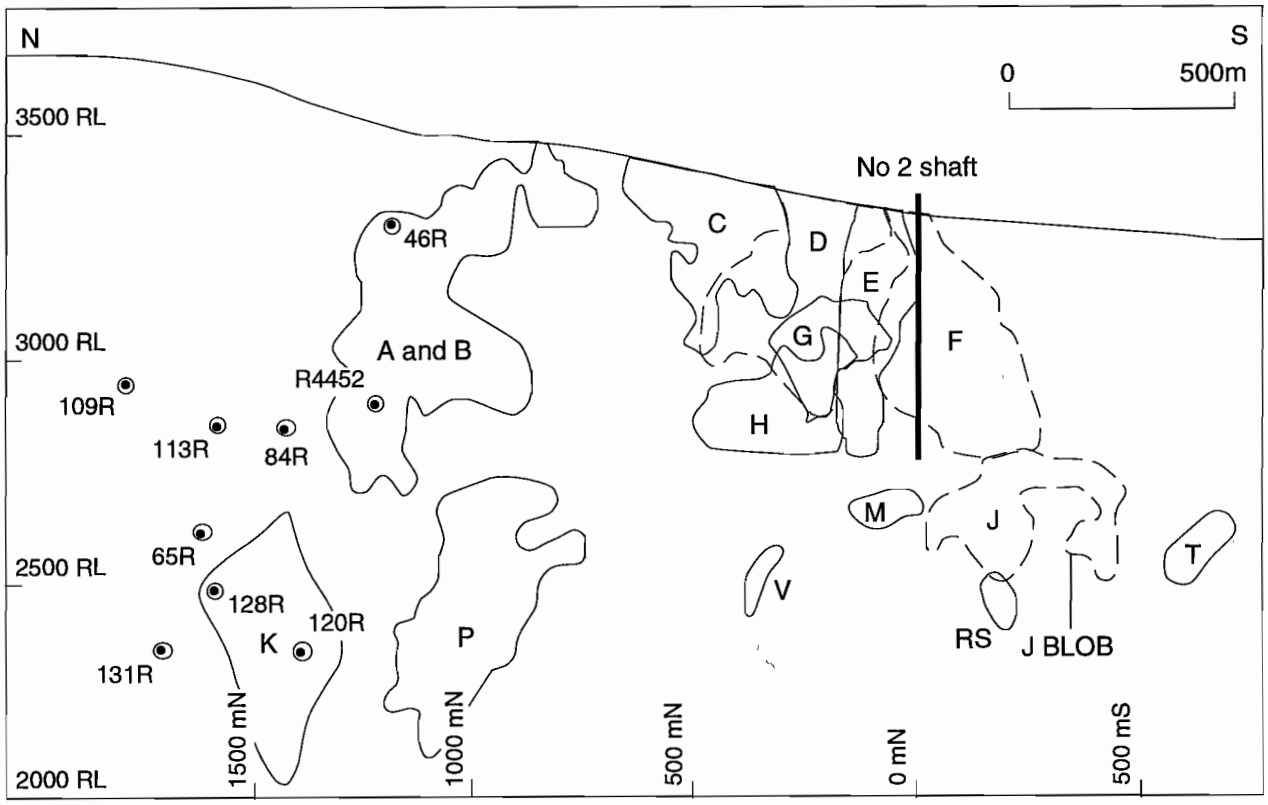

Figure 1 : Long section of Rosebery Mine showing drill holes sampled in this investigation in relation to the ore lenses (modified from Graves et al., 1997).

substituting for octahedral AI. However, except for their Ba content, these phengetic muscovites are similar to those found in non-mineralised areas of the MRV (Herrmann et al., this vol.). Sodic muscovite with up to 0.35 Na/(Na + K) and low phengite content (<0.5 Fe + Mg cations) occur in a zone of volcanic sandstones and black slates overlying the ore deposit. This may be a regional feature, although similar sodic muscovites have not been identified elsewhere on the MRV regional traverses.

Chlorites in the ore lenses, associated Mn-carbonate zone and the hangingwall volcanic sandstone unit are Mg-rich with a Mg number of 50 to 70. This compares with chlorite in the footwall and above the Black Slate which are generally more Fe-rich with Mg number from 20 to 50. More work is required on chlorites at Rosebery to test their relationship to mineralisation.

A study of carbon and oxygen isotopes in carbonates has found no extensive isotope halo at Rosebery, but demonstrates that C/O isotopes can be used to assist in the discrimination of carbonates associated with Cambrian VHMS mineralisation from carbonates related to metamorphism or granite emplacement during the Devonian.

In conclusion this study has identified a series of geochemical vectors and mineralogical/ isotopic criteria that are of considerable importance in the exploration for sheet-style VHMS deposits of the Rosebery type. Listed in approximate order from proximal to distal the key vectors are:

Pb, Zn, MnO, Mg number of chlorite, $\delta^{18}O_{carb}$, Ba, mole % $MnCO_3$ in carbonate, CCPI, Ishikawa AI, Na/(Na + K) muscovite [PIMA AlOH 1], K_2O, Na_2O depletion, Sb and Tl.

Introduction

The Rosebery massive sulfide deposit is a major (>28 million tonnes) sheet-style Zn-Pb-Cu-Ag-Au VHMS within the Mt Read Volcanics of Western Tasmania (Green et al., 1981; Large, 1992).

An investigation of the alteration mineralogy and geochemistry of the northern ore lenses (lens A-B and K) was undertaken as part of AMIRA Project P439 in order to characterise the Rosebery alteration halo and develop vectors to ore useful for mine scale exploration.

Previous AMIRA reports

This final report on Rosebery alteration summarises and brings together the results from all previous AMIRA P439 reports on the Rosebery-Hercules deposits and emphasises the conclusions relevant to mineral exploration. Previous reports are:

- Allen R.L. and Large R.R., 1996, Rosebery Alteration Study : AMIRA P439 Report 3, October 1996, p143–152.
- Large, R.R., 1997, The Hercules-Mt Read traverse: Relationships between volcanic mineralogy, alteration and geochemistry : AMIRA P439, Report 3, October 1996, p153–233.
- Large, R.R. and Allen, R.L., 1997, Preliminary report on the Rosebery lithochemical halo study : AMIRA P439, Report 4, May 1997, p259–330.
- Allen, R.L., 1997, Rosebery alteration study and regional alteration studies in the Mount Read Volcanics. The record of diagenetic alteration in the strongly deformed, felsic volcaniclastic succession enclosing the Rosebery and Hercules massive sulfide deposits : AMIRA P439, Report 5, October 1997, p135–145.
- Large, R.R., Allen, R.L. and Blake, M., 1997, Carbonate and muscovite mineral chemistry, Rosebery VHMS deposit, Tasmania : AMIRA P439, Report 5, October 1997, p147–173.

Sampling strategy

A total of 255 samples were collected and analysed from nine drill holes at the northern end of the Rosebery deposit (Fig. 1). The north end was selected due to the relatively simple structure and the lower degree of late metasomatic alteration related to Devonian granites compared to the south end of the deposit. Four of the drill holes intersect the ore lenses (DDH 120R, 128R, R4452 and 46R) and the other five intersected the host stratigraphy at varying distances west of the ore lenses; from 100 to 500m west (DDH 131R, 65R, 84R, 113RDI, 109R).

Where possible samples were collected over a stratigraphic thickness of 500 m from the base of the Mt Black Volcanics, through the hangingwall sequence, the host rocks and the immediate footwall volcanics.

All samples were analysed for the major elements by XRF. Trace elements were analysed by XRF or ICP-MS according to the following scheme:

XRF	As, Ba, Ce, Cr, Cu, La, Nd, Ni, Pb, Rb, S, Sc, Sr, Th, V, Y, Zn, Zr
ICP-MS	Ag, As,Bi, Cd, Cs, Mo, Sb, Tl, U

Ore deposit characteristics

Form of orebody: The Rosebery deposit comprises a series of stratiform massive sulfide ore lenses with an average thickness of 2–10 m, strike of 100–400 m and down dip extent of 100 to 500 m.

Host rocks: The ore lenses occur in feldspar-phyric pumice- and/or crystal-rich rhyolitic volcaniclastic rocks of breccia to coarse sand grainsize, near the top of a several hundred metre thick succession of rhyolitic pumiceous breccia within the Central Volcanic Complex of the Mt Read Volcanics.

Size and Grade: The global mining resource of the Rosebery deposit is 28.3 Mt at 14.3% Zn, 4.3% Pb, 0.6% Cu, 145 ppm Ag and 2.4 ppm Au. Resource statistics for the individual ore lenses are shown in Table 1 (Edwards pers. comm. 1998).

Sulfide mineralogy: Sphalerite, galena, pyrite, chalcopyrite, tetrahedrite with lesser arsenopyrite and pyrrhotite.

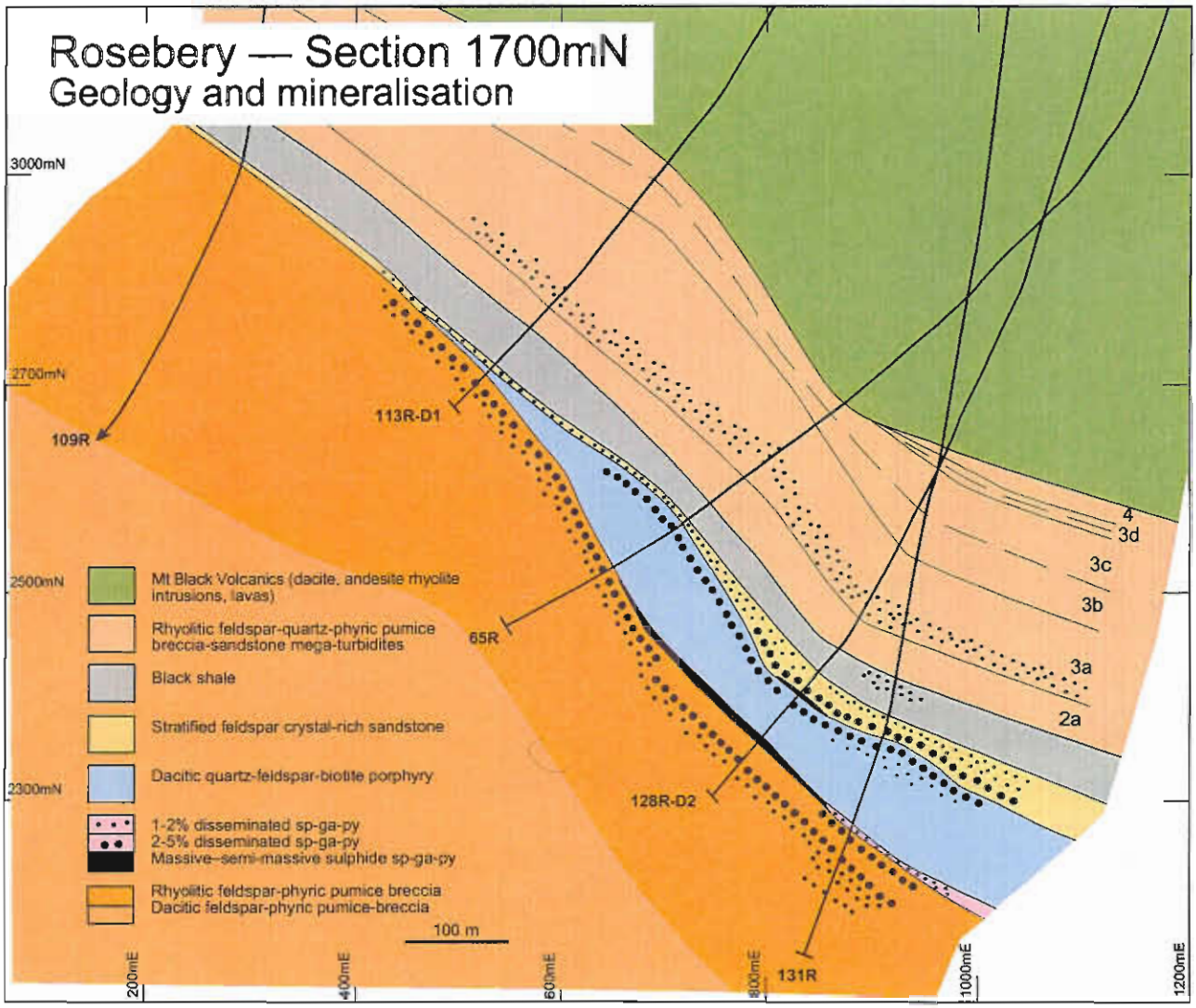

Figure 2 : Geological cross-section 1700 mN. (a) Geology and mineralisation.

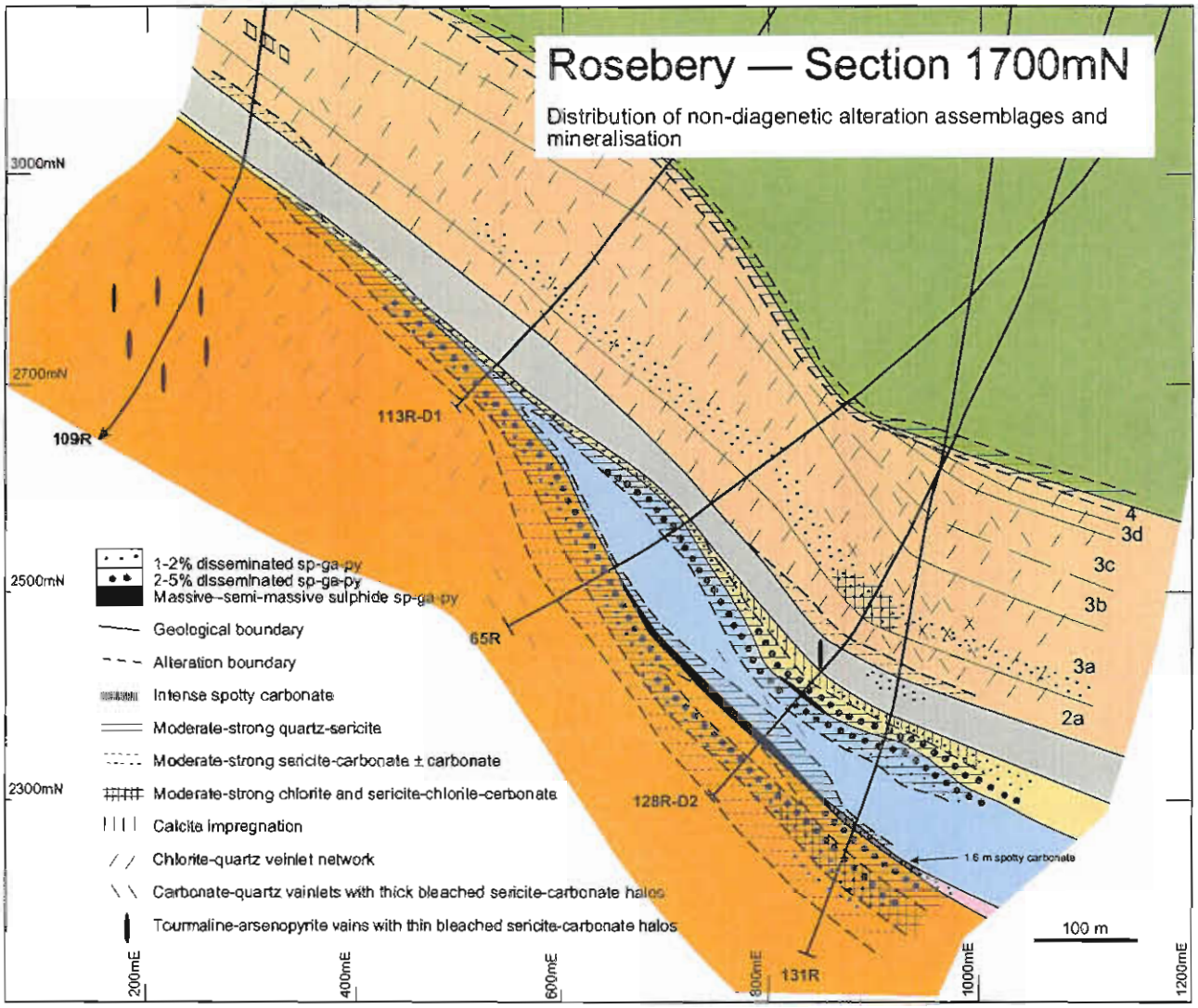

Figure 2 : Geological cross-section 1700 mN. (b) Distribution of non-diagenetic alteration assemblages and mineralisation.

Alteration mineralogy: Sericite, chlorite, Mn-carbonates, barite, quartz, with minor tourmaline, biotite, magnetite, fluorite, hematite.

Deformation: The Rosebery ore deposit varies from moderately to strongly deformed, and occurs on the eastern limb of a regional anticline that forms the hangingwall to the Rosebery thrust fault (Allen, 1997). Two main regional foliations, one main generation of folding and several generations of faulting have been recognised by Allen (1991, 1994). Further details on the deformation of the ores are to be found in Aerden (1994), Allen (1994, 1997) and Berry (1997). Textural studies by Allen (1997), which form part of this AMIRA project, demonstrate that the main phase of zinc-lead-copper mineralisation is Cambrian syn-volcanic and prior to the main deformation that probably occurred in the Devonian.

Volcanic facies architecture

The lowest stratigraphic unit exposed in the Rosebery-Hercules area is a greater than 800 m thick, poorly stratified, rhyolitic to dacitic pumice deposit, with subordinate coherent to hyaloclastic sills (Footwall Volcanics; Allen, 1991, 1994a). This unit is overlain by a well stratified, up to 300 m thick, succession of black mudstone and rhyolitic pumiceous mass flow units (Fig. 2; Hangingwall Volcaniclastics). These are in turn overlain by more than 1 km of rhyolitic pumice breccias, lavas and dacitic intrusions known informally as the Mount Black volcanics (Allen, 1991, 1994a; Gifkins, 1997). Locally, a 0-50 m thick package of stratified, felsic, crystal-pumice-lithic sandstones and siltstones occurs at the boundary between the Footwall Volcanics and

Table 1. Rosebery Mine, production plus resource statistics and mineral associations, by lens. (From Edwards pers. comm. 1998)

LENS	PRODUCTION PLUS RESOURCES						
	Tonnes (Mt)	Pb (%)	Zn (%)	Cu (%)	Ag (g/t)	Au (g/t)	Fe (%)
A	0.98	4.7	18.9	0.4	463	0.9	11.7
B	3.42	4.9	13.8	0.3	129	2.1	11.1
BP	0.30	2.2	3.0	0.1	218	3.3	2.8
C	2.84	4.6	19.4	0.5	170	1.6	17.3
D	2.18	3.6	12.5	1.2	123	2.2	22.3
E	3.16	3.7	12.8	1.3	106	2.7	23.3
F	4.98	4.3	14.6	0.7	125	3.1	10.5
G	1.64	4.2	12.8	0.8	135	2.2	11.5
H	2.33	3.7	11.1	0.4	84	2.2	8.1
J	2.22	3.3	12.4	0.5	125	2.0	14.6
K	2.77	6.2	16.7	0.4	193	3.4	8.6
M	0.08	4.9	15.3	0.1	88	1.7	10.1
P	1.10	4.0	15.5	0.4	154	3.2	6.5
Q	0.08	1.1	11.4	0.3	37	0.6	6.9
RS	0.21	2.7	11.9	0.2	105	1.2	21.7
T	N/A	-	-	-	-	-	-
Total	28.29	4.3	14.3	0.6	145	2.4	13.5

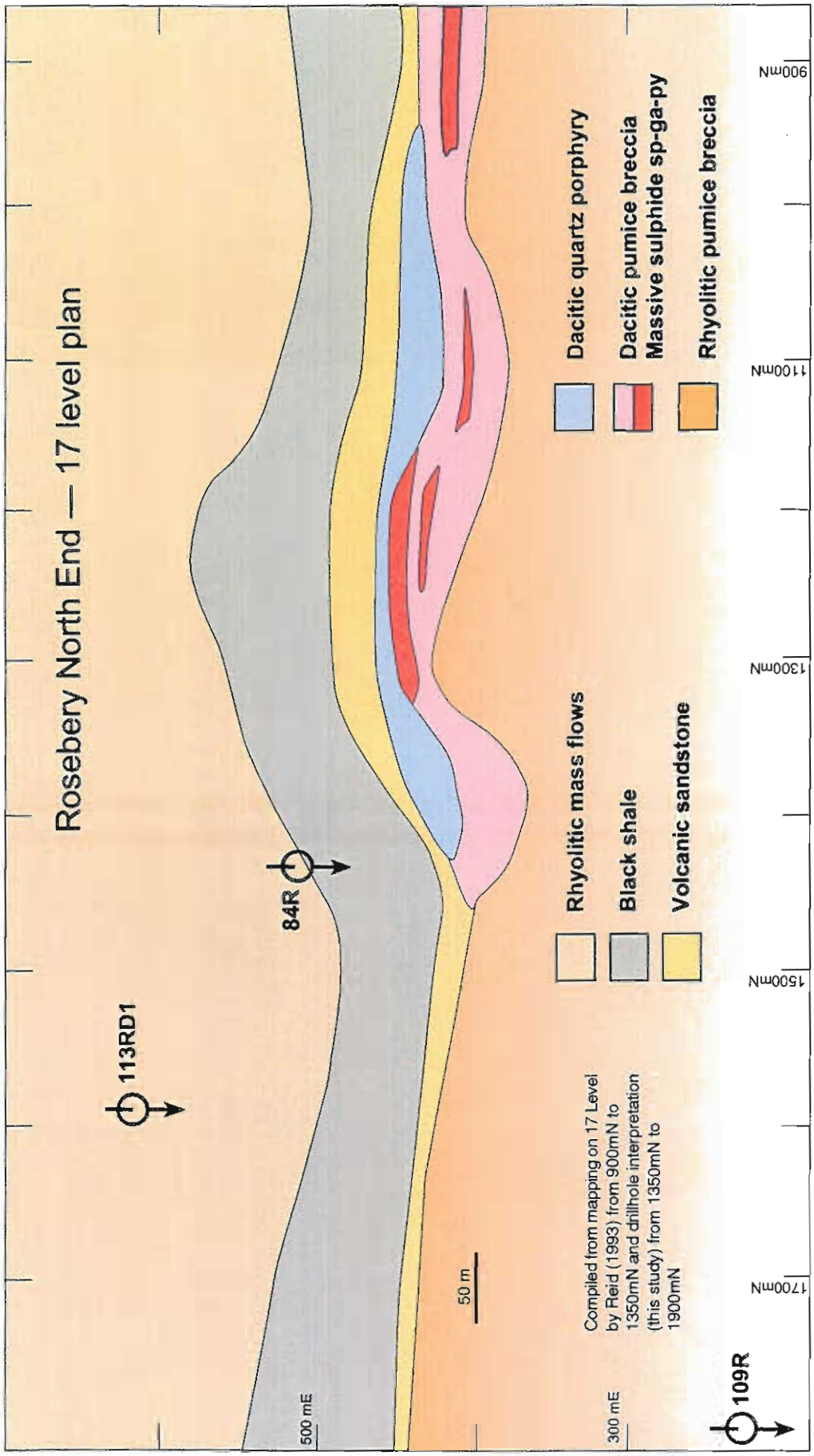

Figure 3. Geology Plan 17 level.

Hangingwall Volcaniclastics (Fig. 2). This package is termed "host rock" by Rosebery Mine staff and the Transitional Stratified Volcaniclastics (TSV) by Allen (1991, 1994a,b). Ore lenses occur within the top of the Footwall Volcanics pumice breccia and within the lower part of the Transitional Stratified Volcaniclastics (Allen, 1991, 1994b). The textures and geochemistry of representative examples of each rock unit are given in the Rosebery Alteration Data Sheets at the end of this report.

The pumiceous units of the Footwall Volcanics and Hangingwall Volcaniclastics are mainly interpreted as submarine mass flow deposits, that were fed directly (syneruptively) from large, subaerial to show water, magmatic pyroclastic eruptions (Allen, 1990, 1991, 1994a; Allen and Cas, 1990). The Footwall Volcanics pumice breccia is interpreted to have ponded within a large caldera subsidence structure, whose subsidence accompanied eruption of the pumice breccia (Green et al., 1983; Allen, 1994a). The Transitional Stratified Volcaniclastics is interpreted mainly as slightly to moderately reworked pyroclastic debris, derived mainly from the Footwall Volcanics pumice deposit (Allen, 1991, 1994a).

Chemostratigraphy

Immobile element lithogeochemical studies have been used to assist the volcanic stratigraphic interpretation at both Rosebery and Hercules, especially close to the ore lenses where the intensity of hydrothermal alteration makes it difficult to interpret primary lithologies (Large. 1996; Large and Allen, 1997). The approach used has been outlined by Herrmann (this volume).

The Ti/Zr ratio has proved to be the most useful parameter, showing a good correlation with volcanic stratigraphy (Table 1, and Figs 4 and 5). The major conclusions to emerge from the immobile element chemostratigraphic study are (Large and Allen, 1997):

- The main footwall pumice breccia mass flow deposits at Rosebery and Hercules have a very consistent rhyolitic composition, with Ti/Zr = 7 to 9, indicating eruption from a homogenous magma chamber, and deposition without significant mechanical fractionation of components, or at least a consistent fractionation.
- The carbonate-altered, pumice-bearing host to the ore lenses (A-B and K lens) has a similar appearance to the underlying rhyolitic pumice breccia, but has a more dacitic composition (Ti/Zr = 12 to 14). This indicates that a slightly more dacitic batch of magma was tapped at the end of the footwall pumice eruptions, and the ore commonly occurs at this stratigraphic level.
- The intrusive feldspar-quartz-biotite porphyry sill overlying the ore lenses has a similar Ti/Zr ratio to the dacitic pumice-bearing host-rocks.
- The hangingwall volcanic sandstones (TSV) have a range of Ti/Zr ratios (10 to 30) that result from the great variation in the relative proportions of felsic pumice, feldspar crystals and mafic lithic clasts from bed to bed .
- The hangingwall Black Shale has a high Ti/Zr ratio (~35) due to either (1) a sedimentary fractionation process or (2) derivation from mafic volcanic rocks.

Alteration mineralogy and zonation

Alteration Paragenesis

Allen (1997) discusses the sequences of alteration events at Rosebery; (1) early diagenesis, (2) hydrothermal ore-related alteration, (3) metamorphic alteration, and (4) post S_2 granite-related alteration (Table 2).

Different alteration types were distinguished according to mineralogy, alteration texture, and overprinting relationships with respect to foliations and other alteration types. The relative timing of each alteration type is shown in Table 1 as both the maximum time span possible according to overprinting relationships (widely spaced dashes), and the interpreted most likely timing (closely spaced dashes).

Hydrothermal alteration mineral changes

Mineralogical changes associated with hydrothermal alteration have been studied in detail in DDH 120R through the centre of K lens. A mineral percentage bar chart for a series of samples through the stratigraphic host sequence is shown in Fig. 6. The

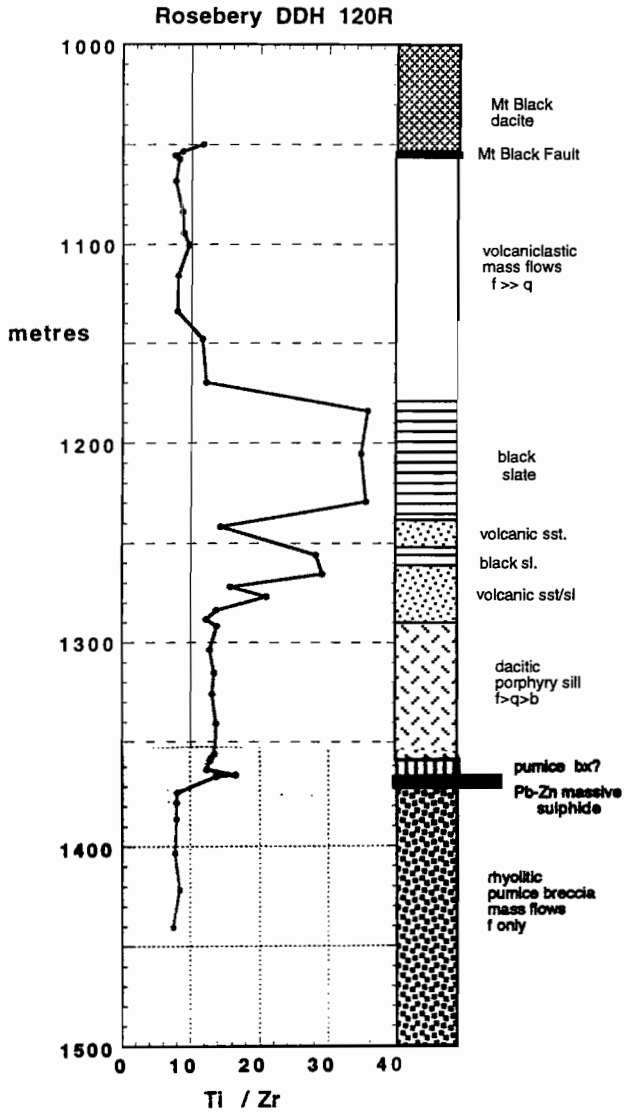

Figure 4 : Chemostratigraphy Ti/Zr variation in DDH 120R.

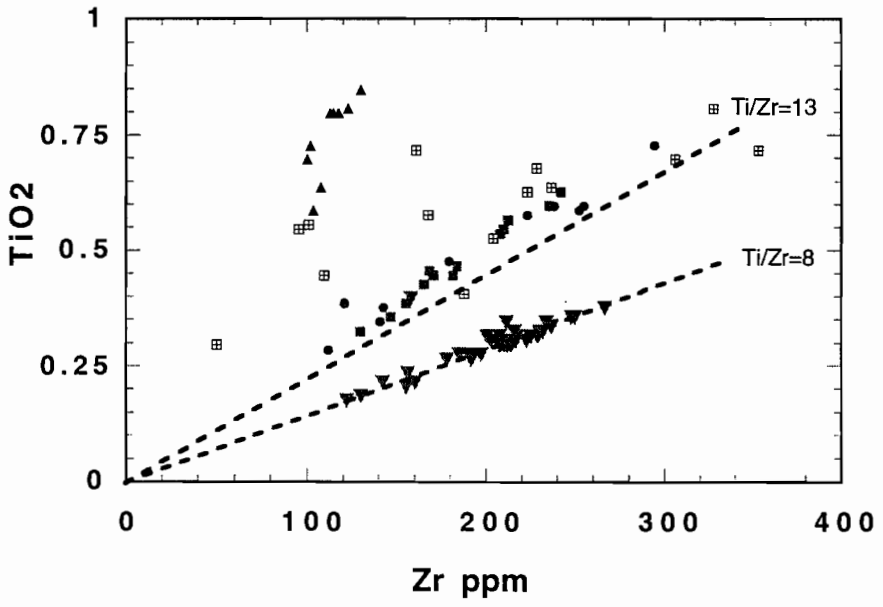

Figure 5 : Relationship between TiO2 and Zr for the major lithologies at Rosebery, showing the different trends relating to varying Ti/Zr ratios for each lithology.

mineral percentages have been calculated from the whole rock analyses by the least sequences method outlined by Herrmann (this volume) and show good agreement with the thin section estimates provided by Allen (1997) for these samples (Herrmann, this volume, Fig. 21).

The key conclusions from this bar chart (Fig. 6) are:

- Passing stratigraphically upwards through the footwall rhyolitic pumic breccias towards the K lens, albite content decreases while muscovite, quartz, chlorite and minor Mn-carbonate increases.
- Maximum chlorite concentration occurs immediately below the ore lens (data sheet 120R–138.6).
- Maximum Mn-carbonate concentration occurs in the dacitic pumice unit, directly above the ore lens (data sheet 120R–135.7). At other locations, maximum Mn-carbonate concentration can occur directly below the ore lens (e.g. R4452).
- The basal four meters of the hangingwall dacitic quartz porphyry sill show intense muscovite alteration and albite depletion.
- The central zone of the porphyry sill shows no effects of hydrothermal alteration (data sheet 120R–135.3).
- The volcanic sandstone unit (TSV) above the porphyry sill may be moderately to strongly hydrothermally altered in the lower section (samples 1284, 1288, 1292) exhibiting muscovite enrichment and albite depletion (data sheets 120R–1265.5 and 120R–1122).
- Hangingwall rocks above 1280 m (i.e., 90 m above the ore lens) show no strong mineralogical effects of hydrothermal alteration, except for scattered stratabound zones of calcite impregnation that may be related to the ore-forming hydrothermal system (data sheet 120R–1147).
- Chlorite and calcite enrichment in the hangingwall volcanic sandstone (TSV) unit could in part be a primary compositional feature related to the greater abundance of feldspar crystals and mafic lithic clasts in this unit (see also Chemostratigraphy section).

Alteration mineral zonation

The major hydrothermal alteration minerals at Rosebery and Hercules are Mn-carbonate (rhodochrosite, kutnohorite and Mn-ankerite), quartz, chlorite and sericite. Based on all nine drill holes studied we conclude that these minerals form a series of overlapping zones around the ore lenses (Figs 2b and 7).

Quartz-sericite zone: Ore and intense mineralization mainly occurs in one or more strata-parallel zones of bleached quartz-sericite-sulphide composition (Fig. 2b). Rock textures vary from homogeneous to spotty and augen schist textured (see data sheet 84R-843), the latter comprising an anastomosing fabric of strongly foliated sericite > quartz domains wrapping around siliceous knots of quartz>sericite. At the lateral margins of ore grade mineralization, the quartz-sericite zone continues with 1-10% disseminated sulphide. Sulphide is typically disseminated and preferentially occurs in the siliceous spots or augen (e.g. data sheet 84-843).

Mn-carbonate zone: The mineralized quartz-sericite zone is overlain (e.g. DDH 120R) and/or locally underlain (e.g. DDH R4452) by a zone of intense Mn-bearing carbonate alteration, up to 10 m thick (data sheet 120R–1357). Intense Mn-carbonate is spatially closely associated with massive sulphide, but locally extends several tens of metres beyond the limits of known massive sulphide (e.g. down-dip of the K-lens intersection on section 1700 mN, Fig. 2b). The Mn-carbonate typically has a spotty texture, comprising 25-60% Mn-carbonate spots in a strongly sericite-altered, or locally a chlorite-altered, matrix. This alteration zone is generally poor in sulphides.

Chlorite zone: Chlorite is concentrated in the immediate footwall of the ore lenses, varying in content from 15 to 50 wt% (data sheet 120R–1386. Thickness of the intense chlorite alteration is generally less than 5 m in the drill holes studied. The thickest and most intense chlorite alteration is associated with the footwall zone to the copper-rich lenses elsewhere at Rosebery. A narrow zone of chlorite alteration extends along strike in the footwall of the ore position (Fig. 7). Preliminary microprobe and whole-rock analyses indicate that the chlorite in the footwall alteration zone is Fe-rich, whereas chlorite in the Mn-carbonate zone and stratigraphically overlying volcanic sandstone unit (TSV) is Mg-rich.

Sericite-carbonate zone: A broad alteration zone of sericite with scattered Mn-bearing carbonate blebs overlaps and extends beyond the chlorite, Mn-carbonate and chlorite zones (Figs. 2b, 7) (data sheets

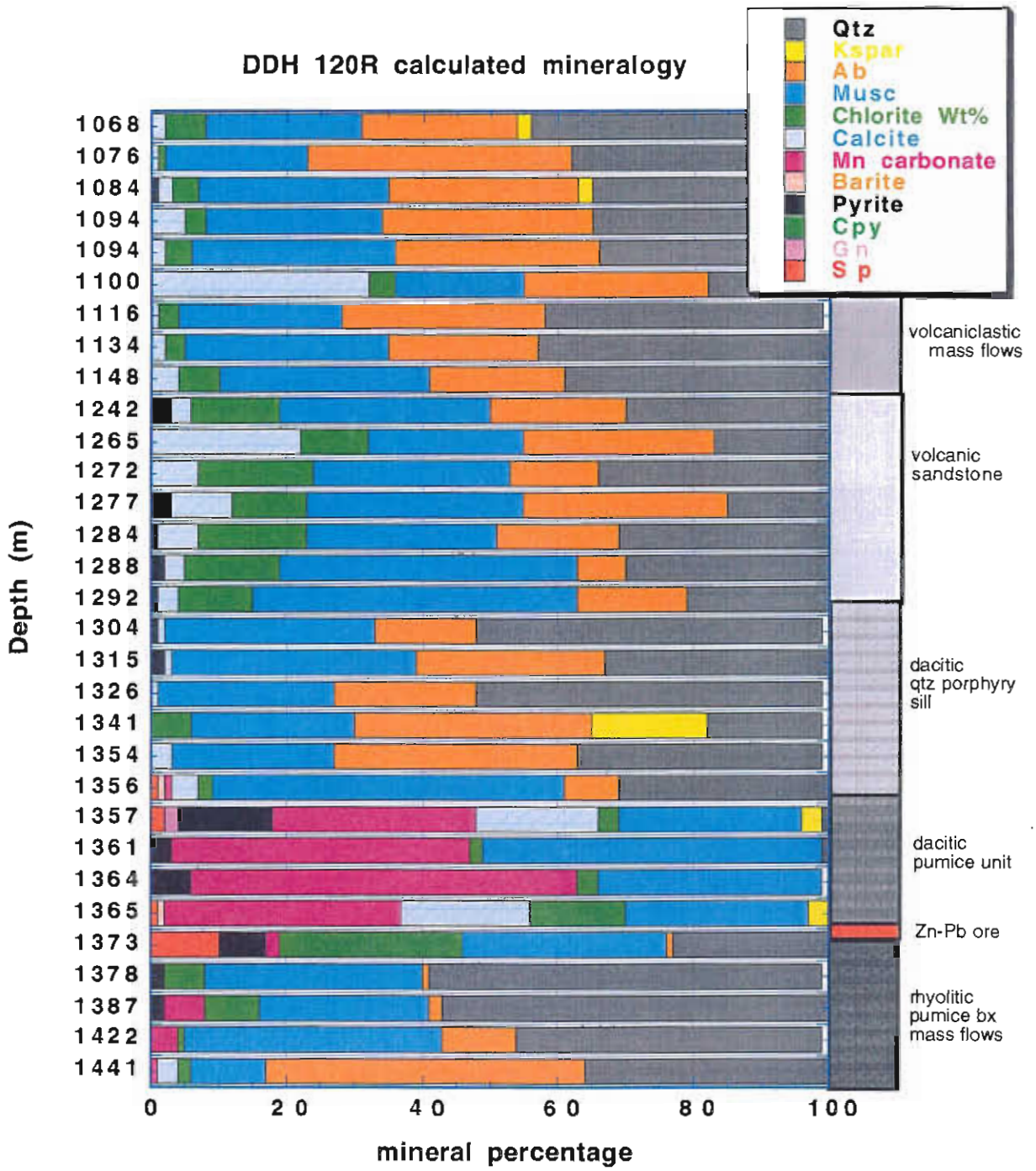

Figure 6 : Variation in mineral distribution in a series of samples from DDH 120R through K lens. The mineral percentages have been calculated from the whole rock analyses using a least squares procedure (Herrmann et al., this volume).

Table 2 Alteration types and their relative timing, Rosebery-Hercules area

Table 2 Alteration types and their relative timing, Rosebery-Hercules area

	Regional + ORE RELATED alteration	Time ---------->
		| Si | S2 |
	Deposition of pumice breccia	-
(1)	Smectite (montmorlllonite) (glass surfaces)	---------- - - -
(2)	SPHEROIDAL MN-CARBONATE (concentric layered, concretionary)	--- - - - - -
(3)	Mordenite-clinoptilolite (replaces glass)	---- - - - - - -
	Sphene-leucoxeneihematite	---------- - - - - -
(4)	?Analcite (replaces mordenite-clinoptilolite)	----- - - - - -
	Kfeldspar-quartz (overgrowths on plag phenos)	----- - - - - -
(5)	Burial compaction, smectite/sericite fiamme	- - - - ---------- - -
(6)	SPOTTY MN-CARBONATE (not concretionary)	---------- - - - - - -
	SUB-SPHEROIDAL Mn-CARBONATE VEINS	---------- - - - - - - -
(7)	SERICITE-CARBONATE-LEUCOX	---------- - - - - - - - - -
(8)	QUARTZ±SERICITE-Py-Sp ±Gn-Cpy	---- - - - - - - - - -
(9)	CHLORITE±QUARTZ ±Py-Sp-Gn-Cpy	---- - - - - - - - - -
(10)	Calcite impregnation ± sp (in TSV,hangingwall)	---------- - - - - -
(11)	Albite (replaces K-feldspar ±analcite; deep subseafloor)	- - ---------- - - -
(12)	Stylolitic Sl	- ---------- -
	Chlorite/sericite pseudofiamme	- ---------- -
(13)	Metamorphic albite-chl-epid-carb-mag-leucox	- - ---------- -
	Metamorphic biotite + retrograde chlorite	- - ---------- -
(14)	Reactivated Sl ±sericite or chlorite	- --- - -
(15)	Syn-S2 sericite-calcite (cleavage related)	- ---------- -
(16)	Syn-S2 quartz- calcite ±ser±sp-py-gn veins	- ---------- -
(17)	Syn/late-S2 FeMn-carb ±arspy veins, bleached haloes	- - - - - - - - --------- -
(18)	Syn/late-S2 network chlorite veins (fault-related)	- - ------- -
(19)	Late/post-S2 quartz-carbonate veins, bleached halos	- ----- - -
(20)	Post-S2 biot-tour, chl-mag, carb-fluor-tour-arspy veins (with sericite-dark carbonate vein selvages)	------ - -
		| Si | S2 |

---------- Interpreted main growth interval
- - - - - - - - Time span that is possible from overprinting relationships

128R–1230, 84R–875). Muscovite content varies from 20 to 60 wt% through this zone. Distinct sericite-carbonate alteration can be mapped by eye and chemistry along the ore position (upper contact of footwall pumice breccia) beyond the limit of sampling (Fig. 2b), i.e., at least 500 m west of A-B lens.

Halo Geochemistry

Down hole variation of major and trace elements around the ore lenses has been previously outlined and discussed by Large and Allen (1997). Some of the drill hole data has been compiled onto a composite cross-section at 1700 mN (Figs 8, 9) and plan of 17 level (Fig. 10). The critical geochemical halo patterns evident from these figures are discussed below.

Zinc and lead distribution: The distinctly ore-related zinc and lead halo is of limited extent, reaching about 300 m along the potential ore position (top of pumice breccias) and only about 50 m across strike into the footwall. A poorly defined zone of disseminated sphalerite (100–1000 ppm zinc) occurs in the hangingwall volcaniclastics above the quartz porphyry sill. A more extensive study is required to determine whether this hangingwall low-level zinc anomaly is spatially related to the Rosebery orebody, or whether it is a regional zinc anomaly within the hangingwall mass flow succession. However, the occurrence of widespread zinc dispersion above a major zinc deposit is likely to be more than coincidence, and we suggest that this halo is worthy of further consideration in the future. This hangingwall zinc zone is not accompanied by anomalous lead.

Manganese distribution: MnO forms a limited halo, confined to the Mn-carbonate alteration zone, and the inner parts of the sericite-carbonate zone, which tend to be richer in Mn-carbonate blebs. Minor MnO extends further into the footwall sericite alteration zone, but exhibits background values (<0.5 wt%) throughout the hangingwall and most of the footwall,

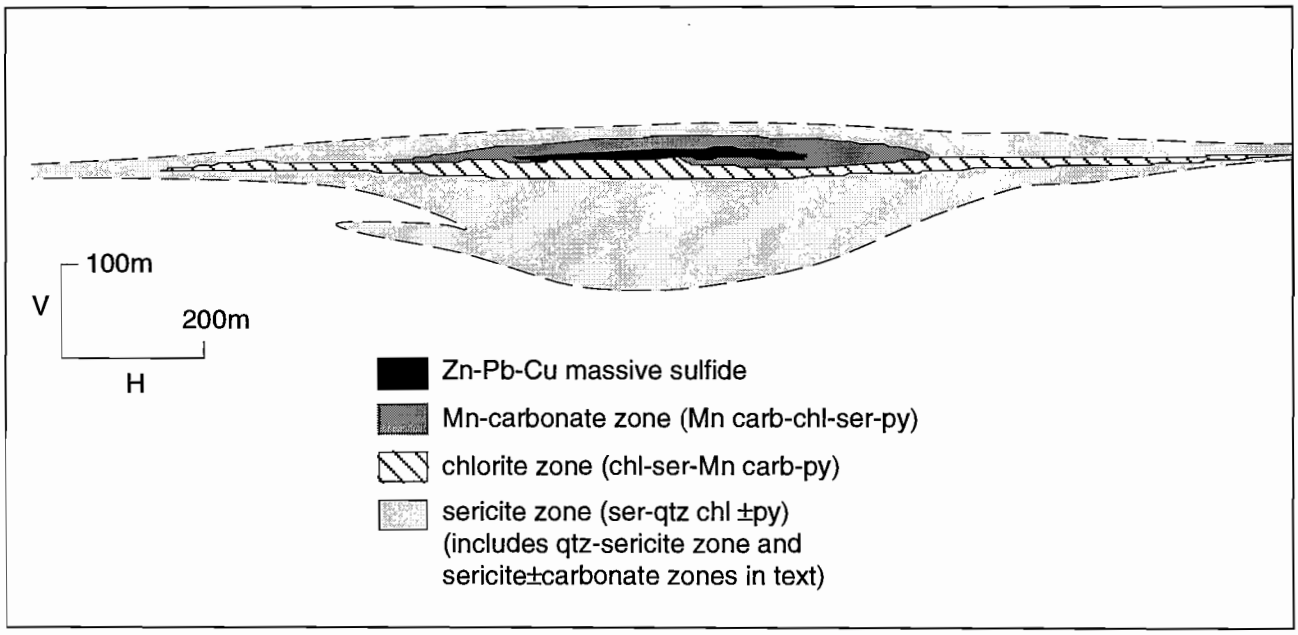

Figure 7: Diagrammatic model of alteration mineral zones surrounding the K lens, Rosebery.

except for local increases (spikes in the down-hole geochemical plots) related to local bleached sericite-carbonate alteration haloes around syn-tectonic and post-tectonic veins (Fig. 2b). For example, the patch of anomalous MnO deep in the footwall in DDH 109R is related to carbonate-arsenopyrite-pyrite-tourmaline veins with carbonate-bearing haloes. Petrographic studies by Rod Allen indicate these veins range from syn- to post-S2 cleavage (Devonian deformation). Carbon and oxygen isotope analyses indicate they have similar isotopic values to the massive sulfide lenses and are distinctly different to Devonian syn-tectonic or granite-related mineralisation. This suggests they could represent Devonian remobilisation of Cambrian alteration-mineralisation, and may be worthy of further investigation.

Sodium distribution: Albite replacement by sericite ± chlorite ± quartz leads to strong sodium depletion (to <0.1 wt%) throughout the footwall alteration zones to the Rosebery ore lenses. This zone thins latterally and grades into a narrow zone of sodium depletion at the top of the footwall pumice breccia that underscores the potential ore position for more than 500 m to the west of A-B and K lenses. Sodium depletion occurs in two other zones at Rosebery:

(1) Along the Black Slate horizon where it is related to primary sedimentary processes rather than hydrothermal processes;
(2) In a narrow zone of sericite±carbonate, quartz-sericite and tourmaline alteration along the Mt Black Fault (Fig. 2b), probably due to the passage of metamorphic fluids along this fault during Devonian deformation and granite intrusion.

Potassium distribution: Elevated K_2O occurs in a zone surrounding the ore lenses and extending into the overlying quartz-porphyry sill (Fig. 8). The highest levels of K_2O (>5 wt%) occur in a stratiform sericite alteration band about 50 m below the ore lenses. A narrow band of K_2O enrichment also coincides with the sodium depletion zone along the Mt Black Fault.

*Thallium and Antimony distribution:*Thallium and antimony are the only trace elements investigated in this study which show a clearly developed and widespread halo around the ore lenses (Large and Allen, 1997). Smith and Huston (1992) previously reported significant Tl and Hg halos surrounding the ore lens at Rosebery, however their sampling was limited and the full extent of the halos was not defined.

In DDH 120R (Fig. 11) thallium exhibits an amazingly systematic pattern, defining a halo at least 270 m across stratigraphy surrounding the ore position. The main features of the Tl halo are:

- The halo of Tl in the hangingwall units (porphyry sill, volcanic sandstone and black slate) varies systematically from 10 ppm down to 1 ppm over a distance of 200 m, passing away from the ore body.

- The footwall halo is less extensive, but penetrates at least 70 m below the ore lens.

- A second Tl peak occurs at the upper contact of the porphyry sill/volcanic sandstone suggesting a second zone of mineralization at this level (this mineralised position is confirmed in DDH 128R).

On section 1700 mN and the 17 level plan (Figs 9, 10) the thallium halo (above 1 ppm) forms an envelope about 200 to 300 m wide which surrounds the ore lens and extends along strike, defining the favourable ore position, for at least 500 m west (beyond DDH 109R). Regional studies in the Hercules area (Large, 1996; and Herrmann et al., 1997) indicate that anomalous Tl values occur at the White Spur Formation–CVC contact 3.5 km south of the Hercules deposit.

This research indicates the potential to use thallium as a identifier for regional favourable ore horizons, and locally on the mine scale to identify proximity to an ore lens.

Antimony shows a similar distribution to thallium outlining a broad halo around the ore lenses at Rosebery (Fig. 9). However Sb values tend to be not as systematic as thallium and should therefore only be used in support of the Tl data. There is a good correlation between Tl and Sb for the complete Rosebery data set (Fig. 12) giving an indication of the variation in these trace elements throughout the halo to the K and A-B lenses.

Previous workers have concluded that Tl most likely substitutes for K-bearing minerals in the halo of base metal deposits. The data from Rosebery (Fig. 13) shows a rough correlation between Tl and K_2O suggesting that Tl is present in muscovite in the alteration halo. The data also suggests that both the background and anomalous populations of thallium

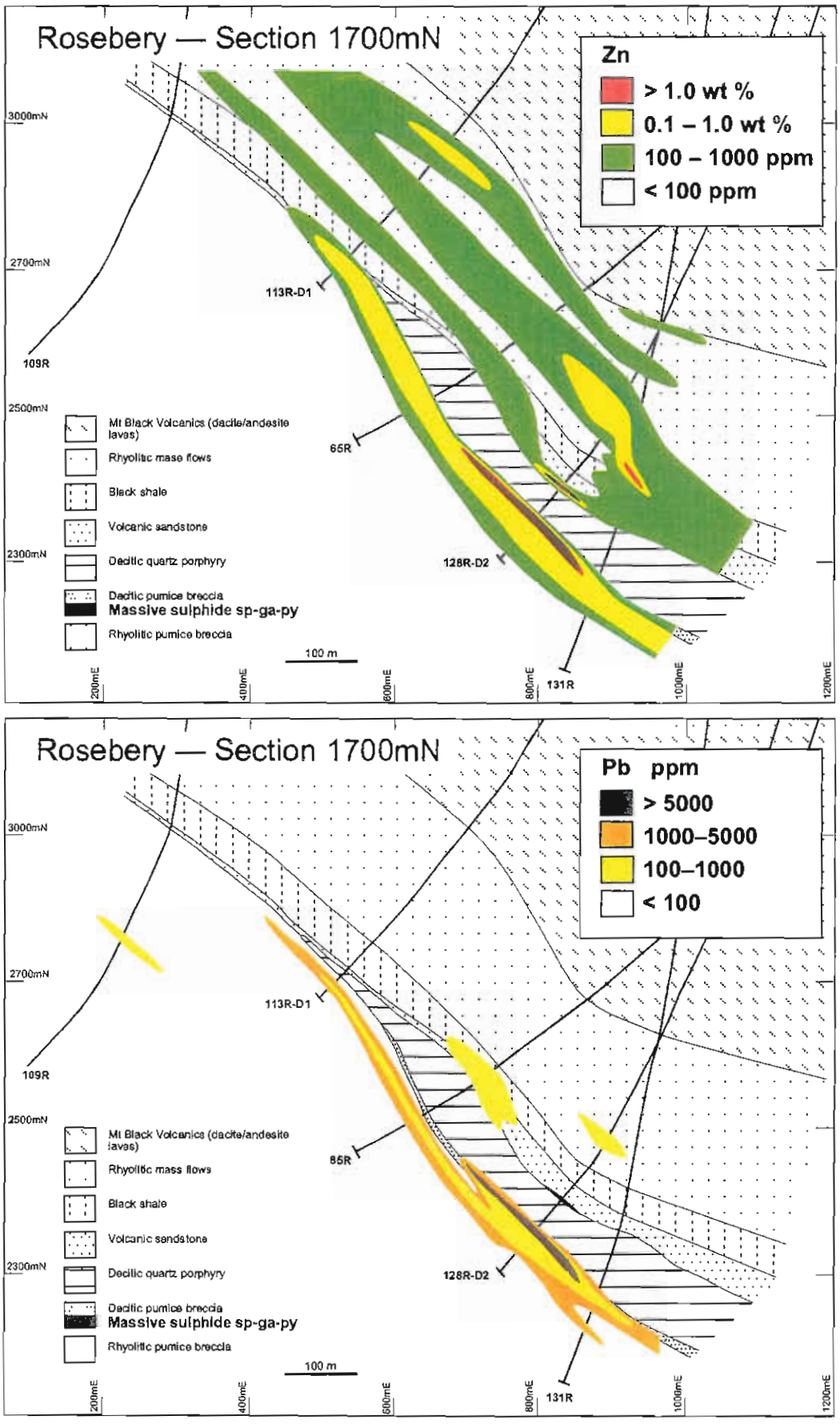

Figure 8. Composite section at 1700 mN showing the geology and geochemical dispersion around the K lens: Zn, Pb, Na_2O, K_2O, MnO.

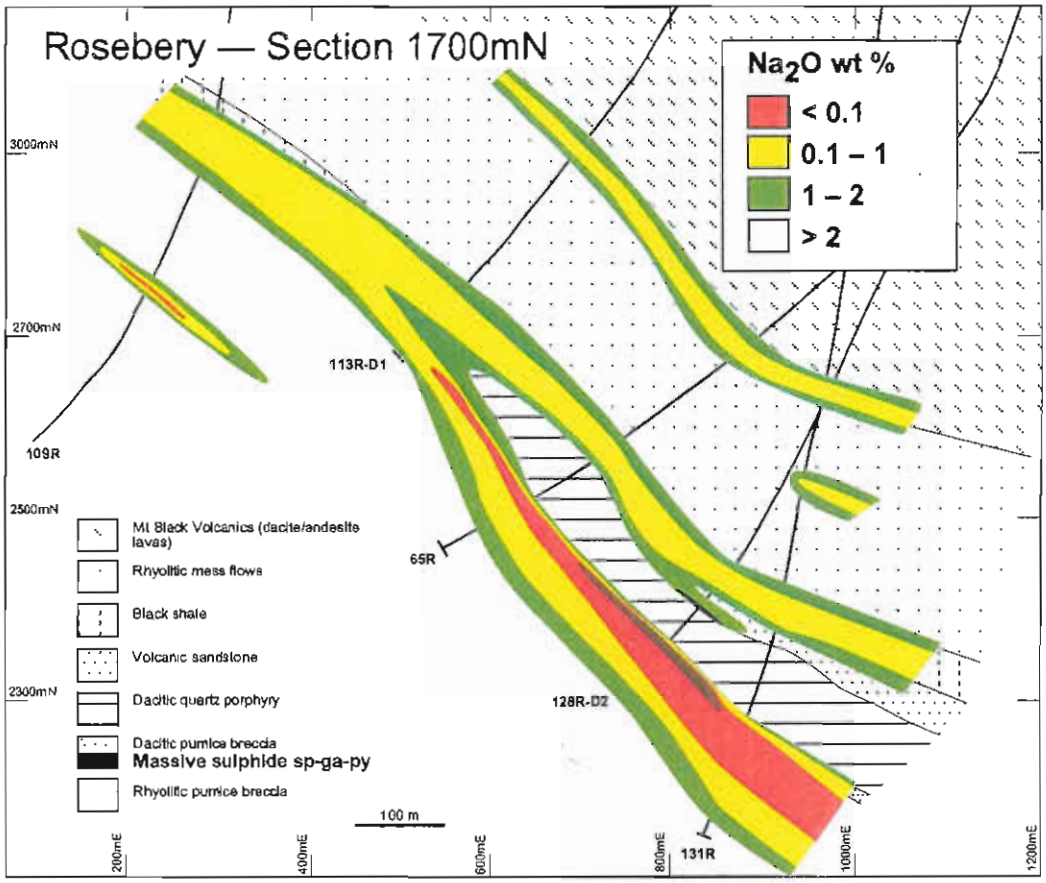
Rosebery — Section 1700mN
Na2O wt %
< 0.1
0.1 – 1
1 – 2
> 2
3000mN
2700mN
2500mN
2300mN
113R-D1
109R
65R
128R-D2
131R
Mt Black Volcanics (dacite/andesite lavas)
Rhyolitic mass flows
Black shale
Volcanic sandstone
Dacitic quartz porphyry
Dacitic pumice breccia
Massive sulphide sp-ga-py
Rhyolitic pumice breccia
100 m
200mE
400mE
600mE
800mE
1000mE
1200mE

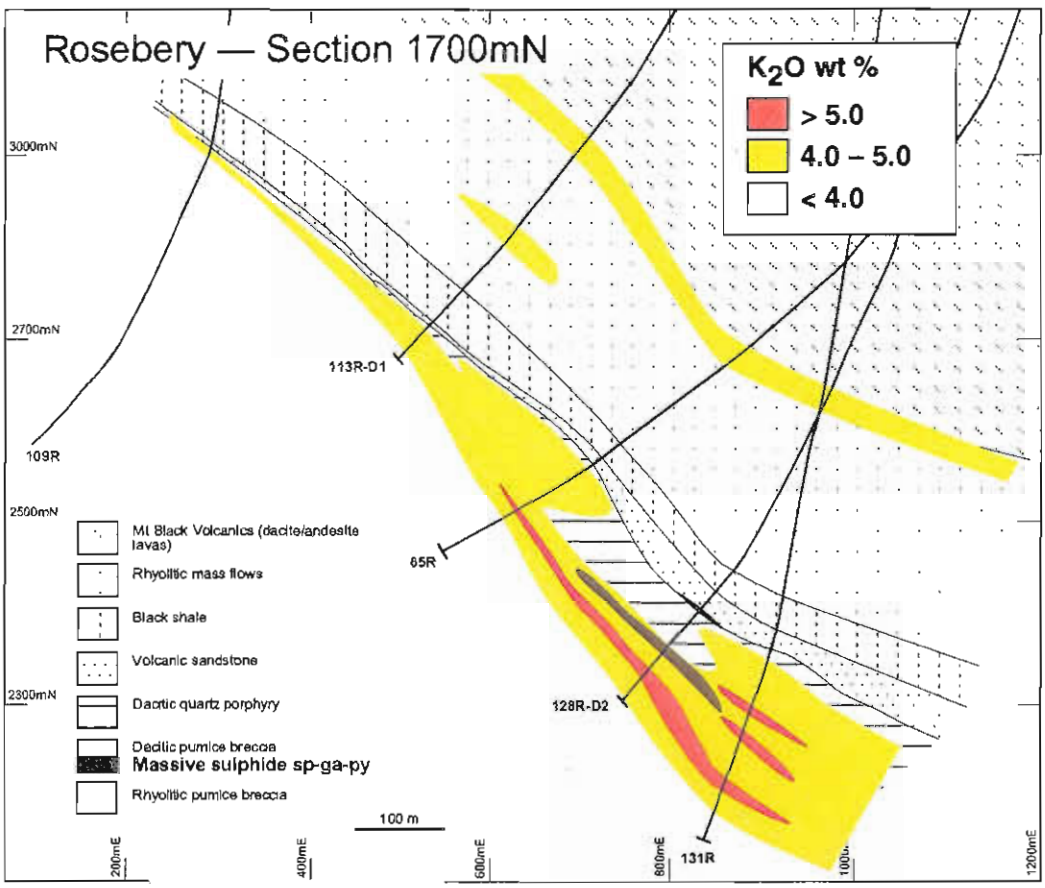
Rosebery — Section 1700mN
K2O wt %
> 5.0
4.0 – 5.0
< 4.0
3000mN
2700mN
2500mN
2300mN
113R-D1
109R
65R
128R-D2
131R
Mt Black Volcanics (dacite/andesite lavas)
Rhyolitic mass flows
Black shale
Volcanic sandstone
Dacitic quartz porphyry
Dacitic pumice breccia
Massive sulphide sp-ga-py
Rhyolitic pumice breccia
100 m
200mE
400mE
600mE
800mE
1200mE

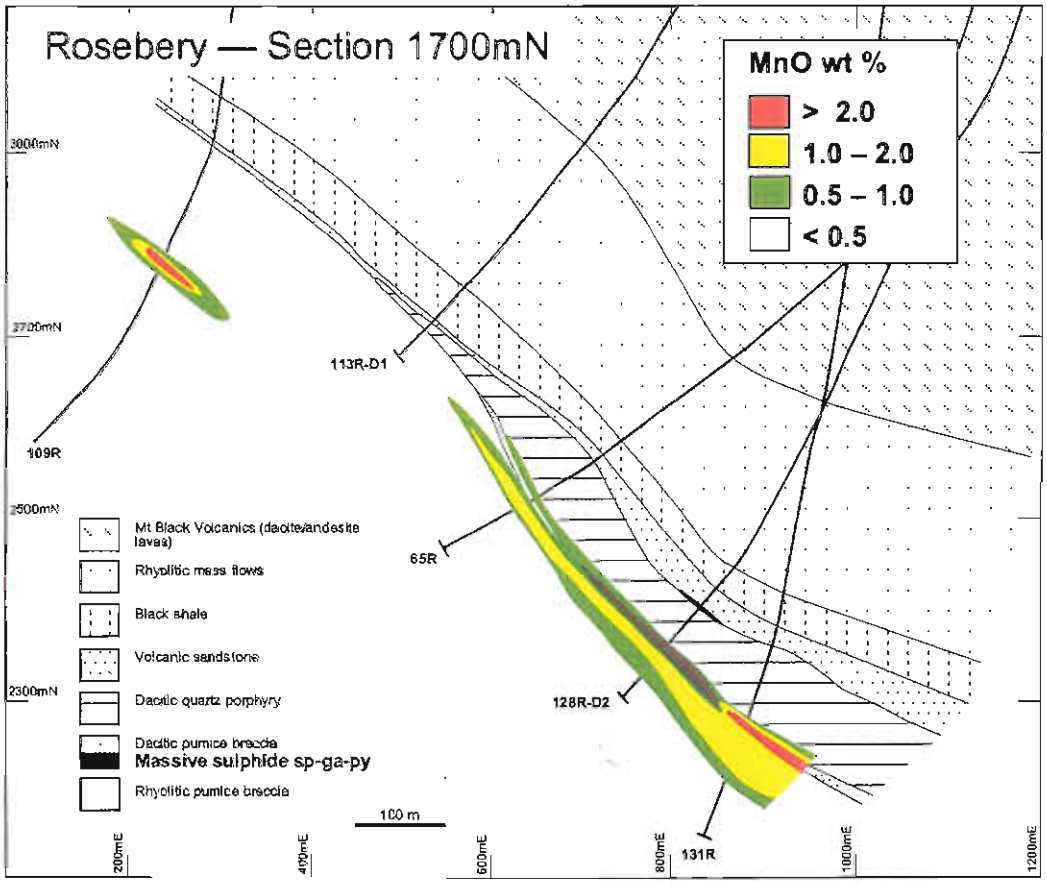
Rosebery — Section 1700mN
MnO wt %
> 2.0
1.0 – 2.0
0.5 – 1.0
< 0.5
3000mN
2700mN
2500mN
2300mN
113R-D1
109R
65R
128R-D2
131R
Mt Black Volcanics (dacite/andesite lavas)
Rhyolitic mass flows
Black shale
Volcanic sandstone
Dacitic quartz porphyry
Dacitic pumice breccia
Massive sulphide sp-ga-py
Rhyolitic pumice breccia
100 m
200mE
400mE
600mE
800mE
1000mE
1200mE

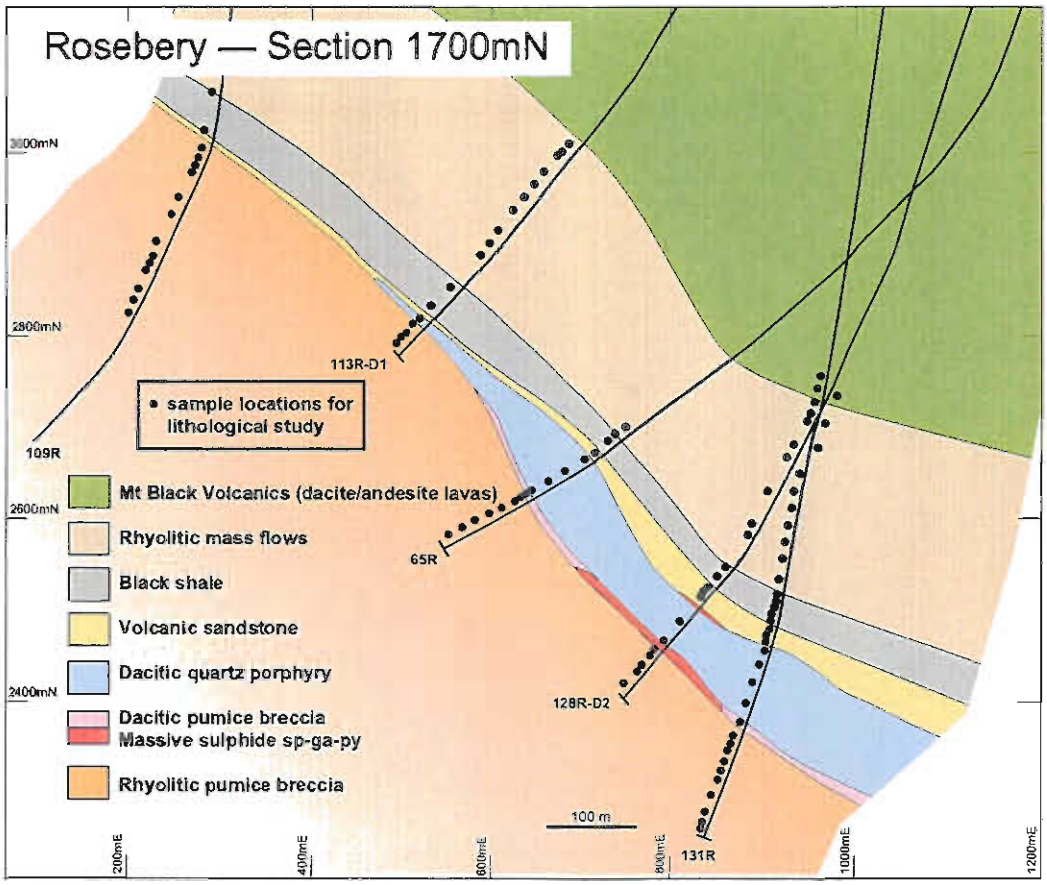
Rosebery — Section 1700mN
3000mN
2800mN
2600mN
2400mN
113R-D1
109R
65R
128R-D2
131R
• sample locations for lithological study
Mt Black Volcanics (dacite/andesite lavas)
Rhyolitic mass flows
Black shale
Volcanic sandstone
Dacitic quartz porphyry
Dacitic pumice breccia
Massive sulphide sp-ga-py
Rhyolitic pumice breccia
100 m
200mE
400mE
600mE
800mE
1000mE
1200mE

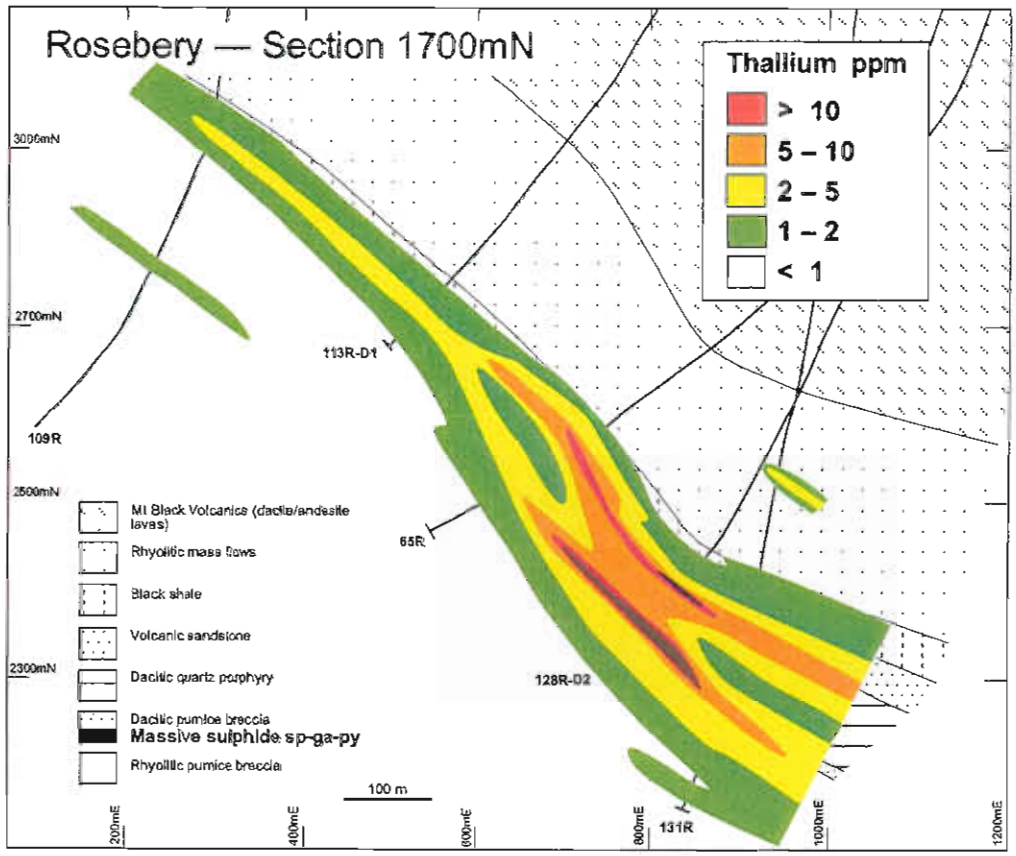

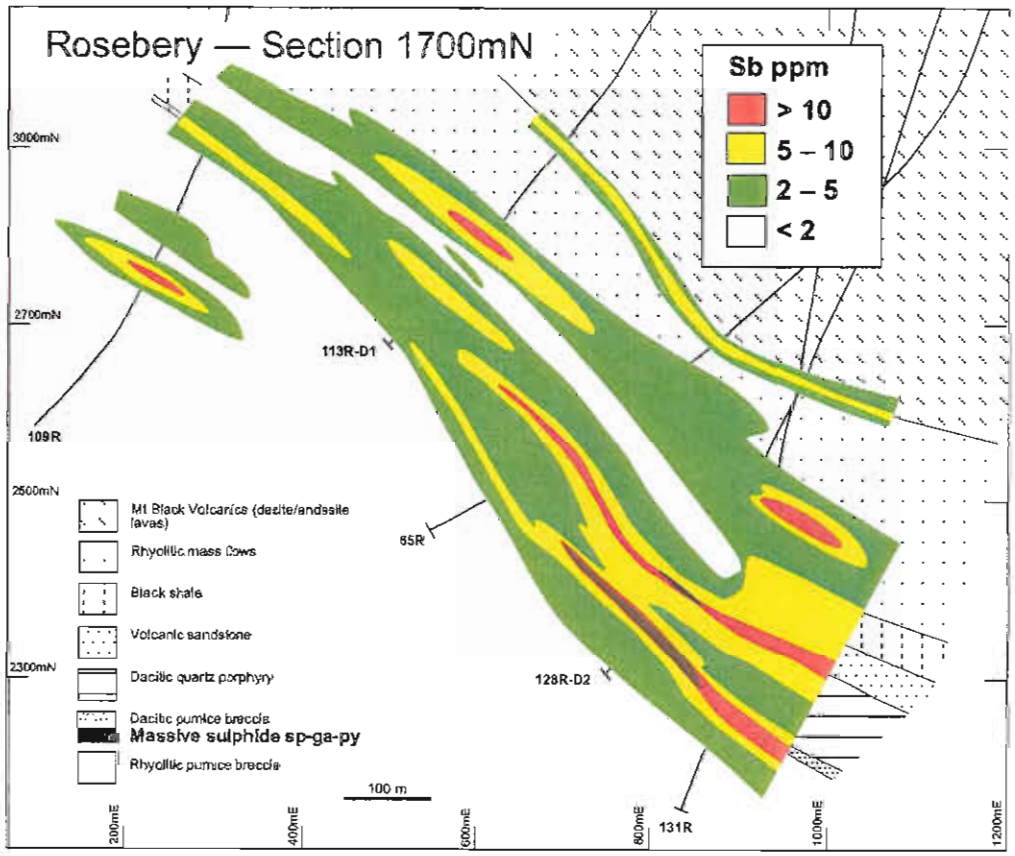

Figure 9. Composite section at 1700 mN show the geology and geochemical dispersion around the K lens: Tl, Sb, Ishikawa Al and Ba/Sr ratio.

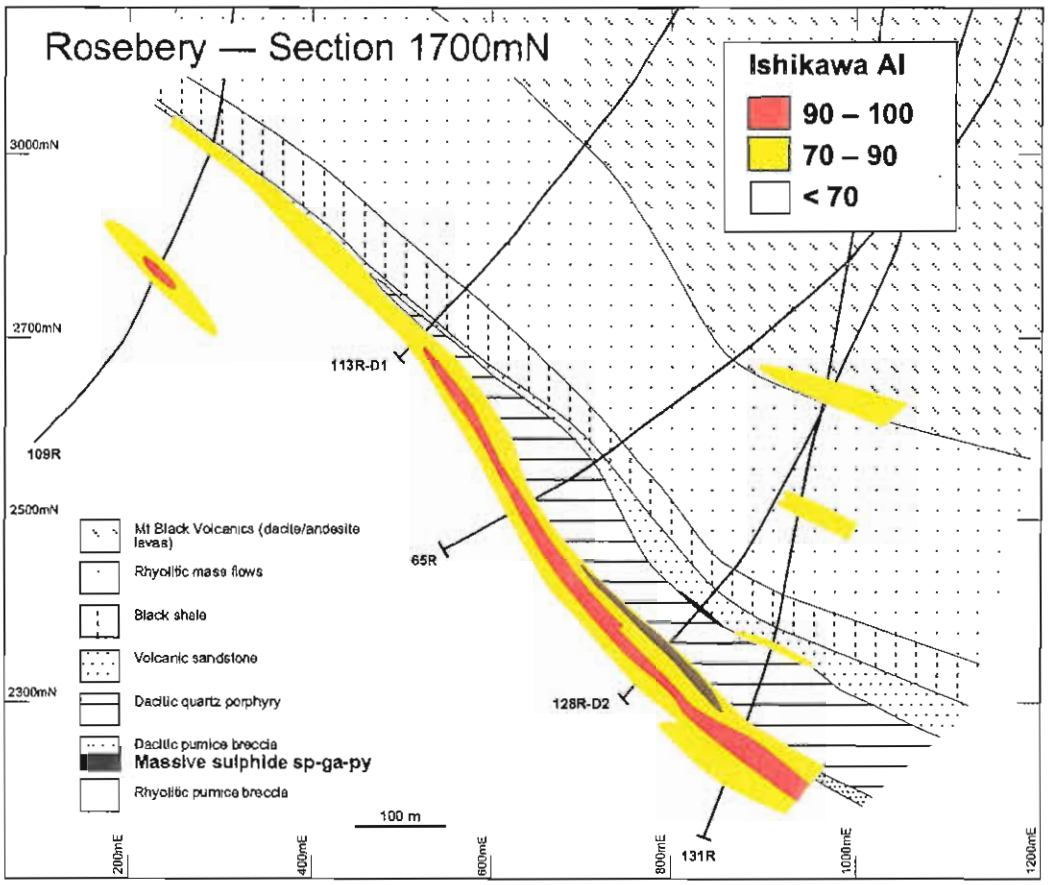
Rosebery — Section 1700mN
Ishikawa AI
90 – 100
70 – 90
< 70
3000mN
2700mN
2500mN
2300mN
113R-D1
109R
65R
128R-D2
131R
Mt Black Volcanics (dacite/andesite lavas)
Rhyolitic mass flows
Black shale
Volcanic sandstone
Dacitic quartz porphyry
Dacitic pumice breccia
Massive sulphide sp-ga-py
Rhyolitic pumice breccia
100 m
200mE
400mE
600mE
800mE
1000mE
1200mE

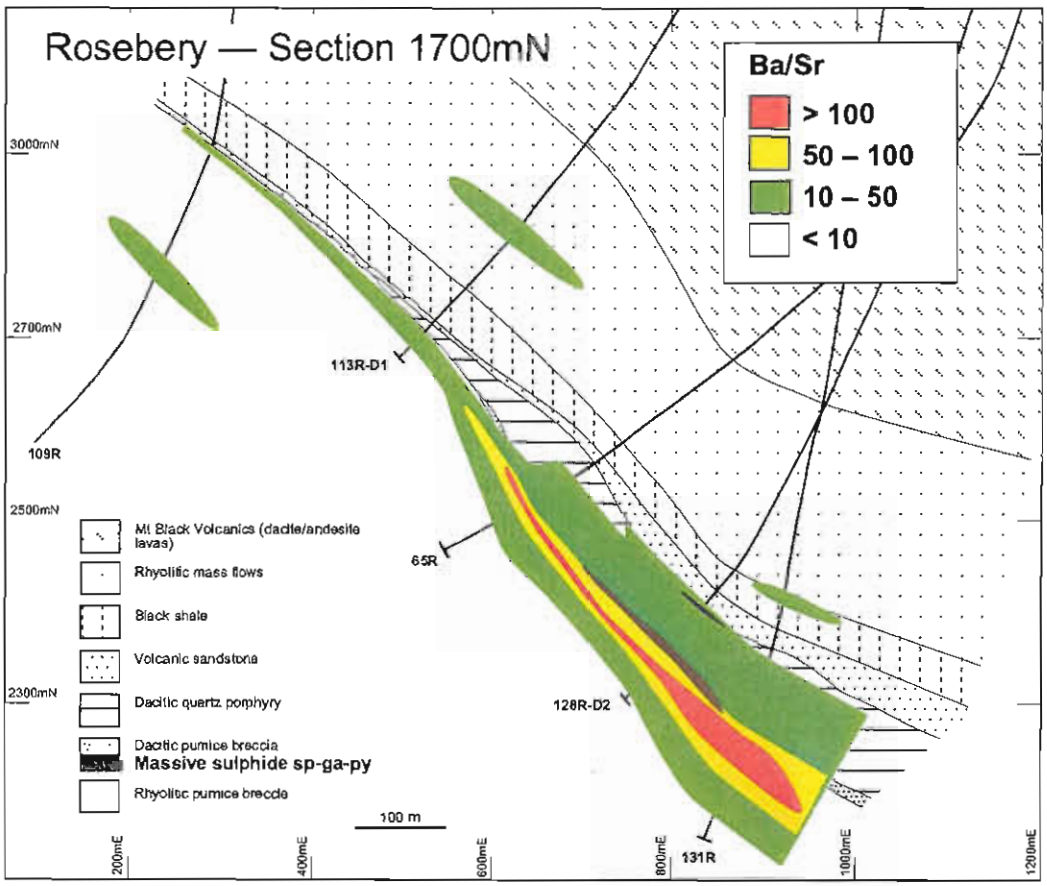
Rosebery — Section 1700mN
Ba/Sr
> 100
50 – 100
10 – 50
< 10
3000mN
2700mN
2500mN
2300mN
113R-D1
109R
65R
128R-D2
131R
Mt Black Volcanics (dacite/andesite lavas)
Rhyolitic mass flows
Black shale
Volcanic sandstone
Dacitic quartz porphyry
Dacitic pumice breccia
Massive sulphide sp-ga-py
Rhyolitic pumice breccia
100 m
200mE
400mE
600mE
800mE
1000mE
1200mE

blank

blank

blank

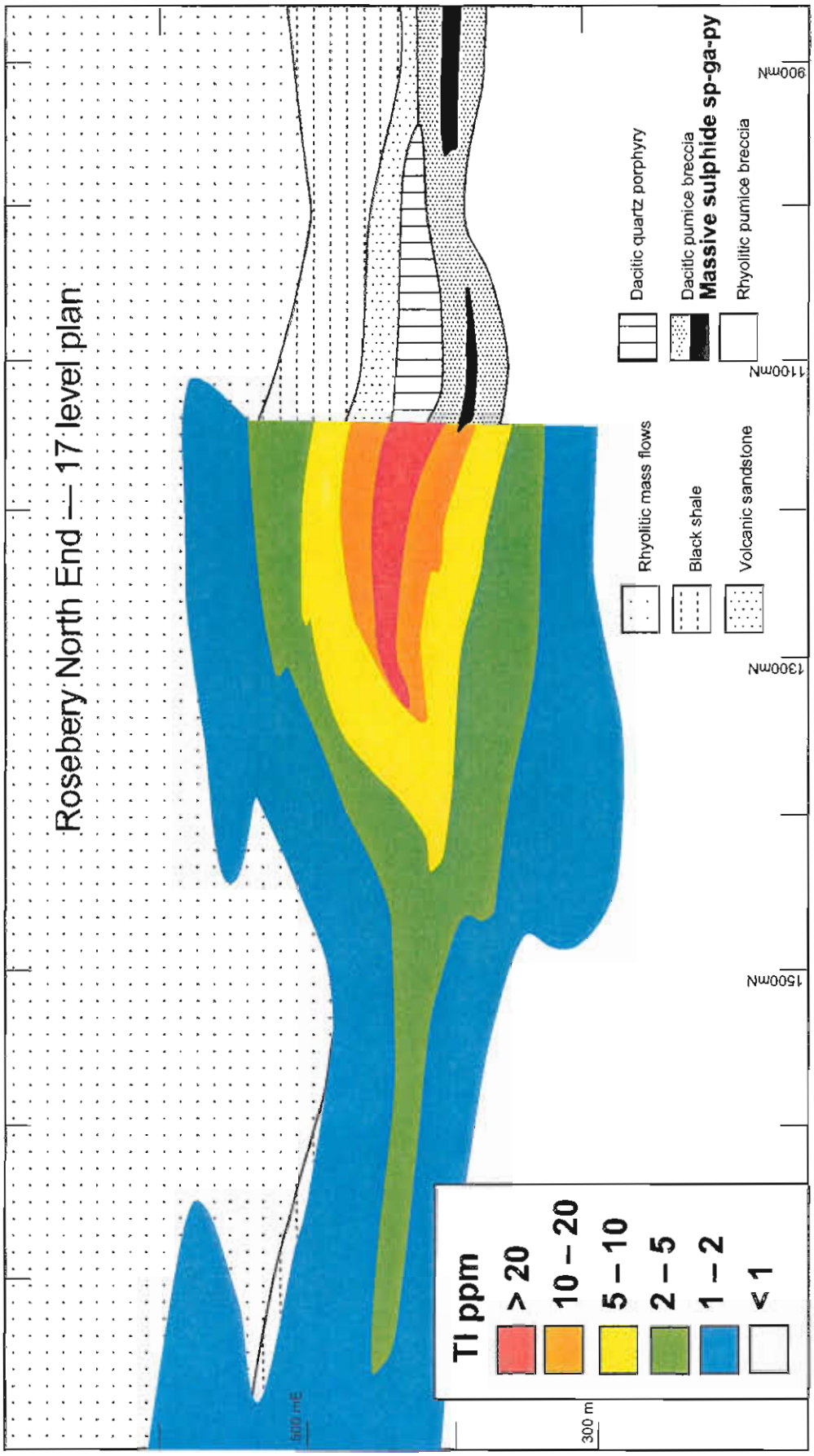

Figure 10: Rosebery north end 17 level plan and thallium distribution based on DDH's R4452, 84R, 113RDI and 109R.

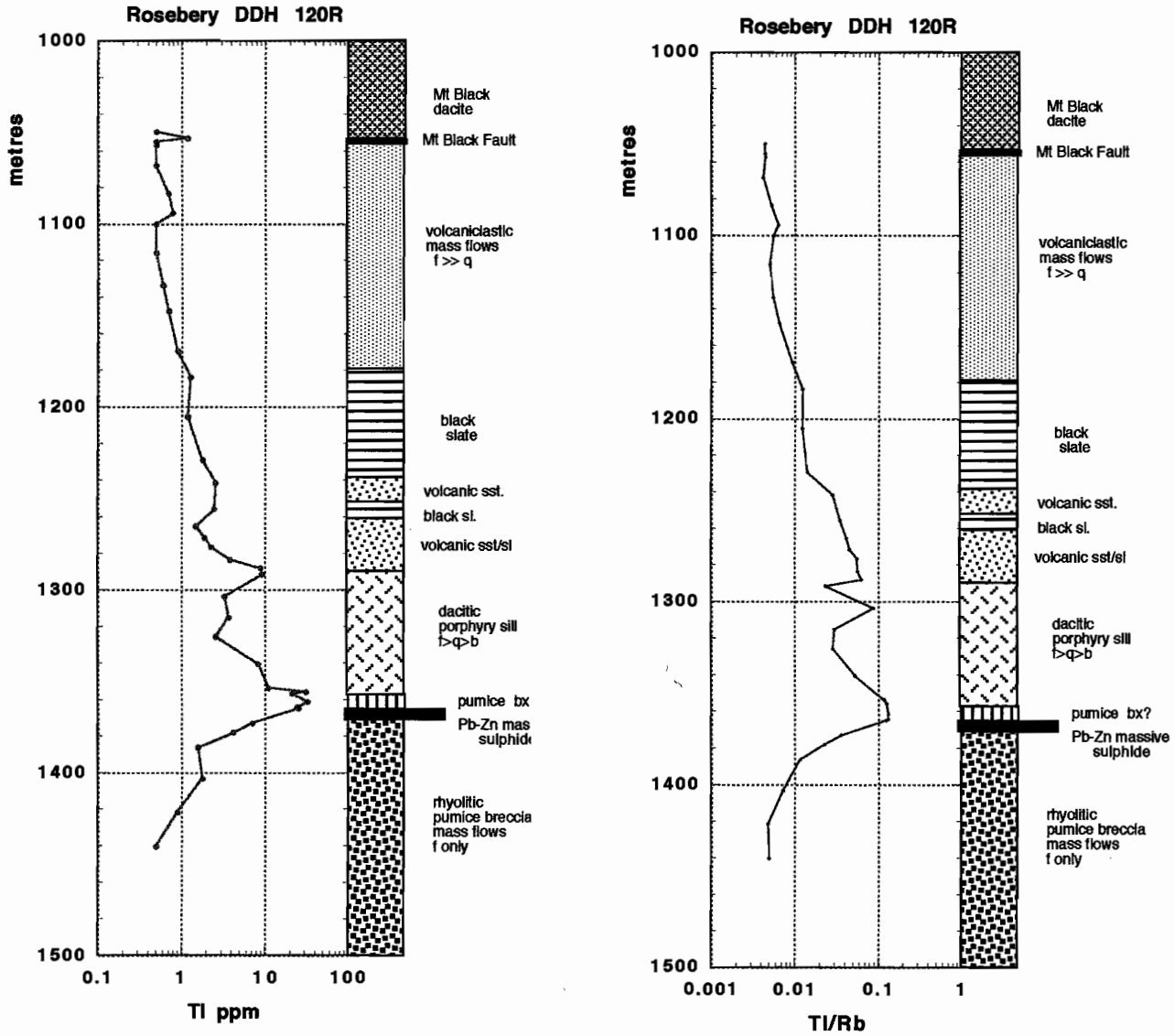

Figure 11: (a) Thallium distribution in DDH 120R, showing a systematic decrease from the massive sulfide ore lens for over 300 m through the hangingwall succession. (b) Tl/Rb ratio for DDH 120R, shows a smoother pattern than Tl above.

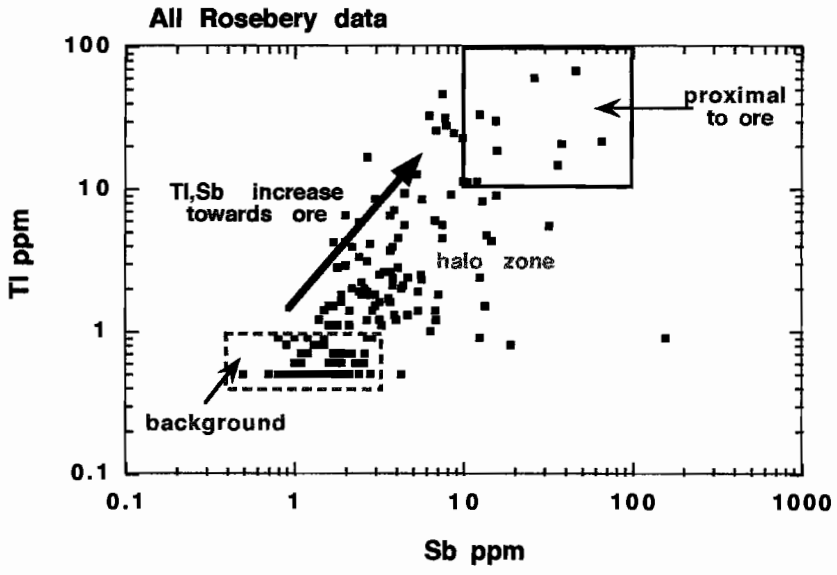

Figure 12 : Relationship between Tl and Sb for the ore zone and halo at Rosebery; based on data from nine drill holes in the Rosebery north end.

are partly controlled by the muscovite content of the volcanic rocks.

Because both Tl and Rb substitute for K in muscovite, then the Tl/Rb ratio shows a very smooth and well developed halo around the Zn=Pb ore lenses at Rosebery (Fig. 11b).

Alteration Indices

A number of alteration indices and element ratios have been tested on the Rosebery data set. They are discussed below in order of their value for use as vectors to ore.

S/Na_2O ratio

Varies through five orders of magnitude from values of 0.01 in albite-rich, pyrite poor unaltered volcanics to over 100 for pyrite-rich, albite depleted highly altered volcanics (Fig. 14). The ratio is an excellent vector within footwall sericite and pyrite-bearing alteration zones, and for up to 50 m into the hangingwall, but is of little use in weakly developed hangingwall alteration, which typically lacks significant sulfide development or albite destruction. The ratio provides a good vector for the Rosebery ore stratigraphic position at distal locations up to several hundred metres from ore.

Ishikawa Alteration Index

$100\ (MgO + K_2O)/(MgO + K_2O + CaO + Na_2O)$

This index relates to the replacement of plagioclase by sericite and chlorite during hydrothermal alteration. The index is elevated to values of 70 to 100 throughout the footwall alteration zone (Fig. 14), and extends along the favourable horizon making an excellent indicator of the ore position (Fig. 9). However at Rosebery the index is slightly less anomalous in the direct hangingwall to ore than the S/Na2O ratio, is unable to detect weak alteration further into the hangingwall, and is unresponsive to carbonate alteration.

Chlorite, carbonate, pyrite index CCPI

$CCPI = 100(FeO + MgO)/(FeO + MgO + K_2O + Na_2O)$

This index measures the degree of chlorite, (Fe, Mg) carbonate and/or pyrite alteration related to VHMS deposits (Large, 1996; Large and Allen, 1997). The index exhibits a systematic increase (from 10 to 80) through the footwall alteration zone to the ore position (Fig. 14). It is also elevated through the hangingwall volcanic sandstones (TSV) and black slate due to the chlorite-carbonate-bearing mineralogy of these sedimentary rocks. This index is less useful due to its variation with primary rock composition, and in the Rosebery data set is a slightly less distinct vector than S/Na2O and the Ishikawa Alteration Index (Fig. 14).

Ba/Sr ratio

This ratio reaches a peak in the ore zone alteration due to the fact that Ba substitutes for K in the muscovite structure, while Sr is depleted due to albite destruction. As shown in Fig. 14 the Ba/Sr ratio increases abruptly through the footwall sericite/chlorite alteration zones, reaching a peak in the ore zone. A broad halo of elevated Ba/Sr extends up to 80 m through the hanging wall sequence. This ratio is superior to the other indices (but not thallium) in the hangingwall directly above ore (Fig. 14) and for some distance lateral to ore (Fig. 9) but becomes a less distinct vector at distal positions from ore.

The Al-CCPI box plot

Our previous research has shown that the AI-CCPI box plot is very useful for classifying altered rhyolitic volcanics in the Rosebery-Hercules district (Large, 1997). The value of this graphic representation relates to the fact that whole rock geochemistry can be directly related to alteration mineralogy. Least altered rhyolitic volcanics plot within a restricted field on the box plot (Fig. 15a), and alteration such as chloritisation, sericitation, carbonate alteration, epidote alteration, albite alteration or K-feldspar alteration is represented by trends lines away from the least altered box.

Both whole-rock analyses and microprobe mineral analyses can be plotted on the box plot, and show a clear relationship between alteration mineral assemblages and whole-rock geochemistry (fig. 15b). At Rosebery, hydrothermal alteration zones with the assemblage sericite-chlorite-Mn carbonate (± quartz) plot in the top right-hand sector of the box plot. This assemblage is present in all four major alteration zones surrounding the deposit (Fig. 7). Volcanic rocks with the assemblage albite-K-feldspar-calcite-

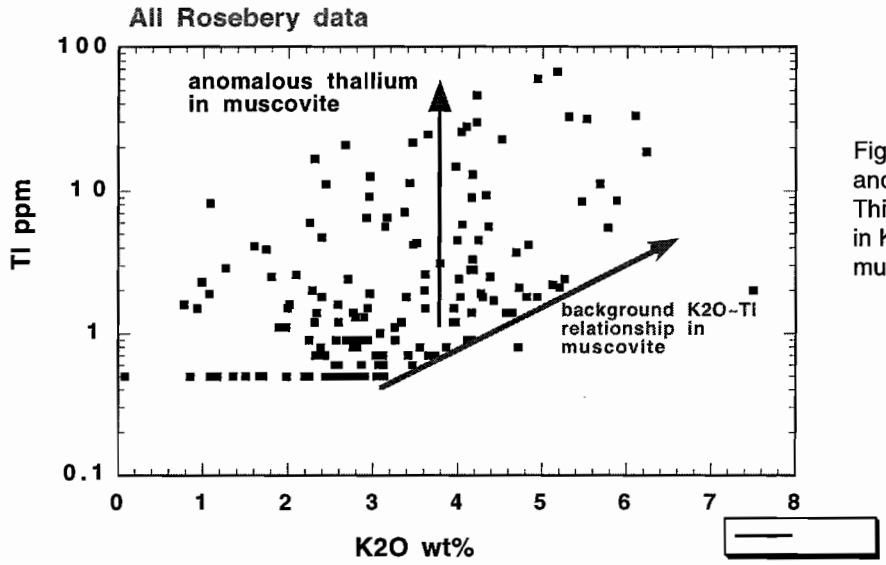

Figure 13 : Relationship between Tl and K_2O for all Rosebery samples. This pattern suggests that Tl is present in K_2O-bearing minerals (principally muscovite) in the alteration halo.

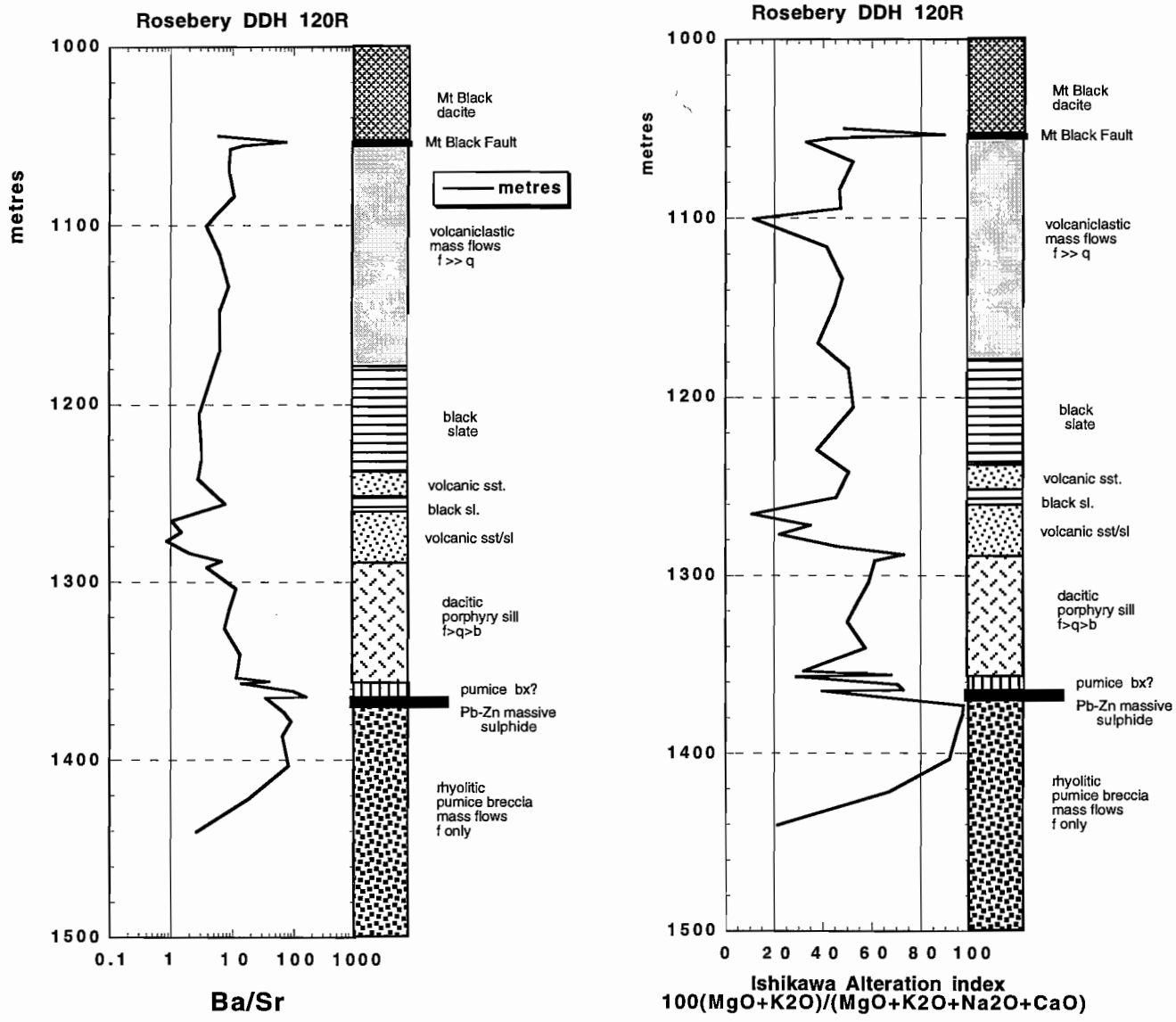

Figure 14 (continued on opposite page) : Comparison of the patterns of various alteration indices and ratios in DDH 120R: Ba/Sr, Ishikawa AI, CCPI, and S/Na_2O ratios.

sericite±chlorite±epidote plot in the lower left-hand corner of the box plot and represent diagenetic and/or metamorphic assemblages with little or no associated hydrothermal alteration (Fig. 15b).

Five fields can be identified on the box plot, that define the major alteration types at Rosebery:

Field 1. Least altered rhyolitic volcanics fall within a box bounded by AI = 20 to 65 and CCPI = 20 to 45.

Field 2. Weak sericite alteration in the deep footwall or hangingwall has AI >65 and CCPI <45.

Field 3. Intense footwall alteration typically exhibits AI >75 and CCPI >25 to 45 and plots adjacent to the sericite-chlorite/pyrite join.

Field 4. Altered rocks within the Rosebery-Hercules ore horizon fall in a triangular zone (carbonate-sericite-chlorite) with AI <75.

Field 5. Diagenetically altered, albitised rocks, well removed from hydrothermal alteration typically have AI <20.

A previous study (Large and Allen, 1997) has shown that the AI-CCPI box plot should only be used for studying alteration in relatively primary

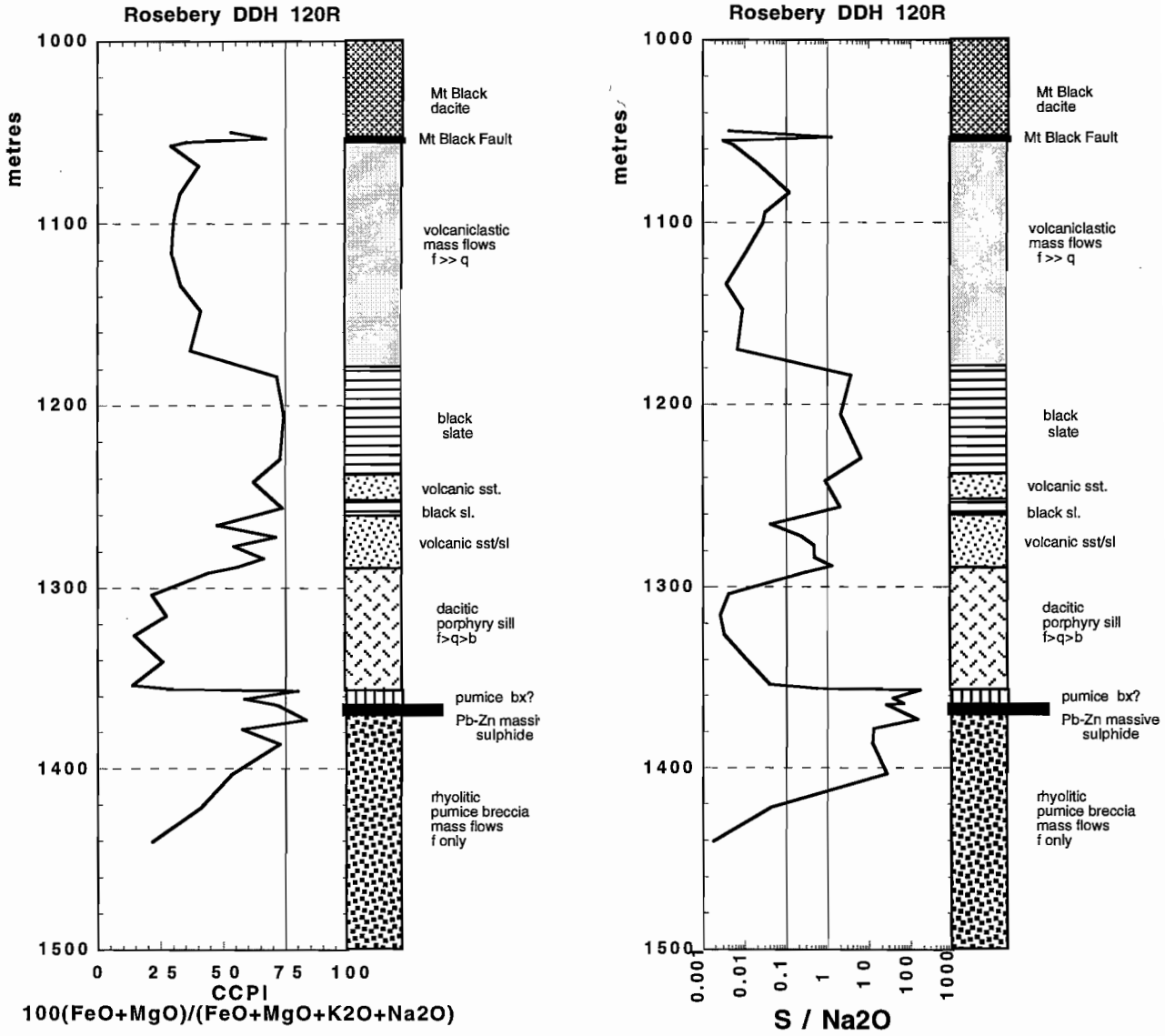

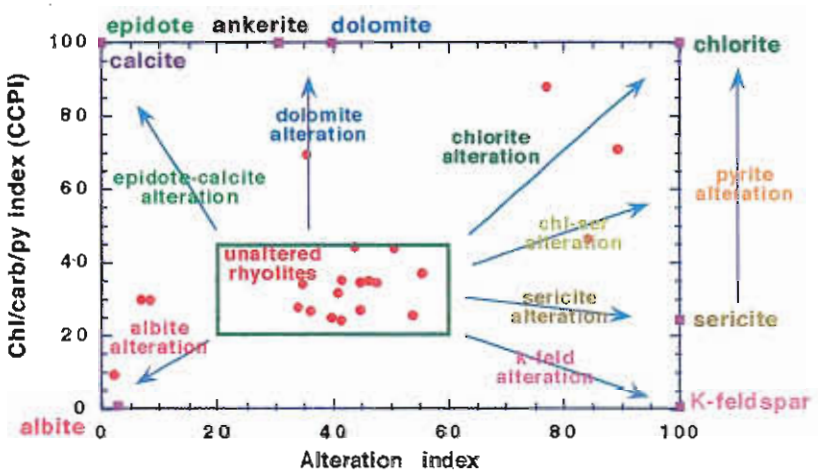

Figure 15a. Alteration index box plot showing the field of least altered rhyolitic volcanics and theoretical trend lines for various types of alteration. The red dosts are data from DDH 109R.

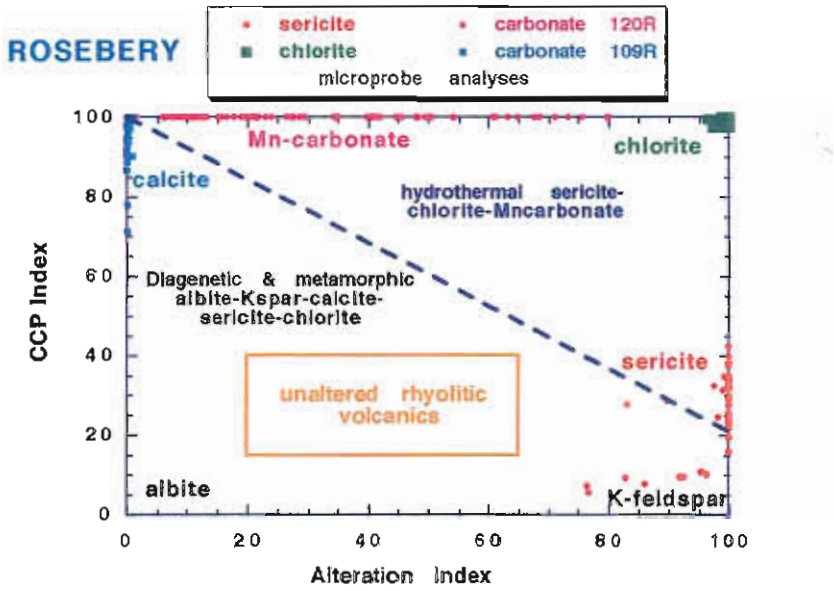

Figure 15b. Microprobe analysis of Mn-carbonate, calcite, chlorite and sericite from DDH 120R and DDH 109R shown on the alteration index box plot.

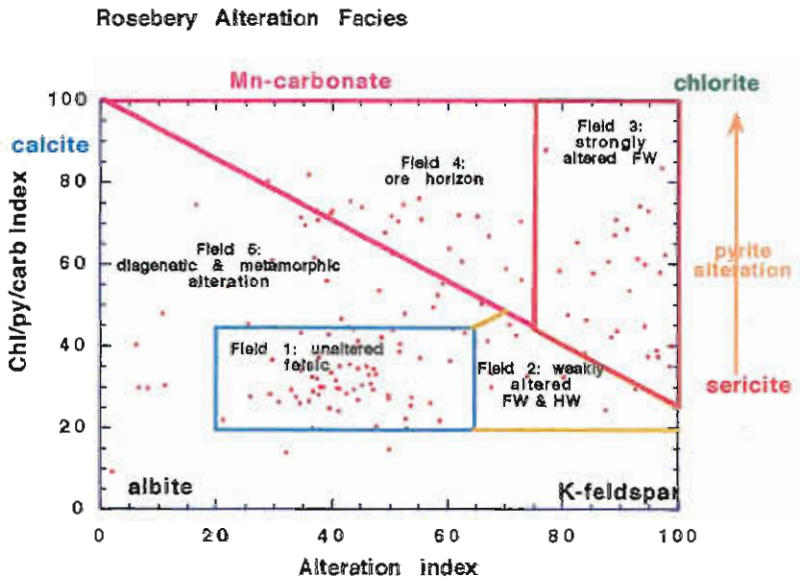

Figure 16 : Alteration index box plot showing the classification into least altered and the various hydrothermal alteration fields relevant to the Rosebery-Hercules district.

volcanics (lavas, pyroclastics, porphyry intrusives, syn-eruptive mass flows). Moderately to strongly reworked volcanics and sediments such as the TSV and Black Slate should be treated with care and may not show the alteration features discussed above.

Alteration mineral chemistry

A detailed study of muscovite and carbonate chemistry in selected samples through the volcanic stratigraphy and ore zone in DDH 120R was previously reported by Large et al. (1997). Since then further microprobe data has been collected on DDH 109R (500 m west of A-B lens) and all samples from the nine drill holes at Rosebery have been analysed by PIMA to test for mineral chemistry correlations in muscovite. Herrmann et al. (this volume) has undertaken a detailed study of the Rosebery PIMA spectra, and their relationship to mineral chemistry of muscovite and chlorite. A brief summary of the key concusions from this work are outlined below.

Muscovite composition

Microprobe analyses of 129 muscovites in 35 samples from Rosebery DH109R and 120R fall into two groups:

- Phengitic muscovites with between 0.5 and 1.0 Fe+Mg cations substituting for octahedral Al, and negligible Na. These exist in intensely altered proximal, and weakly altered distal, footwall alteration zones; in the weakly altered dacite sill overlying the sulfide lens and in the sequence above the Mt Black Fault (Fig. 17). Their compositional range is similar to muscovites in essentially fresh Mt Read Volcanics at Hercules and Mt Black.
- Sodic muscovites with up to 0.35 Na/Na+K and low phengite contents (<0.5 Fe+Mg cations). The Na exists either as a substitution for K in muscovite, or in fine mixtures of paragonite and muscovite. Muscovites of this type are restricted to the volcaniclastic sandstone (and associated black shale?) unit/s in the lower part of the hangingwall sequence (Fig. 12). The most sodic and least phengitic members of this group exist in close proximity to the ore lenses. It is likely that the unusual muscovite composition is associated with high chlorite content in these units and their probable mafic provenance, and may indirectly be related to the massive sulfide forming hydrothermal system (Fig. 18).

The down-hole variation of muscovite composition in DDH 120R is shown in Fig. 16, and described in detail in Herrmann et al. (this volume). The only feature of muscovite composition that is obviously related to mineralization is the increased substitution of Ba for K in the muscovite structure close to ore (Large et al., 1997). The contoured section of PIMA AlOH wavelength for muscovite (Fig. 18) shows a zone of low wavelength sodic muscovite corresponds to the volcanic sandstone unit in the hangingwall of the K lens.

Chlorite chemistry

Averaged analyses of 83 chlorites in 22 samples from DDH 109R and 120R indicate compositions ranging in Mg Number from 25 to 70 and in Si cations from 5.2 to 6.0 (Fig. 19). Chlorite compositional variations are not obviusly related to intensity of hydrothermal alteration, or spatially to sulfide lenses and the favourable horizon. However, the data are sparse in the footwall pumice breccia. Chlorites associated with the sulfide lens in DDH 120R, and in the anomalous hangingwall sandstone unit in both 120R and 109R have Mg numbers in the range 50–70 (Fig. 19a) compared to chlorites in the footwall and hangingwall mass flow units which are more iron-rich with Mg numbers in the range 20–50. This relationship between Fe-rich chlorite and Mg-rich chlorite is supported by thewhole-rock least squares calculations shown in Fig. 20.

Carbonate chemistry

Previous studies by Brathwaite (1974), Dixon (1980), Green et al. (1981) and Khin Zaw (1991) reported a manganese-rich suite of carbonates, including the following minerals in order of abundance: rhodochrosite ($MnCO_3$), ferroan rhodochrosite [(Mn,Fe) CO_3], kutnahorite [$CaMn(CO_3)_2$], manganoan siderite [Fe,(Mn) CO_3], dolomite [$CaMg(CO_3)_2$] and calcite ($CaCO_3$).

A total of 218 microprobe analyses of carbonate minerals from DDH 120R and 109R have been collected as part of this AMIRA study. Data from

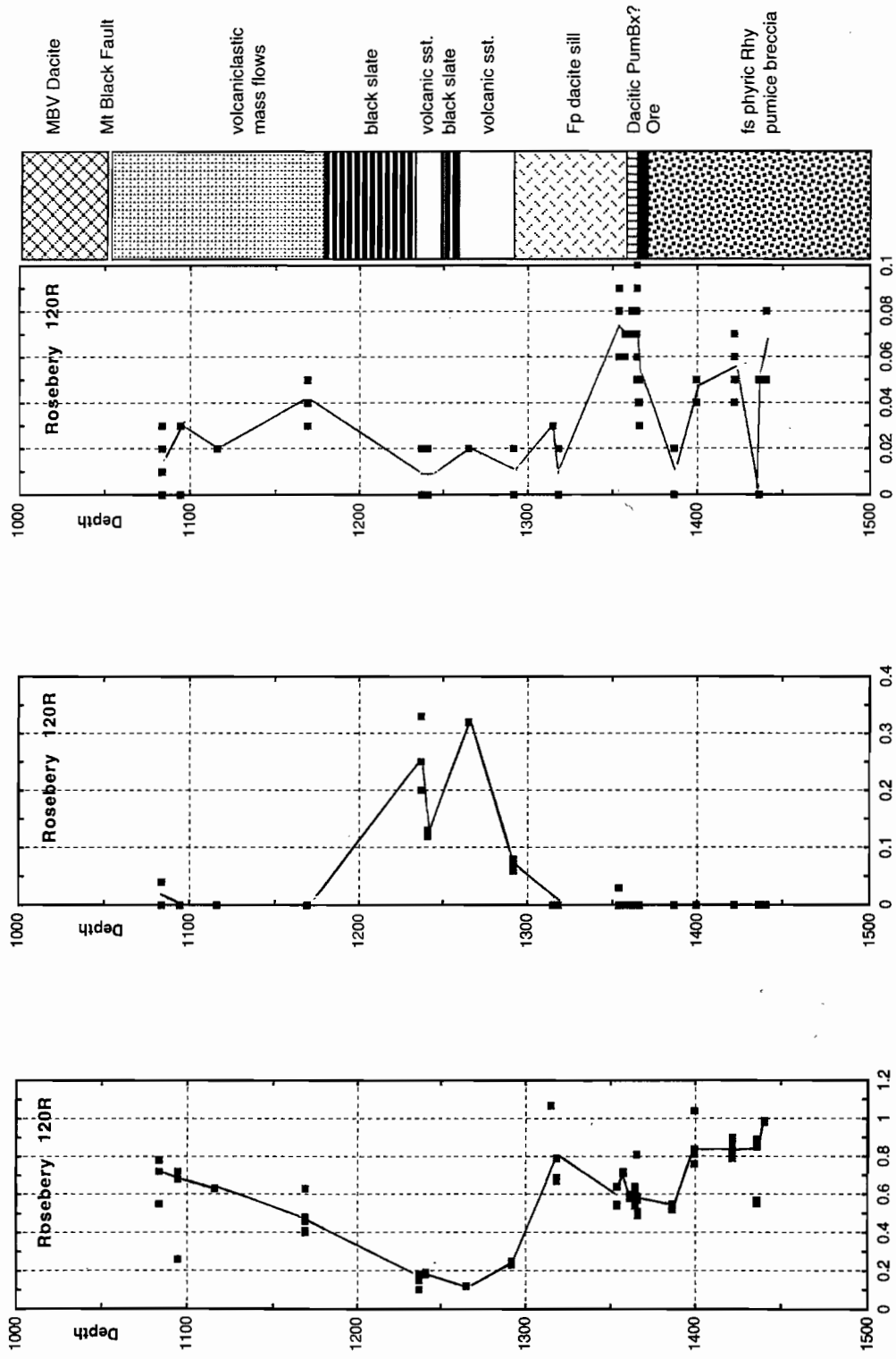

Figure 17: Down-hole variation in muscovite chemistry in DDH 120R. (a) Fe + Mg cations. (b) Na/(Na + K). (c) Ba cations

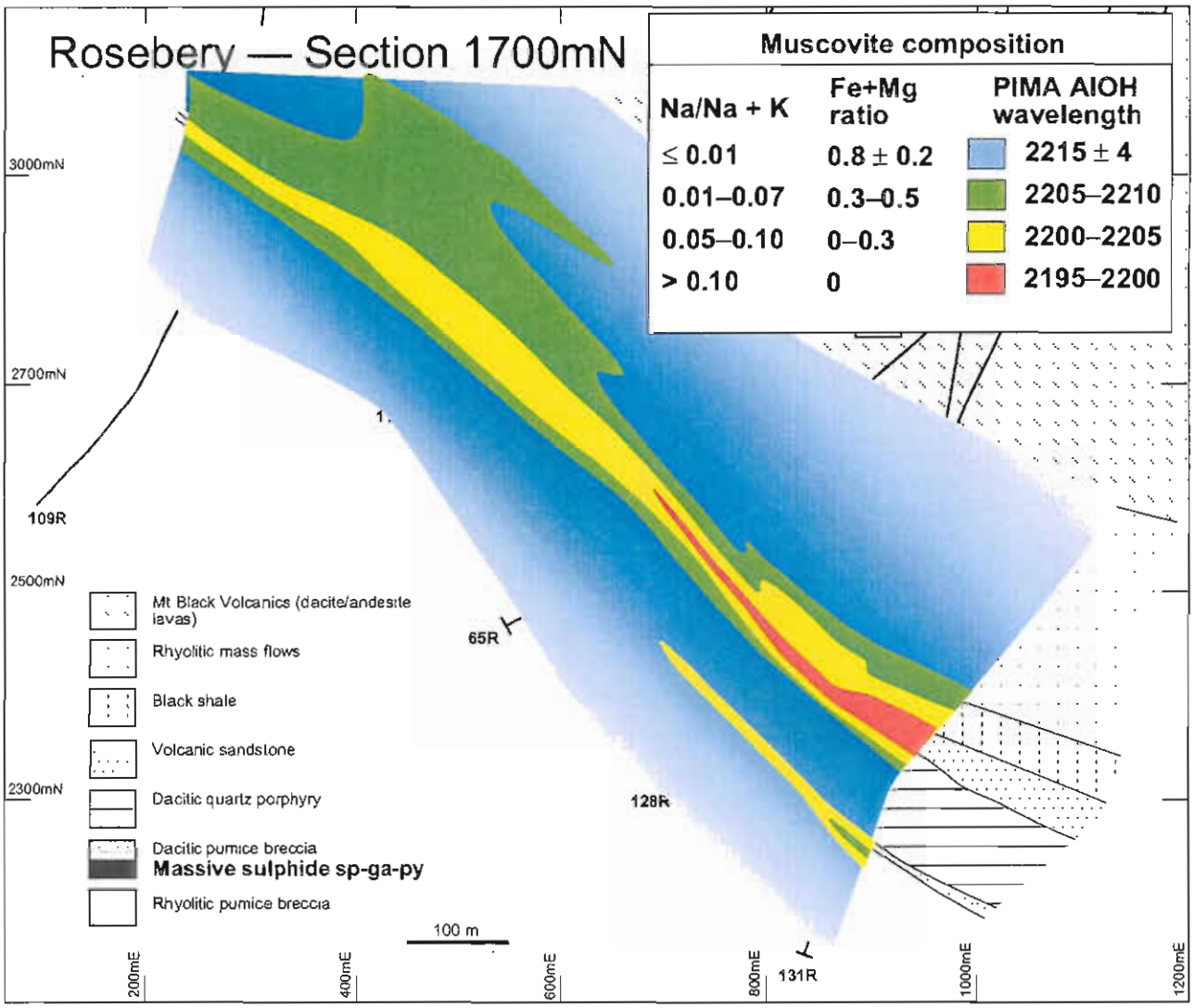

Figure 18: Contours of AlOH wavelength of muscovite on Rosebery section 1700 mN determined from PIMA spectra. The most sodic muscovites with lowest AlOH wavelengths are confined to the volcanic sandstones in the hangingwall of K lens.

DDH 120R was previously reported by Large et al. (1997), and the results are summarised below along with the new findings from DDH 109R (outside the ore zone). A more detailed report on the relationship between carbonate paragenesis and carbonate chemistry at Rosebery is provided by Allen et al. (this volume).

DDH 120R

Plots of the microprobe data from this study (Fig. 22) show that the carbonates in DDH 120R fall into three main groups.

Group 1: rhodochrosite-ferroan rhodochrosite-manganoan siderite ;
- dominantly carbonates from the dacitic pumice breccia horizon that hosts the massive sulfide ore lenses;
- also includes some footwall carbonate alteration (ferroan rhodochrosite with 10 to 40 mole % $FeCO_3$).

Group 2 : kutnahorite-ankerite
- dominantly ore horizon carbonates with some footwall carbonates at the ankerite end of the spectrum.

Group 3 : calcite
- confined principally to the hangingwall volcanics and volcaniclastics above the base of the dacitic porphyry sill. The deepest sample in the footwall (70m below the ore lens) also contains calcite.

Down-hole variation in carbonate chemistry is shown in Figure 21. These plots clearly show the marked change in carbonate chemistry between the hangingwall sequence and the ore-horizon/footwall sequence below the porphyry sill. These chemical features are summarised below:

Hangingwall carbonate: always calcite with very minor substitution of $FeCO_3$ (<3 mole %), $MnCO_3$ (<3 mole %) and $MgCO_3$ (<2 mole %). It is interesting that the most Mn-poor and "purest" calcites were found in the volcanic sandstone and black slate overlying the dacite porphyry. These lithologies also host the most Fe, Mg-poor muscovite, with highest paragonite component.

Ore horizon : within the ore lens and overlying dacitic pumice breccia unit the carbonates are Mn-rich varieties (>20 mole % $MnCO_3$): rhodochrosite, ferroan rhodochrosite and ferroan kutnahorite.

Footwall alteration zone : carbonate compositions are similar to the ore-horizon but with examples concentrated at the Fe-rich end of the spectrum; ferroan rhodochrosite and ankerite.

DDH 109R

Carbonates in this remote hole, 500 m west of the A-B lens, are dominantly calcite with less than 3 mole % $MnCO_3$ and $FeCO_3$. There does not appear to be any development of $MnCO_3$ at the ore position (top of the rhyolitic pumice breccias, or the overlying volcanic sandstones) in this drill-hole (Fig. 23). However manganoan siderite with 25 to 45 mole % $MnCO_3$ is present as a series of carbonate-arseno-pyrite–pyrite veins with associated alteration deep in the footwall 160 m below the ore position. The significance of this Mn-carbonate alteration zone is discussed elsewhere in this report.

Comparison of calculated $MnCO_3$ and microprobe data

Because microprobe analyses are expensive and not normally available from commercial laboratories an alternative method of estimating the Mn content of carbonates from whole-rock analyses has been investigated.

This procedure assumes that all the whole-rock MnO is present within manganese carbonate minerals. This is a partly valid assumption for the Rosebery-Hercules area, although minor MnO may be present in chlorite. The relationship used for estimating $MnCO_3$ mole % from whole-rock data is

$$MnCO_3 \text{ mole \%} = \frac{MnO_{WR}/71.8}{CO_{2WR}/44}$$

where MnO_{wr} and CO_{2wr} are the whole-rock analyses of these components.

A comparison of the down-hole $MnCO_3$ variation between microprobe and whole-rock data for DDH 120R and 109R are shown in Fig. 25. These plots show very similar trends and demonstrate that useful information is available from the whole-rock calculation method. For DDH 120R (Fig. 25) the

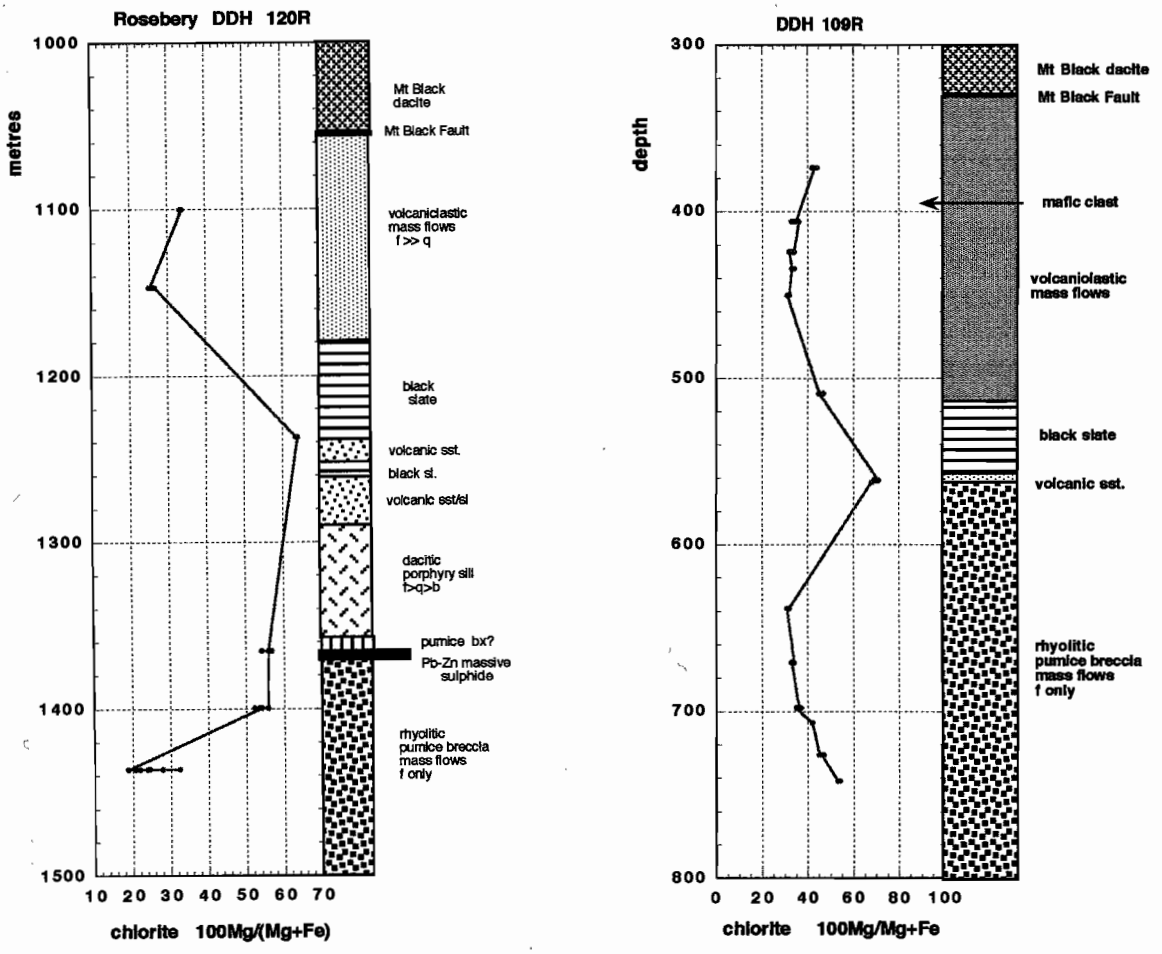

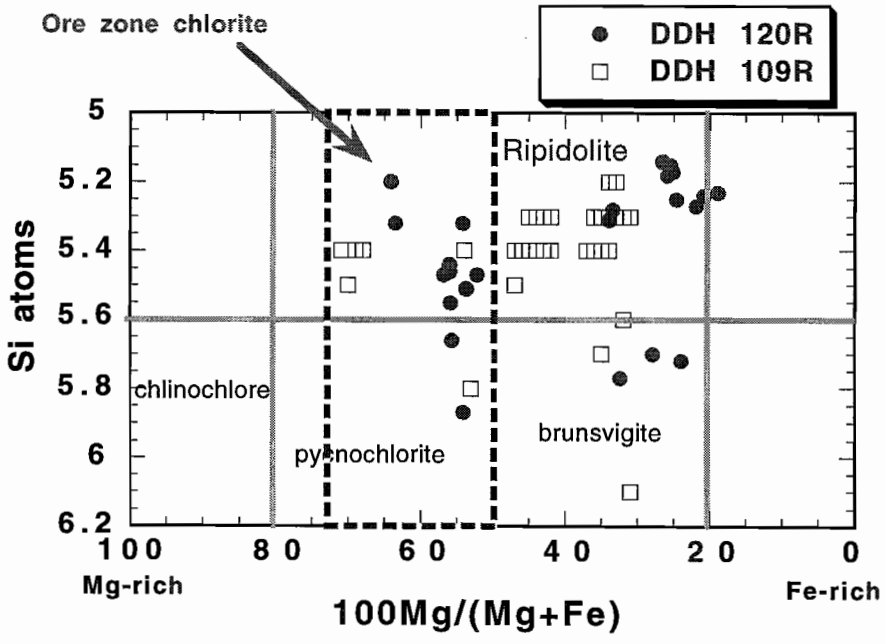

Figure 19 : (a) Down-hole variation in microprobe Mg number of chlorites from DDH 120R and 109R. (b) Variation in composition of chlorites from Rosebery. the ore-related chlorite fall in the box between Mg number 50 and 75.

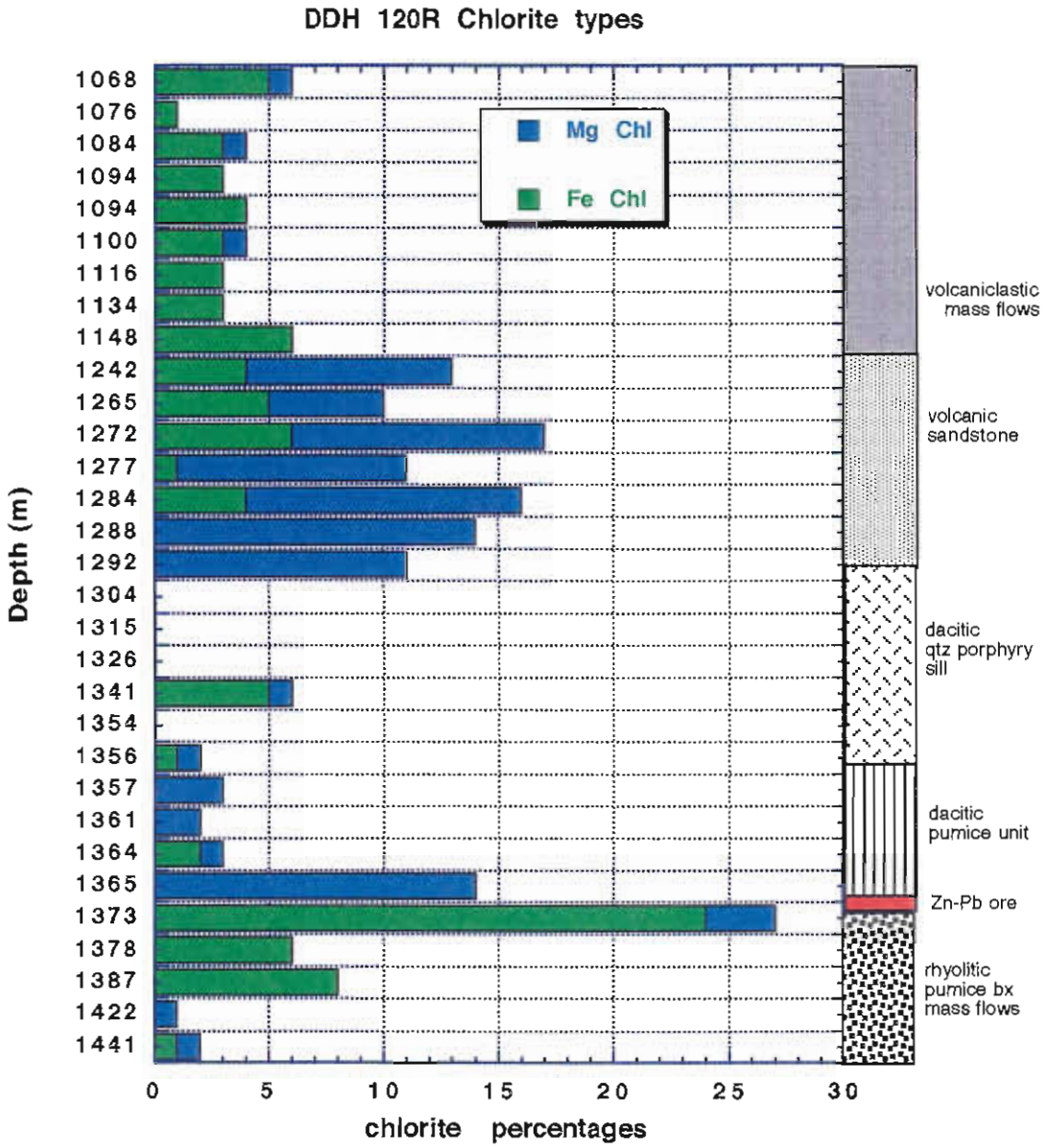

Figure 20: Distribution of Mg-rich chlorite and Fe-rich chlorite in DDH 120R calculated from the whole-rock geochemical datausing the least squares method (Herrmann, this volume).

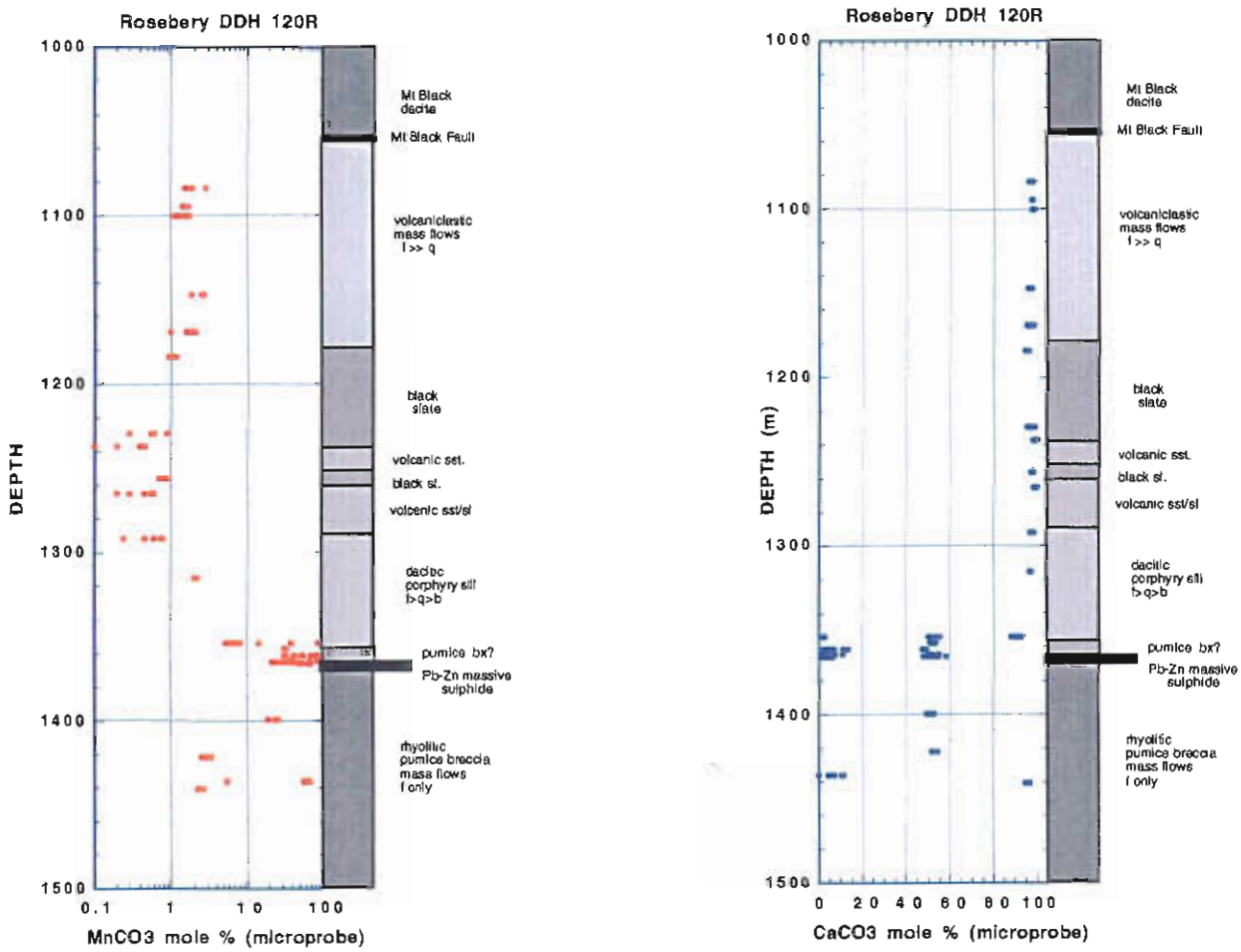

Figure 21: Down-hole plots of carbonate microprobe data in DDH 120R (a) $MnCO_3$ content, (b) $CaCO_3$ content.

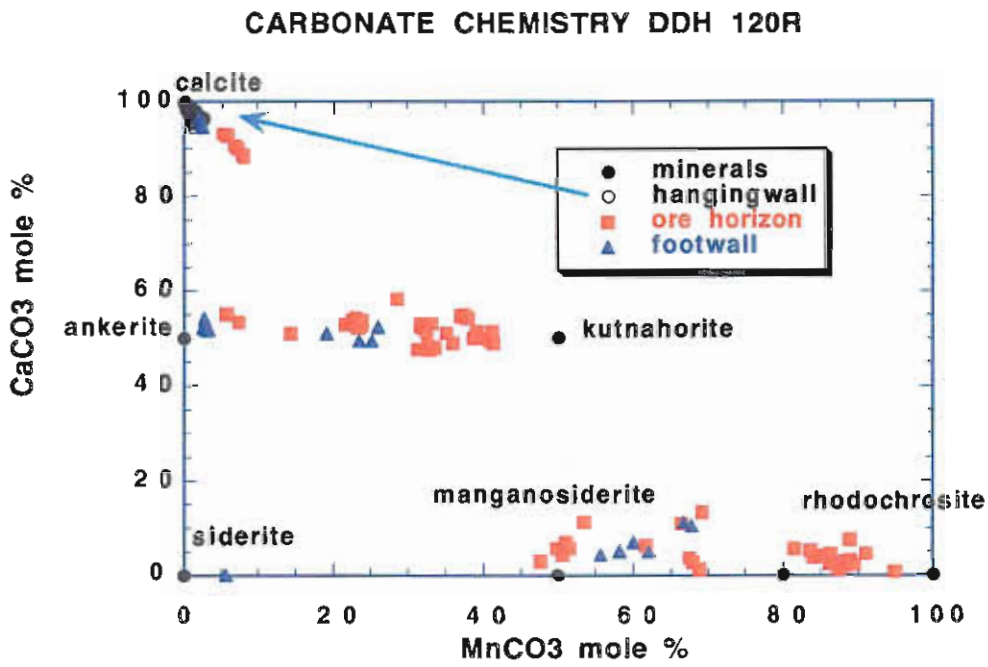

Figure 22: DDH 120R carbonate analyses showing the three major groups (rhodochrosite-ferroan rhodochrosite-siderite, kutnahorite-ankerite, and calcite) (from Large et al., 1997)

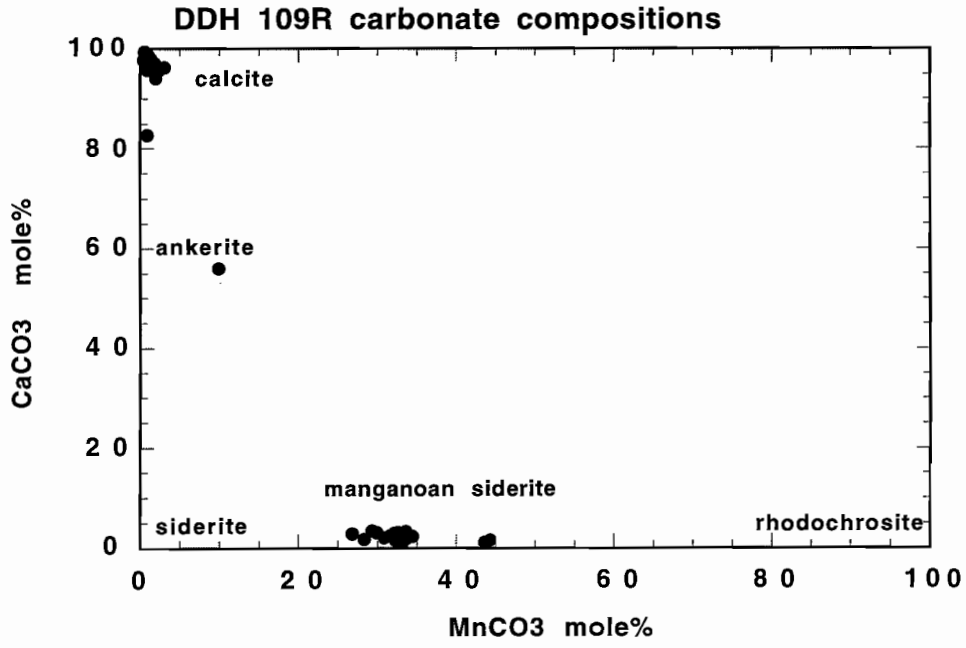

Figure 23: DDH 109R carbonate microprobe analyses.

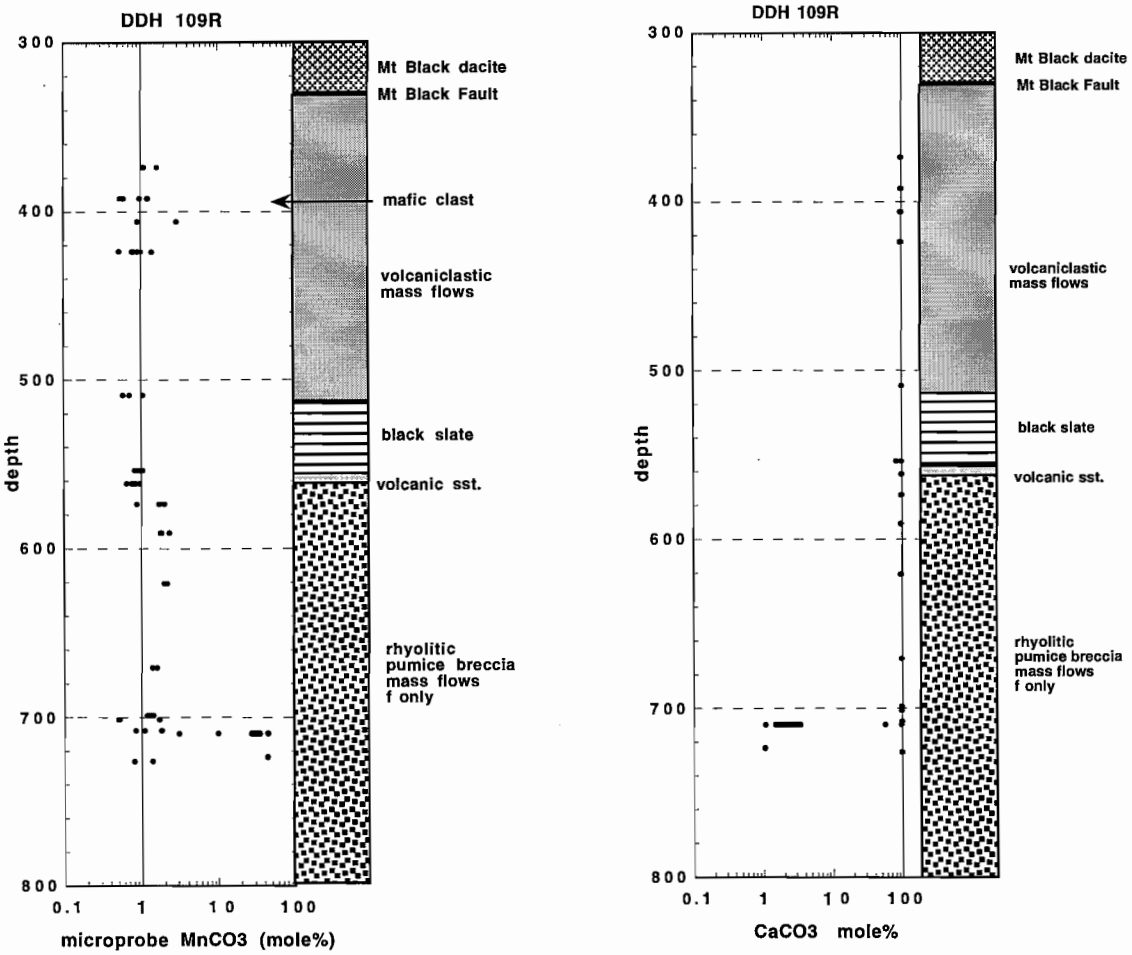

Figure 24: Down-hole plots of carbonate microprobe data in DDH 109R. (a) $MnCO_3$ content; b) $CaCO_3$ content.

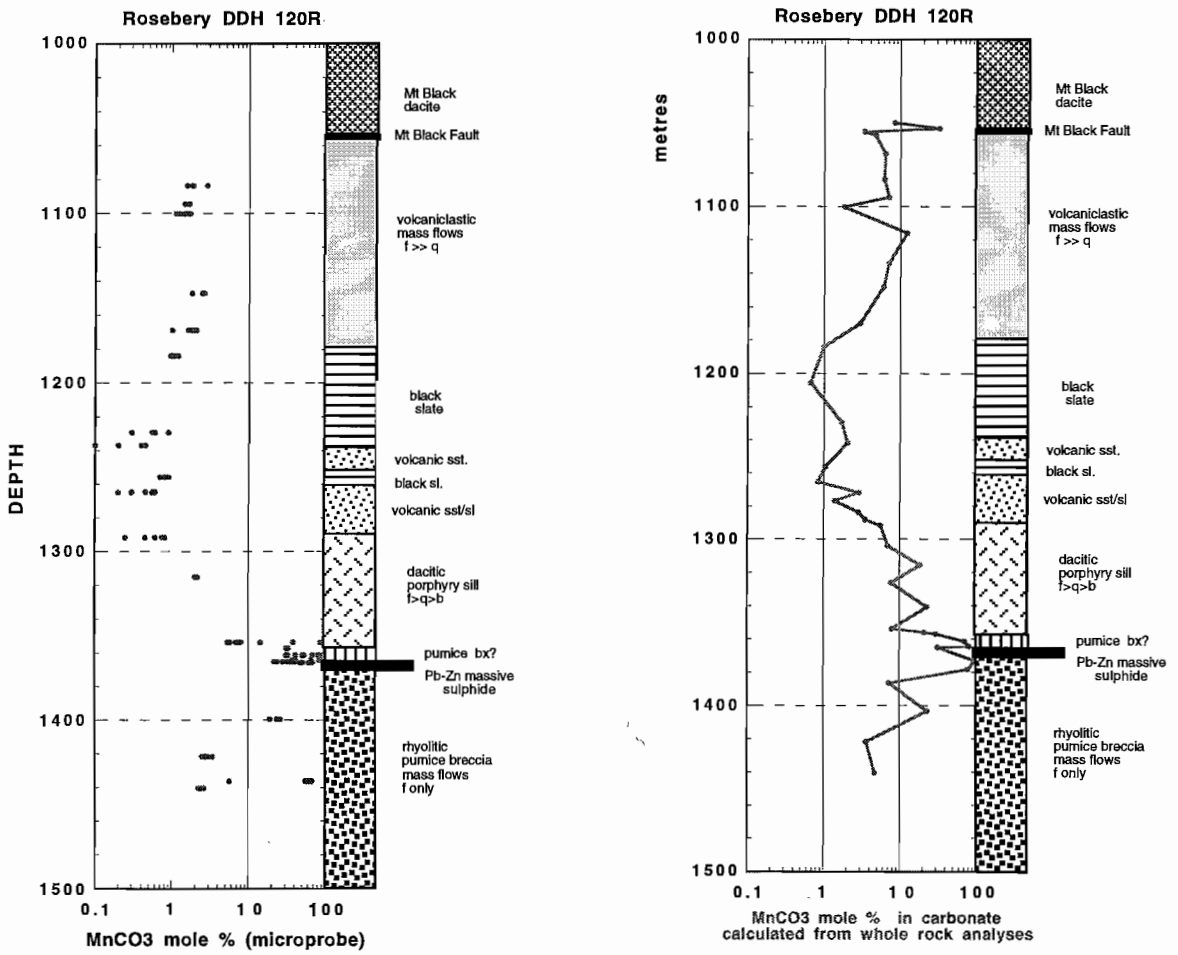

Figure 25: Comparison of $MnCO_3$ content of carbonate from (a) whole-rock calculation and (b) microprobe data for DDH 120R.

whole-rock calculation shows that mole % $MnCO_3$ is an excellent vector to mineralisation increasing gradually over a 100 m interval (1220 m to 1320 m) down toward the ore lens through the hangingwall volcanic sandstones and the dacitic porphyry sill.

Caution should be used when applying this approach to other ore systems, especially in intermediate or mafic host-rocks where Mn-chlorite is likely to be a significant component.

Isotope halos

Carbon and oxygen isotopes in carbonates

Previous studies on sediment-hosted Zn-Pb-Ag deposits (e.g., Large et al., 1995; McGoldrick et al., 1998) have shown that extensive oxygen and carbon isotope halos are developed within carbonate minerals surrounding the ore lenses. The isotope halos which are associated with enrichment of Mn in the carbonate minerals are caused by an increase in $\delta^{18}O$ and decrease in $\delta^{13}C$ compared to the background sedimentary dolomite. These variations are due to the interaction of evolved high salinity connate brines with carbonate minerals in the ore environment.

A study of carbonate C/O isotopes was undertaken at Rosebery to test for similar isotope halo development. Matrix and vein carbonates were drilled from selected samples from DDH 120R and DDH 109R and analysed for carbon and oxygen isotopes at the University of Tasmania CSL using conventional methods. The results are provided as down-hole plots (Fig. 26) and as C-O plots compared with other available data (Fig. 27).

The major conclusions to be drawn from this Rosebery data set are:

1. No extensive halo of carbon or oxygen isotopes in carbonate minerals can be defined at Rosebery, although the ore-zone carbonates generally (but not always) exhibit a distinct isotopic signature.

2. Mn-bearing carbonates in the ore zone of DDH 120R usually have distinctly low $\delta^{18}O$ values from 8.5 to 10.0 per mil. compared with other calcic carbonates in the hangingwall and footwall of the deposit (10.5 to 14.0 per mil.). However, overall there is no relationship between C-O isotope values and $MnCO_3$ content of carbonates (Fig. 27a).

3. The C/O isotope trend for samples in the halo to the Rosebery deposit (Fig. 27b) indicates the mixing of two separate isotope compositions in carbonate phases. Cambrian carbonates related to VHMS formation have isotopic compositions in the range:
   $\delta^{18}O$ = 7 to 13 per mil.
   $\delta^{13}C$ = -0.5 to -4 per mil.

   Devonian metamorphic carbonates are commonly lighter in carbon (-4 to -10 per mil.) and heavier in oxygen (12 to 17 per mil.) than the Cambrian VHMS carbonates. The light $\delta^{13}C$ values exhibited by metamorphic calcite is probably related to oxidation of organic carbon from the Black Slates and adjacent reduced volcanosedimentary facies.

4. Devonian magmatic carbonates (e.g., Renison hydrothermal carbonates, Kitto, 1994) generally exhibit more elevated $\delta^{18}O$ values in the range 10 to 22 per mil., however there is considerable overlap with the Cambrian Rosebery volcanics and Black Slate carbonate isotope patterns.

Although this C-O isotope study has not defined a halo to the Rosebery ore lenses it has confirmed the potential for discriminating VHMS ore-related carbonate alteration from background metamorphic carbonates and granite-related hydrothermal carbonates.

Whole-rock oxygen isotopes

No whole-rock oxygen isotope studies were undertaken at Rosebery in this AMIRA project. However previous studies by Green and Taheri (1992) at Hercules and Hellyer have demonstrated the usefulness of this technique as a vector to VHMS mineralisation. Their work has shown that whole rock $\delta^{18}O$ values decrease towards ore in the footwall alteration zone from values of 11.0 per mil. to 14.0 per mil. in the unaltered volcanic to values <7.0 per mil. in the highly altered stringer zone or chlorite alteration pipe. A similar pattern was recorded by Stolz and Large (1992) in the footwall pipe to the Que River deposit. Green and Taheri also showed that fuchsite-carbonate altered basalts in the hangingwall to Hellyer have depleted $\delta^{18}O$ values (10.6 ± 1.2) compared with unaltered basalts (11.8 ± 2.2). Further research is required at Rosebery to relate the oxygen isotope variation to stratigraphy and alteration and test its usefulness as a proximal or distal vector.

Significance of alteration veins in DDH 109R

A zone of carbonate-pyrite ± arsenopyrite ± tourmaline veins occurs in DDH 109R (from 710 to 725 m) deep in the footwall rhyolitic pumice massflow sequence about 150 m stratigraphically below the ore position, and 500 m west of the closest ore lens (data sheet 109R–723).

Two samples from this zone gave very anomalous geochemistry and the signature expected from altered rocks close to massive Zn-Pb-Ag ore. Geochemically the samples show strongly anomalous MnO, depletion of Na_2O, elevated AI (>80) and CCPI (>60), Ba/Sr >10 and S/Na_2O >1, elevated Tl, Sb, and As (Large et al., 1997, p311–318).

Although the mineralised veins are syn or post tectonic in nature, the geochemistry suggests that they are the result of remobilisation from Cambrian VHMS style mineralisation. This is supported by microprobe and C/O isotope data on the carbonates which identifies the carbonate as Mn-rich siderite with a similar isotopic pattern to other Mn-carbonates in the immediate halo (within 10 m) to the massive sulfide lenses (Fig. 26). The chemistry and isotopic character of the carbonates deep in DDH 109R are very different to other syn-tectonic carbonates elsewhere in the hangingwall and footwall sequence at Rosebery. It is thus concluded that the carbonate bearing alteration zone in DDH 109R is possibly related to a Cambrian massive sulfide lens, close to, but off-section from this intersection point in DDH 109R.

Lithogeochemical halo model and vectors to ore

A composite alteration halo model for Rosebery B–K lens is given in Figure 28. The model shows alteration mineral zones (left hand side) and the most useful geochemical vectors related to these zones (right hand side). A tabulation of the best proximal and distal geochemical vectors is provided in Table 3. A simplified halo model showing the interpreted extent of the three major geochemical halos (a) Zn-Pb-Mn, (b) Ba/Sr, and (c) Tl–Sb is given in Fig. 29.

In summary, the geochemical vectors can be grouped in the following way:

1. Proximal vectors that may detect ore lenses within 200–500 m along strike and 5–50 m across strike. These include Zn, Pb, MnO, Ba and $\delta^{18}O_{carbonate}$.

2. Medial vectors that may predict the presence of ore 500–1000 m along strikes, 10–80 m into the hangingwall and 60–120 m into the footwall; S/Na_2O, Ba/Sr, K_2O, Na_2O depletion, Ishikawa AI, CCPI and Mn content of carbonate.

3. Distal vectors that may predict the presence of ore at greater than 1000 m along strike, 200–300 m into the hangingwall and 60–100 meters into the footwall. Only Tl and Sb.

Acknowledgement

Special thanks to Pasminco for providing access to Rosebery mine to allow this study to take place.

References

Aerden, D., 1994, Formation of the Rosebery and Hercules ore deposits, Tasmania by syntectonic mobilization of metals and wallrock replacement about structural traps. Contentious issues in Tasmanian Geology Symposium 1994, Geological Society of Australia Tasmanian Division, Extended Abstracts volume, p. 83-88.

Allen, R.L., 1990, Subaqueous welding, or alteration, diagenetic dompaction and tectonic dissolution? IAVCEI International Volcanological Congress, Mainz, Germany, Abstracts volume.

Allen, R.L., 1991, Stratigraphy, structure volcanology and ore genesis of the Rosebery–Hercules Zn-Pb-Cu-Au massive sulfide district, Tasmania. Unpublished report to Pasminco Exploration, Melbourne Australia. 3 volumes.

Allen, R.L., 1994a, Volcanic facies analysis indicates large pyroclastic eruptions, sill complexes, syn-volcanic grabens, and subtle thrusts in the Cambrian "Central Volcanic Complex" volcanic centre, western Tasmania. Contentious Issues in Tasmanian Geology Symposium, Geological Society Australia Tasmania Division, Hobart. Abstracts number 39, p. 31–32.

Allen, R.L., 1994b, Syn-volcanic, subseafloor replacement model for Rosebery and other massive sulfide ores. Contentious Issues in Tasmanian Geology Symposium, Geological Society Australia Tasmania Division, Hobart. Abstracts number 39, p. 89–91.

Allen, R.L., 1997, Rosebery alteration study and regional alteration studies in the Mount Read Volcanics. The record of diagenetic alteration in the strongly deformed, felsic volcaniclastic succession enclosing the Rosebery and Hercules massive sulfide deposits : AMIRA P439, Report 5, October 1997, p. 135–145.

Allen, R.L. and Cas, R.A.F., 1990, The Rosebery controversy : Distinguishing prospective submarine ignimbrite-like units from true subaerial ignimbrites in the rosebery-Hercules Zn-Cu-Pb massive sulfide district, Tasmania. 10th Australian Geological Convention. Geological Society Australia, Abstracts 25, p. 31-32.

Allen, R.L. and Large, R.R., 1996, Rosebery Alteration Study : AMIRA P439 Report 3, October 1996, p. 143–152.

Berry, R., 1997, Geochemical evidence for the structure of the Rosebery deposit, AMIRA project P291 Report 2, p. 51–66.

Brathwaite, R.L., 1974, The geology and origin of the Rosebery Ore Deposit, Tasmania, Economic Geology, v. 69, p. 1086–1101.

Dixon, 1980,

Gifkins, C., 1997, Background alteration in the Mount Black Volcanics, mineralogy and geochemistry : AMIRA/ARC Project P439, Report 5, p. 85–134.

Green, G.R. and Taheri, 1992, Stable isotopes and geochemistry as exploration indicators : in Tasmania : an island of potential, Geol. Survey Bull, 70, Tas. Dept Mines, p. 84–91.

Green, G.R., Solomon, M. and Walshe, J.L., 1981, The formation of the volcanic-hosted massive sulfide ore deposit at Rosebery, Tasmania. Econ. Geol. 76, p. 304–338.

Herrmann, et al., (this volume), Application of PIMA and FTIR to VHMS alteration studies : AMIRA P439, Final Report, May 1998, p. .....

Herrmann, W., Allen, R. and McPhie, J., 1977, Preliminary geochemical data from the Dobson Creek–White Spurr traverses : AMIRA/ARC Project P439, Report 5, p. 193–199.

Khin Zaw, 1991, The effect of Devonian metamorphism and metasomatism on the mineralogy and geochemistry of the Cambrian VMS deposits in the Rosebery-Hercules district, Western Tasmania, Unpub. PhD thesis, University of Tasmania, pp. 342.

Large, R.R., 1992, Australian volcanic-hosted massive sulfide deposits : features, styles and genetic models, Econ. Geol., v.87, p. 471–510.

Large, R.R., 1997, The Hercules-Mt Read traverse : Relationships between volcanic mineralogy, alteration and geochemistry : AMIRA P439, Report 3, October 1996, p. 153–233.

Large, R.R. and Allen, R.L., 1997, Preliminary report on the Rosebery lithochemical halo study : AMIRA P439, Report 4, May 1997, p. 259–330.

Large, R.R., Allen, R.L. and Blake, M., 1997, Carbonate and muscovite mineral chemistry, Rosebery VHMS deposit, Tasmania : AMIRA P439, Report 5, October 1997, p. 147–173.

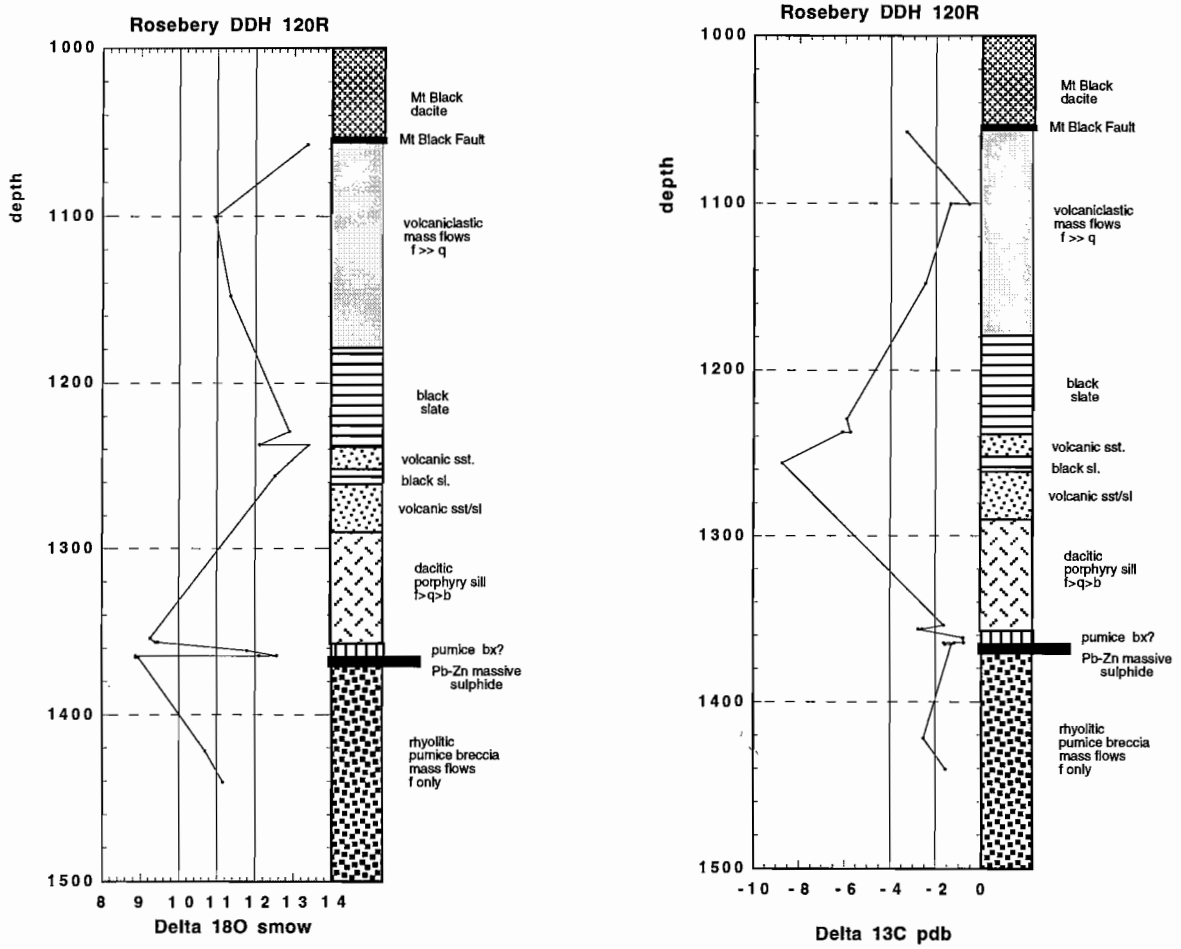

Figure 26 (continued on opposite page): Down-hole carbon and oxygen isotope variation in carbonates from DDH 120R and DDH 109R.

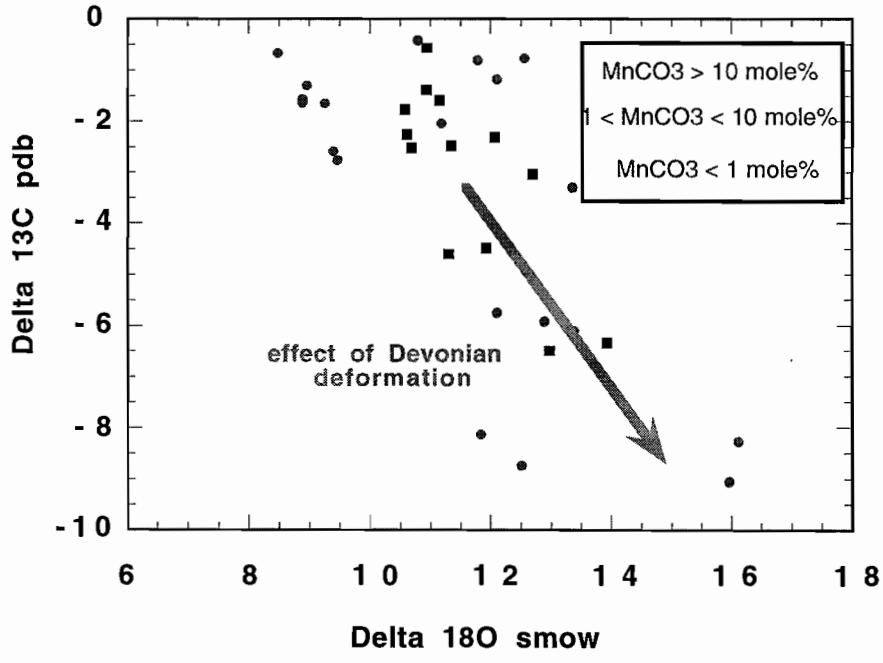

Figure 27: (a) Variation in δC–δO carbonates from DDH 120R and 109R, showing no relationship to $MnCO_3$ content of carbonates.

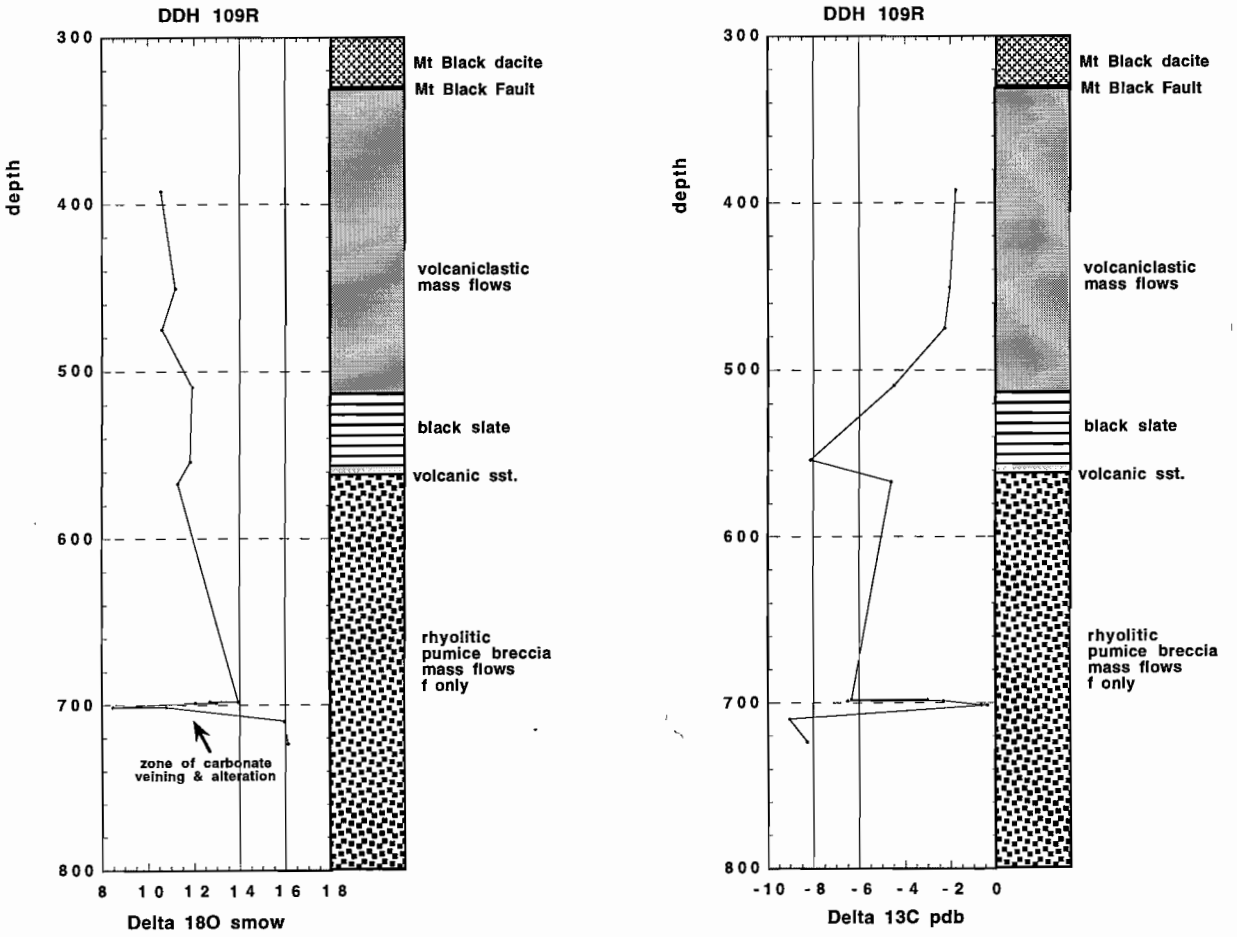

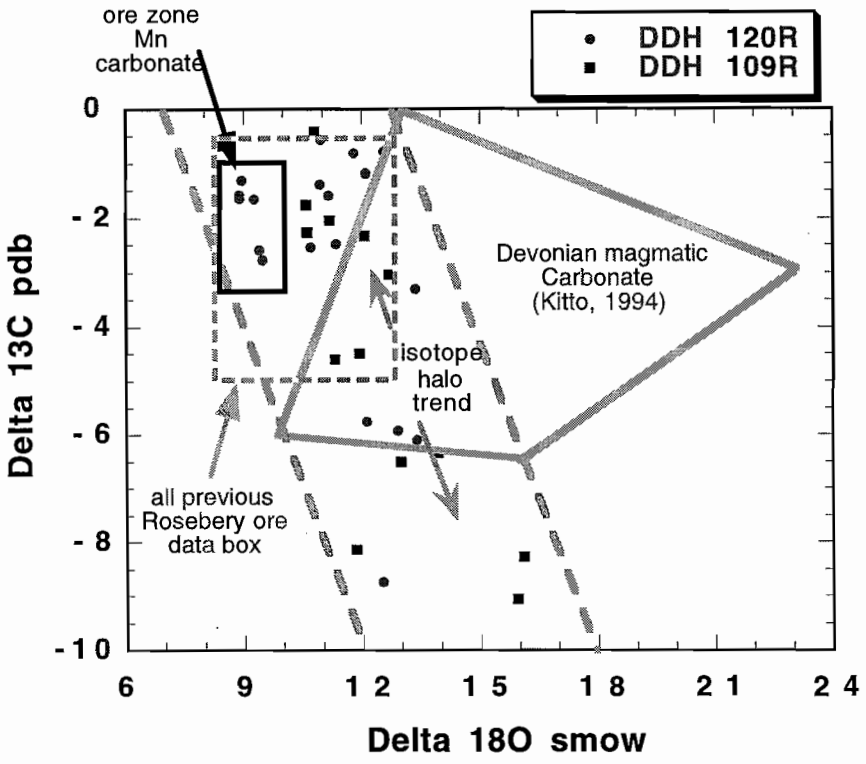

Figure 27b: Variation in δC–δO for Rosebery DDH 120R and 109R carbonates compared with Devonian magmatic carbonates from Kitto (1994).

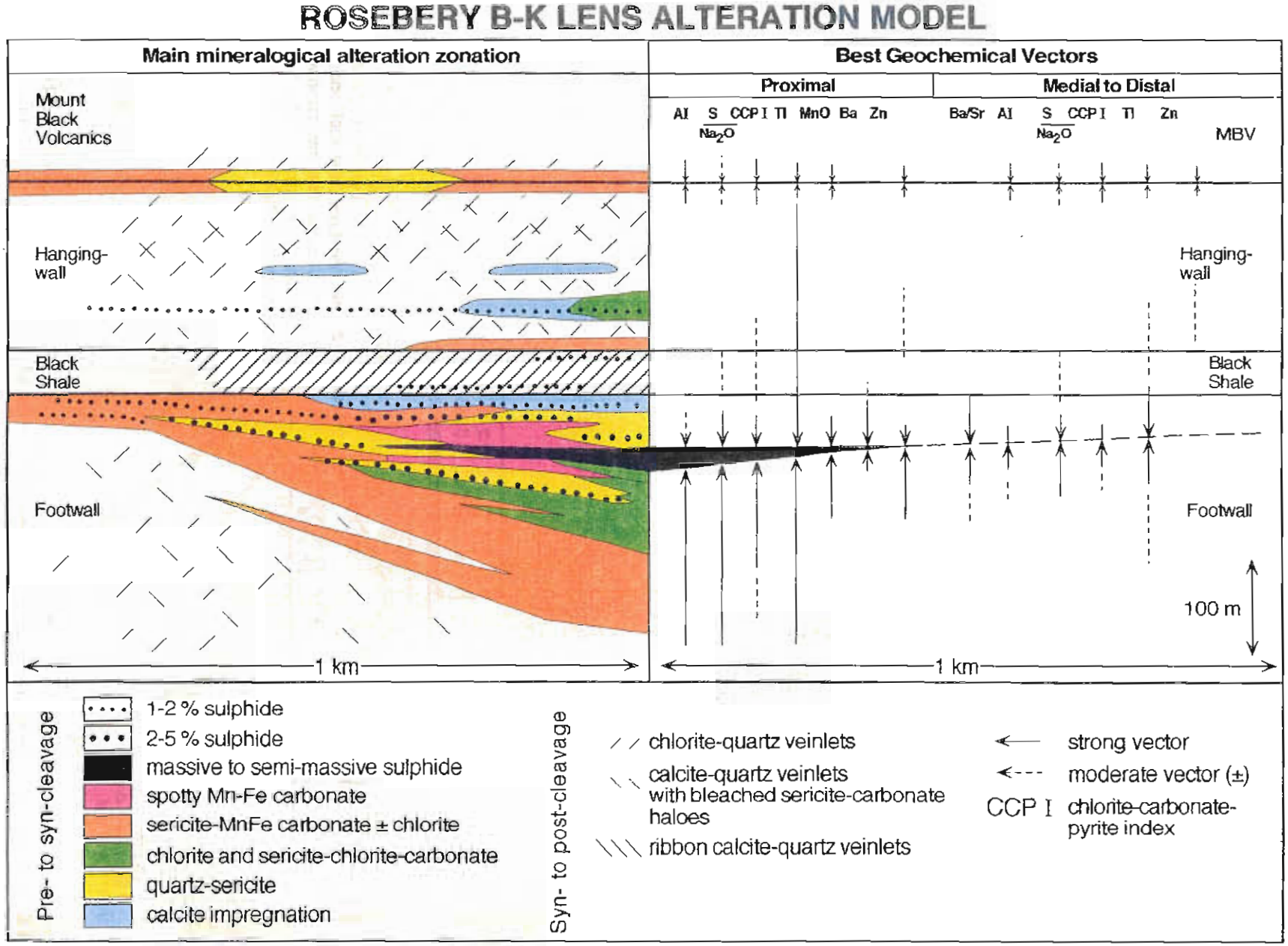

Figure 28: Rosebery B–K lens alteration model and best geochemical vectors.

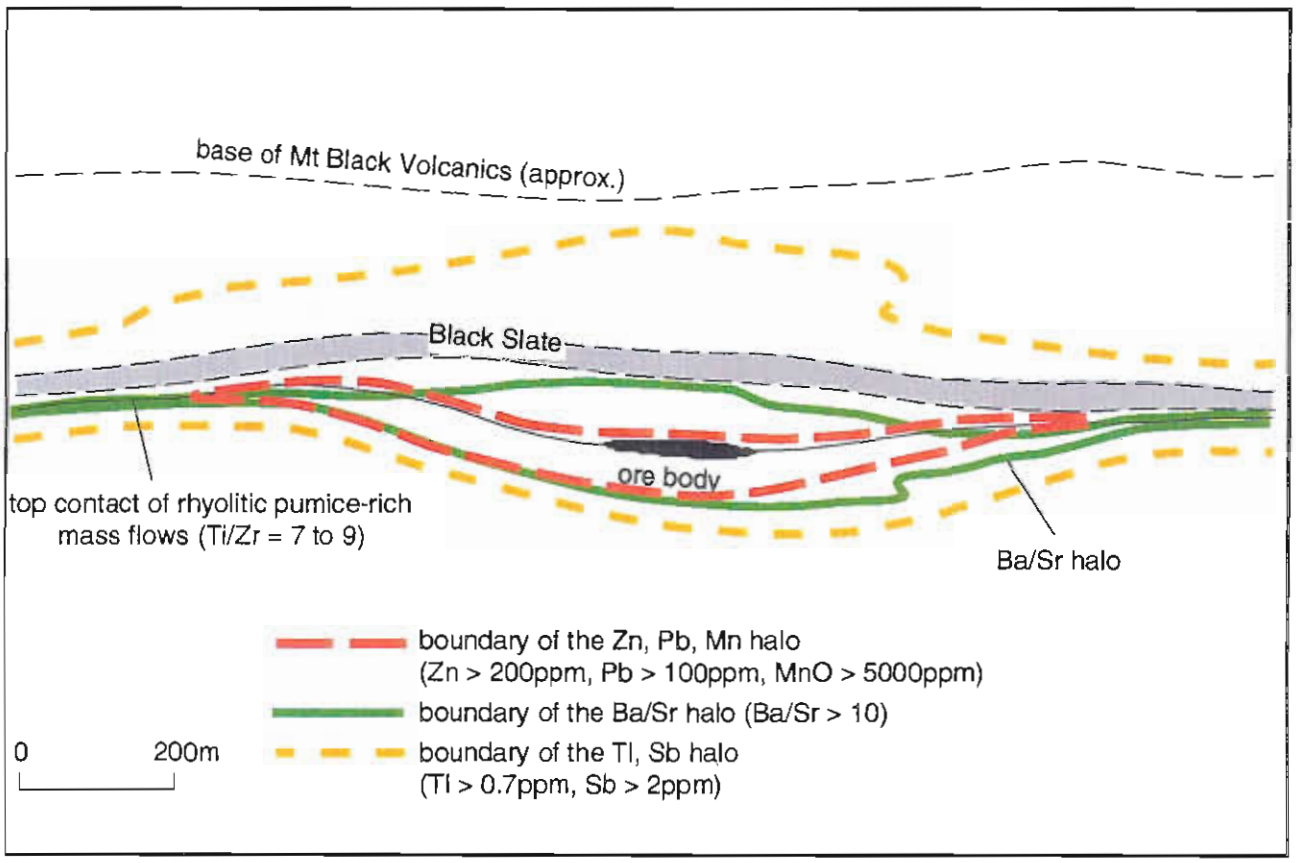

Figure 29: Diagrammatic representation of the extent of the three major geochemical halos at Rosebery (based on the B and K lenses).

Table 3: Summary of geochemical vectors to ore at Rosebery

Distal Vectors	Hangingwall maximum penetration (m)	Footwall maximum penetration (m)	Along strike extent (m)	Typical anomalous range max.	to min.
Thallium	200 - 300	100	500 to 2000+?	100 ppm	0.7 ppm
Antimony	200+	60	500 to 2000+?	100 ppm	2.0 ppm
Ba/Sr	100	60 to 80	500+	100	1 to 10
K_2O	10 to 80	60 to 100	500+	6%	3 to 4%
Na_2O depletion	10 to 20	60 to 100	500 to 1000+?	<0.1%	1 to 2%
Ishikawa AI	10 to 20	60 to 100	500 to 1000+?	90 to 99	50 to 60
S/Na_2O	0 - 10	70 to 120	500 to 1000+m	10 to 200	0.1 to 1
CCP Index	10 - 15	60 - 80	500	80 to 95	40 to 80
Mole % $MnCO_3$ in carbonate*	60 to 100	50	300 to 500?	20 to 100%	2 to 10%
Proximal Vectors					
Zn	10 - 20*	20 - 40	300 - 500	30%	100 to 500ppm
Pb	5 - 10	10 - 40	300 - 400	10%	100 to 200ppm
MnO	5 - 10	40 - 60	200 - 300	30%	0.1 to 0.3%
Ba	80 to 100	0 - 10	100 - 200	>1%	0.1 to 0.2%
$\_^{18}O$ carbonate	5 - 10	5 - 10?	250?	9.5 per mil.	8.5 per mil.
$^{206}Pb/^{204}Pb$ whole rock	10 - 15	5 - 10	200 - 300?	18.4	18.25

* Mole % $MnCO_3$ in carbonate can be determined by microprobe or calculated from whole rock analyses.

Large, R.R., Kitto, P.A. and McGoldrick, P.J., 1995, Variation of carbon and oxygen isotopes in the halo of the Lady Loretta deposit - implications for exploration and ore genesis: AMIRA P384 Final Report, p289-303.

McGoldrick, P.J., Kitto, P.A. and Large, R.R., 1995, Variation of carbon and oxygen isotopes in the halo of the Lady Loretta deposit - implications for exploration and ore genesis: In Arehart and Hulston (eds), Water-Rock Interaction, A.A. Balkema,1998, p561-564.

Reid, L.G., 1993, Aspects ofnorth end mineralisation, Rosebery Mine, Western Tasmania, unpub. Master of Econ. Geol. thesis, CODES, University of Tasmania, pp 82.

Smith, R.N. and Huston, D.L., 1992, Distribution and association of selected trace elements at the Rosebery deposit, Tasmania, Economic Geology, v. 87, p. 706–719.

Stolz, J. and Large, R.R., 1992, Evaluation of the source-rock control on precious metal grades in VHMS deposits from western Tasmania, Econ. Geol., v.87, p. 720–738.

Sample No. 120R - 1265.5
Location Rosebery Mine, K lens, DDH 120R 1265.5 m.
Alteration zone Hangingwall, calcite
Formation Mt Read Volcanics, Central Volcanic Complex

Description Weakly quartz - sericite altered and moderately calcite impregnated, moderately foliated, diffusely stratified, medium to coarse grained, albite crystal rich sandstone.
Facies Interp Volcaniclastic sandstone derived from re - working of footwall pumice deposit.

Alteration Intensity	none	(weak)	moderate	strong	intense	Py - Po 1%
Alteration Style	(patchy)	(pervasive)	veined		cleavage control	
Alteration Mineralogy	Groundmass	sericite - quartz - calcite				
	Feldspars	weak sericite - calcite				
	Mafics	-				
Interpretation	diagenetic	(metamorphic)	syntectonic		hydrothermal	
Relict Mineralogy						

Geochemistry

SiO_2	TiO_2	Al_2O_3	Fe_2O_3	MnO	MgO	CaO	Na_2O	K_2O	P_2O_5	S	CO2	Al	CCPI	Ti/Zr
50.86	0.55	16.03	3.24	0.11	1.13	13.2	3.5	0.93	0.11	0.15	9.64	11	48	29

Rb	Ba	Cu	Pb	Zn	Sb	Tl	Zr	Nb	Y
35	451	9	4	60	2	1	114	8	24

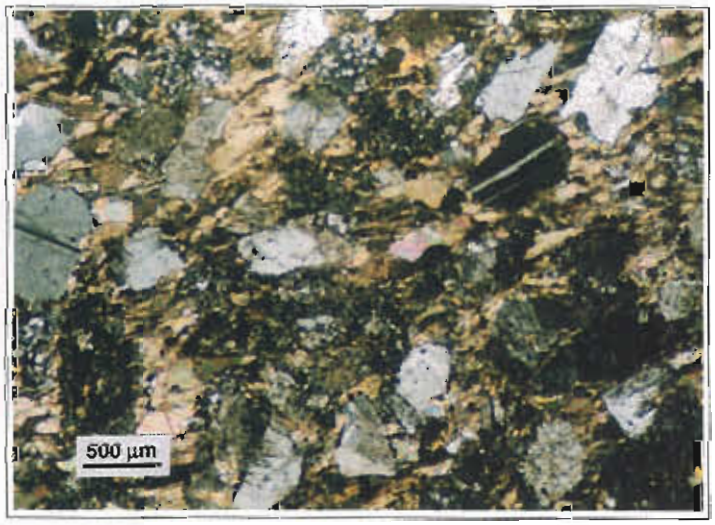

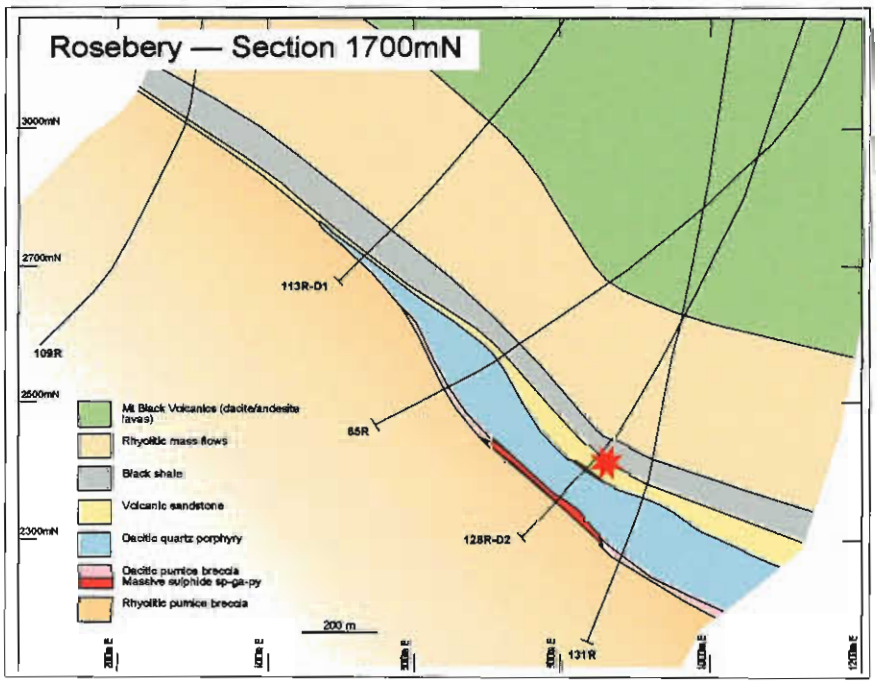

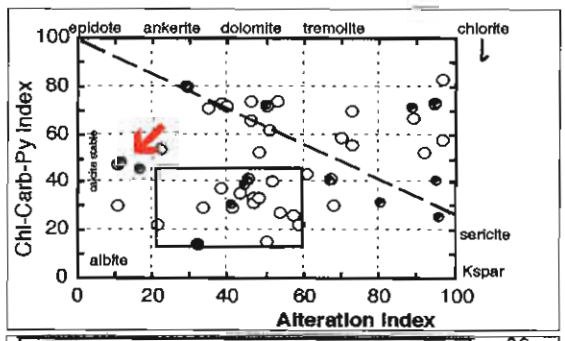

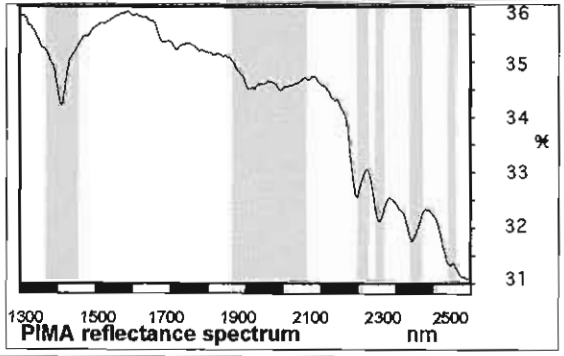

Rosebery Alteration Data Sheet

Sample No. 128R - 1122
Location Rosebery Mine, K lens, DDH 128R 122.4 m.
Alteration zone Hangingwall, calcite
Formation Mt Read Volcanics, Central Volcanic Complex

Description Calcite impregnated, strongly foliated, diffusey stratified, medium to coarse grained, feldspar crystal - rich, crystal - lithic pebbly sandstone
Facies Interp Volcaniclastic sandstone derived from reworking of footwall pumice deposit.

Alteration Intensity none (weak) (moderate) strong intense Py 1%
Alteration Style (patchy) pervasive veined cleavage control
Alteration Mineralogy Groundmass calcite > sericite - quartz
Feldspars weak sericite - calcite
Mafics -
Interpretation diagenetic (metamorphic) syntectonic (hydrothermal)
Relict Mineralogy feldspar phenocrysts, feldspar - microlitic lithic clasts

Geochemistry

SiO_2	TiO_2	Al_2O_3	Fe_2O_3	MnO	MgO	CaO	Na_2O	K_2O	P_2O_5	S	CO2	Al	CCPI	Ti/Zr
44.48	0.73	11.98	4.96	0.21	2.93	16.77	1.79	0.77	0.14	1.03	14.45	16	45	28

Rb	Ba	Cu	Pb	Zn	Sb	Tl	Zr	Nb	Y
29	426	5	16	102	4	4	151	10	24

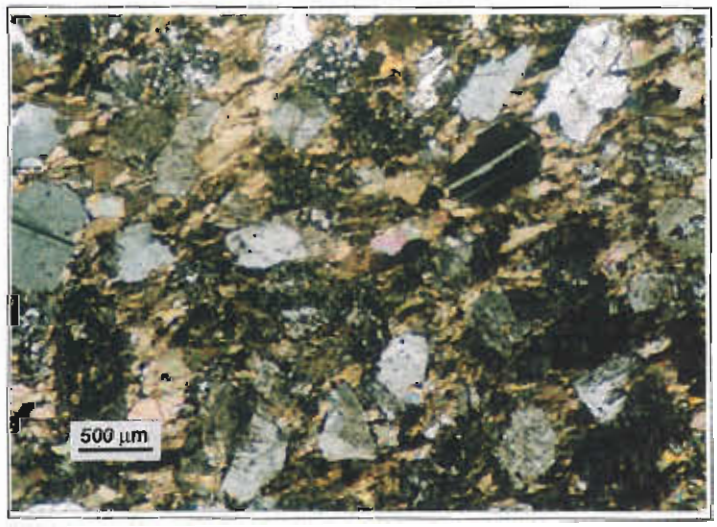

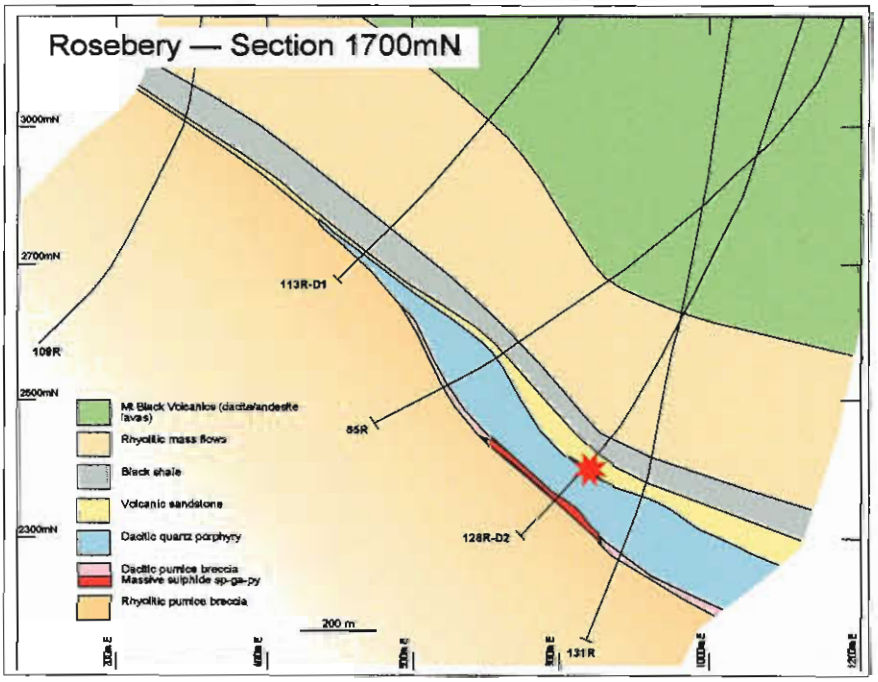

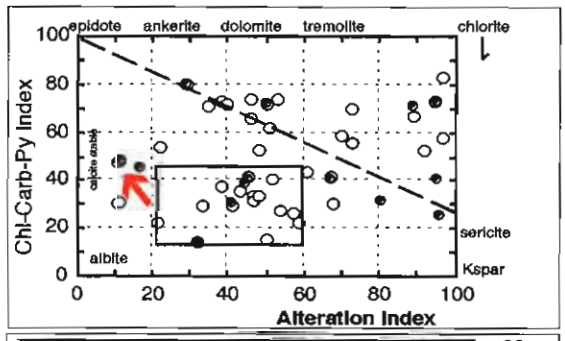

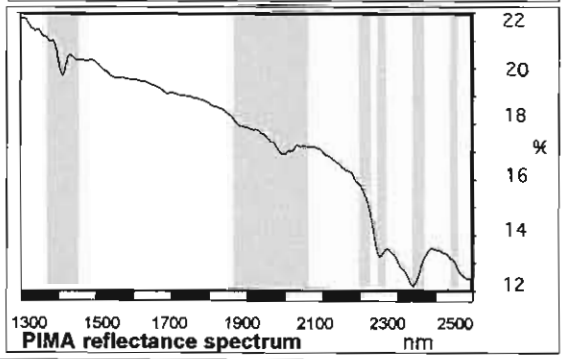

Sample No.	**120R - 1357**
Location	Rosebery Mine, K lens, DDH 120R 1357.4 m.
Alteration zone	Ore zone, spotty carbonate
Formation	Mt Read Volcanics, Central Volcanic Complex

Description Spotty to massive, intensely carbonate - sericite altered, carbonate veined, moderately foliated rock.

Facies Interp Context in drill core indicates this is a part of a non welded, subaqueous deposit of rhyolitic/dacitic pumice.

Alteration Intensity	none	weak	moderate	strong	(intense)	Py 5%, Sp <1%
Alteration Style	patchy	(pervasive)	veined		cleavage control	
Alteration Mineralogy	Groundmass	carbonate - sericite				
	Feldspars	sericite				
	Mafics	-				
Interpretation	diagenetic	metamorphic	syntectonic	(hydrothermal)		
Relict Mineralogy	none					

Geochemistry

SiO_2	TiO_2	Al_2O_3	Fe_2O_3	MnO	MgO	CaO	Na_2O	K_2O	P_2O_5	S	CO2	Al	CCPI	Ti/Zr
17.98	0.35	9.31	12.91	9.96	2.44	14.33	0.05	3.46	0.1	8.06	17.47	29	80	12.8

Rb	Ba	Cu	Pb	Zn	Sb	Tl	Zr	Nb	Y
150	3392	668	13800	10900	66	22	164	6	0

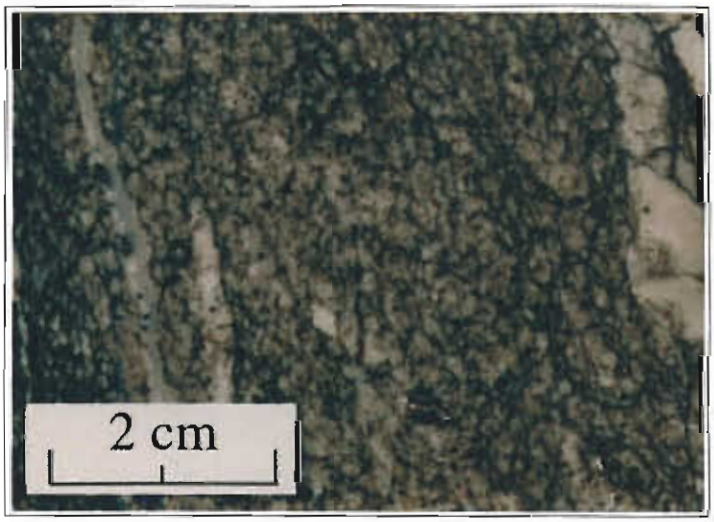

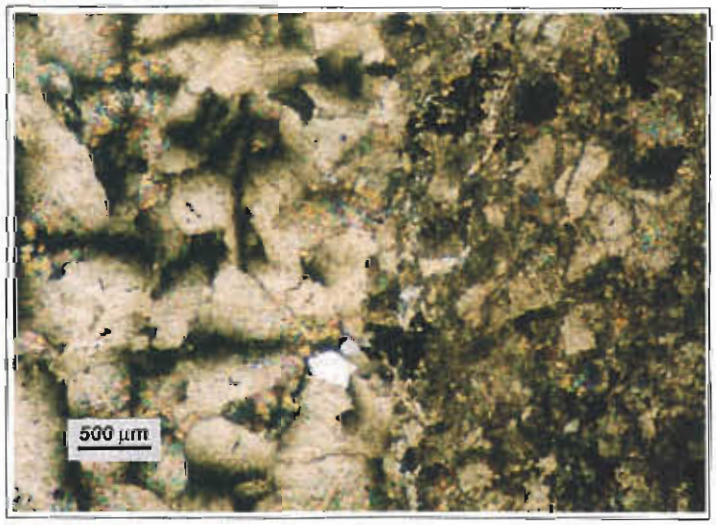

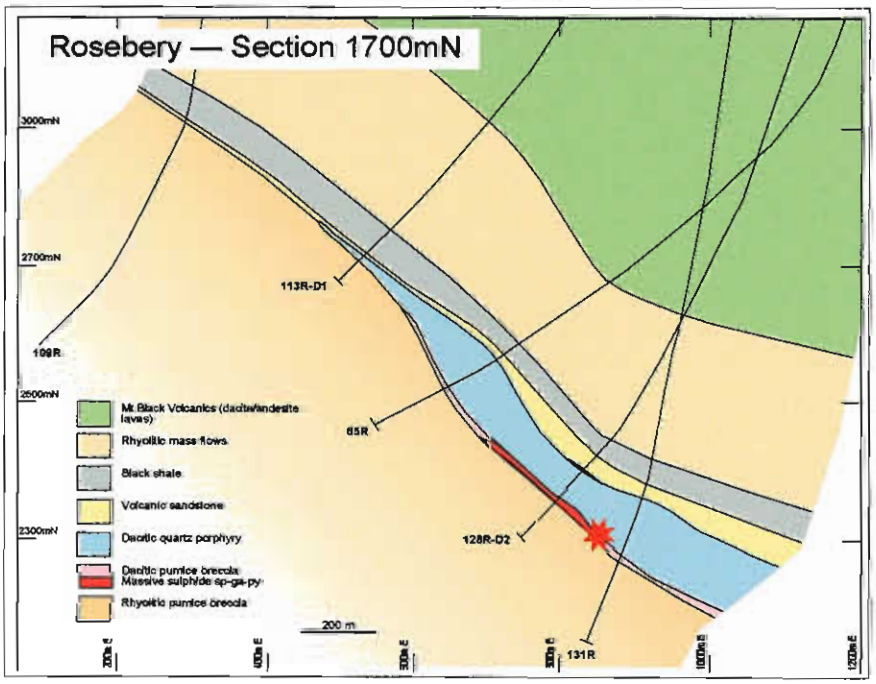

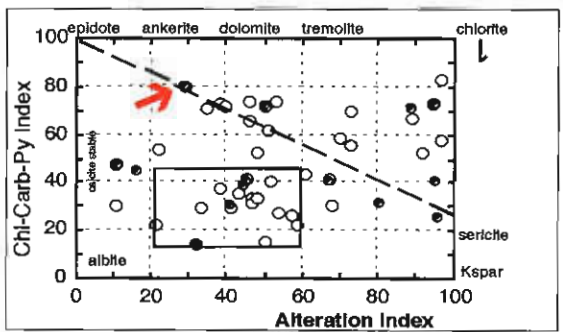

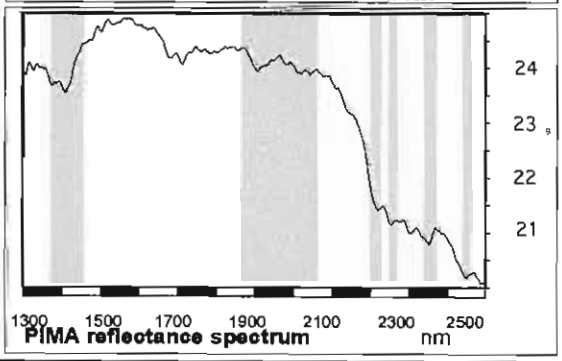

Sample No.	**120R - 1353**
Location	Rosebery mine, K lens, DDH 120R 1353.8 m.
Alteration zone	Hangingwall sill, quartz - sericite
Formation	Mt Read Volcanics, Central Volcanic Complex

Description	Weakly to moderately quartz - altered, moderately foliated, massive, feldspar - quartz - biotite porphyritic dacite - rhyolite.
Facies Interp	Early synvolcanic felsic sill; has peperitic intrusive margins.

Alteration Intensity	none	(weak)	moderate	strong	intense	Py 1%	
Alteration Style	patchy	(pervasive)	veined		cleavage control		
Alteration Mineralogy	Groundmass	sericite - quartz - feldspar					
	Feldspars	weak carbonate - sericite					
	Mafics	biotite : strong sericite - sphene - leucoxine					
Interpretation	(diagenetic)	metamorphic	syntectonic	hydrothermal			
Relict Mineralogy	Quartz and feldspar phenocrysts, recrystallised spherulites in groundmass						

Geochemistry

SiO_2	TiO_2	Al_2O_3	Fe_2O_3	MnO	MgO	CaO	Na_2O	K_2O	P_2O_5	S	CO2	Al	CCPI	Ti/Zr
72.18	0.43	14.21	0.73	0.16	0.41	1.83	4.2	2.44	0.12	0.17	2.74	32	14	13.5

Rb	Ba	Cu	Pb	Zn	Sb	Tl	Zr	Nb	Y
88	2290	15	68	100	11	11.1	191	11	21

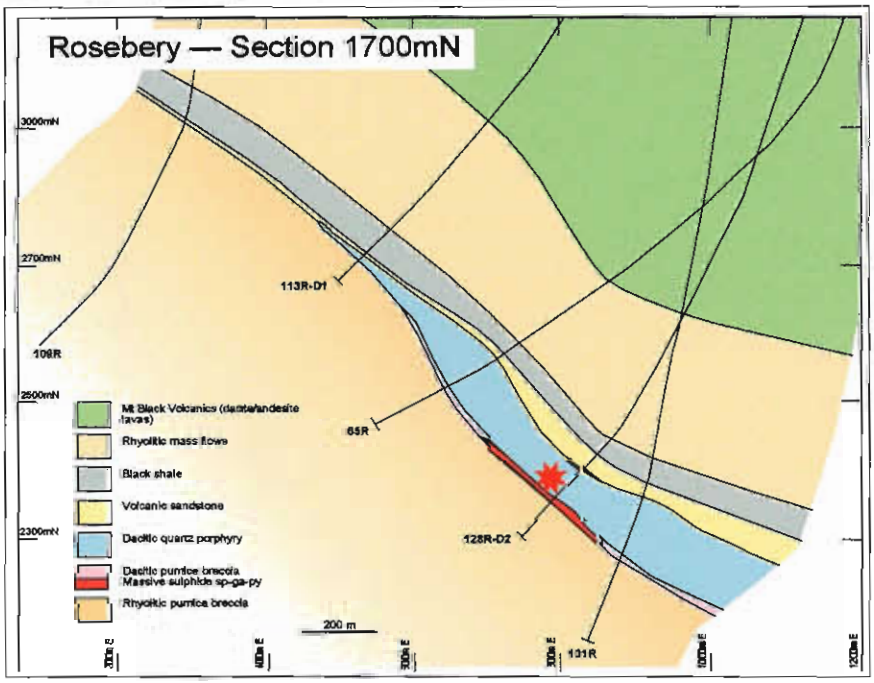

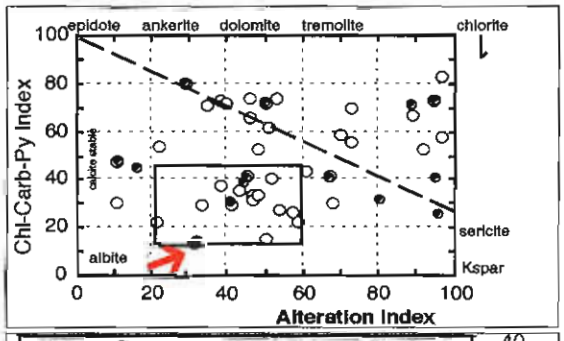

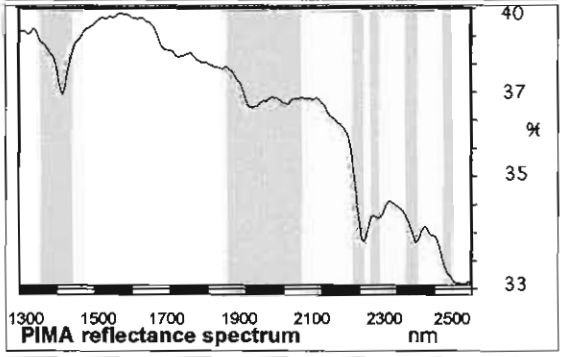

Sample No. 109R - 726.0
Location Rosebery Mine, north of B lens, DDH 109R 726.0 m.
Alteration zone Footwall, least altered
Formation Mt Read Volcanics, Central Volcanic Complex

Description Weakly albite altered, moderately foliated, massive, plagioclase phyric, rhyolitic pumice breccia

Facies Interp Non - welded, subaqueous mass flow deposit of rhyolitic pumice clasts

Alteration Intensity	none	(weak)	moderate	strong	intense	Py trace
Alteration Style	(patchy)	pervasive	veined	cleavage control		
Alteration Mineralogy	Groundmass	albite - Kspar - quartz - sericite				
	Feldspars	weak sericite				
	Mafics	-				
Interpretation	(diagenetic)	metamorphic	syntectonic	hydrothermal		
Relict Mineralogy	feldspar phenocrysts partially preserved					

Geochemistry

SiO_2	TiO_2	Al_2O_3	Fe_2O_3	MnO	MgO	CaO	Na_2O	K_2O	P_2O_5	S	CO2
73.2	0.32	14.13	2.11	0.03	0.97	0.99	3.87	2.38	0.04	0.01	

AI	CCPI	Ti/Zr
41	31	7.5

Rb	Ba	Cu	Pb	Zn	Sb	Tl	Zr	Nb	Y
110	865	1	3	26	2		256	14	33

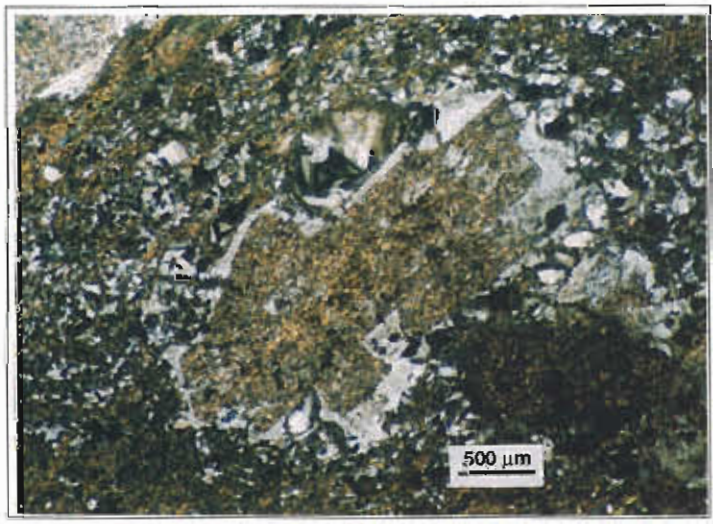

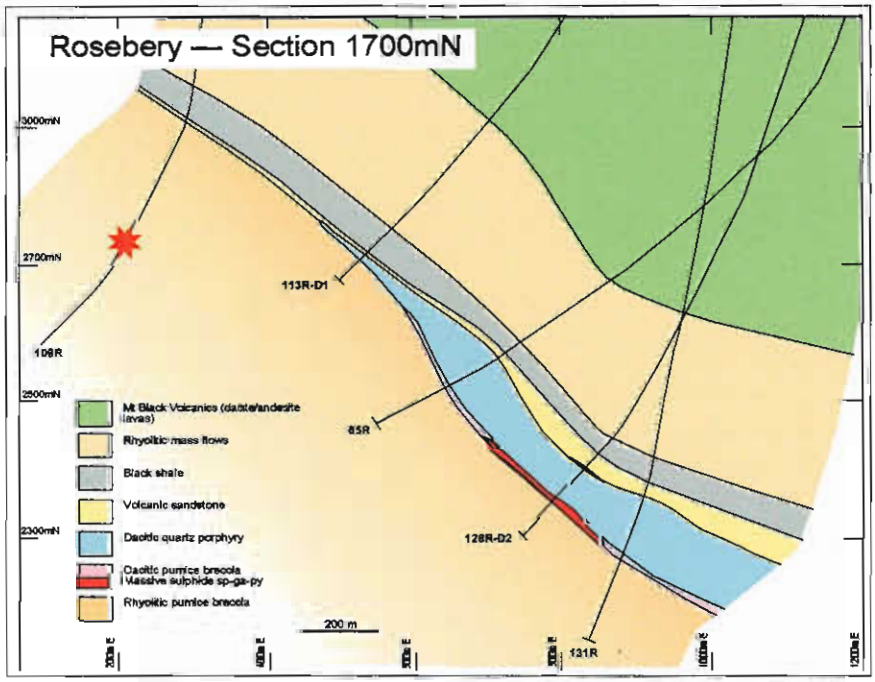

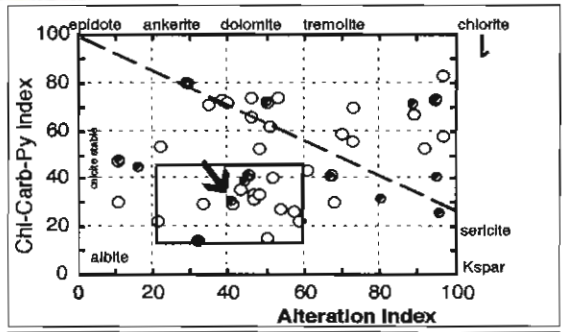

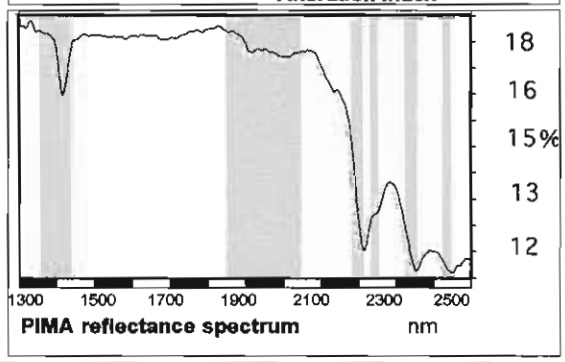

Sample No. 113RD1 - 865
Location Rosebery Mine, north of B lens, DDH 113RD1, 865.4 m.
Alteration zone Hangingwall, vein related ser - carb
Formation Mt Read Volcanics, Central Volcanic Complex

Description Weak sericite > carbonate altered, moderately foliated, feldspar - quartz - phyric, rhyolitic, pumice - crystal sandstone.

Facies Interp Upper, well sorted part of a non - welded, subaqueous mass flow bed of rhyolitic pumice and crystals.

Alteration Intensity none (weak) (moderate) strong intense Py trace
Alteration Style patchy pervasive (veined) cleavage control
Alteration Mineralogy
Groundmass sericite - quartz - feldspar
Feldspars sericite > carbonate
Mafics - **veins** 1. quartz + chlorite, 2. Fe - Mn bearing carbonate
Interpretation diagenetic metamorphic (syntectonic) hydrothermal
Relict Mineralogy quartz phenocrysts, minor relict feldspar in feldspar phenocrysts

Geochemistry

SiO_2	TiO_2	Al_2O_3	Fe_2O_3	MnO	MgO	CaO	Na_2O	K_2O	P_2O_5	S	CO2
68.7	0.35	14.26	3.5	0.26	0.76	1.28	3.24	2.86	0.05	0.01	

Al	CCPI	Ti/Zr
44	39	10.8

Rb	Ba	Cu	Pb	Zn	Sb	Tl	Zr	Nb	Y
111	929	2	19	16	2	1	195	11	29

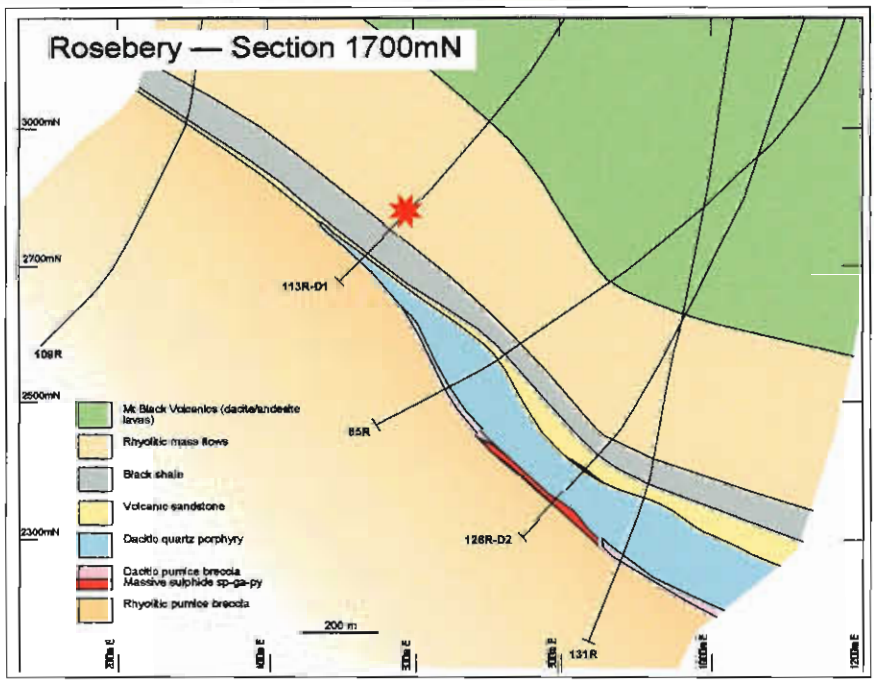

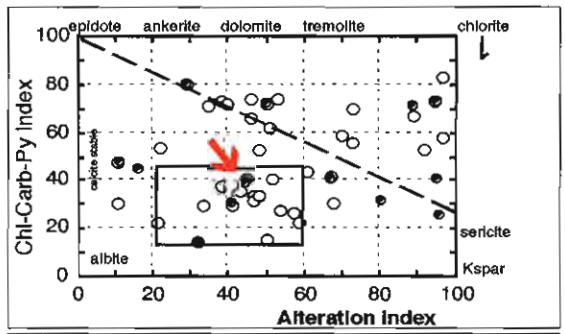

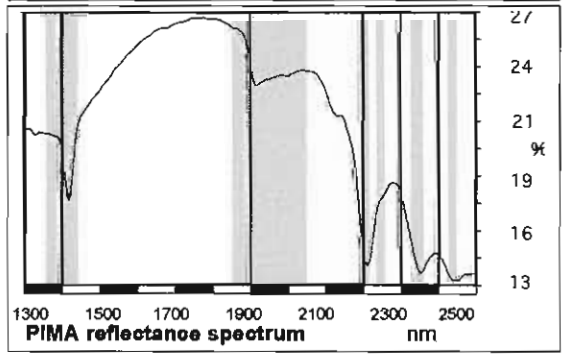

Sample No.	**120R 1147**
Location	Rosebery Mine, K Lens, DDH 120R 1147.8 m.
Alteration zone	Hangingwall, sericite - carbonate
Formation	Mt Read Volcanics, Central Volcanic Complex

Description Moderately sericite > carbonate altered, moderately foliated, feldspar - quartz - phyric, rhyolitic, pumice crystal sandstone

Facies Interp Middle, well sorted part of a non - welded, subaqueous mass flow bed of rhyolitic pumice and crystals

Alteration Intensity	none	weak	(moderate)	strong	intense	Py > Sp 2%
Alteration Style	patchy	(pervasive)	veined		cleavage control	
Alteration Mineralogy	Groundmass	sericite > quartz				
	Feldspars	calcite - sericite				
	Mafics	-				
Interpretation	diagenetic	metamorphic	syntectonic	(hydrothermal)		
Relict Mineralogy	quartz phenocrysts, minor relict feldspar in feldspar phenocrysts					

Geochemistry

SiO_2	TiO_2	Al_2O_3	Fe_2O_3	MnO	MgO	CaO	Na_2O	K_2O	P_2O_5	S	CO2	Al	CCPI	Ti/Zr
68.71	0.4	14.82	3.2	0.14	0.84	2.63	2.23	3.11	0.08	0.02	3.56	45	41	11.5

Rb	Ba	Cu	Pb	Zn	Sb	Tl	Zr	Nb	Y
107	1629	5	63	130	2	1	209	9.6	34

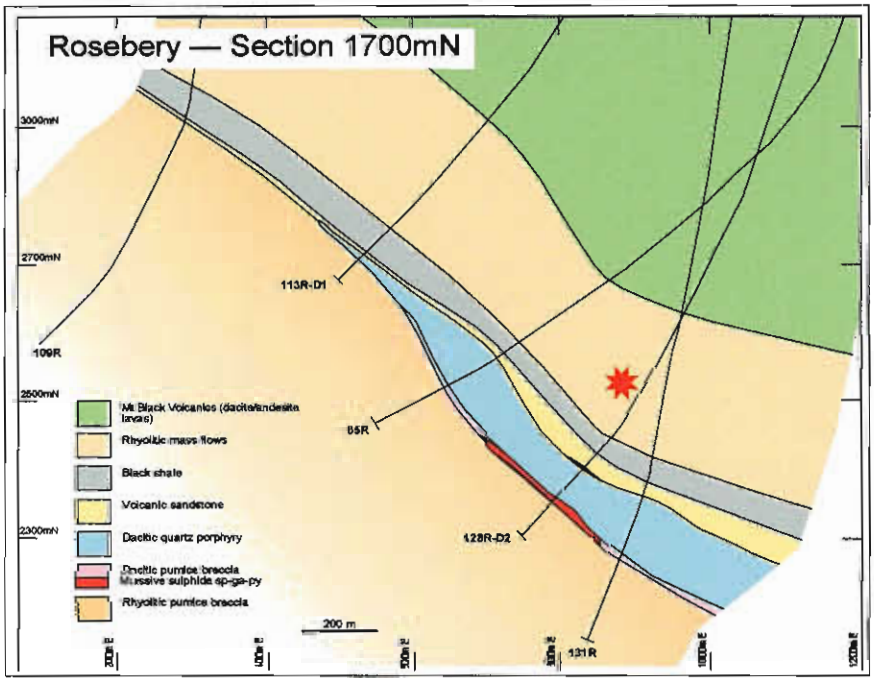

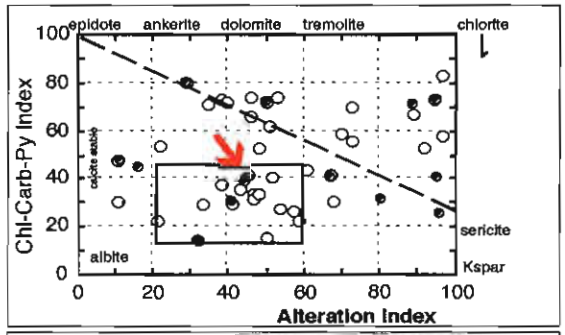

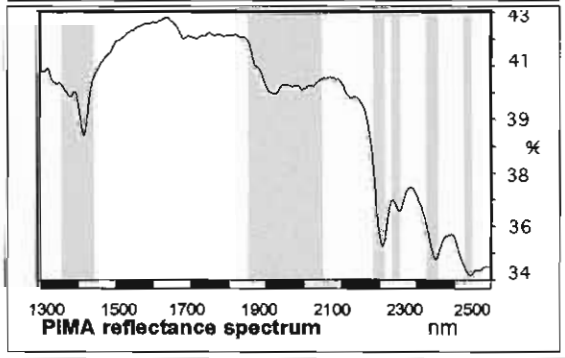

Sample No. 120R 1184
Location Rosebery Mine, K lens, DDH 120R 1184.0 m

Alteration zone Hangingwall slate with calcite - quartz veins
Formation Mt Read Volcanics, Central Volcanic Complex

Description Strongly calcite - quartz veined, black slate

Facies Interp Subaqueous hemipelagic mudstone sediment

Alteration Intensity none (weak) moderate strong intense Py - Po 2 - 3%
Alteration Style patchy pervasive (veined) cleavage control
Alteration Mineralogy Groundmass sericite - quartz - carbon
Feldspars -
Mafics - **Veins** calcite - quartz - pyrite - pyrrhotite
Interpretation diagenetic metamorphic (syntectonic) hydrothermal
Relict Mineralogy Black slate outside the veins is only weakly altered

Geochemistry

SiO_2	TiO_2	Al_2O_3	Fe_2O_3	MnO	MgO	CaO	Na_2O	K_2O	P_2O_5	S	CO2	Al	CCPI	Ti/Zr
63.8	0.8	12.2	7.45	0.09	2.02	4.25	0.57	2.89	0.15	2.06	6.18	50	72	35.6

Rb	Ba	Cu	Pb	Zn	Sb	Tl	Zr	Nb	Y
110	567	77	18	98	4	1	135	13	25

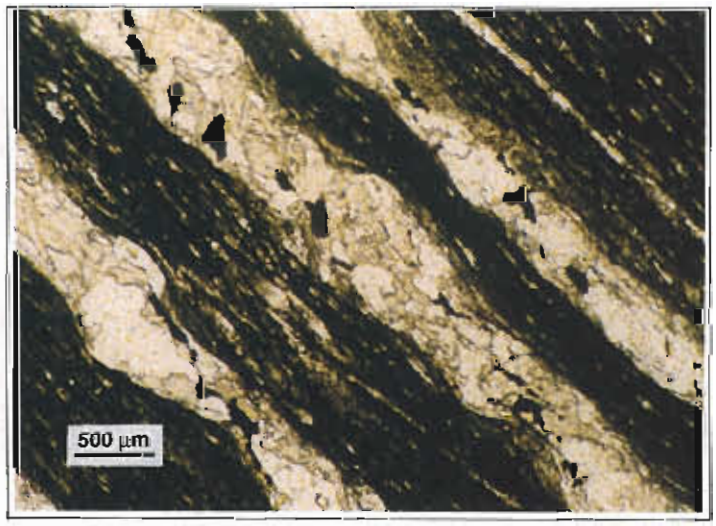

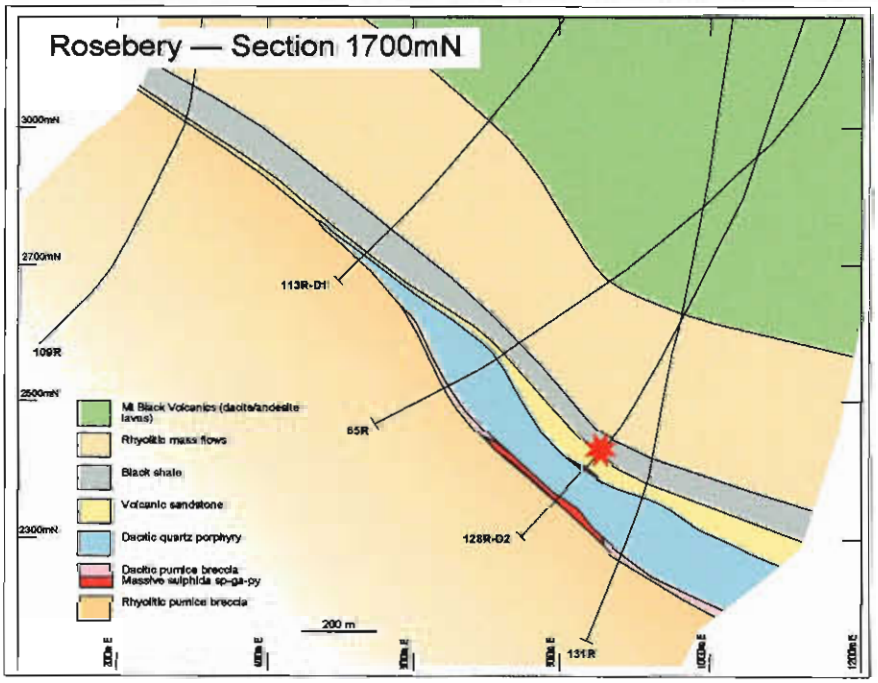

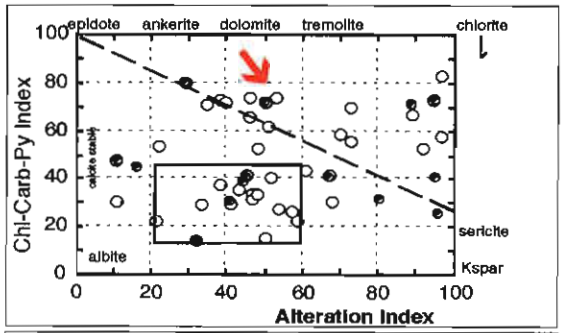

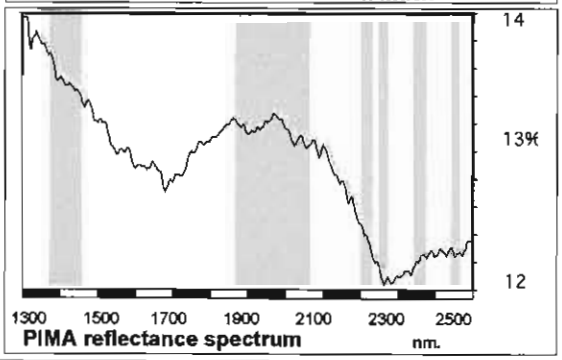

Rosebery Alteration Data Sheet

Sample No. 120R - 1421
Location Rosebery Mine, K lens, DDH 120R 1421.8 m.
Alteration zone Footwall, sericite - carbonate
Formation Mt Read Volcanics, Central Volcanic Complex

Description Moderately sericite - carbonate altered, massive, plagioclase phyric, rhyolitic pumice breccia.

Facies Interp Non - welded, subaqueous mass flow deposit of rhyolitic pumice clasts

Alteration Intensity none weak (moderate) strong intense Py < 1%
Alteration Style patchy (pervasive) veined cleavage control
Alteration Mineralogy Groundmass sericite > quartz
Feldspars carbonate > sericite
Mafics -
Interpretation diagenetic metamorphic syntectonic (hydrothermal)
Relict Mineralogy Feldspar phenocrysts partially preserved

Geochemistry

SiO_2	TiO_2	Al_2O_3	Fe_2O_3	MnO	MgO	CaO	Na_2O	K_2O	P_2O_5	S	CO2	Al	CCPI	Ti/Zr
71.46	0.32	12.93	2.44	0.11	1.65	1.49	1.36	4.16	0.06	0.06	3.89	67	41	8.3

Rb	Ba	Cu	Pb	Zn	Sb	Tl	Zr	Nb	Y
182	1042	3	5	29	0.9	229.9	32		

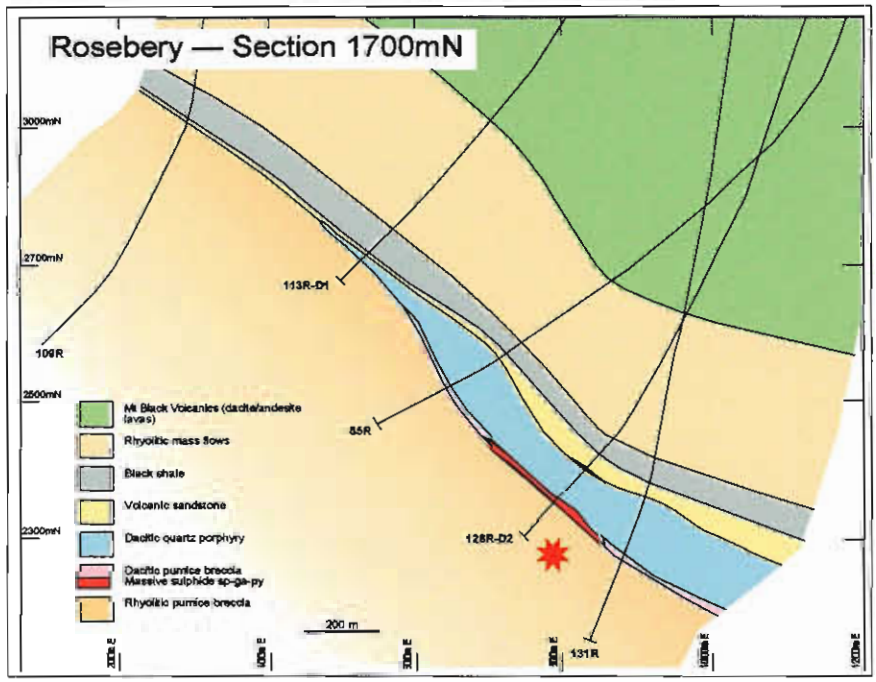

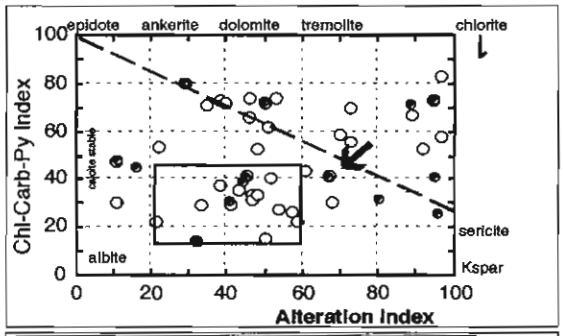

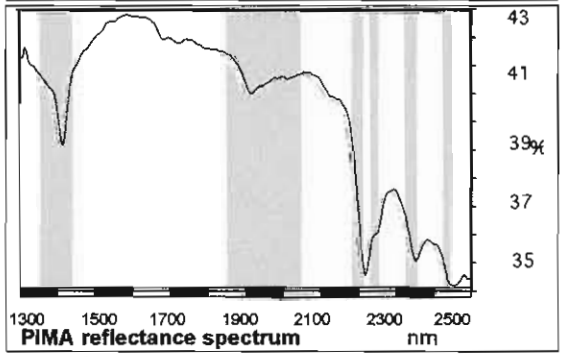

Sample No.	**128R - 1230**
Location	Rosebery Mine, K Lens DDH 128R 1230.4 m.
Alteration zone	Footwall , sericite - carbonate
Formation	Mt Read Volcanics, Central Volcanic Complex

Description Strongly sericite - quartz - carbonate altered, moderately foliated, massive feldspar - phyric, rhyolitic pumice breccia with dark sericite fiamme like lenses.

Facies Interp Non - welded, subaqueous mass flow deposit of rhyolitic pumice clasts.

Alteration Intensity	none	weak	moderate	(strong)	intense	Py - Sp - Ga 2%
Alteration Style	(patchy)	(pervasive)	veined		cleavage control	
Alteration Mineralogy	Groundmass	sericite - quartz > carb				
	Feldspars	carbonate - sericite - sp - ga - py				
	Mafics	-				
Interpretation	diagenetic		metamorphic		syntectonic	(hydrothermal)
Relict Mineralogy	none					

Geochemistry

SiO_2	TiO_2	Al_2O_3	Fe_2O_3	MnO	MgO	CaO	Na_2O	K_2O	P_2O_5	S	CO2	Al	CCPI	Ti/Zr
72.37	0.26	12.18	1.8	0.92	1	1.22	0.29	5.2	0.04	0.27	3.78	80	33	8

Rb	Ba	Cu	Pb	Zn	Sb	Tl	Zr	Nb	Y
239	1638	203	1800	1800			194	11.6	32

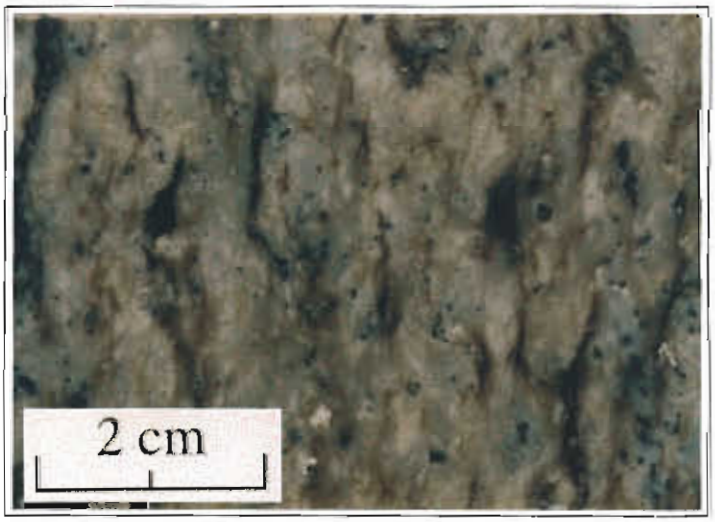

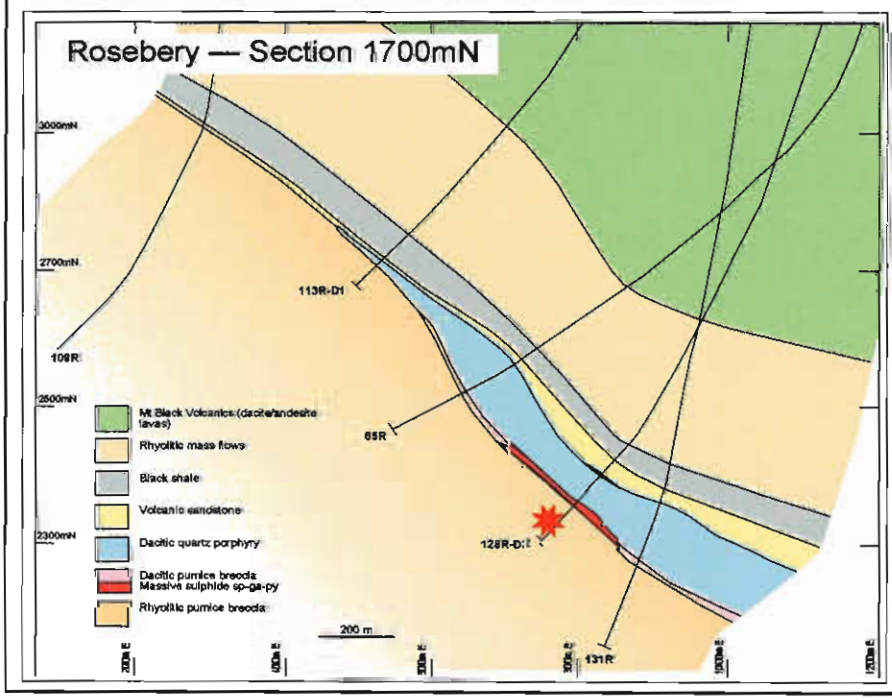

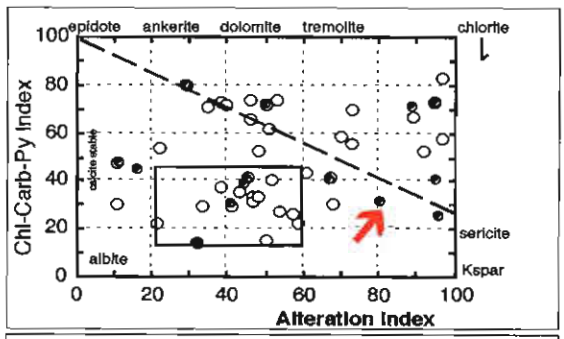

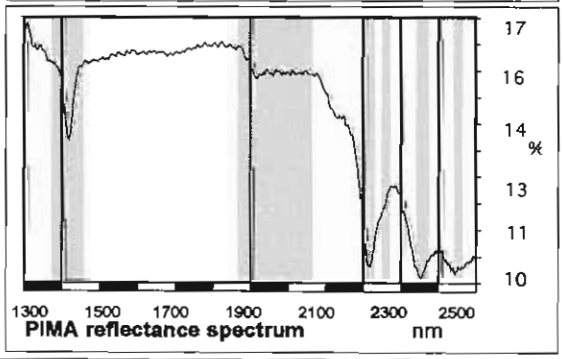

Rosebery Alteration Data Sheet

Sample No. 109R - 723
Location Rosebery Mine, north of B lens, DDH 109R 723.5 m.
Alteration zone Footwall, carb - tour - aspy veins
Formation Mt Read Volcanics, Central Volcanic Complex

Description Manganiferous carbonate - tourmaline - arsenopyrite vein with Bleached sericite - carbonate halo, in moderately foliated, massive feldspar - phyric rhyolitic pumice breccia
Facies Interp Non - welded, subaqueous mass flow deposit of rhyolitic pumice clasts

Alteration Intensity	none	weak	moderate	(strong)	intense	Py - Aspy 1%
Alteration Style	patchy	pervasive	(veined)		cleavage control	
Alteration Mineralogy	Groundmass	sericite - carbonate				
	Feldspars	sericite				
	Mafics -	veins: carbonate - quartz - flourite - tourmaline - chlorite - py - aspy				
Interpretation	diagenetic	metamorphic	(syntectonic)	(hydrothermal)		
Relict Mineralogy	none					

Geochemistry

SiO_2	TiO_2	Al_2O_3	Fe_2O_3	MnO	MgO	CaO	Na_2O	K_2O	P_2O_5	S	CO2
60.85	0.24	11.07	8.75	3.87	1.07	0.46	0.09	3.61	0.04	0.3	

Al	CCPI	Ti/Zr
89	71	8

Rb	Ba	Cu	Pb	Zn	Sb	Tl	Zr	Nb	Y
247	636	11	81	102			181	10	33

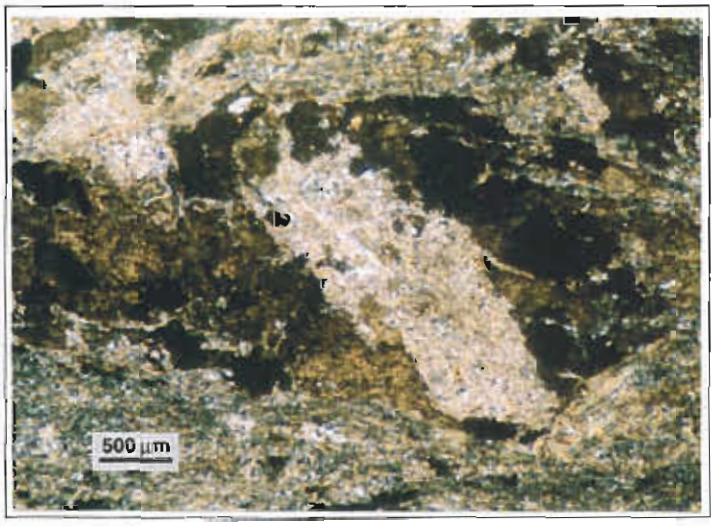

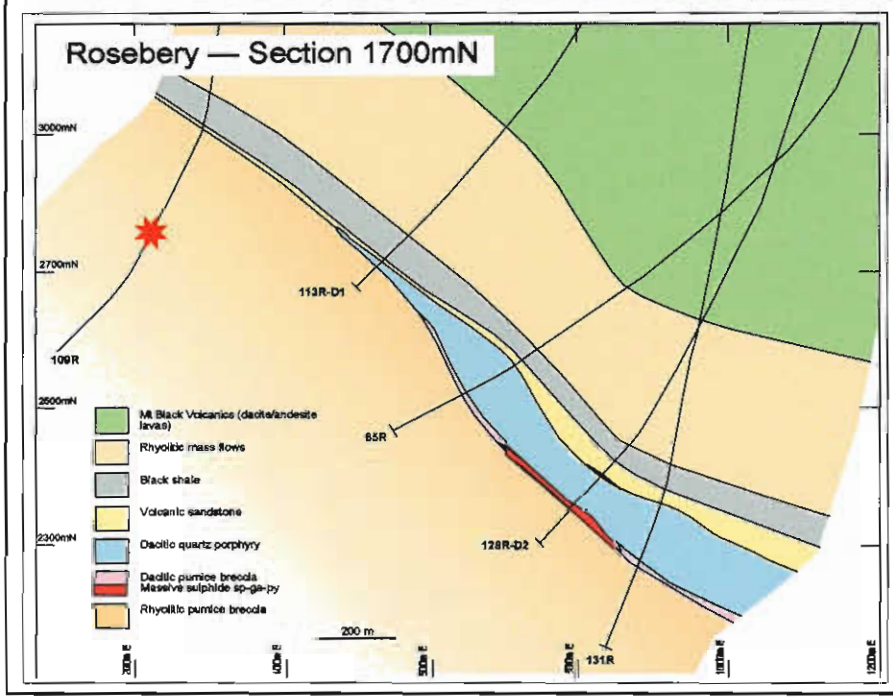

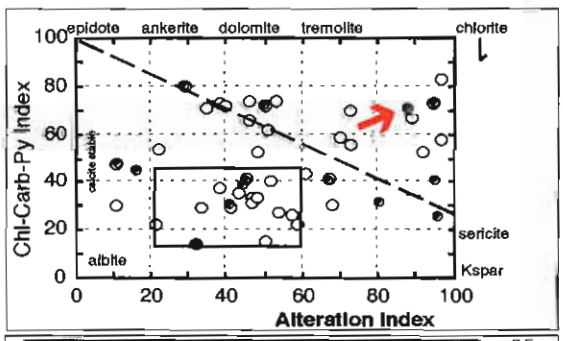

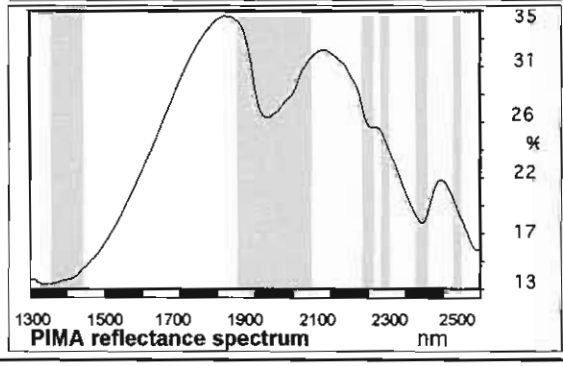

Sample No. 120R - 1386
Location Rosebery Mine, K lens, DDH 120R 1386.5 m.
Alteration zone Footwall, chlorite
Formation Mt Read Volcanics, Central Volcanic Complex

Description Strong quartz - chlorite - sericite altered, strongly foliated, massive, feldspar phyric, rhyolitic pumice breccia

Facies Interp Non - welded, subaqueous mass flow deposit of rhyolitic pumice clasts.

Alteration Intensity	none	weak	moderate	(strong)	intense	Py 2%
Alteration Style	patchy	(pervasive)	veined		cleavage control	
Alteration Mineralogy	Groundmass	quartz - chlorite - sericite				
	Feldspars	quartz - py				
	Mafics	-				
Interpretation	diagenetic	metamorphic	syntectonic	(hydrothermal)		
Relict Mineralogy	none					

Geochemistry

SiO_2	TiO_2	Al_2O_3	Fe_2O_3	MnO	MgO	CaO	Na_2O	K_2O	P_2O_5	S	CO2	Al	CCPI	Ti/Zr
75.5	0.2	9.8	6.5	0.4	1.3	0.1	0.1	2.6	0.05	1.1	2.88	95	73	8

Rb	Ba	Cu	Pb	Zn	Sb	Tl	Zr	Nb	Y
133	549	344	31	398	2	2	165	9	

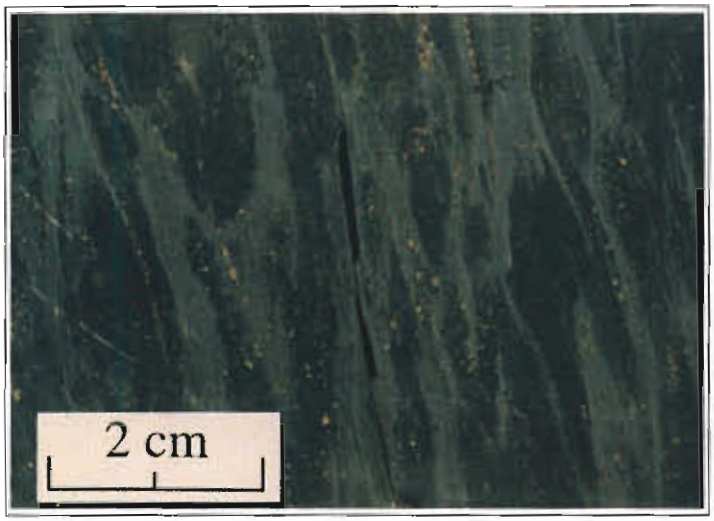

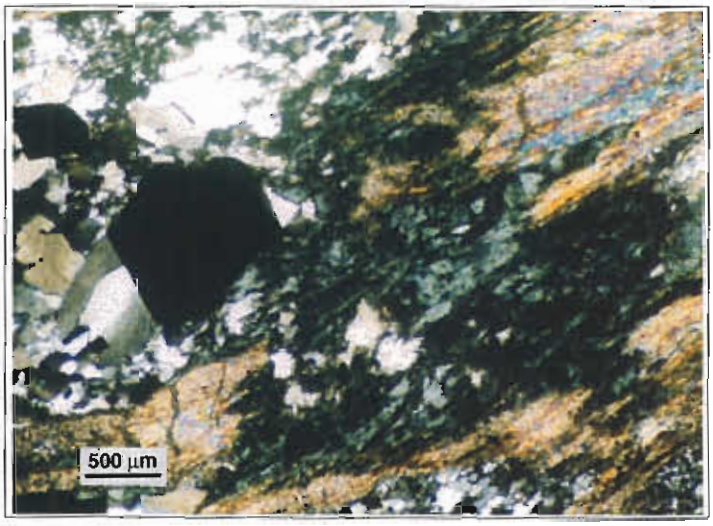

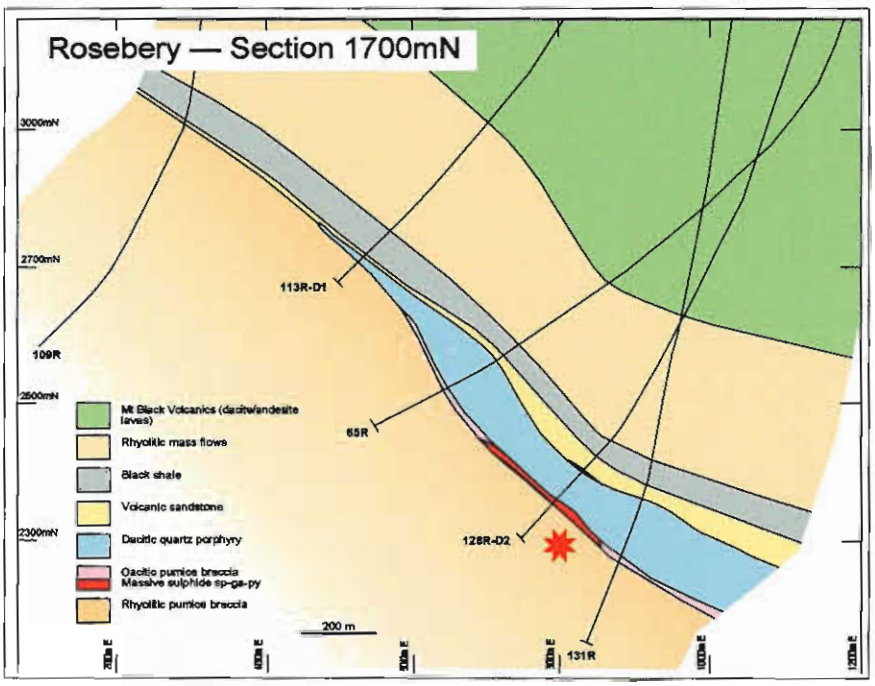

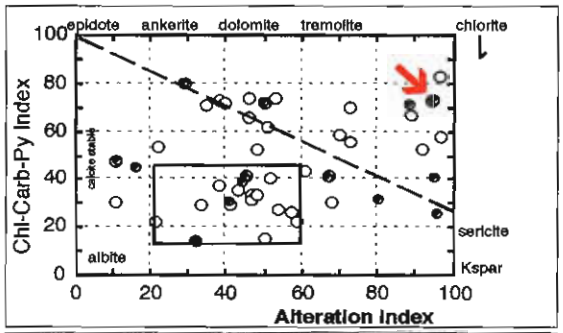

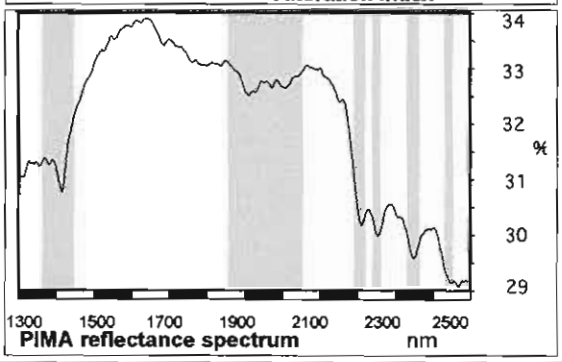

Sample No.	**84R - 843**
Location	Rosebery Mine, edge of B Lens, DDH 84R 843.8 m.
Alteration zone	Footwall, quartz - sericite
Formation	Mt Read Volcanics, Central Volcanic Complex

Description	Very strongly spotty quartz - sericite altered, moderately foliated, massive, feldspar - phyric, rhyolitic pumice breccia.
Facies Interp	Non - welded, subaqueous mass flow deposit of rhyolitic pumice clasts.

Alteration Intensity	none	weak	moderate	(strong)	intense	Py Sp-Ga-Py 3%
Alteration Style	(patchy)	(pervasive)	veined	cleavage control		
Alteration Mineralogy	Groundmass	quartz - sericite				
	Feldspars	quartz - sericite - sp - ga - py				
	Mafics	-				
Interpretation	diagenetic	metamorphic	syntectonic	(hydrothermal)		
Relict Mineralogy	none					

Geochemistry

SiO_2	TiO_2	Al_2O_3	Fe_2O_3	MnO	MgO	CaO	Na_2O	K_2O	P_2O_5	S	CO2	Al	CCPI	Ti/Zr
72.95	0.27	12.86	2.58	0.17	1.14	0.27	0.05	4.74	0.04	1.94	3.57	95	43	7

Rb	Ba	Cu	Pb	Zn	Sb	Tl	Zr	Nb	Y
202	1767	239	4300	6900			224	13.2	35

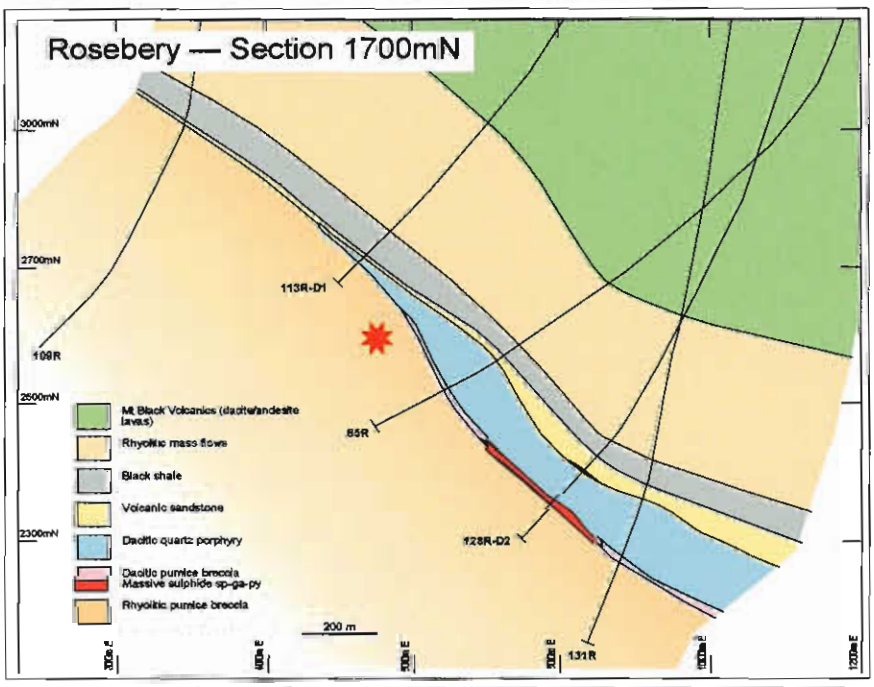

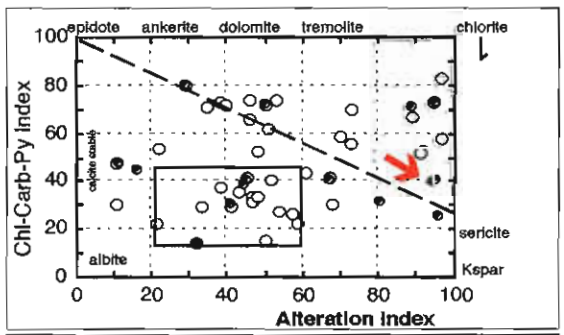

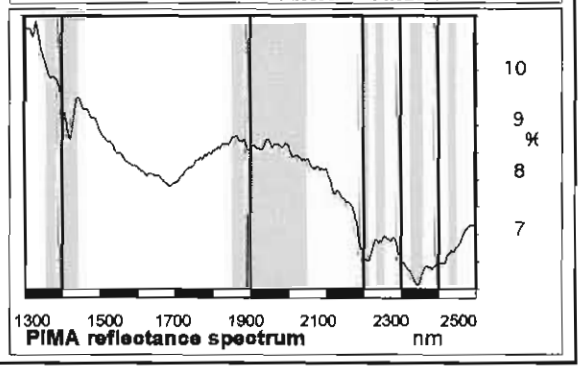

Rosebery Alteration Data Sheet

Sample No.	**84R - 875**
Location	Rosebery Mine, north of B lens, DDH 84R 875.5 m.
Alteration zone	Footwall, quartz - sericite
Formation	Mt Read Volcanics, Central Volcanic Complex

Description	Strongly quartz - sericite altered, strongly foliated, massive, feldspar - phyric, rhyolitic pumice breccia with dark sericite fiamme like lenses
Facies Interp	Non welded, subaqueous mass flow deposit of rhyolitic pumice clasts.

Alteration Intensity	none	weak	moderate	strong	(intense)	Py - Sp 1%
Alteration Style	(patchy)	(pervasive)	veined		cleavage control	
Alteration Mineralogy	Groundmass	quartz - sericite				
	Feldspars	carbonate - quartz - sericite - py - sp				
	Mafics	-				
Interpretation	diagenetic	metamorphic	syntectonic	(hydrothermal)		
Relict Mineralogy	none					

Geochemistry

SiO_2	TiO_2	Al_2O_3	Fe_2O_3	MnO	MgO	CaO	Na_2O	K_2O	P_2O_5	S	CO2	Al	CCPI	Ti/Zr
74.49	0.32	13.78	2.26	0.15	0.93	0.13	0.07	4.94	0.05	0.85	2.8	96	26	8

Rb	Ba	Cu	Pb	Zn	Sb	Tl	Zr	Nb	Y
242	1067	8	92	348	3	2	239	12	36

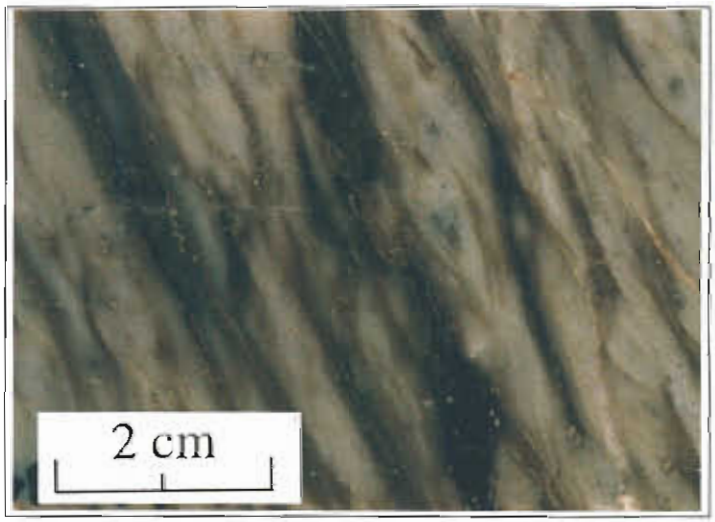

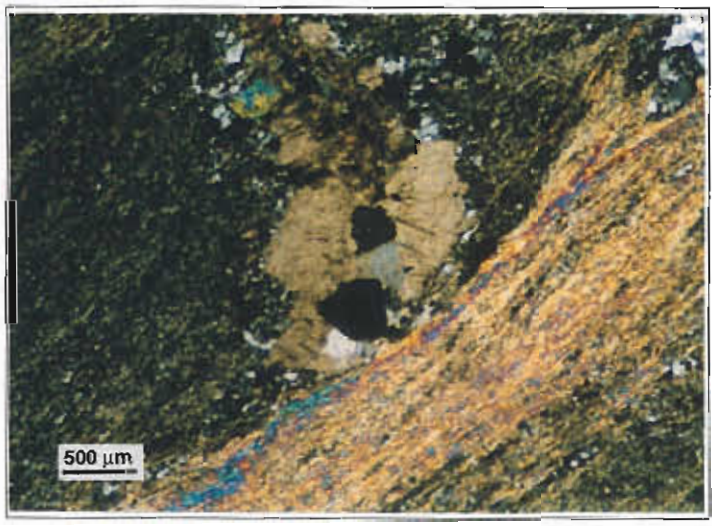

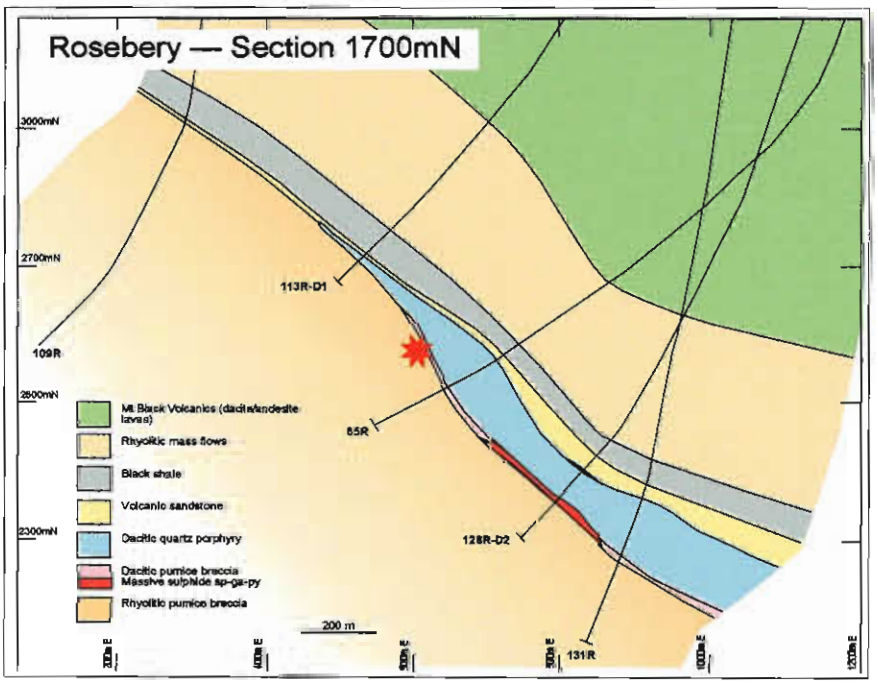

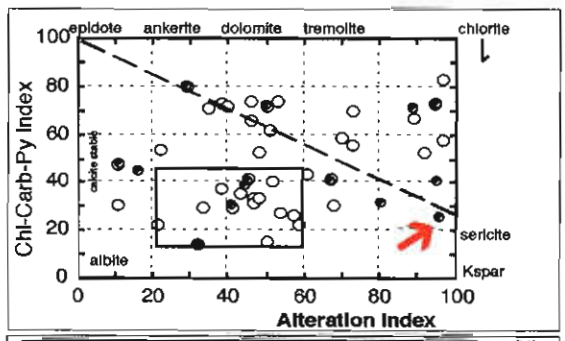

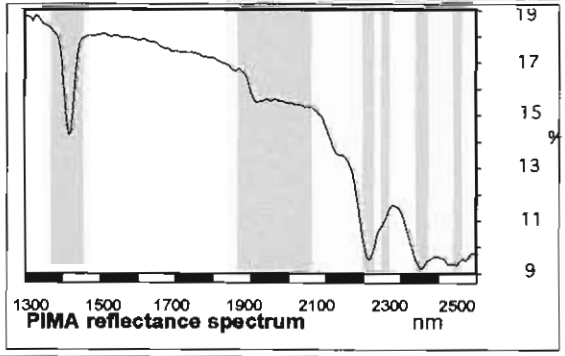

Alteration halo model for the Hellyer VHMS deposit, western Tasmania

J. Bruce Gemmell and Russell Fulton
Centre for Ore Deposit Research

Introduction

The Hellyer massive sulfide deposit is a major (16 million tonnes), high grade (13.9% Zn, 7.1% Pb, 0.4% Cu, 168 g/t Ag, 2.5 g/t Au, 2.2% Ba, 1.2% As), mound-style polymetallic VHMS within the Mt Read Volcanics of Western Tasmania (Gemmell and Large, 1992; McArthur, 1996).

A study of the hangingwall alteration and geochemistry by Fulton was undertaken as part of AMIRA Project P439 in order to characterise the alteration developed above the ore body in the Hellyer basalt and to develop vectors to ore for use on a district and local scale. No detailed study of the alteration mineralogy of the hangingwall has previously been undertaken apart from some research which formed a portion of a MSc project (Jack, 1989). Fulton's information has been combined with previous information on the footwall alteration and geochemistry by Gemmell (1990) and Gemmell and Large (1992) to produce an overall model for the alteration associated with the Hellyer VHMS deposit.

Previous AMIRA Reports

- Fulton, F and Gemmell, J.B., 1995, Hellyer hangingwall study: AMIRA P439 Report 1, November 1995, p. 123-126.

- Fulton, F., 1996, Mineral chemistry of the hangingwall alteration, zone at the Hellyer mine, western Tasmania: AMIRA P439 Report 2, May 1996, p. 63-94.

- Fulton, R., 1996, Hellyer alteration study: AMIRA P439 Report 3, October 1996, p. 291-300.

- Fulton, R. and Gemmell, J.B., 1997: Mineralogy and Geochemistry of the hangingwall alteration, Hellyer deposit : AMIRA P439 Report 5, October 1997, 29 pp. (handout)

Sampling strategy

A total of 160 samples were collected and analysed from 10 drill holes that intersected the hangingwall alteration plume above the deposit and from drill holes away from the deposit, primarily on an east-west section (Fig. 1). Samples were collected from the different alteration assemblages encountered throughout the Hellyer basalt. These data have been combined with the unaltered Hellyer Basalt data from Stanley and Gemmell (see database).

All samples from both data sets were analysed for the major elements by XRF. The trace elements were analysed by XRF or ICP-MS as follows:

XRF	As, Ba, Ce, Cr, Cu, La, Nd, Ni, Pb, Rb, S, Sc, Sr, Th, V, Y, Zn, Zr
ICP-MS	Ag, As, Bi, Cd, Cs, Mo, Sb, Tl, U

Ore Deposit Characteristics

Form of orebody: Footwall rocks consist of massive and fragmental (autobrecciated, quench-fragmented, hyaloclastic) andesitic and basaltic lavas with intercalated polymict epiclastic mass flow sediments. Massive sulfide mound with dimensions of 800 m north-south and 200 m east-west with an average vertical thickness of 45 m (Fig. 2). Above the

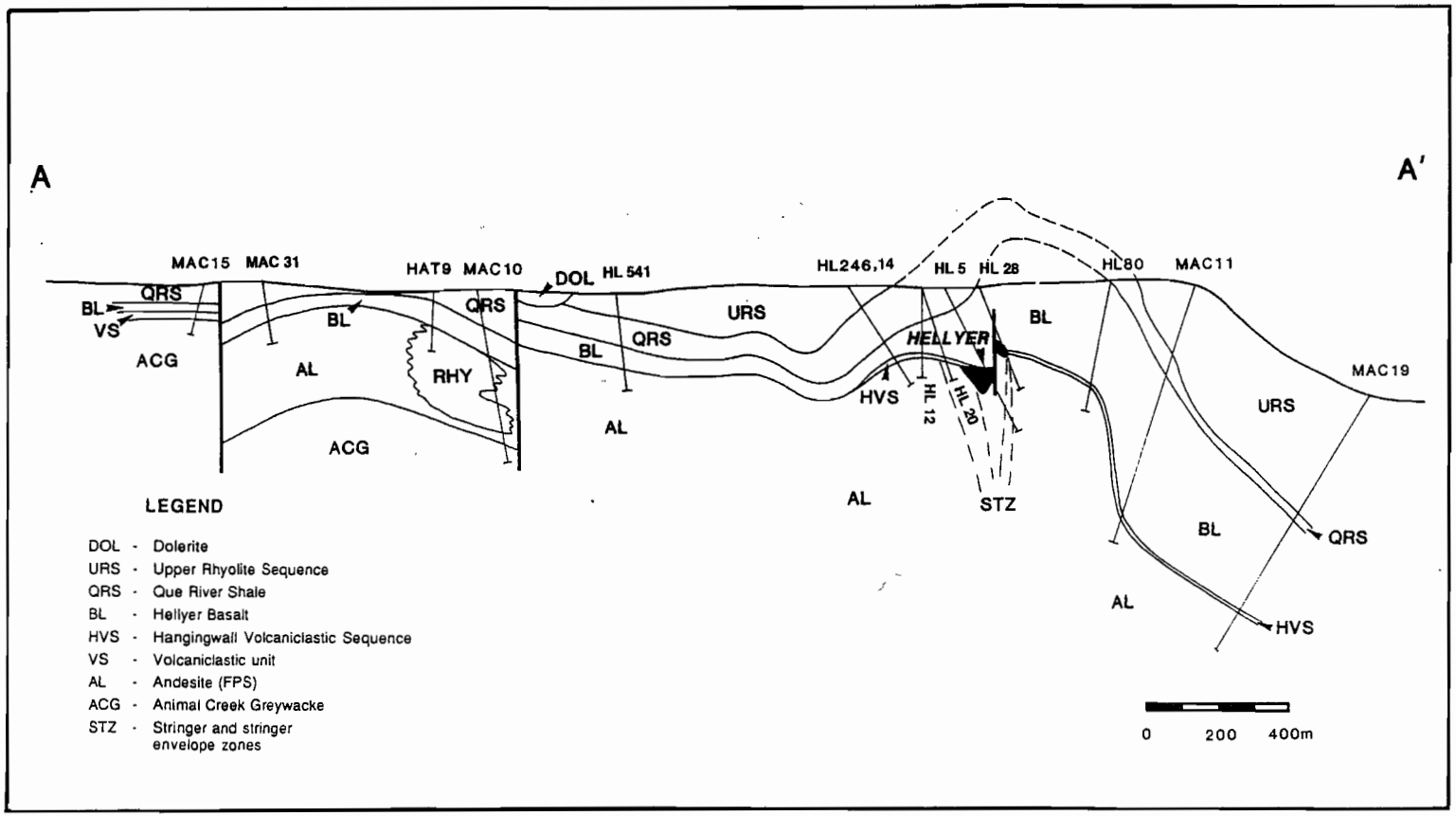

Figure 1a A schematic model of the seafloor environment at the time of deposition of the Hellyer deposit. In this model the sea floor topography is controlled by a series of north-south trending normal block faults associated the regional extensional tectonics. Several normal faults may have created a of tilted, upthrown blocks which would represent lava ridges. Submarine debris flows shed off these upthrown blocks would collect in the troughs. From Gemmell (1990)

Figure 1b (opposite page) Surface geology map of the Hellyer region including drill collars of the holes used in this study.

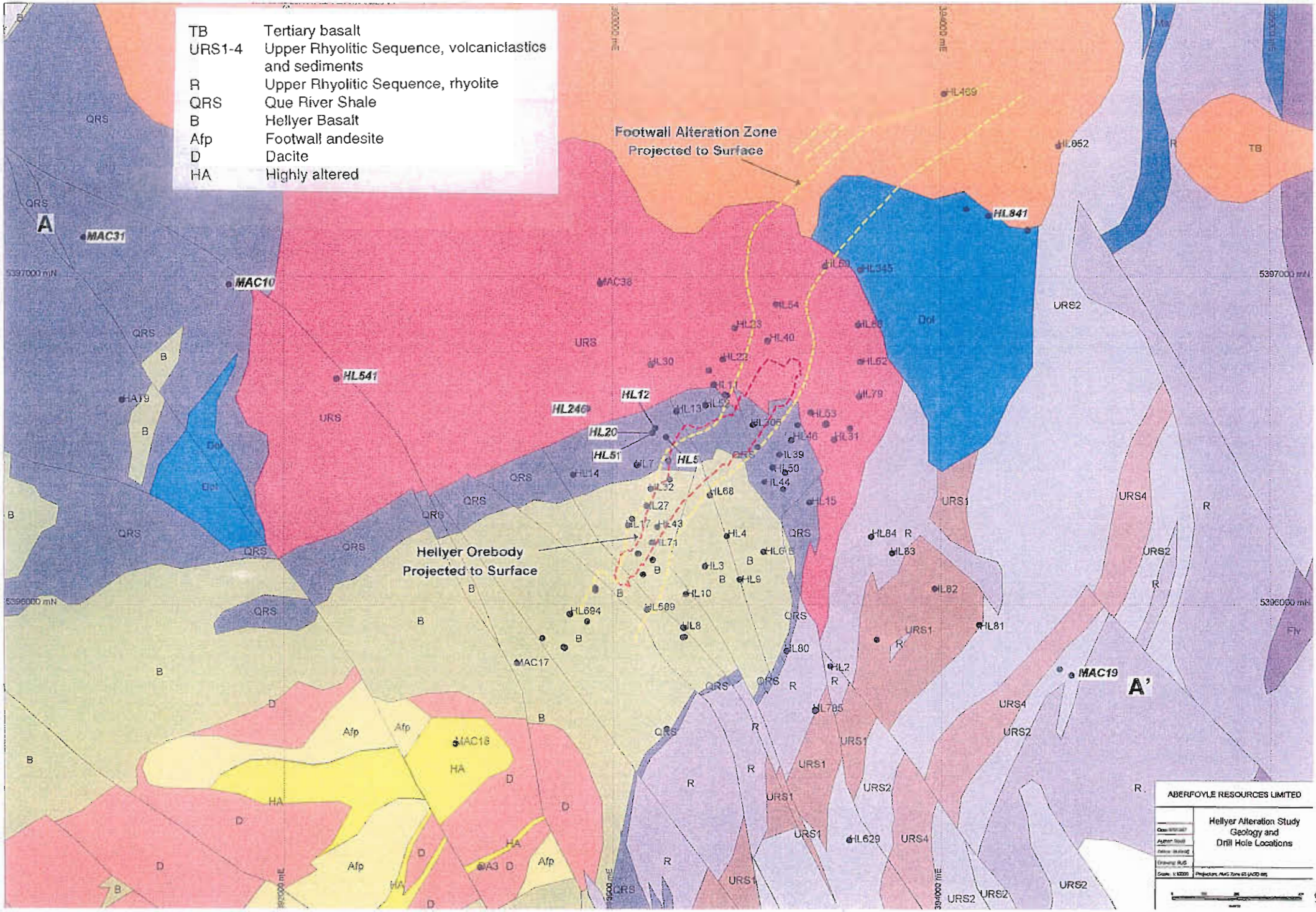
TB Tertiary basalt
URS1-4 Upper Rhyolitic Sequence, volcaniclastics and sediments
R Upper Rhyolitic Sequence, rhyolite
QRS Que River Shale
B Hellyer Basalt
Afp Footwall andesite
D Dacite
HA Highly altered
Footwall Alteration Zone Projected to Surface
Hellyer Orebody Projected to Surface
A
A'
MAC31
MAC10
MAC38
MAC17
MAC18
MAC19
HL541
HL246
HL12
HL20
HL51
HL5
HL841
HL852
HL694
HL589
HL629
HL785
5397000 mN
5396000 mN
394000 mE
ABERFOYLE RESOURCES LIMITED
Hellyer Alteration Study
Geology and
Drill Hole Locations

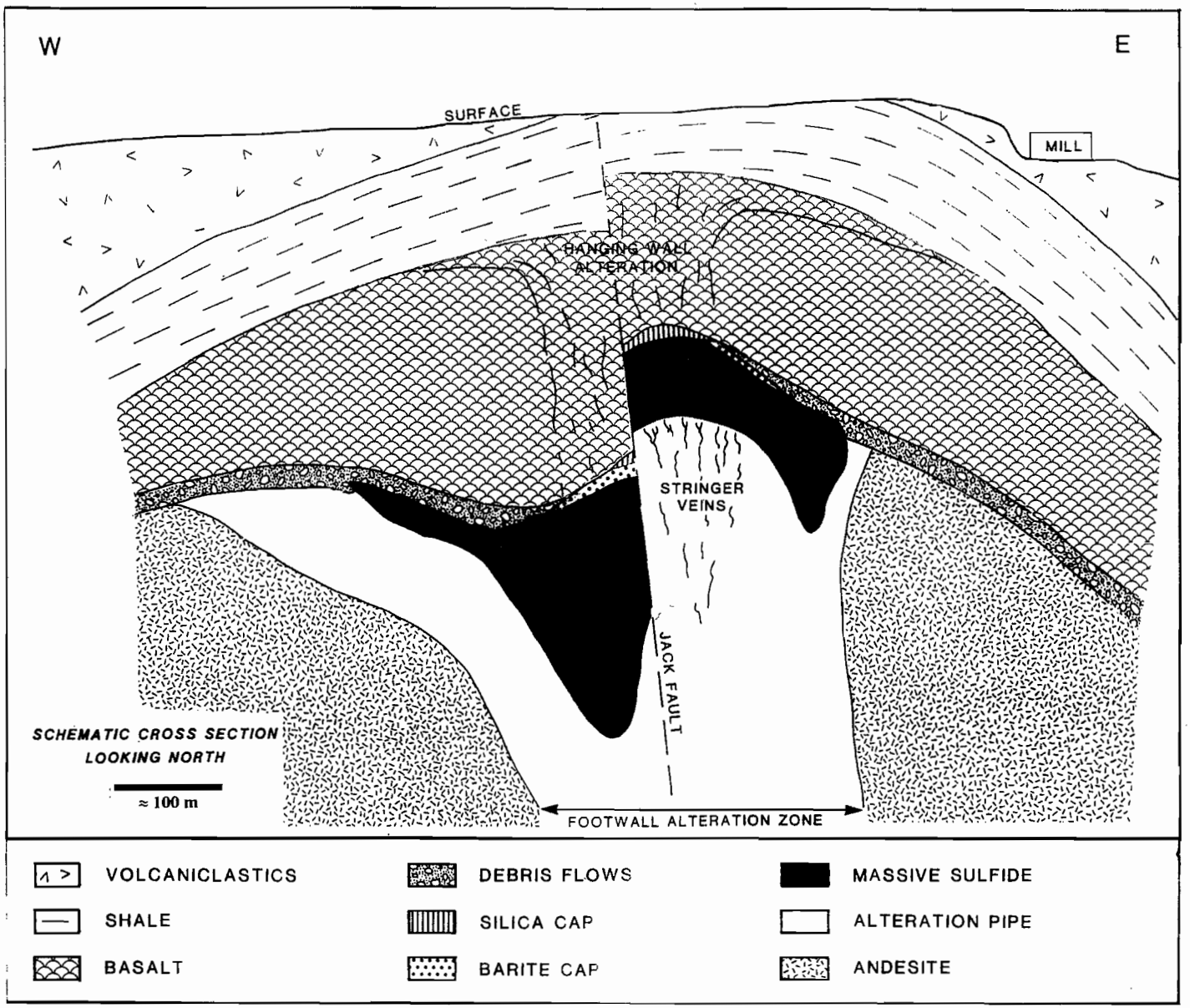

Figure 2 Schematic cross section of the Hellyer deposit showing the geologic setting of the deposit. Abbreviations: SEZ-stringer envelope zone (quartz-sericite-pyrite alteration), Stringer zone - intense footwall alteration, from core to rim; quartz→chlorite→sericite. From Gemmell and Large (1993).

central portion of the deposit on the stratigraphic hangingwall occurs a small zone of silica-pyrite which is surrounded by a 10–15 m thick barite cap. Onlapping, but not totally covering the deposit, is a 0–40 m thick volcaniclastic sequence consisting of polymict mass flow breccias and laminated ash. Massive and pillow basalt lavas (Hellyer Basalt) cover the volcaniclastic sediments and the massive sulfide deposit. Overlying the basalt is the Que River Shale and interbedded rhyolitic tuffs, volcaniclastics, shales, and graywackes, locally called Upper Rhyolitic Sequence.

Size and grade: 17 million tonnes at 13.0% Zn, 6.8% Pb, 0.3% Cu, 160 g/t Ag, 2.3 g/t Au. Within the deposit a classic metal zonation exists with elevated Cu-Fe in the lower and inner regions and grading upwards and outwards to a zone of Pb, Zn, Ag, As, and Au enrichment.

Sulfide mineralogy: Sulfide mineralization averages 54% pyrite, 20% sphalerite, 8% galena, 2% arsenopyrite and 1% chalcopyrite with minor tetrahedrite. The remaining 15% is gangue consisting of quartz, barite, calcite, chlorite, sericite and siderite. Ore textures include banded (both primary and deformational), massive, recrystallized, and reworked fragmental types.

Alteration mineralogy: Footwall alteration contains chlorite, dolomite or Fe-dolomite, sericite, and quartz (Gemmell and Large, 1992; Bradley, 1997). Hangingwall alteration consists of chlorite, white mica (including sericite and "fuchsite"), carbonate (calcite, Fe-dolomite, ankerite), albite and quartz (Jack, 1989; this study).

Deformation and metamorphism: East–west compression during the Devonian Tabberabberan Orogeny has resulted in open anticlines with tight, locally isoclinal synclines within the massive sulfide deposit and one episode of folding and a later wrench faulting event are recognized within the mine area (Drown and Downs, 1990). Strain has been strongly partitioned into the phyllosilicate-rich rock in both the footwall and hangingwall alteration zones, and into the galena-sphalerite rich outer zones of the orebody. A major north-south sub-vertical wrench fault, the Jack fault, cuts acutely across the center of the deposit with post-mineralization and post-folding sinistral movement; the east block moved 130 m north and 30 m up.

In the Que–Hellyer area, Cambrian hydrothermal alteration associated with mineralisation has been overprinted by regional Devonian prehnite–pumpellyite facies metamorphism (Jack, 1989). This has been expressed by the formation of epidote, pumpellyite and prehnite in the footwall andesites, but only rarely are these minerals developed within the Hellyer basalt.

Volcanic facies architecture

The Que-Hellyer Volcanics are a 1 km thick suite of Late Middle Cambrian mafic to felsic lavas and volcaniclastics that lie within the Dundas Group and are considered part of the Mount Read Volcanics. Characteristics of the volcanic rocks hosting the Hellyer deposit (Fig. 3) have been outlined by Waters and Wallace (1992) and updated by Fulton (1996). Below is a short summary of the petrologic and volcanologic characteristics of the host, these include the Lower Basalt, Footwall Andesite and Epiclastic Debris Flows, Hangingwall Volcaniclastic Sequence, Hellyer Basalt, Que River Shale and the Upper Rhyolitic sequence.

Lower basalt

Basaltic volcanics underlie the footwall andesitic volcanics and overlie the Animal Creek Greywacke. This unit consists of massive to pillowed lavas and peperitic breccias.The Lower Basalt has a limited, patchy distribution and appears to be thickest around the Que River mine.

Footwall andesite lavas and epiclastic debris flows (FPS)

The footwall to the Hellyer deposit was originally considered to consist of andesitic lavas but it has been recognised that a large proportion of the footwall, especially in the immediate vicinity of the massive sulphide mineralisation, consists of primary and re-sedimented volcaniclastic debris. Autobrecciated and quench fragmentated, polymict volcaniclastic rocks are dominant, with massive or coherent andesite lavas making up a minor

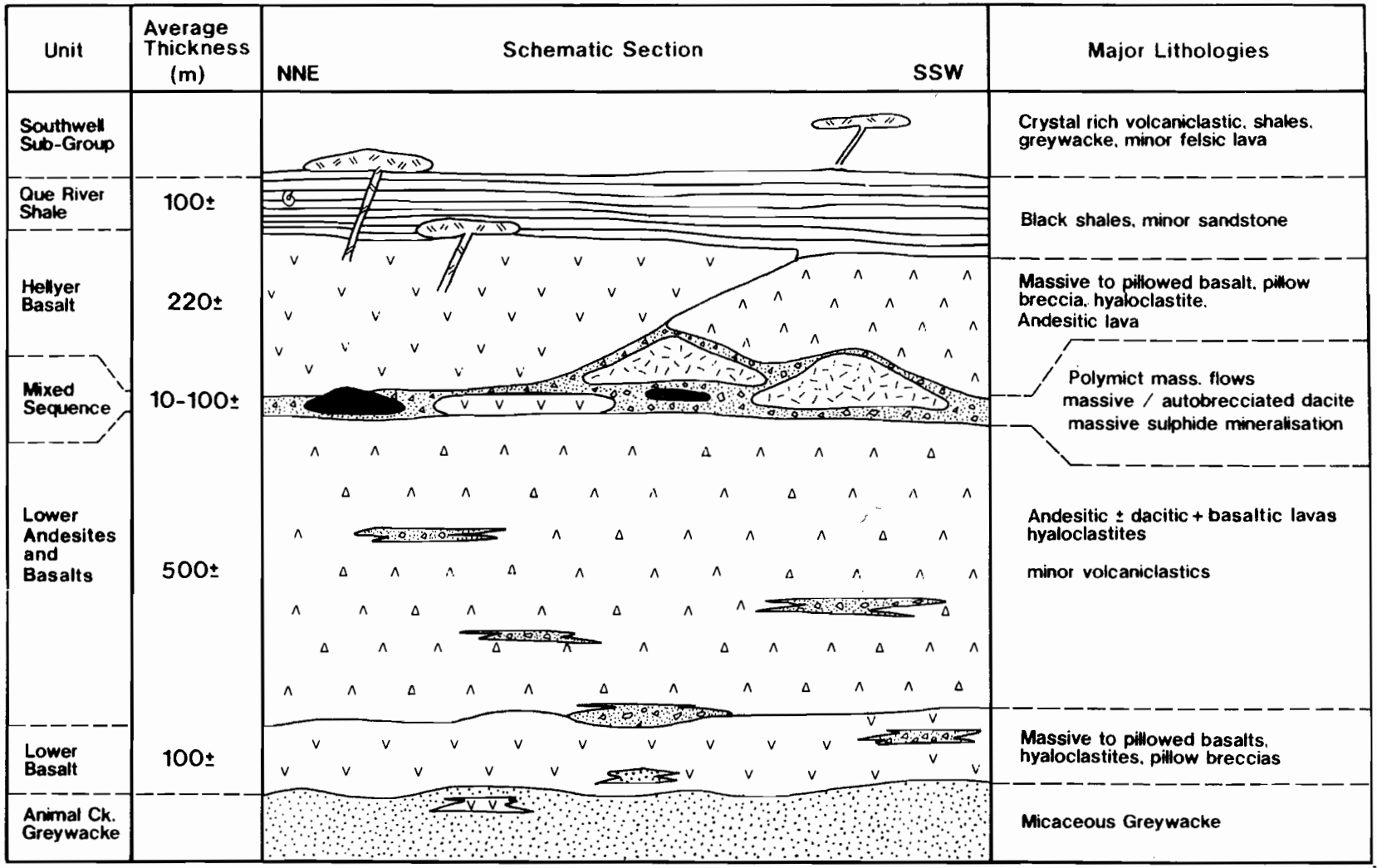

Figure 3 Schematic stratigraphic section through Que-Hellyer Volcanics (not to scale). From Waters and Wallace (1992).

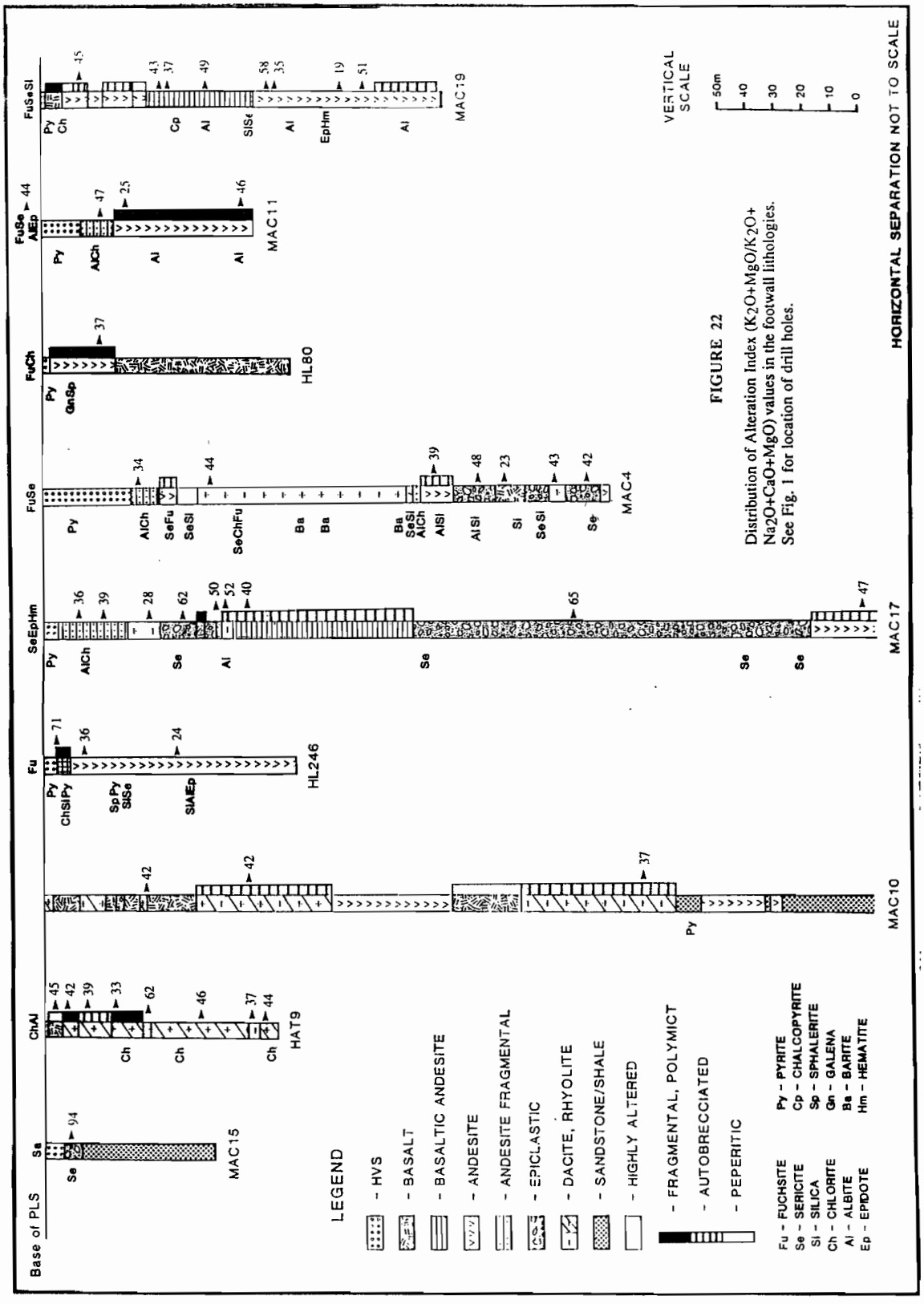

FIGURE 22

Distribution of Alteration Index ($K_2O+MgO/K_2O+Na_2O+CaO+MgO$) values in the footwall lithologies. See Fig. 1 for location of drill holes.

Figure 4 Distribution of lithologies, alteration and Alteration Index in footwall rocks in the Hellyer district. See Fig. 1b for drill hole locations. From Gemmell (1990).

proportion. The massive andesitic lava consists of intervals of 10's of metres of massive feldspar porphyritic andesite lava. This lava is poorly to non-vesicular and consists of phenocrysts and glomerocrysts of plagioclase set in a matrix of dominated by feldspar and varies from pilotaxitic to hyalopilitic, with the later often perlitically fractured. Footwall volcaniclastics are generally weakly graded, very poorly sorted, lithic breccias. Fragments are composed dominantly of andesite with minor amounts of basalt, dacite and micaceous sedimentary/metasedimentary lithics.

Within the Que-Hellyer district, andesite lavas and breccias dominate to the east of Hellyer with minor polymict epiclastic debris flow sediments (Fig. 4). To the west the footwall lithologies are a complex mixture of andesite lavas and breccias, rhyolitic lavas or shallow intrusives/domes and minor interbedded sandstones and shales. To the south of Hellyer the footwall is dominated by epiclastic debris flow sediments and dacite lavas or shallow intrusives/dome complexes with minor andesite and basalt lavas and breccias.

Hangingwall Volcaniclastic Sequence (HVS)

The Hangingwall Volcaniclastic Sequence is a sequence of polymict breccias, volcaniclastics and minor shales with an average thickness of 10 m (McArthur, 1986). Several sedimentary facies have been recognised in the HVS; a volcanic lithic breccia, which is thought to be a mass flow unit or a high concentration turbidity current, and very fine to coarse-grained sands and thin interbeds of finer-grained sediments, which formed from small scale, high concentration, turbidity currents associated with the mass flow deposits. The HVS contains more basaltic and dacitic fragments and less andesitic material differs compared to the footwall volcaniclastics. One distinctive feature of the HVS is that it contains fragments of sulphide and barite mineralisation.

Dacitic and rhyolitic material in the forms of lavas, lava domes and autoclastic breccias, both primary and resedimented, have a close spatial association with the ore horizons of both the Hellyer and Que River deposits. Two facies have been identifed; massive dacitic lava facies and a brecciated dacitic lava facies. The massive dacitic lava facies consists of massive porphyritic dacitic to rhyodacitic lavas which appear to be a result of relatively short flow, small volume sub-aqueous effusive eruptions. This facies characteristically forms the centre or core of dome shaped bodies which occur throughout the Que-Hellyer Volcanics at or about the ore horizon. The brecciated dacitic lava facies consists of auto-brecciated to quench fragmented dacitic lavas and resedimented equivalents. The breccia facies is best developed around the margins of the massive dacitic domes, which are interpreted as being very shallow intrusives to extrusives as indicated by the abundant primary and resedimented autoclastic breccias.

Hellyer Basalt — Pillow Lava Sequence (PLS)

The Hellyer Basalt or Pillow lava sequence (PLS) at Hellyer consists of a 80-250 m thick sequence of pillowed to massive basaltic lavas, hyaloclastites and interbedded sediments overlying the HVS (McArthur, 1986). The lavas vary from aphyric to porphyritic with phenocrysts of plagioclase and clinopyroxene set in a groundmass consisting of microcrystalline plagioclase, clinopyroxene and alkali feldspar. Vesicles filled with calcite and/or quartz are a distinguishing feature of the Hellyer basalt.

The pillow lava facies is volumetrically the most dominant facies of the Hellyer basalt. This facies contains pillowed basaltic and basaltic-andesite lavas with associated interpillow sediments and breccias. The pillow lava facies is a result of the extrusion of lava into water or water saturated sediments. The massive basaltic lava facies consists of massive, dominantly non-vesicular porphyritic lava in the form of sheet flows. This unit is commonly peperitic, having large volumes of sedimentary material between fragments. Fragments range from porphyritic to aphyric with planer to cuspate margins and some show insitu brecciation ("jigsaw" fit). The matrix to the fragments is very fine silts and muds that are similar in appearance to the Que River Shale.

The Hellyer basalt can be interpreted as a series of subaqueous flows of massive sheet lavas and pillow lavas with associated hyaloclastites. Extrusion of the basalt in places was onto wet unconsolidated sediments and locally the flows burrowed into the wet sediments as indicated by the peperitic tops to some flow units. The presence of sheet flows indicate local voluminous out pourings of lava or a more

proximal volcanic facies. Slowing supply rates or increased distance from the source led to the formation of pillows. During extrusion, the rapid cooling of the lava in association with continued growth of pillows with chilled carapaces led to fragmentation

Que River Shale (QRS)

The Que River Shale consists dominantly of muds and silts with minor intervals of fine to medium-grained sands that generally occur towards the base of the unit. The average thickness of the Que River Shale is approximately 100 m. Paleontological evidence suggests a late Middle Cambrian age and marine depositional conditions.

Upper Rhyolitic Sequence (URS)

The upper most unit of the Que-Hellyer volcanics exposed in the vicinity of the Hellyer deposit is the Upper Rhyolitic Sequence. This unit overlies the Que River Shale and consists of crystal-lithic volcaniclastics of rhyolitic composition, greywackes and crystal-rich siltstones or mudstones, some pumiceous in character. The first evidence of explosive volcanism and pyroclastic material (cuspate/concave grain boundaries on volcanic quartz, typical of explosively fractured crystals produced during pyroclastic eruptions) above the Hellyer ore position occurs within this unit. Average true thickness of the URS is 500 m (McArthur, 1986).

Chemostratigraphy

Footwall

Whole rock geochemistry indicates a bimodal suite of unaltered footwall lithologies, andesites and rhyolites, for the district wide footwall rocks (Fig. 5a) (Gemmell, 1990). The andesites have increased concentrations of TiO_2, Al_2O_3, total Fe, MnO, CaO, Na_2O, P_2O_5, Ni, Cr, Ba and Ti/Zr and decreased contents of SiO_2, MgO, K_2O, and Zr compared to the rhyolites (Gemmell, 1990). Unaltered andesites have Ti/Zr values that range from 22 to 42, averaging 32, while unaltered rhyolites have Ti/Zr values that range from 5 to 7, averaging 6. The mixed sequence dacites have Ti/Zr values that range from 9 to 22, averaging 13. Hydrothermally altered lithologies in the footwall outside the Hellyer stringer zone have Ti/Zr values that vary between those of the andesites and rhyolites. These data indicate that the Ti/Zr ratio does not remain constant during moderate degrees of hydrothermal alteration and illustrates that the Ti/Zr ratio is an unreliable method to determine the original protolith in footwall altered rocks surrounding the Hellyer deposit (Gemmell, 1990). The occurrence of rhyolites in the footwall sequence is unusual as felsic lavas are generally confined to the overlying Mixed Sequence, the stratigraphic package hosting the Que River and Hellyer ore deposits. Based on their petrologic characteristics and chemical composition the rhyolites in the footwall sequence to the west of Hellyer (Fig 1a) are not related to the Mixed Sequence dacites and may represent a separate felsic eruptive centre. The rhyolites may mark a separate, potential ore horizon in the footwall below the recognised Que-Hellyer ore position (Gemmell, 1990).

Hangingwall

Geochemically, the Hellyer basalt has been assigned to Suite III of the five major geochemical suites defined by Crawford et al. (1992). Suite III basalts and andesites have a distinctive and variable chemistry. They range from rocks with low TiO_2 (0.5%), low P_2O_5 (0.1%) and Ti/Zr values of 30–40, to rocks with low TiO_2 (0.4–0.8%), high P_2O_5 (0.4–1%), light REE enriched and Ti/Zr ranging from 19 to 25. The former have affinities with transitional medium to high K calc-alkaline lavas from modern arcs such as Sunda, whilst the latter have been described as "remarkably P_2O_5 and REE-enriched shoshonites with no compositional equivalents in the Andes or modern arc systems." (Crawford et al., 1992). A whole rock geochemistry database was set up by Jack (1989) and the majority of analyses are in the Ti/Zr range of 30–40, with a minor number of analyses down in the 20–30 range. A more primitive core lava, with higher MgO, Cr, Ni, and Ti/Zr of ≈53, has been identified (Jack, 1989) and occurs immediately above the Hellyer ore body.

A TiO_2 vs Zr plot (Fig. 5b), based on basalt geochemical data from this study and data from Stanley and Gemmell (1997), indicates that the majority of unaltered and altered basalt samples have Ti/Zr ratio in the range 20-30 with a few samples

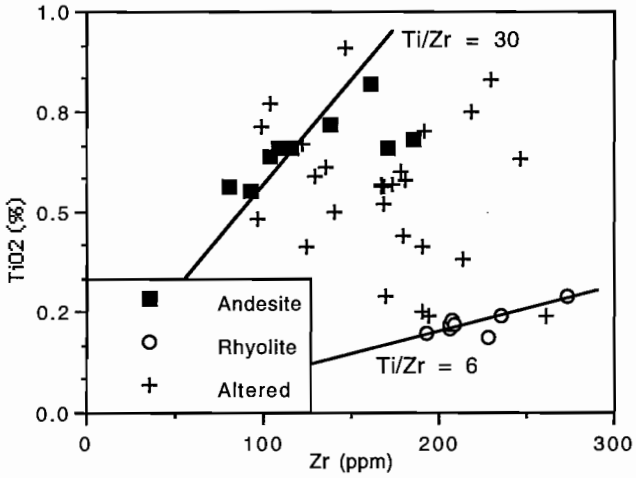

Figure 5a Plot of Zr vs TiO_2 for unaltered and altered footwall samples surrounding Hellyer. The unaltered and altered footwall lithologies do not lie on linear arrays that project back to the origin, suggesting that Zr and TiO_2 are mobile during alteration. From Gemmell (1990).

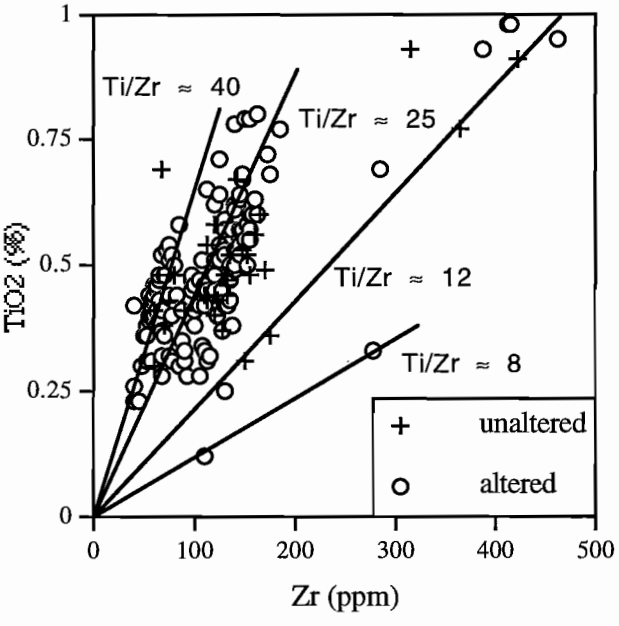

Figure 5b Plot of Zr vs TiO_2 for unaltered and altered Hellyer basalt samples. These data suggest thet there are three magmatic suites represented: Ti/Zr ≈ 55 ("core lava"), Ti/Zr ≈ 40 and Ti/Zr ≈ 25. Altered samples plot along the same trends as the unaltered samples suggesting that that Zr and TiO_2 are immobile during hangingwall alteration.

having Ti/Zr ratios approximately 40 and two samples having higher Ti/Zr values of approximately 55 (similar to Jack's core lava). These data suggest that there are three distinct magma types within the Hellyer Basalt with the "core lava" situated directly above the deposit and the other more evolved basalts occurring above the corer lava and away from the deposit. The majority of data in this study and the Stanley and Gemmell study come from drill holes 100's to 1000's of metres away from the deposit and primarily have Ti/Zr ratios of 20-40.

An analysis of the Ti/Zr ratio between basalt facies indicates that all of the basalts, including the "core lava" occur as massive lavas (Fig. 6a). The other two basalt families, Ti/Zr ≈ 40 and Ti/Zr ≈ 25 occur as lava, pillow and breccia facies (Fig. 6b, c).

Alteration mineralogy and zonation

Footwall

Underlying Hellyer is a zoned alteration pipe and stringer vein system. Mineralogical zoning exists within a footwall alteration pipe, with a central siliceous core giving way to zones of chlorite, chlorite-carbonate, sericite, and finally sericite-quartz (stringer envelope zone) on the margins (Fig. 7). Pervasive alteration started with development of sericite-quartz that was subsequently overprinted by sericite, then chlorite and finally quartz as hydrothermal activity became focused towards the center of the alteration zone (Gemmell and Large, 1992). The Hellyer stringer zone contains distinct thick syn-mineralization veins that represent the channelways for hydrothermal solutions passing up through the alteration zone to the sea floor. Eight stages of veining are distinguished in the stringer zone: one stage of pre-mineralization (stage 1), three stages of syn-mineralization (stages 2A, 2B, 2C), and four stages of post-mineralization veining (stages 3–6). Syn-mineralization veining closely follows the formation of the pervasive footwall alteration and is most intense in the siliceous core (Gemmell and Large, 1992)

An investigation of the district wide footwall geology was undertaken to determine the environment of deposition during formation of the Hellyer stringer zone (Gemmell, 1990). This investigation concentrated on the nature of the footwall lithologies

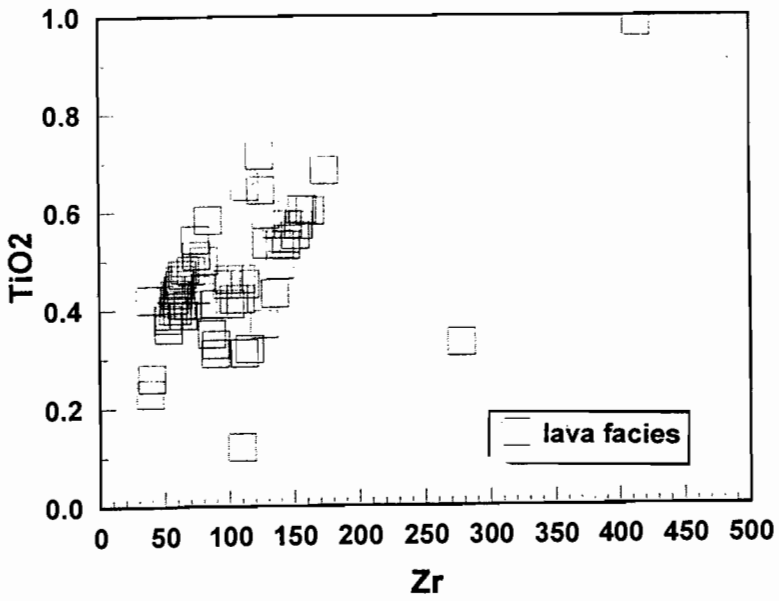

Figure 6a Plot of Zr vs TiO_2 for unaltered and altered, lava facies, Hellyer basalt samples. This facies occurs in all three basalt magmatic suites.

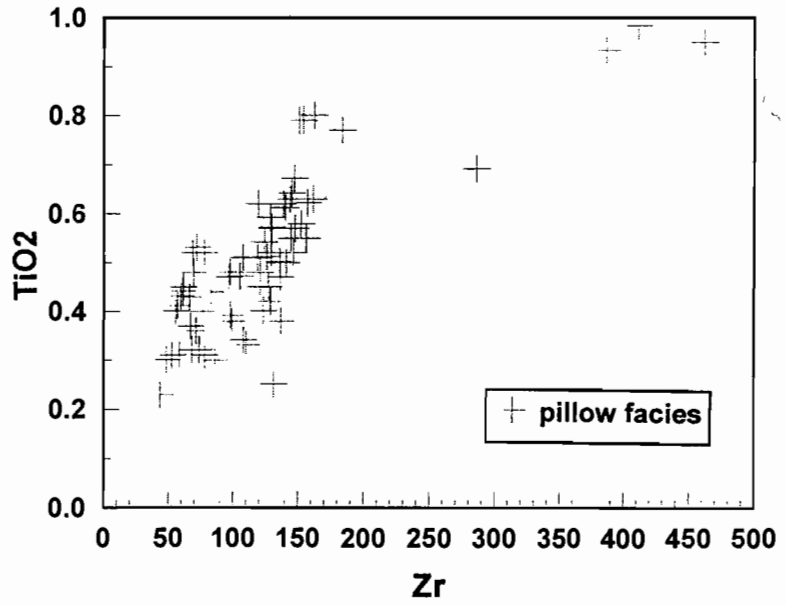

Figure 6b Plot of Zr vs TiO_2 for unaltered and altered, pillow facies, Hellyer basalt samples. This facies occurs only in the Ti/Zr ≈ 40 and Ti/Zr ≈ 25 basalt magmatic suites.

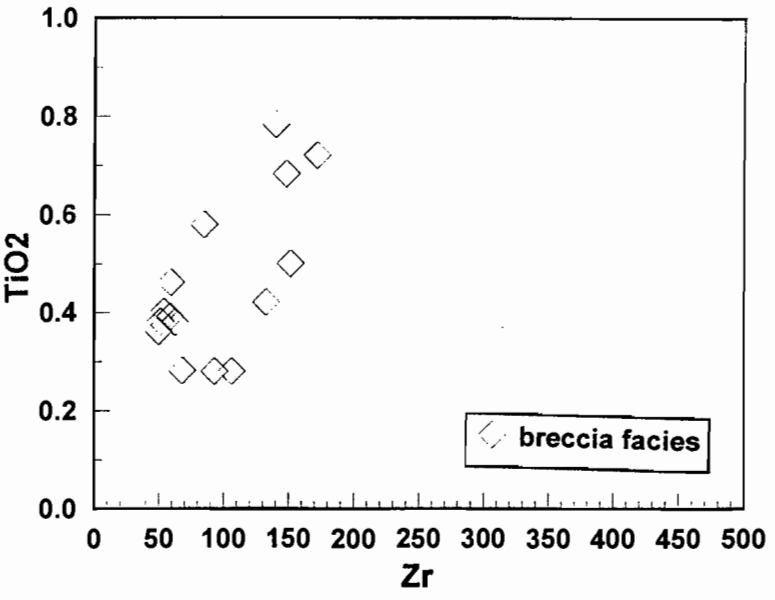

Figure 6c Plot of Zr vs TiO_2 for unaltered and altered, breccia facies, Hellyer basalt samples. This facies occurs only in the Ti/Zr ≈ 40 and Ti/Zr ≈ 25 basalt magmatic suites.

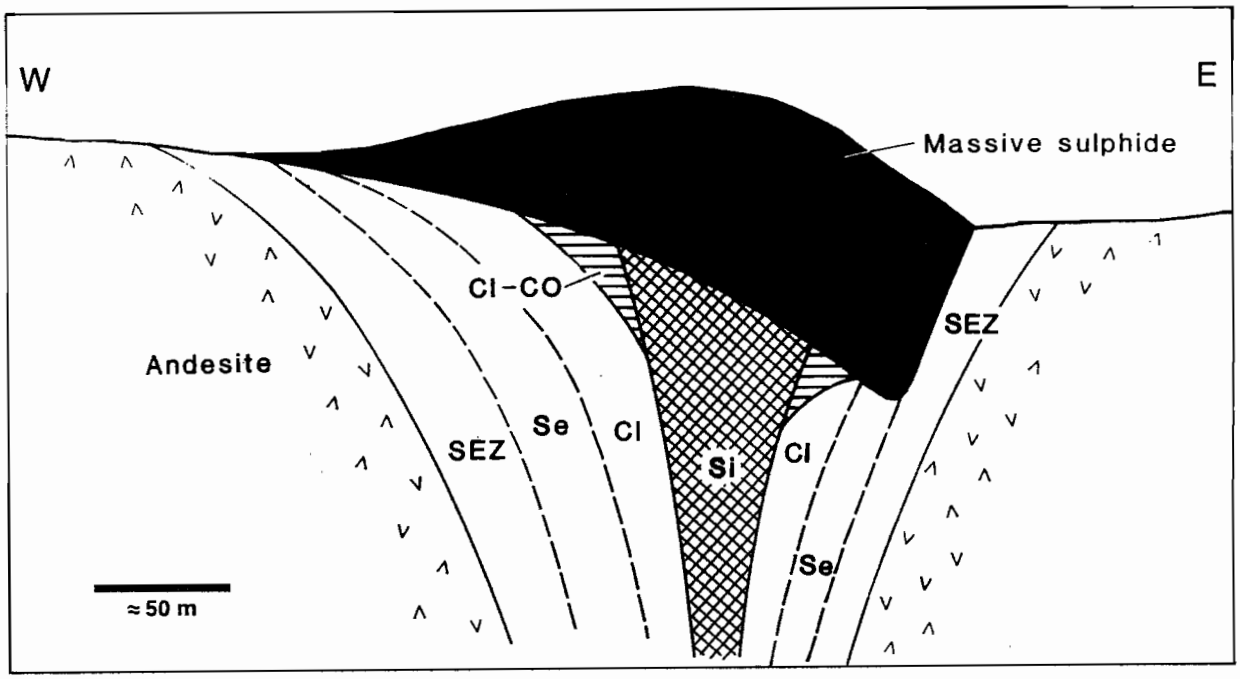

Figure 7 Schematic pre-Jack fault reconstruction of the alteration zones in the center of the hydrothermal system (approximately 10900 N). Abbreviations: SEZ - stringer envelope zone (sericite-quartz alteration), Si - quartz, Se - sericite, Cl - chlorite, CO - carbonate (primarily dolomite). From Gemmell and Large (1992).

and the regional alteration signature, with an aim to determine if a regional alteration signature or trend can be used as an exploration vector. Alteration is confined to patchy silicification, albitisation, chloritisation, and minor sericitisation, epidotisation and hemitisation of the footwall lithologies east of Hellyer, with only patchy sericitisation and chloritisation observed to the west (Fig. 4). In general the alteration is fairly weak compared to the totally destructive alteration within the Hellyer stringer zone. The sericite-quartz-pyrite alteration that distinguishes the Hellyer stringer envelope zone was not observed in drill cores away from the Hellyer deposit. The intense footwall alteration characteristic of the Hellyer stringer zone is confined to the immediate vicinity of the deposit. Veining equivalent to the syn-mineralising Stage 2 veins of the Hellyer stringer system are noticeably absent in the footwall rocks outside the stringer zone. Veining related to the Devonian deformation, equivalent to the post-mineralisation Stage 3-6 veins of the stringer system, are common throughout the footwall lithologies surrounding Hellyer.

Hangingwall

Previous research by Jack (1989) determined that the hangingwall alteration was in a plume–shaped zone directly above the deposit (Fig. 2) that consisted of pervasive calcite-fuchsite, accessory Fe-chlorite patches, calcite veining, increased amounts of interpillow pyrite and albite alteration extending outwards from the plume. The primary alteration phase to affect the Hangingwall Volcaniclastic Sequence (HVS) is sericite and pyrite (Jack, 1989).

In order to ascertain whether there is hangingwall alteration zonation above the ore body two approaches were undertaken. The first was detailed core logging of hangingwall alteration from drill holes directly above the deposit and from holes drilled up to 2 km away from the ore body. The second approach was an analysis of previous drill core logging work. The Hellyer core logging system allows for up to four basic alteration types to be allocated for each core log entry made; the entry "FuCOSePy", for instance, indicates a piece of core which exhibits fuchsite + carbonate + sericite + pyrite alteration. As part of the alteration logging undertaken by

Aberfoyle, geologists assigned an intensity rank from 1 (low intensity) to 5 (high intensity) for each alteration interval logged. As a further filter on the drill core data, only alteration with a intensity rank of 3 or more is used in this study. In the Hellyer database are 365 different combinations of alteration minerals. As this is an unworkable number of mineral assemblages, we have amalgamated the data to form five major alteration assemblage types, based on frequency of occurrence and on importance as determined by the mine experience of Aberfoyle's geologists at Burnie. The major hangingwall alteration assemblages are characterised by the dominant alteration mineral and the associated alteration assemblages. These are

- silica-ablite, silica, silica-ablite-chlorite
- fuchsite, fuchsite-carbonate
- carbonate, carbonate-silica, carbonate-sericite
- chlorite, chlorite-sericite, chlorite-fuchsite
- sericite, sericite-fuchsite

Figures 8 to 10 illustrate the hangingwall alteration zonation based on these five assemblages. In general, there is a zonation (fuchsite→ carbonate-chlorite→ silica-albite) from the middle of the hangingwall alteration zone to the outsides, although there is some asymmetry. Figure 8 is a cross section view, looking north, of the hangingwall alteration and shows that this alteration is best developed directly above the middle and northern portions of the deposit and laterally away from the deposit to the south. Fuchsite-dominated alteration occupies the central portion of the hangingwall alteration. Chlorite and chlorite-carbonate alteration envelops the fuchsite zone with carbonate–rich zones near to the ore deposit and chlorite-rich zones extend above and to the sides of the carbonate. The outermost alteration zone is characterised by silica-ablite alteration, which is best developed to the south and extends laterally away from the deposit for up to 250 m. To the east the silica-albite zone is best developed near the orebody.

A longitudinal view of the hangingwall alteration is given in Figure 9. The fuchsite alteration zone is best developed above the middle and northern portions of the deposit. Outwards from the fuchsite-zone is chlorite-carbonate alteration with carbonate-rich alteration passing outwards to chlorite-rich alteration both north and south. Silica-albite alteration is best developed in the south and extends away from the deposit for 200m. In the north the silica-albite zone lies between the fuchsite and carbonate-rich alteration zones.

Figure 10 is a view of the hangingwall alteration looking down from the surface. The fuchsite zone is best developed above the middle and northern portions of the deposit. To the south there is a distinct zonation from fuchsite to chlorite-carbonate to silica-albite. To the north the alteration is more irregular with carbonate alteration occurring to the west of the deposit, carbonate-chlorite-sericite alteration to the north and silica-albite alteration to the west.

Offler and Whitford (1992) have outlined textural criteria for discriminating between hydrothermal alteration and metamorphic overprinting. Minerals of hydrothermal origin occur in sheaf like, spherulitic, atoll-like, botryoidal, colloform or radiating. They also exhibit primary depositional features, such as growth banding, exhibit non-preferred orientation and pleochroism distinctive from their metamorphic counterparts, are wrapped around by any schistosity present, are euhedral and associated with other minerals lacking a preferred orientation and commonly display a void-filling habit. Minerals of metamorphic origin have a strong preferred orientation, commonly exhibit a fibrous growth habit and occur in extension fractures or pressure shadows and exhibit annealing or dynamic recrystallisation textures. Minerals with a burial metamorphic origin, such as plagioclase altered to white mica and/or carbonates, may be difficult to distinguish from the same minerals formed through hydrothermal processes.

Preservation of hydrothermal alteration textures in the hangingwall basalt is very common, whereas obvious metamorphic textures such as preferred orientation of minerals, fibrous growth habits and dynamic recrystallisation or annealing are uncommon. Common hydrothermal features are spherulites; ellipsoidal or lobate structures sometimes ringed by pyrite; atoll-like structures ringed with fine grained Ti-rich opaques; growth banded mineral aggregates; colloform or botryoidal textures; and euhedral quartz, pyrite. Fresh clinopyroxene was found in some samples, however in other samples, clinopyroxene is replaced by carbonate plus varying

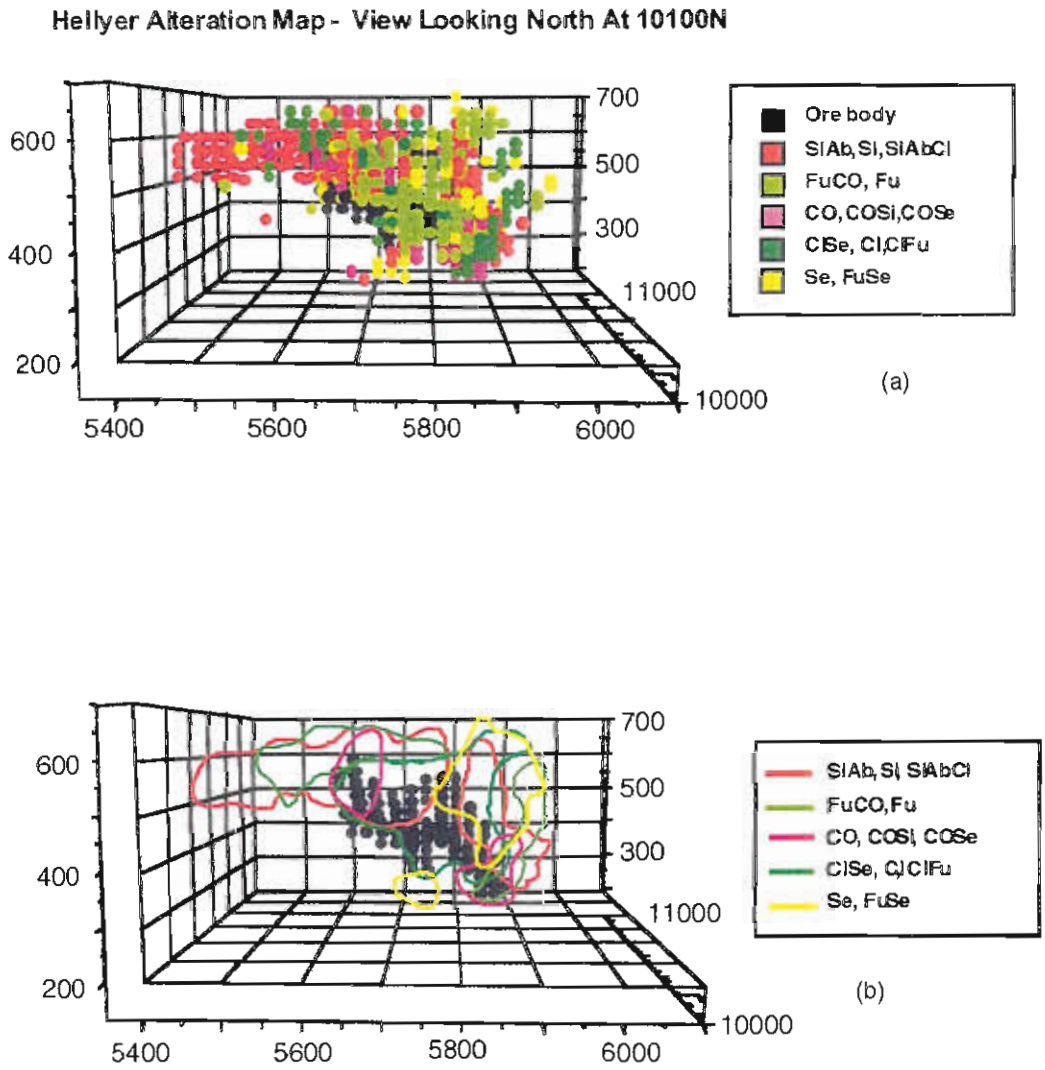

Figure 8 Computer generated cross-section of the hangingwall alteration, view looking north at 101000N. This diagram constructed by taking the hangingwall alteration as logged by the Hellyer geologists, selected holes logged by RF, and combining the various alteration mineralogies into 5 major assemblages, as shown in the legend. A computer program then took the 3D data and divided it into 25m³ blocks for plotting (Fig 8a). Fig. 8b is simplified diagram showing that fuchsite-dominated alteration occupies the central portion of the hangingwall alteration. Chlorite and chlorite-carbonate alteration envelops the fuchsite zone with carbonate–rich zones near to the ore deposit and chlorite-rich zones extend above and to the sides of the carbonate. The outermost alteration zone is characterised by silica-ablite alteration, which is best developed to the south and extends laterally away from the deposit for up to 250m. To the east the silica-albite zone is best developed near the orebody.

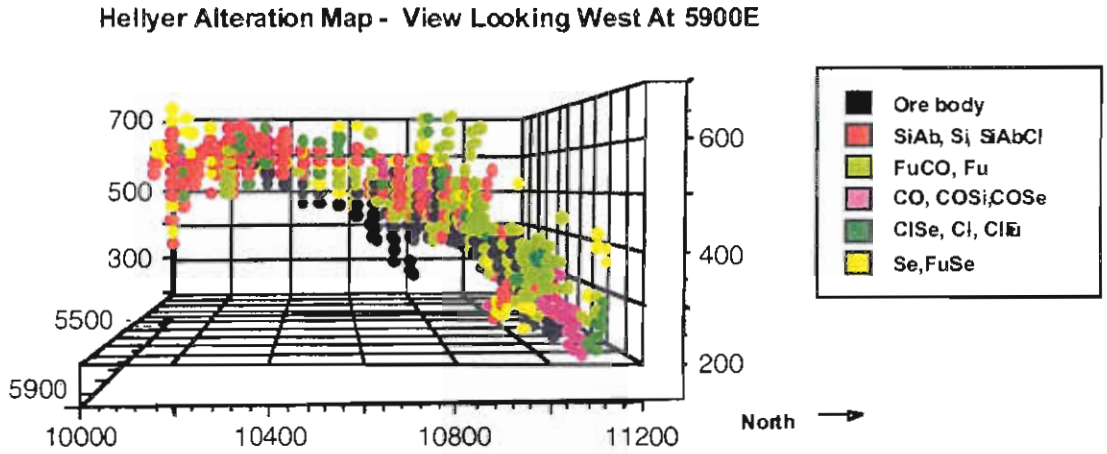

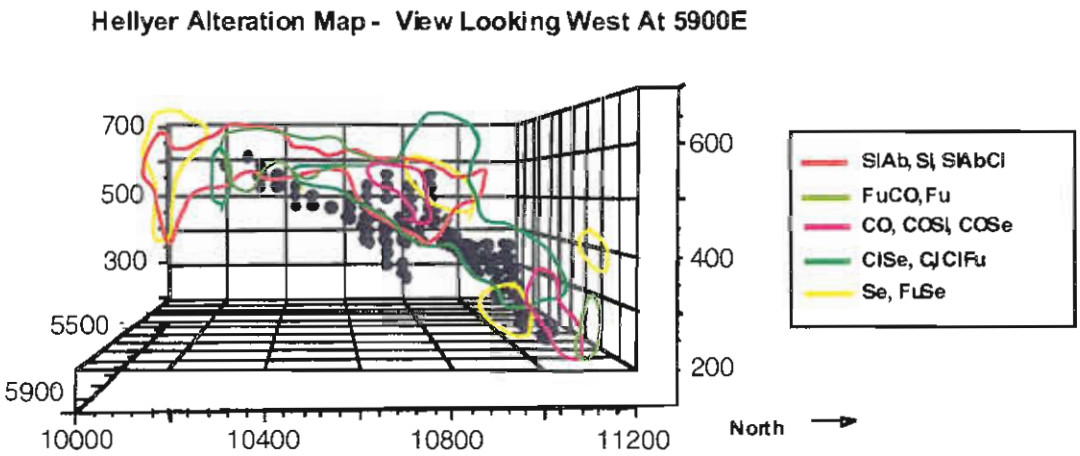

Figure 9a Computer generated longitudinal section of the hangingwall alteration, view looking west at 5900E. This diagram was constructed using the method outlined in Fig 8. Fig. 9b is simplified diagram showing that the fuchsite alteration zone is best developed above the middle and northern portions of the deposit. Outwards from the fuchsite-zone is chlorite-carbonate alteration with carbonate-rich alteration which passes outwards to chlorite-rich alteration both north and south. Silica-albite alteration is best developed in the south and extends away from the deposit for 200m. In the north the silica-albite zone lies between the fuchsite and carbonate-rich alteration zones.

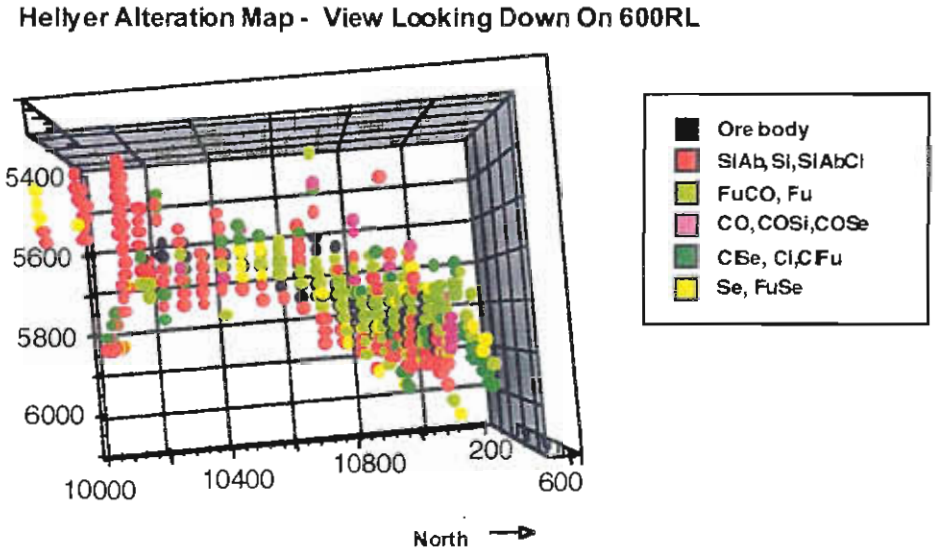

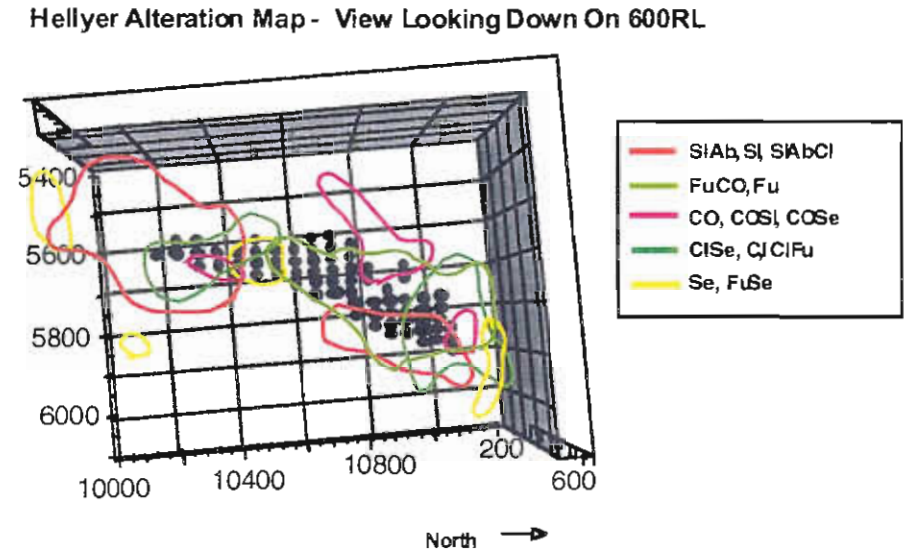

Figure 10a Computer generated view of the hangingwall alteration, looking down form the land surface. This diagram was constructed using the method outlined in Fig 8. Fig. 10b is simplified diagram showing that the fuchsite zone is best developed above the middle and northern portions of the deposit. To the south there is a distinct zonation from fuchsite to chlorite-carbonate to silica-albite. To the north the a is more irregular with carbonate alteration occurring to the west of the deposit, carbonate-chlorite-sericite alteration to the north and silica-albite alteration to the west.

amounts of quartz and/or chlorite. Chlorite occurs in very fine grained intergrowths with varying amounts of quartz, carbonate, white mica and albite; at the centre of ellipsoidal, spheroidal or lobate structures and displaying a radiating habit or rimming these structures when they contain quartz or carbonate; in colloform growth with white mica, quartz and carbonate. Occasionally, chlorite exhibits a preferred orientation and fibrous growth habit. Carbonates occur as irregular aggregates; in spheroidal or ellipsoidal structures rimmed by quartz and/or chlorite, or rimming quartz and/or chlorite; in colloform growths; and in veins. It can display either a sheaflike habit within large spherulites or ellipsoids, or be a optically continuous clear grains up to 10mm. Carbonate occurs in very fine grained intergrowths with varying amounts of chlorite, quartz, white mica and albite. Quartz occurs in very fine grained intergrowths with varying amounts of chlorite, carbonate, white mica and albite; filling small to large ellipsoidal, spheroidal or lobate structures, usually being coarse grained at the centre and finer grained at the rims; as euhedral crystal in carbonate filled amygdules; as irregular aggregates. A minor amount of fibrous quartz in the pressure shadow of pyrite. White mica occurs mostly in very fine grained intergrowths with varying amounts of chlorite, carbonate, quartz and albite Albite is mainly distributed throughout the groundmass, intergrown with other minerals and displaying a very fine grained habit, occasionally coarsening up to small lathes. Pyrite occurs as discrete euhedral crystals; partially or completely rimming spheroidal, ellipsoidal or lobate structures; in veins; finely disseminated.

Halo geochemistry

Footwall

The alteration pipe underlying the Hellyer deposit displays distinct geochemical characteristics (Fig. 11, see next page) (Gemmell and Large, 1992). Compared to unaltered footwall andesite the siliceous core is enriched in SiO_2, K_2O, MnO, Y, Fe_2O_3 and S but depleted Na_2O and CaO. Additions of MgO, MnO, Fe_2O_3, S, and Y and losses of Na_2O and CaO occur in the chlorite zone. In the sericite zone SiO_2, MgO, K_2O, MnO, Fe_2O_3, and S are gained but Na_2O and CaO are depleted. Only Na_2O is depleted while MnO, K_2O, P_2O_5, S, Y, and SiO_2 are gained in the stringer envelope zone (Gemmell and Large, 1992). Investigation of the major and minor element geochemistry of the district wide footwall rocks indicates that Na_2O (Fig. 12) tends to decrease in concentration with distance away (up to 2 km) from the Hellyer alteration pipe (Gemmell, 1990).

Hangingwall

The HVS unit displays some very interesting variations in geochemistry (Fig. 12) even though it is a polymict rock composed of a variety of compositions. The HVS unit has Ti/Zr ratios that vary from 13 to 24, reflecting the dominance of either felsic or intermediate to mafic compositions. From a distance of 2 km away from the deposit the Ti/Zr ratio decreases towards the ore deposit (Fig. 12) with the lowest Ti/Zr ratios occurring in the HVS adjacent to, or covering, the deposit. These data suggest that there is a higher proportion of felsic material, primarily dacite in the HVS near the deposit and a higher proportion of andesite to basalt detritus in the HVS away from the deposit. K_2O, Tl and Sb all decrease in concentration (Fig. 12 b–d) away from the deposit over a distance of 2 km while P_2O_5, CaO and MnO and increase in concentration away from deposit (distance of 2 km) (Fig. 12e–g).

Owing to the various alteration mineral assemblages and intensity of alteration, the variations in lithogeochemistry in the Hellyer basalt are complex with few geochemical vectors. The distinctive and potentially useful geochemical vector in the hangingwall is Sb (Fig. 13). Antimony shows a systematic increase in concentration from values of a few ppm at a distance of 2 km to values over 50 ppm in the basalt overlying the deposit. Antimony also tends to increase in concentration towards the top of the Hellyer basalt in several holes away from the deposit (Fig. 14, see next page).

Jack (1989) determined that the hangingwall calcite-fuchsite alteration had major additions of CaO, CO2, Al_2O_3, K_2O and Ba and major losses in SiO_2, MgO and Fe_2O_3 compared to unaltered Hellyer basalt. The albite alteration has major gains in SiO_2, CaO, CO_2, Na2O, Pb and Zn with major losses in MgO, Fe_2O_3 and Ba compared to unaltered Hellyer basalt.

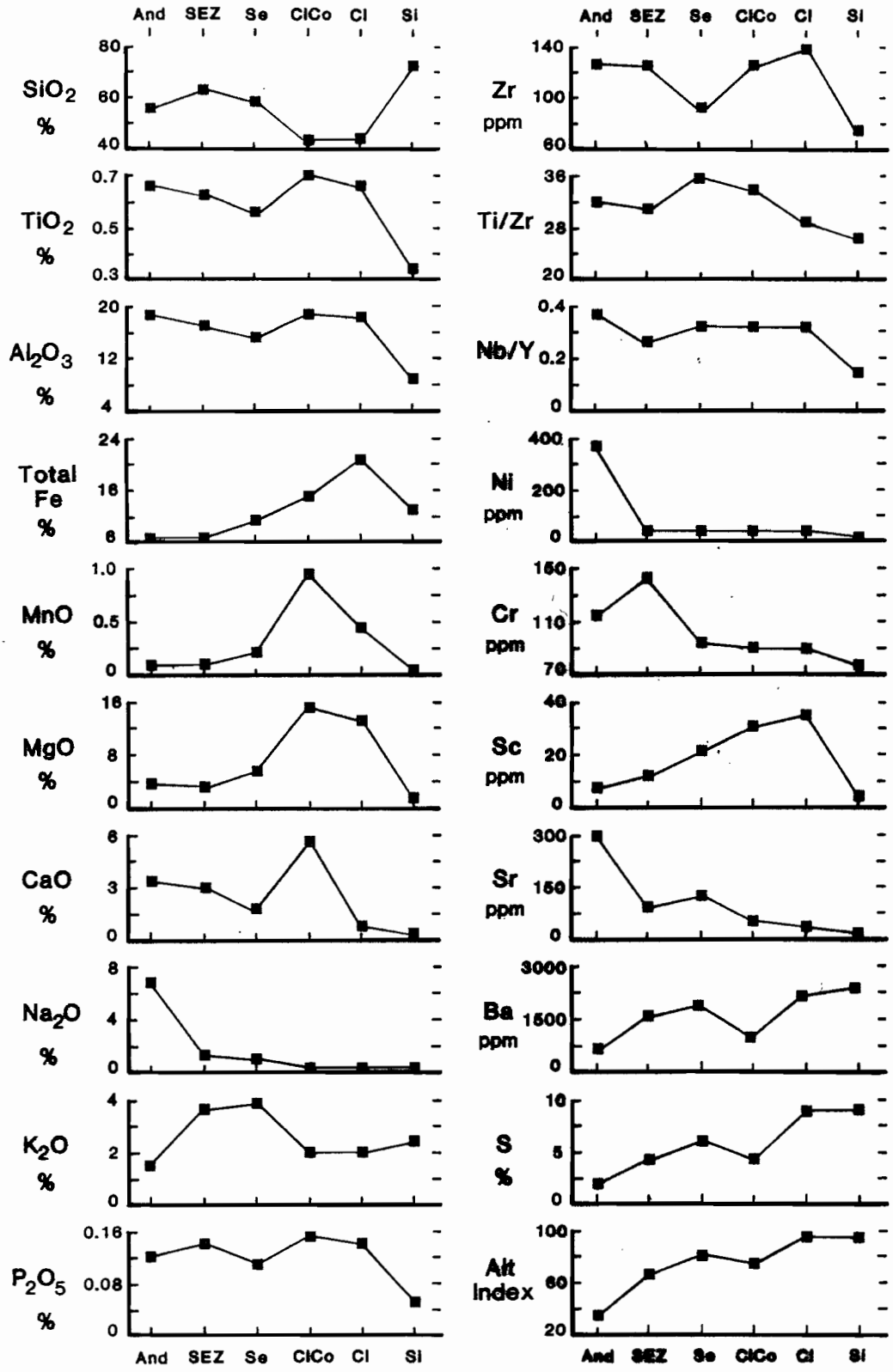

Figure 11 Distribution of major and trace element geochemistry between unaltered footwall andesite and various zones in the footwall alteration pipe. Abbreviations: And - unaltered andesite, SEZ - stringer envelope zone, Si - siliceous core, Se - sericite, Cl - chlorite, Co - carbonate (primarily dolomite). From Gemmell and Large (1992).

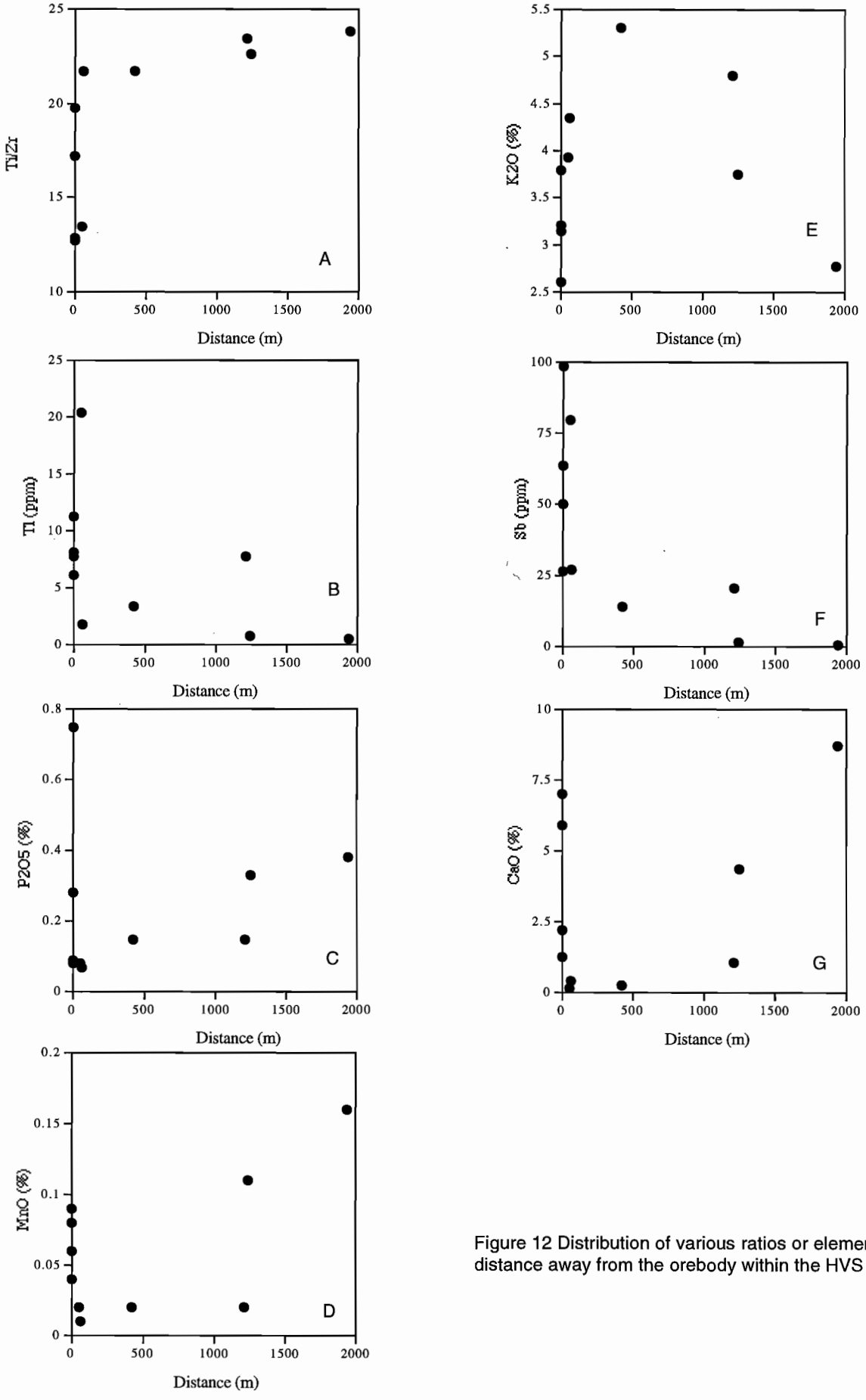

Figure 12 Distribution of various ratios or elements with distance away from the orebody within the HVS unit.

Alteration Indices

A number of alteration indices and element ratios have been tested on the footwall, HVS and Hellyer basalt data sets. The Ishikawa Alteration Index (AI) $100(MgO + K_2O)/(MgO + K_2O + CaO + Na_2O)$ relates to the replacement of plagioclase by sericite and chlorite during hydrothermal alteration. The index was developed for use on felsic volcanic rocks but as the Hellyer footwall data demonstrates it is equally applicable on intermediate to mafic volcanics as well (Gemmell and Large, 1992). The Chlorite-carbonate-pyrite index (CCPI) $100(MgO + FeO)/(MgO + FeO + K_2O + Na_2O)$ measures the degree of chlorite, (Fe, Mg) carbonate and/or pyrite alteration related to VHMS deposits (Large, 1996; Large and Allen, 1997).

Footwall

The AI becomes progressively larger (Figs 9, 15), with increasing intensity of alteration, from the unaltered andesite (AI=36) towards the siliceous core (AI=91) of the footwall alteration pipe (Gemmell and Large, 1992). The CCPI also becomes progressively larger, with increasing intensity of alteration, from the unaltered andesite (AI=59) towards the siliceous core (AI=94) of the footwall alteration pipe.

Analysis of AI and CCPI values in the district wide footwall altered samples indicates that they are not significantly different from the unaltered lithologies (Gemmell, 1990). Overall there does not appear to be a significant regional AI or CCPI alteration signature in the footwall lithologies in the district, over a distance of three km, pointing towards the alteration pipe and deposit.

HVS

Alteration index values vary from 43 to 93 in the HVS unit. There is an interesting relationship between the AI and distance away from Hellyer (Fig. 16). Over a distance of 2 km the AI increases systematically from 55 to 93 towards the ore body. However the HVS right at the orebody has AI values between 75 and 43. This sudden decrease in the AI at the can be explained by the increased CaO (in carbonate) and decrease in K_2O (decrease in sericite content) in the HVS at the ore body. CCPI values vary from 52 to 82 in the HVS but the values are distributed erratically, with no systematic relationship, with distance away from Hellyer.

Hangingwall Basalt

Alteration index values range from 2 to 97 in the altered Hellyer basalt (Fig. 17). Although the highest AI values are found in samples (intense sericite alteration) above the ore position there is no systematic trend of decreasing AI with distance away

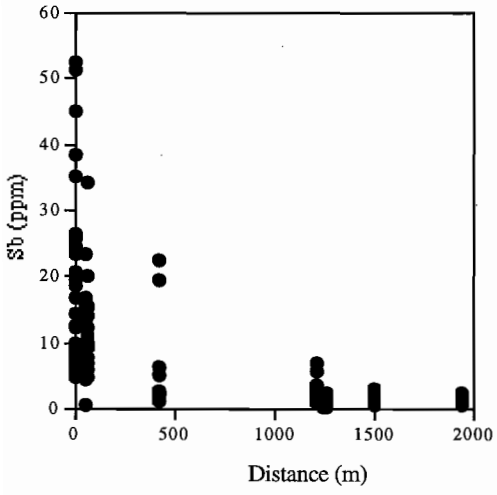

Figure 13 Distribution of Sb with distance away from the orebody within the Hellyer basalt. There is a distinct decrease in Sb concentration from approx. 50 ppm near the deposit to approx. 2 ppm at a distance of 2 km.

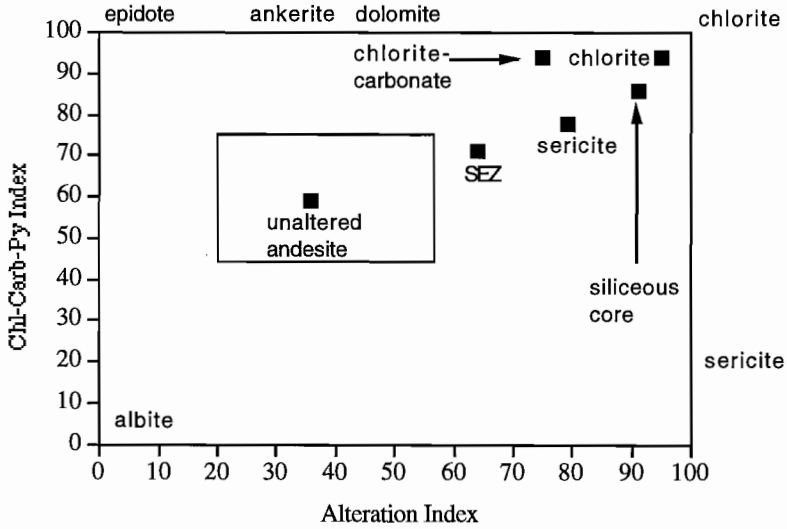

Figure 15 Plot of Alteration Index $[100(MgO + K_2O)/(MgO + K_2O + CaO + Na_2O)]$ vs Chlorite-carbonate-pyrite Index $[100(MgO + FeO)/(MgO + FeO + K_2O + Na_2O)]$ for average analyses from the footwall alteration zones.

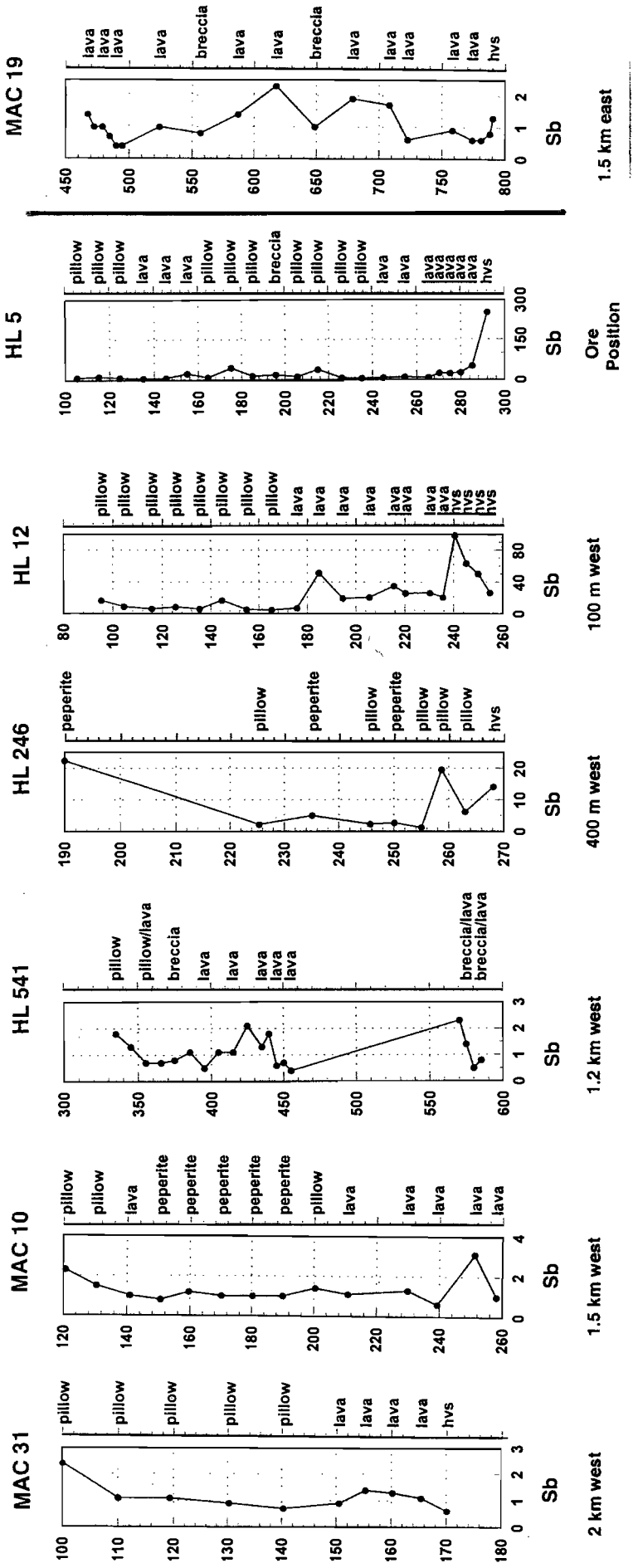

Figure 14 Vertical variation of Sb (ppm) in the Hellyer Basalt and HVS with distance from the Hellyer deposit. Locations of drill holes on Figiurs 1a and 1b. Data from Fulton and Gemmell (1997).

from the deposit. CCPI values vary from 18 to 97. As with the AI, the highest CCPI values (carbonate-chlorite alteration) occur above the deposit and again there is no systematic variation of CCPI with distance away from the deposit.

The AI-CCPI box plot (Fig. 17a) indicates that the majority of hangingwall alteration samples analysed lie within the field of unaltered Hellyer basalt as determined by Stanley and Gemmell (1997). The altered samples that lie within the unaltered box are weakly altered samples from all the various hangingwall alteration assemblages. The remaining samples are more intensely altered samples that plot toward the end-member alteration minerals species that characterise the various alteration (Fig. 17b). Interestingly, the samples that plot towards the chlorite corner are samples identified as sericite or silica-ablite alteration and not chlorite alteration. However the samples that plot near sericite are intensely sericitised samples. None of the fuchsite altered samples plots towards the sericite field. The most intensely silica-albite altered samples plot towards the albite corner. Samples described as carbonate-or carbonate-chlorite plot towards the calcite axis (same as AI=0) with a few samples plotting towards the ankerite-dolomite points.

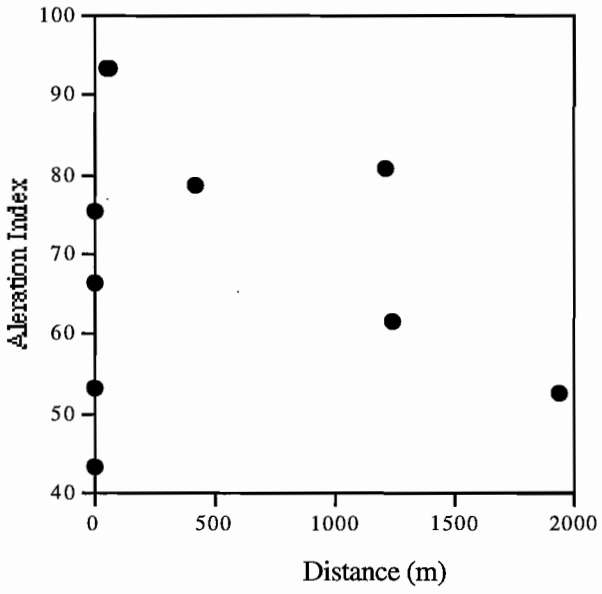

Figure 16 Distribution of the Alteration Index [100(MgO + K2O)/(MgO + K2O + CaO + Na2O)] with distance away from the orebody within the HVS unit. The AI increases towards the orebody and then decreases suddenly in value at the orebody position.

Alteration Mineral Chemistry

Mineral analyses were carried out on a CAMECA SX50 electron microprobe by wavelength dispersive methods using an accelerating voltage of 15kV and beam currents of 20nA for clinopyroxenes, 15nA for feldspars and 10nA for chlorites, micas and carbonates. The structural formulae were calculated on the basis of 28 oxygens for chlorite, 22 oxygens for white micas, 8 oxygens for feldspars and 6 oxygens for clinopyroxenes.

Footwall

Chlorite: Urabe et al. (1983) determined that the Fe/(Fe+Mg) ratio of chlorite is a useful parameter for quantifying hydrothermal alteration associated with volcanic-hosted massive sulfide deposits. The Fe/(Fe+Mg) ratio in chlorites usually increases with distance from the core of the alteration pipe . However, the opposite relationship (decrease in chlorite Fe/(Fe+Mg) with distance from the alteration core) has also been documented. Jack (1989) determined that chlorites in the footwall alteration zone are Mg-rich, (Fe/(Fe+Mg) = 0.14–0.28), while chlorites in the footwall andesites outside the stringer zone were Fe-rich, (Fe/(Fe+Mg) = 0.44–0.46).

White mica: Pima investigations of the footwall (Yang et al., 1997) showed that the higher wavelengths of AlOH in the white micas, corresponding to increased Fe and Mg content, were observed wityhin the footwall alteration pipe compared to the surrounding rocks.

Hangingwall

Chlorite: The majority of chlorites analysed (Fig. 18a) have similar chemistries and are classified as ferro-clinochores (Bayliss, 1975). The chlorites from outside the haningwall alteration plume (Hl 14) are remarkably similar with Mg/Mg + Fe values ranging from ≈63 to 70. Chlorites from within the fuchsite-carbonate plume (Hl 28) have a greater range of Mg/Mg + Fe values, from ≈42 to 81. The low Mg/Mg + Fe chlorites form a distinctive group and are from the most intensely fuchsite-carbonate altered core sample in drill hole HL28, immediately above the ore body. These low Mg/Mg + Fe chlorites are magnesio-chamosites, previously identified as Fe-

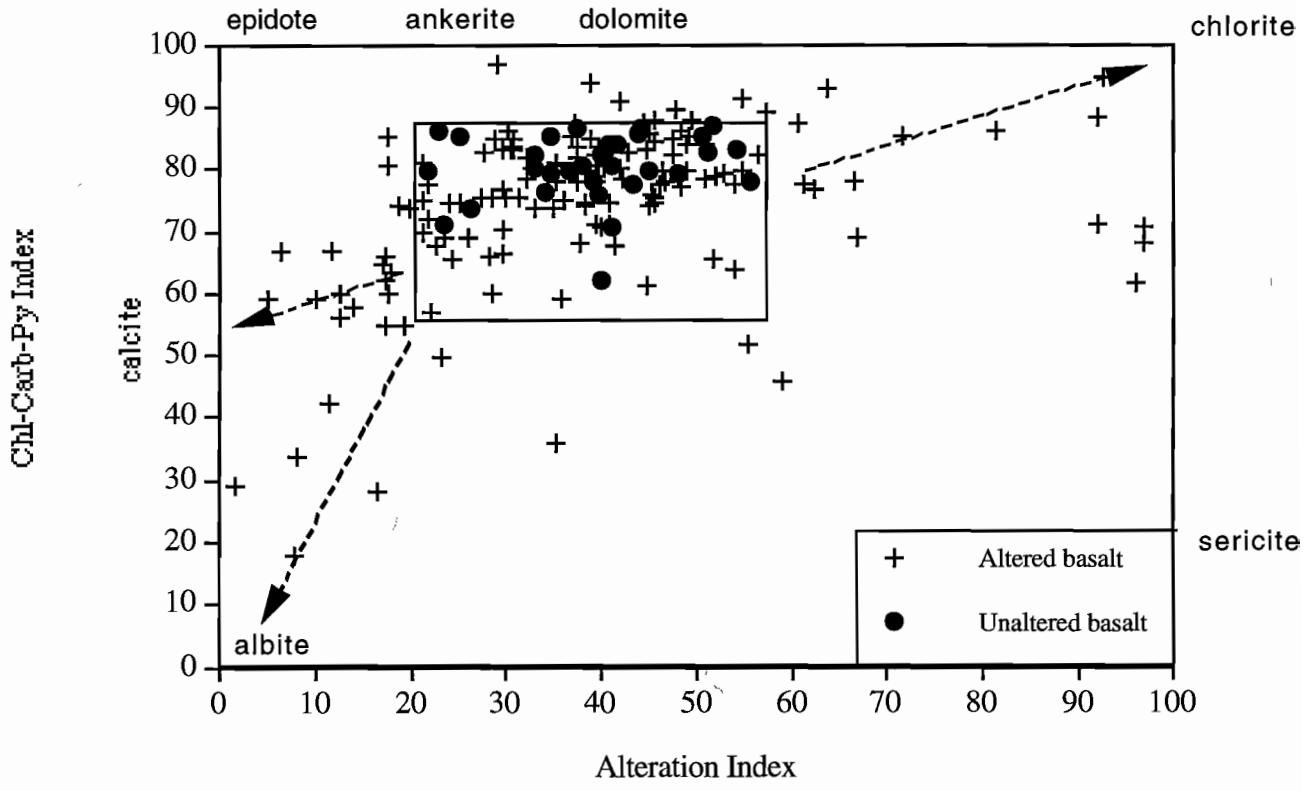

Figure 17a Plot of Alteration Index [100(MgO + K2O)/(MgO + K2O + CaO + Na2O)] vs Chlorite-carbonate-pyrite Index [100(MgO + FeO)/(MgO + FeO+ K2O + Na2O)] for the unaltered and altered Hellyer basalt samples. The unaltered box is based on samples from Stanley and Gemmell (1997).

chlorites. Figure 18b indicates that, overall, there to be no particular relationship between the Fe:Mg ratio in chlorite and proximity to the deposit. A down hole comparison of chlorite chemistry was made in HL5 (Fig. 18c) and although chlorites with the lowest mg# are closest to the orebody no systematic variation uphole was observed.

A small group of chlorites have lower Al and higher Mg/Mg + Fe and also contain significant amounts of Cr, up to 1.91 wt % Cr_2O_3. The chlorites from an intensely fuchsite-carbonate altered sample had a maximum of only 0.11 wt % Cr_2O_3. The chromium content of chlorites is significant and is higher than the chromium contents of the white micas. There is no relationship between chromium content and distance from the deposit, with high Cr-bearing chlorites occurring both above (HL5) and distal (MAC10) to the deposit (Fig. 18d), although the highest Cr values are from chlorites within the hangingwall alteration plume.

White micas: Good analyses of white micas (sericite and "fuchsite") have proved difficult to obtain due to their fine grained nature. Many analyses have been rejected due to impurities from accidental inclusion of the edges of neighbouring minerals. White mica analyses from an intensely fuchsite-carbonate altered sample in HL28, show there is very little Cr enrichment. The nomenclature of chrome micas is not entirely clear - the term fuchsite is defined as a chromian muscovite containing more than 1 wt % Cr_2O_3 (Deer et al., 1962), and having a Si to tetrahedral Al ratio of 6:2, whilst the term mariposite has been used for Cr bearing micas which have a ratio of Si to tetrahedral Al of 7:1 and may have lower Cr contents (Heinrich, 1965). Bailey (1984) suggested that varietal names such as fuchsite and mariposite be abandoned in favour of the use of adjectival modifiers with ideal end members, e.g. chromian muscovite for fuchsite and chromian phengite for mariposite. However, the term fuchsite

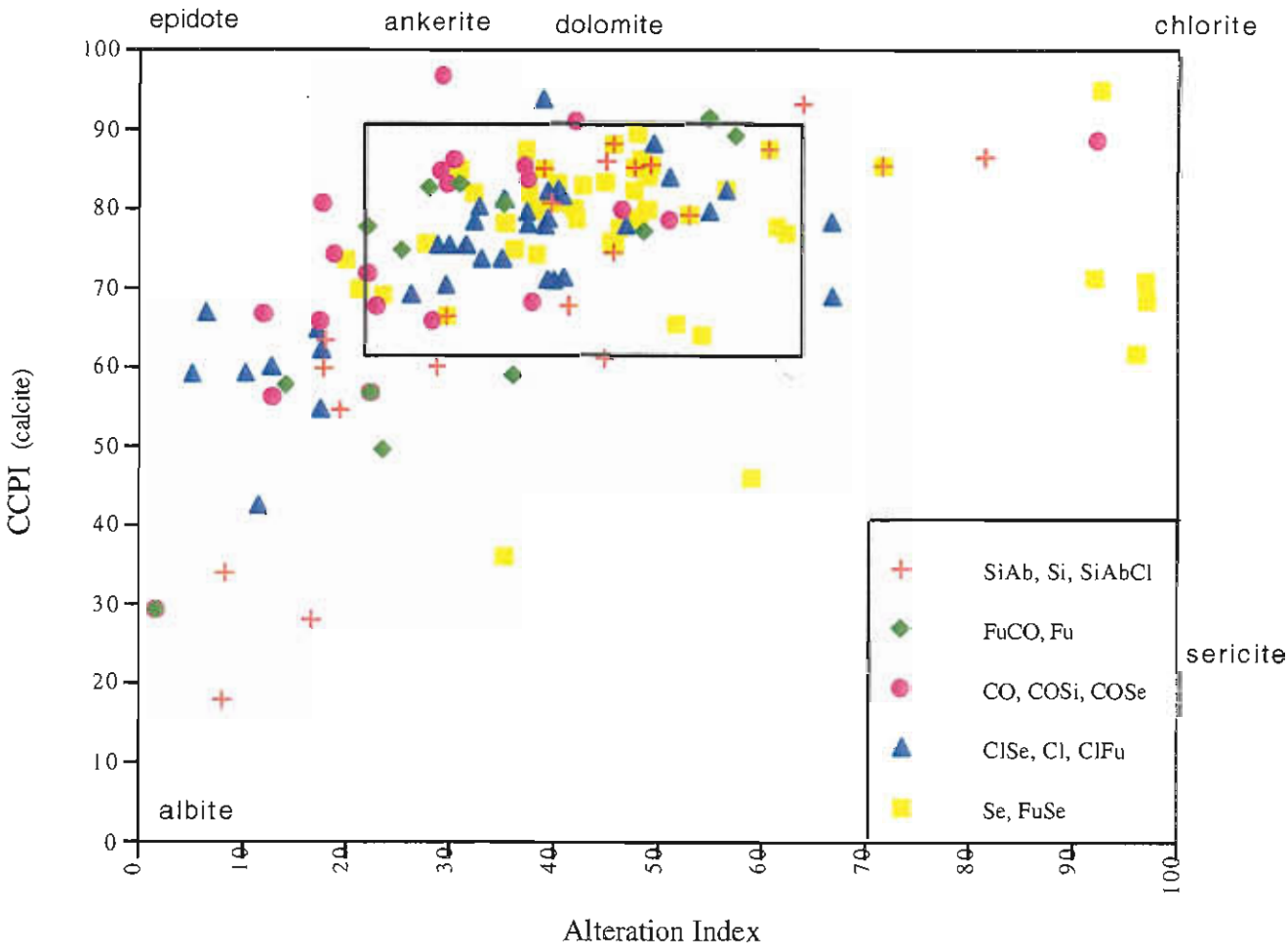

Figure 17b Similar plot to Fig 17a that highlights the various alteration types and where they plot in relation to end member alteration minerals. Most altered samples fall within the unaltered box. Samples that plot towards the chlorite corner are samples identified as sericite or silica-ablite alteration and not chlorite alteration. However the samples that plot near sericite are intensely sericitised samples. None of the tuchsite altered samples plots towards the sericite field. The most intensely silica-albite altered samples plot towards the albite corner. Samples described as carbonate-or carbonate-chlorite plot towards the calcite axis (same as AI=0) with a few samples plotting towards ankerite-dolomite. Black box is tield of unaltered basalt from Fig. 17a.

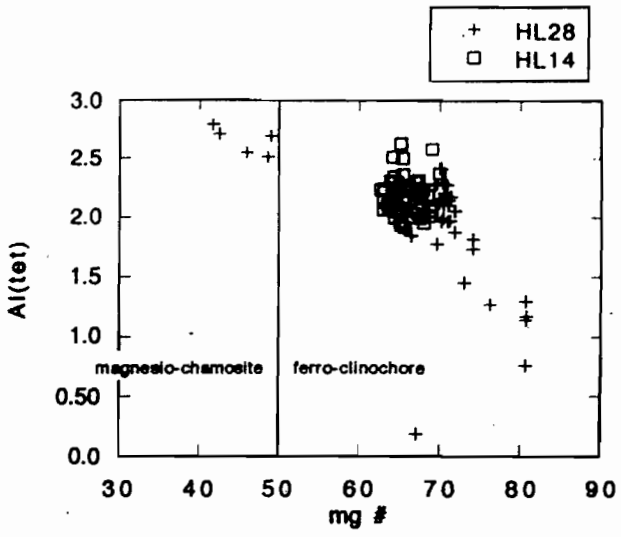

Figure 18a Composition of chlorites in terms of tetrahedral Al and mg# (Mg/Mg+Fe) for drill hole HL 28 (within the hangingwall alteration plume) and HL 14 (400 to the west of the alteration plume).

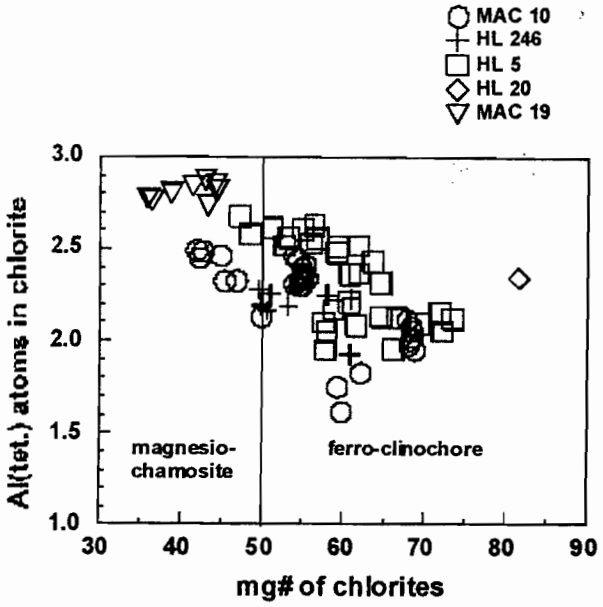

Figure 18b Composition of chlorites in terms of tetrahedral Al and mg# (Mg/Mg+Fe) for drill holes HL 5 and 20 (within the hangingwall alteration plume) and HL 246 (400 to the northwest of the alteration plume), MAC 10 (approx. 1.5 km to the west) and MAC 19 (approx. 1.5 km to the east).

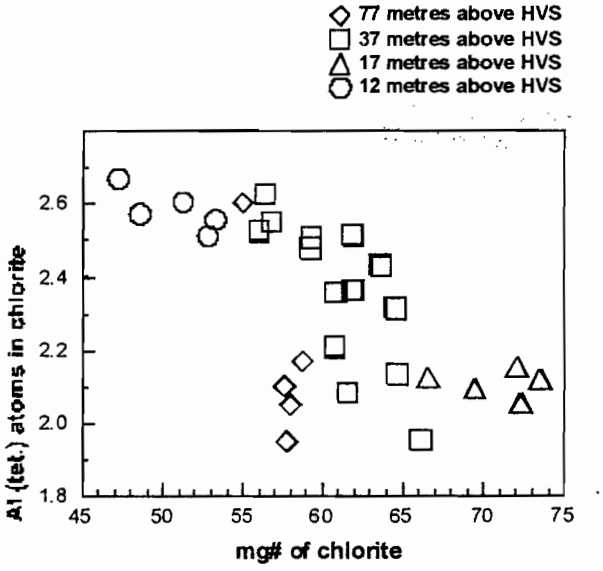

Figure 18c Composition of chlorites in terms of tetrahedral Al and mg# for drill hole HL 5, within the hangingwall alteration plume.

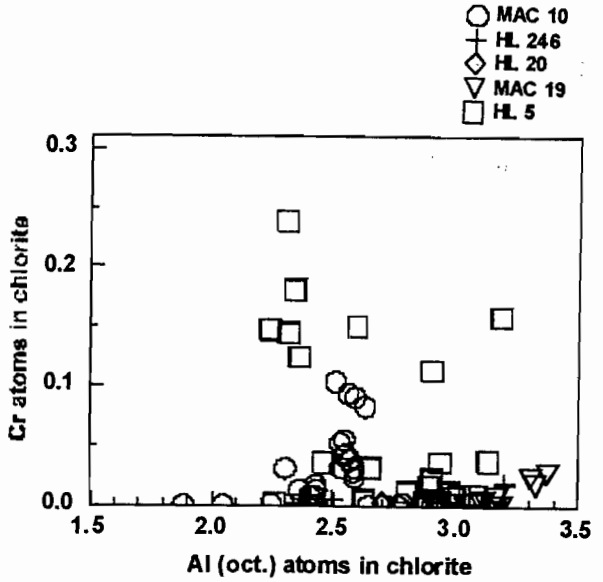

Figure 18d Composition of chlorites in terms of octahedral Al and Cr atoms for drill holes HL 5 and 20 (within the hangingwall alteration plume) and HL 246 (400 to the northwest of the alteration plume), MAC 10 (approx. 1.5 km to the west) and MAC 19 (approx. 1.5 km to the east).

is well established in the Mt Read Volcanics for "bright green mica" and so use of that name will be made here as per the definition of Deer et al. (1962). On that basis, of all the analyses only one is true fuchsite, (1.11 wt % Cr_2O_3), and this was a mica which was immediately adjacent to a large euhedral chromite. Micas not adjacent to chromites had a range of 0.00 to 0.30 wt % Cr_2O_3. Other workers have recorded high Cr content in white micas at Hellyer (Jack, 1989), and at Que River (Offler and Whitford, 1992). Jack (1989) analysed several white micas from the intensely fuchsite-carbonate alteration plume and recorded up to 1.0 wt % Cr_2O_3, and used the term fuchsite to indicate mica that is light-chrome green macroscopically. It seems unlikely that the source of Cr in the white micas and chlorites is from chromites except where the micas or chlorites are immediately adjacent, and even then the source may be disseminated chromite. At Hellyer, a more likely source is probably the breakdown of Cr-rich clinopyroxene. Clinopyroxenes in the Hellyer basalt have a high Cr_2O_3 content, up to 1.3 wt % Cr_2O_3, and have been completely replaced by carbonate ± quartz in the samples where high Cr content chlorites occur.

Microprobe analyses have indicated that there is not as much white mica in the hangingwall basalt as indicated from core logging. Low K in whole rock geochemical analyses and absence of AlOH peak in PIMA spectra for many samples confirms this suggestion. Although it is therefore difficult to make meaningful comparisons of white mica chemistry down holes and between holes, the following observations can be made:

- relatively low Cr content in white mica from rocks which visually appear to be strongly fuchsite altered. Maximum Cr_2O_3 content analysed was 0.28%.
- majority of white micas analysed were phengitic (Si:Al of 3:1 with Fe, Mg substitution for Al). No relationship between amount of phengite and distance from ore deposit.
- up to 1.20% BaO in white micas Ba content of micas decreases with distance away from the orebody (Fig. 19a).
- Fe + Mg content vs Al in the octahedral site in white mica has a limited range near the orebody but erratic values away from the deposit (Fig. 19b)
- white micas in MAC19 indictae a mixing trend with paragonite (Na-rich white mica)

Carbonates

The carbonates analysed in the Hellyer hangingwall alteration are calcites, ferroan dolomites and ankerites (Fig. 20a, b). The dolomites and ankerites containing the greatest amounts of Mg and Fe are found further within the zone of intense fuchsite-carbonate alteration (Fig. 20a), and carry up to ≈6 wt % $MnCO_3$. Petrographically these carbonates are "dirty" in appearance, but give good analysis totals. Most of the carbonates outside the hangingwall alteration plume are calcites (Fig. 20a) with the exception of some small veins which have up to ≈4.5 wt % $MnCO_3$ and one ankeritic vein.

Figure 20b shows the distribution of hangingwall carbonate chemistry away from orebody. The composition of hydrothermal carbonates shows a systematic change of increasing Mn at roughly similar Fe+Mg (although Mg >Fe) as the orebody is approached.

Isotope halos

Sulphur isotopes

Distinct $\delta^{34}S$ variations exist between vein stages within the stringer and stringer envelope zones of the footwall alteration pipe Gemmell and Large, 1992; 1993). The main base-metal rich stage 2B veins display lower sulfur isotope values (3.8–8.9‰, mean = 6.9‰) than the earlier stage 2A veins (5.7–11.1‰, mean = 9.9‰). $\delta^{34}S$ values for stage 2A veins in the stringer envelope zone are significantly higher $\delta^{34}S$ values (11.9–40.7‰, mean = 25.0 ‰) than those from the stringer zone. Variations in $\delta^{34}S$ can be explained by a model where the hydrothermal fluid initially consists of totally to partially reduced seawater sulfate that evolves into a fluid dominated by igneous sulfur (ore-forming fluid) as the convection system intensified and penetrated deeper into the footwall. At the end of the hydrothermal system's life sulfate becomes more abundant in the fluid, and eventually dominant.

Oxygen isotopes

Forty whole-rock oxygen isotope analyses were preformed on the variably altered andesites and rhyolites collected as part of the district wide footwall alteration study (Gemmell, 1990). The intense pervasive alteration of the alteration pipe has $\delta^{18}O$

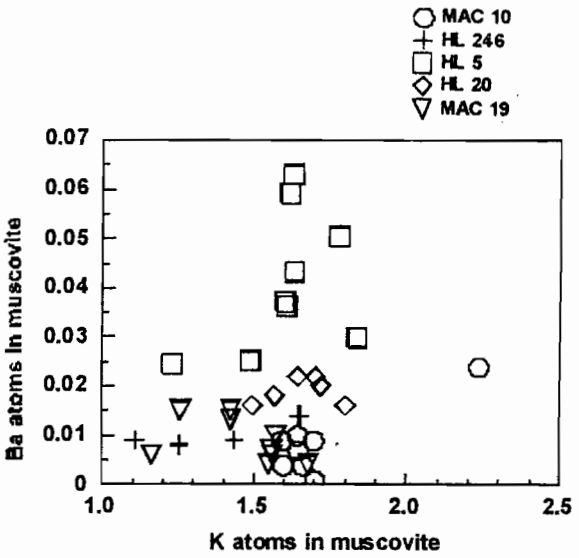

Figure 19a Composition of white micas in terms of K atoms and Ba atoms for drill holes HL 5 and 20 (within the hangingwall alteration plume) and HL 246 (400 to the northwest of the alteration plume), MAC 10 (approx. 1.5 km to the west) and MAC 19 (approx. 1.5 km to the east).

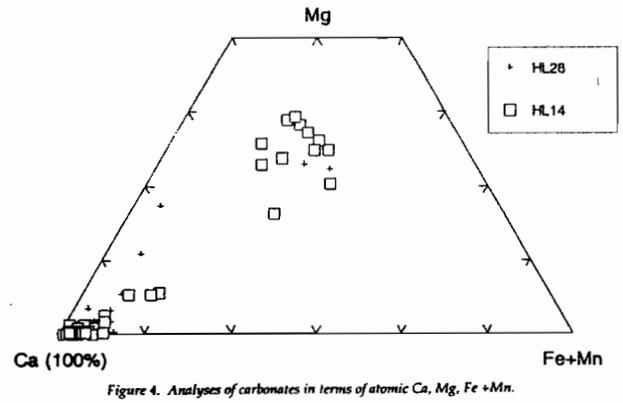

Figure 4. Analyses of carbonates in terms of atomic Ca, Mg, Fe +Mn.

Figure 20a Composition of carbonates for drill holes HL 28 (within the hangingwall alteration plume) and HL 14 (400 to the west of the alteration plume).

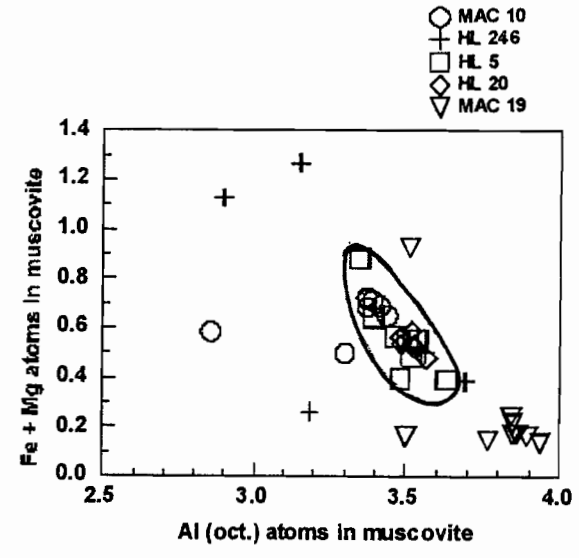

Figure 19b Composition of chlorites in terms of octahedral Al and Fe + Mg atoms for drill holes HL 5 and 20 (within the hangingwall alteration plume) and HL 246 (400 to the northwest of the alteration plume), MAC 10 (approx. 1.5 km to the west) and MAC 19 (approx. 1.5 km to the east).

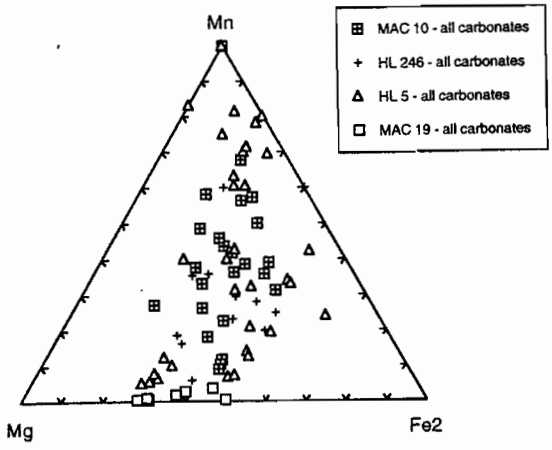

Figure 20b Composition of carbonates for drill holes HL 5 and 20 (within the hangingwall alteration plume) and HL 246 (400 to the northwest of the alteration plume), MAC 10 (approx. 1.5 km to the west) and MAC 19 (approx. 1.5 km to the east).

values of between 6 and 8‰. Oxygen isotope values are between 10 and 11‰ within a kilometre of the pipe and increase to values between 12 and 14‰ at a distance of 2–3 km away.

Whole rock oxygen isotope data for altered and unaltered Hellyer basalt samples have been reported by Green and Taheri (1992). They note that there is a distinction between samples from the fuchsite alteration zone ($\delta^{18}O$ = 9–12‰) and unaltered basalt away from the deposit ($\delta^{18}O$ = 10–14‰).

Lithogeochemical halo model and vectors to ore

A lithogeochemical halo model, which includes vectors to ore, is shown in Figure 21. This model includes geochemical vectors for the district-wide footwall lithologies, the alteration pipe, the Hangingwall Volcaniclastic Sequence (HVS), the Hellyer Basalt and Que River Shale.

Important exploration vectors are:

District-wide Footwall:

- decrease in Cu, Zn and As away from alteration pipe
- increase in whole rock $\delta^{18}O$ values from 6-8 (within pipe) to 10-11‰ (within 1 km) to 12-14‰ at a distance of 2-3 km away

Footwall Alteration Pipe:

- distinct mineralogical zonation (from core to rim: quartz →chlorite(± carbonate) →sericite →quartz-sericite)
- decrease in AI, Ba, S, Ca, Fe, Cu, Pb and Zn from interior to edge of pipe
- increase in Na_2O, Ni, Cr, Sr, Al and $\delta^{34}S$ in stringer veins from interior to edge of pipe

Hangingwall Volcaniclastic Sequence (HVS)

- decrease in AI, K_2O, Tl and Sb away from deposit (distance of 2 km)
- increase in P_2O_5, CaO and MnO away from deposit (distance of 2 km)

Hellyer Basalt

- basalt overlying deposit (Core Lava) has Ti/Zr ≈ 55, basalt above and away from deposit (to a distance of 3 km) have Ti/Zr between 20 and 40
- alteration zonation (outwards from deposit: fuchsite→carbonate-chlorite→silica-ablite)
- Ba in muscovite increases towards the deposit
- Mn in carbonate increases towards the deposit
- decrease in Sb away from deposit (to a distance of 3 km)
- increase in whole rock $\delta^{18}O$ values from 9–12 (within hangingwall alteration) to 10–14‰ in unaltered basalts away from the deposit

Que River Shale (QRS)

- no visible alteration
- increase in SiO_2, Ba and pyrite in QRS overlying hangingwall alteration
- decrease in FeO, MgO and CaO in QRS overlying hangingwall alteration
- zone of increased Pb, Zn, Fe, Ni, V, As and Sb lies approx. 50 m vertically into QRS (source and significance of this metal enrichment is unknown)

References

Bailey, S.W. 1984. Classification and structures of the micas. In Bailey, S.W. (ed): Reviews in mineralogy 13. Mineralogical Society of America.

Bayliss, P. 1975. Nomenclature of the trioctahedral chlorites. Canadian Mineralogist 13:178-180.

Bradley, A., 1997, The Geology and genesis of the chlorite-carbonate alteration in the footwall of the Hellyer Volcanic-hosted massive sulphide (VHMS) deposit, unpub. Honours thesis, University of Tasmania, 101 p.

Corbett, K.D., 1992. Stratigraphic-volcanic setting of massive sulfide deposits in the Cambrian Mount Read Volcanics, Tasmania. Economic Geology 87: 564-586.

Crawford, A.J., Corbett, K.D., and Everard, J.L. 1992. Geochemistry of the Cambrian volcanic-hosted massive sulfide-rich Mount Read Volcanics. Economic Geology 87: 597-619.

Deer, W.A., Howie, R.A. and Zussman, J. 1962. Rock forming minerals 3: sheet silicates. Longmans: 371pp.

Drown, C.G. and Downs, R.C., 1990, Deformational style and strain partitioning at the Hellyer volcanogenic massive sulphide deposit: Geol. Soc. Australia, Spec. Pub. No. 25, p. 176-177.

Gemmell, J.B., 1990, Hellyer Stringer Zone Project: Progress Report No. 3, Aberfoyle Resources Ltd. (Australia), 76 p.

Gemmell, J.B. and Large, R.R., 1992, Stringer system and alteration zones underlying the Hellyer volcanogenic massive sulphide deposit, Tasmania, Australia, Economic Geology, V. 87, No. 3, p. 620-649.

Gemmell, J.B. and Large, R.R., 1993, Evolution of a VHMS hydrothermal system, Hellyer deposit, Tasmania, Australia: sulphur isotope evidence, Resource Geology, No. 17, p. 108-119.

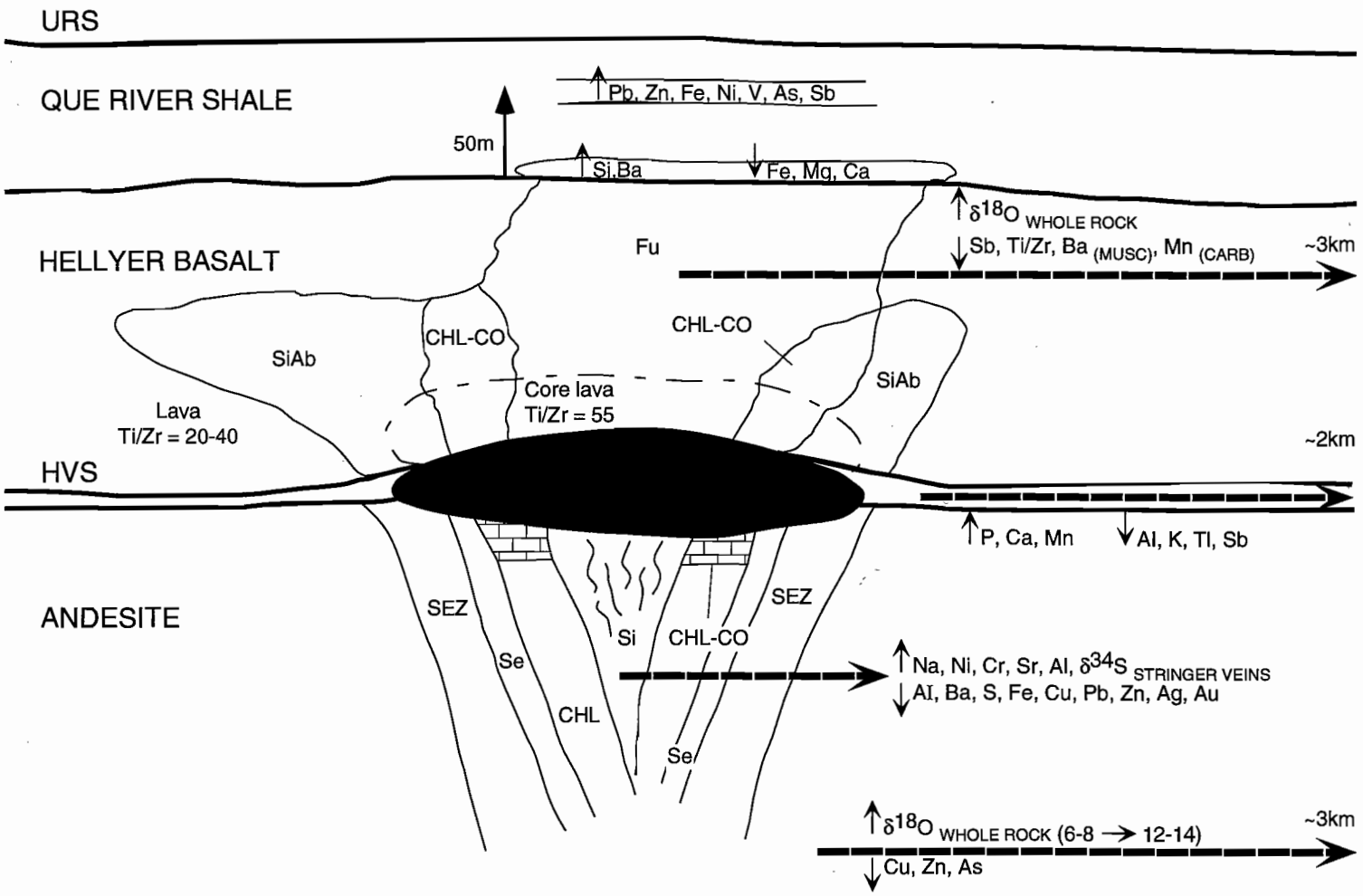

Figure 21 Schematic model of the lithogeochemical halo model and vectors to ore for the footwall alteration pipe, footwall lithologies within the district, Hangingwall Volcaniclastic Sequence (HVS), Hellyer Basalt and Que River Shale. Data from Gemmell (1990), Gemmell and Large (1992; 1993), Jack (1989), Sinclair (1994), Green and Taheri (1992) and this study.

Green, G.R. and Taheri, J., 1992, Stable isotopes and geochemistry as exploration indicators, Tasmanian Geological Survey Bulletin 70, p. 84-91.

Heinrich, E.W. 1965. Further information on the geology of chromian muscovites. American Mineralogist. 50: 758-765.

Jack, D.J., 1989. Hellyer Host Rock Alteration. Unpubl. MSc thesis, University of Tasmania: 182 pp.

McArthur, G.J., 1986, The Hellyer massive sulphide deposit, in Large R.R. (ed.) The Mount Read Volcanics and associated ore deposits, Geol. Soc. Aus., Tasmania Division, p. 11-19.

McArthur, G.J., 1996. Textural evolution of the Hellyer massive sulphide deposit. Unpubl. PhD thesis, University of Tasmania: 272 pp. and 2 appendix volumes.

McLeod, R.L. and Stanton, R.L. 1984. Phyllosilicates and associated minerals in some Palaeozoic stratiform sulfide deposits of southeastern Australia. Economic Geology 79: 1-22.

Offler, R. and Whitford, D.J. 1992. Wall-rock alteration and metamorphism of a volcanic-hosted massive sulfide deposit at Que River, Tasmania: petrology and mineralogy. Economic Geology 87: 686-705.

Sinclair, B.J., 1994, Geology and geochemistry of the Que River Shale, western Tasmania, unpub. Honours thesis, University of Tasmania, 114 pp.

Urabe, T., Scott, S.D., and Hattori, K., 1983, A comparison of footwall-rock interaction and geothermal systems beneath some Japanese and Canadian volcanogenic massive sulphide deposits: in Ohmoto, H. and Skinner, B.J., eds., The Kuroko and Related Volcanogenic Massive Sulfide Deposits, Econ. Geol., Monograph 5, p. 345-364.

Waters, J.C. and Wallace, D.B., 1992. Volcanology and sedimentology of the host succession to the Hellyer and Que River volcanic-hosted massive sulfide deposits, western Tasmania. Economic Geology 87: 650-666.

Yang, K, Hunnington, J.F., Gemmell, J.B. and Fulton, R., 1997, PIMA-II spectral analysis of hydrothermal alteration associated with the Hellyer VHMS deposit: new results, AMIRA Project P439, Report 5, p. 175-192.

Sample No. **Average andesite sample**
Location Hellyer

Alteration zone Outside footwall zones
Formation Que - Hellyer Volcanics

Description Plagioclase-phyric andesite lava. Minor sericitisation of plagioclase phenocrysts, groundmass consists of minor chlorite, sericite and carbonate after glass, plagioclase and pyroxene.

Facies Interp Massive and fragmental (autobrecciated, quench fragmented, hyaloclastic) andesite lavas

Alteration Intensity (none) weak moderate strong intense PY < 1%
Alteration Style patchy pervasive veined cleavage control
Alteration Mineralogy Groundmass chlorite, sericite and carbonate
Feldspars minor sericite
Mafics minor chlorite
Interpretation diagenetic metamorphic syntectonic hydrothermal
Relict Mineralogy plagioclase, pyroxene

Geochemistry

SiO_2	TiO_2	Al_2O_3	Fe_2O_3	MnO	MgO	CaO	Na_2O	K_2O	P_2O_5	S	LOI	Al	CCPI	Ti/Zr
56.94	0.67	18.66	7.97	0.09	3.95	3.27	6.72	1.61	0.12	1.92	3.96	36	59	32

Rb	Ba	Cu	Pb	Zn	Sb	Tl	Zr	Nb	Y	Sr
68	744	1700	62	1433			125	7	19	299

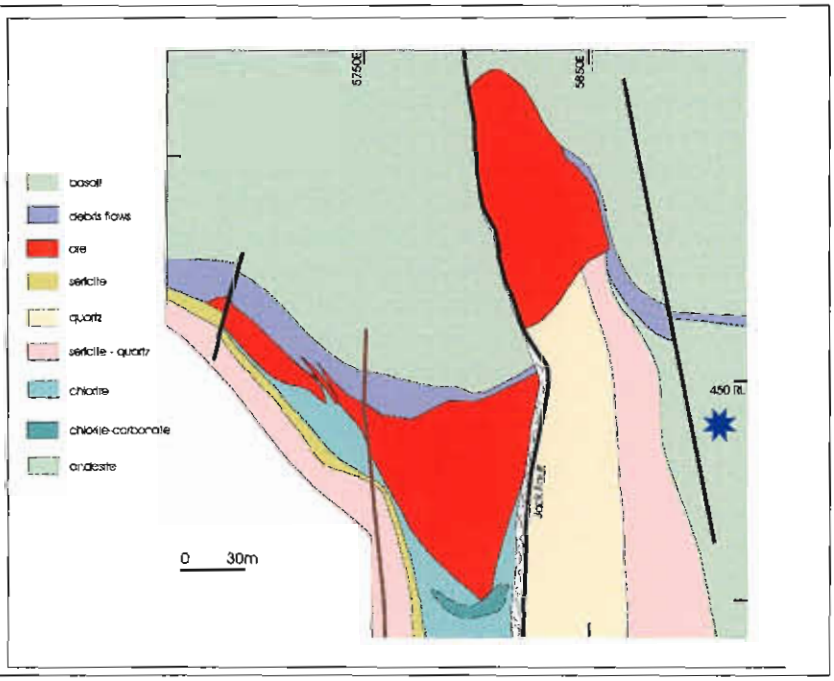

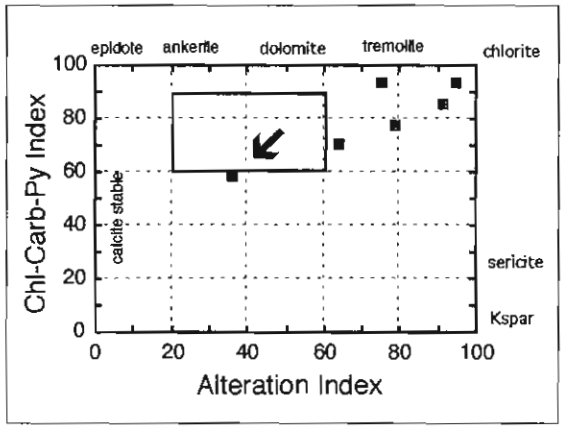

Sample No. Average sample
Location Hellyer

Alteration zone Footwall, Stringer envelope zone
Formation Que - Hellyer Volcanics

Description Low intensity sericite quartz, and minor carbonate alteration. This style of alteration does not destroy the original textures of the host rocks

Facies Interp Polymict debris flow.

Alteration Intensity none (weak) moderate strong intense PY 8%
Alteration Style patchy (pervasive) veined cleavage control
Alteration Mineralogy Groundmass sericite, quartz, pyrite, carbonate
Feldspars sericitised
Mafics sericitised
Interpretation diagenetic metamorphic syntectonic (hydrothermal)
Relict Mineralogy quartz phenocrysts and siliceous rock fragments

Geochemistry

SiO_2	TiO_2	Al_2O_3	Fe_2O_3	MnO	MgO	CaO	Na_2O	K_2O	P_2O_5	S	LOI	Al	CCPI	Ti/Zr
62.29	0.63	16.64	8.42	0.11	3.81	2.94	1.40	3.63	0.14	4.15	7.89	64	71	31

Rb	Ba	Cu	Pb	Zn	Sb	Tl	Zr	Nb	Y	Sr
127	97	1587	312	4523	1697		123	7	26	97

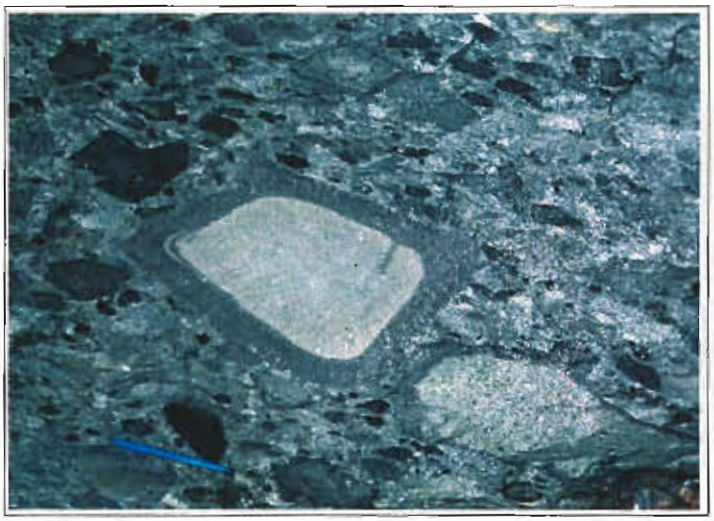

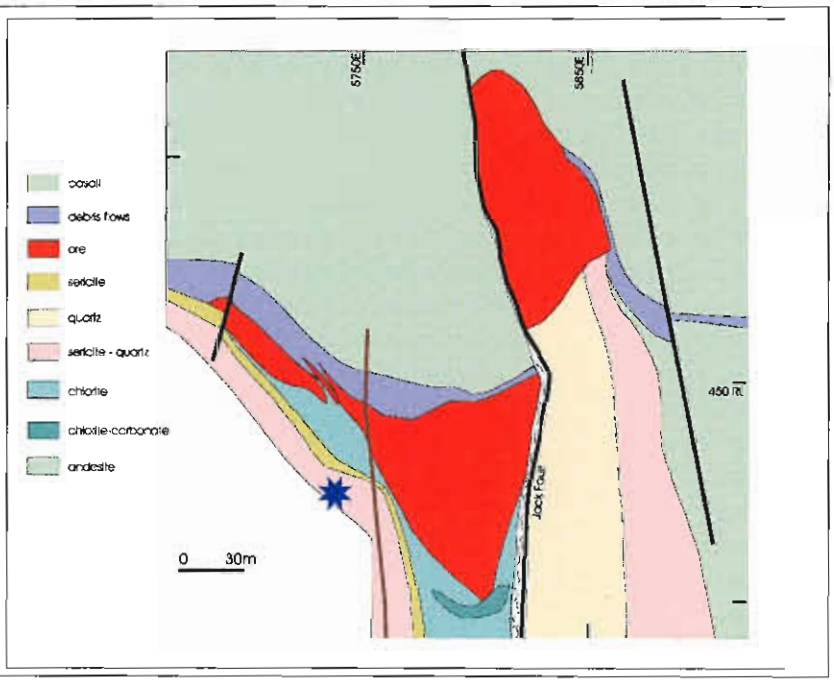

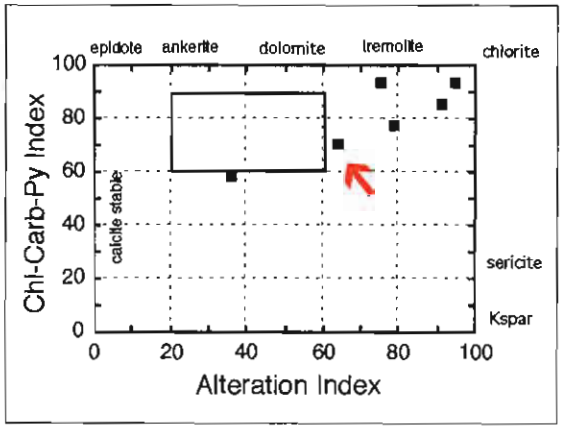

Sample No.	**Average sample**
Location	Hellyer
Alteration zone	Footwall, chlorite-carbonate zone
Formation	Que - Hellyer Volcanics

Description	Abundant dolomite crystals (0.1–5 mm) set in a matrix of chlorite with disseminated pyrite
Facies Interp	Andesite lava

Alteration Intensity	none	weak	moderate	strong	(intense)	PY	10%
Alteration Style	patchy	(pervasive)	veined		cleavage control		
Alteration Mineralogy	Groundmass	chlorite, carbonate, pyrite					
	Feldspars	destroyed					
	Mafics	destroyed					
Interpretation	diagenetic	metamorphic	syntectonic	(hydrothermal)			
Relict Mineralogy	ghosts of plagioclase phenocrysts						

Geochemistry

SiO_2	TiO_2	Al_2O_3	Fe_2O_3	MnO	MgO	CaO	Na_2O	K_2O	P_2O_5	S	LOI	Al	CCPI	Ti/Zr
41.23	0.71	18.47	15.24	0.94	15.45	5.75	0.01	2.04	0.15	4.13	15.40	75	94	34

Rb	Ba	Cu	Pb	Zn	Sb	Tl	Zr	Nb	Y	Sr
66	1074	67	257	526			124	9	28	58

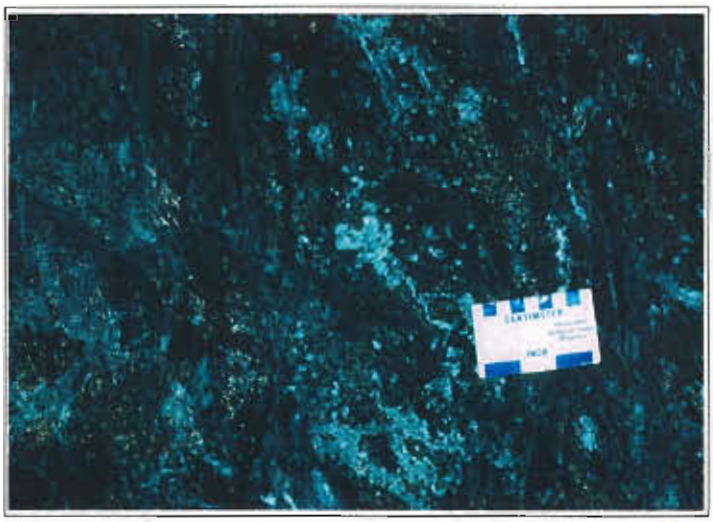

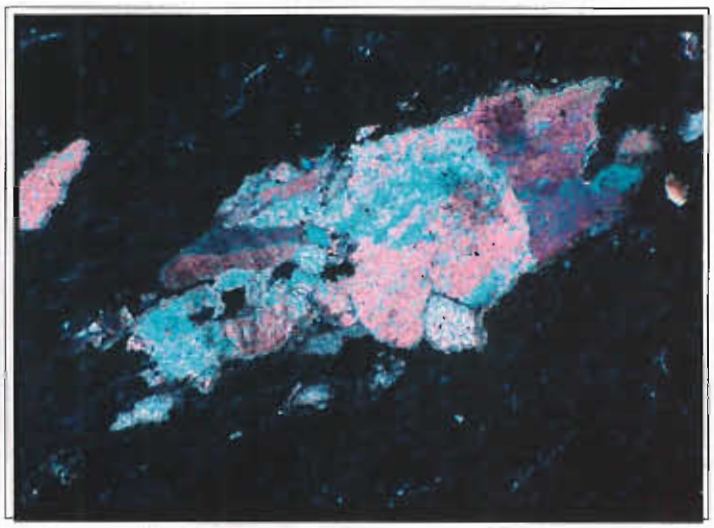

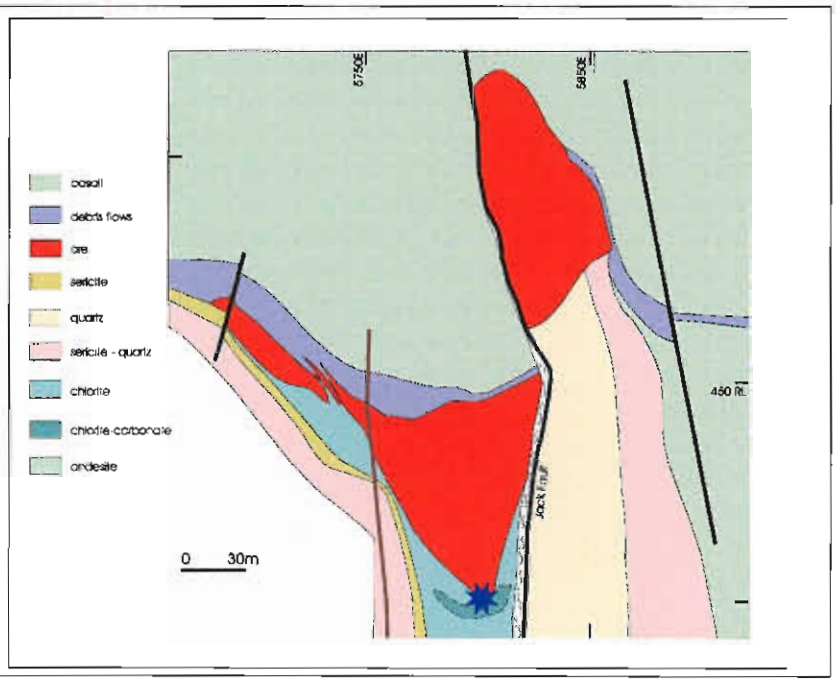

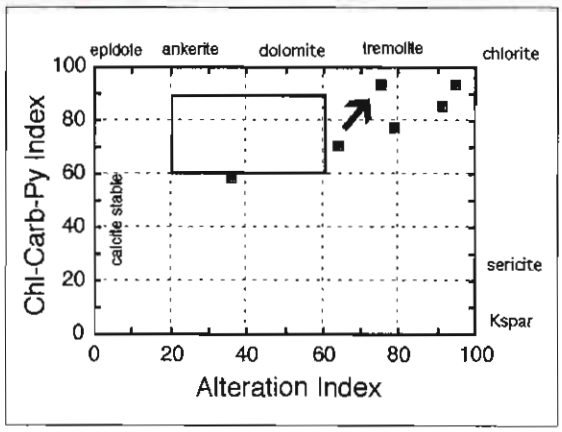

Sample No. Average sample
Location Hellyer

Alteration zone Footwall, Sericite zone
Formation Que - Hellyer Volcanics

Description Fine-grained sericite (up to 70%) and disseminated pyrite with minor chlorite and carbonate

Facies Interp andesite lava

Alteration Intensity	none	weak	moderate	strong	(intense)	PY	8%
Alteration Style	patchy	(pervasive)	veined		cleavage control		
Alteration Mineralogy	Groundmass	sericite, pyrite, chlorite, carbonate					
	Feldspars	destroyed					
	Mafics	destroyed					
Interpretation	diagenetic	metamorphic	syntectonic	(hydrothermal)			
Relict Mineralogy	pseudomorphs of feldspar phenocrysts or rock fragments observed						

Geochemistry

SiO_2	TiO_2	Al_2O_3	Fe_2O_3	MnO	MgO	CaO	Na_2O	K_2O	P_2O_5	S	LOI	Al	CCPI	Ti/Zr
59.31	0.57	15.79	11.90	0.23	5.62	1.60	0.98	3.90	0.11	6.02	8.22	79	78	36

Rb	Ba	Cu	Pb	Zn	Sb	Tl	Zr	Nb	Y	Sr
117	1986	119	392	500			123	7	26	121

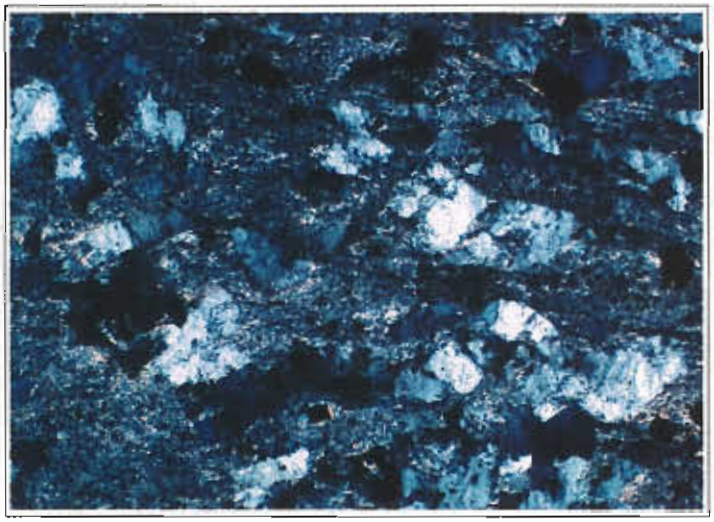

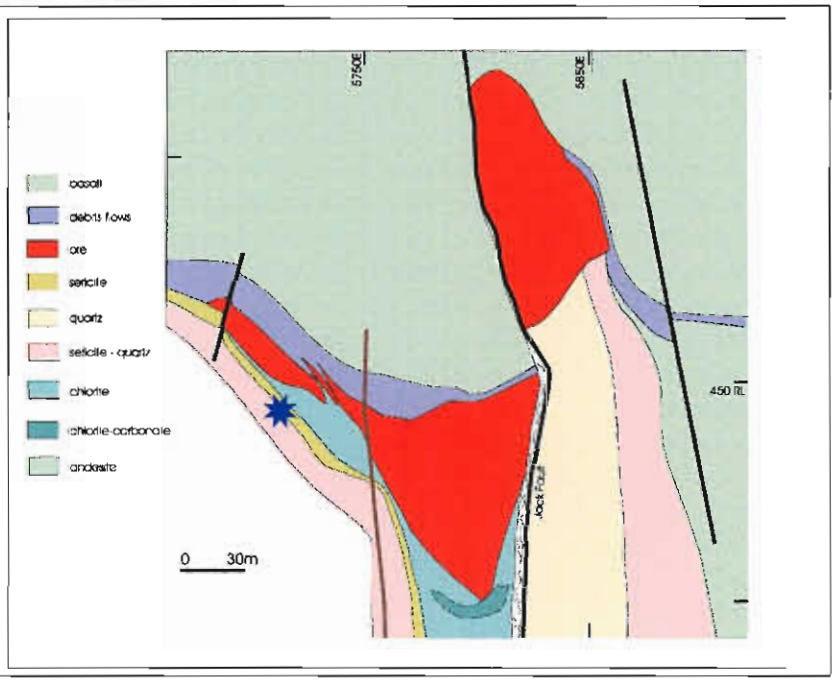

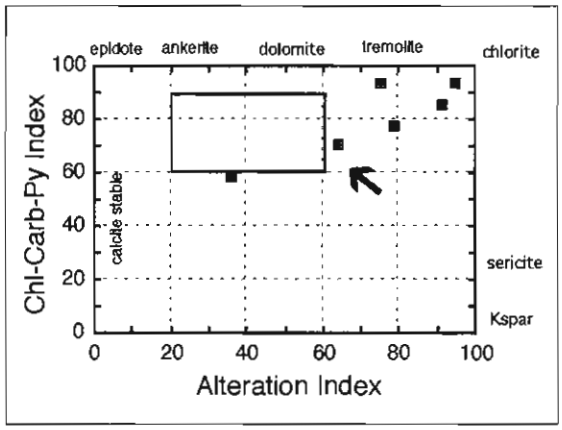

Sample No. Average sample
Location Hellyer

Alteration zone Footwall, Siliceous Core
Formation Que - Hellyer Volcanics

Description Intense quartz-pyrite and quartz-sericite-pyrite±chlorite alteration obliterates all original lithologies

Facies Interp

Alteration Intensity	none	weak	moderate	strong	(intense)	PY	10%
Alteration Style	patchy	(pervasive)	veined		cleavage control		
Alteration Mineralogy	Groundmass	quartz, sericite, chlorite, pyrite					
	Feldspars	destroyed					
	Mafics	destroyed					
Interpretation	diagenetic	metamorphic		syntectonic	(hydrothermal)		
Relict Mineralogy	none						

Geochemistry

SiO_2	TiO_2	Al_2O_3	Fe_2O_3	MnO	MgO	CaO	Na_2O	K_2O	P_2O_5	S	LOI	Al	CCPI	Ti/Zr
73.08	0.33	8.81	13.37	0.08	1.54	0.35	0.03	2.35	0.05	8.87	7.74	91	86	27

Rb	Ba	Cu	Pb	Zn	Sb	Tl	Zr	Nb	Y	Sr
79	2429	308	3892	2948			74	4	28	15

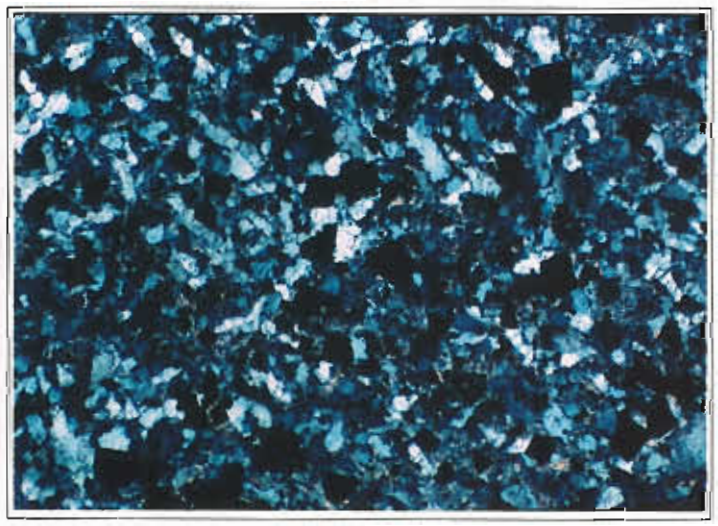

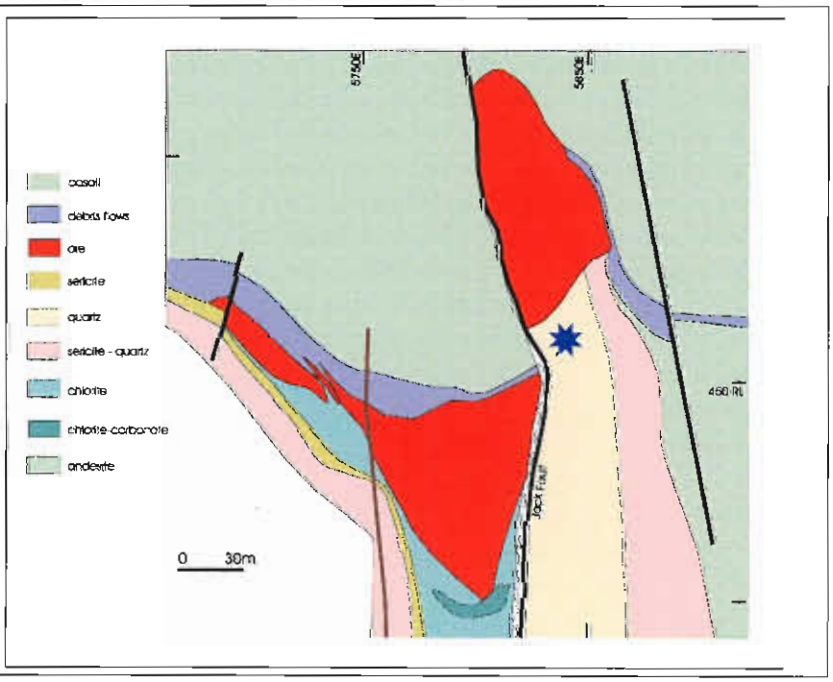

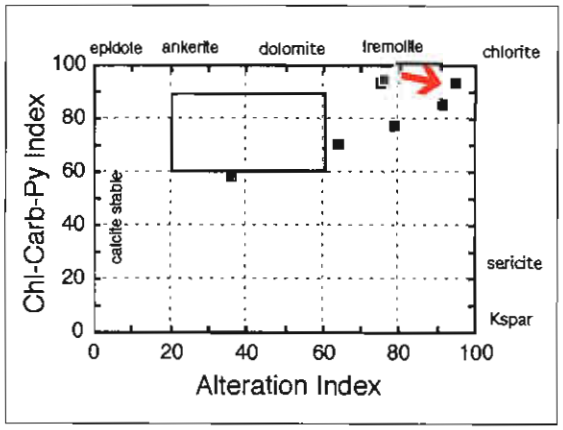

Sample No. Average sample
Location Hellyer
Alteration zone Footwall, Chlorite zone
Formation Que - Hellyer Volcanics

Description Massive, very fine-grained chlorite makes up more than 50% by volume of the rock, and occurs with fine-grained disseminated pyrite and minor sericite, quartz, and carbonate.
Facies Interp andesite lava

Alteration Intensity	none	weak	moderate	strong	(intense)	PY	15%
Alteration Style	patchy	(pervasive)	veined		cleavage control		
Alteration Mineralogy	Groundmass	chlorite, pyrite					
	Feldspars	destroyed					
	Mafics	destroyed					
Interpretation	diagenetic	metamorphic	syntectonic	(hydrothermal)			
Relict Mineralogy	pseudomorphs of feldspar phenocrysts or rock fragments observed						

Geochemistry

SiO_2	TiO_2	Al_2O_3	Fe_2O_3	MnO	MgO	CaO	Na_2O	K_2O	P_2O_5	S	LOI	Al	CCPI	Ti/Zr
42.97	0.67	18.33	21.50	0.47	12.97	0.73	0.14	2.07	0.14	8.65	12.29	95	84	29

Rb	Ba	Cu	Pb	Zn	Sb	Tl	Zr	Nb	Y	Sr
79	2235	1116	139	39			140	8	25	39

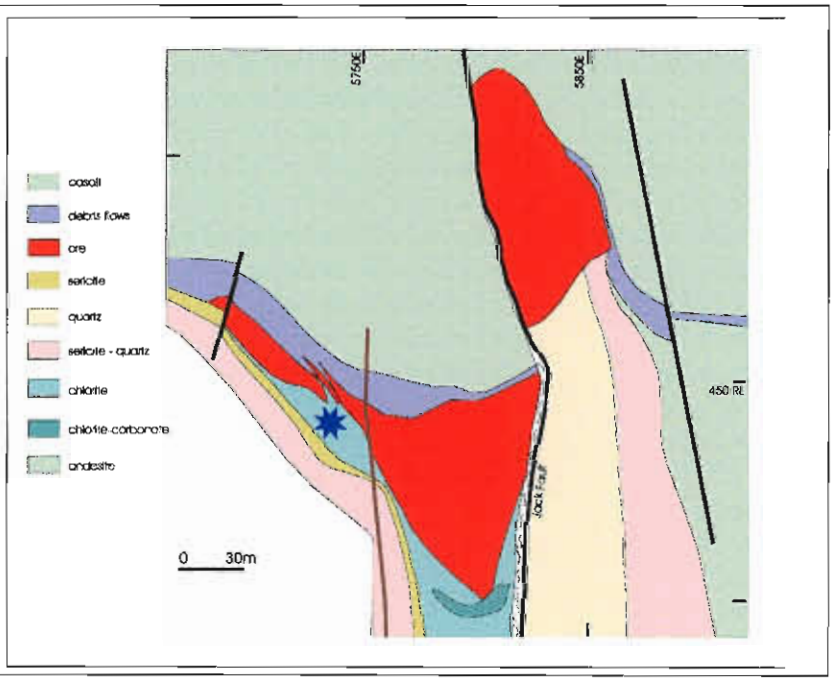

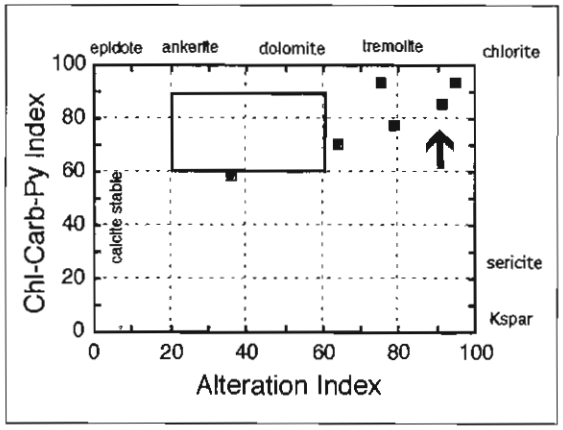

Hellyer Hangingwall Alteration

Sample No.	**628453**
Location	Hellyer
Alteration zone	Silica-albite
Formation	Hellyer Basalt Mt Read Volcanics, Central Volcanic Complex

Description	Strongly silica-albite altered, clinopyroxene-phyric basalt.
Facies Interp	Pillowed basaltic lava.

Alteration Intensity	none	weak	moderate	(strong)	intense	Py 1%
Alteration Style	patchy	(pervasive)	veined		cleavage control	
Alteration Mineralogy	Groundmass	silica-albite				
	Feldspars	silica-albite				
	Mafics	silica±chlorite±carbonate				
Interpretation	diagenetic	metamorphic	syntectonic	(hydrothermal)		
Relict Mineralogy	none					

Geochemistry

SiO_2	TiO_2	Al_2O_3	Fe_2O_3	MnO	MgO	CaO	Na_2O	K_2O	P_2O_5	S	LOI	AI	CCPI	Ti/Zr
73.65	0.25	13.83	1.29	0.01	0.41	1.20	7.02	0.29	0.08	0.71	1.78	8	18	11.5

Rb	Ba	Cu	Pb	Zn	Sb	Tl	Zr	Nb	Y	Sr
9	311	40	9	24	20	0.5	131	9	21	586

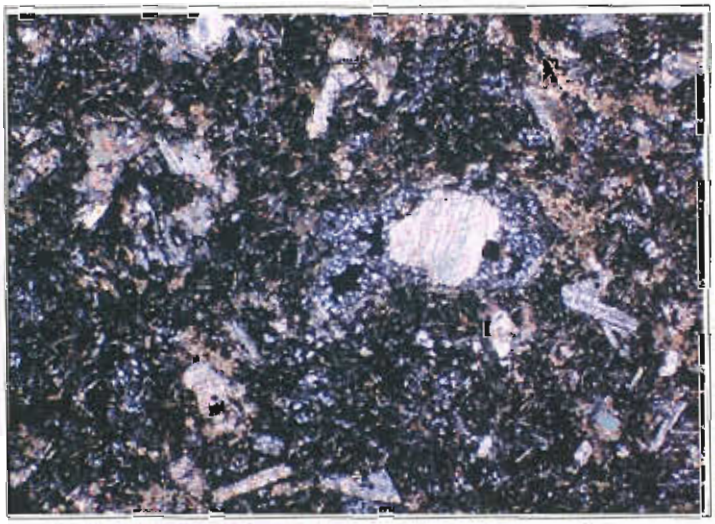

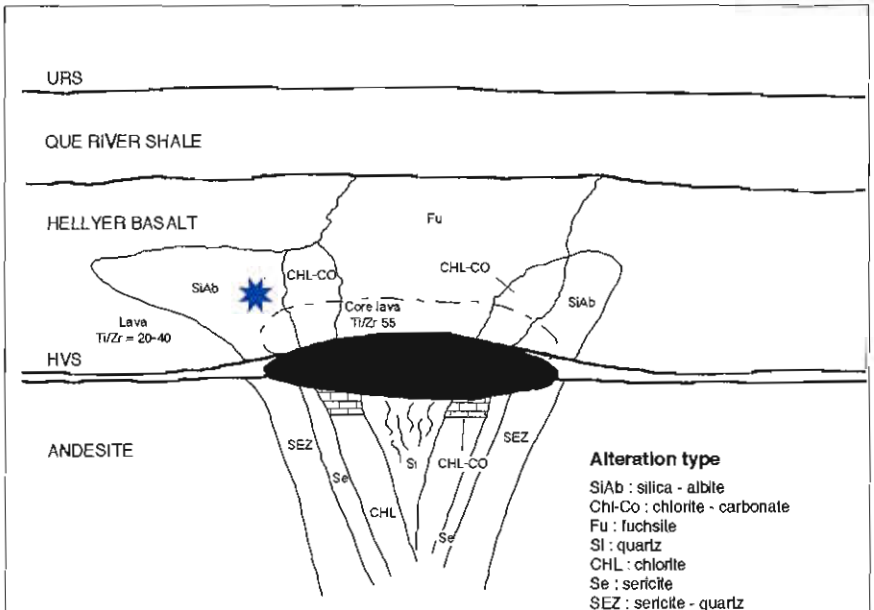

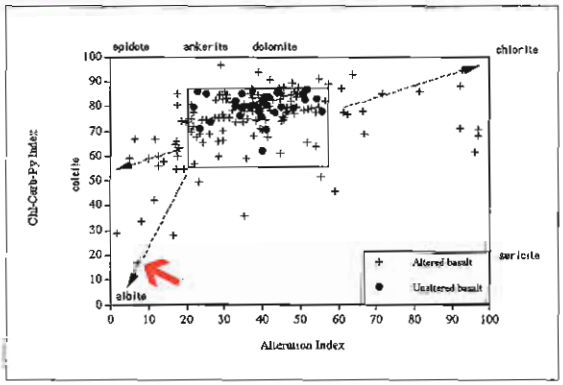

Hellyer Hangingwall Alteration

Sample No.	**628520**
Location	Hellyer
Alteration zone	Carbonate-chlorite-sericite
Formation	Hellyer Basalt Mt Read Volcanics, Central Volcanic Complex

Description Strongly carbonate-chlorite-sericite altered clinipyroxene-phyric basalt.

Facies Interp Massive basaltic lava.

Alteration Intensity	none	weak	moderate	(strong)	intense	Py 1%
Alteration Style	patchy	(pervasive)	veined		cleavage control	
Alteration Mineralogy	Groundmass	carbonate, chlorite, sericite				
	Feldspars	carbonate, white mica				
	Mafics	carbonate, chlorite				
Interpretation	diagenetic	metamorphic	syntectonic	(hydrothermal)		
Relict Mineralogy	chromite					

Geochemistry

SiO_2	TiO_2	Al_2O_3	Fe_2O_3	MnO	MgO	CaO	Na_2O	K_2O	P_2O_5	S	LOI	Al	CCPI	Ti/Zr
31.89	0.39	12.04	6.16	0.21	3.45	21.53	0.00	2.58	0.17	0.8	20.03	22	78	36

Rb	Ba	Cu	Pb	Zn	Sb	Tl	Zr	Nb	Y	Sr
73	2672	54	8	55	52	4.1	65	4	14	295

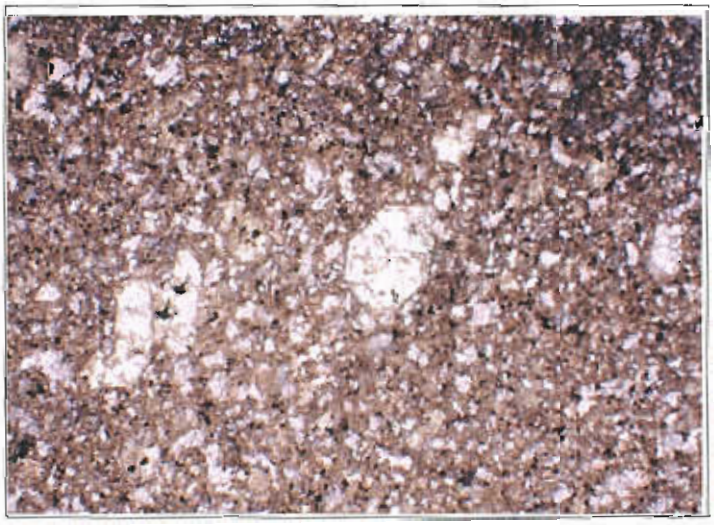

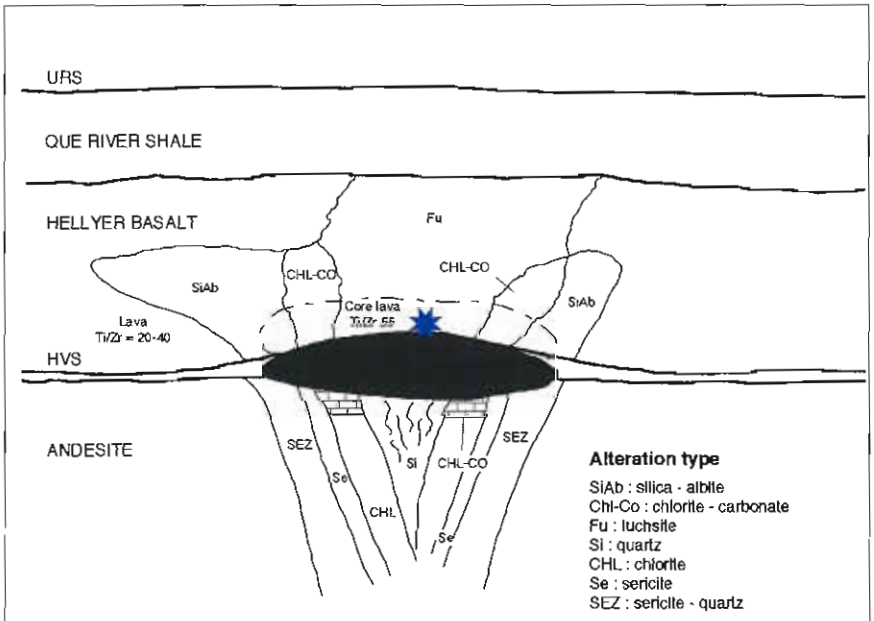

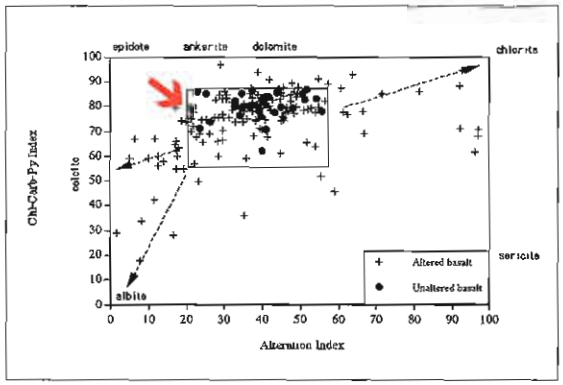

Hellyer Hangingwall Alteration

Sample No.	**628516**
Location	Hellyer
Alteration zone	Fuchsite-Carbonate
Formation	Hellyer Basalt
	Mt Read Volcanics, Central Volcanic Complex

Description Intensely fuchsite-carbonate altered basalt

Facies Interp Massive basaltic lava.

Alteration Intensity	none	weak	moderate	strong	(intense)	Py < 1%
Alteration Style	patchy	(pervasive)	veined		cleavage control	
Alteration Mineralogy	Groundmass	white mica, carbonate				
	Feldspars	carbonate, white mica				
	Mafics	carbonate, whith mica				
Interpretation	diagenetic	metamorphic	syntectonic	(hydrothermal)		
Relict Mineralogy	chromite					

Geochemistry

SiO_2	TiO_2	Al_2O_3	Fe_2O_3	MnO	MgO	CaO	Na_2O	K_2O	P_2O_5	S	LOI	Al	CCPI	Ti/Zr
26.32	0.54	17.35	3.38	0.25	1.88	22.67	0.00	5.00	0.21	0.08	21.13	23	50	43.9

Rb	Ba	Cu	Pb	Zn	Sb	Tl	Zr	Nb	Y	Sr
143	4473	162	2	43	8.1	3.3	74	5	17.9	176

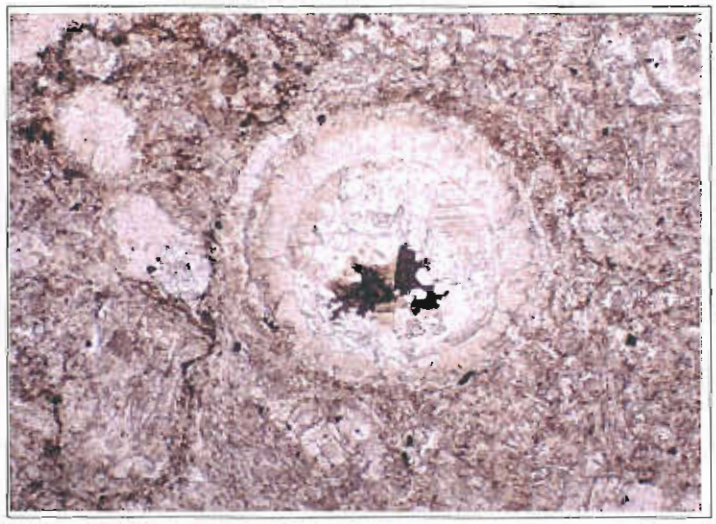

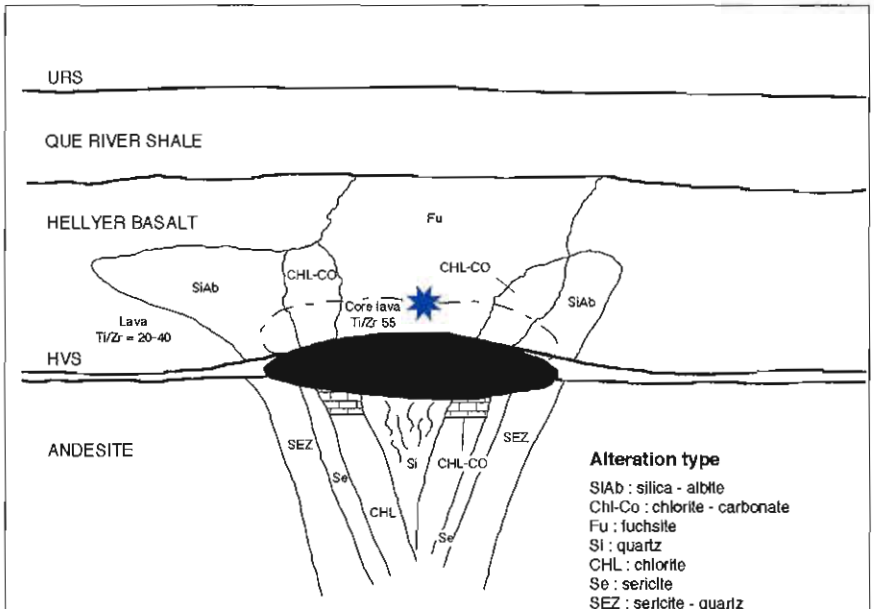

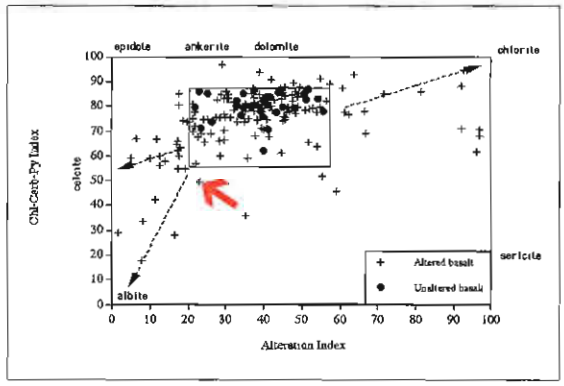

Hellyer Hangingwall Alteration

Sample No.	**628435**
Location	Hellyer
Alteration zone	Unaltered
Formation	Hellyer Basalt Mt Read Volcanics, Central Volcanic Complex

Description	Clinopyroxene-phyric basaltic lava. Some carbonate after glass in groundmass.
Facies Interp	Massive basaltic lava.

Alteration Intensity	none	(weak)	moderate	strong	intense	Py	< 1%
Alteration Style	patchy	pervasive	veined		cleavage control		
Alteration Mineralogy	Groundmass	minor carbonate					
	Feldspars						
	Mafics						
Interpretation	(diagenetic)	metamorphic	syntectonic	hydrothermal			
Relict Mineralogy	clinopyroxene, plagioclase, chromite						

Geochemistry

SiO_2	TiO_2	Al_2O_3	Fe_2O_3	MnO	MgO	CaO	Na_2O	K_2O	P_2O_5	S	LOI	Al	CCPI	Ti/Zr
51.14	0.55	14.77	8.82	0.21	5.56	5.44	4.19	0.42	0.6	0.06	8.17	38	75	22

Rb	Ba	Cu	Pb	Zn	Sb	Tl	Zr	Nb	Y	Sr
21	226	745	6	147	1	0.5	151	7	21	125

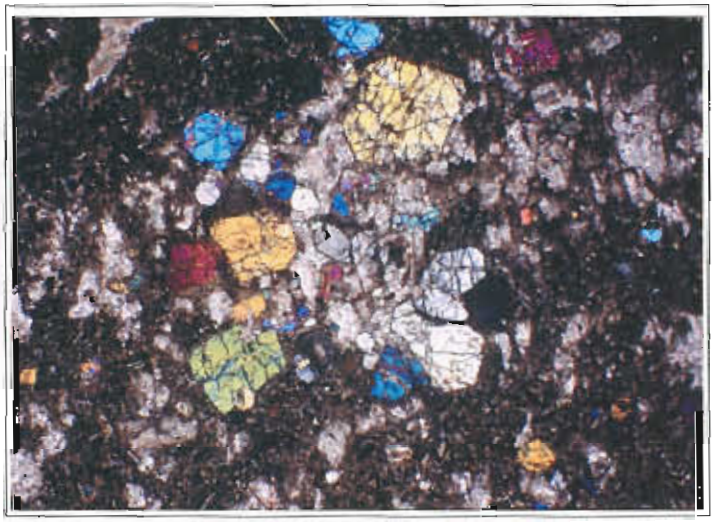

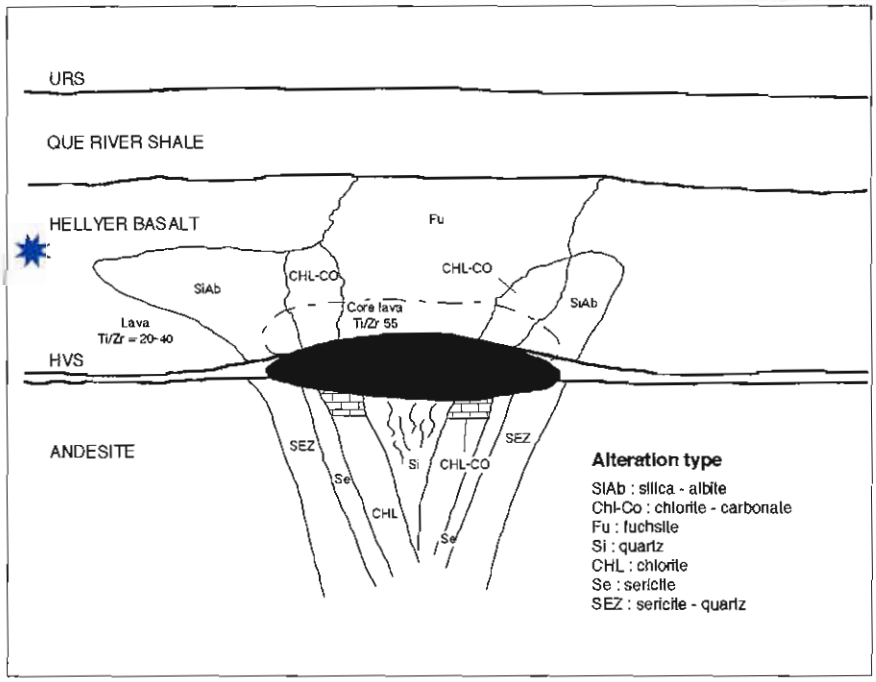

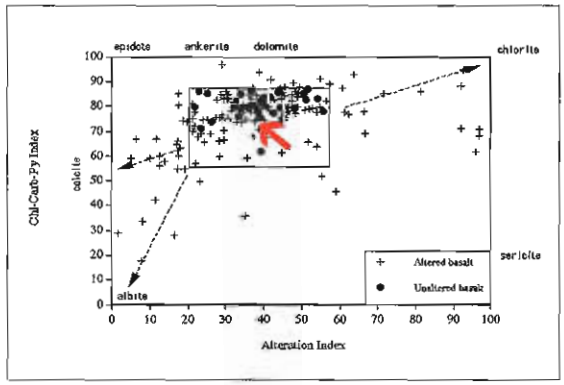

Hellyer Hangingwall Alteration

Sample No.	**628475**
Location	Hellyer
Alteration zone	Chlorite
Formation	Hellyer Basalt Mt Read Volcanics, Central Volcanic Complex

Description Moderately chlorite-carbonate altered clinopyroxene-phyric basalt.

Facies Interp Massive basaltic lava

Alteration Intensity	none	weak	(moderate)	strong	intense	Py < 1%
Alteration Style	patchy	(pervasive)	veined		cleavage control	
Alteration Mineralogy	Groundmass	chlorite, carbonate				
	Feldspars					
	Mafics	chlorite				
Interpretation	diagenetic	metamorphic	syntectonic	(hydrothermal)		
Relict Mineralogy	plagioclase, chromite					

Geochemistry

SiO_2	TiO_2	Al_2O_3	Fe_2O_3	MnO	MgO	CaO	Na_2O	K_2O	P_2O_5	S	LOI	Al	CCPI	Ti/Zr
45.37	0.45	14.04	8.34	0.16	10.09	8.95	1.89	0.49	0.17	0.02	9.87	49	88	44

Rb	Ba	Cu	Pb	Zn	Sb	Tl	Zr	Nb	Y	Sr
18	622	109	3	67	15	0.5	62	4	14	267

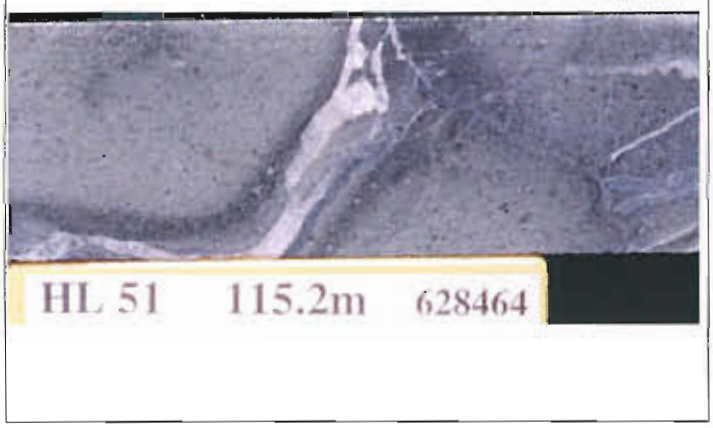

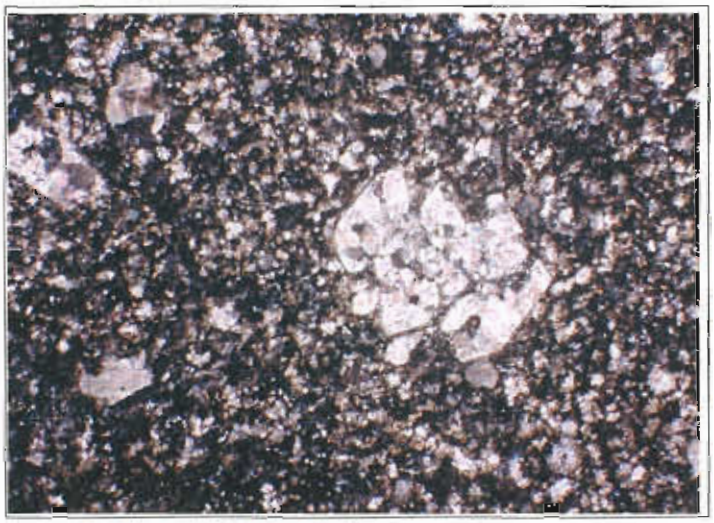

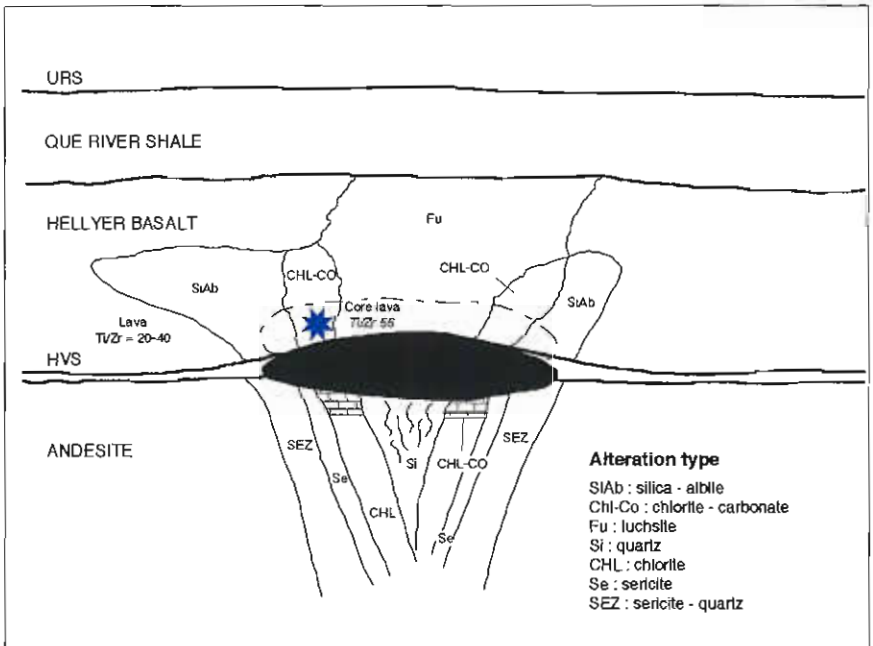

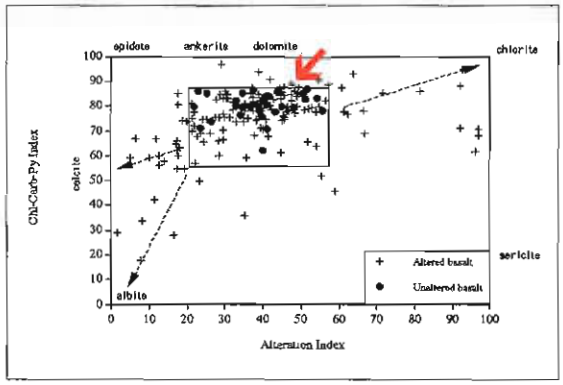

Alteration zonation and geochemical dispersion at the Western Tharsis deposit, Mt Lyell, Tasmania: a summary

by David Huston and Julianne Kamprad
Australian Geological Survey Organisation

Summary

The Western Tharsis deposit occurs within a sequence of dominantly felsic volcaniclastic rocks with lesser clastic and coherent intermediate volcanic rocks in the Central Volcanic Complex. This sequence is overlain by a thin lens of Tyndall quartz-phyric rhyolitic volcanics, which, in turn is overlain by the Owen Conglomerate.

Lithogeochemical, mineral chemistry and PIMA analyses define vectors to ore that can be used in deposit and prospect scale exploration for Western Tharsis-type mineral deposits. As the studies were limited to within 500 m of the ore position, no regional or district-scale vectors were established.

Between 500 to 200 m from ore, rocks surrounding the Western Tharsis deposit are characterised by albitic rocks that have been moderately to strongly quartz-chlorite-sericite or chlorite±sericite altered. This zone is characterised by abundant carbonate minerals that vary from ankeritic composition distal from ore to sideritic compositions more proximal to ore. Increasing proximity to ore is also characterised by a decrease in Mg/(Mg+Fe) ratios of chlorite. This carbonate-rich zone is characterised by positive C-Zn-Tl-Mn-Ca anomalism.

Within 200 m of ore, host rocks to the deposit have been strongly quartz-sericite altered, with the Fe-bearing carbonate minerals supplanted by pyrite. Apatite is an accessory mineral in this and more proximal alteration zones at Western Tharsis. This pyritic zone is characterised by low level Cu, As, Bi, Mo, Ni, S and Se anomalism and by depletion of the Zn-Tl-C-Mn-Ca assemblage. Positive Ba anomalism extends somewhat further than 200 m from the ore position. Although chlorite is not present in this zone, decreasing phenigite content of sericite is a good indication of approach to ore. This is also reflected in PIMA spectra, where $\lambda_{Al\text{-}OH}$ decreases towards ore.

Within 70 m of ore, the orebodies are flanked by zones of extreme depletion in K and Cs. This anomalism is probably related to the development of acid-sulfate alteration assemblages dominated by pyrophyllite, but also including topaz, zunyite, fluorite and woodhouseite. These acid-sulphate assemblages are strongly associated with a zone of bornite-dominant mineralisation that overprints the dominant pyrite-chalcopyrite ore assemblage at Western Tharsis.

The alteration assemblage of pyrophyllite-topaz-zunyite-woodhouseite, which is associated with bornite-dominant mineralisation, is characteristic of acid-sulphate epithermal systems elsewhere in the world. Moreover, the close relationship of this alteration assemblage to the more prevalent quartz-sericite and quartz-chlorite-sericite alteration assemblages associated with disseminated pyrite-chalcopyrite mineralisation suggests that these two types of mineralisation are two stages of one mineralising event, not two separate events as accepted presently. Geological relationships and radiogenic isotope data are consistent with a Delamerian (~460 Ma) timing for Mt Lyell Cu-Au mineral deposits; this mineralisation may be related to the geologic event that formed the Haulage Unconformity. These observations potentially indicate a new exploration model for mineralisation in the Mt Read Volcanic belt and in surrounding Ordovician rocks.

Introduction

Of the deposits studied in AMIRA project P439, the Western Tharsis is unique in both its metal assemblage and style of mineralisation. This deposit, which is one of about twenty deposits in the Mt Lyell mineral field, is characterised by a Cu-Au metal assemblage and a disseminated style of mineralisation in contrast to the Zn-Cu-Pb assemblage and massive sulphide style of mineralisation in the other deposits studied. In addition, the Mt Lyell deposits are the only deposits studied for which a magmatic hydrothermal origin to the mineralisation has been previously inferred (e.g.Large et al., 1996).

Previous reports

This report is one of three describing the geology, alteration mineralogy and zonation and geochemical dispersion about the Western Tharsis deposit. Other reports are entitled "Research program and preliminary results of alteration studies at the Western Tharsis deposit, Mt Lyell field" (Huston, 1997a), and "Geochemical variations in the alteration zone surrounding the Western Tharsis deposit and their utility in exploration" (Huston, 1997b). Herrmann et al. (this volume) describe the mineral chemistry and PIMA responses of the alteration zones surrounding the Western Tharsis deposit.

Research techniques

During February-April and July-August 1997, twelve diamond drill holes, totalling 5.3 km, were logged and sampled from the Western Tharsis deposit. These drill holes were selected along three cross sections: 8600N, 8850N and 9100N. Section 8850N passes through the centre of the orebody, whereas the other two holes pass roughly 100 m along strike from the orebody margins. A total of 215 drill core samples were analysed for major elements and a suite of trace elements using XRF, ICP-MS, LECO titration and hydride generation AAS at the University of Tasmania and Analabs in Perth. Huston (1997b) gives a more detailed summary of the analytical techniques.

The same samples were also analysed with PIMA at AGSO, and about 50 thin sections were cut. Of the thin sections, 25 were analysed using the electron microprobe at the Australian National University to determine the compositions of sericite, chlorite, carbonate and other minerals. Laser Raman analysis of these sections was also undertaken to determine TiO_2 polymorphs and to identify unknown minerals.

In addition, surface traverses corresponding to the above cross sectional lines were conducted in July-August 1997. Rock chip samples were collected every 10-50 m along the traverse from the least weathered exposures present. A total of 39 of these samples were analysed for a suite of elements using ICP (Na, K, Cu, Mn, Sr, Bi, Mo, Pb and Zn), XRF (Ba), hydride generation AAS (As) and Leco titration (S) at Analabs in Burnie.

The results of all of these analyses are appended to this report in the accompanying CD.

Geology of the Mt Lyell mineral field

The Western Tharsis is the only major undeveloped ore deposit presently known in the Mt Lyell field. It and most other orebodies in the field occur in the Mine Sequence, which is dominated by strongly silicified and sericitised felsic volcaniclastic rocks. Four different deposit types occur within the Mine Sequence: (1) disseminated pyrite-chalcopyrite orebodies of which Prince Lyell is the largest example, (2) bornite-chalcopyrite orebodies as exemplified by North Lyell, (3) massive pyrite-chalcopyrite orebodies like The Blow, and (4) stratiform massive pyrite-galena-sphalerite-galena-pyrite orebodies such as Lyell Comstock (Walshe and Solomon, 1981). The disseminated orebodies, which constitute most of the resource at Mt Lyell, mostly occur at a lower stratagraphic interval than the bornite-chalcopyrite orebodies. Although the Western Tharsis deposit is characterised mainly by disseminated pyrite-chalcopyrite, limited bornite-bearing zones may indicate a local transition towards North Lyell style mineralisation.

Geological setting of the Western Tharsis deposit

The Western Tharsis deposit occurs within a moderately to strongly altered sequence of felsic and intermediate volcanic rocks of the Central Volcanic Sequence. Figure 1, which is based on core logging and Zr/TiO_2 ratios, illustrates the original lithological variation of the ore-bearing sequence. Five different rock types are present: (1) felsic volcaniclastic rocks, (2) sandstone, (3) intermediate volcaniclastic rocks, (4) intermediate lavas and/or sills, (5) quartz-phyric rhyolitic volcanic rocks, and (6) siliciclastic conglomerate.

Felsic volcanistic rocks are typically aphyric to sparsely quartz-phyric and have Zr/TiO_2 ratios between 0.05 and 0.12. Two major felsic volcaniclastic units are present at Western Tharsis. The first, which occurs in the stratagraphic footwall (structural hanging wall) to the ore lens, is at least 200 m thick and is interbedded with about 20-30% sandstone. The second unit is separated from the lower felsic unit by a narrow unit of intermediate volcanics. This felsic unit hosts the ore lens and varies between 200 and 300 m thick. These felsic volcaniclastic units typically contain ash to lapilli sized clasts, although the overprinting alteration assemblages commonly obscure the original clastic textures.

Volcanogenic sandstone, siltstone and shale form signicant lenses within the stratagraphically lowermost felsic unit. These lenses are generally laterally continuous and vary from 10 to 50 m in true thickness. Variable Zr/TiO_2 ratios in the sediments suggest a mixed parentage.

Intermediate volcanic rocks, which are characterised by Zr/TiO_2 ratios of between 0.015 and 0.05, form two significant units. The lowermost unit, which is 10-50 m thick, separates the two major felsic units. This unit consists of volcaniclastic rocks with ash-sized fragments and massive, locally amygdaloidal andesite. The andesitic units may include both flows and sills, and weakly altered kernels are relatively common even within the intense alteration zone surrounding the Western Tharsis deposit.

The second major unit containing intermediate volcanics overlies the ore-bearing felsic unit, and extends 200-300 m to the angular contact with the quartz-phyric rhyolitic volcaniclastic unit. In addition to intermediate volcaniclastic rocks, this unit also contains interbedded felsic volcaniclastic rocks. Coherent intermediate volcanic rocks are not common in this volcaniclastic-dominated package.

A thin (<3 m) thick unit of quartz-phyric volcanic rock has an angular contact with the felsic-intermediate sequence. This unit is characterised by the presence of up to 5% 1-2 mm quartz phenocrysts, and resembles the Tyndall Group.

The quartz-phyric volcanic unit is in contact with hematitic, clast- and matrix-supported, pebble-cobble conglomerate of the Owen Conglomerate. This unit, which is highly siliceous, is characterised by sub-angular to rounded, polymictic clasts in a hematitic sandy matrix.

Ore deposit characteristics

The Western Tharsis deposit, which has an indicated and inferred resource totalling 12.4 Mt at 1.3% and 0.3 g/t Au, is a stratiform, disseminated pyrite-chalcopyrite body that occurs near the stratagraphic base of the Mine Sequence at or about the same stratagraphic level as the Prince Lyell deposit. The ore zone does not crop out, but comes within 20 m of surface. It dips steeply to grid west (southwest) and is overturned. The ore zone extends approximately 300 m along strike and has a thickness of up to 150 m. Current drilling indicates that it extends 1000 m below surface and is open at depth (Fig. 1).

Although the Western Tharsis deposit is dominated by a simple pyrite-chalcopyrite ore mineral assemblage, local zones (Fig. 1) are characterised by a North Lyell-like assemblage of pyrite-bornite-chalcopyrite-chalcocite-mawsonite-enargite. Textural studies indicate that the latter assemblage overprints the original pyrite-chalcopyrite assemblage (Manning, 1990; this study). Both ore mineral assemblages are accompanied by quartz, sericite and/or pyrophyllite (see below), although pyrophyllite appears to be more closely associated with the bornite-dominant assemblage.

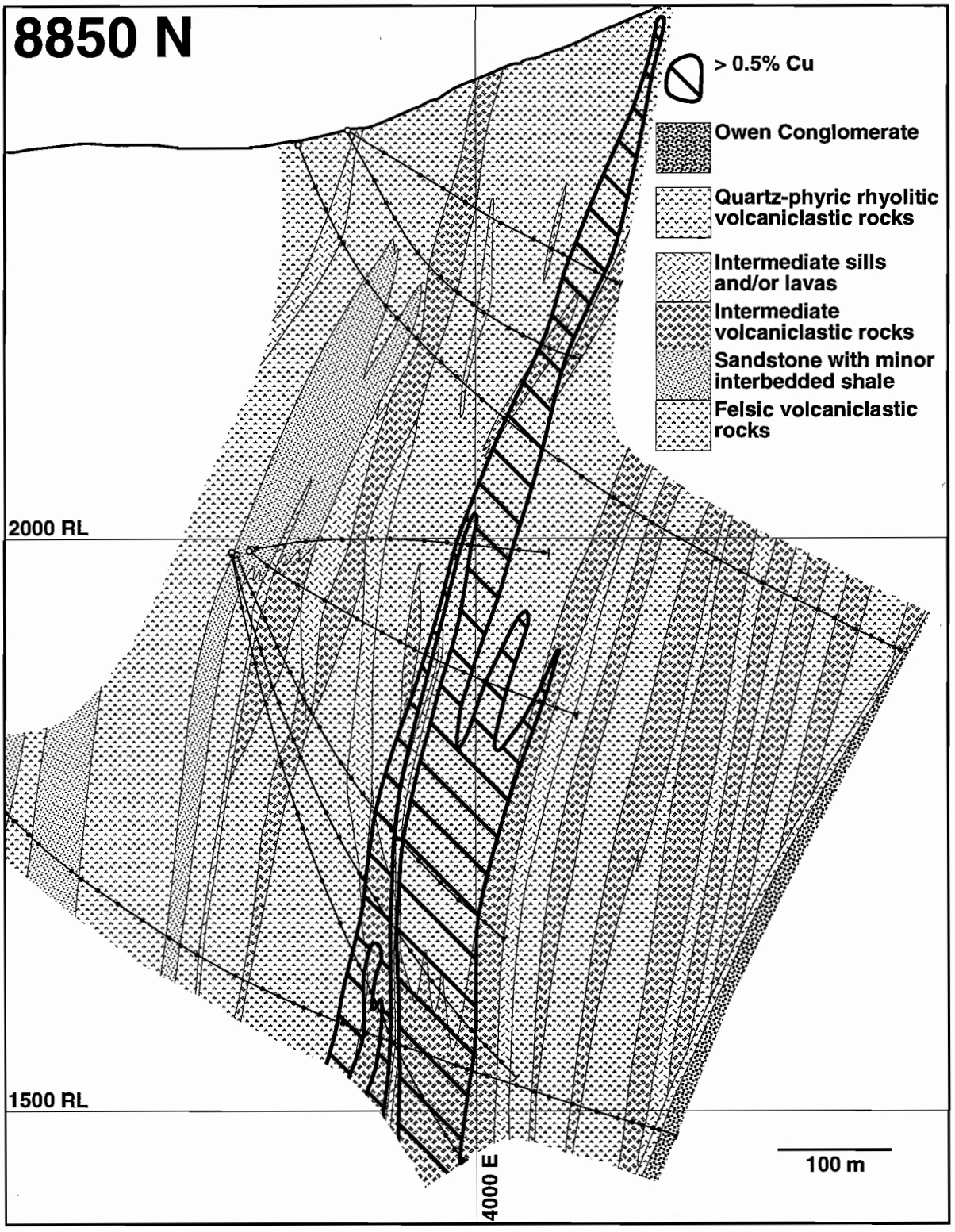

Figure 1. Geological cross section, 8850N, Western Tharsis deposit.

Zonation of alteration assemblages

Alteration at Western Tharsis was characterised by the development of zonation in both phyllosilicate and Fe-S-O-C mineral assemblages. These two mineral groups have significantly different zonation patterns. Summary sheets describing the alteration assemblages are appended.

Silicate alteration assemblages

Based on core logging, PIMA analyses and whole rock geochemical analyses, four major phyllosilicate alteration assemblages are recognised at Western Tharsis (Fig. 2). The least altered assemblage, which occurs some 200-300 west of the orebody in the stratagraphic footwall, is characterised by a weakly developed quartz-sericite assemblage that generally contains significant albite as indicated by core logging and Na_2O analyses. Albite-bearing assemblages do not occur in volcanic units in the stratagraphic hanging wall of the deposit.

The lower part of the ore zone is centred on quartz-chlorite-sericite assemblage. This quartz-chlorite-bearing zone extends from the at least 1450 RL to approximately 2100 RL and does not extend appreciably from the ore zone. A second quartz-chlorite-sericite zone occurs 100-200 m in the footwall to the ore zone. This second zone is not associated with significant copper anomalism, and its stratigraphic base is locally albitic.

The marginal quartz-chlorite-sericite zone is also associated with a chlorite-bearing zones that lack visible quartz (e.g. chlorite, chlorite-sericite and sericite-chlorite assemblages). This zone is best developed in intermediate rocks distal to the ore zone, and Na_2O analyses indicate that it is locally albitic. A second chlorite-bearing zone occurs 200-300 m in the hanging wall of the ore zone.

The central quartz-chlorite-sericite zone is surrounded by quartz-sericite ± pyrophyllite assemblages. These assemblages extend from the ore zone to the marginal chlorite-bearing zones. Quartz-sericite assemblages are the most extensive: these zones extend to the Owen contact. Trace quantities of apatite have been recognised in quartz-sericite altered rocks that lack pyrophyllite.

Pyrophyllite-bearing zones, as identified using PIMA analysis, are restricted to three zones. A large pyrophyllite zone, which is centred on the bornite-bearing zone in hole WT0050, extends between ~2000 RL and ~2300 RL and between 3950E and 4150E. This zone appears to wrap the central quartz-chlorite-sericite zone. Minor gangue minerals that occur within this pyrophyllite-bearing zone include topaz, fluorite, woodhousite and barite.

A second, smaller, pyrophyllite-bearing zone occurs along the western (stratagraphic footwall) margin of the central quartz-chlorite-sericite zone. The third, smallest pyrophyllite-bearing zone occurs at the end of WT0050 near the contact with the Tyndall Group. Zunyite, which is characterised by a characteristic PIMA absorption feature at 2137 nm, occurs within this third pyrophyllite-bearing zone and in a sample that stratagraphically underlies the ore-bearing central quartz-chlorite-sericite alteration zone.

Fe-S-O-C alteration assemblages

Major Fe-bearing minerals at Western Tharsis include chlorite, pyrite, siderite, ankerite and hematite. The distribution of pyrite, siderite and hematite displays a symmetrical distribution about the ore lens (Fig. 3). Pyrite forms an inner halo (>1% by volume) that extends from ~100 m in the stratagraphic footwall to ~200 m in the stratagraphic hanging wall. Within this halo, pyrite occurs as disseminated grains, irregular 1-20 mm stringers and planar 2-50 mm veins. Outside of this halo, the abundance of pyrite generally does not exceed 0.5%. The major exception to this generalisation is in the lowermost ~100 m of hole WT0050.

Siderite, ankerite and minor calcite form an outer halo that extends both into the footwall and hanging wall of the pyrite halo. These carbonate minerals occur as early, 1-5 mm, irregular veins, as 1-10 mm lenticular domains and in late 1-30 mm, planar veinlets. Microprobe analyses (Herrmann et al., this volume) indicate that siderite occurs along the inner margin of this halo, but that ankerite is the main carbonate within the outer part of the carbonate halo. The late veinlets appear to be composed of calcite.

The pyrite and carbonate halos have only minimal overlap. The carbonate halo generally fades out when the pyrite contend exceeds 1-2%. However, hematitic zones are developed at or near the boundaries between the pyrite and carbonate halos (Fig. 3). In

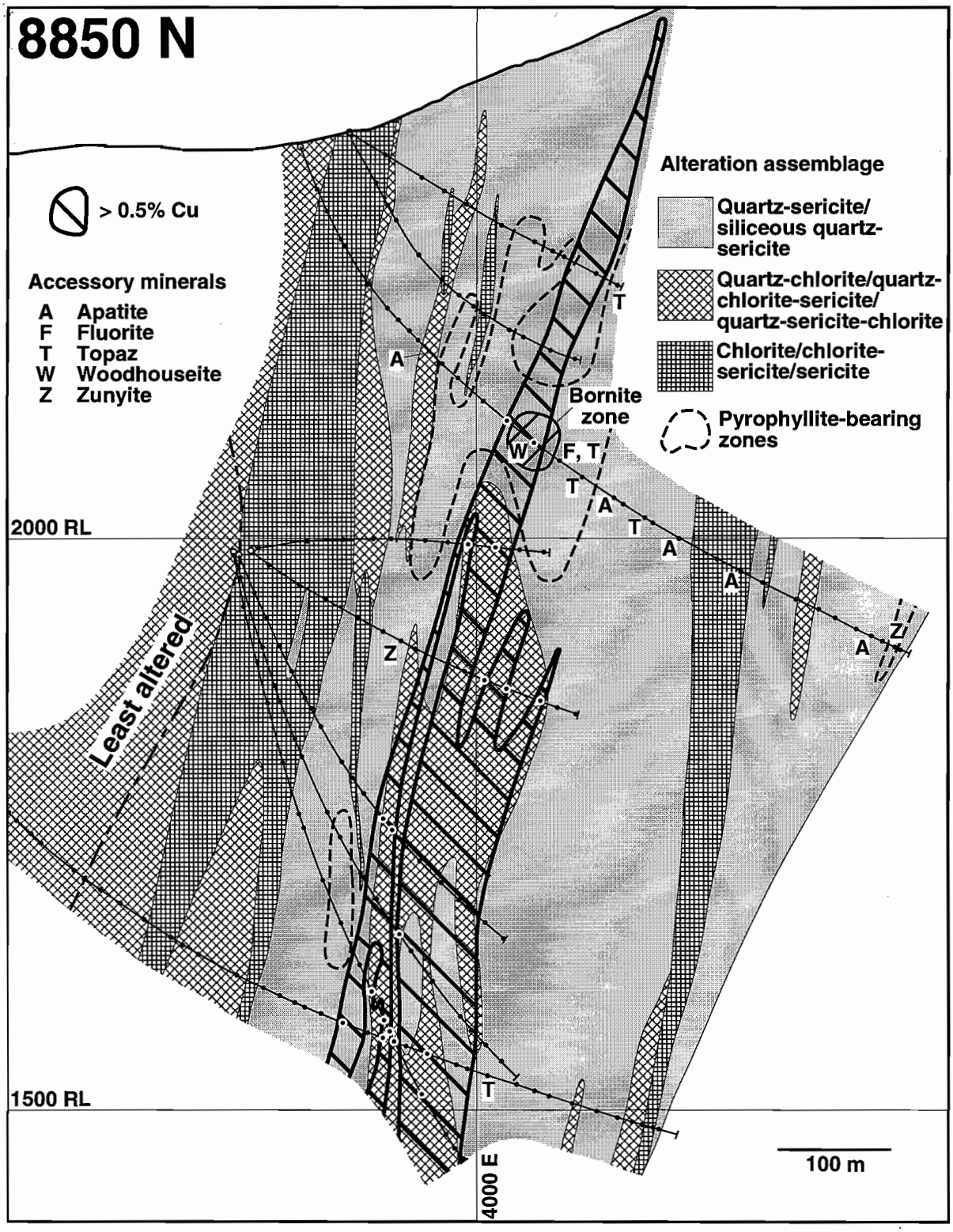

Figure 2. Phyllosilicate alteration assemblages, section 8850N, Western Tharsis deposit.

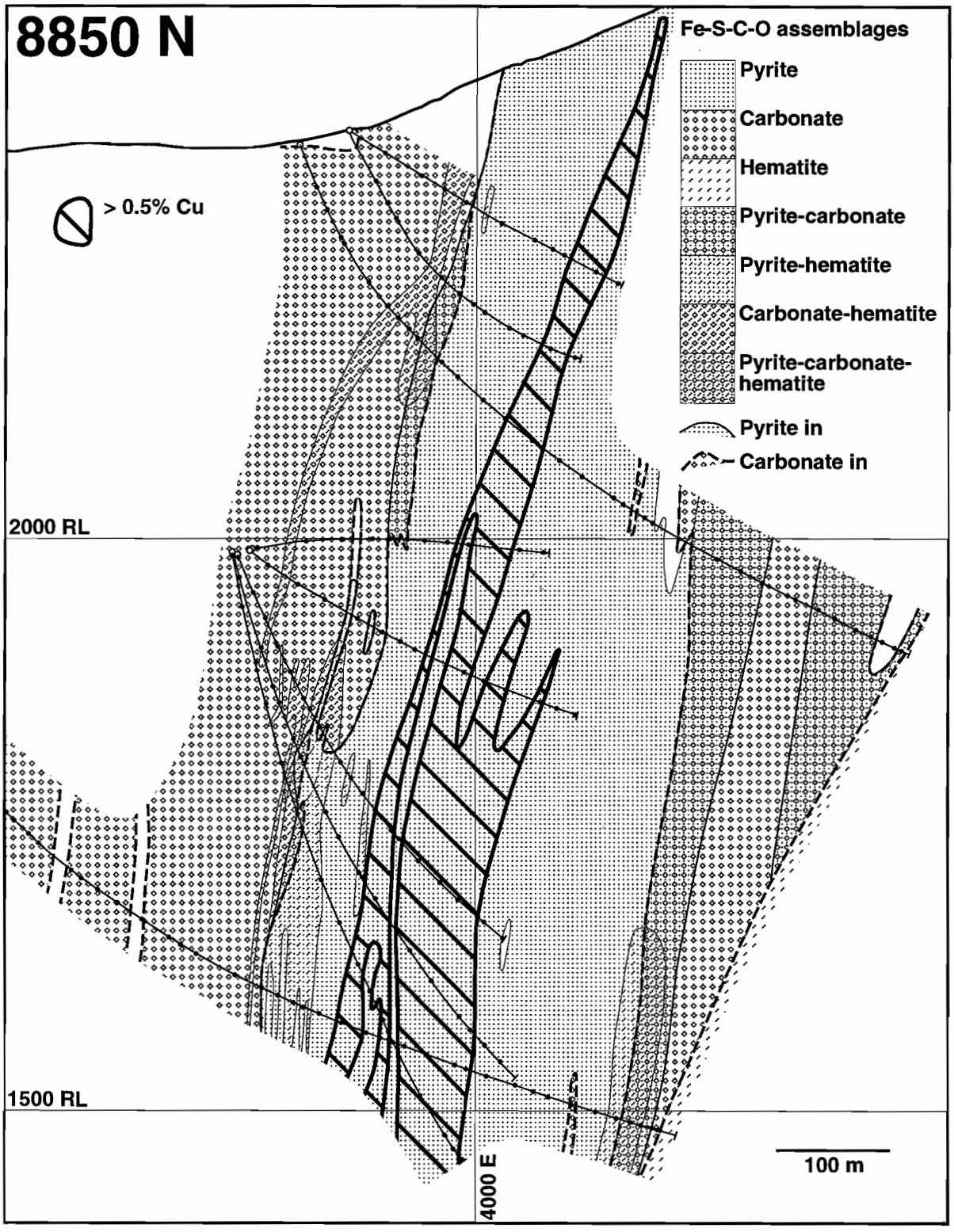

Figure 3. Fe-S-O-C alteration assemblages, section 8850N, Western Tharsis deposit.

drill core, hematitic alteration gives the rock a characteristic purplish tinge, and in thin section, the hematite occurs as disseminated laths and in irregular veinlets. Examination of thin sections indicates that the hematite content that gives the purplish tinge is commonly less that 1% by volume. Laser Raman analysis indicates that the hematite is, in fact, maghemite. In some thin section carbonate minerals appear to mantle or replace hematite.

Mineral chemistry of alteration minerals

To evaluate the usefulness of mineral chemistry as a vector to ore, all samples were analysed using PIMA (portable infrared mineral analyser), and a suite of 25 thin sections from WT0050 were analysed using electron microprobe and laser Raman analysis. The results of this study are described in detail by Herrmann et al. (this volume).

PIMA analyses

The PIMA proved to be highly successful at Western Tharsis in establishing a vector to ore using the wavelength shift in the Al-OH absorption band ($\lambda_{Al\text{-}OH}$) for sericite. The ore zone occurs within a broad zone in which $\lambda_{Al\text{-}OH}$ is less than 2200 nm (Fig. 4). This zone extends approximately 150 m into the footwall and 200 m into the hanging wall of the ore zone. Outside of this zone, $\lambda_{Al\text{-}OH}$ ranges from 2200 to 2210 nm, as shown on section 8850N (Fig. 4). $\lambda_{Al\text{-}OH}$ values in drill hole WT0048, which passes 100-150 m north of the orebody range from 2199 to 2205 nm, with the lower values associated with a weakly mineralised zone near the base of the hole. Within the zone with $\lambda_{Al\text{-}OH}$ less than 2200 nm, the orebody is very closely associated with values below 2198 nm. Comparison of $\lambda_{Al\text{-}OH}$ with the composition of sericite determined from electron microprobe analysis indicates that this PIMA response in due to variations in the phengite content of the sericite (Herrmann et al., this volume).

A second important use of the PIMA in this study was the rapid identification of unusual alteration minerals. Definition of the pyrophyllite halo at Western Tharsis is mainly based on PIMA analyses: pyrophyllite and sericite are very difficult to differentiate in hand specimen or thin section. In addition, PIMA spectra were the first indication of topaz and zunyite (samples 95970006S and 95970007I, respectively) in the Western Tharsis system. Both minerals have characteristic absorption features and seem to be highly responsive (i.e. the presence of zunyite can probably be detected at sub-percent levels).

Electron microprobe analyses

Electron microprobe analyses on samples from hole WT0050 confirmed previous mineral identifications using PIMA and thin section. In addition, electron microprobe analysis identified woodhouseite as an alteration mineral closely associated with the bornite assemblage and indicated that Western Tharsis topaz is fluorine-rich.

Systematic analyses of thin section from hole WT0050 were also undertaken to establish variations in the compositions of sericite, carbonate minerals and chlorite as exploration vectors. Systematic decreases in the phengite content of sericite (as measured by Mg+Fe) towards the ore zone was noted (Herrmann et al., this volume). This variation in mineral chemistry is the direct cause of the $\lambda_{Al\text{-}OH}$ vector described previously.

A smaller number of analyses indicates that the Mg/(Mg+Fe) ratio in chlorite decreases (i.e. becomes more Fe-rich) towards the ore zone, but that this trend is limited by the presence of chlorite as an alteration mineral. Moreover, chlorite in the hanging wall appears to have higher Mg/(Mg+Fe) ratios than that in the stratagraphic footwall (Herrmann et al., this volume).

Finally, electron microprobe analyses indicate that carbonate minerals at Western Tharsis include ankerite, siderite and calcite. The latter mineral occurs as late veinlets that cut the foliation, and hence did not form during ore-related alteration. Of the two other minerals, ankerite occurs mainly in the lowermost part of the footwall carbonate halo, and siderite occurs in the upper footwall carbonate halo and in the hanging wall carbonate halo. Consequently, the Fe content of the carbonates increases towards ore from the footwall. The Mn content of carbonate minerals is signficantly higher in the hanging wall than in the footwall (Herrmann et al., this volume).

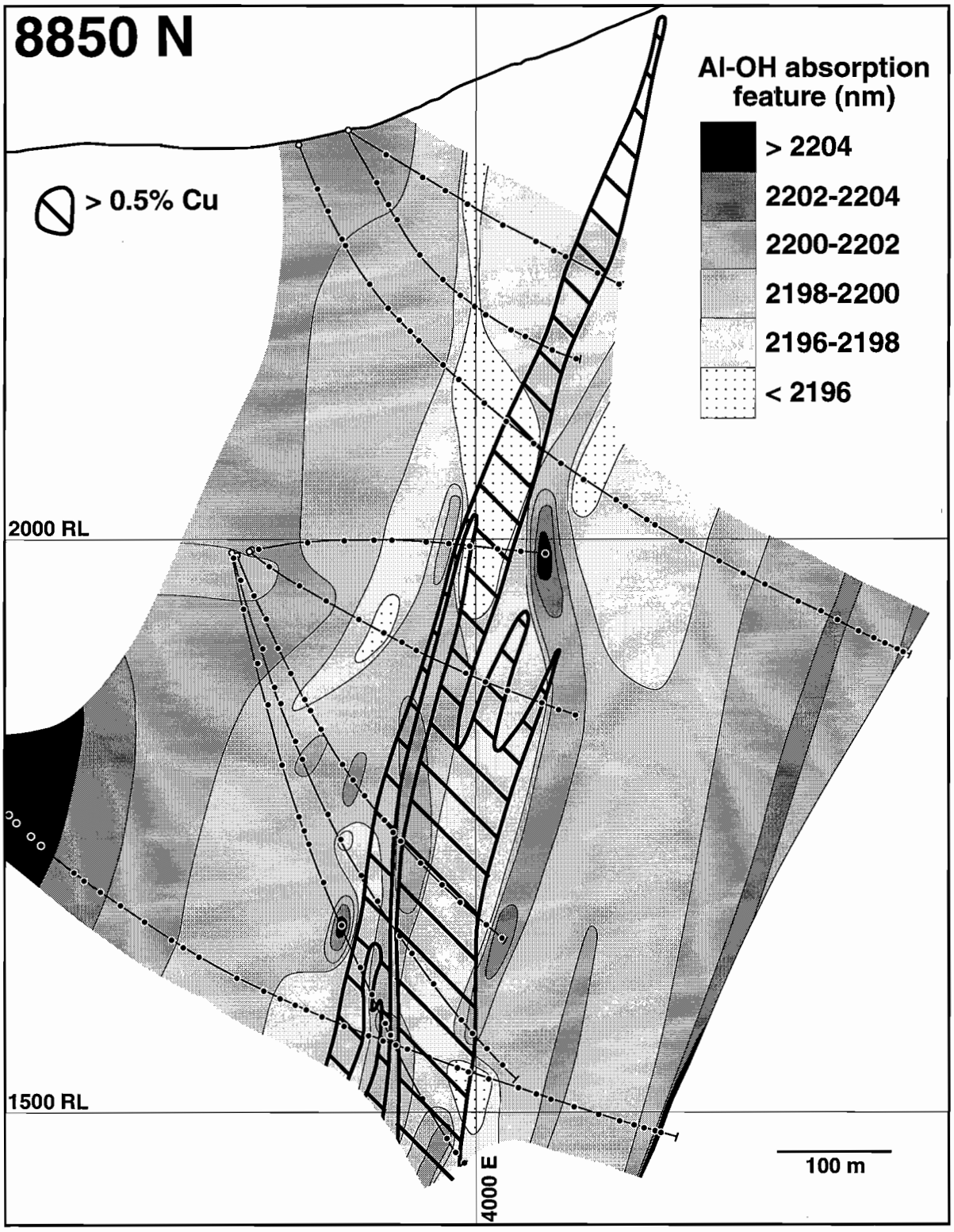

Figure 4. Variation in the wavelength of the Al-OH absorption feature, section 8850N, Western Tharsis deposit.

Lithogeochemical halos

Based on detailed geochemical analyses of fresh drill core samples from the alteration zones surrounding the Western Tharsis deposit, Huston (1997b) defined four main groups of elements with characteristic geochemical dispersion patterns (Table 1). The first group, which includes Cu, As, Bi, Mo, Ni, S and Se, shows extreme enrichment in the ore zone and less extreme enrichment in the flanking pyrite halo, particularly in the stratagraphic hanging wall. The second group, which inclues Ba and Sr, is enriched in the ore and barren pyrite zone and may extend into the peripheral carbonate zone. The third group, which includes Zn, Tl, C, Mn and Ca, is enriched in the peripheral carbonate zone, but is generally depleted in the ore and barren pyrite zone. The final group, which includes K and Cs, is characterised by extreme depletion in narrow zones peripheral to the ore zones, but within the barren pyrite zone. Other elements, such as Na, Mg and Sb has less well defined or less useful dispersion patterns. Finally, Y appears to be strongly depleted in the pyrophyllitic alteration zones: this results in unusually high (>1.0) values for the supposedly immobile Nb/Y ratio.

Surfical dispersion

As described previously, surface traverses were conducted along three traverses corresponding to the three cross sections discussed previously. Of the elements determined, Mo and Sr appear to be the most useful of the elements enriched within the ore and pyrite halos (Fig. 5). Anomalous Mo values (>10 ppm) extend up to 50-150 m from the ore position, and anomalous Sr values (>50 ppm) extend up to 100-150 m from the ore position. Zinc and Mn may also be of use in that they show significant and consistent depletion anomalies that extend up to 50-150 m from the ore position (Fig. 5). Anomalous zones for all four of these elements are apparent on traverses 8850N and 8650N, which both pass over sub-economic to economic mineralised zones. In contrast, no significant anomaly was found on traverse 9100N, which passes north of significant mineralised zones. Suprisingly, the response of Cu at the ore position is weak and offset 100 m into the footwall of the ore position (Fig. 5).

Vectors to ore

Lithogeochemical, mineral chemistry and PIMA analyses define vectors to ore that can be used in deposit and prospect scale exploration for Western Tharsis-type mineral deposits. As the studies were limited to within 500 m of the ore position, no regional or district-scale vectors were established.

From 500 to 200 m from ore, rocks surrounding the Western Tharsis deposit are characterised by albitic rocks that have been moderately to strongly quartz-chlorite-sericite or chlorite±sericite altered. This zone is characterised by abundant carbonate minerals that vary from ankeritic composition distal from ore to sideritic compositions more proximal to ore. Increasing proximity to ore is also characterised by a decrease in Mg/(Mg+Fe) ratios of chlorite. This carbonate-rich zone is characterised by positive C-Zn-Tl-Mn-Ca anomalism.

Within 200 m of ore, host rocks to the deposit have been strongly quartz-sericite altered, with the Fe-bearing carbonate minerals supplanted by pyrite. Apatite is an accessory mineral in this and more proximal alteration zones at Western Tharsis. This pyritic zone is characterised by low level Cu, As, Bi, Mo, Ni, S and Se anomalism and by depletion of the Zn-Tl-C-Mn-Ca assemblage. Positive Ba anomalism extends somewhat further than 200 m from the ore position. Although chlorite is not present in this zone, decreasing phenigite content of sericite is a good indication of approach to ore. This is also reflected in PIMA spectra, where $\lambda_{Al\text{-}OH}$ decreases towards ore.

Within 70 m or ore, the orebodies are flanked by zones of extreme depletion in K and Cs. This anomalism is probably related to the development of acid-sulfate alteration assemblages dominated by pyrophyllite, but also including topaz, zunyite, fluorite and woodhouseite. These acid-sulphate assemblages are strongly associated with a zone of bornite-dominant mineralisation that overprints the dominant pyrite-chalcopyrite ore assemblage at Western Tharsis.

Table 1. The distribution of selected elements with potential exploration utility at the Western Tharsis deposit, Mt Lyell, Tasmania.

As, Bi, Mo and S These four elements are characterised by extreme enrichments in the ore zone flanked by less extreme enrichments in the barren pyrite zone and background values in the carbonate zone. In the case of Mo, enrichment in the barren pyrite zone is very limited, and Bi and S enrichments in the hanging wall are very erratic. Arsenic has the "smoothest" distribution. The following summarises the abundances of these elements:

	Ore zone	Barren pyrite zone		Carbonate zone
		Footwall	Hanging wall	
As (ppm)	10-100	5-20	5-10	<5
Bi (ppm)	0.5-1.3	0.5-2	0.5-6	<0.5
Mo (ppm)	20-800	1-10	<5	<1
S (%)	2-20	1-10	1-10	<1

Se Selenium has a broadly similar distribution to the suite As-Bi-Mo-S. Although enriched in the ore zone (2-10 ppm), the highest values (5-50 ppm) occur marginal to the orebody, particularly in the hanging wall. Values in the hanging wall are highly erratic, although they drop off ~50 m from the Owen contact.

K_2O and Cs K_2O and Cs are generally characterised by relatively uniform values (2-4% and 1.5-3 ppm, respectively) throughout, except in 20-30 m wide, stratiform zones that occur 20-70 m both above and below the margins of the ore zone. These zones are characterised by extreme depletion (0.06-0.9% and 0.1 -0.9 ppm, respectively).

C, Zn Carbon(ate)-rich (>0.5% C) zones occur within the peripheral carbonate zone that starts 50-250 m from the ore lens margin both in the footwall and in the hanging wall. Within the barren pyrite zone, C values are <0.1%, although slightly higher values (0.2-0.5%) occur locally in the ore zone. In several drill holes, C values increase gradually in the footwall carbonate zone (from 0.5 to 2%) and then dramatically decrease when the pyrite zone is reached. Zinc has a similar distribution, with low order anomalism (100-300 ppm) along the upper margin of the lower carbonate zone. In the upper carbonate zone, Zn anomalism is erratic but with higher maximum values (to 1200 ppm). In the barren pyrite zone Zn values are typically 5-50 ppm, but in the ore zone, Zn values are up to 50 ppm.

Tl Thallium is characterised by anomalous values (0.5-1.2 ppm) in the peripheral carbonate zones and a depleted zone (<0.5 ppm) in the barren pyrite and ore zones. Although the anomaly in the hanging wall carbonate zone extends to the Owen contact, the anomaly only occurs in the upper 100-150 m of the footwall carbonate zone.

Sb Antimony does not display a consistent distribution pattern, with most values between 0.5 and 2 ppm. There is an anomalous zone (2-3 ppm) in the upper 100 m of the footwall carbonate zone.

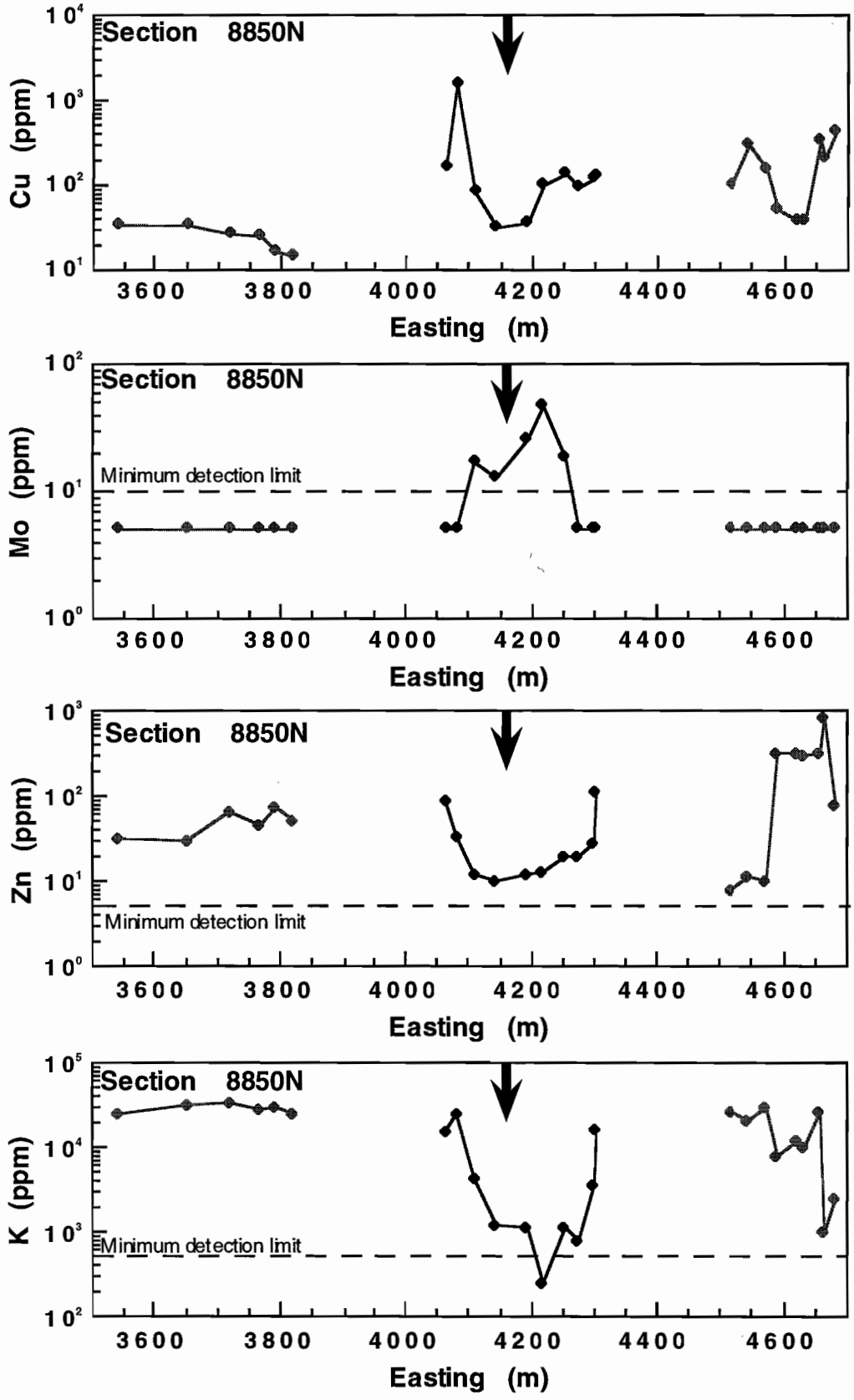

Figure 5. Variation in the concentrations of Cu, Mo, K and Zn, traverse 8850N, Western Tharsis deposit.

Genetic implications

Evidence presented previously in this report indicates that two styles of mineralisation are present in the Western Tharsis mineral deposit: a dominant, disseminated pyrite-chalcopyrite assemblage, which is overprinted by a subordinate, bornite-dominant assemblage. The two assemblages correspond to the Prince Lyell and North Lyell styles of mineralisation, respectively; Western Tharsis is one of the few orebodies where both assemblages are present.

Moreover, paragenetic and spatial relationships indicate that the disseminated pyrite-chalcopyrite assemblage is associated with quartz-chlorite-sericite and quartz-sericite silcate alteration assemblages. These two assemblages are also characterised by the presence of accessory hydrothermal apatite.

In contrast, the bornite-dominant ore assemblage is associated with a quartz-pyrophyllite±sericite alteration assemblage with accessory topaz, fluorite, zunyite and woodhouseite. The assemblage pyrophyllite-topaz-zunyite-woodhouseite is characteristic of alteration assemblages associated with "acid-sulphate (or high sulphidation) epithermal" deposits. Moreover, the presence of topaz indicates a magmatic-hydrothermal origin to at least the quartz-pyrophyllite assemblage and the bornite-dominant sulphide assemblage.

The timing of Mt Lyell mineralisation

The origin and timing of the Mt Lyell orebodies has long been contentious. Walshe and Solomon (1981) inferred a Cambrian timing, but, more recently, a model advocating a dual timing has been advanced (Arnold and Carswell in Solomon and Carswell, 1989; Berry, 1992). In this model, the Prince Lyell-type deposits formed during the Cambrian, whereas the North Lyell-type deposits formed by remobilisation of this mineralisation during Devonian deformation. However, these results of the present investigation call this dual timing model into question.

Did the Prince Lyell and North Lyell styles form ~140 Ma apart? Studies at Western Tharsis suggests that the alteration associated with North Lyell-style bornite-dominant assemblages has a systematic spatial distribution to quartz-chlorite-sericite assemblages associated with Prince Lyell-style disseminated pyrite-chalcopyrite assemblages. This relationship, the common telescoping of "acid-sulphate epithermal" deposits on genetically related, precursor deposits (e.g. Sillitoe, 1994), and the unlikely coincidence of Cambrian sub-seafloor disseminated deposits and Devonian "acid-sulphate" mineral deposits makes it more likely that the Prince Lyell-type and North Lyell-type orebodies formed as two stages of a single mineralising event.

What is the timing of this Mt Lyell mineralising event? The timing of the Mt Lyell mineral deposits are constrained to between the deposition of the Central Volcanic Complex at approximately 500 Ma and the Devonian Tabberabberan Orogeny at about 360 Ma by the facts that the deposits are hosted by the Central Volcanic Complex and that the alteration assemblages and sulphide assemblages are affected by Tabberabberan folliations.

The timing of the Mt Lyell mineralising event is even more constrained by the extension of sericite-hematite alteration assemblages into the Owen Conglomerate and the Pioneer Beds (Berry, 1992). Recent palaeontological dating of the Pioneer Beds constrains this unit the upper Darriwilian Stage of the Ordovician, which corresponds to an age of ~460 Ma (Laurie, 1996). Hence, the Mt Lyell mineralising event is constrained by geological relationships to between ~460 Ma and ~360 Ma. This interpretation is not consistent with a Cambrian age for Prince-Lyell style ore deposits at Mt Lyell.

A Delamerian age for the Mt Lyell mineralising event? The fact that the alteration assemblages at Mt Lyell are foliated by Tabberabberan cleavages indicates that the mineralisation formed either early during or predated this deformation event. However, Tabberabberan granitoids in Tasmania are post-kinematic (Solomon, 1981), and the Mt Lyell event appears to be magmatically related. Moreover, "acid-sulphate" alteration assemblages are not known to be associated with Tabberabberan (or Cambrian) Granitoids in Tasmania. These relationships suggest that a Devonian timing might not be appropriate for the Mt Lyell mineralising event.

Although a Delamerian influence on western Tasmanian geology has been long suggested, the influence has been inferred to be local. However, the recent dating of Haulage Unconformity (Pioneer Beds) as upper Darriwilian (Laurie, 1996), evidence of a protracted thermal event between 500 Ma and

450 Ma from Ar-Ar dating of sericite in the Hellyer region (Perkins et al., 1995), and the recognition of ~490 Ma granitoids in the northeast extention of the Mt Read Volcanics (Black et al., 1997), suggests that Delamerian actvity is widespread in western Tasmania.

Although mineralisation in the Mt Lyell field has not been dated directly, inferences can be made from the Pb isotope ratios reported by Gulson and Porritt (1987; Fig. 6). Gulson and Porritt (1987) documented that the lead isotope ratios of the strataform, Zn-Pb-rich orebodies of the Comstock Valley are similar to those of the Rosebery deposit, but different from those of the Prince Lyell and Crown Lyell deposits. Part of this difference lies in the sample medium: most Prince Lyell samples were of Pb-poor pyrite, whereas the Comstock Valley samples were Pb-rich. Hence, much of the dispersion towards more radiogenic ratios for the Prince Lyell samples stems in part from the high U/Pb ratios of the sampling medium (Gulson and Porritt, 1987).

However, the four least radiogenic samples from Prince Lyell form a tight cluster with a $^{206}Pb/^{207}Pb$ ratio intermediate between the Comstock Valley and Rènison (Devonian Sn deposit) ratios. These least radiogenic samples include both relatively Pb-rich pyrite and galena, suggesting that they probably are the primary Prince Lyell values. On interpretation of the difference between the Prince Lyell least radiogenic ratio and the Comstock Valley ratio is a different timing of mineralisation. If this hypothesis is accepted, the difference in the ratios corresponds to an approximately 40 Ma difference in ages: the Prince Lyell- (and probably the North Lyell-) type deposits could have formed at ~460Ma, at about the time of the Haulage Unconformity. This interpretation is most consistent with all geological and isotopic data (including Sr data of Whitford et al., 1992).

A hypothesis for the formation of the Mt Lyell mineral system

Four signicant styles of mineralisation occur in the Mt Lyell field. A fifth, minor style of mineralisation, which consists of clay-hosted native copper and cuprite, occurs in shales and limestones at the base of the Gordon Group (Solomon and Carswell, 1989). At Western Tharsis, the two most important styles of mineralisation are juxtaposed and seem to be genetically related. This observation and the apparent

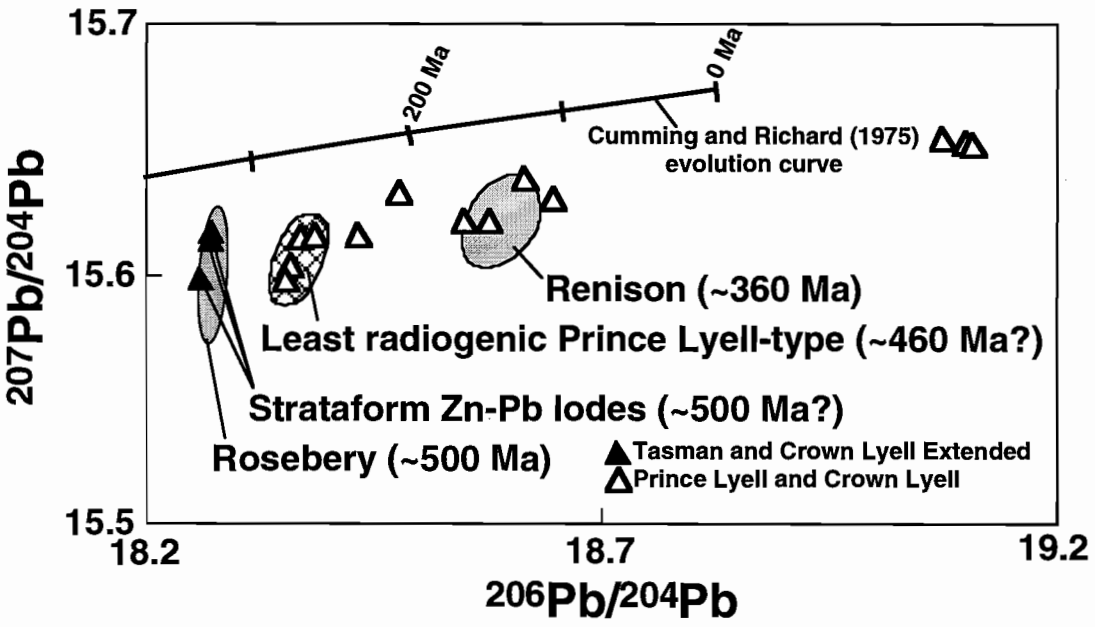

Figure 6. Lead isotope systematics of Mt Lyell deposits in comparison with Rosebery and Renison (modified after Gulson & Porritt, 1987).

age differences between the strataform Zn-Pb lodes in the Comstock Valley and the Prince Lyell disseminated deposits leads to the following hypothesis for the formation of the Mt Lyell deposits.

Event one. As indicated by Pb isotope ratios and their geological occurrence, the strataform Zn-Pb deposits in the Comstock Valley formed at ~500 Ma as syngenetic VHMS deposits. This event was then followed by a period of ~40 Ma, during which Delamerian tectonism occurred and the Haulage Unconformity formed.

Event two, stage one. Near the end of this period, the Prince Lyell type deposits formed by the interaction of high temperature, probably magmatic-hydrothermal fluids with ambient fluids (evolved Ordovician seawater?) along palaeo-aquifers formed by felsic volcaniclastic rocks. Ore deposition resulted from temperature decrease and acid neutralisation. During this time, quartz-sericite and quartz-chlorite-sericite alteration assemblages formed in the Central Volcanic Complex and extended into the Owen Conglomerate and possibly the Pioneer Beds.The massive sulphide bodies at The Blow and South Lyell formed by the interaction of the magmatic-hydrothermal (?) fluids with Ordovician seawater flowing along the contact between the Central Volcanic Complex and the Owen Conglomerate.

Event two, stage two. During this second magmatic-hydrothermal event, changes in either the source granitoid or the overall geological environment resulted an increase in the acidity and oxidation state of the ore fluids, producing an "acid-sulfate" mineralising fluid. Interaction of this fluid with ambient fluids resulted in pH neutralisation and temperature drops, resulting in the formation of the bornite-bearing, North Lyell mineral assemblage.

Acknowledgements

Terry Mernagh is thanked for his help with laser Raman analyses, Nick Ware is thanked for his assistance with electron microprobe analyses, and Mike Blake is thanked for formatting the acompanying data sheests.

References

Berry, R. F., 1992, Mount Lyell mine leases: summary: Unpub. CODES P291 AMIRA Report, v. 4, p. 67-75.

Black, L. P., Seymour, D. B., Corbett, K. D., Cox, S. E., Streit, J. E., Bottrill, R. S., Calver, C. R., Everard, J. L., Green, G. R., McClenaghan, M. P., Pemberton, J., Taheri, J., and Turner, N. J., 1997, Dating Tasmania's oldest geological events: AGSO Record 1997/15.

Cumming, G. L., and Richards, J. R., 1975, Ore lead isotope ratios in a continuously changing earth: Earth and Planetary Science Letters, v. 28, p. 155-171.

Gulson, B. L., and Porritt, P. M., 1987, Base metal exploration of the Mount Read Volcanics, Western Tasmania: Pt. II. Lead isotope signattures and genetic implications: Economic Geology, v. 82, p. 291-307.

Hermann et al., this volume,

Huston, D. L., 1997a, Research program and preliminary results of alteration studies at the Western Tharsis deposit, Mt Lyell field: Unpub. CODES P439 AMIRA Report, v. 4, p. .

Huston, D. L., 1997b, Geochemical variations in the alteration zone surrounding the Western Tharsis deposit and their utility in exploration: Unpub. CODES P439 AMIRA Report, v. 5, p. 1-34.

Large, R., Doyle, M., Raymond, O., Cooke, D., Jones, A., and Heasman, L., 1996, Evaluation of the role of Cambrian granites in the genesis of world class VHMS deposits in Tasmania: Ore Geology Reviews, v. 10, p. 215-230.

Laurie, J. R., 1996, Correlation of Lower-Middle Ordovician clastics in Tasmania: AGSO Record 1996/23.

Manning, C. G., 1990, The geology and mineralisation of the Western Tharsis copper deposit, Mt Lyell, Tasmania: Unpub. B. Sc. Honours thesis, University of Tasmania.

Perkins, C., Walshe, J. L., and Morrison, G., 1995, Metallogenic episoteds of the Tasman Fold Belt System, eastern Australia: Economic Geology, v. 90, p. 1443-1466.

Sillitoe, R. H., 1994, Erosion and collapse of volcanoes: causes of telescoping in intrusion-centered deposits: Geology, v. 22, p. 945-948.

Solomon, M., 1981, An introduction to the geology and metallic ore deposits of Tasmania: Economic Geology, v. 76, p. 194-208.

Solomon, M., and Carswell, J. T., 1989, Mt Lyell: Geological Society of Australia Special Publication 15, p. 125-132.

Walshe, J. L., and Solomon, M., 1981, An investigation into the environment of formation and the volcanic-hosted Mt. Lyell copper deposits using geology, mineralogy, stable isotopes, and a six-component chlorite solid solution model: Economic Geology, v. 76, p. 246-284.

Whitford, D. J., Korsch, M. J., and Solomon, M., 1992, Strontium isotope studies of barites: implications for the origin of base metal mineralization in Tasmania: Economic Geology, v. 87, p. 953-959.

Sample No.	**97950006S**
Location	Western Tharsis DDH WT0050 @ 448.7 - 449.0
Alteration zone	Pyritic halo/quartz - sericite zone
Formation	Mt Read Volcanics, Central Volcanic Complex

Description Brecciated rhyoliti volcanic rock with highly siliceous domains cut by anastomising topaz veins

Alteration Intensity	none	weak	moderate	strong	(intense)
Alteration Style	(patchy	pervasive	veined)	cleavage control	
Alteration Mineralogy	Groundmass	quartz - topaz - carbonate pyrite			
	Feldspars				
	Mafics				
Interpretation	diagenetic	metamorphic	syntectonic	(hydrothermal)	
Relict Mineralogy	Nil				

Geochemistry

SiO_2	TiO_2	Al_2O_3	Fe_2O_3	MnO	MgO	CaO	Na_2O	K_2O	P_2O_5	S	CO2	Al	CCPI	Ti/Zr
68.25	0.28	18.13	1.35	0.30	1.12	2.05	<0.05	0.06	0.07	0.37	3.12	35	95	4

Rb	Ba	Cu	Pb	Zn	Sb	Tl	Zr	Nb	Y
1	171	10	21	14	0.1	0.5	364	14	10

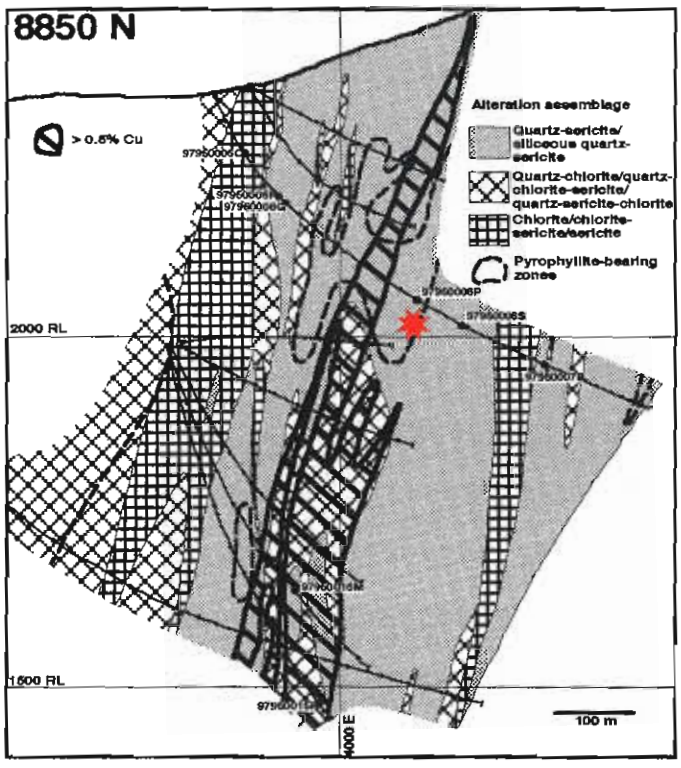

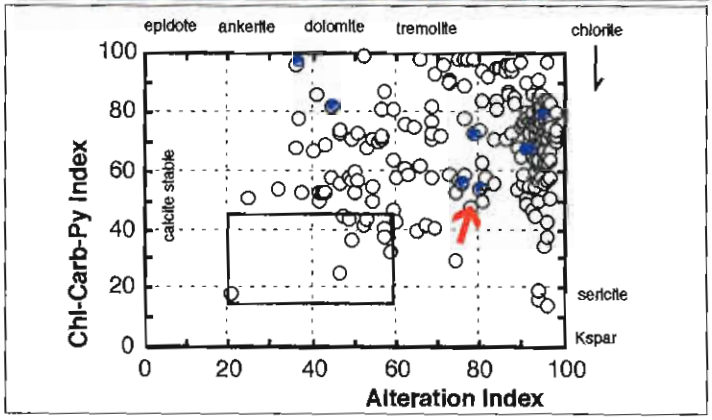

Sample No.	**97950006f**
Location	Western Tharsis DDH WT0050 @ 87.0 - 87.4
Alteration zone	Outer Carbonate halo/chlorite-sericite
Formation	Mt Read Volcanics, Central Volcanic Complex

Description Siliceous, quartz - sericite - carbonate altered, tuffaceous sandstone

Alteration Intensity	none	weak	moderate	strong	(intense)
Alteration Style	(patchy)	(pervasive)	veined	cleavage control	
Alteration Mineralogy	Groundmass	quartz - sericite - carbonate			
	Feldspars				
	Mafics				
Interpretation	diagenetic	metamorphic	syntectonic	(hydrothermal)	
Relict Mineralogy	Nil				

Geochemistry

SiO_2	TiO_2	Al_2O_3	Fe_2O_3	MnO	MgO	CaO	Na_2O	K_2O	P_2O_5	S	CO2	Al	CCPI	Ti/Zr
70.51	0.24	12.81	4.39	0.25	1.14	1.50	0.12	3.89	0.03	<0.01	3.89	44	81	42

Rb	Ba	Cu	Pb	Zn	Sb	Tl	Zr	Nb	Y
46	367	10	6	199	0.8	0.5	72	3	17

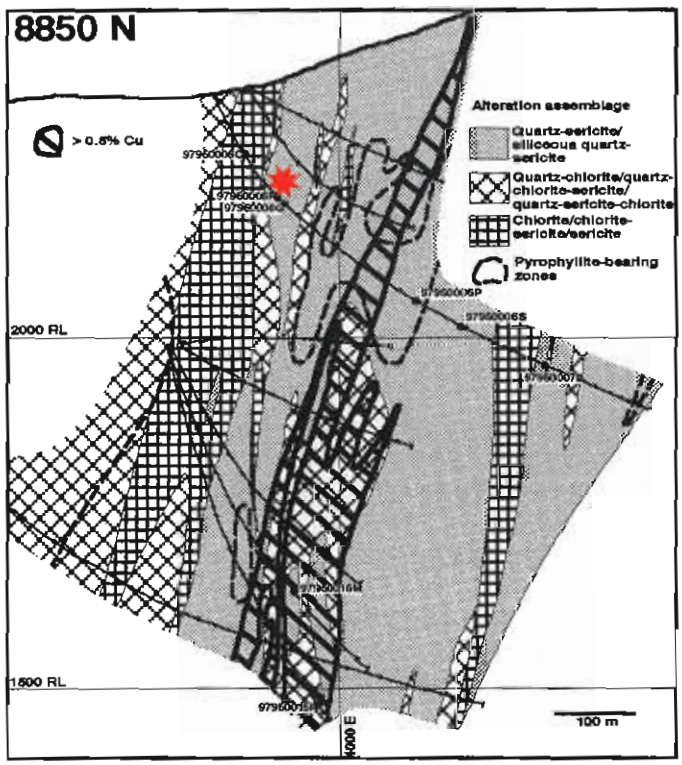

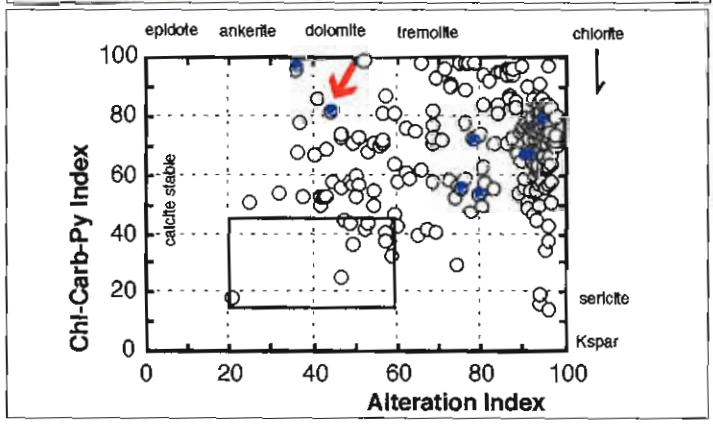

Sample No.	**97950006C**
Location	Western Tharsis, DDH WT0050 @ 87.0 - 87.4
Alteration zone	Outer carbonate halo/chlorite - sericite
Formation	Mt Read Volcanics, Central Volcanic Complex

Description Sheared to massive, chlorite - carbonate altered, andesitic volcanic rock with carbonate veins (not in photo)

Alteration Intensity	none	weak	(moderate)	strong	intense
Alteration Style	patchy	(pervasive)	(veined)		cleavage control
Alteration Mineralogy	Groundmass	chlorite - carbonate			
	Feldspars	albite			
	Mafics				
Interpretation	diagenetic	metamorphic	syntectonic	(hydrothermal)	
Relict Mineralogy					

Geochemistry

SiO_2	TiO_2	Al_2O_3	Fe_2O_3	MnO	MgO	CaO	Na_2O	K_2O	P_2O_5	S	CO2	Al	CCPI	Ti/Zr
47.78	0.51	14.56	12.59	0.19	4.63	5.53	2.07	1.47	0.09	0.04	7.85	44	81	42

Rb	Ba	Cu	Pb	Zn	Sb	Tl	Zr	Nb	Y
46	367	10	6	199	0.5	0.5	72	3	17

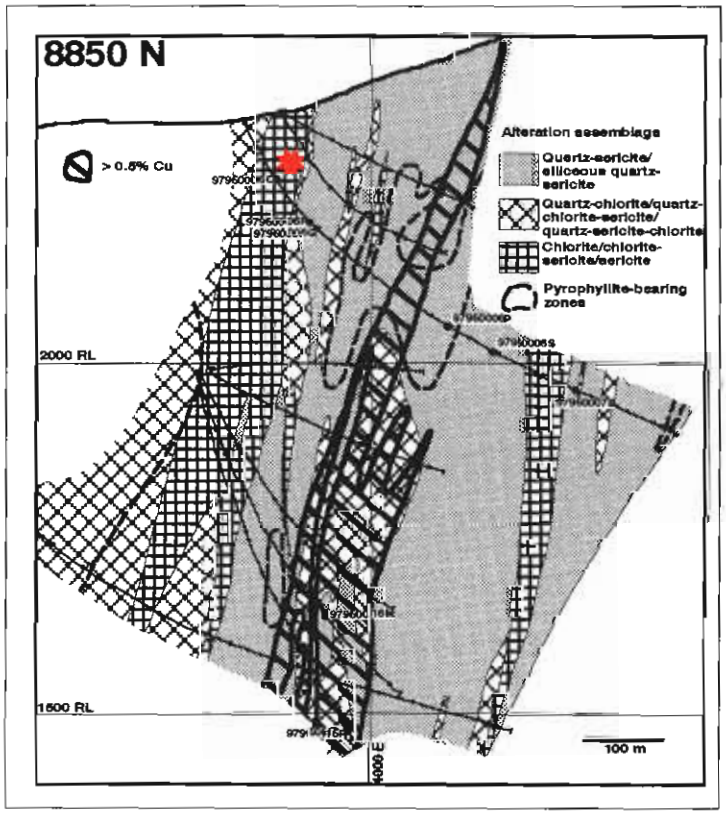

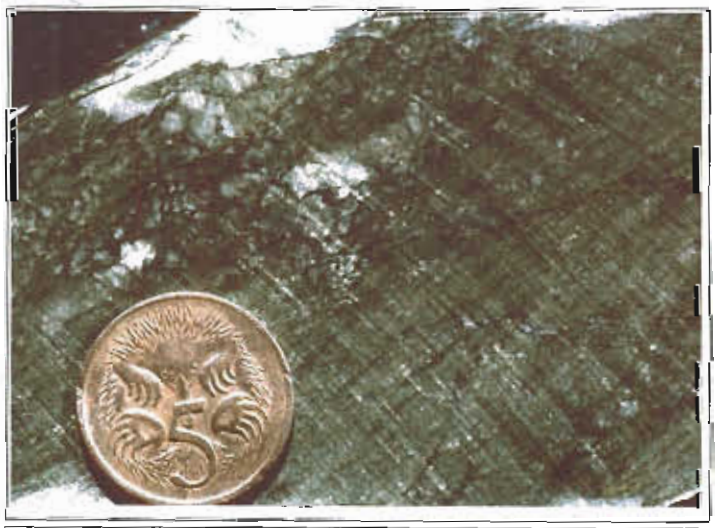

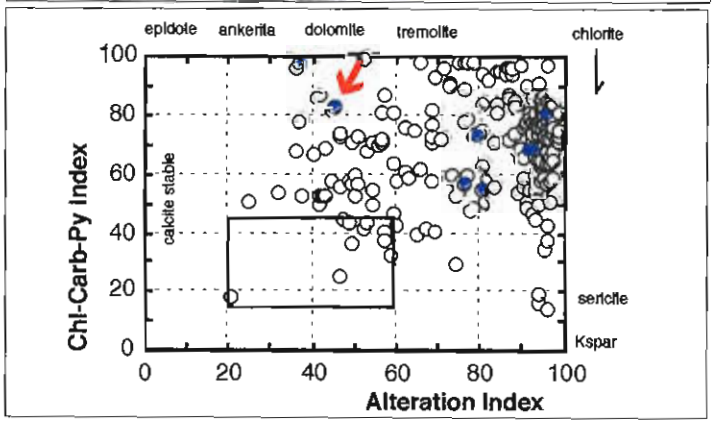

Sample No.	**97950006G**
Location	Western Tharsis DDH WT0050 @ 159.4 - 159.9
Alteration zone	Outer carbonate halo/ quartz - sericite zone
Formation	Mt Read Volcanics, Central Volcanic Complex

Description Quartz - sericite - carbonate - hematite altered rhyolitic volcaniclastic rock

Alteration Intensity	none	weak	moderate	strong	(intense)
Alteration Style	(patchy)	(pervasive)	veined	cleavage control	
Alteration Mineralogy	Groundmass	Quartz - sericite - carbonate - hematite			
	Feldspars				
	Mafics				
Interpretation	diagenetic	metamorphic	syntectonic	(hydrothermal)	
Relict Mineralogy	Nil				

Geochemistry

SiO_2	TiO_2	Al_2O_3	Fe_2O_3	MnO	MgO	CaO	Na_2O	K_2O	P_2O_5	S	CO2	Al	CCPI	Ti/Zr
70.58	0.23	12.12	8.03	0.11	0.68	0.16	0.21	3.63	0.04	0.02	3.12	75	55	5

Rb	Ba	Cu	Pb	Zn	Sb	Tl	Zr	Nb	Y
141	731	6	5	59	2	0.9	266	13	47

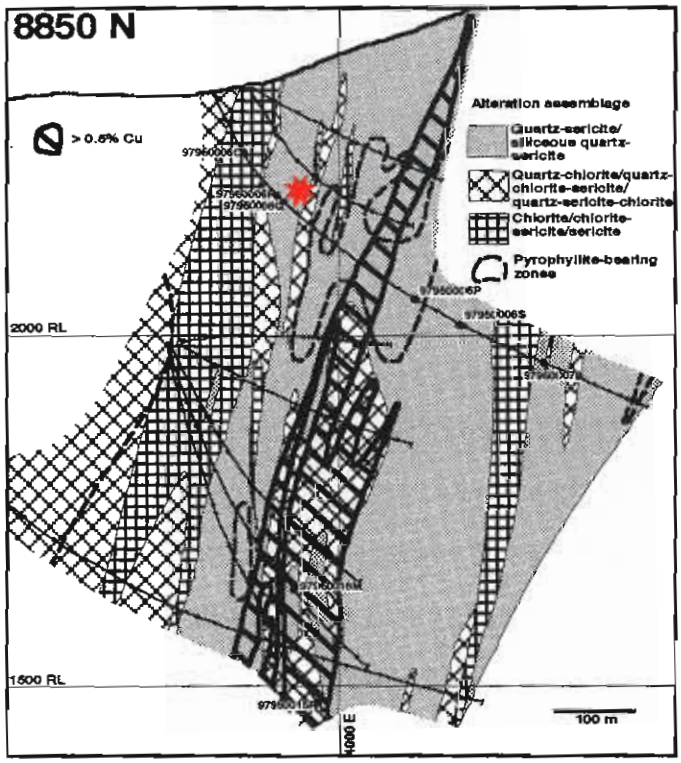

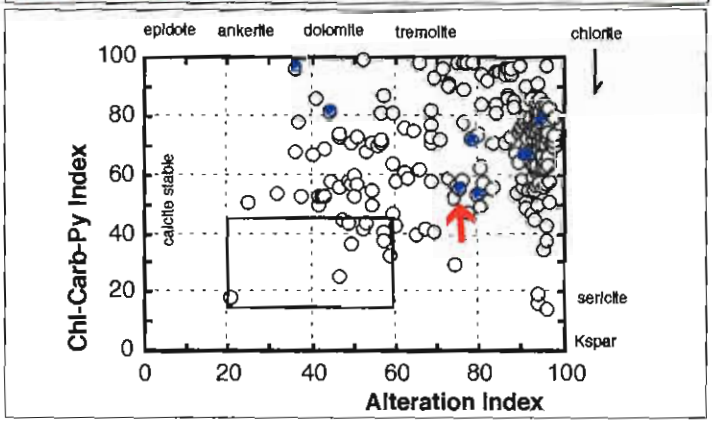

Sample No.	**97950007B**
Location	Western Tharsis DDH WT0050 @ 563.0 - 564.0
Alteration zone	Pyritic halo/quartz - sericite zone
Formation	Mt Read Volcanics, Central Volcanic Complex

Description Quartz - sericite - carbonate - pyrite altered fragmental ? dacitic volcanic rock cut by anastomosing pyrite stringers

Alteration Intensity	none	weak	moderate	strong	(intense)
Alteration Style	patchy	(pervasive	veined)		cleavage control
Alteration Mineralogy	Groundmass	quartz - sericite - pyrite - carbonate			
	Feldspars				
	Mafics				
Interpretation	diagenetic	metamorphic	syntectonic	(hydrothermal)	
Relict Mineralogy	Quartz microphenocrysts				

Geochemistry

SiO_2	TiO_2	Al_2O_3	Fe_2O_3	MnO	MgO	CaO	Na_2O	K_2O	P_2O_5	S	CO2	Al	CCPI	Ti/Zr
60.29	0.35	12.84	10.77	0.52	1.08	1.26	0.13	3.97	0.08	6.28	2.64	78	72	11

Rb	Ba	Cu	Pb	Zn	Sb	Tl	Zr	Nb	Y
120	1737	88	214	138	0.1	1	182	9	23

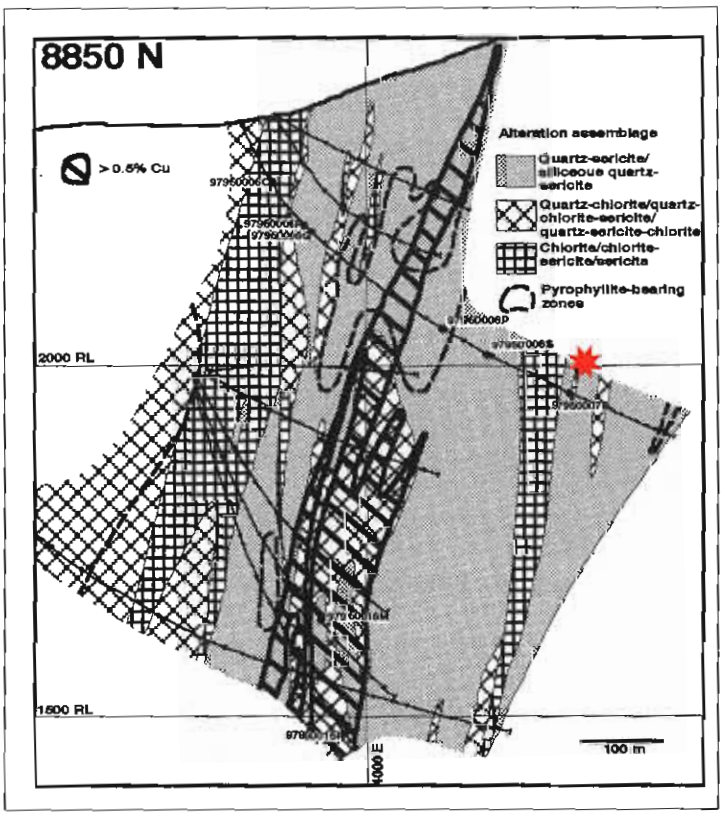

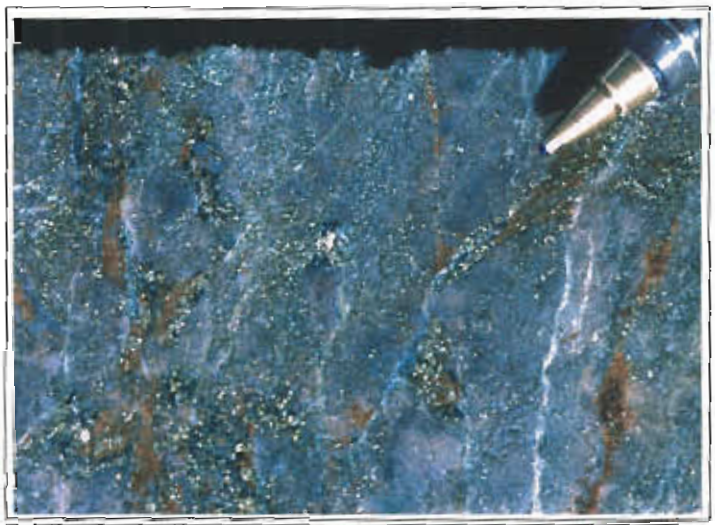

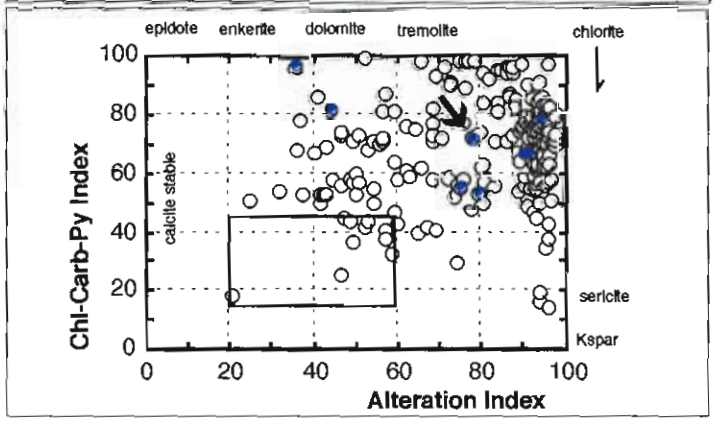

Sample No.	**97950006P**
Location	Western Tharsis DDH WT0050 @ 384.3 - 384.8
Alteration zone	Pyritic halo/quartz - sericite zone - prophyllite subzone
Formation	Mt Read Volcanics, Central Volcanic Complex

Description Siliceous quartz - pyrophyllite - sericite altered rhyolitic volcanic rock

Alteration Intensity	none	weak	moderate	strong	(intense)
Alteration Style	(patchy	pervasive)	veined		cleavage control
Alteration Mineralogy	Groundmass	quartz - pyrophyllite - sericite - pyrite - topaz - barite			
	Feldspars				
	Mafics				
Interpretation	diagenetic	metamorphic	syntectonic	(hydrothermal)	
Relict Mineralogy	Nil				

Geochemistry

SiO_2	TiO_2	Al_2O_3	Fe_2O_3	MnO	MgO	CaO	Na_2O	K_2O	P_2O_5	S	CO2	Al	CCPI	Ti/Zr
80.78	0.24	12.25	2.21	<0.01	0.12	0.03	0.36	1.43	0.05	1.61	0.4	79	54	5

Rb	Ba	Cu	Pb	Zn	Sb	Tl	Zr	Nb	Y
31	1170	72	7	6	0.6	0.5	249	13	6

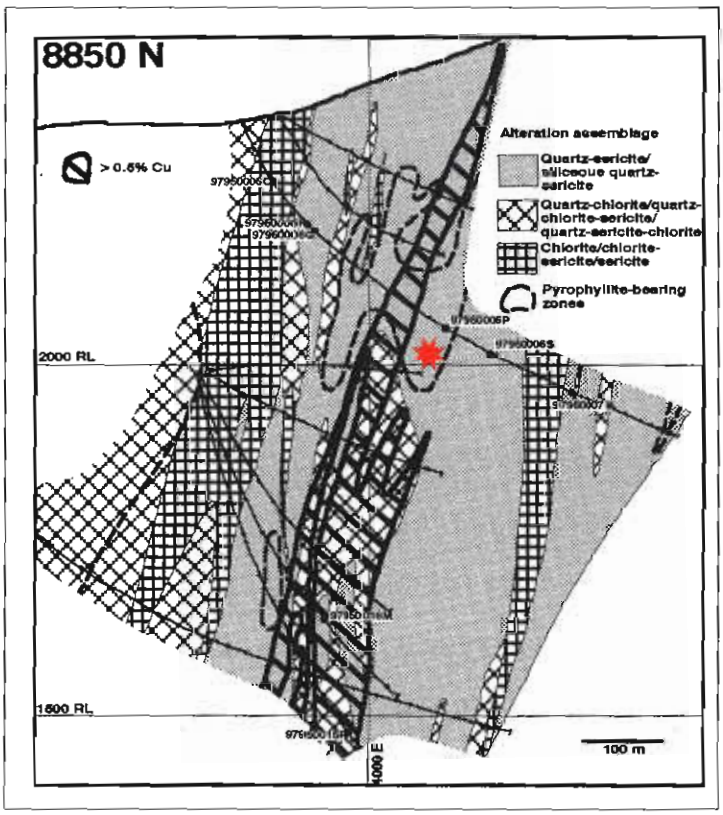

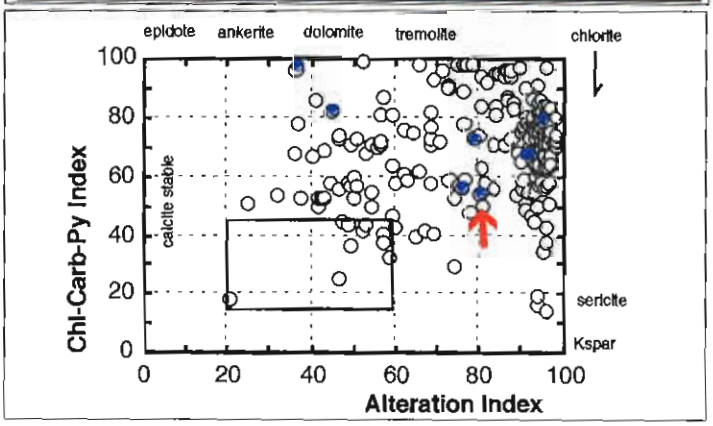

Sample No. 97950016M
Location Western Tharsis DDH 95WTD0091 @ 389.0 - 390.0
Alteration zone Ore zone/quartz - sericite zone

Formation Mt Read Volcanics, Central Volcanic Complex

Description Siliceous quartz - sericite altered rhyolitic volcaniclastic rock with 5 - 7% disseminated pyrite and chalcopyrite in irregular sericitic intersticies

Alteration Intensity none weak moderate strong (intense)
Alteration Style (patchy) (pervasive) veined cleavage control
Alteration Mineralogy Groundmass Quartz - chlorite - sericite - pyrite - chalcopyrite
Feldspars
Mafics
Interpretation diagenetic metamorphic syntectonic (hydrothermal)
Relict Mineralogy Nil

Geochemistry

SiO_2	TiO_2	Al_2O_3	Fe_2O_3	MnO	MgO	CaO	Na_2O	K_2O	P_2O_5	S	CO2	Al	CCPI	Ti/Zr
72.75	0.22	10.11	6.11	0.01	0.36	0.33	0.05	2.8	0.35	4.17	0.0	89	67	6

Rb	Ba	Cu	Pb	Zn	Sb	Tl	Zr	Nb	Y
64	1330	13800	21	32	99	20	200	11	12

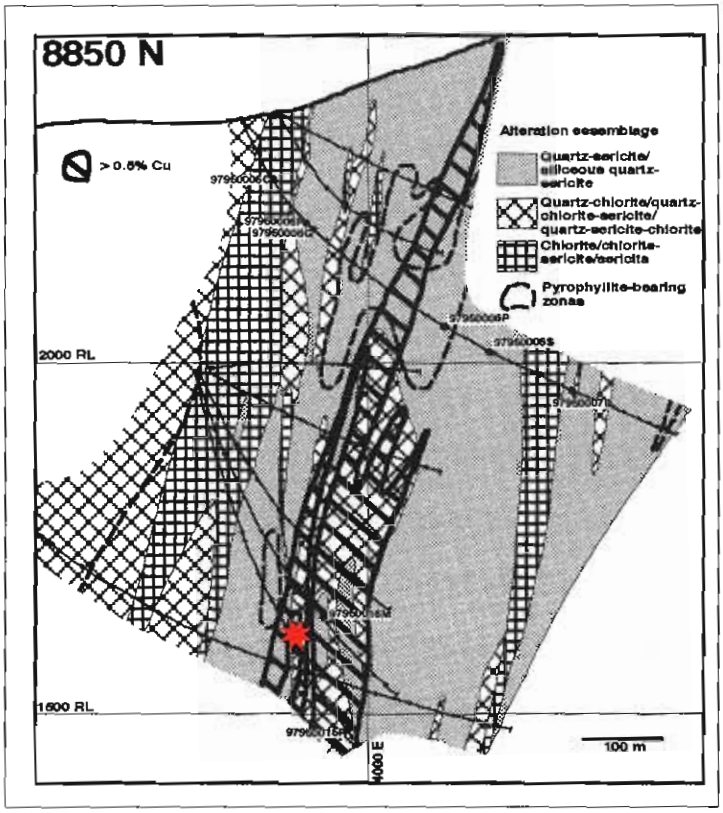

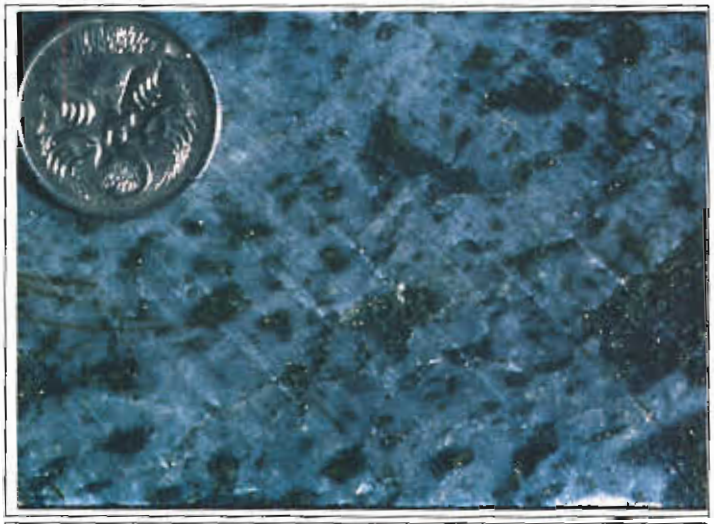

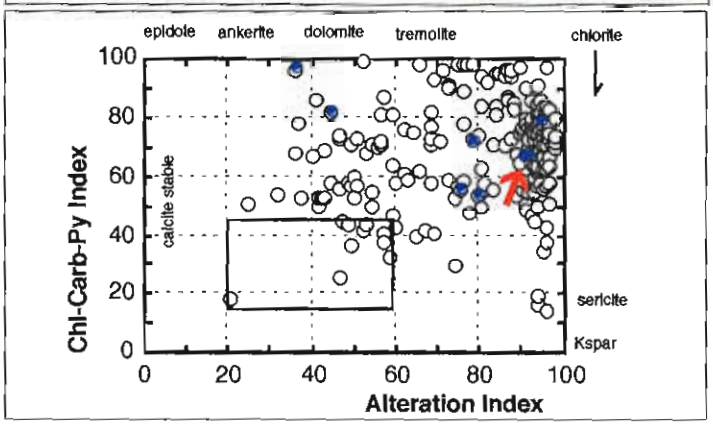

Sample No.	**97950015P**
Location	Western Tharsis DDH 95WTD0090 @ 546.0 - 547.0
Alteration zone	Ore zone/quartz - chlorite - sericite zone
Formation	Mt Read Volcanics, Central Volcanic Complex

Description quartz - chlorite - sericite altered andesitic volcaniclastic rock with disseminated and stringer pyrite and chalcopyrite.

Alteration Intensity	none	weak	moderate	strong	(intense)
Alteration Style	patchy	(pervasive	veined)		cleavage control
Alteration Mineralogy	Groundmass	Quartz - chlorite - sericite - pyrite - chalcopyrite			
	Feldspars				
	Mafics				
Interpretation	diagenetic	metamorphic	syntectonic	(hydrothermal)	
Relict Mineralogy	Nil				

Geochemistry

SiO_2	TiO_2	Al_2O_3	Fe_2O_3	MnO	MgO	CaO	Na_2O	K_2O	P_2O_5	S	CO2	Al	CCPI	Ti/Zr
58.74	0.49	13.65	12.66	0.23	1.75	0.26	0.03	3.45	0.27	5.38	0.17	94	79	17

Rb	Ba	Cu	Pb	Zn	Sb	Tl	Zr	Nb	Y
92	2097	12000	15	99	0.9	0.5	167	13	99

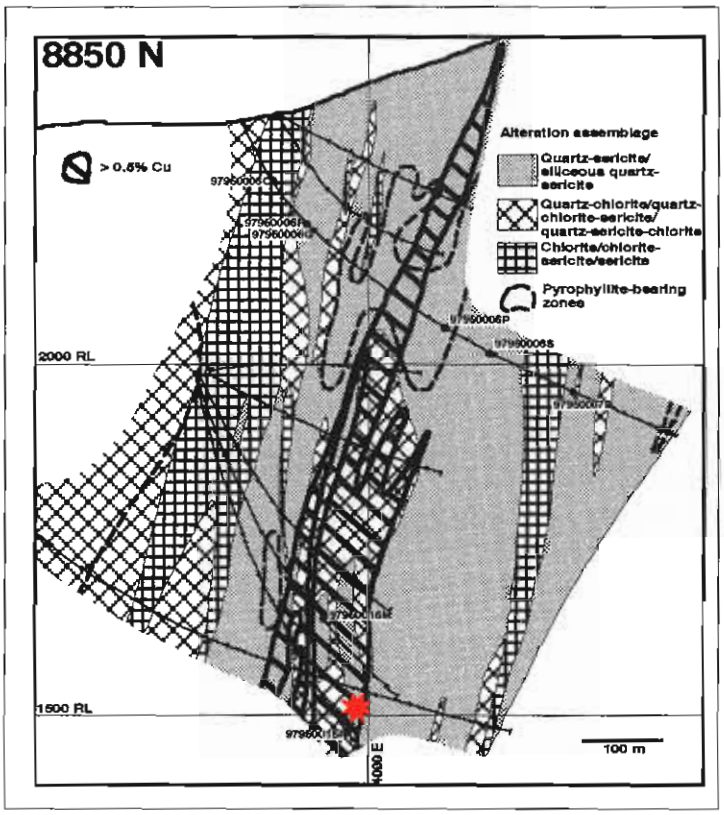

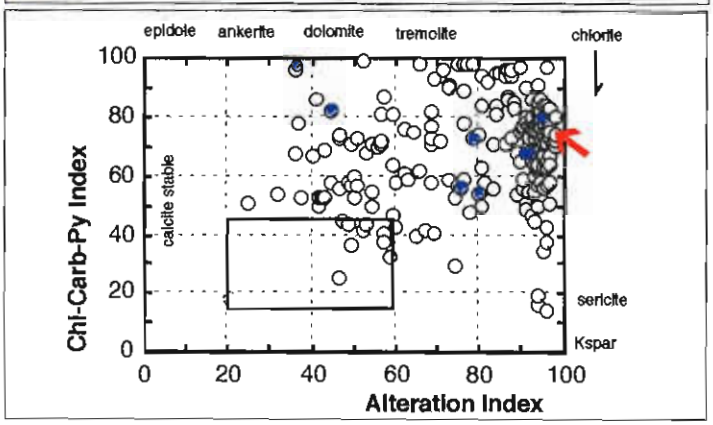

Alteration halo model for the Zone 96 volcanogenic gold deposit, Henty gold mine, western Tasmania

Jason Beckton
Goldfields Exploration, Kalgoorlie.

Introduction

The Zone 96 deposit is a small tonnage (@ 506000 t) , high grade (26 ppm Au) volcanogenic gold deposit hosted within the Late Cambrian Tyndall Group of the Mount Read Volcanics of Western Tasmania.

The following report details structural and geochemical features of the Zone 96 deposit and the surrounding host lithologies. The influence of structure and protolith on the geometry of the alteration system and selected elements within it, will be assessed.

Previous AMIRA report

The previous AMIRA report investigated influence of structure and protolith on the geometry of one alteration type, MQ (Massive Quartz), which is host to most Au metal within the deposit. Exploration vectors towards the entire envelope of alteration and mineralisation styles will be the focus of the following report.

- Beckton J.M. 1997. Geological and Geochemical Characteristics of Zone 96. P439 Report 5, October 1997, p2-3.

Sampling strategy

During reserve definition drilling a total of 240 diamond drill holes were drilled at a spacing of approximately 15x15 m. The following suite of elements have been used in orebody halo analysis as was analyzed for most of the drillholes:

Au - Fire Assay, AAS Finish.
Ag, As, Bi, Cu, Pb, Zn. Determination by AAS or ICP-AES depending on upper detection limit.

Multi-element analysis was undertaken on alteration types to assist in determination of protolith and to attempt to develop a chemostratigraphy for the Zone 96 deposit. Studies concentrated on the MQ alteration type.

Au, Ag, As, Ba, Br, Ca, Ce, Co, Cr, Cs, Eu, Fe, Hf, Ir, K, La, Lu, Mo, Na, Rb, Sb, Sc, Se, Sm, Ta, Te, Th, U, W, Yb, Zn, Zr. Determination by NAA.

Al_2O_3, SiO_2, TiO_2, Fe_2O_3, MnO, CaO, K_2O, MgO, P_2O_5, Na_2O. Determination by XRF.

Ore deposit characteristics

Form of Orebody The Zone 96 Deposit comprises stratabound lenses of Silica–Sericite–Sulphide alteration within Tyndall Group volcaniclastics and epiclastics. Alteration assemblages are differentiated on the basis of silica-sericite-sulphide content. In long projection the deposit has dimensions of 300 m in length and 250 m from top to bottom. Thickness of the alteration system is approximately 50 m. The deposit is located approximately 400 m below the surface.

Size and Grade The Zone 96 1996 reserves are 526,000 t at 26.2 g/t Au, containing 442,678 ounces of gold. Annual gold production is estimated to average 90,000 ounces over a period of 4.5 years. During the 1996–97 financial year, Henty produced 74,930 t at 21.1 g/t Au, recovering 48,377 ounces (De Mark & Callaghan 1997).

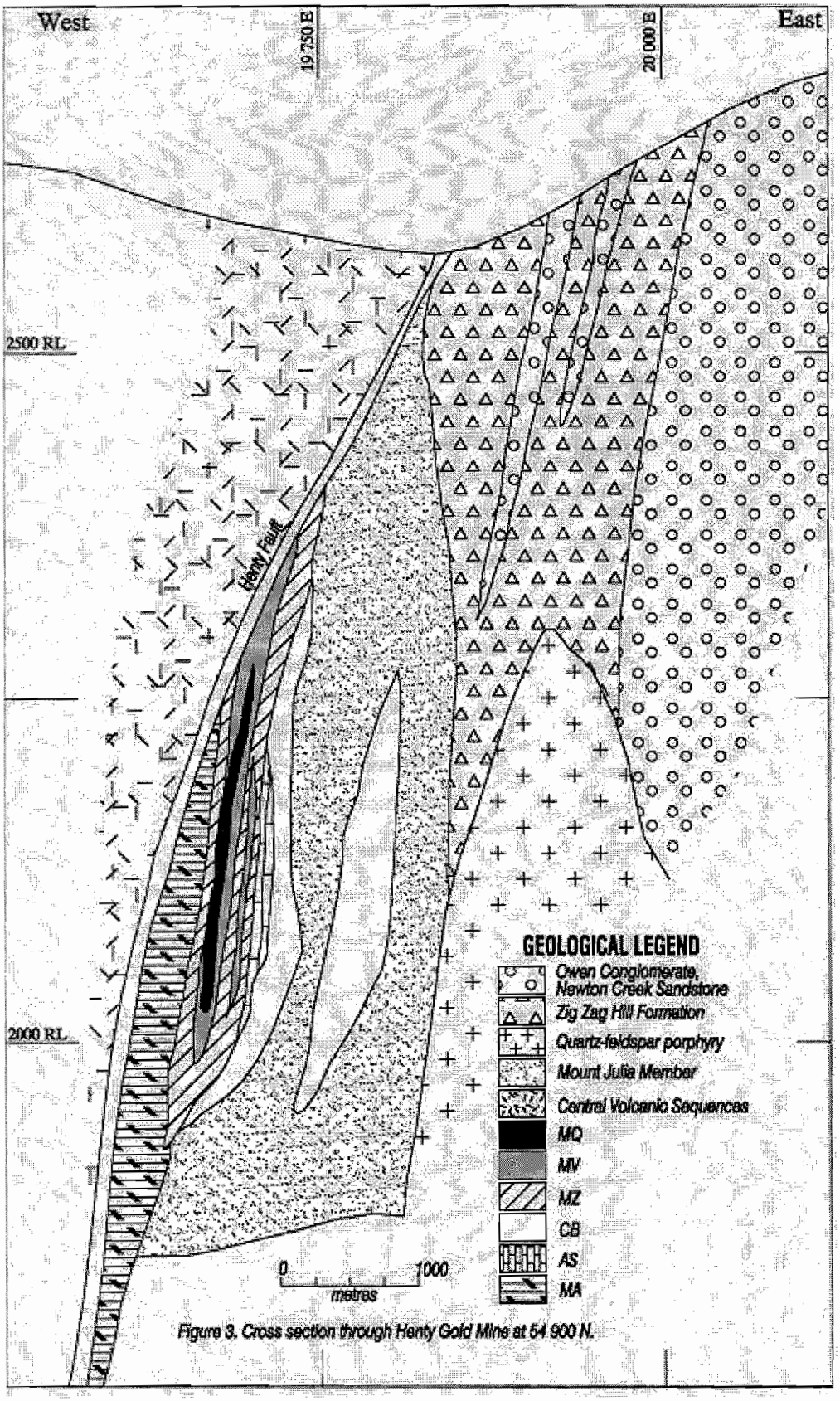

Figure 1: Cross section of the Henty deposit showing host lithologies and alteration system.

Sulphide Mineralogy: Pyrite, chalcopyrite, galena, bismuth (sulphosalts), sphalerite, hessite.

Alteration Mineralogy: Sericite, silica, albite, pyrite.

Deformation: The structural evolution of Zone 96 is related a series of interrelated Devonian events related to noted regional structural evolution as noted above.

NE-SW directed compression which has resulted in resulted in a dominant regional S2 foliation orientated NW oblique to the N-S strike of A-Zone. NW orientated folding has also resulted during this compression phase. **Sulphide and gold has been remobilised from quartz-carbonate-sulphide-gold veinlets within the MQ into developing sericite dominated S2 cleavage.**

High angle reverse faulting related to granite intrusion may have provided fluorite seen within sericite-carbonate-fluorite shears which mark the final stage of S2 cleavage formation.

Dextral wrench has involved a change in azimuth of the principal stress from NE-SW to NNE-SSW. This has resulted in asymmetric geometry of Devonian folds. **Considerable thickening of A Zone units has resulted around an azimuth of WSW.** In long projection an interference pattern that reflects this orientation is evident.

Late sinistral strike slip movement of the Henty Fault has resulted in the generation of brittle faults which are considered to be generally contemporaneous.

Volcanic facies architecture

Regional volcanic facies

Deposit geology is dominated by a regional structural feature, the Henty Fault. The Henty Fault is striking NW and dipping 70° to the West in the vicinity of the deposit. It is a bimodal fault with a Eastern 'puggy' component and an Western mylonitic component. Central volcanics occur to the West of the deposit and mineralised Tyndall Group volcaniclastics and epiclastics occur to the East. The Tyndall group host lithologies generally trend NE and have subvertical dip.

Host-rock volcanic facies

Tyndall Group is divided into Upper and Lower units by Goldfields geologists. This equates to Zig Zag Hill Formation and Comstock Formation.

- Comstock Formation subdivided into the lower Lynchford and Upper Mt Julia Member.
- The Lynchford Member consists coarse, polymict, matrix supported volcaniclastics which host the Zone 96 mineralisation.
- The Mt Julia member is referred to as the Comstock Tuff by RGC geologists. Greater qtz pheno content than Lynchford member.

The main features of Henty mine lease stratigraphy are:

1. Dominantly intermediate, submarine volcaniclastic sedimentation and carbonate deposition of the Lynchford member.
2. Rhyolitic to dacitic submarine volcaniclastic and extrusive/intrusive activity of the Mt Julia member.
3. Extensive quartz porphyry intrusions/extrusions associated with the Zig Zag Hill formation.
4. Gradational and possibly erosional upper contact of the Zig-Zag Hill Owen conglomerate units. (White & McPhie 1996, Callaghan 1996)

Chemostratigraphy

Multielement analysis was undertaken on the main host to mineralisation the MQ. When Th, Sc and Ti are plotted on a ternary diagram after rank

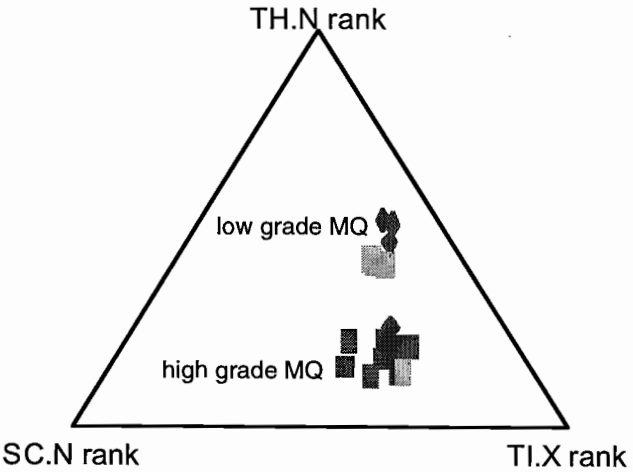

Figure 2. Ternary diagram using multi-element data to distinguish MQ types.

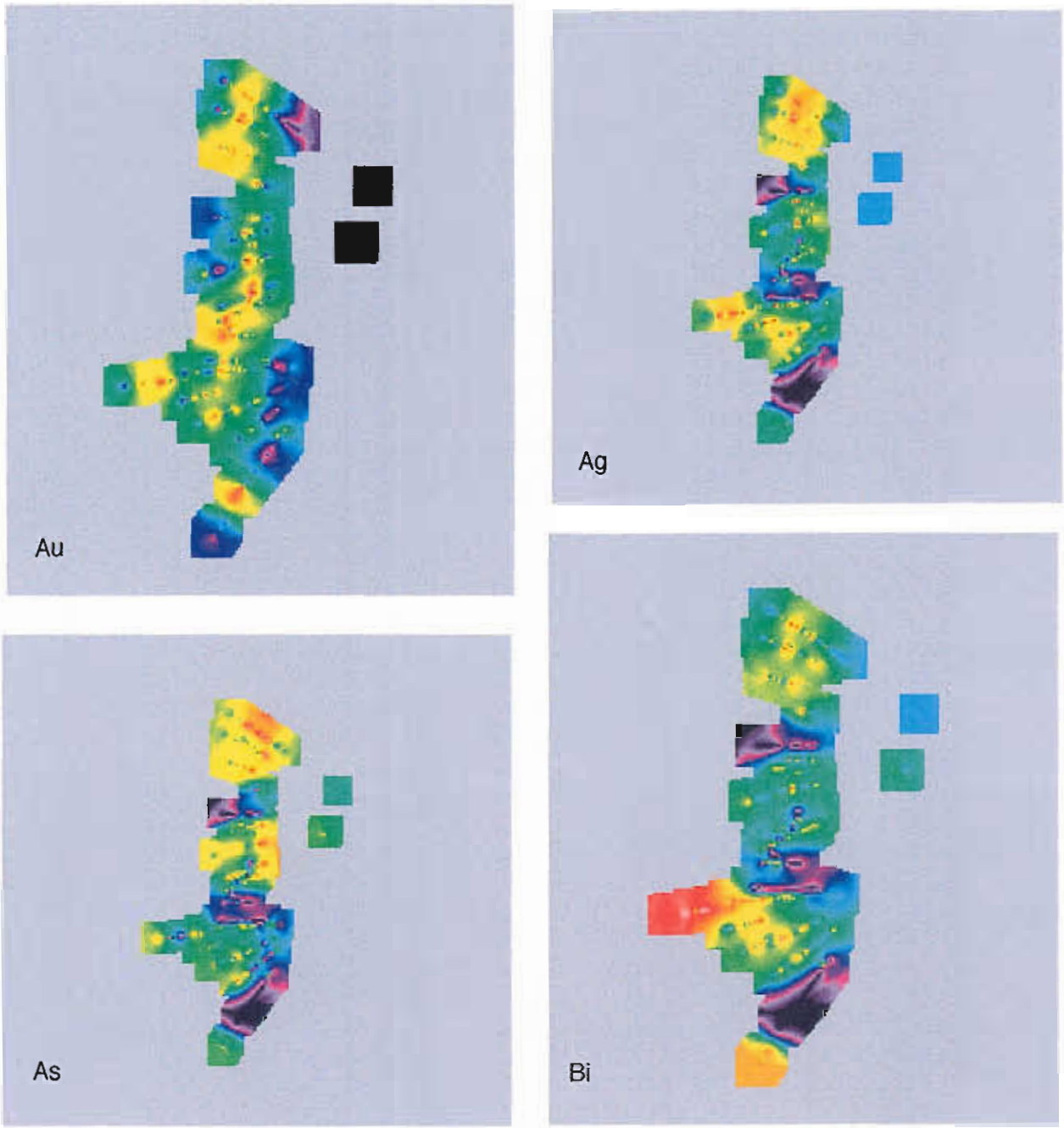

Figure3. Au, Ag, As, Bi, Cu, Pb, Zn, Fe cross sections.

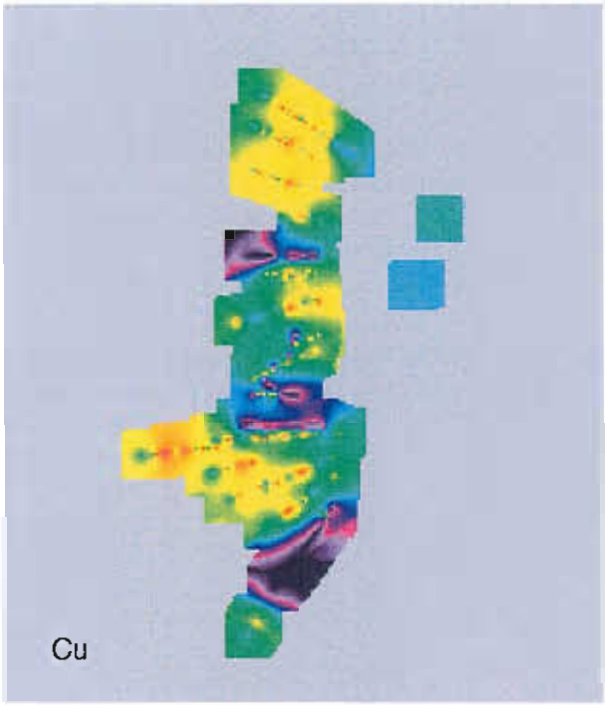
Cu

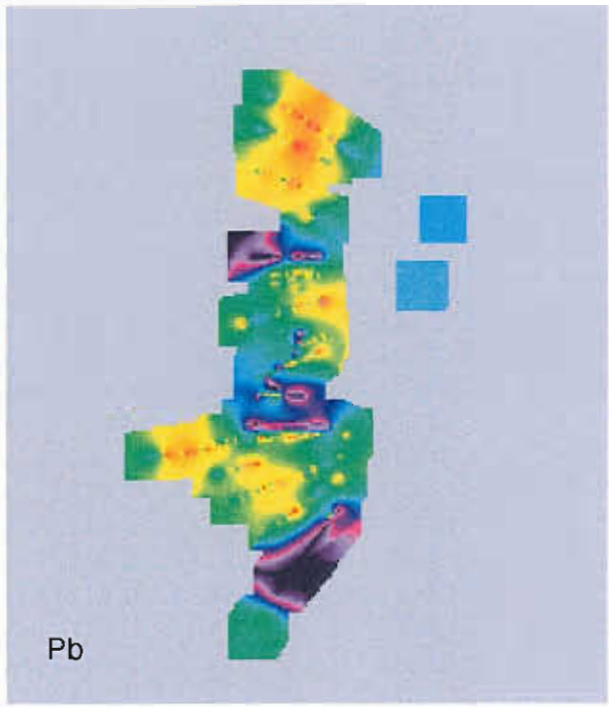
Pb

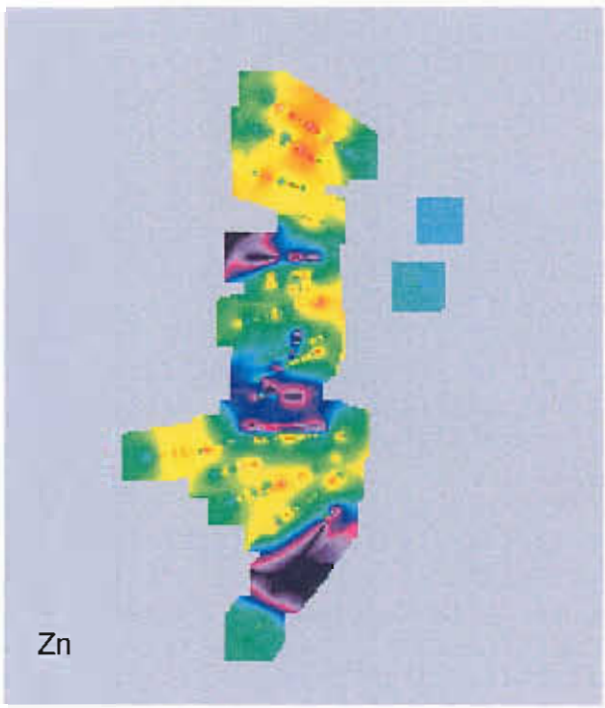
Zn

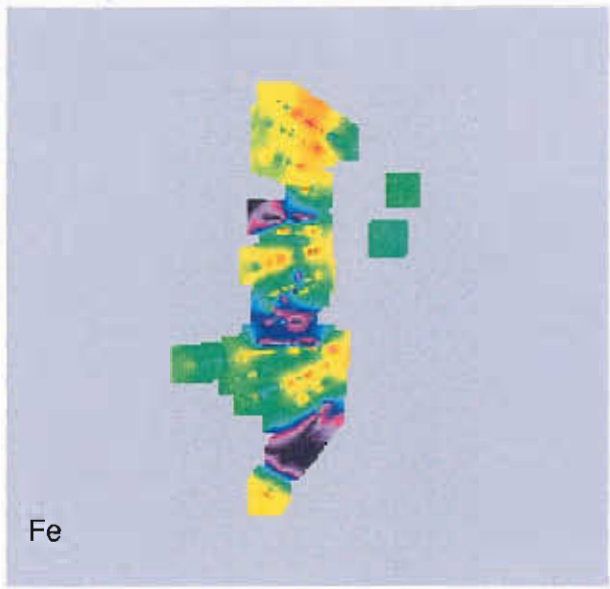
Fe

transforming the data, it is possible to differentiate high grade MQ low grade MQ and from Mount Julia MQ. The protolith for the MQ is thought to most likely a rhyodacitic volcaniclastic. Compositional variations to the north and south may explain Th.

Alteration mineralogy and zonation

The stratigraphy of the alteration system has been described in detail in the previous Amira report. In summary the alteration system is characterised by asymmetry.

Footwall

The stratigraphic footwall is moderately altered with feldspar destruction incomplete and volcaniclastic textures still recognizable. The footwall alteration is labelled MA (moderately altered)and is highly foliated. It is in contact with the Henty fault to the West and the MQ/MZ position to the East.

Ore position

The main ore position comprises Silica-sulphide-(gold) (MQ) enveloped by Silica-sericite (MV) and Sericite-silica-sulphide (MZ) alteration. MV alteration occurs predominately on the stratigraphic hanging-wall side of the MQ and occurs along strike. In thin section the matrix of the MV resembles the MQ, however it is dominated by a sericite overprint.

Hangingwall

MZ alteration texturally in many places closely resembles epiclastic shale seen in the stratigraphic hangingwall. It is volumetrically the most significant alteration assemblage.

Carbonate lenses occur predominantly stratigraphically above the MQ but also below. These units are interpreted from meso and micro scale to have overprinted epiclastic shales. This alteration is probably predating the main silica-sulphide and later sericite forming events. Along strike away from the main alteration zone, chlorite-calcite is the dominant assemblage of this alteration unit.

The hangingwall of the deposit has in many places been Na enriched. Albite-silica alteration (AS) occurs in the stratigraphic hangingwall and appears to have replaced a coherent lithology such a rhyolite sill. This alteration lithology is thickest (up to 20 m) directly above the thickest zones of the MQ alteration.

Halo geochemistry

A series of cross sections (Fig. 3), Level Plans (Fig. 4) and Long Projections (Fig. 5) through the middle of the orebody illustrate Au, Ag, As, Cu, Pb, Zn, Bi and total Fe zonations.

In section Ag and Bi have a strong positive corellation with Au. Cu, Pb, Zn and Fe have negative correlation mostly due to predominance of sulphides within the enveloping MZ and MV assemblages and possible remobilisation during Devonian deformation.

As seems to be mainly associated with the contact between the alteration units and the Henty Fault. Spatial relationship between structural features and As anomalism is a common feature mesothermal Au deposits but may have some application for structural features associated with Henty style mineralisation.

Significant ***negative*** correlation can be seen between Au and Zn. Maximum Zn concentrations occur in the hanging and footwall positions as opposed to the main MQ/Au zone which occurs within the centre of the alteration zone.

Maximum Au concentration is closely enveloped by Zn and Bi in long projection. Arsenic maxima occurs along the trace with the Henty Fault and may also be associated with flat Devonian east dipping faults.

Lithogeochemical halo model and vectors to ore

Henty may be loosely associated with the Cu-Au VHMS classification (eg Mt Lyell). Geochemical exploration for this deposit type must factor in the negative correlation of Zn. Cu, Fe and Pb have a less distinct negative correlation and are probably less useful as halo elements.

Tracing and extrapolation of structural features may be possible with As.

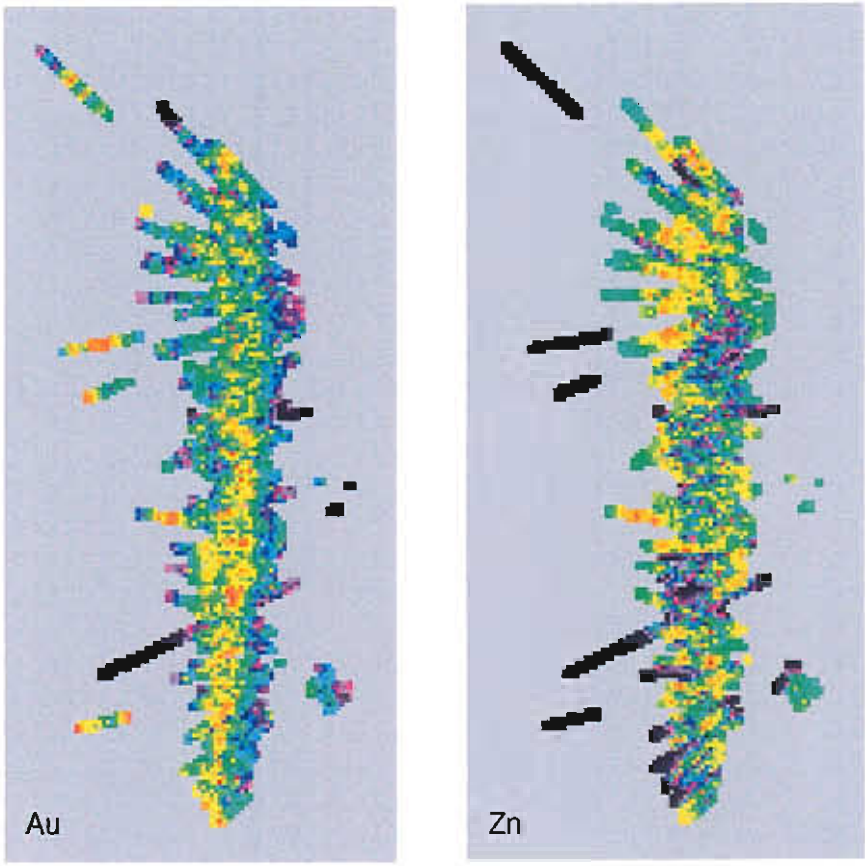

Figure 4. Imaged Au and Zn in level plan

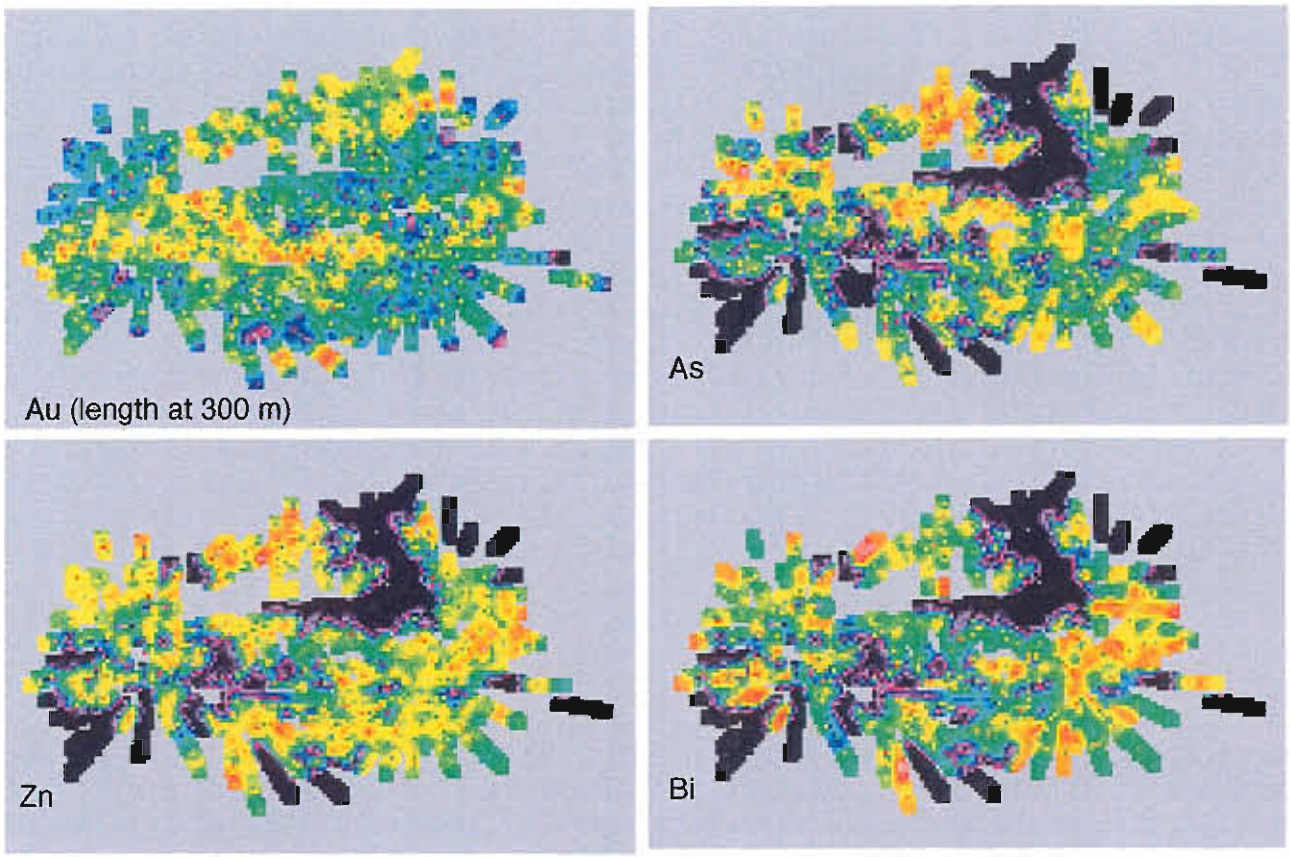

Figure 5. Long projections

Henty system genesis

Henty is interpreted to have been a shallow water gold rich VHMS deposit that has been deformed in the Devonian (Halley and Roberts 1997).

During the deformation episode, sulphides are interpreted to have been remobilised. The main host to Au mineralisation, the MQ failed in a brittle manner during this deformation. Zn appaers to have been remobilised into the surrounding sericite-silica zones during this deformation. Cu, Pb and Bi do not appear to have been as mobile.

High grade gold is associated with the dominant cleavage formed during this deformation however on a deposit scale gold is largely stratabound within the MQ alteration. From structural relationships noted underground (Beckton 1997), the MQ is interpreted to have formed prior to deformation.

Lithogeochemical Halo features noted above are largely thought to be the result of pre-deformation alteration.

References

Beckton J.M. 1997. Geological and Geochemical Characteristics of Zone96. P439 Amira Report 5, October 1997, p2-3.

Callaghan, T. 1996. Stratigraphy of the Henty Mine Lease. RGC Exploration Report.

De Mark, P. and Callaghan, T. 1997. An Overview of the Henty Gold Mine, Tasmania. Within notes for AUSIMM Mine Geologists conference. Launceston.

Halley, S.W. and Roberts, R.H. 1997. Henty: A Shallow Water, Gold Rich VMS Deposit in Western Tasmania. Econ. Geol. Vol. 92, pp. 438-447.

White, M.J. and McPhie, J. 1996. Stratigraphy and paleovolcanology of the Cambrian Tyndall Group, Mt Read Volcanics, Western Tasmania. Aust. Jour. Of Earth Sciences. Vol. 43, pp. 147-159.

Mt Julia–Henty gold mine: Summary of alteration study

Tim Callaghan
Goldfields Tasmania Ltd.

Introduction

The Mt Julia–Henty gold deposits are a series of small tonnage (<500,000 t) high grade (10–30 g/t Au) sheet like lenses hosted in an extensive package (>20Mt) of silica-sericite altered volcanics (Fig. 1) in the Mt Read Volcanics of western Tasmania.

An investigation of the alteration mineralogy and geochemistry of the southernmost lens (Mt Julia) and its similarities with the whole system was undertaken as a thesis for a Masters of Economic Geology at the University of Tasmania. A summary is included in AMIRA Project P439.

Previous AMIRA reports

This final report on the Mt Julia–Henty alteration system summarises some of a previous AMIRA P439 report and documents brief summaries of further research.

The previous report is:

* Callaghan T.J., 1997, Preliminary Investigations on the Geology and Geochemistry of the Mt Julia Prospect: AMIRA P439 Report 5, October 1997.

Ore deposit characteristics

Form of orebody

The alteration system forms a subvertically dipping tabular sheet bound updip by the South Henty Fault and down dip by rapidly decreasing alteration intensity (see figure 2). Mineralisation is confined to lenses within the subvertically dipping alteration system.

Deformation

The alteration system is strongly deformed due to reactivation of the South Henty Fault. The sericitic alteration is strongly foliated and mylonitised and the orebody is now located on the steeply west dipping, overturned limb of a broad shallowly plunging syncline.

Tonnes and grade

The 1996 Reserves for Henty were 526,000t @ 26.2 g/t Au. The 1997 Inferred Resource for Mt Julia is 731,000t @ 7.6 g/t Au.

Ore mineralogy

Pyrite and chalcopyrite with lesser galena–sphalerite and minor gold, electrum, galenobismuth and native bismuth.

Alteration mineralogy

Alteration mineralogy is dominated by silica-carbonate (MQ), silica-sericite-carbonate (MV), silica-sericite-chlorite-pyrite (MZ), albite-silica-chlorite (AS) and carbonate.

Volcanic facies architecture

The Mt. Julia–Henty alteration system is hosted at the base of the Tyndall Group, the highest stratigraphic unit in the Mt. Read Volcanics. Rapid facies changes and discontinuous bedforms are a feature of the Tyndall Group, particularly on the Henty Mine Lease.

Much of the footwall volcanics have been faulted away by the South Henty Fault. Where they are present and identifiable they consist of porphyritic

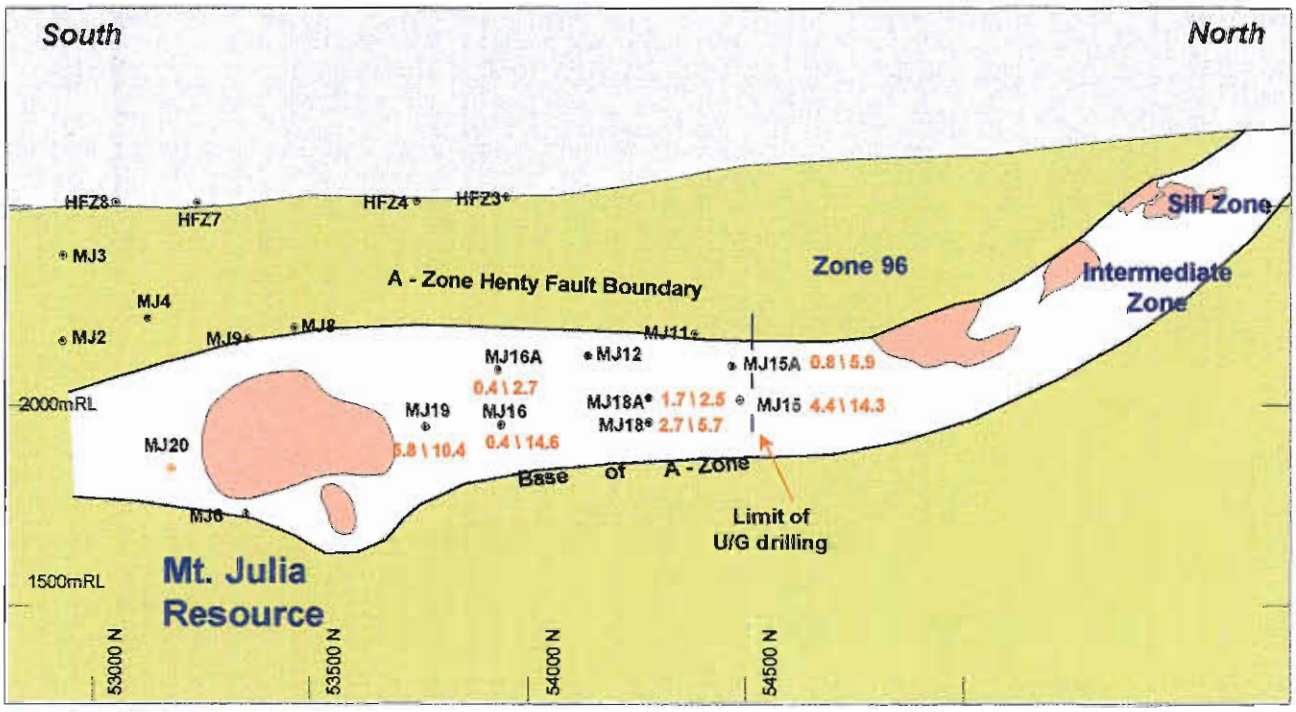

Figure 1. Henty–Mt Julia long projection

rhyolite and polymict volcaniclastic massflows, possibly belonging to the Lynchford Member of the Tyndall Group or the top of the underlying Central Volcanic Complex.

Mineralisation and alteration is hosted in predominantly dacitic feldspar crystal-lithic volcaniclastic sandstones and massflows interbedded with shallow water carbonates and clastic carbonates of the Lynchford Member. Positive identification of the host rock after alteration is difficult, but is assisted by overprinting relationships and immobile element geochemistry. Locally overlying the Lynchford Member at Mt Julia are coherent to hyaloclastic quartz-porphyritic rhyolites and rhyolitic volcaniclastics of the Mt Julia Member (Figure 2). These are overlain by rhyolitic volcaniclastic massflows, quartz crystal sandstones, rhyolitic coherent volcanics and minor siliciclastic conglomerates and shales of the Zig Zag Hill Formation.

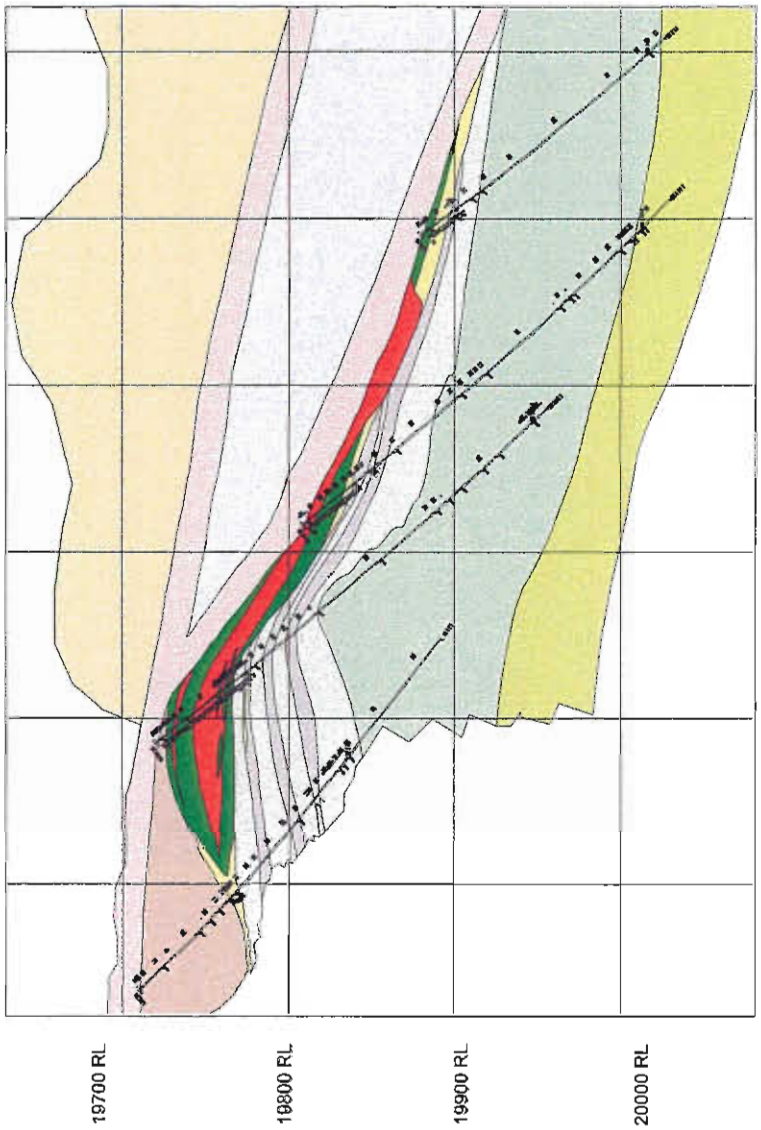

GEOLOGICAL LEGEND - Cross Sections

Ctt	..... Mainly crystal-rich volcanic sandstone and lithic greywacke (quartz-feldspar phyric) Mt Julia Member, Comstock tuff and correlates.
Cttl	..... Crystal-rich volcanic sandstone (feldspar-pyroxene phyric), lithic-rich bases with minor ash, sandstone, siltstone and limestone Lynchford Member, Lynchford tuff and correlates.
Ctl	. .... Quartz-feldspar phyric lava and intrusives.
Ccarb	... ... Exhalitive carbonate horizon
Ccv	..... Mainly felsic pyroclastic rocks, dominantly feldspar phyric, including pumice bearing tuff and breccia, crystal vitric tuff, vitric tuff and minor shale and sandstone
Chs	..... Siltstone and sandstone
MQ	..... Massive quartz-sulphide+carbonate+gold breccia
MV	..... Quartz-sericite+carbonate+sulphide schist
MZ	.. .... Sericite-quartz-sulphide schist
MA	..... Sericite+pyrite+carbonate alteration
	..... Fault

Figure 2. Mt Julia section 53350N.

Chemostratigraphy

The chemostratigraphy is summarised in Figure 3.

Alteration mineral assemblages

The alteration of the Mt Julia Prospect is distinctly asymmetric (Fig. 4) and can be subdivided into three categories, footwall alteration, alteration associated with mineralisation (A-Zone) and hangingwall alteration. Alteration is similar to that of Zone 96 and the Sill Zone but generally has a lower sulphide content. Other small alteration zones associated with gold mineralisation occur higher in the stratigraphic sequence (B-Zone, C-Zone etc.).

Footwall alteration

Footwall alteration at Mt. Julia consists of intensely foliated to mylonitic sericite-pyrite-carbonate-silica (MA) altered rhyolitic volcaniclastics, lavas and sills. Minor fuchsite-sericite altered dykes are characteristic of the footwall alteration. Late carbonate veining is common throughout footwall altered rocks. Occasionally relict clastic textures of mass flows and porphyritic textures of rhyolites are preserved in an intensely sericitised and foliated matrix. Pyrite content varies from 0–2%.

A-Zone alteration

A-Zone at Mt Julia is dominated by silica-sericite schists (MV) with lesser silica-carbonate alteration (MQ) and silica-sericite-pyrite (MZ) schists. This is quite different from Zone 96 where A-Zone is dominated by MZ with lesser MV and MQ, reflecting the overall lower sulphide content of the Mt Julia deposit.

MQ is an intensely silicified and brecciated, possibly intermediate volcanic. The rock is composed dominantly of silica and carbonate veins with lesser sericite. Contacts with MV are often interfingered and gradational with increasing sericite contents. Occasional jasper clasts are preserved within both MQ and MV type alteration.

MV is an intensely silicified and sericitised indeterminate though possibly intermediate volcanic. The rock is intensely deformed and contains numerous silica-carbonate veins.

MZ often interfingers with MV and appears to be a similar rock but contains variable amounts of disseminated pyrite to 5% and is less silicified.

The asymmetry of A-Zone is apparent as very minor massive sulphide (MS) and massive pyrite (MP) is associated with carbonate horizons concentrated near the top of the A-Zone alteration. Most of the massive sulphides appear to be massive sphalerite-galena veins with lesser disseminated and banded sphalerite and galena.

Carbonates (CB) can occur as massive, white to pink limestones but more commonly as carbonate impregnated volcaniclastics. Carbonates, although frequently occurring near the top of A-Zone, are not restricted to this position and occur at the base of A-Zone on some sections (MJ013). Jasper nodules or clasts are a feature of the sediments hosting the carbonate horizons. There is no barite associated with the carbonates or massive sulphides. The carbonates formed earlier and possibly independently from the gold mineralising event.

The sericite-silica-sulphide alteration overprints earlier carbonate and jasper alteration and albite-silica alteration.

Hangingwall alteration

Rocks in the immediate hangingwall to mineralisation are strongly to intensely albite-silica (AS) and albite-silica-chlorite altered depending on the chemistry of the protolith. Albite forms zoned euhedral crystals nucleated on pre existing feldspars giving a pseudo porphyritic texture to some rocks, but more commonly occurs as pervasive fine grained albitisation of the entire rock mass. The albitisation varies from a complete, pervasive texture destructive alteration, to a bleaching of volcaniclastics with orange albitic reaction rims, to alteration of the fine grained matrix of coherent volcanics whilst preserving most primary textures. Hangingwall alteration can extend up to 100 m above the mineralised horizon.

The alteration zone has not been closed of to the north and south. Drillholes MJ008, MJ004 and MJ009 close off the mineralisation updip and MJ006 and MJ007A close it off down dip.

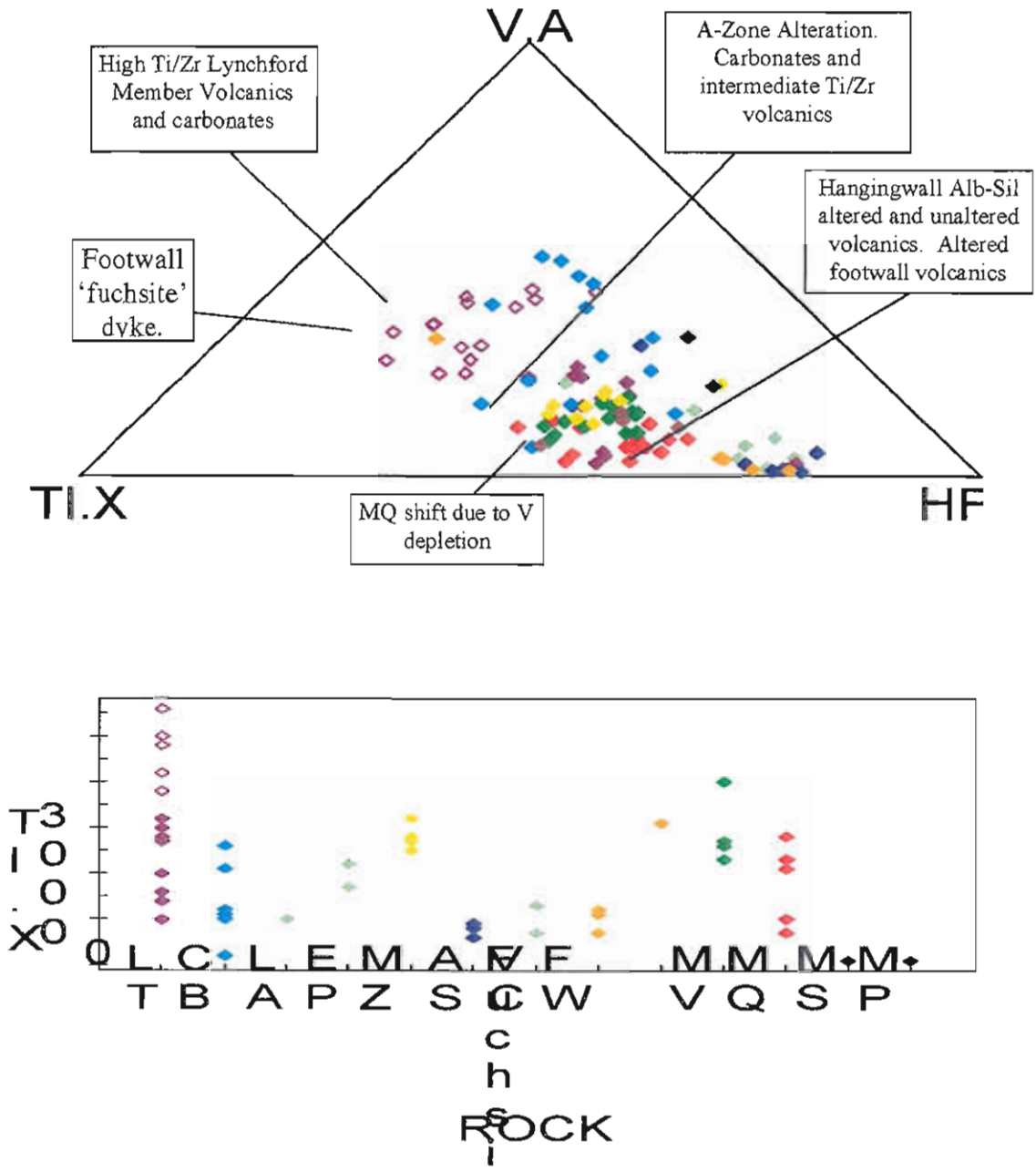

Figure 3. Chemostratigraphy of Mt Julia Legend — LT = Lynchford Member, CB = carbonates, LA = Mount Julia Member rhyolite, EP = Mount Julia Member rhyolitic epiclastics, MZ = A-Zone silica-pyrite-sericite schist, AS = Mount Julia Member intensely albitised rhyolite, VC = Mount Julia Member volcaniclastics, FW = footwall sericite-pyrite-carbonate altered rhyolites, Fuchsite = footwall sericite-fuchsite altered dyke, MV = A-Zone silica-sericite schist, MQ = A-Zone intense silica-sulphide alteration, MS = massive sulphide, MP = massive pyrite.

Wholerock geochemical halos

Useful geochemical haloes for exploration can be divided into two categories, wholerock geochemical haloes, and metal zonation haloes within A-Zone. As the metal zonation has not been documented yet it will be dealt with in a separate section.

Na_2O–K_2O

The most useful wholerock geochemical halo is the variation of Na_2O and K_2O through the system. The footwall and A-Zone alteration is intensely Na_2O depleted and K_2O enriched. This directly related to the feldspar destruction and sericitisation of the footwall and A-Zone rocks. The hangingwall alteration is strongly Na2O enriched at the expense of K_2O. This is a reflection of the albitisation prevalent in the hangingwall rocks. The boundary between Na_2O depleted and Na_2O enriched zones is generally sharp.

Immobile elements

Immobile elements Al2O3, Sc, V, Nb and Y have been depleted and Th enriched in the MQ alteration. However the analysis of, and plotting of the local variations of these elements is not a practical exploration tool as only the MQ is depleted and this is the target alteration.

Metal zonation haloes

Introduction

Routine sampling of drillcore on the Henty Mine lease has involved analysis of half core for Au, Ag, As, Cu, Pb, Zn and Bi. Sampling has occurred generally on 1m lengths with respect for geological boundaries. All A-Zone sulphide-sericite-silica alteration has been analysed. Discontinuous sampling has occurred in the footwall and hangingwall alteration packages. Not all of the above mentioned elements have been assayed routinely resulting in some areas of missing data throughout the data base.

A large database over more than 2 km of strike length between Mt. Julia and the Sill Zone has provided some useful information on the mineralising system, particularly metal zonation within the alteration package.

The data is stored in an Access database at the Henty Mine and has been manipulated in Datamine prior to analysis using RGC's in-house geochemical analysis system (GAS). Metal concentrations for A-Zone intersections have been composited and the weighted average grades and metal accumulations for each intersection log transformed and used to model metal zonation in long projection.

Results

Colour imaging of log values of both A-Zone averages and A-Zone metal accumulations for the above mentioned elements in both N–S longprojection and E–W sections have been created. Both the metal accumulations and metal averages show similar trends with the accumulations giving more prominent anomalies with the exception of the thinner lenses such as the Sill Zone and the MJ016 area (53900N). Metal accumulations only are presented in this report (Figs 6 to 11).

Several trends are obvious on the long projections including:

- The metal accumulation plots highlight the high Au lenses of the Sill Zone, Intermediate Zone, Zone 96, MJ015 and two discrete lenses within the Mt. Julia resource area (Fig. 5). Several other smaller, high Au zones are present, one below the Sill Zone, drillhole HP134, and another above Zone 96, associated with several holes around the discovery hole HFZ5.

- Ag forms a strong positive correlation with the high Au zones (Fig. 6). Ag appears to be more tightly focused on the highest grade Au zones than even Au grades. This is evident in both long projection and section. There is not a strong Ag anomaly on the northern lens of the Mt Julia deposit suggesting that the MJ005E lens is on the periphery of a high grade lens. The prominent Ag anomalies on MJ015 and the southern Mt Julia lens suggest that these are good targets for defining further high grade resources.

- As forms broad, dispersed highs surrounding the high Au zones with lows centred over the high Au centres (Fig. 7). Unfortunately much of the Mt.

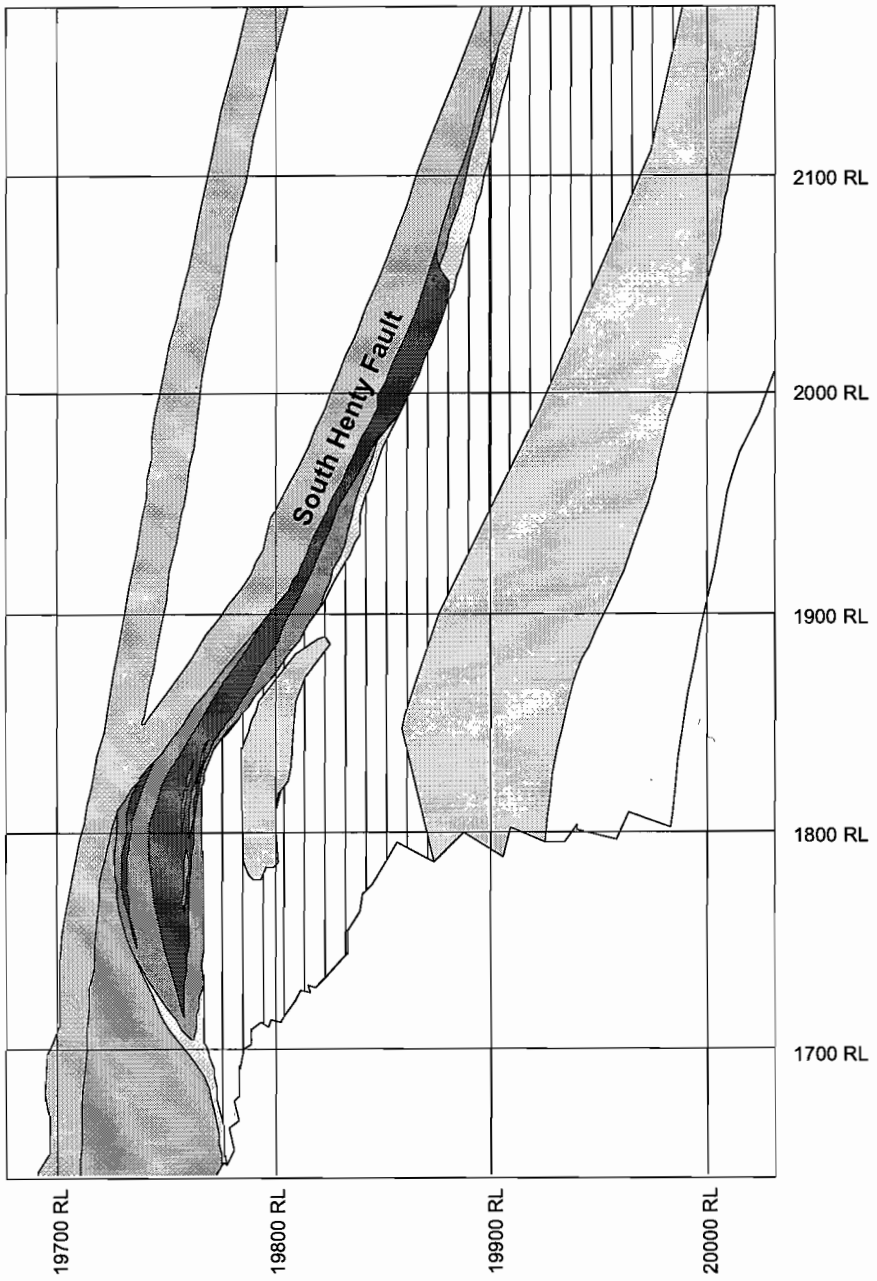

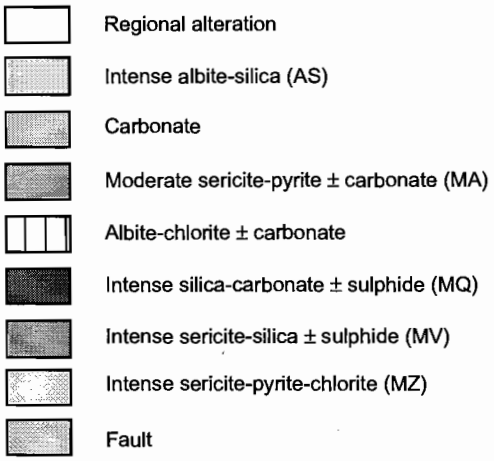

Figure 4. Mt Julia alteration section 53350N.

Julia core has not been routinely sampled for As. Because not all intersections have been analysed for As and some of the As analysis have been calculated with different detection limits, this data should be handled with caution.

- There is a positive association of Bi, Cu and Pb with high Au zones but these elements form distinct proximal halos of highest accumulations around the high Au zones (Figs 8, 9, 10). The southern Mt Julia lens and the MJ015 lens appear to have significant Bi, Cu and Pb haloes again suggesting these are prime targets for identifying a high grade resource. In section Cu forms a broad halo around the gold mineralisation, with most Cu in the hangingwall and footwall. Pb forms a positive correlation with Au but also concentrates laterally, above the high Au Zone.

- There is a negative correlation of Zn with the high Au zones but Zn forms a distinct, strong proximal halo to the Zone 96 resource with most zinc concentrating on the updip side (Fig. 11). Again the southern Mt Julia lens and MJ015 area are good followup targets for resource drilling.

Lithogeochemical halo model and vectors to ore

Distal halos and vectors

Albite-silica, albite-silica-chlorite, albite-silica-chlorite-carbonate alteration of hangingwall (lithology dependant).

Sericite-pyrite-carbonate alteration of footwall and A-Zone margins.

Immobile element lithogeochemistry to identify favourable stratigraphy.

Bedded carbonates as stratigraphic markers?

Na_2O depletion and K_20 enrichment of the footwall.

Na_2O enrichment and K_2O depletion of the hangingwall.

Proximal vectors

Alteration zonation from sericite-chlorite-pyrite to sericite-silica to silica. Carbonate is ubiquitous but bedded carbonates generally occur near the stratigraphic top.

Depletion of Al_2O_3, Y, Nb, Sc and V.

Addition of Th (Mt Julia only).

A-Zone metal accumulation halos.

Broad distal As halo.

Localised distal Zn halo

Positive Bi-Cu-Pb correlation with Au with prominent halos surrounding local high Au zones.

Strong Au-Ag correlation.

Genetic Considerations

The Henty deposits have been considered to be gold-rich, shallow water VHMS style deposits (Taheri and Green, 1992, Halley and Roberts, 1997, Yeats 1989). This is based mainly on the asymmetry of the alteration with the carbonates and small massive sulphides representing an exhalative facies of mineralisation. Sulphur isotope data (Taheri and Green, 1992, Yeats 1989) suggest the sulphides have formed from reduced Cambrian seawater.

However there are a few problems with this model. One is the position of the alteration system at the time of formation (seafloor or sub seafloor). The other is a probable magmatic component of the fluid.

The carbonates are probably not directly related to the mineralising fluids for the following reasons:

They occur at many stratigraphic levels over a strike length of approximately 20 km, commonly not associated with hydrothermal systems. This is supported by their varied lithogeochemical signature whilst A-Zone has a unique signature.

They are overprinted by the albite silica alteration as well as the sericite-silica alteration.

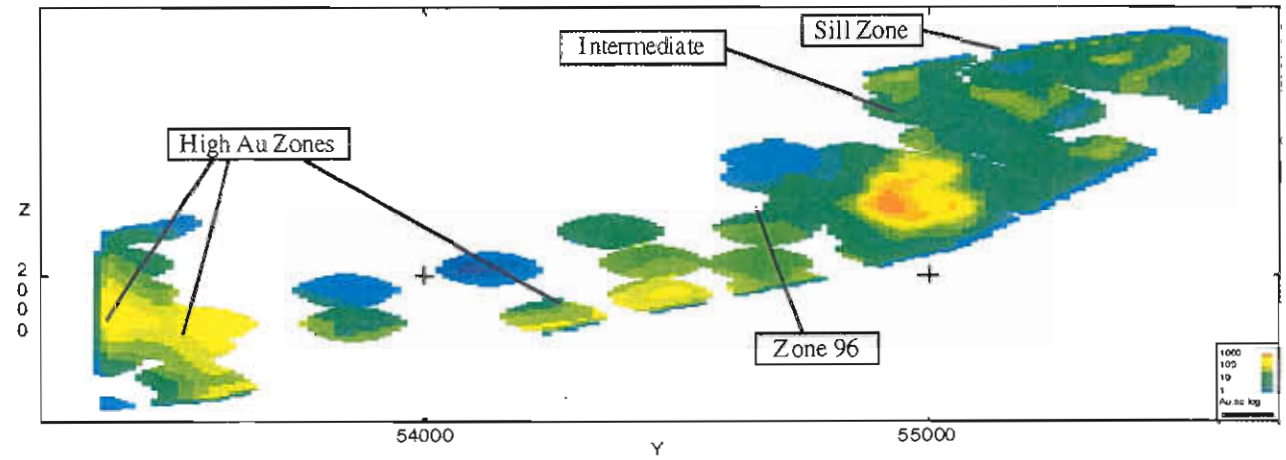

Figure 5. Colour imaging of A-Zone Au accumulations (gmetres). Henty-Mt Julia Long Projection

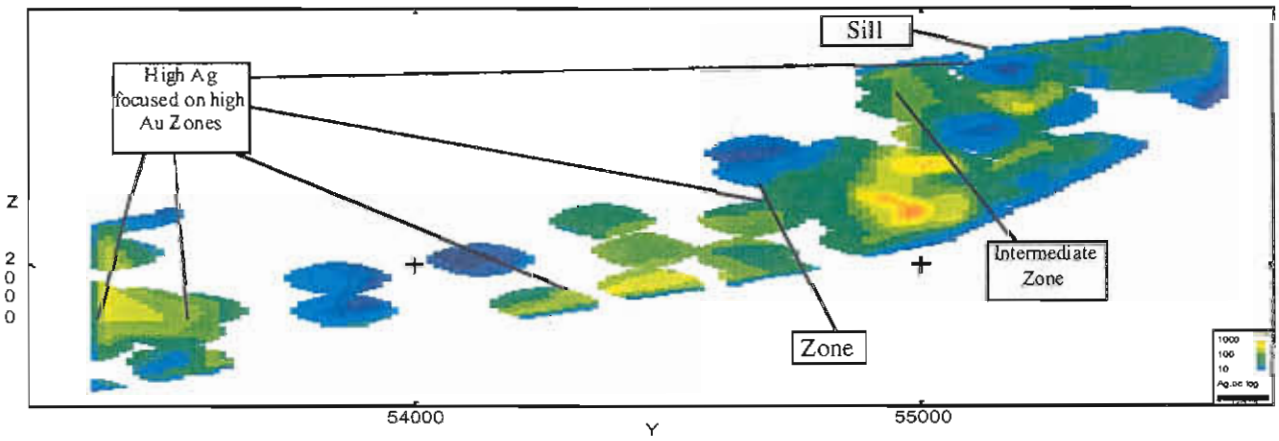

Figure 6. Colour imaging of A-Zone Ag accumulations (gmetres). Henty-Mt Julia Long Projection

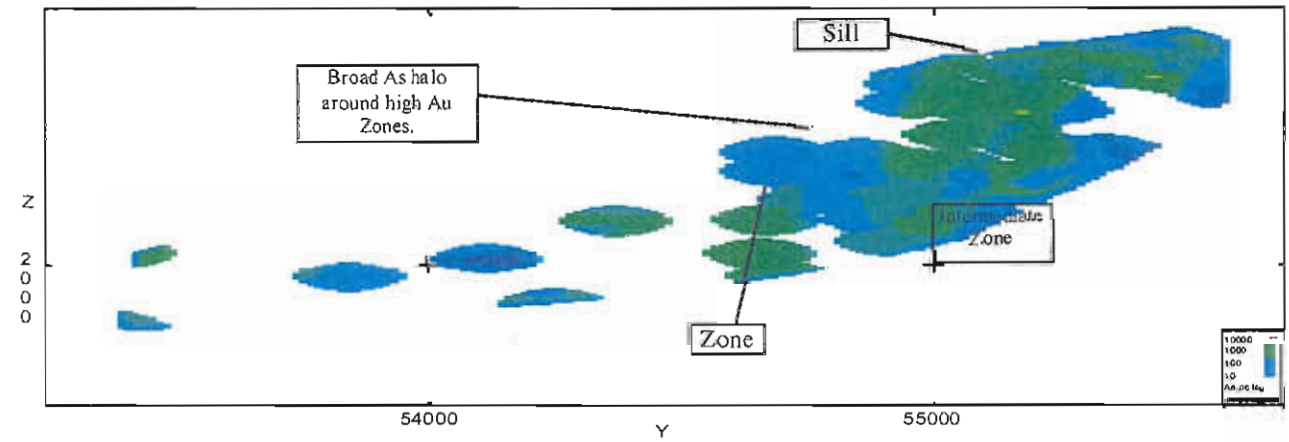

Figure 7. Colour imaging of A-Zone As accumulations (gmetres). Henty-Mt Julia Long Projection.

The carbon and oxygen stable isotopes of carbonates throughout the district (unpublished company data) exhibit trends that can be explained by water–rock interaction at the Henty–Mt Julia deposits (G. Davidson, unpublished Resolute Ltd. company report).

Carbonate and jasper clasts have been reworked and occur as clasts in many stratigraphic positions throughout the district. MQ and AS clasts have not been identified in clastic rocks (as yet).

Therefore the carbonates are not good evidence for the Henty system to have formed at the Cambrian seafloor. It is more likely that the deposits occurred subseafloor. The massive sulphides have quite probably replaced the carbonates in the pyrite stable alteration zone (MZ).

A magmatic component to the mineralising fluid is suggested by the following criteria:

Cu–Bi association.

The intense depletion of MQ is atypical of VHMS systems, but can occur in advanced argillic and leached silica alteration associated with high sulphidation (acid sulphate) and copper porphyry systems. The alteration zonation from strongly depleted silica (MQ) to silica-sericite stable (MV) to silica-sericite-pyrite-chlorite stable (MZ) indicates an increase in pH of the hydrothermal fluid, perhaps as a result of buffering with bicarbonate rich fluids present in the volcanics and carbonates.

Fluorite association. There are late flourite veins in MV alteration formed from liberation of fluorine during recrystallisation of sericite. The flourine rich sericite may indicate some fluorine input from a magmatic source during the mineralisation event.

It is most likely that the Henty–Mt Julia deposits are sub-seafloor epigenetic deposits formed from high sulphidation magmatic fluids with a lesser VHMS component.

References

Halley, S W and Roberts, R H, 1997. Henty: A shallow water, gold rich VMS deposit in Western Tasmania, *Economic Geology*, V92, pp438–447.

Taheri, J and Green, G R, 1991. The origin of the gold mineralisation at the Henty prospect, *Department of Resources and Energy, Division of Mines and Mineral Resources, Report* (unpublished)

Yeats, C. J. 1989. The Geology and mineralisation of the Henty Prospect, Honours Thesis, University of Tasmania Geology Department, 1989.

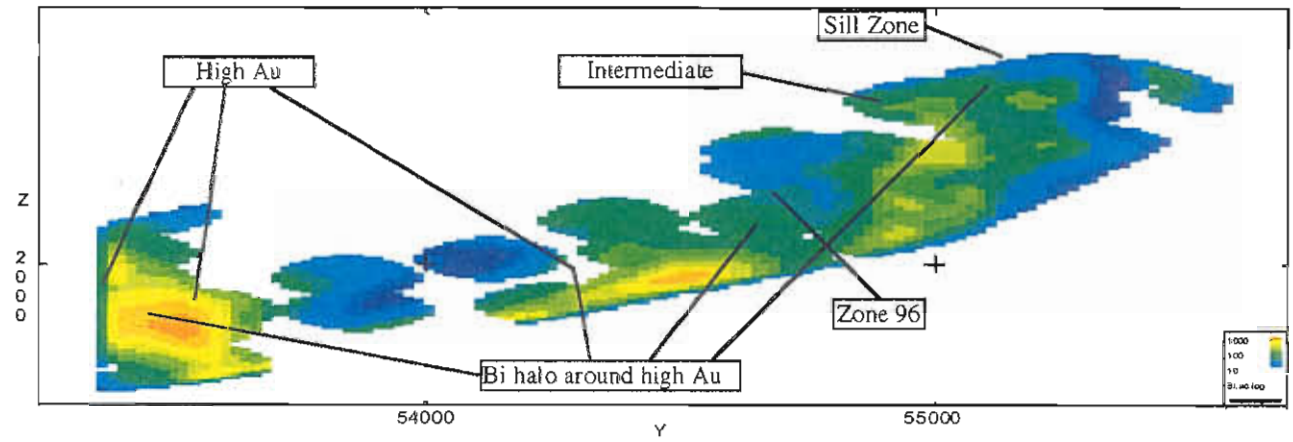

Figure 8. Colour imaging of A-Zone Bi accumulations (gmetres). Henty-Mt Julia Long Projection

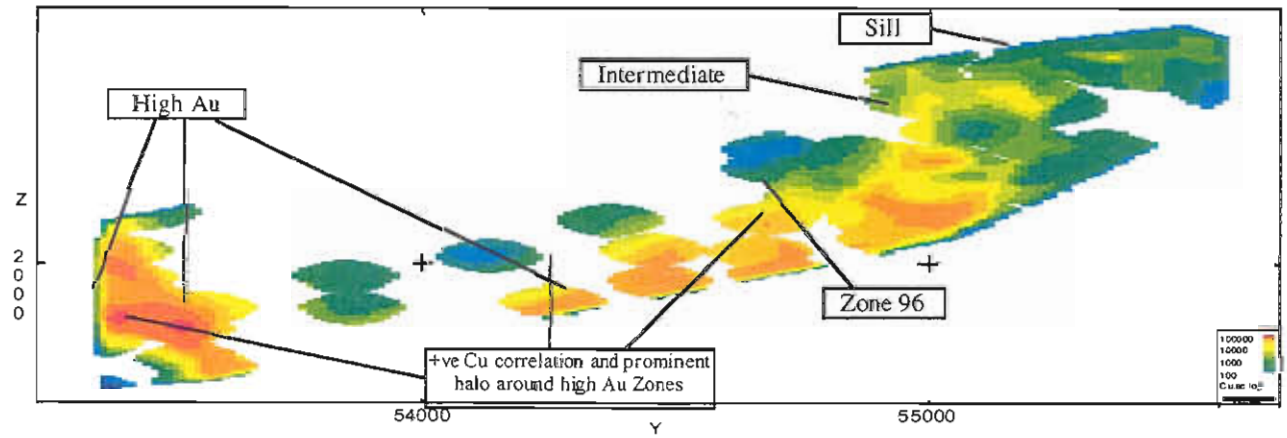

Figure 9. Colour imaging of A-Zone Cu accumulations (gmetres). Henty-Mt Julia Long Projection

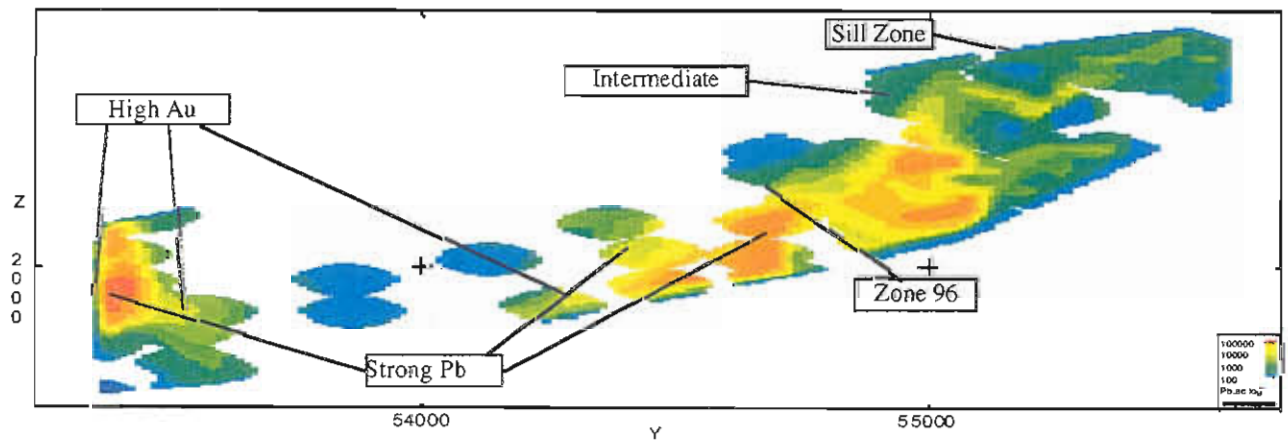

Figure 10. Colour imaging of A-Zone Pb accumulations (gmetres). Henty-Mt Julia Long Projection.

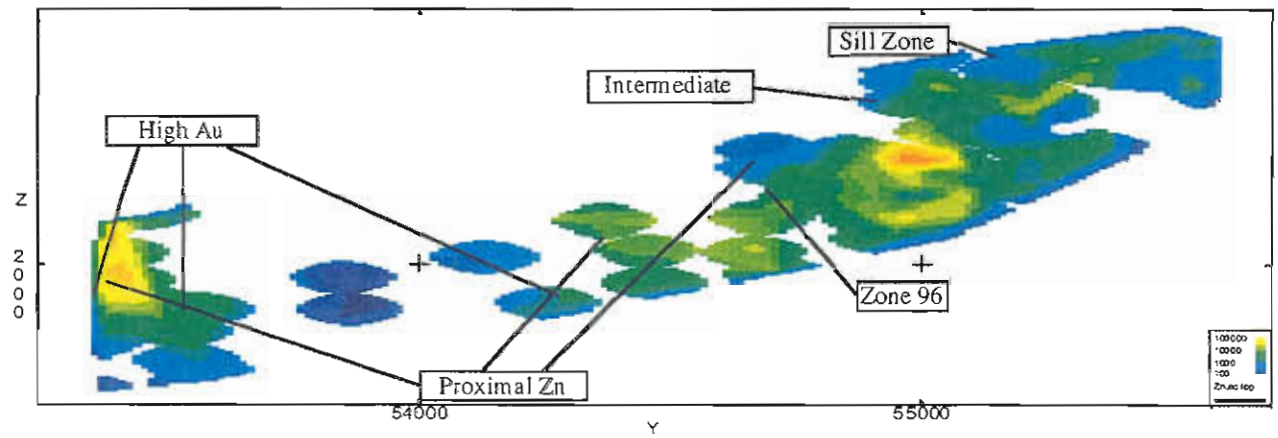

Figure 11. Colour imaging of A-Zone Zn accumulations (gmetres). Henty Mt. Julia Long Projection

Figure 12. Schematic section of Henty post mineralisation but pre-deformation, demonstrating wholerock and immobile element vectors

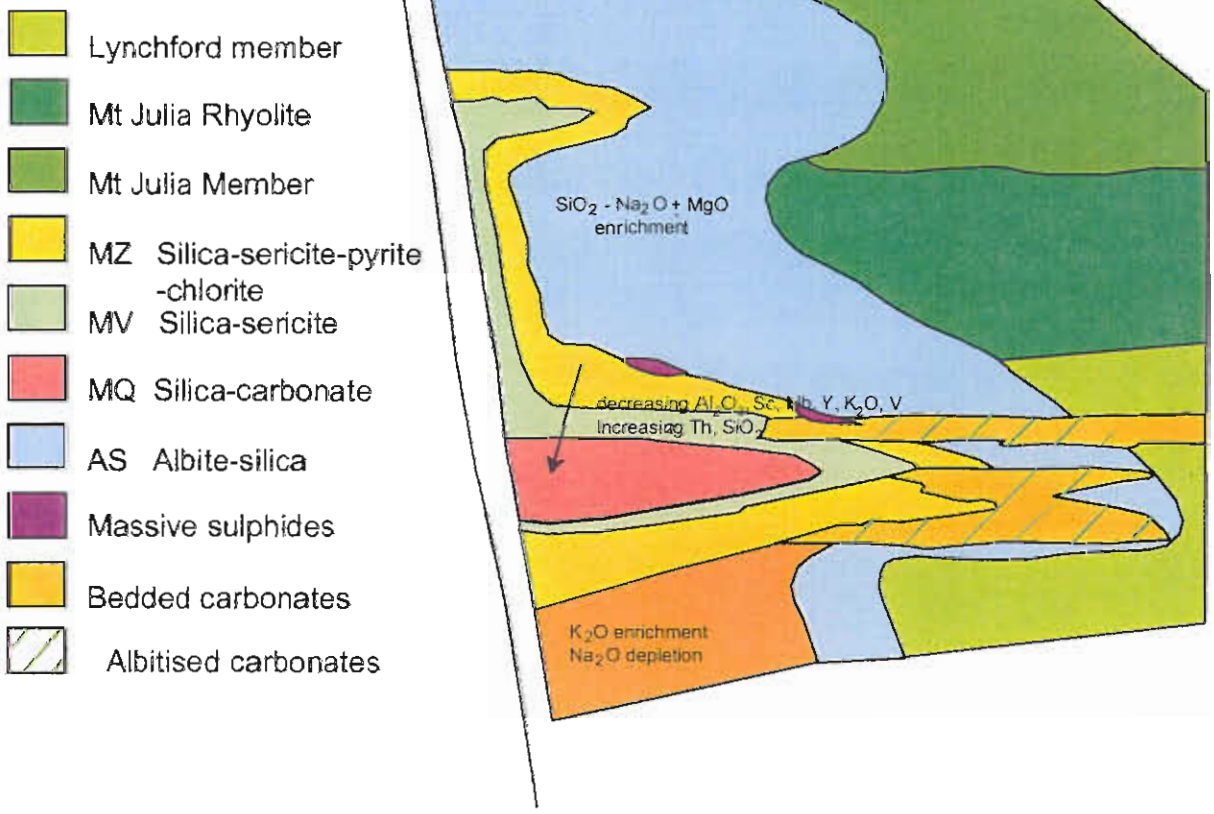

Alteration halo of the Thalanga VHMS deposit, north Queensland

Holger Paulick
Centre for Ore Deposit Research

Introduction

The Thalanga volcanic-hosted massive sulphide deposit is located close to the western end of the E–W striking, Cambro-Ordovician Mount Windsor Subprovince in north Queensland, approximately 180 km inland from Townsville. It has been deformed during regional metamorphism under upper greenschist facies conditions (biotite grade). The initial geological reserve was ~6 Mt of Zn-Pb-Cu-Ag-Au mineralisation in sheet-style, semi-connected ore lenses.

This study was part of AMIRA project P439 and the main objectives were

- to unravel the volcanic facies architecture of the footwall and the hangingwall, and
- to characterise the textural, mineralogical, and geochemical effects of hydrothermal alteration associated with the mineralisation.

Previous AMIRA reports

Previous progress reports on this PhD research project discuss several aspects of the volcanic facies architecture and geochemical features in detail and will be referenced throughout this final report which focuses on alteration facies and alteration geochemistry.

Previous reports are:

- Paulick, H. (1995): A comparison of volcanic facies architecture and alteration styles of felsic and mafic volcanic host sequences to massive sulfide deposits–Thalanga (north Queensland) and Teutonic Bore (Western Australia). AMIRA/ARC project P439, report 1, 147–149.
- Paulick, H. (1996): Facies architecture, alteration, and metamorphism of the volcanic host rock sequence at the Thalanga massive sulphide deposit, north Queensland, Australia. AMIRA/ARC project P439, report 2, 147–155.
- Paulick, H. (1997): Volcanic facies analysis, alteration, and geochemistry of the host rock sequence to VHMS-style mineralisation at Thalanga (north Queensland). AMIRA/ARC project P439, report 4, p 185–223.

Sampling and geochemical analysis

The geology and geochemistry of the Thalanga mine sequence has been studied in six cross sections in the mine area and in the railway cutting locality approximately 5 km to the west of the Thalanga mine (Fig. 1). Diamond drill core logging was the main source of geological information because of the paucity of surface outcrop in the Thalanga mine area. In total, 14,000 m of drill core were examined and the selection of drill holes and sampling strategy are detailed in a previous report (Paulick, 1997, AMIRA report no. 4, p.188, Tables 1, 2). The results of 184 geochemical analyses (XRF and ICP-MS) and REE data for a sub-set of 40 samples are reported in the database compiled for this AMIRA project.

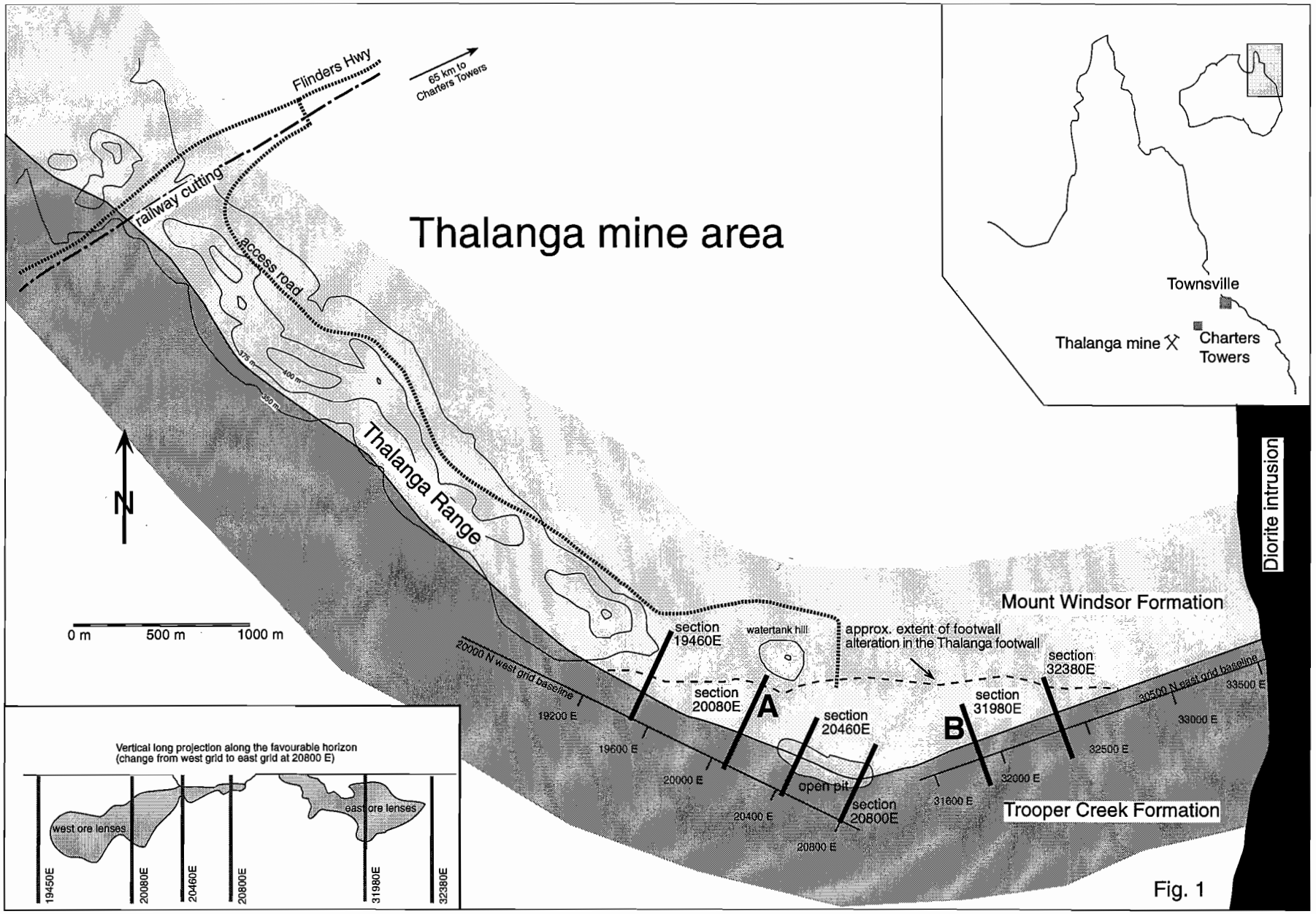

Fig 1: Map of the Thalanga mine area showing the locations of cross sections examined during this project and the cross section selected for presentation in this report (A and B).

Analyses for major elements and a range of trace elements were performed by the XRF laboratory at the School of Earth Sciences (University of Tasmania). Low abundance trace elements were measured by ICP-MS with one batch (104 samples from sections 20080E, 20800E, 31380E and the railway cutting) analysed by the Central Science Laboratory (University of Tasmania) and another batch (80 samples) by Analabs. The concentrations of REE of a selected subgroup of samples was measured by ICP-MS at the Central Science Laboratory on the same solutions used for the measurement of low abundance trace elements.

method and laboratory/elements
XRF (School of Earth Sciences)
Si, Ti, Al, Fe, Mn, Mg, Ca, Na, K, P, S Ba, Cu, Pb, Zn, As, Bi, Cr, Nb, Ni, Rb, Sr, Th, V, Y, Zr
ICP-MS (Central Science Laboratory)
Ag, Bi, Cd, Cs, Mo, Sb, Th, Tl, U
REE measurements: Y, Ba, La, Ce, Pr, Nd, Sm, Eu, Gd, Tb, Dy, Ho, Er, Tm, Yb, Lu
ICP-MS (Analabs)
Ag, As, Bi, Cd, Cs, Mo, Sb, Th, Tl, U

This database was supplemented by 100 XRF analyses from previous studies on samples from drill holes examined during this project (Wills, 1985; Stolz, 1991; Herrmann, 1994; Hill, 1996). Furthermore, 300 multi-element analyses of major and trace elements by ICP-MS and other methods on variably altered footwall rhyolite from section 20080E, 20800E and 31980E were provided by RGC Exploration (Stolz, 1997). Miscellaneous geochemical data on samples from exploration drilling in 1997 and assay data (mainly Cu, Pb, and Zn) from the ore horizon in sections 19450E, 20080E, 20800E, 31980E, and 32380E was made available by Thalanga mine geologists.

Ore deposit characteristics

Form of ore body: Thalanga consists of a series of stratiform, sheet-like massive sulphide lenses with a thickness of 1–5 m, lateral width of 100 to 300 m and a down dip extend of 50 to 400 m.

Size and grade: The initial geological resource of the Thalanga deposit was 6.35 Mt of ore with an average grade of 12.4% Zn, 3.9% Pb, 2.2% Cu, 99 g/t Ag and 0.6 g/t Au (Gregory et al, 1990)

Sulfide mineralogy: Sphalerite, pyrite, galena, chalcopyrite, minor magnetite, tetrahedrite, arsenopyrite (Hill, 1996)

Alteration mineralogy: Footwall: quartz, sericite, chlorite, biotite, pyrite

Favourable Horizon: quartz, chlorite, sericite, carbonate, tremolite, barite, pyrite

Hangingwall: epidote, albite, minor actinolite, biotite, chlorite, hematite

Deformation and metamorphism: The Thalanga sequence was folded into a sub-vertical orientation during regional metamorphism (D2, Berry et al., 1992; Hill, 1996) which produced strongly foliated biotite in micaceous rocks. A later (post-D2) contact metamorphic event was associated with the intrusion of a large diorite body cross cutting stratigraphy east of the Thalanga ore bodies. Peak metamorphic conditions are constrained by garnet-chlorite and garnet-biotite assemblages and microprobe data show that garnets are spessartine-rich and pyrope-poor. Therefore, it can be estimated that peak metamorphic temperatures were in the range of 450–480°C (cf. Spear, 1993, p. 352–354) with pressure conditions in the range of 2–4 kbar (Hill, 1996).

Volcanic facies architecture

The Thalanga mineralisation is hosted within a felsic succession of rhyolite and dacite which were emplaced in a below wave-base, sub-aqueous environment (Paulick, 1997). The deposit is located at the stratigraphic contact of regionally extensive rhyolite of the Mount Windsor Formation (MWF) in the footwall, and a dacite dominated volcano-sedimentary succession of the Trooper Creek Foramtion (TCF) in the hangingwall. Rhyolite of the MWF from the railway cutting locality (Fig. 1) was dated by SHRIMP U-Pb yielding a crystallisation age of 479 ± 5 Ma (Perkins, 1993). The ore hosting stratigraphic position is referred to as the Favourable Horizon and consists of various volcaniclastic deposits, coarsely quartz-feldspar porphyritic coherent rhyolite, laminated mudstone, carbonaceous 'pseudo-exhalite' (Herrmann, 1994) and massive to semi-massive sulphides with carbonate-rich, siliceous

Figure 2 (on following two pages): Geology of cross sections A and B through the Thalanga sequence in west and east Thalanga. Diamond drill holes shown have been examined for this study. The geometry of the ore bodies is based on mapping of underground exposure and logging of underground production drilling by Thalanga mine staff.(a) Geology of cross section A (West Thalanga, 200080 E), (b) Geology of cross section B (East Thalanga, 31380 E)

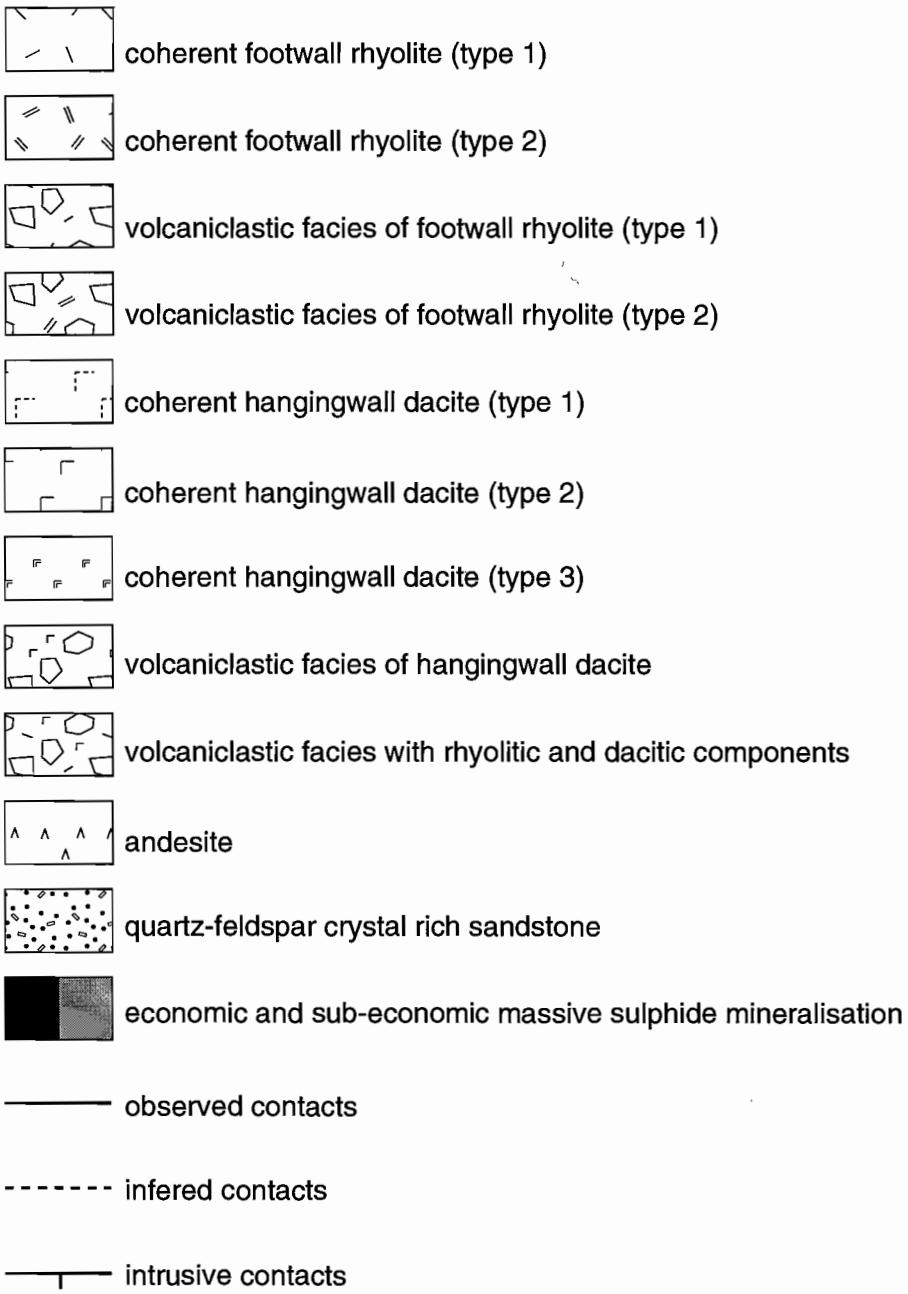

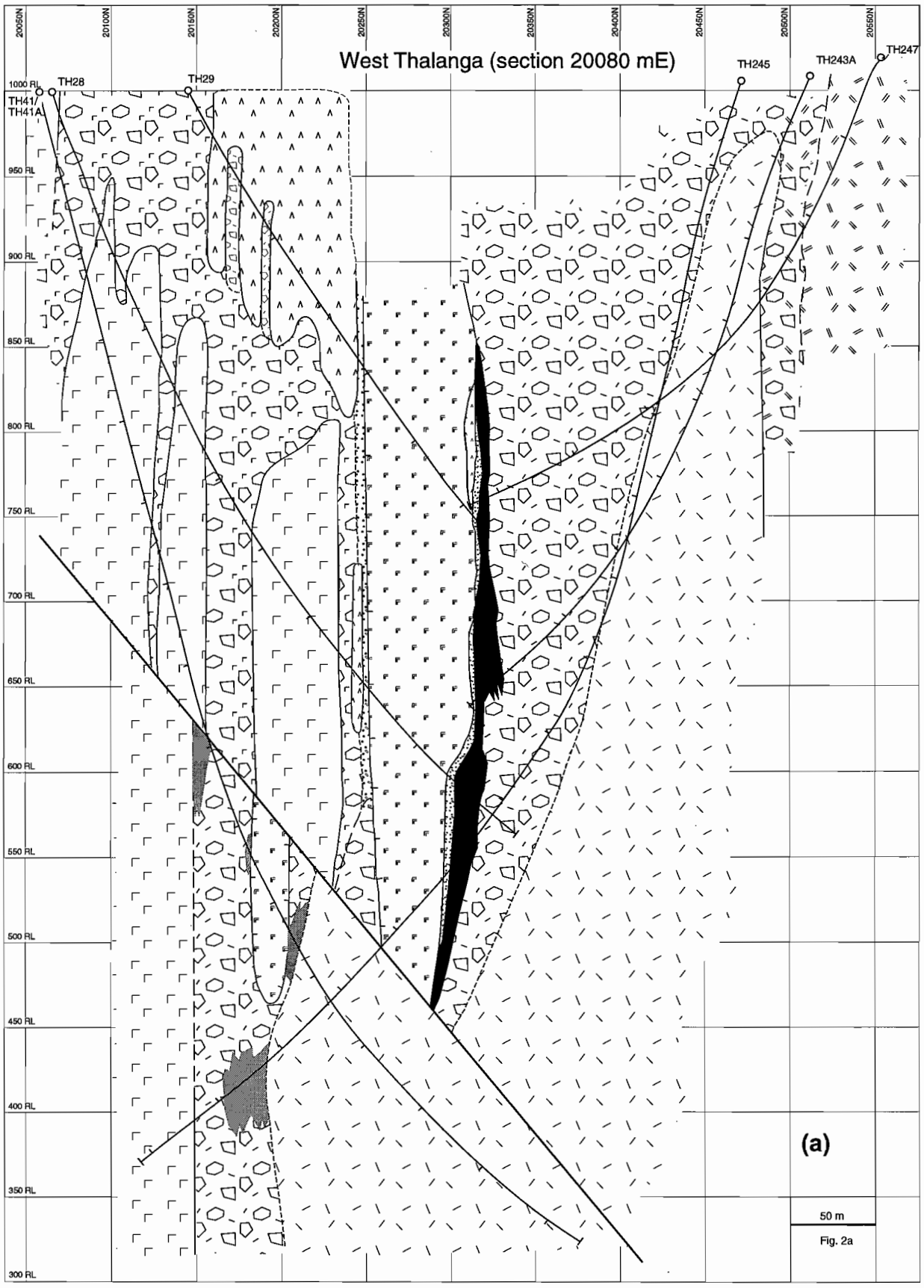
West Thalanga (section 20080 mE)
20050N
20100N
20150N
20200N
20250N
20300N
20350N
20400N
20450N
20500N
20550N
1000 RL
950 RL
900 RL
850 RL
800 RL
750 RL
700 RL
650 RL
600 RL
550 RL
500 RL
450 RL
400 RL
350 RL
300 RL
TH28
TH29
TH41/
TH41A
TH245
TH243A
TH247
(a)
50 m
Fig. 2a

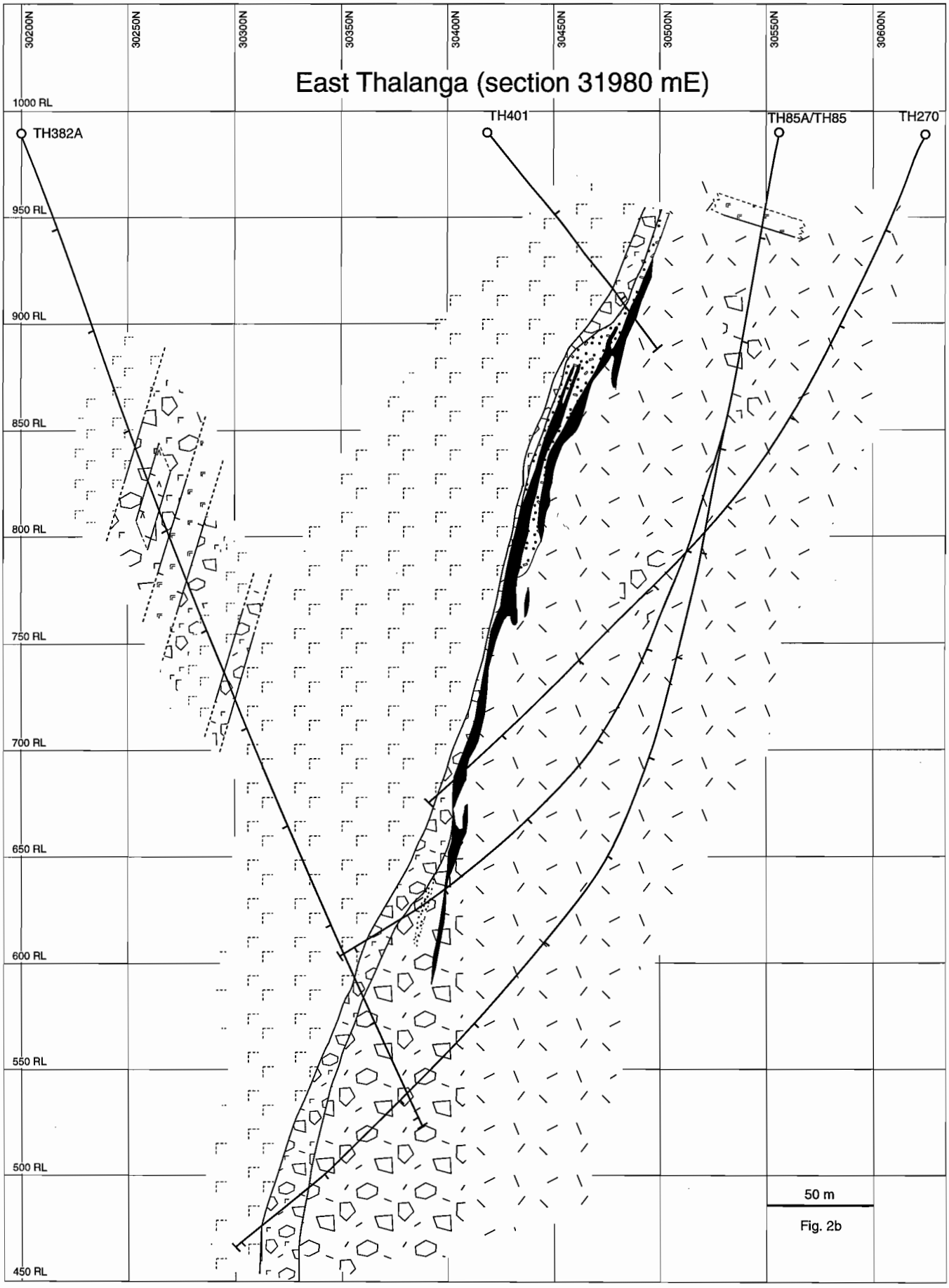
East Thalanga (section 31980 mE)
30200N
30250N
30300N
30350N
30400N
30450N
30500N
30550N
30600N
1000 RL
950 RL
900 RL
850 RL
800 RL
750 RL
700 RL
650 RL
600 RL
550 RL
500 RL
450 RL
TH382A
TH401
TH85A/TH85
TH270
50 m

Fig. 2b

Table 1: Types of footwall rhyolite types and hangingwall dacite in the Thalanga sequence

name	description	alteration	occurrences
rhyolite type 1	poorly to moderately quartz-feldspar phyric, fine to medium rhyolite phenocrysts: 1 - 5 vol%; ≤ 1 - 2 mm feldspar phenocrysts pseudomorphed or obliterated in intensely altered areas geochemistry: Ti/Zr: 3.9 ± 0.4 Ti/Th: 45 ± 12	moderate to strong alteration common	immediate footwall to Thalanga mineralisation in all sections
rhyolite type 2	highly quartz-feldspar phyric medium rhyolite phenocrysts: 7 - 15 vol%; mainly 2-5mm geochemistry: Ti/Zr: 3.9 ± 0.4 Ti/Th: 45 ± 12	fresh (water tank hill) to weakly altered	in lower part of east and west Thalanga, outcropping at watertank hill
rhyolite type 3	moderately to highly quartz phyric, fine to medium rhyolite (feldspar phenocrysts absent or subordinate in fresh and altered specimen) phenocrysts: 8-15 vol%; <1 to 2 mm geochemistry: Ti/Zr: 3.9 ± 0.4 Ti/Th: 45 ± 12	fresh to weakly altered, strongly altered in central Thalanga	railway cutting, west Thalanga (TH410), central Thalanga (TH18, TH38)
rhyolite type 4 (previously referred to as QEP = 'Quartz Eye Porphyry' or QFP = 'Quartz Feldspar Porphyry')	very highly quartz-feldspar phyric, coarse rhyolite phenocrysts: 20-25 vol%; mainly 4-8 mm quartz phenocrysts are commonly blue geochemistry: three sub-types of rhyolite type 4 can be defined based on immobile element ratios: type 4a: Ti/Zr: 4 - 5.5 Ti/Th: 30 - 45 type 4b: Ti/Zr: 5.6 - 11.5 Ti/Th: 95 - 155 type 4c: Ti/Zr: 15.7 Ti/Th: 300	unaltered to weakly altered	intrusions within footwall, at Favourable Horizon position, in hangingwall of west Thalanga
dacite type 1	poorly feldspar phyric, fine dacite (or aphyric dacite) phenocrysts: < 1 vol%, < 1 mm geochemistry: Ti/Zr: 12.4 ± 0.4 Ti/Th: 244 ± 7	hematite altn, diss. or vein controlled epidote altn, diss. chlorite and biotite, locally minor diss. actinolite	East Thalanga
dacite type 2	moderately feldspar phyric, medium (to fine) dacite phenocrysts: 1-5 vol%; mainly 1-3 mm geochemistry: Ti/Zr: 11.1 ± 0.9 Ti/Th: 244 ± 20	epidote (± carbonate ± actionlite) alteration, hematite alteration, diss. chlorite-biotite	West Thalanga, Central Thalanga
dacite type 3	highly feldspar phyric, fine dacite phenocrysts: 8-15 vol%; ≤ 1 mm geochemistry: Ti/Zr: 18.7 ± 1.0 Ti/Th: 390 ± 30	epidote alteration, biotite-chlorite alteration	West, Central and East Thalanga

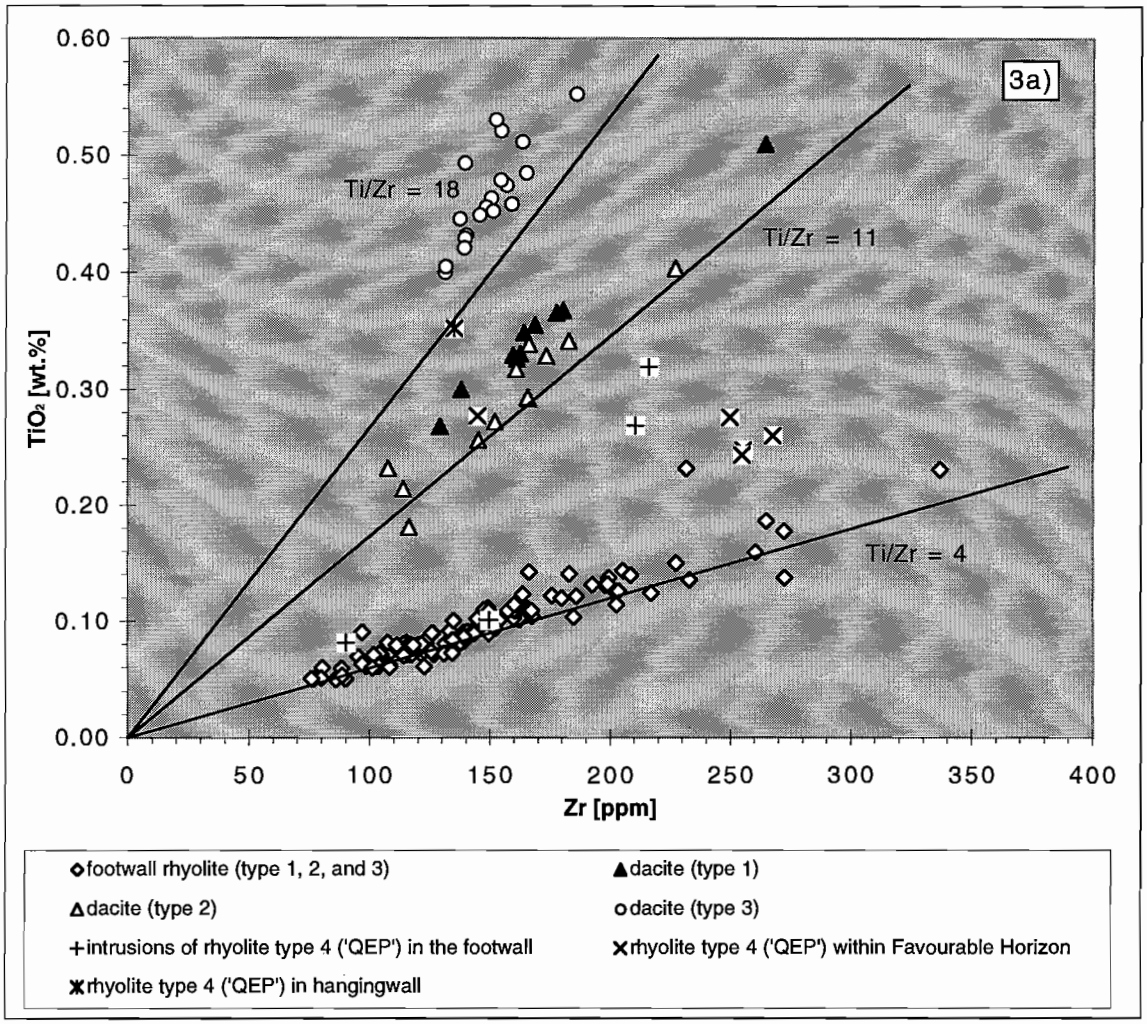
3a)
Ti/Zr = 18
Ti/Zr = 11
Ti/Zr = 4
TiO2 [wt.%]
Zr [ppm]
0.00
0.10
0.20
0.30
0.40
0.50
0.60
0
50
100
150
200
250
300
350
400
footwall rhyolite (type 1, 2, and 3)
dacite (type 1)
dacite (type 2)
dacite (type 3)
intrusions of rhyolite type 4 ('QEP') in the footwall
rhyolite type 4 ('QEP') within Favourable Horizon
rhyolite type 4 ('QEP') in hangingwall

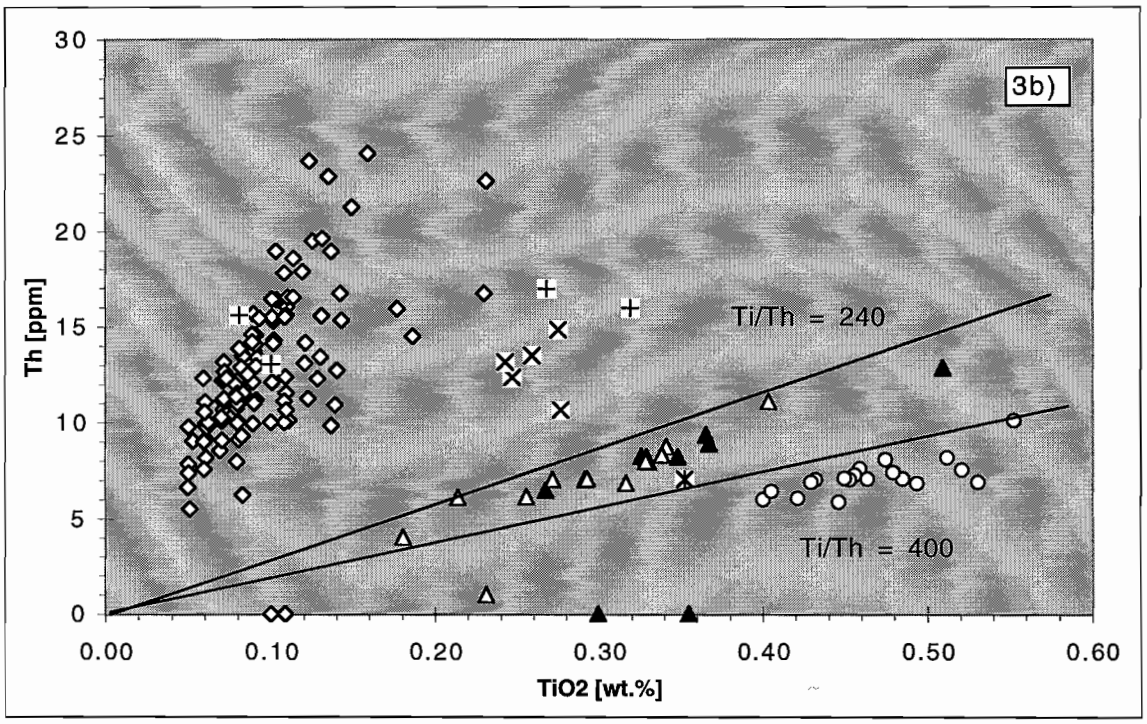
3b)
Ti/Th = 240
Ti/Th = 400
Th [ppm]
TiO2 [wt.%]
0
5
10
15
20
25
30
0.00
0.10
0.20
0.30
0.40
0.50
0.60

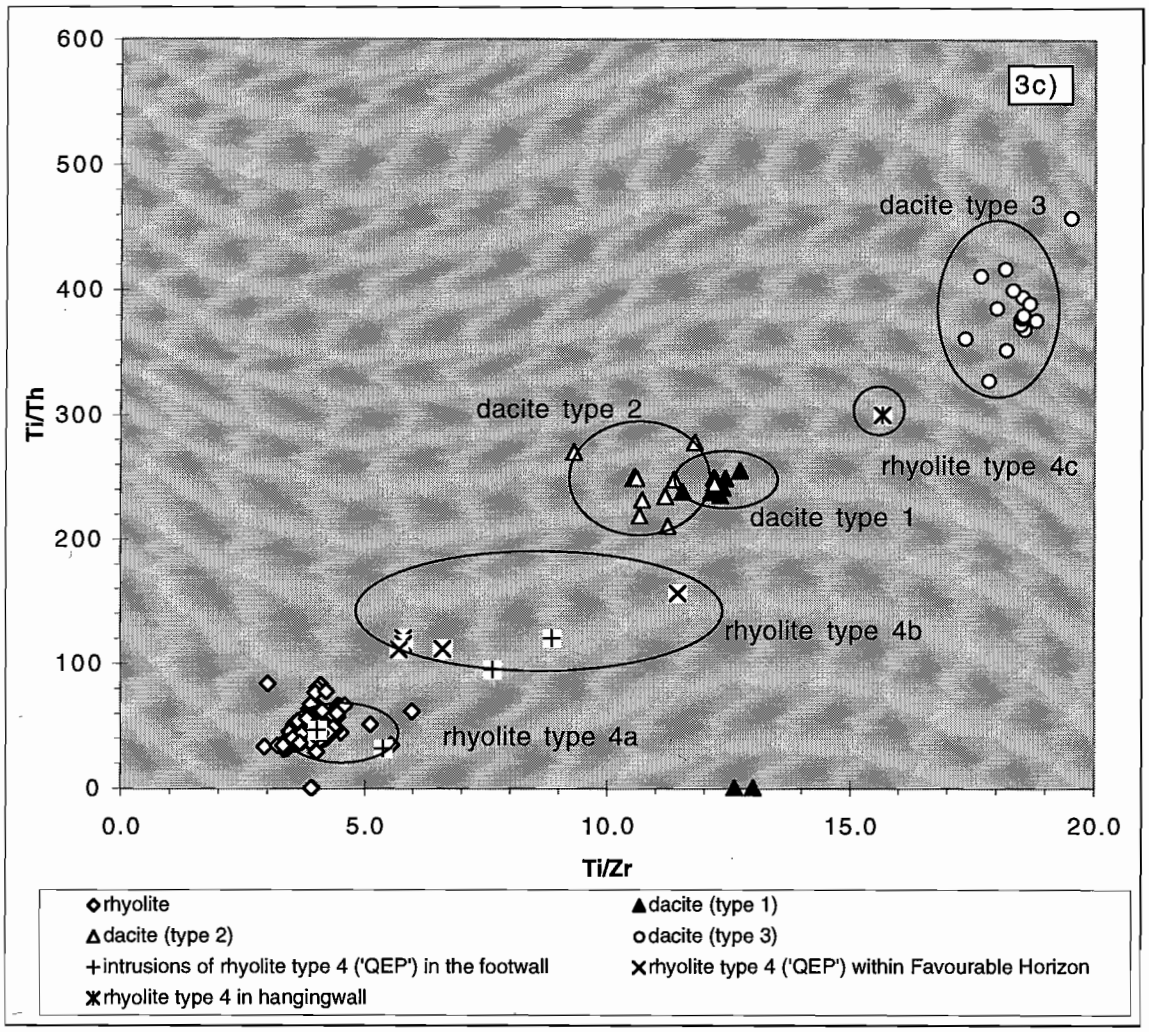

Fig 3: Immobile element plots demonstrating the compositional differences between the principal volcanic units of the Thalanga sequence (data: this study, see also Table 1 for averages and standard deviation).
(a) The analyses of ~ 100 variably altered footwall rhyolite samples (rhyolite type 1, 2 and 3) fall on a very tightly constrained line with a Ti/Zr ratio of about 4. This indicates that the elements Ti and Zr were immobile on hand specimen scale during alteration of the footwall (MacLean & Barrett, 1993). Analyses of hangingwall dacite fall into two groups: while samples of dacite types 1 and 2 have a Ti/Zr ratio of 10 - 12, samples of dacite type 3 have a significantly and consistently higher Ti/Zr ratio (18 - 20). Samples of rhyolite type 4 from different stratigraphic positions have variable Ti/Zr ratios ranging from ~ 4 upto ~ 16.
(b) The analyses of variably altered footwall rhyolite have a somewhat larger scatter in a Th versus TiO_2 plot compared to the Zr vs. TiO_2 plot which may indicate that Th was mobile during footwall alteration or that the Th content of the rhyolite was originally inhomogeneous. Analyses of dacite fall into two separate groups with data from type 1 and 2 defining a linear trend with a Ti/Th ratio of ~ 250 whereas dacite type 3 have higher concentrations of TiO_2 (Ti/Th ratio ~ 400). Analyses of rhyolite type 4 fall into 3 separate area: 1) overlapping with the rhyolite field, 2) intermediate between the rhyolite and the dacite type 1 and 2 line, and 3) between the high and low Ti/Th dacite suites.
(c) The petrogenetic groups present in the Thalanga sequence are effectively separated on a plot of Ti/Zr ratio versus Ti/Th ratio. Analyses of footwall rhyolite (type 1, 2, and 3) fall into a tightly constrained field with low values for both ratios. Hangingwall dacite of type 1 and type 2 belong to one petrogenetic group with Ti/Th ratio of 220 to 280 and Ti/Zr ratios between 10.5 and 12 whereas hangingwall dacite of type 3 form a group with higher Ti/Zr and Ti/Th ratios (ranging between 17.5 to 20 and 340 to 440, respectively). The analyses of rhyolite type 4 fall in 3 separate fields warranting the definition of three subtypes of rhyolite type 4 based on these immobile element ratios. Type 4a has comparable ratios to footwall rhyolite types 1,2, and 3 and occurs as intrusions in the footwall. Type 4b has a Ti/Th ratios ranging between 100 and 150 and Ti/Zr ratios between 5.5 and 11.5. This rhyolite type occurs in the Favourable Horizon and as intrusion in the footwall. Type 4c has a Ti/Th ratio of 300 and a Ti/Zr ratio of 15.7 and occurs in the hangingwall of west Thalanga ~ 200 m stratigraphically above the Favourable Horizon (DDH TH62C interval 0 to 60 m).

Fig. 4 on pages162, 163): Alteration zonation of cross sections A and B through the Thalanga sequence in west and east Thalanga. Diamond drill holes shown have been examined for this study. The geometry of the ore bodies is based on mapping of underground exposure and logging of underground production drilling by Thalanga mine staff. (a) Alteration zonation of cross section A (West Thalanga, 200080 E), (b) Alteration zonation of cross section B (East Thalanga, 31380 E)

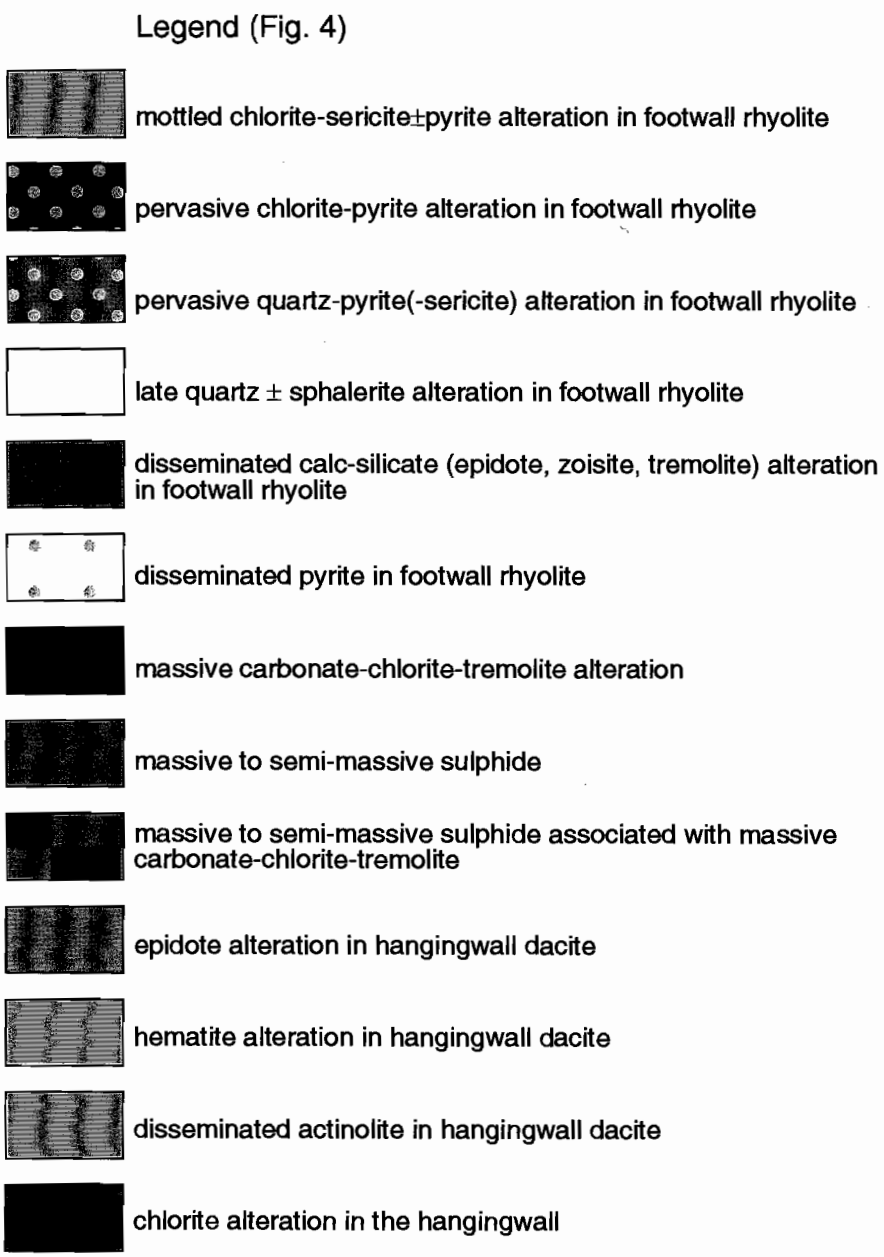

or phyllosilicate-rich gangue. Silica-ironstones occur locally in the Favourable Horizon position along strike to the west of the Thalanga mine and in up dip parts of west Thalanga ore lens (Duhig et al, 1992). The geology of the Favourable Horizon was studied in detail by Hill (1996). The footwall rhyolite, the lithologies of the Favourable Horizon and the hangingwall succession are collectively referred to as the 'Thalanga sequence' in this report.

Several types of rhyolite have been identified in the MWF based on textural observations which include the size range, abundance and relative proportions of quartz and feldspar phenocrysts and contact relationships (Table 1). The footwall to the ore bodies in the mine area is dominated by a weakly to strongly altered, poorly to moderately quartz (-feldspar) phyric rhyolite with phenocrysts ranging from < 1 mm to 2 mm in diameter (rhyolite type 1). Locally, poorly porphyritic rhyolite with ~1 % quartz phenocrysts and moderately porphyritic rhyolite with 3–5 % quartz phenocrysts can be distinguished. However, contacts between these rhyolite emplacement units appear to be gradational or obliterated by alteration. Commonly, a highly porphyritic rhyolite with quartz and feldspar phenocrysts in the size range of 1–5 mm (rhyolite type 2) occurs at about 200 m stratigraphically below the Favourable Horizon (Fig. 2a). The unaltered rhyolites in the railway cutting are moderately quartz-phyric (diameter mainly 1–2 mm) but contain only minor feldspar phenocrysts and are therefore considered to represent a separate type of rhyolite (type 3).

Highly porphyritic rhyolite with abundant coarse quartz and feldspar phenocrysts has previously been called 'Quartz-Feldspar Porphyry' (QFP) or 'Quartz-Eye Porphyry' (QEP') and constitutes the rhyolite type 4 in the Thalanga sequence. This rhyolite occurs as intrusions in the footwall to the Thalanga mineralisation, within the Favourable Horizon, and in the hangingwall. Based on immobile element ratios three subtypes can be defined (see below).

Three texturally distinct dacite types can be distinguished in the hangingwall based on feldspar phenocrysts size range and abundance (Table 1). Dacite type 1 is poorly porphyritic with fine (< 1 mm diameter) feldspar phenocrysts and locally appears aphyric in drill core. It occurs in the immediate hangingwall to the Favourable Horizon in east Thalanga (Fig. 2b). Dacite type 2 is moderately porphyritic with feldspar phenocrysts mainly in the 1–3 mm diameter size range and occurs in west and central Thalanga (Fig. 2a). Dacite type 3 is highly porphyritic with fine feldspar phenocrysts ranging in abundance between 8 and 15 %. However, altered samples of dacite type 3 may contain less feldspar phenocrysts than their fresh counterparts. Dacite type 3 occurs in west, central and east Thalanga and intrusive top contacts have been recognised.

Chemostratigraphy

Examination of immobile element ratios is an important tool in the study of altered volcanic rocks in order to define petrogenetically related groups. At Thalanga, plots of TiO_2 versus Zr and TiO_2 versus Th were found to be the most useful in separating lithological groups with distinctive immobile element ratios (Fig. 3).

Analyses of footwall rhyolite and hangingwall dacite define distinctive trends in plots of TiO_2 versus Zr and TiO_2 versus Th (Fig. 3a, b). The data of least altered to strongly altered footwall rhyolite follow a tightly constrained straight line in the TiO_2 versus Zr plot indicating that the Ti/Zr ratio of all samples was originally between 3.5 and 4.5 and was not affected by hydrothermal alteration or metamorphism. Data for hangingwall dacite define two separate linear trends on TiO_2 versus Zr and TiO_2 versus Th diagrams. Samples of dacite type 1 and 2 have a Ti/Zr ratio of ~12 and Ti/Th ratio of ~240 whereas samples of dacite type 3 have consistently higher ratios (Ti/Zr ~18.5 and Ti/Th ~390). Rhyolite of type 4 ('Quartz Eye Porphyry') can be divided into three sub-groups based on their immobile element ratios (Fig. 3c). Rhyolite type 4a has similar Ti/Zr and Ti/Th ratios as footwall rhyolite (type 1, 2, 3) and occurs as intrusions in the footwall. Rhyolite of type 4b have consistently higher Ti/Zr and Ti/Th ratios than footwall rhyolite spanning a comparatively large range of Ti/Zr ratios (5.5–11.5) and occur in the Favourable Horizon position and within the footwall. Analyses of 'Quartz-Feldspar Porphyry' from the Favourable Horizon by Hill (1996) have a similar range of Ti/Zr ratios indicating that those samples could also be classified as type 4b rhyolite.

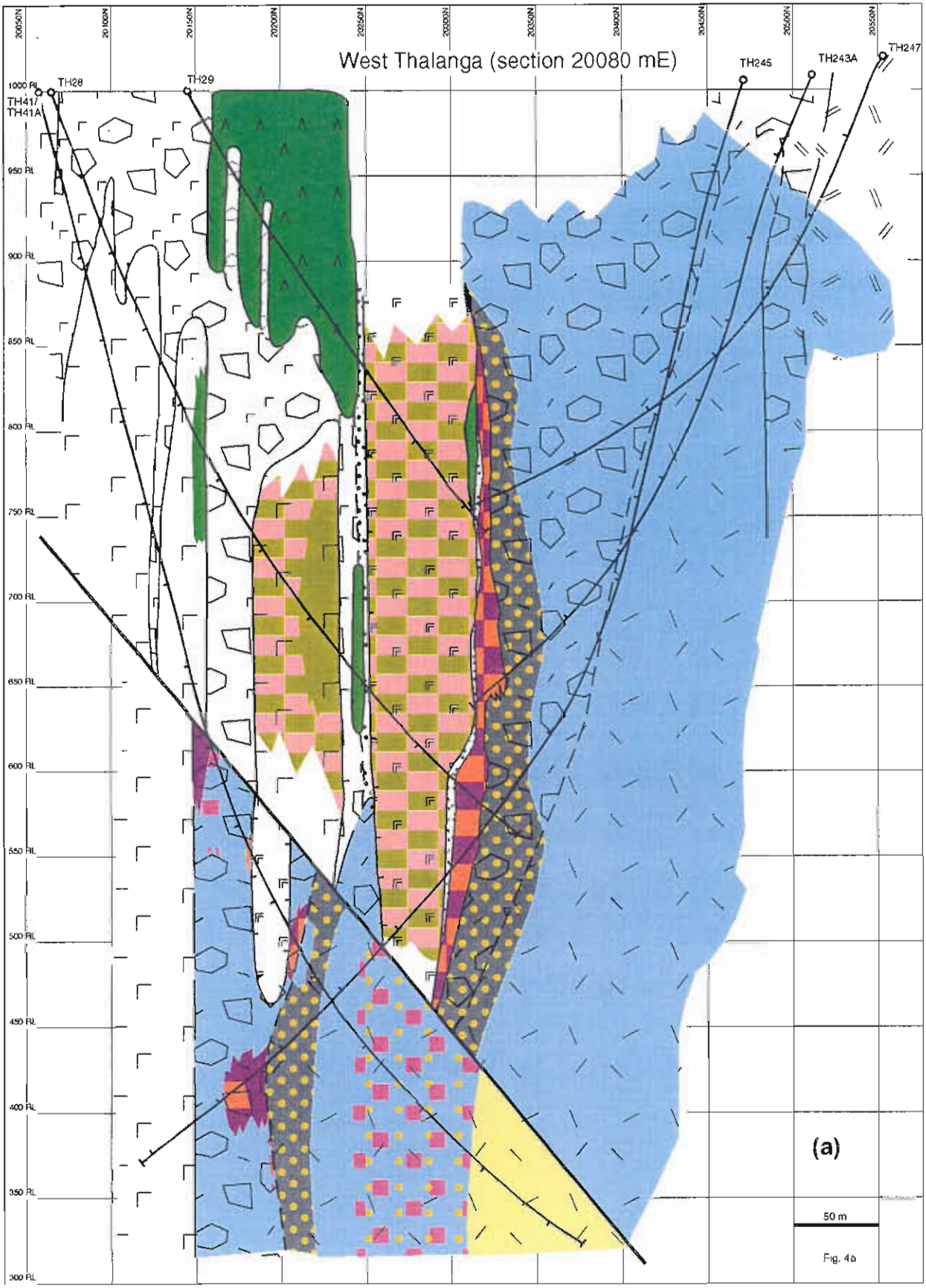
West Thalanga (section 20080 mE)
TH28
TH29
TH41/
TH41A
TH245
TH243A
TH247
20050N
20100N
20150N
20200N
20250N
20300N
20350N
20400N
20450N
20500N
20550N
1000 RL
950 RL
900 RL
850 RL
800 RL
750 RL
700 RL
650 RL
600 RL
550 RL
500 RL
450 RL
400 RL
350 RL
300 RL
(a)
50 m

Fig. 4a

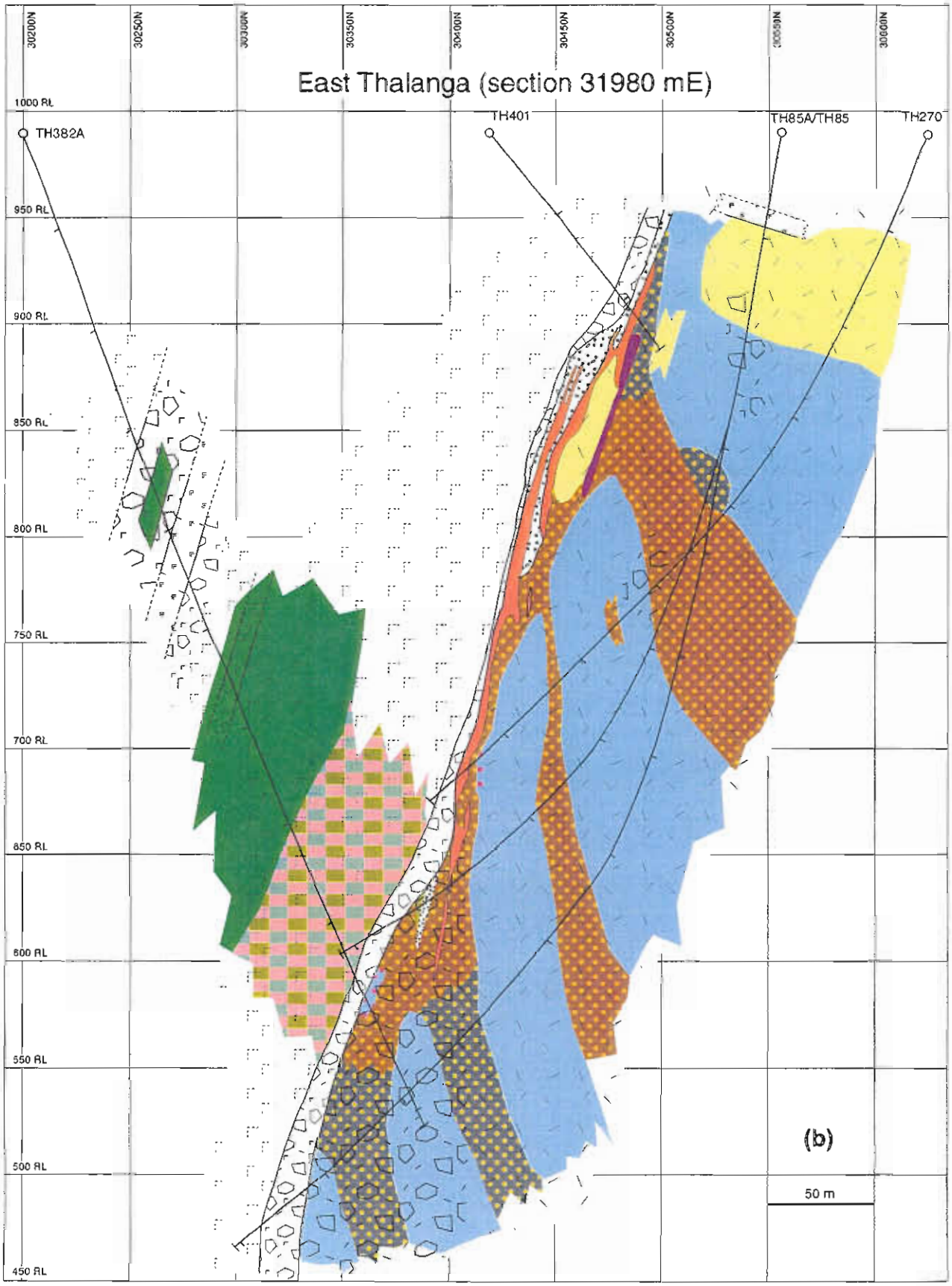
East Thalanga (section 31980 mE)
30200N
30250N
30300N
30350N
30400N
30450N
30500N
30550N
30600N
1000 RL
950 RL
900 RL
850 RL
800 RL
750 RL
700 RL
650 RL
600 RL
550 RL
500 RL
450 RL
TH382A
TH401
TH85A/TH85
TH270
(b)
50 m

A sample of type 4 rhyolite from the hangingwall in west Thalanga (section 19450E, DDH TH62C, interval 0 to 60 m) has comparatively high immobile element ratios (Ti/Zr: 15.7 and Ti/Th: 300). Therefore, it is interpreted to represent a petrogenetically distinct sub-group (rhyolite type 4c).

Alteration mineralogy and zonation

Alteration types and zonation

Alteration of the footwall to the Thalanga ore bodies is texturally and compositionally diverse and small scale variations are commonly observed in drill core. However, alteration types may be defined based on dominant mineral assemblages and general intensity of alteration.

The principal alteration types in the footwall are: mottled chlorite-sericite ± pyrite alteration, intense quartz(-sericite)-pyrite and chlorite-pyrite alteration, late quartz (± sphalerite ± k-feldspar) alteration and carbonate-calc-silicate (epidote-zoisite-tremolite) alteration. Biotite is associated with mottled chlorite-sericite alteration and chlorite-pyrite alteration and is inferred to be entirely of metamorphic origin. Sample sheets for least-altered and variably altered rhyolites illustrate the textural and compositional variability of the Thalanga footwall (see Appendix).

Massive to semi-massive assemblages of carbonate-chlorite-tremolite ('CCT') commonly occur within or close to the Favourable Horizon in west Thalanga (Fig. 4a). These have been studied in detail by Herrmann (1994) who concluded that this rock type is not an exhalite but represents extreme footwall rhyolite alteration.

The most intense, texturally destructive types of alteration in the footwall are dominated by quartz(-sericite)-pyrite or chlorite-pyrite mineral assemblages. These alteration types are commonly accompanied by pyrite veins and occur in distinctive zones within the footwall and in an upto 50 m wide stratabound zone parallel to the Favourable Horizon (Fig. 4). In east Thalanga, zones of intense chlorite-pyrite alteration within the footwall can be outlined from exploration drill core (Fig. 4b). These zones alternate with mottled chlorite-sericite alteration and intercept the Favourable Horizon with an angle of 30–50°. Such zones of intense chlorite-pyrite alteration have not been identified in the footwall of west Thalanga (Fig. 4a) where mottled alteration with variable amounts of pyrite dominates and a stratabound zone of strong quartz-pyrite alteration runs parallel to the Favourable Horizon immediately below the mineralisation. Calcareous alteration can be intense close to (or within) the Favourable Horizon and is locally intimately associated with massive sulphide mineralisation.

The mottled chlorite-sericite ± pyrite alteration type has a wide range of textures and common endmembers are: pseudoclastic textures with wispy, phyllosilicate-rich domains and lensoidal quartz-rich domains, phyllosilicate-rich rhyolite with pervasive foliation and rhyolite with blotches of chlorite in a quartz-sericite-rich groundmass (Fig. 5). These different textures are the result of heterogeneous devitrification during and after rhyolite emplacement, alteration caused by the passage of hydrothermal fluids, and subsequent deformation associated with metamorphism. At the fringes of the hydrothermally altered footwall rhyolite, mottled chlorite–sericite ± pyrite alteration is often overprinted by later massive white quartz (± sphalerite ± K-feldspar) alteration. Resulting textures include patchy white quartz domains, white siliceous 'network-shaped' domains ('pseudomatrix') or massive white quartz (drill core intervals of upto 20 m length) with remnant domains of muscovite-biotite-chlorite. Geochemical evidence indicates that late quartz alteration was locally accompanied by K-feldspar alteration (Fig. 6). However, K-feldspar crystals are difficult to recognise in thin section due to the fine grain size of the groundmass.

Alteration of the hangingwall dacite is rarely texturally destructive (Paulick, 1997) and common alteration minerals are disseminated chlorite(-biotite) and epidote (± actinolite). A prominent patchy to vein controlled 'red rock' alteration type occurs frequently and is inferred to be caused by disseminated, sub-microscopic hematite microcrysts (Fig. 5). Geochemical data of dacite show that a large proportion of the dacite have very low (K_2O/K_2O+Na_2O) ratios indicative of Na-metasomatism and albite alteration (Paulick, 1997, report 4, p. 215). Albite altered dacite may appear unaltered in handspecimen (Fig. 5), show hematite alteration and may contain disseminated chlorite-biotite or epidote. Hence, albite alteration has no reliable textural

expression in handspecimen and geochemical analysis is required for reliable identification.

Geochemistry of alteration types

Thalanga footwall rhyolite with weak, moderate and strong alteration can be effectively separated on a plot of alteration index (Ishikawa, 1976) versus carbonate-chlorite-pyrite index (CCP index, Large, 1996). These indices were developed to monitor the relative changes of sodium, potassium, calcium, magnesium and iron concentration commonly observed in alteration systems associated with VHMS deposits.

Least altered footwall rhyolite have an alteration index of 30 to 60 and CCP values of 10 to 30 reflecting the high (unmodified) concentrations of alkalis and low concentrations of FeO and MgO (Fig. 6). Intensely altered rhyolite (quartz-pyrite and chlorite-pyrite alteration) plot in the upper right hand corner of the diagram (alteration index > 90) because of large gains in magnesium and iron and loss of sodium and calcium. The large spread in CCP values (50–100) is due to variable concentrations of potassium which is related to the amount of biotite and muscovite in the samples. Rhyolite with mottled chlorite-sericite ± pyrite alteration have intermediate alteration indices and CCP values partly overlapping with the fields for least altered and intensely altered rhyolite. Data for massive carbonate-chlorite-tremolite alteration of footwall rhyolite from Herrmann (1994) plot along the upper boundary of the diagram (CCP values > 90) and the large spread in alteration indices reflects the proportions of calcite and chlorite in the samples. Analyses of rhyolite with late quartz alteration overlap with the field occupied by mottled chlorite-sericite alteration and least altered samples and trend towards the lower right corner of the diagram which is indicative of K-feldspar alteration. The distribution of rhyolite samples with disseminated epidote-zoisite-tremolite alteration is weakly constrained.

Dacites from the hangingwall have low alteration indices (5–50) and plot mainly in a field to the left of the least altered footwall rhyolite. This indicates that the hangingwall alteration occurred under different conditions than footwall alteration and that Na-metasomatism (albite alteration) played an important role.

The geochemical changes associated with hydrothermal alteration in the Thalanga footwall can be further characterised by comparing the averages of different alteration types (Table 2). The following differences between altered and least altered rhyolite are apparent. Intensely altered rhyolite (chlorite-pyrite and quartz-pyrite alteration) are enriched in iron, magnesium, sulphur, base metals and several trace elements (As, Bi, Mo and Rb) whereas sodium, calcium and strontium have lower concentrations compared to least altered rhyolite. Silica and barium are elevated in quartz-pyrite altered rhyolite but depleted in rhyolite with chlorite-pyrite alteration. Mottled chlorite-sericite alteration is characterised by elevated magnesium, sulphur, barium, base metals, rubidium and low sodium content. The composition of rhyolite with late quartz alteration and disseminated calc-silicate alteration is similar to least altered rhyolite for most elements except for elevated silica, barium and zinc in late quartz alteration and elevated calcium, barium, and strontium in calc-silicate alteration. Samples of massive carbonate-chlorite-tremolite alteration are extremely depleted in silica and alkalis and have very high concentrations of magnesium, calcium, sulphur, barium and base metals.

In order to quantify these general observations a mass balance calculation was performed. The underlying principal of this method is that differences in immobile element concentration between altered and least altered samples can be used as a monitor for mass change and therefore the problem of closure inherent to geochemical analyses can be eliminated. The details and implications of this method are outlined and discussed in MacLean & Kranidiotis (1987), MacLean (1990), MacLean & Barrett (1993), and Barrett & MacLean (1994).

The principal assumptions are that the footwall rhyolite at Thalanga (rhyolite type 1 and 2) had a homogeneous chemical composition prior to alteration and that zirconium was immobile during alteration and metamorphism. Both assumptions are supported by the constant Ti/Zr ratio observed. Using the Zr value of least altered rhyolite samples (143 ppm) mass changes were calculated for each alteration type based on their respective average composition (Table 2). The results show that there are significant mass gains in magnesium and mass loss in sodium for all alteration types (Fig. 7a). However, total mass change for mottled chlorite-sericite and chlorite-pyrite alteration is relatively

Fig.5: Some typical textures of footwall rhyolite and hangingwall dacite from the Thalanga sequence

(a) rhyolite with chlorite-sericite±pyrite alteration and a pseudoclastic texture (sample TH245-224.49, section 20080E)

(b) foliated rhyolite with chlorite-sericite±pyrite alteration (sample TH394-114.0, section 32380E)

(c) rhyolite with chlorite-sericite±pyrite alteration and a pseudoclastic texture with blotches of chlorite (sample TH394-293.0, section 32380E)

(d) rhyolite with pseudoclastic texture due to late quartz alteration (apparent matrix) overprinting chlorite-sericite alteration (sample TH247-322.10, section 20080E)

(e) fresh, moderately feldspar phyric, medium dacite (type 2); $K_2O/(K_2O+Na_2O)$= 0.37 (sample TH28-304.50, section 20080E)

(f) albite altered, highly feldspar phyric, fine dacite (type 3); $K_2O/(K_2O+Na_2O)$= 0.01 (sample TH18-89.70, section 20800E)

(g) poorly feldspar phyric, fine dacite (type 1) with pervasive hematite alteration + epidote alteration; $K_2O/(K_2O+Na_2O)$= 0.56 (sample TH402-321.10, section 32380E)

(h) poorly feldspar phyric, fine dacite (type 1) with vein controlled hematite alteration; $K_2O/(K_2O+Na_2O)$= 0.11 (sample TH402-123, section 32380E)


CM


CI


CM

small with both having lost some SiO_2 whereas quartz-pyrite and late quartz alteration are associated with significant mass gains mainly in the form of silica addition. Rhyolite with quartz-pyrite or chlorite-pyrite have also gained substantial iron and sulphur. These results differ somewhat from the findings of Herrmann (1994) who reported a general silica gain for moderately to strongly altered rhyolite and a progressive increase in Si, Fe, S (± Mg) through mottled zones to quartz-pyrite stringer zones.

Calculated mass change for massive carbonate-chlorite-tremolite alteration is extremely high indicating that the precursor gained ~ 60g/100g of total mass. Mass gains for magnesium, calcium, barium, and base metals (especially lead and zinc) are very high and coupled with substantial silica mass loss.

Chlorite-pyrite alteration is characterised by barium loss and gains in Cu and Zn (Fig. 7b) whereas quartz pyrite alteration shows large gains in barium, zinc and lead but has gained only about half the amount of Cu (~160 g/t) calculated for chlorite-pyrite alteration (~350 g/t). Mottled chlorite-sericite alteration is associated with gains in barium, zinc, lead, and minor amounts of copper. Late quartz alteration shows relatively small gains in barium, zinc and lead and calc-silicate altered rhyolite have gained some barium. The trace elements As, Bi, and Mo are substantially enriched in intensely altered rhyolite (Fig. 7c). Rubidium was added to all altered rhyolite whereas Sr was lost for all types of alteration except rhyolite with disseminated carbonate-epidote-zoisite-tremolite alteration which has gained Sr.

In summary, the geochemical data for the different alteration types within the Thalanga footwall rhyolite may be interpreted as follows:

- the elements Mg, S, Ba, Cu, Pb, Zn, As, Bi, Mo, and Rb were added to the footwall rhyolite during hydrothermal alteration,
- Na was lost, and
- the elements Si, Ca, and Sr appear to have been redistributed within the footwall between zones of different alteration types.

Halo geochemistry

The Thalanga deposit has a geochemical halo extending ~ 100–200 m (stratigraphic thickness) into the footwall (Fig. 4a). The lateral extent of this halo beyond the Thalanga mine area is limited and rhyolite samples from section 19450E (Fig. 1), which contains sub-economic mineralisation, are generally similar in composition to the background. The most prominent geochemical features of the alteration halo are sodium loss, and gains in magnesium, iron, sulphur, base metals and some trace elements (mainly As, Mo, and Bi). However, there are rarely any consistent straight-forward trends in the data when plotted against drill hole location of the sample. Rather, a large scatter in the data is typical which appears to be controlled primarily by the types of alteration intercepted in a specific drill hole. Data from DDH TH247 and TH270, which represent the different styles of footwall alteration observed in west and east Thalanga, are presented in this report (Fig. A1 and A2) to document this observation. Drill hole TH247 exposes ~220 m (true thickness) of footwall rhyolite which shows mottled chlorite-sericite ± pyrite alteration typical for west Thalanga sections and a zone of intense quartz-pyrite-sericite alteration just below the mineralisation (Fig. 4a). Drill hole TH270 in east Thalanga intercepts ~120 m of altered footwall rhyolite in east Thalanga which contains zones of intense chlorite-pyrite alteration (Fig. 4b). As an example for the geochemical composition of the hangingwall dacite data for drill hole TH382A (east Thalanga) was also plotted against sample location (Fig. A3).

In the following the trends of the data from drill holes TH247 and TH270 will be discussed in the light of their usefulness as ore-proximity indicators.

Sodium depletion: The concentration of sodium is well below 0.5% for most altered rhyolite in TH270 whereas sodium depletion is somewhat erratic in TH247. This reflects the dominance of intense alteration in the footwall of east Thalanga.

MgO: MgO content of most samples from TH270 is well above background (2–15 %). most altered rhyolite samples from TH247 have ~2% MgO.

S: Sulphur concentration ranges between <1 % to >2% in TH270 with a general increasing trend towards the Favourable Horizon. In TH247 all

Table 2: Average geochemical composition of main alteration types in the footwall rhyolite of the Thalanga sequence.

	least altered rhyolite		mottled chlorite-sericite (± pyrite) alteration		late quartz (± sphalerite) alteration		chlorite-pyrite alteration		quartz-pyrite alteration		carbonate - calcsilicate alteration		massive to semi-massive carbonate-chlorite-tremolite	
	n= 8		n=31		n=9		n=18		n=10		n=6		n=17	
	av.	std dev	av.	std dev	av.	std dev	av.	std dev	av.	std dev	av.	std dev	av.	std dev
wt %														
SiO2	78.4	2	76.0	5.2	80.1	4.0	70.4	9.4	75.7	7.6	75.7	6.2	31.6	12.7
TiO2	0.10	0.02	0.10	0.02	0.08	0.02	0.09	0.04	0.07	0.03	0.08	0.02	0.06	0.06
Al2O3	11.8	1	12.9	2.9	11.0	2.4	12.7	3.2	10.5	3.8	10.6	1.3	4.4	2.5
Fe2O3	1.4	0.5	1.8	0.8	1.3	0.6	8.3	4.8	7.8	8.5	1.9	1.1	3.3	3.2
MnO	0.03	0.01	0.04	0.03	0.03	0.03	0.12	0.08	0.03	0.04	0.13	0.17	0.52	0.43
MgO	0.5	0.2	2.1	1.3	1.3	1.1	5.2	3.3	2.0	1.2	2.2	1.9	16.7	6.4
CaO	0.8	0.5	0.4	0.6	0.2	0.2	0.05	0.12	0.10	0.20	4.2	4.1	19.0	8.3
Na2O	3.7	1.0	1.4	1.1	1.9	1.6	0.15	0.07	0.21	0.16	1.4	1.1	0.30	0.48
K2O	3.2	0.9	4.7	2.5	3.8	2.2	2.8	1.2	3.1	1.2	3.4	2.7	0.43	0.68
P2O5	0.01	0.005	0.02	0.01	0.01	0.004	0.01	0.005	0.01	0.003	0.03	0.01	0.17	0.18
ppm														
Ba	790	400	2170	4130	990	920	640	930	2150	2840	1140	1240	16940	21330
Cu	12	22	55	180	12	10	350	770	120	290	15	17	4910	5760
Pb	14	7	205	950	70	80	40	60	220	340	37	18	89670	12900
Zn	70	60	710	2080	300	610	590	920	550	780	121	84	26400	33500
Ag-ICP	<0.5		0.68	2.66	<0.2		0.7	1.3	1.5	3.2	0.3	0.4		
As-ICP/XRF	1.5	1.5	4	5	3	3	12	12	16	19	2	3		
Bi-ICP	1	1	0.6	0.7	0.6	0.4	6	4	9.5	8.3	1	1		
Cd-ICP	<0.2		1.8	5.0	0.9	1.7	0.9	1.4	1.5	2.0	0.4	0.3		
Cr	1	1	2	1	1	1	2	1	<1		1	1		
Cs-ICP	0.7	0.4	1.3	0.9	0.7	0.3	0.9	1.2	1.3	1.1	1.1	0.9		
Mo-ICP	0.3	0.3	2.3	3.2	2.9	1.8	5.1	8.3	18	23	1.1	1.1		
Nb	14	2	16	4	14	4	16	6	13	5	15	5	4	3
Ni	2	1	2	1	1	0.3	1	1	3	4	2	0		
Rb	75	21	130	60	92	51	97	66	100	40	86	45		
Sb-ICP	<0.2		1.7	6.9	0.3	0.1	0.28	0.20	1.3	1.7	1.5	2.5		
Sr	68	30	58	68	37	14	10	4	37	66	99	31		
Th	12	3	14	4	12	3	13	4	11	4	12	2		
Tl-ICP	<0.5		2.1	3.8	0.8	0.4	1.6	3.3	1.9	2.0	1.7	1.8		
U-ICP	2.4	0.5	3.2	1.3	2.8	0.8	3.1	1.0	2.6	1.0	3.1	1.5		
V	1	1	3	6	2	3	2	2	3	3	4	4		
Y	37	4	43	13	35	11	40	15	38	11	44	16	10	11
Zr	143	19	151	40	124	32	140	37	117	40	127	19	83	48
S %	0.05	0.05	0.50	0.52	0.47	0.38	2.8	2.2	4.9	5.7	0.37	0.54	3.7	4.2
Ti/Zr	4.2	0.3	3.9	0.3	4.0	0.3	3.8	0.6	3.8	0.3	3.8	0.5	5.8	11.3
Zr/Y	3.9	0.3	3.6	0.7	3.6	0.7	3.7	0.6	3.1	0.7	3.1	0.8		
Ti/Th	51	10	44	7	42	6	42	12	41	7	39	4		
A.I.	46	9	77	17	69	26	97	1	94	5	54	25	48	19
CCP-index	20	5	38	15	30	15	79	10	67	16	43	23	51	19
LOI %	0.58	0.16	1.84	0.83	1.35	0.72	4.7	1.7	5.2	4.1	1.9	1.1	9.9	6.1
CO2													11.2	8.9

Data: this study except massive to semi-massive carbonate-chlorite-tremolite alteration (Herrmann, 1994, table 1, groups 33, 34, and 35)

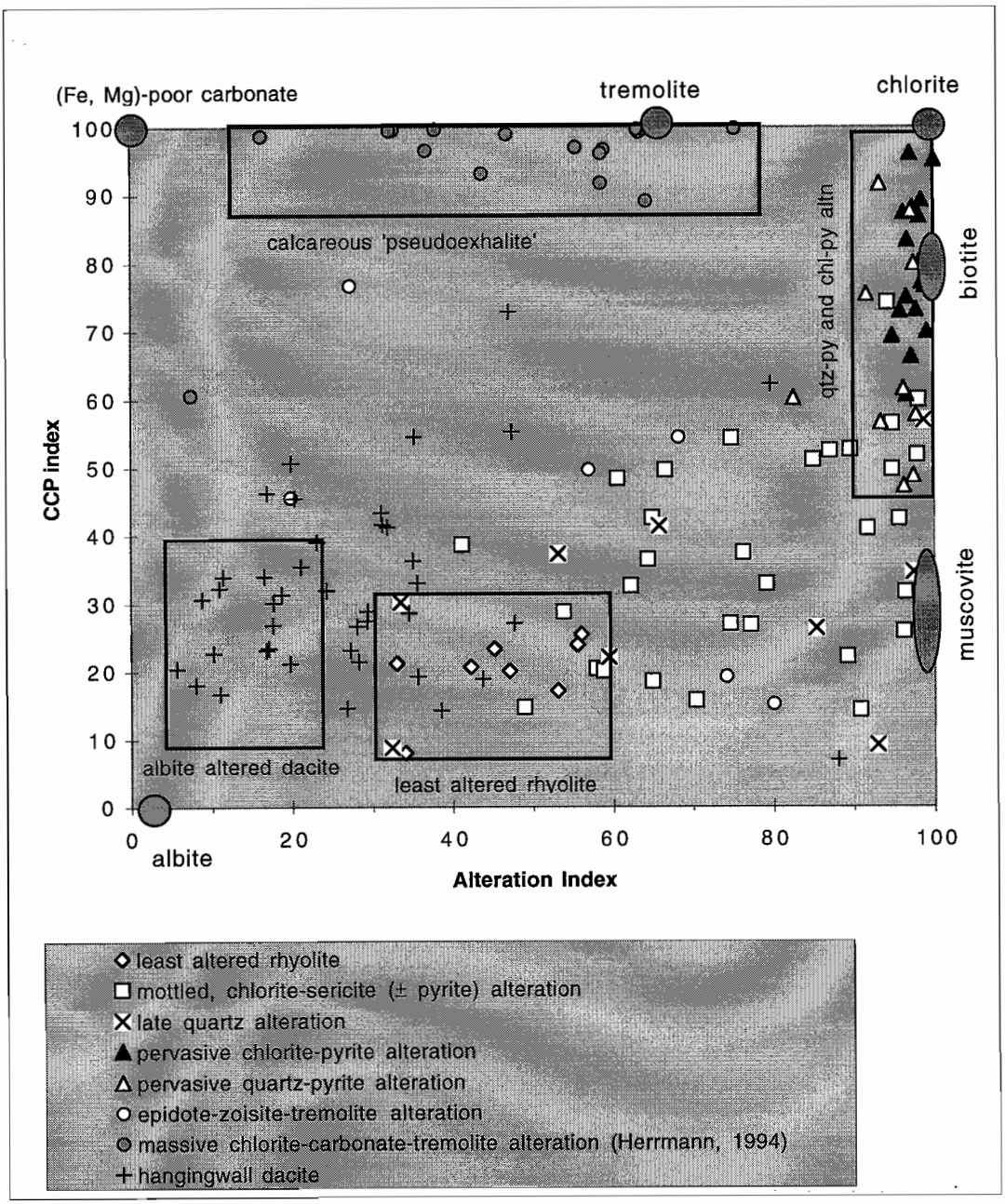

Fig. 6 A plot of alteration index versus carbonate-chlorite-pyrite index (CCP index) separates the rhyolite analyses into distinctive field depending on intensity and type of alteration.
Alteration index: $(K_2O+MgO)/(K_2O+MgO+Na_2O+CaO) * 100$
CCP index: $(MgO+FeO)/(MgO+FeO+Na_2O+K_2O) * 100$
Fields for muscovite, biotite and chlorite composition were calculated from microprobe data.

samples have ~0.5% S except for one sample from the quartz-pyrite-sericite zone just below the mineralisation (2%).

Alteration index: Most samples from TH270 have an alteration index >90 and in TH247 values for the alteration index range unsystematically between 30 and 98.

Carbonate-chlorite-pyrite (CCP) index: The CCP index shows a good positive trend with proximity to ore. It increases from 40 at the start of TH270 to values around 90 close to the Favourable Horizon. In TH247 it increases from 20 in the least altered rhyolite to 50 close to the mineralisation.

S/Na_2O: The S/Na_2O ratio shows a general

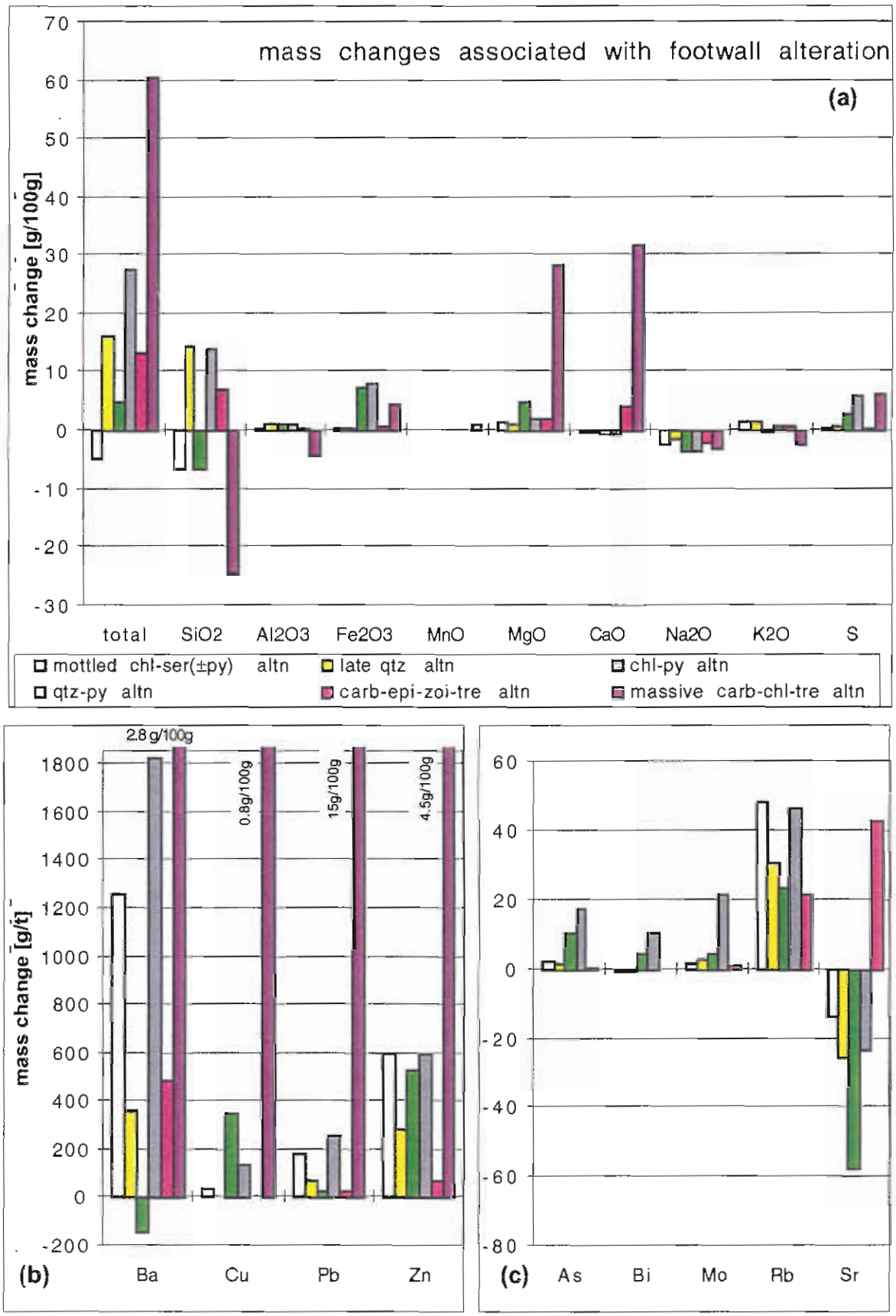

Fig. 7: Results of mass change calculation associated with the various footwall alteration types observed at Thalanga.

increasing trend towards Favourable Horizon in TH270 which has a similar pattern to S. In TH247 only the sample from the quartz-pyrite-sericite zone has an elevated S/Na_2O ratio.

Ba: The Ba concentration is generally decreasing towards the Favourable Horizon in TH270 except for the rhyolite sample closest to mineralisation (8.9 % Ba) which contains substantial barite. In TH247 Ba ranges erratically between 200 and 3000 ppm.

Cu: The Cu concentration in samples from TH270 shows a very good positive correlation with zones of intense chlorite-pyrite alteration whereas in TH247 least altered and strongly altered samples have comparable Cu contents.

Pb and Zn: Pb and Zn concentrations are generally higher than background in TH270 and TH247, however no systematic trend can be observed.

Mo, Bi, and As: Most samples from TH270 have high concentrations of these elements without displaying a consistent systematic increase towards the Favourable Horizon. However the sample just below the mineralisation has the highest Mo value (24 ppm). In TH247 the concentration of these elements in generally far less than in TH270 and often in the order of the background value. Only the sample from the quartz-pyrite-sericite zone just below the mineralisation has consistently elevated concentrations (eg. 50 ppm As).

Tl: Tl concentrations are mostly below 1 ppm for all samples from TH270 and TH247 except for samples just below the Favourable Horizon (2 to 4.2 ppm).

Rb/Sr: The Rb/Sr ratio shows a general increase towards the Favourable Horizon in east and west Thalanga which is somewhat more strongly developed in TH270 (except for the barite-rich sample close to the mineralisation).

The data from DDH TH382A show that there is no reliable geochemical indication for the Thalanga mineralisation in the hangingwall dacite. However, there are occasional samples with elevated trace element concentrations (typically Zn) such as the sample ~ 20 m above the Favourable Horizon in drill hoe TH382A (Fig. A3).

Alteration mineral chemistry

Chlorite, biotite, and muscovite from altered and unaltered Thalanga footwall rhyolite were analysed by microprobe in order to investigate any compositional variation with regard to proximity to ore. Samples from diamond drill hole TH247 (west Thalanga) are most suitable for this purpose because 220 m (true thickness) of variable altered footwall stratigraphy are intersected. In addition to 12 samples from TH247 two samples of least altered rhyolite from the railway cutting were analysed.

The abundance of chlorite, biotite, and muscovite varies strongly between individual samples. In general, least altered samples contain some muscovite and biotite but only accessory chlorite whereas altered rhyolite contain variable amounts of chlorite, biotite and muscovite. Muscovite is especially abundant in a sample from the quartz-pyrite zone directly below the mineralisation (TH247-347). One sample from the Favourable Horizon represents the chlorite-carbonate-tremolite alteration type and lacks any biotite or muscovite (TH247-361.30).

In general, chlorite and biotite from any single sample are homogeneous in composition whereas muscovites show some compositional variability. Average structural formulae for chlorite, biotite, and muscovite were calculated for each sample in order to illustrate the principal compositional changes with proximity to ore (Table 3). In the following, the principal compositional characteristics and trends are discussed.

Chlorite: Chlorites range in composition from chamosite (Fe-rich) to chlinochlore (Mg-rich) and there is a strong linear correlation between iron and magnesium content (Fig. 8a) indicative of a simple Mg <=> Fe exchange substitution. The chlorites contain ~2.1 to 3.2 Al cations per formula unit (pfu) in the octahedral position and slightly less Al cations occur in tetrahedral sites (1.8–2.6 pfu). Manganese is only a minor component in all chlorites analysed. The X_{Mg}-ratio (Mg/Mg+Fe) of chlorite shows a strong positive correlation with proximity to the Favourable Horizon and is a very good vector to ore at Thalanga (Figs 8a, 9). Least altered rhyolite from the railway cutting and the start of diamond drill hole TH247 have accessory chlorite with high iron concentrations (X_{Mg}-ratio = 0.45). Approaching the ore position the

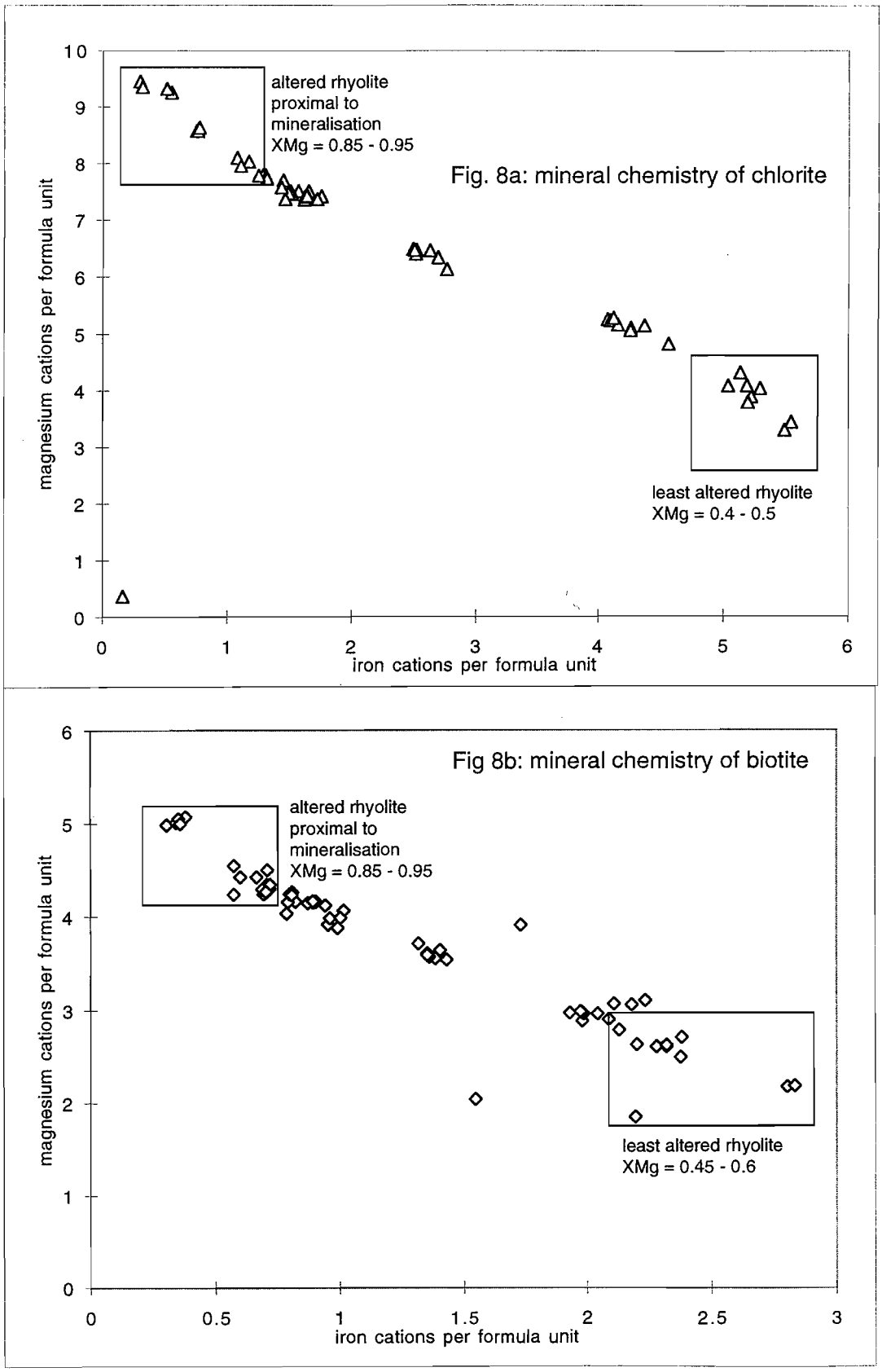

Fig. 8: Relationship between magnesium and iron content of chlorite and biotite in altered and least altered Thalanga footwall rhyolite.

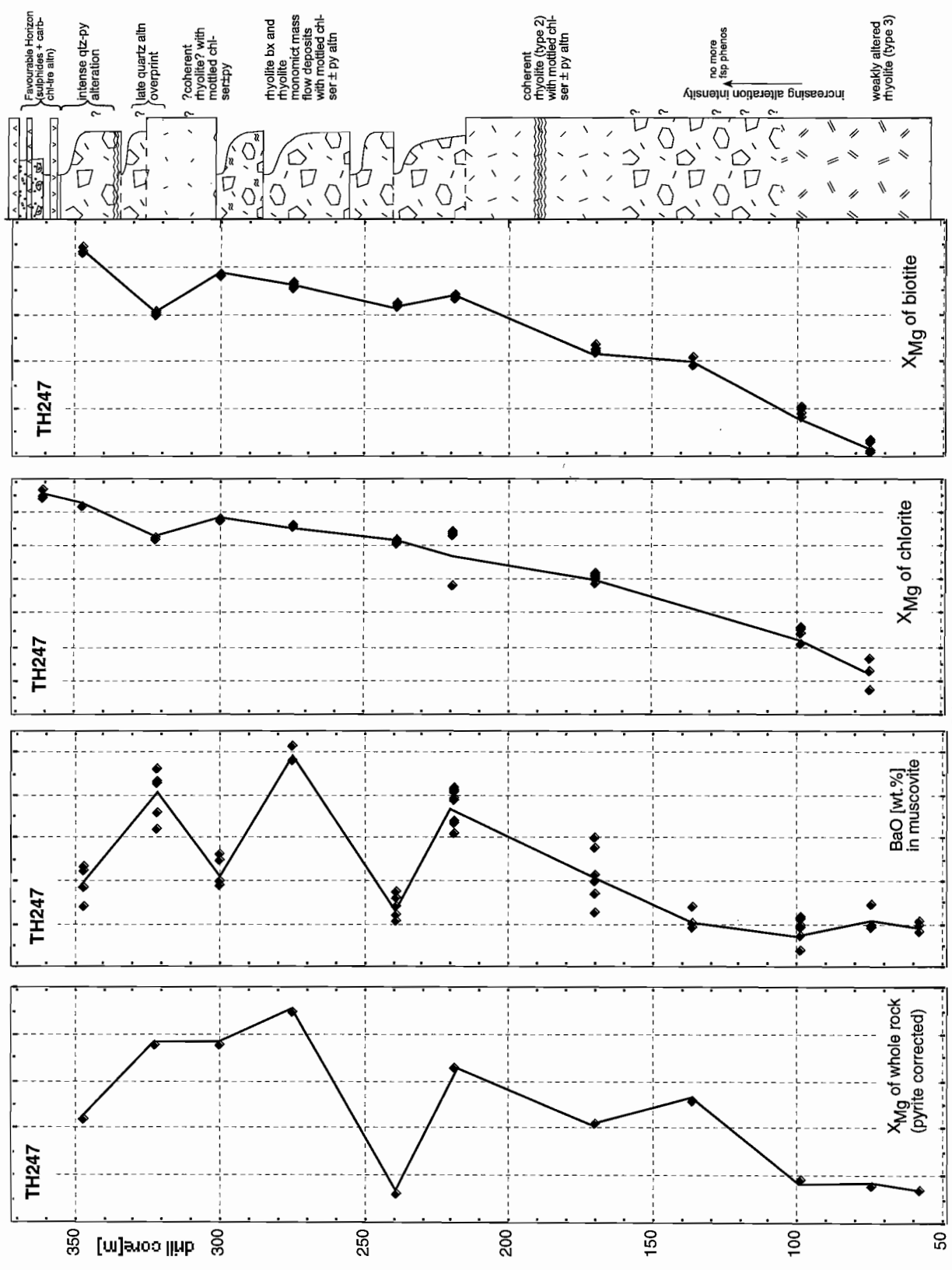

Fig. 9

Fig. 9: Downhole plot of TH247 (west Thalanga, section A) showing the X_{Mg} ratio of chlorite and biotite which increase towards the mineralisation. The X_{Mg} ratio of whole rock XRF analyses is shown for comparison. Barium in muscovite is often elevated in altered Thalanga footwall rhyolite.

- elevated Mo, Bi and As (not always for mottled chlorite-sericite±pyrite alteration)
- increase in Rb/Sr ratio
- increase in X_{Mg}-ratio of chlorite, biotite and whole rock

Geochemical proximity indicators to the Thalanga mineralisation on a mine scale are:

- strongly elevated As, Bi, and Mo
- anomalous Tl
- locally strong Ba enrichment
- fluorine enrichment in biotite (? and whole rock)

Whole rock analyses of rhyolite with mottled chlorite-sericite±pyrite alteration often show inconsistent trends with proximity to ore. By contrast, microprobe analyses of chlorite and biotite reveal that the Mg : Fe ratio of these minerals increases systematically towards the Favourable Horizon with remarkable little scatter. Therefore, increase in the X_{Mg}-ratio of chlorite and biotite is probably the best indicator for potential Thalanga-style mineralisation on an exploration scale.

Genetic consideration

The stratiform aspect of the mineralisation and the marked contrast in alteration style and alteration intensity between the footwall and the hangingwall are strong evidence for the syngenetic origin of the Thalanga VHMS deposit.

Volcanic facies interpretation of footwall rhyolite indecate that the geometry of the hydrothermal system is not controlled by the spatial arrangement of coherent and clastic facies.

The stratabound geometry of zones with intense quartz-pyrite alteration directly below the mineralisation indicate that fluid discharge was unfocussed and that sub-seafloor replacement may have played an important role in the development of proximal alteration zones and some parts of the ore body.

Mass gains of magnesium and the importance of the X_{Mg}-ratio of chlorite and biotite as a vector to ore suggest that Mg-rich fluid (ie. sea-water) was involved in the genesis of the Thalanga massive sulphide deposit.

References

Barrett, T. J., and MacLean, W. H., 1994, Chemostratigraphy and hydrothermal alteration in exploration for VHMS deposits in Greenstones and younger volcanic rocks, in Lentz, D. R., ed., Alteration and alteration processes associated with ore-forming systems, 11. Short Course Notes, Geological Association of Canada, p. 433-467.

Berry, R. F., Huston, D.L., Stolz, A.J., Hill, A.P., Beams, S.D., Kuronen, U. & Taube, A., 1992, Stratigraphy, structure and volcanic hosted mineralisation of the Mt. Windsor Subprovince, North Queensland, Australia: Economic Geology, v. 87, p. 739-763.

Duhig, N. C., Stolz, J., Davidson, G. J., and Large, R. R., 1992, Cambrian microbial and silica gel textures in silica iron exhalites from the Mount Windsor Volcanic Belt, Australia: their petrography, chemistry, and origin: Economic Geology, v. 87, p. 764-784.

Herrmann, W., 1994, Immobile element geochemistry of altered Volcanics and Exhalites at the Thalanga Deposit, North Queensland:. M. Econ. Geol. thesis, University of Tasmania.

Hill, A. P., 1996, Structure, volcanic setting, hydrothermal alteration and genesis of the Thalanga massive sulphide deposit. PhD thesis, University of Tasmania, p. 404.

Ishikawa, Y., Sawaguchi, T., Iwaya, S. & Horiachi, M., 1976: Delineation of prospecting targets for Kuroko deposits based on modes of volcanism of underlying dacite and alteration halos. Mining Geology 26: 105-117. (in Japanese with English abstract)

Large, R.R. 1996, The Hercules-Mount Read traverse: Relationships between volcanic mineralogy, alteration and geochemistry: AMIRA/ARC project P439, report 3, pp. 153-234.

MacLean, W. H., 1990, Mass change calculations in altered rock series: Mineralium Deposita, v. 25, p. 44-49.

MacLean, W. H., and Barrett, T. J., 1993, Lithogeochemical techniques using immobile elements: Journal of Geochemical Exploration, v. 48.

MacLean, W. H., and Kranidiotis, P., 1987, Immobile elements as monitors of mass transfer in hydrothermal alteration: Phleps Dodge massive sulfide deposit, Matagami, Quebec: Economic Geology, v. 82, p. 951-962.

Paulick, H. (1997): Volcanic facies analysis, alteration, and geochemistry of the host rock sequence to VHMS-style mineralisation at Thalanga (north Queensland).- AMIRA/ARC project P439, report 4, p 185–223.

Perkins, C., 1993, Isotopic dating of precious and base metal deposits and their host rocks in Eastern Australia, AMIRA, project P334.

Spear, F. S., 1993, Metamorphic phase equilibria and pressure-temperature-time paths, Mineralogical Society of America, monograph, 788 p.

Stolz, A. J., 1995, Geochemistry of the Mount Windsor Volcanics: Implications for the tectonic setting of Cambro-Ordovician volcanic-hosted massive sulfide mineralization in Northeastern Australia: Economic Geology, v. 90, p. 1080-1097.

Stolz, A.J., 1991, Stratigraphy and geochemistry of Mount Windsor Volcanics and associated exhalites. In: Mount Windsor Project Research Report No.2, March 1991, CODES, University of Tasmania, p. 23–84.

Stolz, A.J., 1997, Thalanga footwall study–geochemical vectors to mineralisation, Report to RGC Exploation, p. 78.

Wills, K. J. A., 1985, Thalanga Comprehensive Study–Final Report, Pennaroya (Australia) P/L.

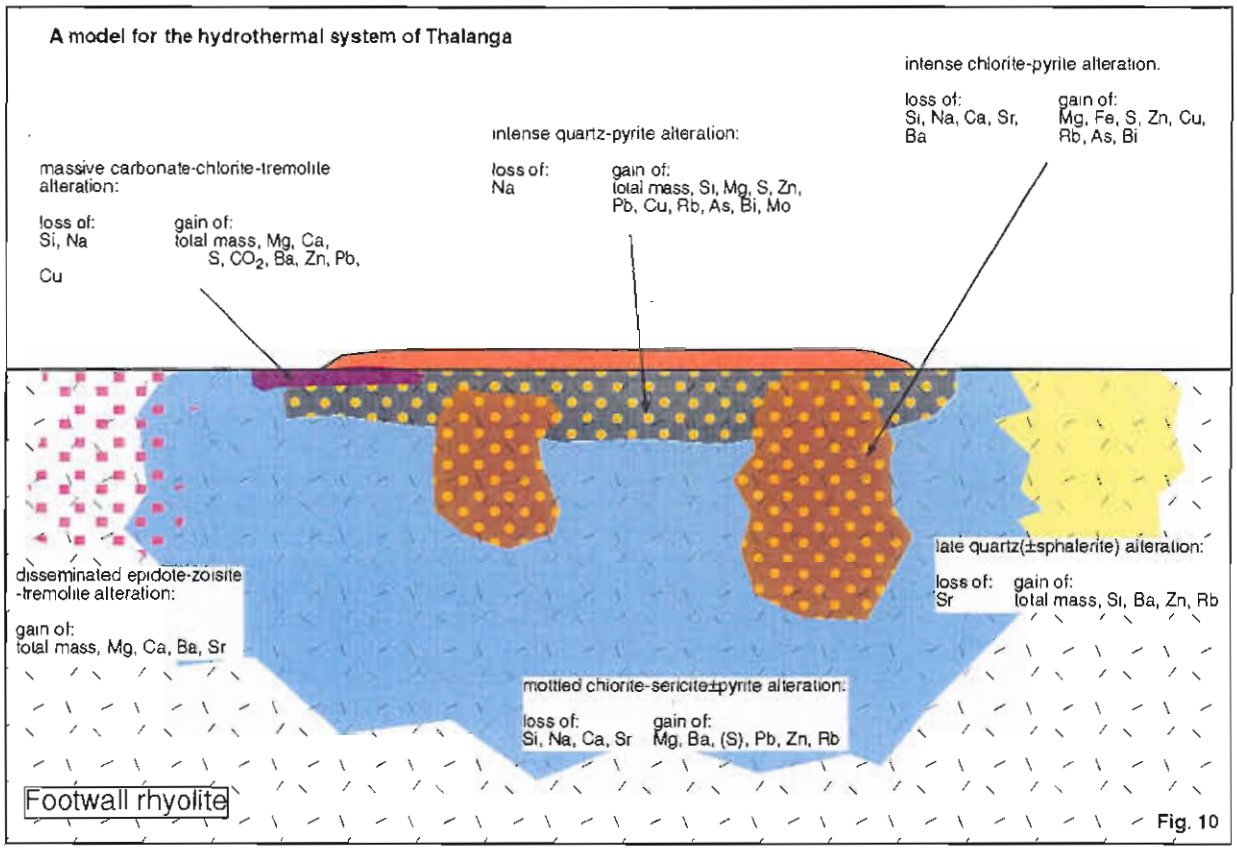

Fig. 10: Model for the Thalanga hydrothermal system outlining the general spatial relationships between alteration types and associated mass change.

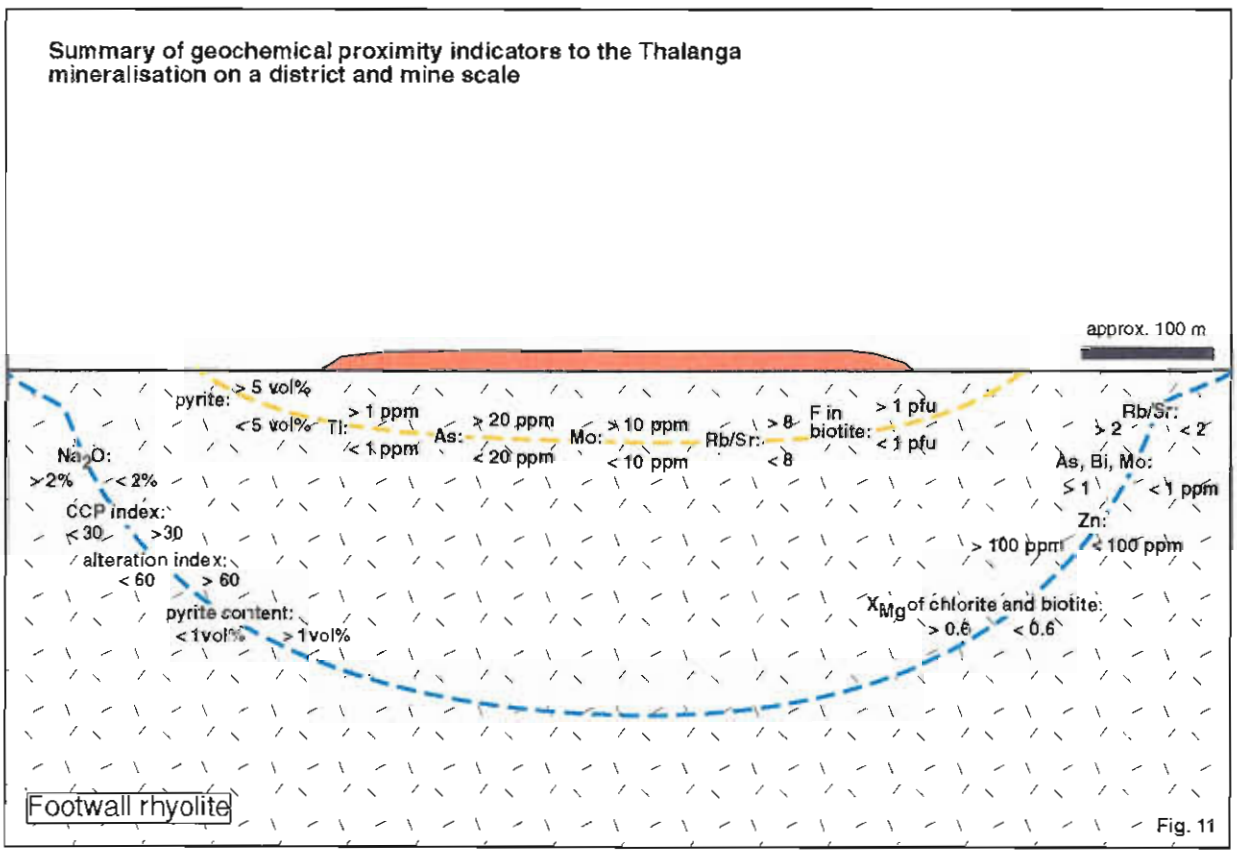

Fig. 11: Summary of geochemical proximity indicators to the Thalanga mineralisation.

Table 3: Structural formulae for chlorite, biotite, and muscovites of altered and unaltered Thalanga footwall rhyolite full data set is included in database compiled for this AMIRA project. THRW1 and THRW5: see report 4 (1994) p. 193 for sample location at railway cutting. equipment: Cameca SX50 (University of Tasmania); acceleration voltage: 15 kV; beam current: 25 nA; beam diameter: 1 µm standards: quartz (Si), ilmenite (Ti), plagioclase (Al), forsterite (Mg), fayalite (Fe), rhodonite (Mn), apatite (Ca), microcline (K), carnegieite (Na), sphalerite (Zn), barite (Ba), NaCl (Cl), and lithiumflourite (F). detection limits (wt.%; 95% confidence): Si: 0.05, Ti: 0.05, Al: 0.05, Fe: 0.13, Zn: 0.19, Mn: 0.14, Mg: 0.05, Ca: 0.06, Na: 0.05, K: 0.05, Ba: 0.13, F: 0.28, Cl: 0.05.

sample	alteration	chlorite	biotite	muscovite*
TH247-361.30	carbonate-chlorite-tremolite altn in the ore horizon	$Mg_{9.3}Fe_{0.4}Al_{2.1}(Al_{1.8}Si_{6.2}O_{20})(OH)_{16}$ (average of 4 analyses on 4 crystals)	-	-
TH247-347	intense quartz-pyrite-sericite	$Mn_{0.1}Mg_{8.6}Fe_{0.8}Al_{2.4}(Al_{2.2}Si_{5.8}O_{20})(OH)_{16}$ (average of 3 analyses on 4 crystals)	$Na_{0.1}K_{1.8}Mg_5Fe_{0.4}Al_{0.5}(Al_{2.2}Si_{5.8}O_{20})(F_{1.7}OH_{2.3})$ (average of 5 analyses on 5 crystals)	$Na_{0.1}K_{1.5}Mg_{0.5}Fe_{0.1}Al_{3.6}(Al_{1.6}Si_{6.4}O_{20})(F_{0.2}OH_{3.8})$ (average of 5 analyses on 5 crystals)
TH247-322.20	mottled chl-ser±py altn with late qtz overprint	$Mn_{0.2}Mg_{7.5}Fe_{1.6}Al_{2.6}(Al_{2.5}Si_{5.5}O_{20})(OH)_{16}$ (average of 3 analyses on 3 crystals)	$K_{1.8}Mn_{0.1}Mg_4Fe_1Al_{0.7}Ti_{0.1}(Al_{2.4}Si_{5.6}O_{20})(F_{0.3}OH_{3.7})$ (average of 6 analyses on 6 crystals)	$Na_{0.1}K_{1.5}Mg_{0.4}Fe_{0.2}Al_{3.6}(Al_{1.7}Si_{6.3}O_{20})(OH)_4$ (average of 5 analyses on 5 crystals)
TH247-300	mottled chlorite-sericite±pyrite altn	$Mn_{0.1}Mg_8Fe_{1.1}Al_{2.7}(Al_{2.4}Si_{5.6}O_{20})(OH)_{16}$ (average of 3 analyses on 2 crystals)	$Na_{0.1}K_{1.7}Mg_{4.4}Fe_{0.6}Al_{0.8}Ti_{0.1}(Al_{2.3}Si_{5.7}O_{20})(F_{0.7}OH_{3.3})$ (average of 3 analyses on 2 crystals)	$Na_{0.1}K_{1.5}Mg_{0.4}Fe_{0.2}Al_{3.6}(Al_{1.6}Si_{6.4}O_{20})(F_{0.1}OH_{3.9})$ (average of 4 analyses on 4 crystals)
TH247-274.80	mottled chlorite-sericite±pyrite altn	$Mn_{0.1}Mg_{7.8}Fe_{1.3}Al_{2.7}(Al_{2.5}Si_{5.5}O_{20})(OH)_{16}$ (average of 4 analyses on 3 crystals)	$K_{1.8}Mn_{0.1}Mg_{4.3}Fe_{0.7}Al_{0.7}(Al_{2.3}Si_{5.7}O_{20})(F_{0.5}OH_{3.5})$ (average of 9 analyses on 8 crystals)	$Na_{0.1}K_{1.6}Mg_{1.6}Fe_{0.3}Al_{2.7}(Al_2Si_6O_{20})(F_{0.2}OH_{3.8})$ (average of 2 analyses on 2 crystals)
TH247-238.80	mottled chlorite-sericite±pyrite altn	$Mn_{0.1}Mg_{7.4}Fe_{1.7}Al_{2.6}(Al_{2.5}Si_{5.5}O_{20})(OH)_{16}$ (average of 6 analyses on 3 crystals)	$K_{1.8}Mg_{4.2}Fe_{0.9}Al_{0.7}Ti_{0.1}(Al_{2.3}Si_{5.7}O_{20})(F_{0.9}OH_{3.1})$ (average of 5 analyses on 4 crystals)	$Na_{0.2}K_{1.3}Mg_{0.3}Fe_{0.2}Al_{3.7}(Al_{1.7}Si_{6.3}O_{20})(F_{0.1}OH_{3.9})$ (average of 5 analyses on 7 crystals)
TH247-219	mottled chlorite-sericite±pyrite altn	$Mn_{0.1}Mg_{6.5}Fe_{1.3}Al_{3.2}(Al_{2.1}Si_{5.9}O_{20})(OH)_{16}$ (average of 7 analyses on 4 crystals)	$K_{1.7}Mn_{0.1}Mg_{4.2}Fe_{0.8}Al_{0.7}Ti_{0.1}(Al_{2.3}Si_{5.7}O_{20})(F_{0.7}OH_{3.3})$ (average of 8 analyses on 8 crystals)	$Na_{0.2}K_{1.5}Mg_{0.5}Fe_{0.2}Al_{3.5}(Al_{1.8}Si_{6.2}O_{20})(F_{0.1}OH_{3.9})$ (average of 9 analyses on 9 crystals)
TH247-169.80	mottled chlorite-sericite±pyrite altn	$Mn_{0.2}Mg_{6.4}Fe_{2.6}Al_{2.8}(Al_{2.6}Si_{5.4}O_{20})(OH)_{16}$ (average of 7 analyses on 7 crystals)	$K_{1.9}Mn_{0.1}Mg_{3.6}Fe_{1.4}Al_{0.7}Ti_{0.1}(Al_{2.4}Si_{5.6}O_{20})(F_{0.6}OH_{3.4})$ (average of 6 anelyses on 6 crystals)	$Na_{0.2}K_{1.5}Mg_{0.8}Fe_{0.5}Al_{3.1}(Al_{1.8}Si_{6.2}O_{20})(F_{0.2}OH_{3.8})$ (average of 7 analyses on 7 crystals)
TH247-136.10	mottled chlorite-sericite±pyrite altn	-	$K_{1.7}Mn_{0.1}Mg_{3.7}Fe_{1.6}Al_{0.6}Ti_{0.1}(Al_{2.5}Si_{5.5}O_{20})(F_{0.5}OH_{3.5})$ (average of 2 analyses on 2 crystals)	$Na_{0.1}K_{1.7}Mg_{0.7}Fe_{0.4}Al_{3.2}(Al_{1.8}Si_{6.2}O_{20})(F_{0.1}OH_{3.9})$ (average of 3 analyses on 3 crystals)
TH247-98.60	mottled chlorite-sericite±pyrite altn	$Mn_{0.2}Mg_{5.1}Fe_{4.2}Al_{2.4}(Al_{2.3}Si_{5.7}O_{20})(OH)_{16}$ (average of 8 analyses on 1 crystal)	$K_{1.8}Mn_{0.1}Mg_3Fe_{2.1}Al_{0.6}Ti_{0.1}(Al_{2.4}Si_{5.6}O_{20})(F_{0.5}OH_{3.5})$ (average of 8 analyses on 8 crystals)	$Na_{0.1}K_{1.5}Mg_{0.6}Fe_{0.5}Al_{3.3}(Al_{1.8}Si_{6.2}O_{20})(F_{0.1}OH_{3.9})$ (average of 9 analyses on 9 crystals)
TH247-74.50	mottled chlorite-sericite±pyrite altn	$Mn_{0.3}Mg_{3.6}Fe_{5.4}Al_{2.5}(Al_{2.3}Si_{5.7}O_{20})(OH)_{16}$ (average of 3 analyses on 1 crystal)	$K_{1.8}Mn_{0.1}Mg_{2.6}Fe_{2.4}Al_{0.5}Ti_{0.2}(Al_{2.4}Si_{5.6}O_{20})(F_{0.6}OH_{3.4})$ (average of 6 analyses on 5 crystals)	$Na_{0.1}K_{1.4}Mg_{0.3}Fe_{0.4}Al_{3.4}(Al_{1.5}Si_{6.5}O_{20})(F_{0.1}OH_{3.9})$ (average of 4 analyses on 3 crystals)
TH247-57.70	mottled chlorite-sericite±pyrite altn	-	-	$Na_{0.1}K_{1.5}Mg_{0.4}Fe_{0.3}Al_{3.5}(Al_{1.5}Si_{6.5}O_{20})(F_{0.1}OH_{3.9})$ (average of 4 analyses on 4 crystals)
THRW5	unaltered rhyolite (railway cutting)	$Mn_{0.2}Mg_4Fe_{5.2}Al_{2.5}(Al_{2.4}Si_{5.6}O_{20})(OH)_{16}$ (average of 5 analyses on 4 crystals)	$Na_{0.1}K_{1.7}Mn_{0.1}Mg_{2.1}Fe_{2.6}Al_{0.7}Ti_{0.2}(Al_{2.4}Si_{5.6}O_{20})(F_{0.2}OH_{3.8})$ (average of 4 analyses on 4 crystals)	$K_{1.5}Mg_{0.4}Fe_{0.6}Al_{3.3}(Al_{1.5}Si_{6.5}O_{20})(F_{0.1}OH_{3.9})$ (average of 8 analyses on 6 crystals)
THRW1	unaltered rhyolite (railway cutting)	-	$K_{1.7}Mn_{0.1}Mg_{2.6}Fe_2Al_{0.9}Ti_{0.1}(Al_{2.3}Si_{5.7}O_{20})(F_{0.5}OH_{3.5})$ (average of 5 analyses on 5 crystals)	$Na_{0.1}K_{1.5}Mg_{0.5}Fe_{0.5}Al_{3.4}(Al_{1.7}Si_{6.3}O_{20})(F_{0.1}OH_{3.9})$ (average of 2 analyses on 2 crystals)

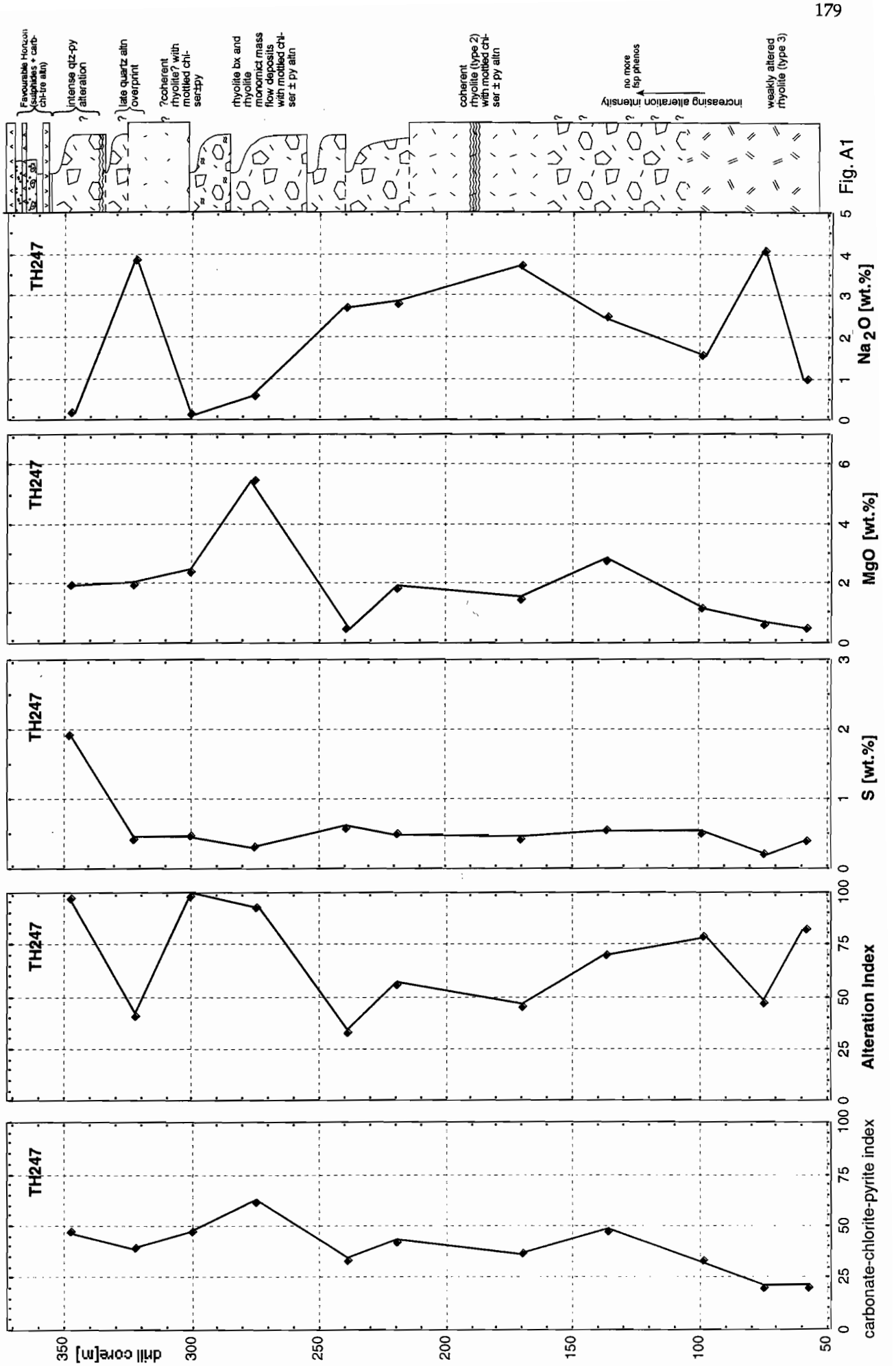

Fig. A1: Downhole geochemical variation of selected elements (Na_2O, MgO, S, Ba, Cu, Pb, Zn, As, Bi, Mo, and Tl) and alteration indices (alteration index, carbonate-chlorite-pyrite index, S/Na_2O and Rb/Sr) in diamond drill hole TH247 (west Thalanga footwall, section A) data: this study and RGC Exploration.

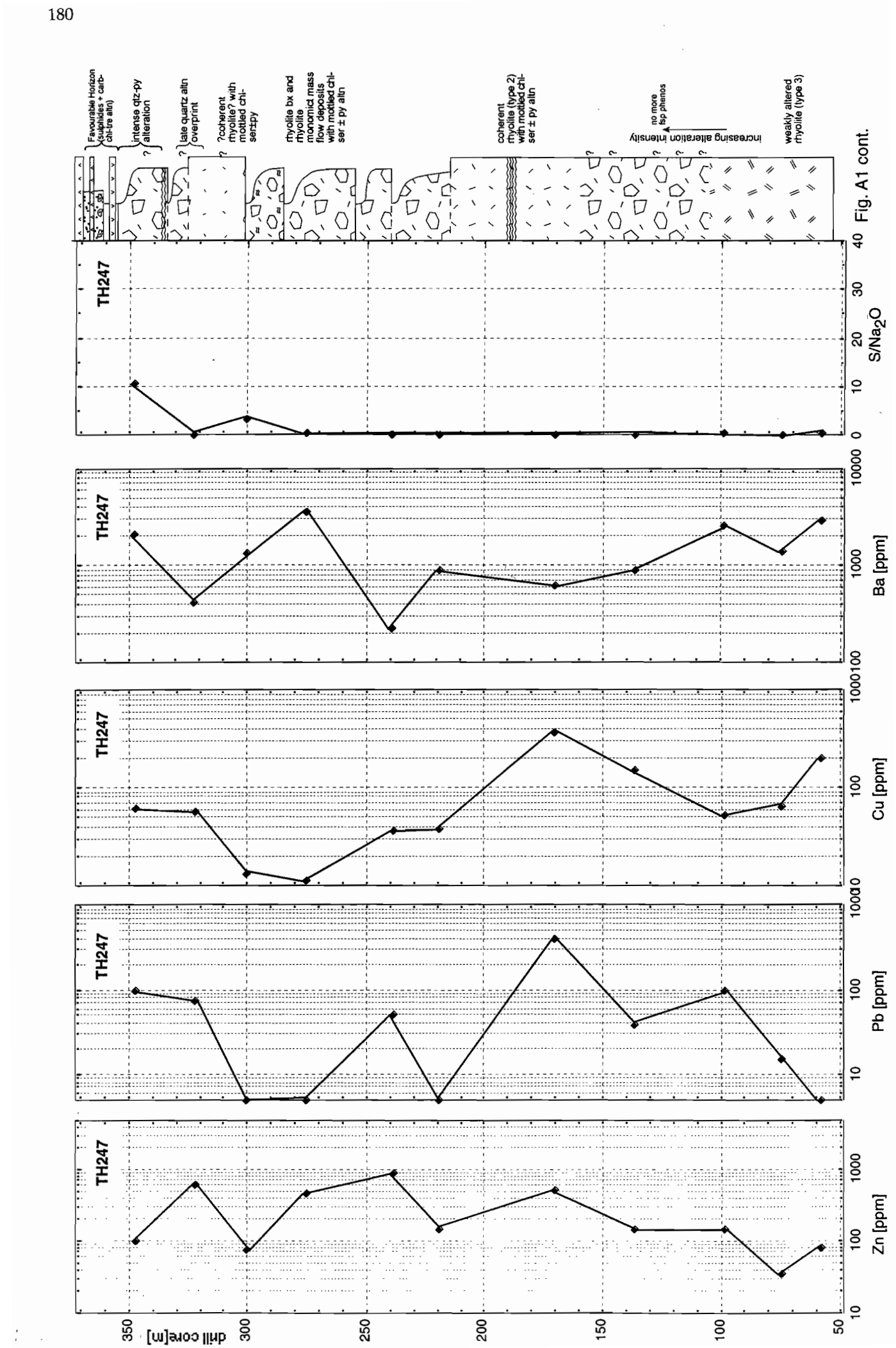
Favourable Horizon (sulphides + carb-chl-tre altn)
intense qtz-py alteration
late quartz altn overprint
?coherent rhyolite? with mottled chl-ser±py
rhyolite bx and rhyolite monomict mass flow deposits with mottled chl-ser ± py altn
coherent rhyolite (type 2) with mottled chl-ser ± py altn
increasing alteration intensity
no more fsp phenos
weakly altered rhyolite (type 3)
TH247
drill core[m]
350
300
250
200
150
100
50
Zn [ppm]
Pb [ppm]
Cu [ppm]
Ba [ppm]
S/Na2O
10
100
1000
10000
0
10
20
30
40

Fig. A1 cont.

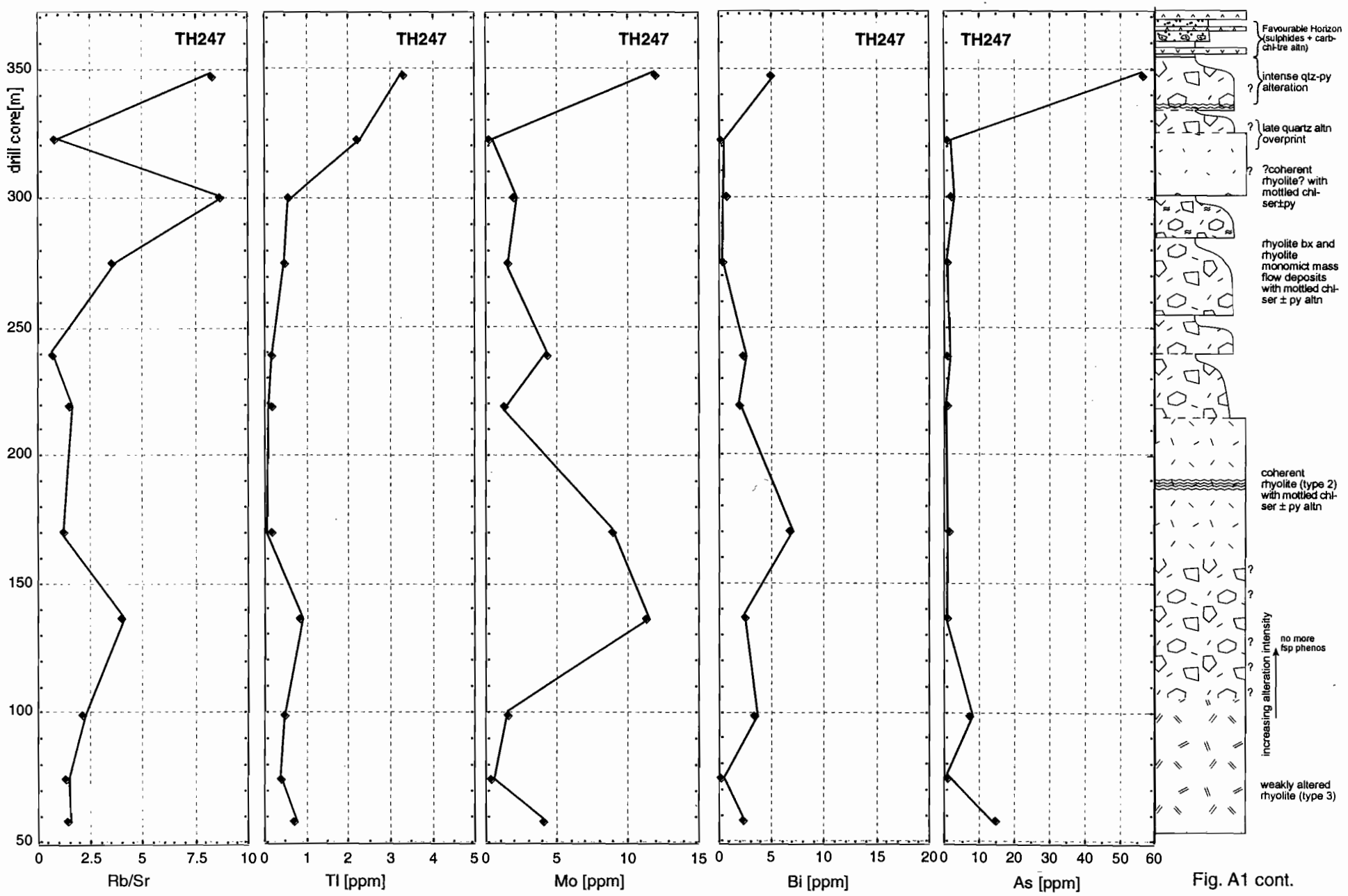
TH247
TH247
TH247
TH247
TH247
drill core[m]
350
300
250
200
150
100
50
0 2.5 5 7.5 10
Rb/Sr
0 1 2 3 4 5
Tl [ppm]
0 5 10 15
Mo [ppm]
0 5 10 15 20
Bi [ppm]
0 10 20 30 40 50 60
As [ppm]
Favourable Horizon (sulphides + carb-chl-tre altn)
intense qtz-py alteration
late quartz altn overprint
?coherent rhyolite? with mottled chl-ser±py
rhyolite bx and rhyolite monomict mass flow deposits with mottled chl-ser ± py altn
coherent rhyolite (type 2) with mottled chl-ser ± py altn
increasing alteration intensity
no more fsp phenos
weakly altered rhyolite (type 3)

Fig. A1 cont.

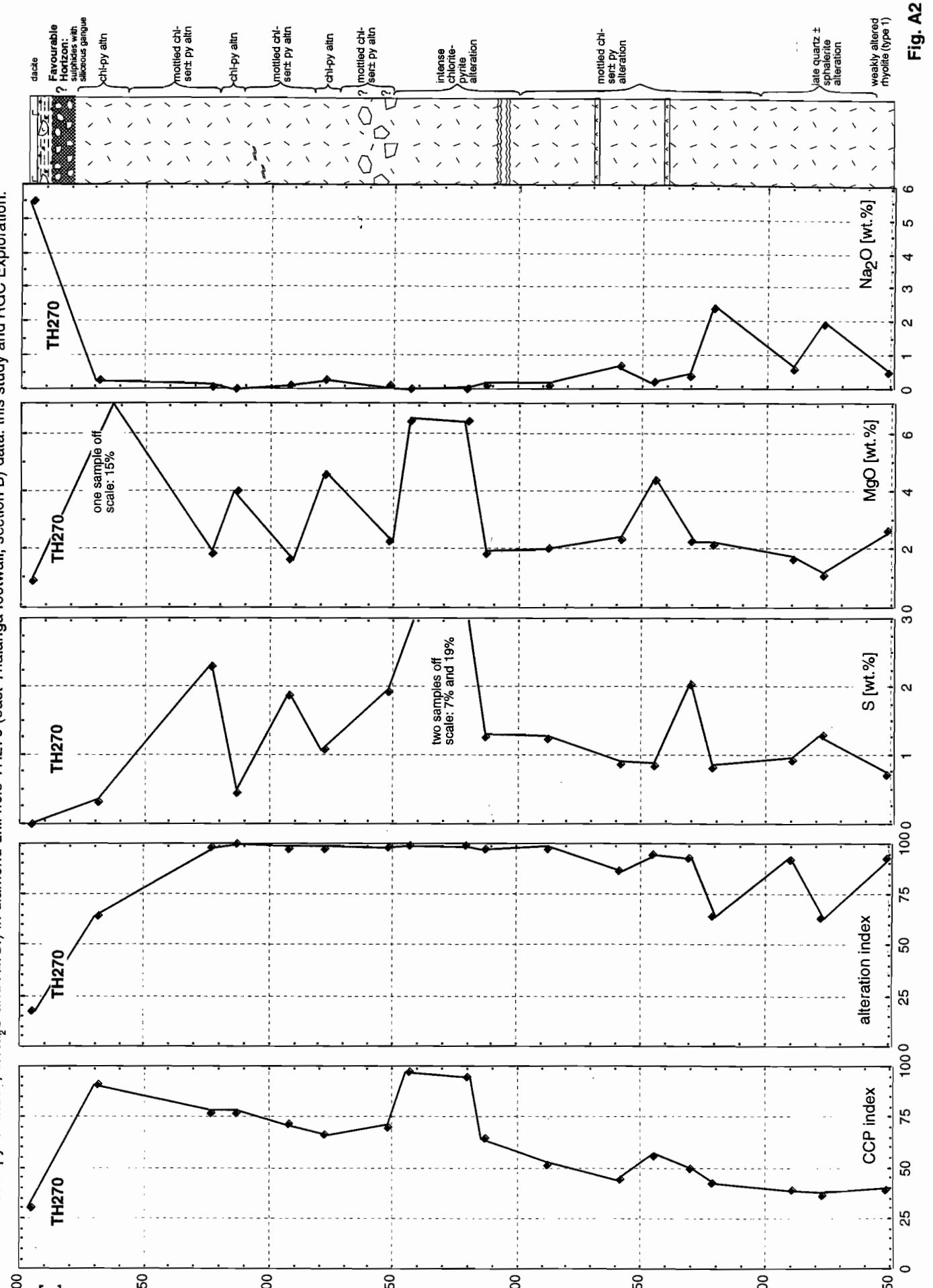

Fig. A2: Downhole geochemical variation of selected elements (Na_2O, MgO, S, Ba, Cu, Pb, Zn, As, Bi, Mo, and Tl) and alteration indices (alteration index, carbonate-chlorite-pyrite index, S/Na_2O and Rb/Sr) in diamond drill hole TH270 (east Thalanga footwall, section B) data: this study and RGC Exploration.

Fig. A2

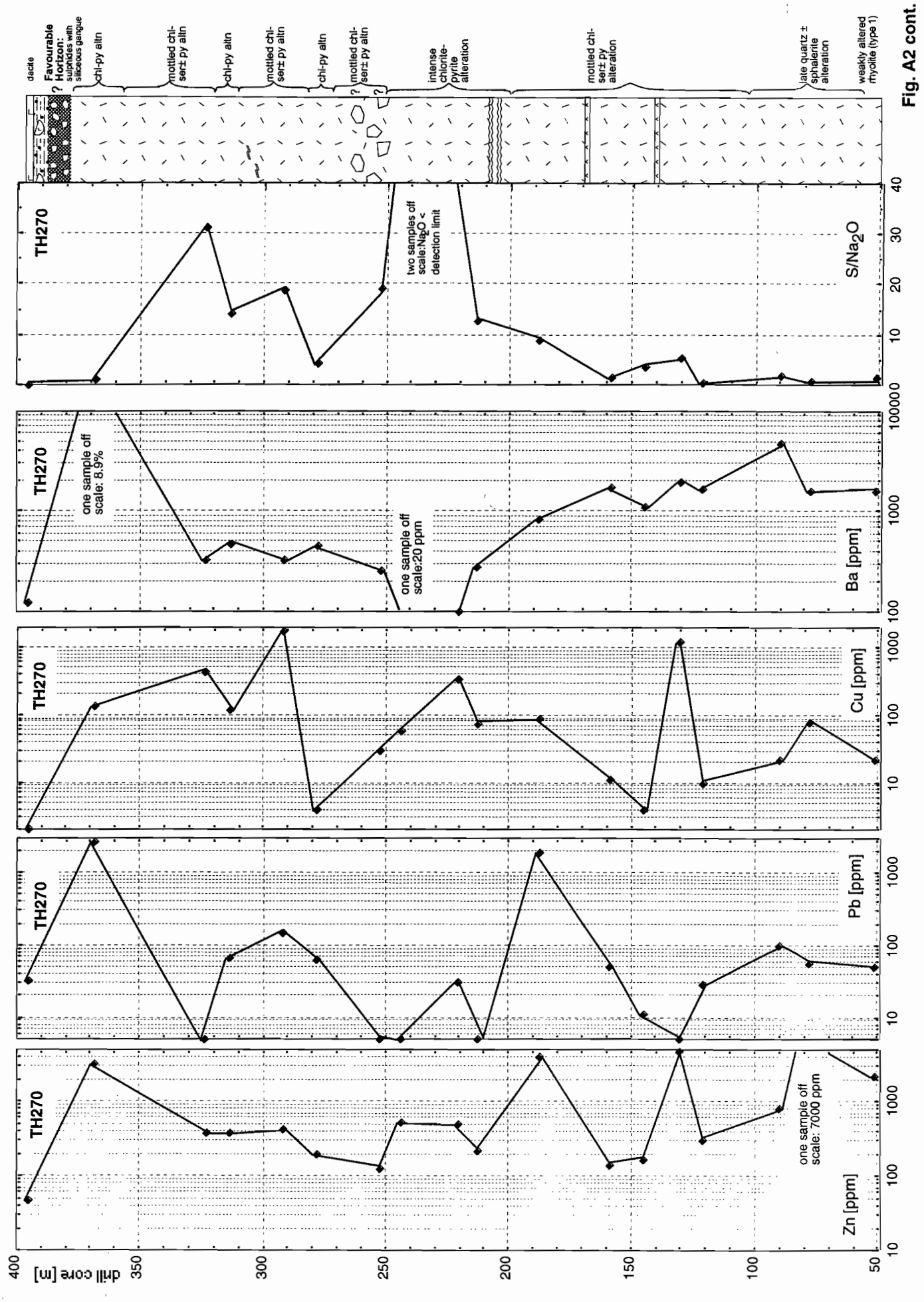
drill core [m]
400
350
300
250
200
150
100
50
TH270
Zn [ppm]
one sample off scale: 7000 ppm
Pb [ppm]
Cu [ppm]
Ba [ppm]
one sample off scale:20 ppm
one sample off scale: 8.9%
S/Na2O
two samples off scale:Na2O < detection limit
10
100
1000
10000
100000
0
10
20
30
40
decke
Favourable Horizon: sulphides with siliceous gangue
chl-py altn
mottled chl-ser± py altn
chl-py altn
mottled chl-ser± py altn
chl-py altn
mottled chl-ser± py altn
intense chlorite-pyrite alteration
mottled chl-ser± py alteration
late quartz ± sphalerite alteration
weakly altered rhyolite (type 1)

Fig. A2 cont.

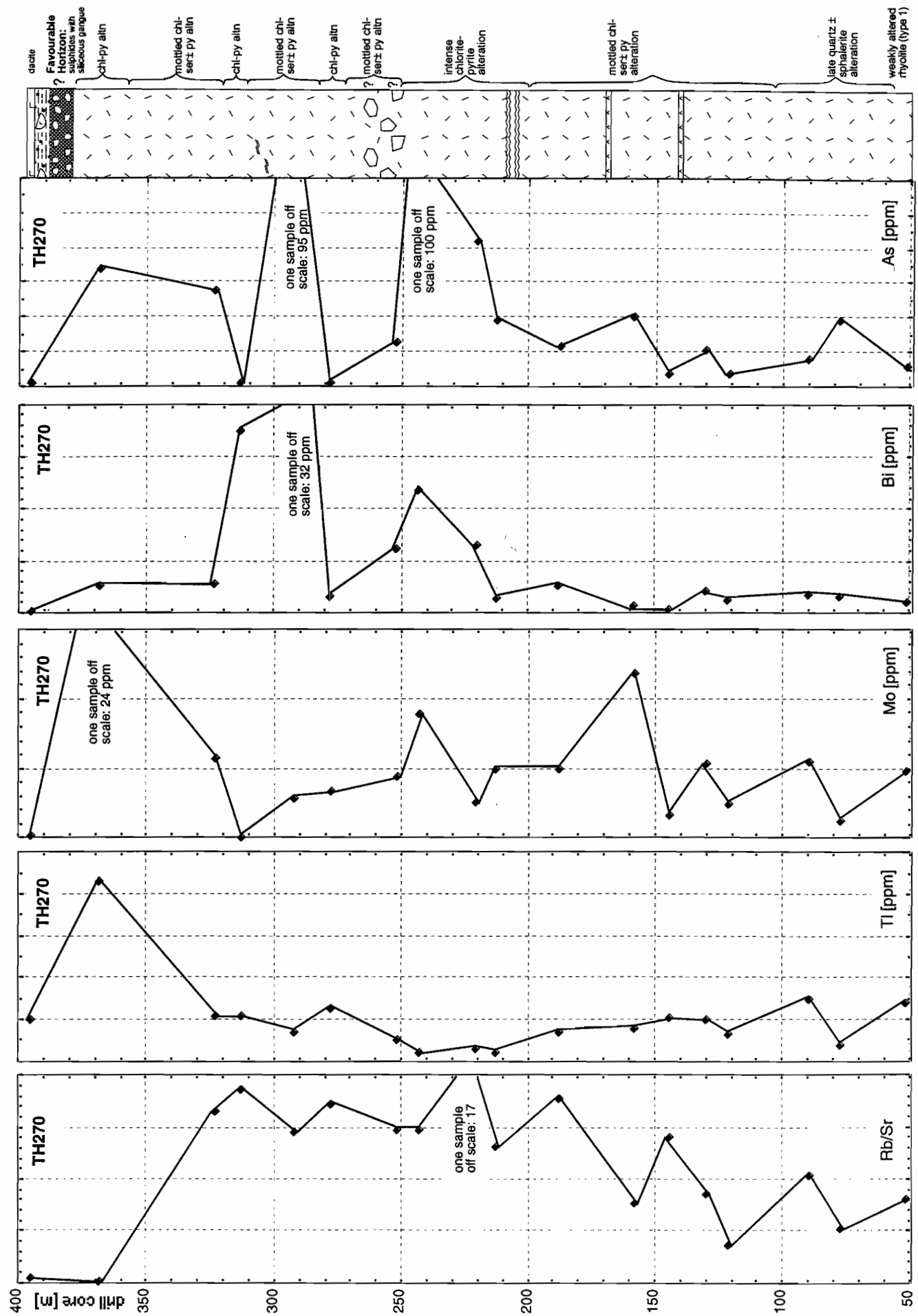
dacite
Favourable Horizon: sulphides with siliceous gangue
chl-py altn
mottled chl-ser± py altn
chl-py altn
mottled chl-ser± py altn
chl-py altn
mottled chl-ser± py altn
intense chlorite-pyrite alteration
mottled chl-ser± py alteration
late quartz ± sphalerite alteration
weakly altered rhyolite (type 1)
TH270
Rb/Sr
one sample off scale: 17
Tl [ppm]
Mo [ppm]
one sample off scale: 24 ppm
Bi [ppm]
one sample off scale: 32 ppm
As [ppm]
one sample off scale: 95 ppm
one sample off scale: 100 ppm
drill core [m]

Fig. A2 cont.

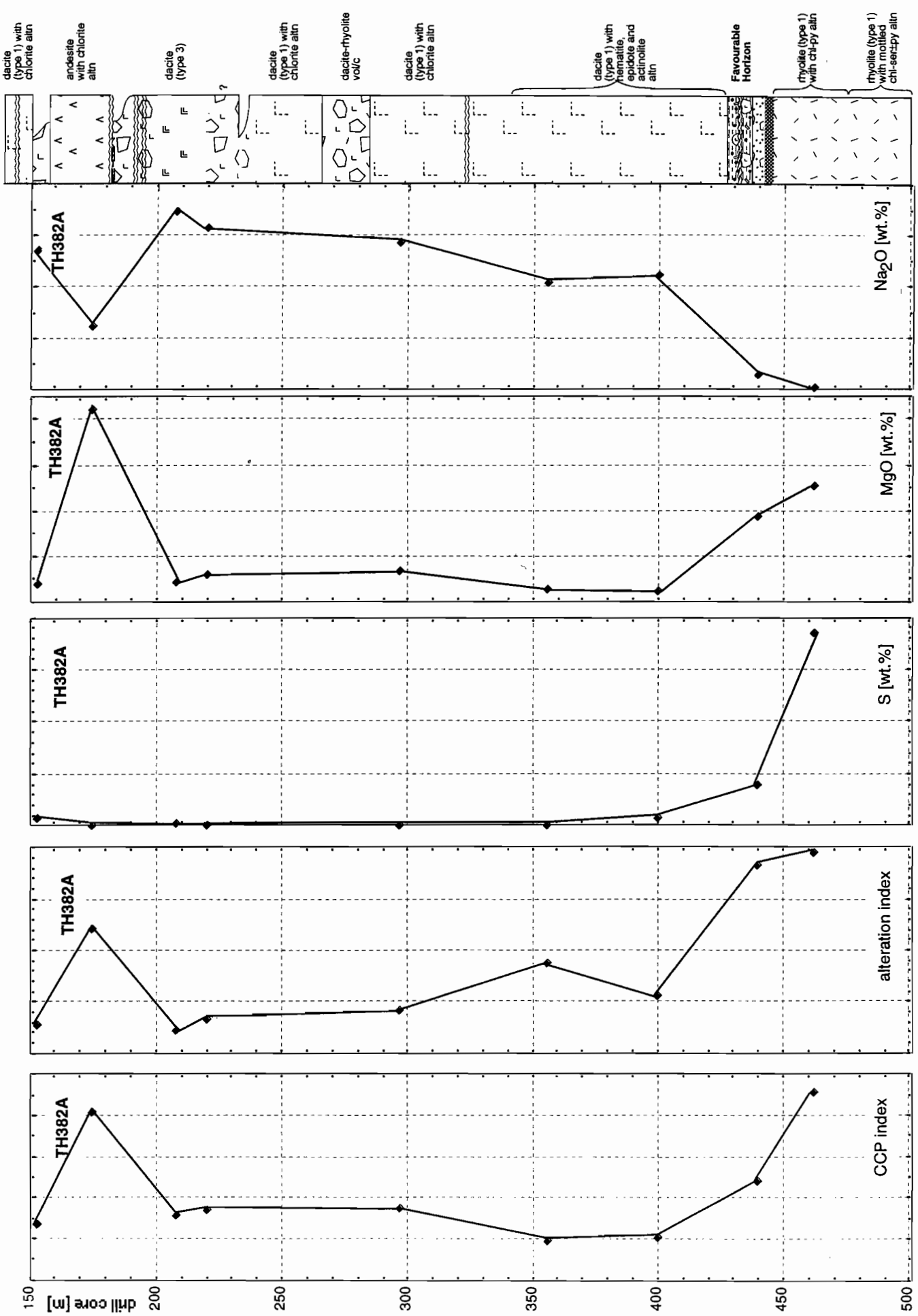

Fig. A3: Downhole geochemical variation of selected elements (Na_2O, MgO, S, Ba, Cu, Pb, Zn, As, Bi, Mo, and Tl) and alteration indices (alteration index, carbonate-chlorite-pyrite index, S/Na_2O and Rb/Sr) in diamond drill hole TH382A (east Thalanga hangingwall, section B) data: this study and RGC Exploration.

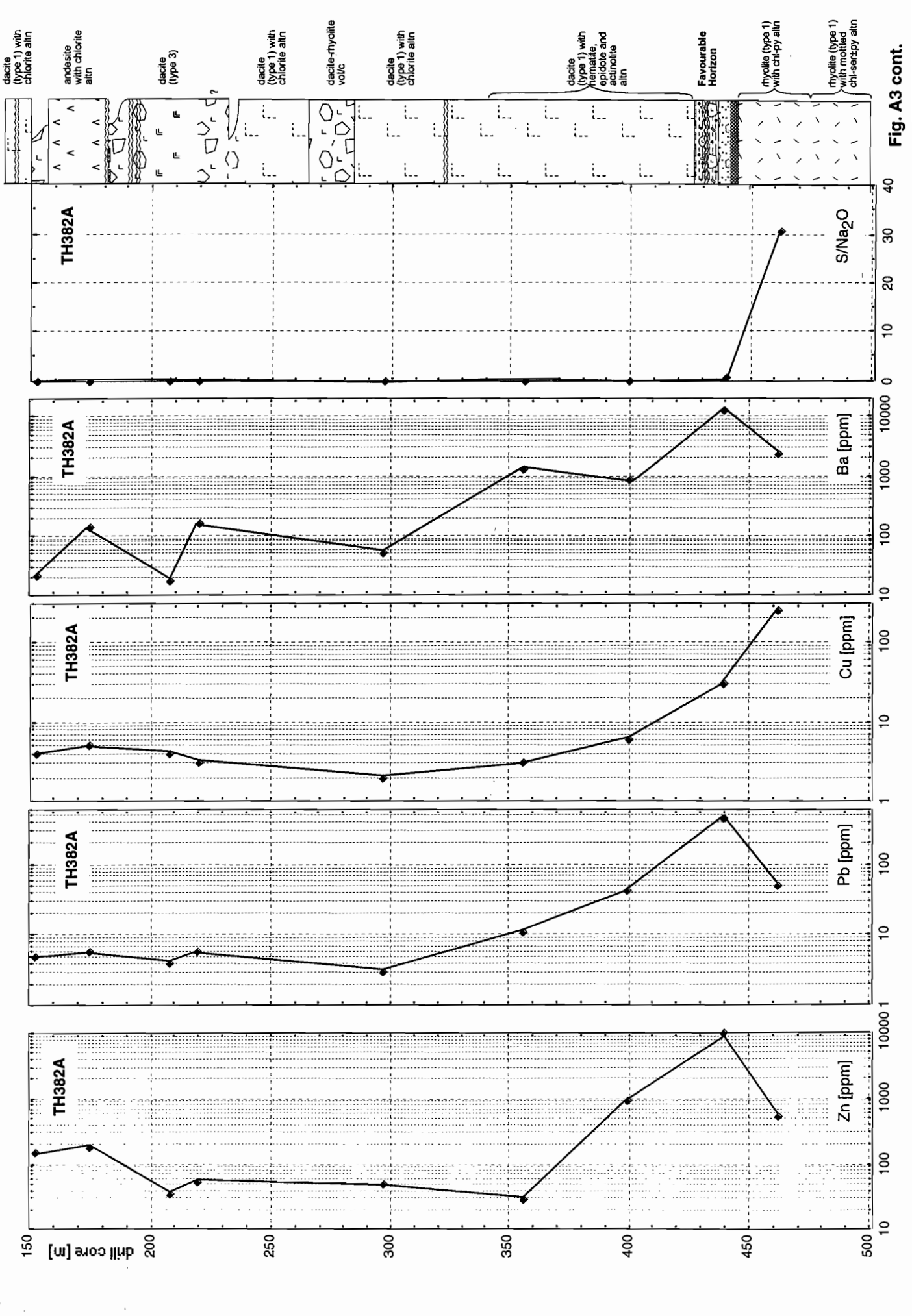
dacite (type 1) with chlorite altn
andesite with chlorite altn
dacite (type 3)
dacite (type 1) with chlorite altn
dacite-rhyolite volc
dacite (type 1) with chlorite altn
dacite (type 1) with hematite, epidote and actinolite altn
Favourable Horizon
rhyolite (type 1) with chl-py altn
rhyolite (type 1) with mottled chl-ser±py altn
TH382A
S/Na2O
Ba [ppm]
Cu [ppm]
Pb [ppm]
Zn [ppm]
drill core [m]
150
200
250
300
350
400
450
500
0
10
20
30
40
1
10
100
1000
10000

Fig. A3 cont.

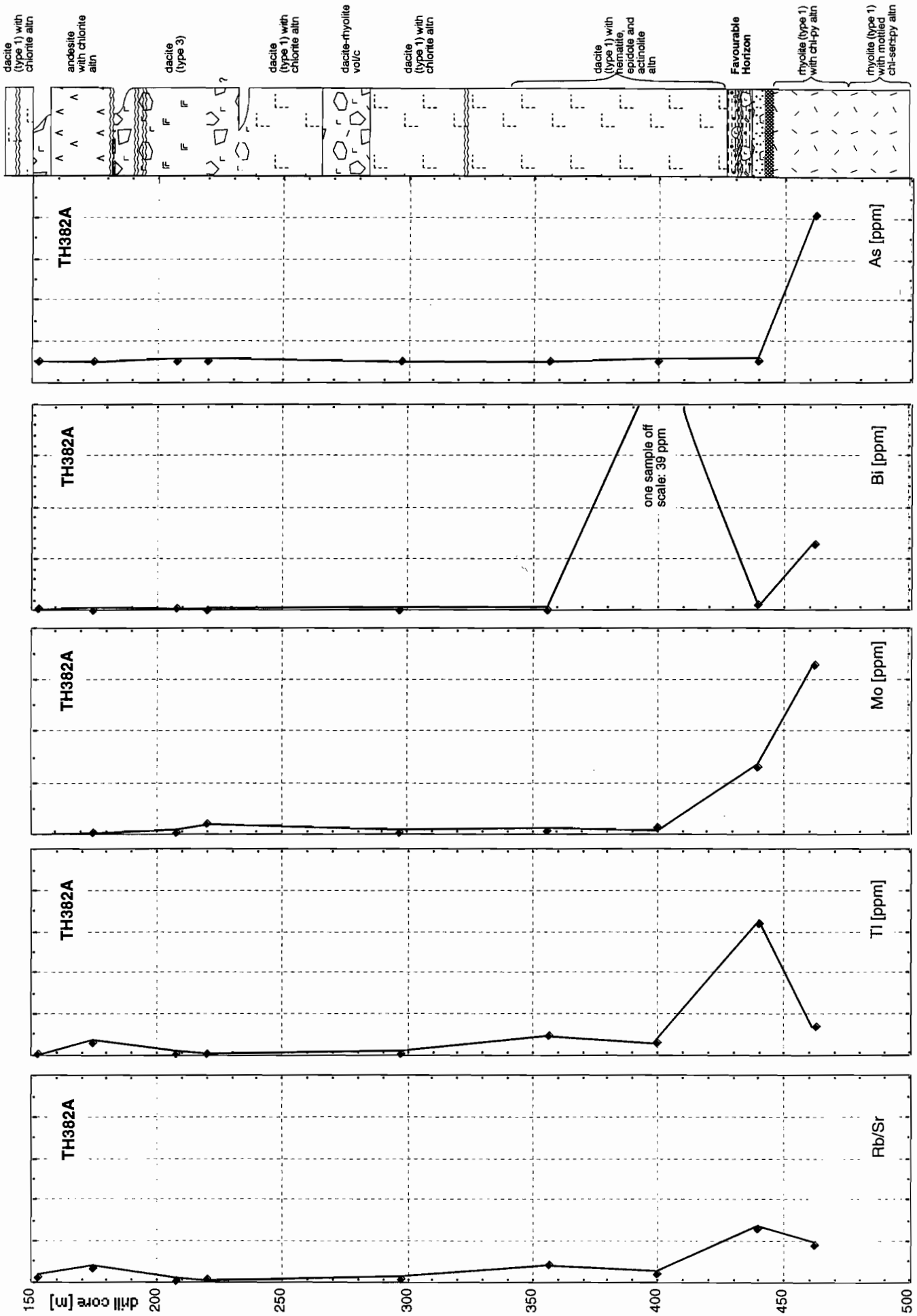
dacite (type 1) with chlorite altn
andesite with chlorite altn
dacite (type 3)
dacite (type 1) with chlorite altn
dacite-rhyolite volc
dacite (type 1) with chlorite altn
dacite (type 1) with hematite, epidote and actinolite altn
Favourable Horizon
rhyolite (type 1) with chl-py altn
rhyolite (type 1) with mottled chl-ser±py altn
TH382A
As [ppm]
TH382A
Bi [ppm]
one sample off scale: 39 ppm
TH382A
Mo [ppm]
TH382A
Tl [ppm]
TH382A
Rb/Sr
drill core [m]
150
200
250
300
350
400
450
500

Fig. A3 cont.

Sample No. TH247-169
Location west Thalanga, section 20080E

Alteration zone footwall rhyolite, mottled chlorite-sericite± pyrite alteration
Formation Mt Windsor Formation

Description foliated, quartz(-feldspar) phyric, fine to medium rhyolite (type 1)

Facies Interp coherent facies of extrusive rhyolite lava

Alteration Intensity none weak (moderate) strong intense Py < 1%
Alteration Style patchy (pervasive) veined cleavage control
Alteration Mineralogy Groundmass quartz-sericite-chlorite-biotite
Feldspars replaced by quartz-sericite-biotite

Interpretation diagenetic - metamorphic syntectonic (hydrothermal)
Relict Mineralogy quartz phenocrysts (feldspar phenocryst relicts)

Geochemistry

SiO_2	TiO_2	Al_2O_3	Fe_2O_3	MnO	MgO	CaO	Na_2O	K_2O	P_2O_5	S	LOI	Al	CCPI	Ti/Zr
75.1	0.1	11.7	2.07	0.06	1.44	0.36	3.7	1.8	< 0.01	0.42		45	37	4.21

Ba	Cu	Pb	Zn	As	Bi	Mo	Nb	Rb	Sb	Sr	Th	Tl	Zr
622	360	400	513	1.7	6.7	9		80	< 0.2	64	12	< 0.5	141

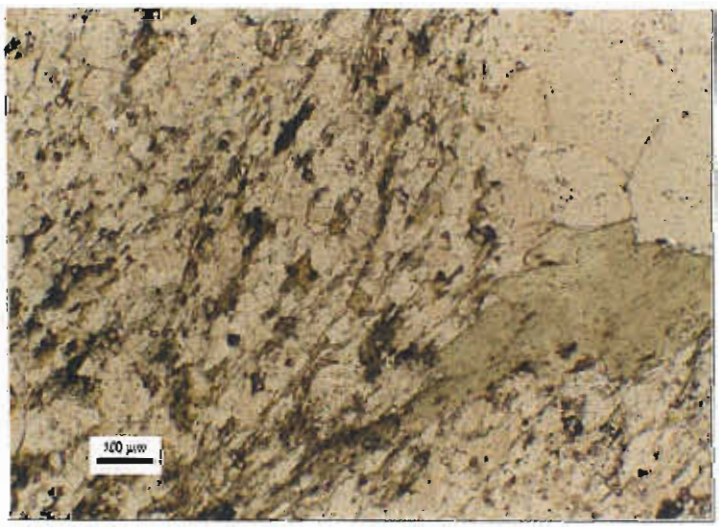

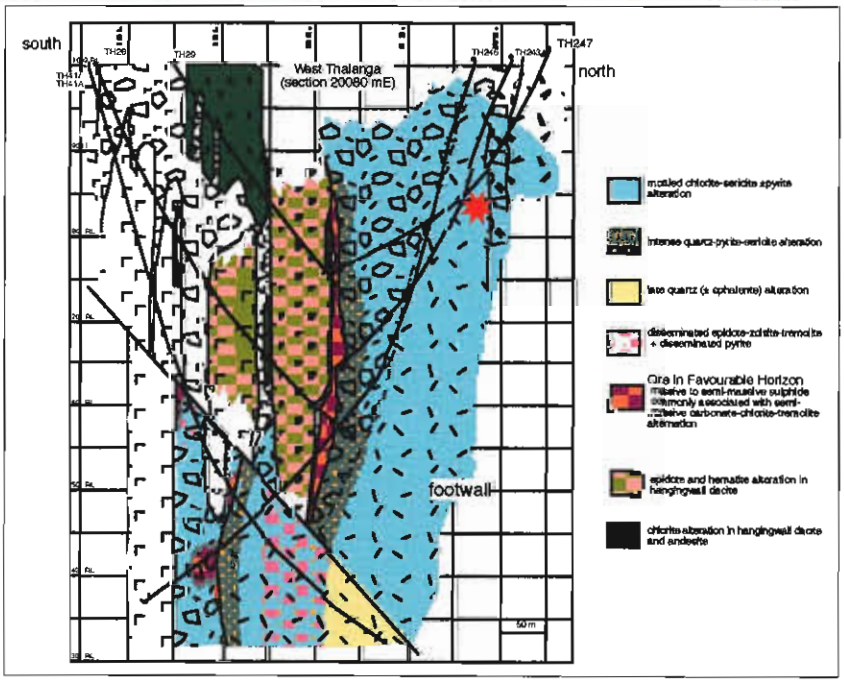

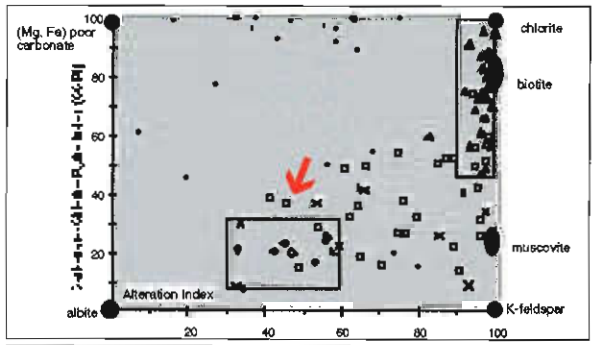

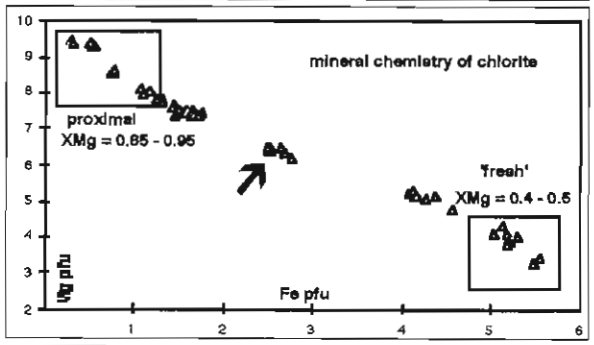

Sample No.	**TH247-75**
Location	west Thalanga, section 20080E
Alteration zone	Footwall rhyolite, least altered
Formation	Mt Windsor Formation

Description weakly altered, highly quartz-feldspar phyric, medium rhyolite (type 2)

Facies Interp coherent facies of extrusive lava

Alteration Intensity	none (weak) moderate strong intense Py trace
Alteration Style	patchy (pervasive) veined cleavage control
Alteration Mineralogy	Groundmass quartz-felddspar-sericite-biotite(-chlorite)
	Feldspars weak sericite-biotite
Interpretation	diagenetic (metamorphic) syntectonic hydrothermal
Relict Mineralogy	quartz phenocrysts, feldspar phenocrysts (partially altered)

Geochemistry

SiO_2	TiO_2	Al_2O_3	Fe_2O_3	MnO	MgO	CaO	Na_2O	K_2O	P_2O_5	S	LOI	Al	CCPI	Ti/Zr
78.3	0.11	11.8	1.4	0.04	0.58	0.24	4.06	3.25	0.02	0.2	0.71	47	20	4.46

Ba	Cu	Pb	Zn	As	Bi	Mo	Nb	Rb	Sb	Sr	Th	Tl	Zr
1410	64	15	36	1.4	0.2	0.4	13	72	<0.2	54	11	<0.5	149

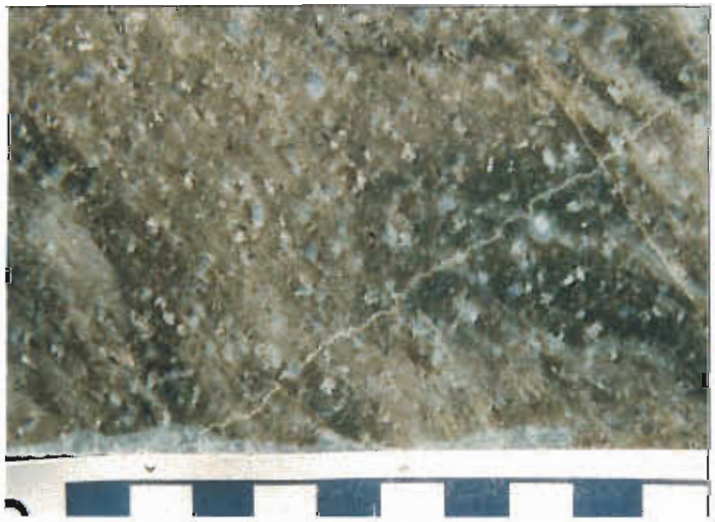

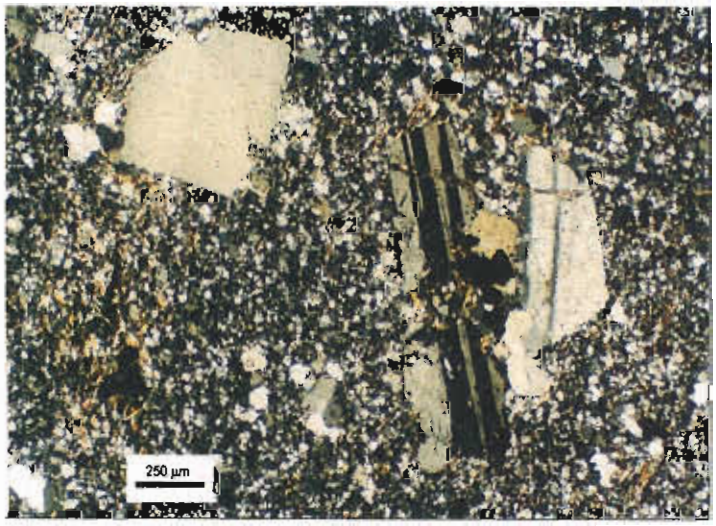

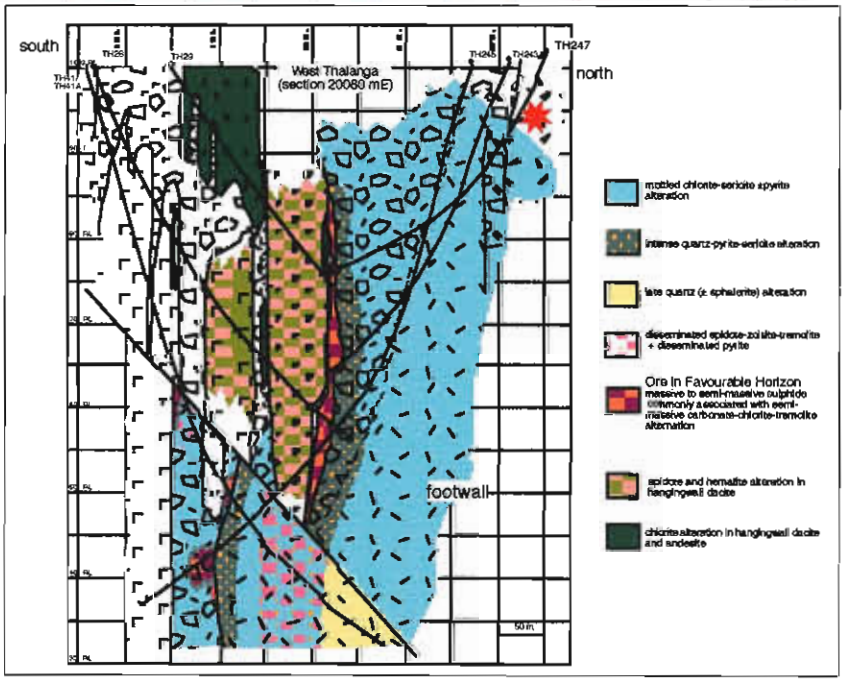

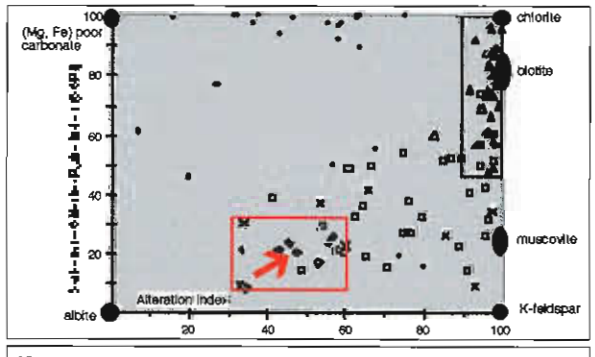

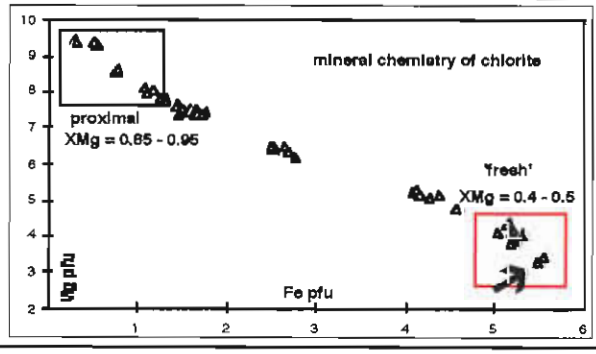

Sample No.	**TH270-77**
Location	east Thalanga, section 31980E
Alteration zone	footwall rhyolite, late quartz (±sphalerite) alteration
Formation	Mt Windsor Formation

Description	white, strongly silicified, moderately quartz phyric, medium rhyolite (type 1) with relict domains of sericite(-chlorite) alteration
Facies Interp	coherent rhyolite

Alteration Intensity	none	weak	(moderate)	strong	intense	Py < 1%
Alteration Style	patchy	(pervasive)	veined		cleavage control	
Alteration Mineralogy	Groundmass	quartz-sericite(-chlorite-pyrite-sphalerite)				
	Feldspars	quartz-sericite				
Interpretation	diagenetic	metamorphic	syntectonic	(hydrothermal)		
Relict Mineralogy	Quartz phenocrysts					

Geochemistry

SiO_2	TiO_2	Al_2O_3	Fe_2O_3	MnO	MgO	CaO	Na_2O	K_2O	P_2O_5	S	LOI	Al	CCPI	Ti/Zr
80.7	0.07	10.85	1.67	0.02	1.08	0.07	1.94	2.57	0.01	1.3	2	64	36	4.13

Ba	Cu	Pb	Zn	As	Bi	Mo	Nb	Rb	Sb	Sr	Th	Tl	Zr
1570	79	56	6950	18.8	1.5	1.3	11	80	<0.2	31	8	<0.5	104

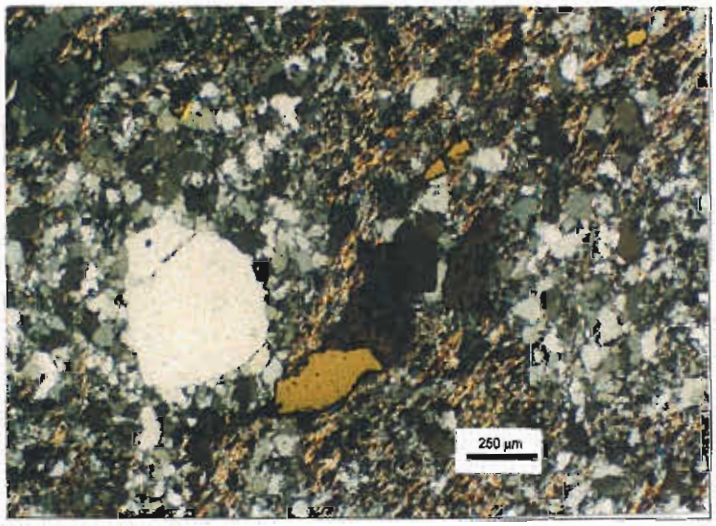

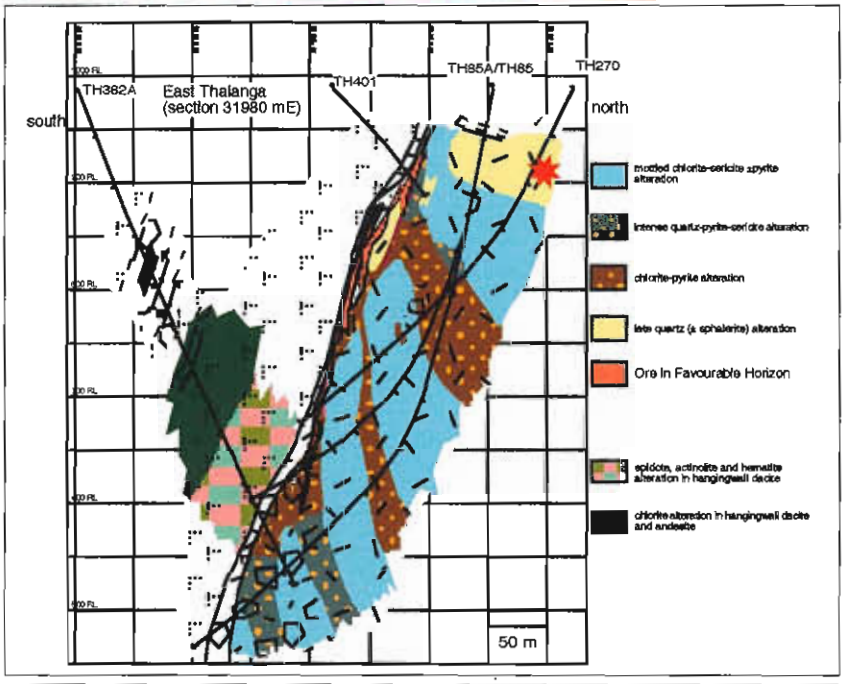

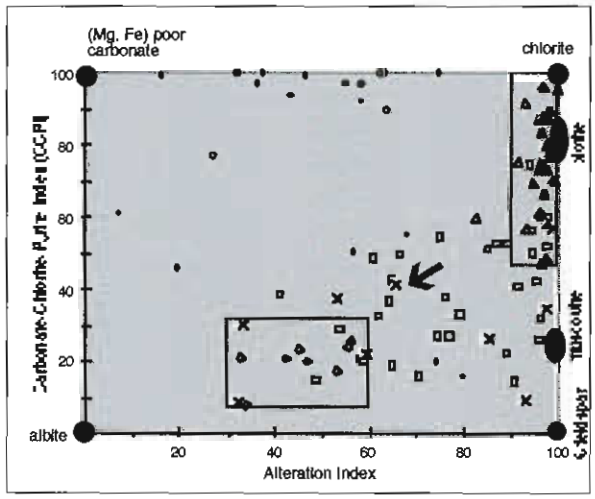

Sample No. TH85A-381
Location east Thalanga, section 31980E

Alteration zone footwall rhyolite, intense chlorite-pyrite alteration
Formation Mt Windsor Formation

Description strongly chlorite-pyrite altered, poorly quartz-phyric, fine rhyolite (type 1), 15 % diss. pyrite and veins

Facies Interp coherent rhyolite

Alteration Intensity	none	weak	moderate	strong	(intense)	Py 15%	
Alteration Style	patchy	(pervasive)	veined	cleavage control			
Alteration Mineralogy	Groundmass	quartz-chlorite-pyrite-sericite-biotite					
	Feldspars	not preserved					
Interpretation	diagenetic	metamorphic	syntectonic	(hydrothermal)			
Relict Mineralogy	quartz phenocrysts						

Geochemistry

SiO_2	TiO_2	Al_2O_3	Fe_2O_3	MnO	MgO	CaO	Na_2O	K_2O	P_2O_5	S	LOI	Al	CCPI	Ti/Zr
60.1	0.11	15.1	15.6	0.15	5.32	0.12	0.2	2.61	0.02	5.9	7.2	96	87	3.89

Ba	Cu	Pb	Zn	As	Bi	Mo	Nb	Rb	Sb	Sr	Th	Tl	Zr
1030	3365	80	1320	39	5.2	1.9	20	66	0.85	20	14	1.6	168

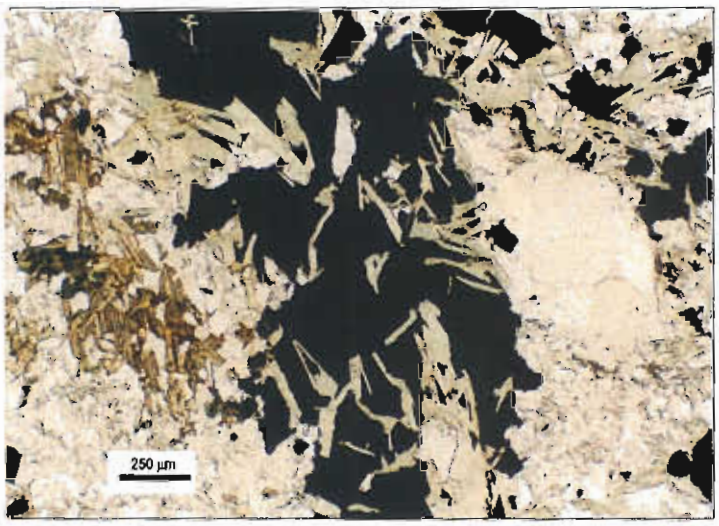

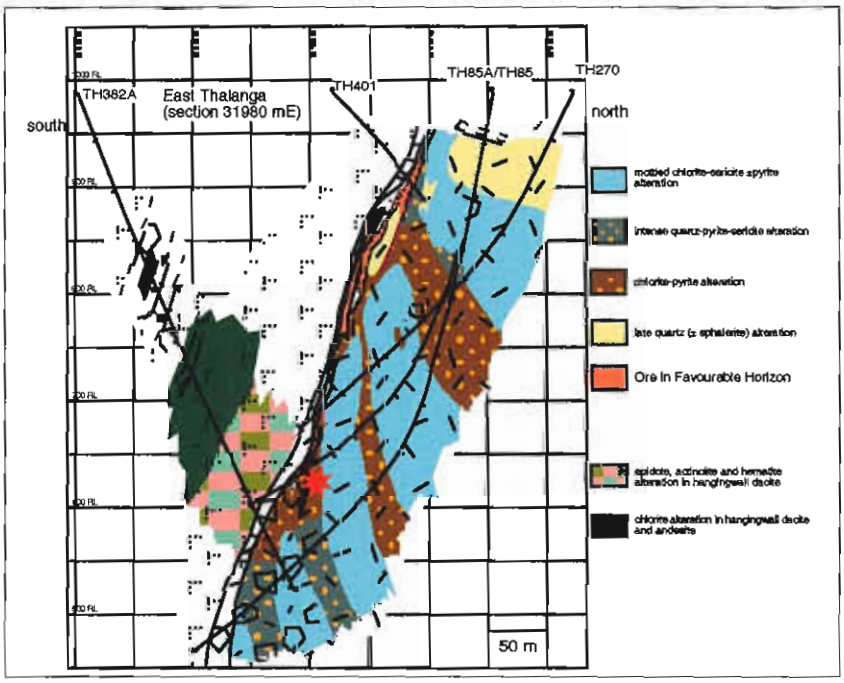

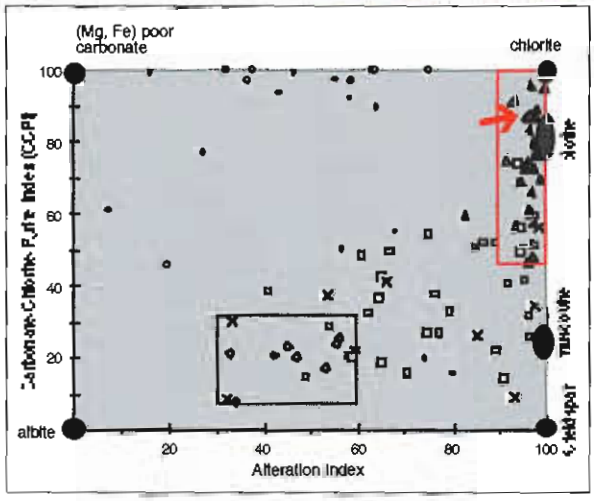

Sample No.	**TH247-347**
Location	west Thalanga, section 20080E
Alteration zone	footwall rhyolite, intense quartz-pyrite-sericite alteration
Formation	Mt Windsor Formation
Description	intensely quartz-pyrite-sericite altered moderately quartz phyric, fine rhyolite, possibly volcaniclastic facies, 10% pyrite diss. and in veins
Facies Interp	?normal graded monomict rhyolitic breccia

Alteration Intensity	none	weak	moderate	strong	(intense)	Py 10 %
Alteration Style	patchy	(pervasive)	veined		cleavage control	
Alteration Mineralogy	Groundmass	sericite > quartz				
	Feldspars	carbonate > sericite				
Interpretation	diagenetic	metamorphic	syntectonic	(hydrothermal)		
Relict Mineralogy	quartz phenocrysts					

Geochemistry

SiO_2	TiO_2	Al_2O_3	Fe_2O_3	MnO	MgO	CaO	Na_2O	K_2O	P_2O_5	S	LOI	Al	CCPI	Ti/Zr
62.9	0.18	17.1	3.53	0.02	1.94	0.05	0.18	5.70	0.02	1.92		97	47	3.87

Ba	Cu	Pb	Zn	As	Bi	Mo	Nb	Rb	Sb	Sr	Th	Tl	Zr
2120	61	100	101	57	5	12		175	1.5	21	19	3.3	274

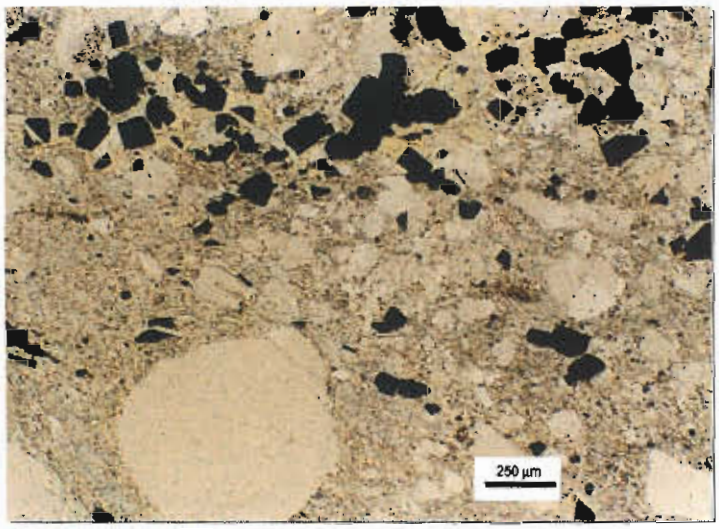

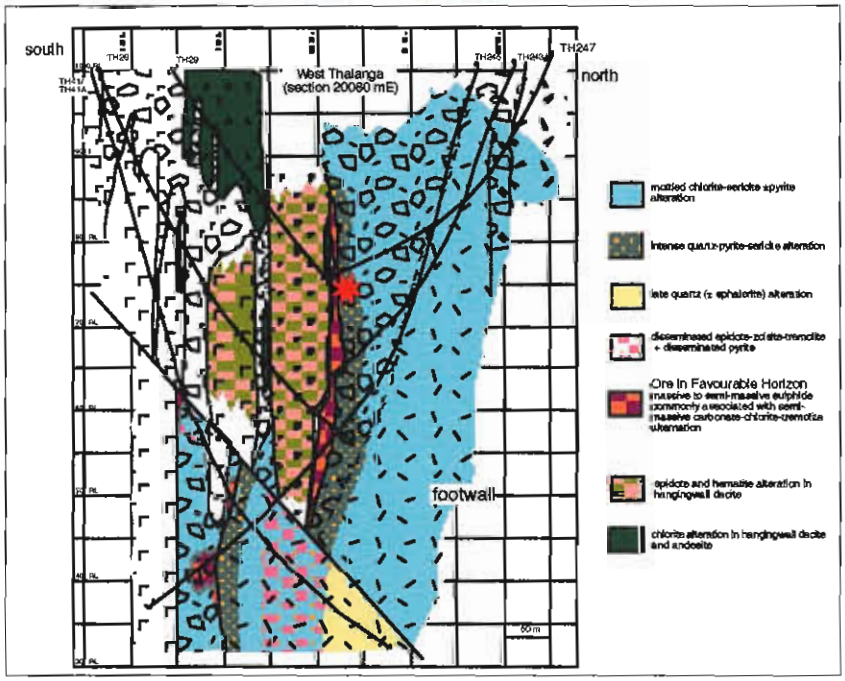

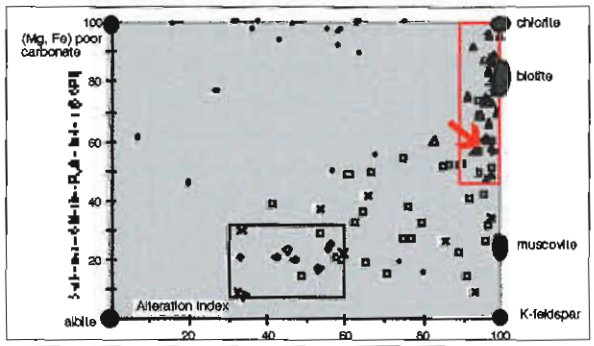

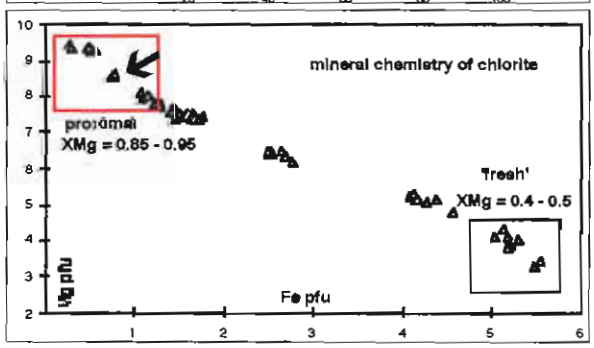

Alteration halo to the Highway–Reward sub-seafloor replacement deposit, Mount Windsor Subprovince, Queensland

Mark G. Doyle
Centre for Ore Deposit Research

Introduction

The Cu-Au Highway-Reward volcanic-hosted massive sulfide (VHMS) deposit is situated approximately 32 km south of Charters Towers within the Cambro-Ordovician Mount Windsor Subprovince of northern Queensland. The deposit provides a rare example of a pipe-style, sub-seafloor replacement VHMS deposit hosted by a submarine syn-sedimentary intrusion-dominated volcanic centre.

Review of previous work

An integrated volcanological, sedimentological and ore deposit study of the Cambro-Ordovician Seventy Mile Range Group has provided insights into the characteristics of Highway-Reward type sub-seafloor replacement deposits. The character, geometry and facies architecture of the submarine host succession, alteration mineralogy and zonation, alteration geochemistry, and interrelationships between volcanic facies, alteration and mineralisation have been addressed in previous reports. These reports are:

- Doyle MG, 1995. Preliminary investigation of alteration at the Highway and Reward deposits, Mount Windsor Volcanics, Queensland. AMIRA - P439, Studies of VHMS-related alteration: geochemical and mineralogical vectors to ore. Report 1: 149-160.

- Doyle MG, 1996. Volcanic influences in the formation of iron oxide-silica deposits in a volcanogenic-massive sulfide terrain, Mount Windsor Volcanic belt, Queensland. AMIRA - P439, Studies of VHMS-related alteration: geochemical and mineralogical vectors to ore. Report 3: 87-142.

- Doyle MG, 1997a. Alteration associated with sub-seafloor replacement style massive sulfide deposits: evidence from the Cambro-Ordovician Highway-Reward deposit, Mount Windsor Subprovince. AMIRA - P439, Studies of VHMS-related alteration: geochemical and mineralogical vectors to ore. Report 4: 231-257.

- Doyle MG, 1997c. Alteration geochemistry of the sub-seafloor replacement style Highway-Reward deposit, Mount Windsor Subprovince. AMIRA - P439, Studies of VHMS-related alteration: geochemical and mineralogical vectors to ore. Report 5: 201-219.

Ore deposit characteristics

Form of orebody

The Highway and Reward pyrite-chalcopyrite pipes are discordant to local bedding and contain relic domains of intensely altered rhyolite to dacite (Fig. 1). Pyrite±quartz stringer veins occur below the pipes, and on some sections also occur in sericite-quartz-altered lithofacies above the pipes. Near-surface pyritic ores have oxidised to form oxide and supergene ores. The pyrite-chalcopyrite pipes are surrounded by a halo of sphalerite-galena-barite-rich mineralisation. Within this envelope there are four styles of mineralisation: (1) strata-bound pyrite-sphalerite-chalcopyrite-barite lenses; (2) disseminated sphalerite within sericite-chlorite-quartz-altered

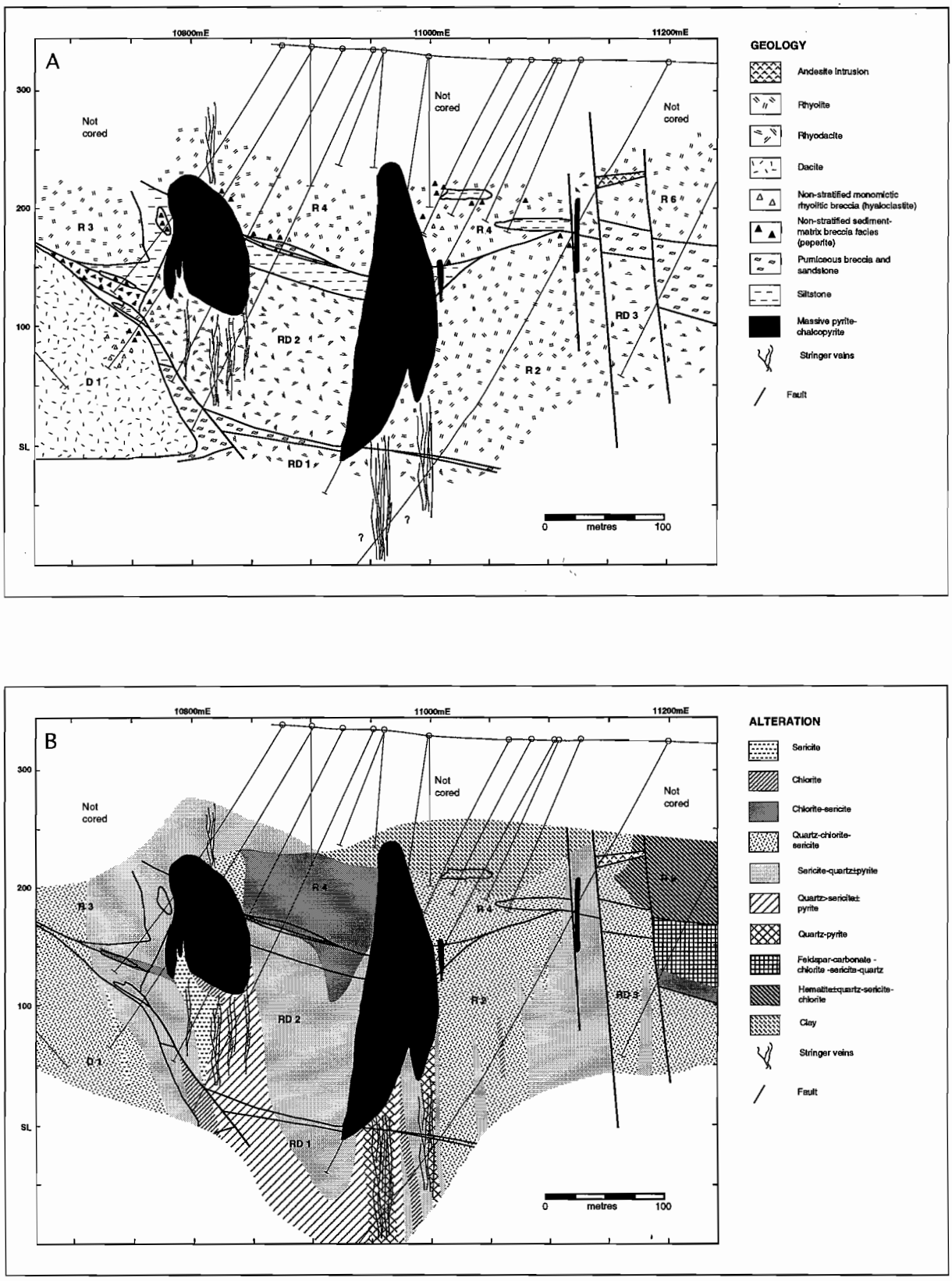

Figure 1. Simplified geological cross section showing the distribution of (A) lithofacies and (B) alteration at 10150N. The position of the massive sulfide bodies is also shown. Dacite D1, rhyodacites RD1-RD3 and rhyolites R2-R4 and R6 are exposed on section 10150mN (after Doyle, 1997b).

rhyolite at the top of the pipes; (3) massive and semi-massive pyrite-sphalerite-chalcopyrite±barite at the margins of the pyrite pipes; (4) veins of sphalerite ± galena-barite in altered volcanic facies along the margins and tops of the pipes.

Size and grade

After Thalanga, the Highway-Reward deposit is the largest known VHMS deposit in the Seventy Mile Range Group. Most of the oxide resource at Highway was mined by North Queensland resources from 1986 to 1988. A significant primary resource remains at Highway and the Reward orebody is presently being developed by RGC (Table 1).

Sulfide mineralogy

Pyrite, chalcopyrite, sphalerite and galena

Alteration mineralogy

Chlorite, sericite, quartz, barite, hematite with minor anhydrite, carbonate, rutile, talc, and fuchsite

Deformation

The Highway and Reward orebodies occur within a major northeast trending D4 shear zone (Policeman Creek Fault Zone of Henderson (1986)) and have the same tectonic fabric as the altered host rocks. The pyrite-chalcopyrite pipes are parallel to S4, have a plunge sub-parallel to a sub-vertical mineral lineation (Berry et al., 1992), and include zones of cataclasite (Doyle, 1997a). Disseminated sphalerite has been drawn out into the S4 cleavage and mineralogical bands in strata-bound pyrite-sphalerite-galene-barite lenses have been folded. The alteration halo has sheared sub-parallel to the S4 cleavage. The foliation wraps around euhedral anhydrite crystals in chlorite-anhydrite-altered lithofacies at the margins of the pipes. This observation indicates a pre- or syn-kinematic timing for anhydrite and is consistent with an Ordovician syn-genetic origin (Doyle, 1997a,b) and not the post-kinematic origin proposed by some previous workers.

Volcanic facies

The Highway-Reward massive sulfide deposit is hosted by a silicic submarine (below storm wave base) syn-sedimentary intrusion-dominated volcanic centre. Detailed mapping of phenocryst populations and contact relationships indicates the presence of more than thirteen distinct porphyritic units in a volume of 1x1x0.5 km (Fig. 1A, Doyle, 1994; Doyle, 1997a,b). Peperitic upper margins suggest that at least 75% of the rhyolites to dacites were emplaced as small (<350 m diameter) syn-sedimentary sills and cryptodomes (Table 2). Another 15% remain as undifferentiated lavas and intrusions, as critical upper contact relationships are not preserved The intrusions have steep margins and are separated from neighbouring intrusions by thin (0.2 to 30 m) disrupted intervals of siltstone, sandstone turbidites, polymictic lithic breccia, and non-welded pumice- and crystal-rich breccia (Table 3). Evidence for extrusion of magma onto the seafloor is limited to a single, partly extrusive cryptodome (rhyolite 4).

The Highway and Reward pyrite-chalcopyrite pipes occur within, but close to, the steep margins of cryptodomes within the host succession (Fig. 1A; Doyle, 1997a,b). The Highway Pipe is bound by four porphyries: Dacite 1 (western margin), rhyodacite 2 (footwall), and rhyolite 3 and 4 (hanging wall, northern margin) (Fig. 1). The upper contact of the Highway orebody partly replaces the peperitic base of the partly extrusive cryptodome (rhyolite 4). The massive sulfides and peperite are not mixed and sulfides have more often replaced rhyolite clasts than siltstone in the matrix or filling fractures. The main Reward pipe is elongate sub-parallel to the boundary of two cryptodomes: rhyodacite 2 (western margin) and rhyolite 2 (eastern margin). The northern extent of the Reward orebody is marked by a northerly thickening cryptodome (rhyolite 9). The southern margin is poorly constrained. The upper margin of the pipe often corresponds to the top of Rhyolite 4. However, several smaller pyrite pipes cut across the overlying resedimented hyaloclastite deposits, pumice breccia beds and hanging wall intrusions (rhyolites 5-6). Pumiceous mass-flow deposits that overlie rhyolite 4 host strata-bound pyrite-sphalerite-galena-barite mineralisation.

Table 1. Grade and tonnage data for the primary, oxide and supergene ore zones at Highway-Reward. The Highway oxide resource is a pre-mining resource estimate. Data from Beams and Dronseika (1995).

	Highway	Reward
Primary	1.2 m.t. @ 5.5% Cu, 6.5 g/t Ag, 1.2 g/t Au	0.2 m.t. @ 3.5 Cu, 13 g/t Ag, 1 g/t Au
Supergene		0.3 m.t @ 11.6% Cu, 21 g/t Ag, 1.8 g/t A
Oxide	0.07 m.t. @ 6.04 g/t Au	0.1 m.t @ 33 g/t Ag, 6.49 g/t Au

Table 2. Form, dimensions and phenocryst populations for sills, cryptodomes and partly extrusive cryptodomes at Highway-Reward (Doyle, 1997b).

Unit	Form	Dimensions (m)			Quartz		Feldspar	
		Length	Width	Thickness	%	size (mm)	%	size (mm)
Dacite 1	cryptodome	250	300	>300	—	—	5	0.5-15
Rhyodacite 1	sill	150	>250	>100	2-3	0.5-2	6-7	1-2
Rhyodacite 2	cryptodome	175	≥275	50-150	sparse	< 1	2-3	0.5-15
Rhyodacite 3	?	>50	>75	>80	2	0.5-3	8-10	1-3
Rhyolite 1	sill	?	?	?	9-10	0.5-4	?	?
Rhyolite 2	cryptodome	>100	>125	120-170	10-12	1-3	6	1-2
Rhyolite 3	cryptodome	175	5 - >150	20-100	6-7	1-3	7	1-3
Rhyolite 4	partly ext.	312	>300	40-120	6-7	1-4	7	1-2
Rhyolite 5	sill	38	25-140	5-10	6-7	1-6	7-8	1-3
Rhyolite 6	sill	150	>300	25 to >60	7	0.5-2	5	1-2
Rhyolite 7	?	>37	>60	>30	4-5	1-3	5	1-3
Rhyolite 8	sill	75	>300	35 to >85	6-7	0.5-7	7	1-2
Rhyolite 9	cryptodome	?	>350	>225	6	1-3	10-12	1-2

Chemostratigraphy

All lithofacies in the host succession to the Highway-Reward deposit have been subject to regional greenschist facies metamorphism and hydrothermal alteration is typically intense. Elements identified as immobile during these alteration events, such as Ti, Zr, Nb, P and Th, have been used to refine petrographic interpretations and to compare the geochemistry of host rocks at Highway-Reward with analyses of coherent volcanic rocks from the remainder of the Seventy Mile Range Group (Doyle, 1997b,c). The principal conclusions to emerge from this research are:

- On a plot of P/Zr vs Ti/Zr, the range of compositions from rhyolite to high-silica dacite fall within linear trends which are consistent with the remainder of the Trooper Creek Formation (Fig. 2A).

- Some lavas that were mapped as rhyolite (because they contain 5-7% modal quartz and feldspar phenocrysts, 1-7 mm long) plot in the high-silica dacite field. Other samples contain less than 1% quartz phenocrysts (mapped as rhyodacite) also plot in the high-silica dacite field.

- The composition of coherent rocks from the footwall and hanging wall to mineralisation are similar.

Table 3. Summary of the principal lithofacies in the host succession to the Highway-Reward deposit.

Lithofacies	Characteristics	Interpretation
Massive rhyolite to dacite	Aphyric or evenly porphyritic; columnar and tortoise shell jointing; massive or flow banded	Coherent facies of lavas and domes, cryptodomes and syn-sedimentary intrusions
Non-stratified rhyolitic to dacitic breccia	Monomictic; poorly sorted; blocky to ragged clasts; clast- to matrix-supported; gradational into coherent facies and/or peperite	Autobreccia and in situ hyaloclastite
Non-stratified sediment-matrix breccia facies	Rhyolitic to andesitic; blocky, ragged and globular shaped clasts; clast- to matrix-supported; jigsaw-fit texture in matrix-poor breccia; matrix may be siltstone, sandstone or pumice breccia; present along the upper or lower contacts of massive andesite to rhyolite facies; 0.1–1 m thick	Peperite (cf. Busby-Spera and White, 1987; Brooks, 1995)
Stratified, monomictic rhyolitic to dacitic breccia facies	Thick (0.5-11 m), internally massive or graded beds; clast-supported; blocky to elongate jagged clasts; often associated with hyaloclastite, peperite and coherent lava	Gravity-driven collapse and resedimentation of unstable hyaloclastite (cf. Dimroth et al., 1978). Deposits from high-concentration sediment gravity flows
Siltstone-matrix rhyolitic to dacitic breccia	Stratified; polymictic, matrix- to clast-supported; thick (< 7 m); internally massive or normally graded; blocky to ragged clasts locally with jigsaw-fit fabric; siltstone matrix and intraclasts	Gravity-driven collapse of unstable hyaloclastite or peperite from the margins of subaqueous lavas or cryptodomes; deposition from high-concentration sediment gravity flows (? debris flows)
Graded dacitic to rhyolitic pumice breccia and sandstone	Essentially monomictic; normally graded; non-welded; 1–80 m thick; equant to ragged tube pumice, crystal fragments, shards and sparse angular lithic clasts	Resedimentation of subaerial or shallow submarine pyroclastic pumice into a deeper submarine setting; syn-eruptive; down-slope transport by high-concentration turbidity currents
Stratified crystal-rich volcanic sandstone	Essentially monomictic; massive or weakly normally graded; grain supported; rich in crystal fragments and pumice with lesser shards and lithic clasts; 1-50 m thick	Syn-eruptive; crystal concentration during eruption and transportation; deposition from high-concentration, granular turbidity currents
Polymictic lithic-pumice breccia facies	Poorly sorted; matrix-supported; weak normal grading; ~12 m thick; clasts (3 cm-2 m) of siltstone, dacite, ironstone and dacite clasts with indurated siltstone rinds; pumiceous matrix	Gravity-driven collapse of pre-existing unstable peperite, pumice breccia and ironstone; down-slope transport by high-concentration sediment gravity flows (? debris flow); deposited and sourced subaqueously
Vitric-crystal-lithic sandstone	Planar, laterally continuous beds; thin (15-70 cm) massive to normally graded crystal-vitric-lithic sandstone and interbedded siltstone; dominantly volcanic; some beds contain non-volcanic detritus	Sandstone beds are deposits from low concentration turbidity currents (Bouma Ta-Te); siltstone predominantly from suspension sedimentation
Massive to laminated siltstone	Laminated or thinly bedded intervals up to 160 m thick; planar, even, continuous beds; in some cases laminae drape small irregularities such as outsize pumice clasts	Predominantly suspension sedimentation; in part water-settled volcanic ash; deposited below storm wave base

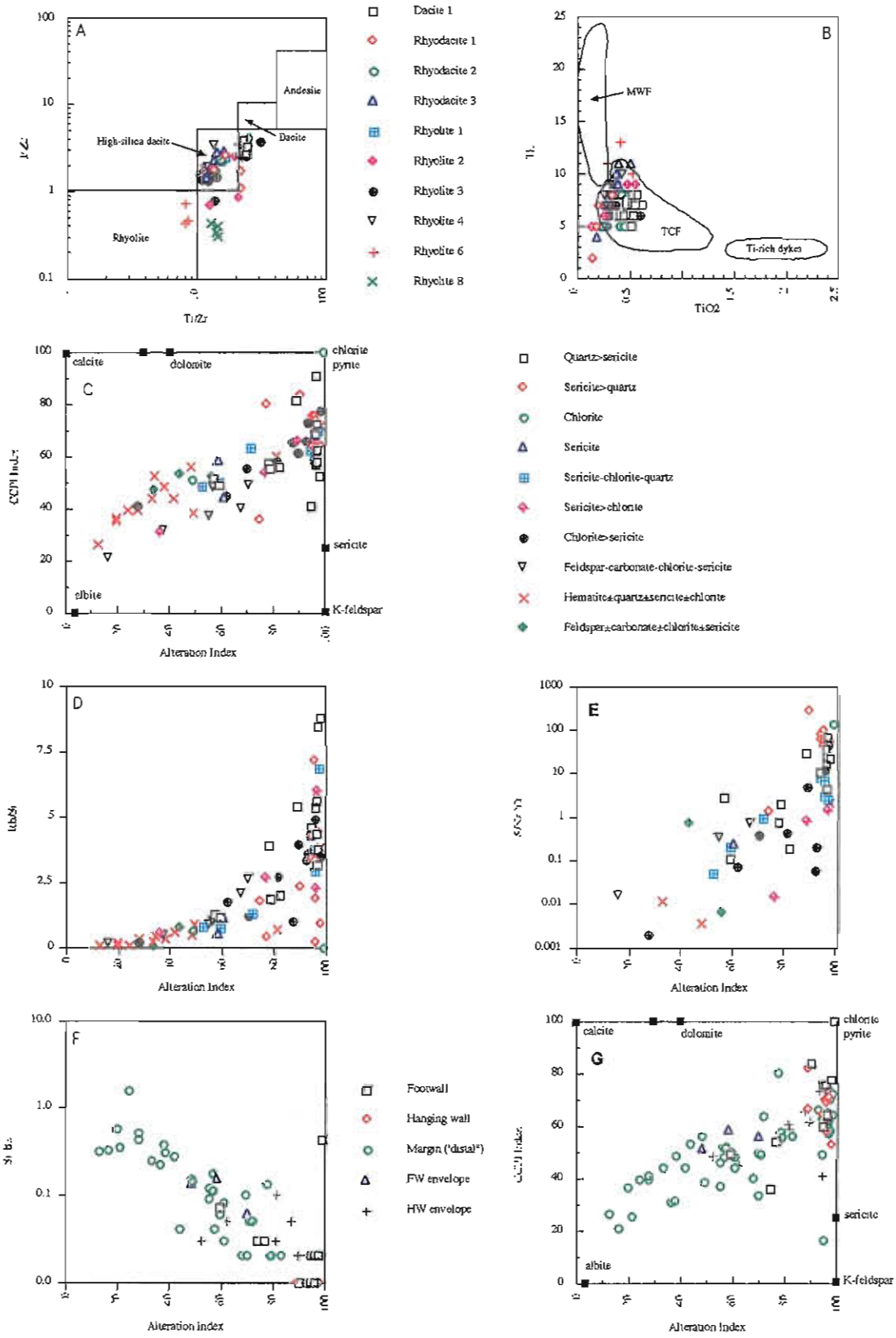

Figure 2: (A-B) Geochemistry of coherent lavas and intrusions at Highway-Reward. Fields in (B) after Stolz (1995) and Doyle (1997b). (C-G) Geochemical plots for hydrothermal alteration zones at Highway-Reward.

- On plots of P/Zr vs. Ti/Zr and Th vs. TiO_2, samples of coherent facies, resedimented hyaloclastite and pumice breccia from the host succession are geochemically similar and fall along trends consistent with the remainder of the Trooper Creek Formation (Fig. 2A-B).

Alteration mineralogy and zonation

Alteration mineralogy and paragenesis

The Highway-Reward deposit is enclosed within a discordant hydrothermal alteration envelope which has a mineralogical zonation defined by assemblages of chlorite±anhydrite, chlorite-sericite, chlorite-sericite-quartz and quartz-sericite±pyrite. Outside the alteration envelope rhyolitic to dacitic coherent and volcaniclastic rocks have altered to various assemblages of feldspar (albit e± K-feldspar), sericite, chlorite, quartz, carbonate and hematite. Feldspar-chlorite-sericite ± carbonate ± quartz alteration is regionally distributed which is consistent with a regional diagenetic or metamorphic origin. Vesicles and former glassy vesicle walls are now optically continuous K-feldspar or have altered to quartz-albite-sericite-chlorite. The feldspar alteration (albite, K-feldspar) or a precursor mineral(s) (zeolite ?) protected pumice clasts from diagenetic compaction, suggesting that the alteration occurred prior to, or during diagenesis. The diagenetic compaction foliation (S1) and associated stylolitic foliation is crenulated by the regional cleavage implying that the alteration was complete prior to regional deformation (Doyle1997a,b). The regional distribution of hematite-rich alteration assemblages suggests that they may not be genetically related to mineralisation. At least some of the hematite-rich alteration is interpreted to reflect hydrothermal convection driven by lavas and intrusions. Circulating fluids leached Fe, Si and other elements from glassy parts of the succession (cf. Sigurdsson, 1977) and redeposited these elements in the host succession (Doyle, 1996, 1997b).

Alteration mineral zonation

Massive sulfide mineralisation is enclosed by a hydrothermal alteration envelope, which extends from at least 150 m below the pyrite pipes to over 60 m above the Highway orebody (Fig. 1B). Although the pyrite-chalcopyrite pipes and associated stringer veining at Highway and Reward are separated by approximately 200 m, the alteration zones associated with each overlap, and some phyllosilicate-rich alteration domains enclose both orebodies. Summary descriptions and interpretations of the principal hydrothermal alteration zones are given in Table 4. The mineralogical and geochemical characteristics of samples from the main alteration zones are illustrated in summary sheets in the Appendix.

Halo geochemistry

A detailed analysis of the major and trace element variations of alteration zones at Highway-Reward was presented by Doyle (1997c) and summarised in Table 5. The principal geochemical halo patterns are briefly reviewed below.

Copper, lead and zinc

A well developed halo of ore-related Cu enrichment (up to 4706 ppm) occurs in hanging wall lithofacies at least 50 m above the pyrite pipes. Anomalous values of greater than 200 ppm Cu also occur in a number of samples from the footwall and margins of the orebodies. Lead and zinc are elevated in some samples.

Sodium and calcium distribution

Depletion in Na_2O and CaO to values typically < 1 wt%, extends to at least 100 m below the orebodies and 40 m above the Highway pipe. The northern and southern extent of the Na_2O and CaO halo is poorly constrained due to limited drill core data. Sodium is generally high (1.5-7.7 wt%) in sericite-chlorite ± feldspar ± carbonate ± quartz-altered lithofacies greater than around 200m from the orebodies.

Magnesium and potassium

Hanging wall and footwall quartz-sericite±pyrite alteration are characterised by elevated K_2O (1-6 wt%), coupled with depletion in MgO (0.2-6 wt%). The K_2O and MgO alteration halos are more erratic than for Na_2O and CaO. Samples from the chlorite ± anhydrite zone contain highly elevated MgO (26 wt%) and low K_2O (0.01 wt%).

Table 4. Summary of the principal alteration zones enveloping the Highway-Reward deposit.

Alteration zone	Mineralogy and characteristics	Distribution
Quartz-sericite±pyrite zone	Relative proportions of quartz, sericite and pyrite vary. Associated stringer veins. Alteration destroys many original volcanic textures. Alteration pervasive, patchy or generates apparent clastic textures.	Footwall and, on some sections, in the hanging wall.
Chlorite± anhydrite zone	Intense pervasive chlorite alteration. Euhedral anhydrite crystals (< 1.5 cm). Cleavage wraps around crystals.	Locally developed in footwall quartz-sericite±pyrite zone.
Sericite zones	Pervasive. Alteration obscures or destroys primary volcanic textures.	Widespread. Shear zones at margins of pipes and as gangue in massive sulfide.
Sericite-chlorite-quartz zone	Varying proportions of chlorite, sericite-quartz and chlorite-sericite. Alteration controlled by volcanic texture (fracture/matrix permeability). Patchy, mottled, wispy and apparent clastic textures.	Outward from quartz-sericite±pyrite zone
Chlorite-sericite zone	Chlorite-sericite & minor carbonate.	Domains within quartz-chlorite-sericite alteration.
Feldspar± carbonate-chlorite-sericite-quartz alteration	Various assemblages of albite, K-feldspar, carbonate, chlorite, sericite and quartz. Pervasive, fracture controlled or patchy. Diagenetic compaction foliation in pumice-crystal breccia beds.	Lithofacies greater than 200 m from orebodies. Selective replacement of glassy units. Regionally distributed (diagenetic) alteration.
Hematite± quartz-sericite-chlorite alteration	Alteration pervasive or domains of hematite, chlorite-sericite and chlorite-carbonate alteration generate patchy, mottled or pseudoclastic textures.	Generally 50-200 m from massive sulfide deposit. Regionally distributed. "Low temperature" hydrothermal alteration associated with accumulation of volcanic pile.

Table 5. Summary of the principal elemental variations in alteration zones at Highway-Reward.

Alteration zone	Depletion	Enrichment
Quartz-sericite±pyrite zone	Na_20, MnO, MgO and CaO ± Cs, Al_2O_3	K_20 Bi, S and Fe_2O_3 elevated at AI>90 Sporadic enrichment in Ag, As, Cd, Mo, Ni, Sb, Cu, Pb & Zn
Chlorite± anhydrite zone	Na_20, K_20 and CaO	MgO, Fe_2O_3, P_2O_5, Al_2O_3 and MnO
Sericite zones	—	Se ± Zn
Sericite-chlorite-quartz zone	Na_20, CaO	Tl, Bi, Cd, V, Cu, Zn, Pb, P_2O_5 and MnO elevated in some samples with AI > 90
Chlorite-sericite zone	Na_20, CaO	Sporadic enrichment in Y, Ag, As, Bi, Cd, Mo, Sb, Se, Cu, Zn and Pb
Feldspar± carbonate-chlorite-sericite-quartz alteration	K_20, Rb and Ba	Na_20
Hematite± quartz-sericite-chlorite alteration	—	MgO, Cs, Bi and Rb ± Y, Th, V, Cu and Zn elevated in samples with high AI

Manganese, aluminium and phosphorous

MnO, Al_2O_3 and P_2O_5 values generally fall within the range of background levels, with sporadic enrichment at AI values greater than 90. MnO enrichment to values of 0.4 wt% characterises zones of intense chlorite alteration at the margins of the pyrite pipes.

Alteration indices

Ishikawa Alteration Index (AI)

The AI is consistently high within hanging wall lithofacies (AI=89-97), and although values for footwall samples are generally greater than 90, rare samples have values as low as 59. Alteration Index values for the remainder of the sample population range from 12 to 98 (Fig. 2C). The highest values are for samples altered to assemblages of sericite-quartz±pyrite (19%), chlorite-sericite (23%), sericite-chlorite-quartz (48%) and hematite±sericite-chlorite-quartz (<1%).

Chlorite, carbonate, pyrite index (CCPI)

In hanging wall lithofacies, CCPI values range between 52 and 81. As the alteration mineralogy in the footwall lithofacies varies, CCPI patterns are more erratic (35-99). The highest values (99) occur within the chlorite-altered pumice breccia from beneath the Highway orebody. CCPI values for samples marginal to the orebodies vary widely (16-79), but are mostly less than 60.

Rb/Sr ratio

Rb/Sr ratios are also a good indicator of intense hydrothermal alteration, and values are generally higher in the hanging wall (mostly 4.2 to 8.7) than the footwall (1.1 to 4.5). Outside the Highway-Reward hydrothermal alteration halo, ratios are generally low in feldspar-chlorite-sericite±carbonate-altered samples (0.4 to 0.91) and hematite-rich samples (generally 0.05-0.88, Fig. 2D).

S/Na_2O ratio

This ratio typically increases from values of less than 2 in hematite and albite-rich lithofacies outside the hydrothermal alteration envelope, to over 95 for intensely quartz-sericite±pyrite-altered samples in the footwall and hanging wall to mineralisation (Fig. 2E). Variable S/Na_2O ratios (0.05-7.88) for sericite-chlorite-quartz-altered samples reflect different alteration mineral percentages and alteration intensities.

Sr/Ba ratio

This ratio measures the substitution of Ba for K in muscovite and the depletion in Sr during albite destruction. The Sr/Ba ratio decreases systematically passing from albitised and hematite-altered lithofacies distal to mineralisation into the hydrothermal alteration envelope surrounding the Highway-Reward deposit (Fig. 2F). Values are lowest at AI >90, the exception being intensely chloritised samples. The halo of depleted Sr/Ba ratios extends at least 40 m into hanging wall lithofacies.

AI-CCPI box plot

The AI-CCPI box plot is useful in delineating hydrothermal alteration at Highway-Reward. The critical points are:

- Intense quartz-sericite±pyrite-altered samples from the footwall and hanging wall generally fall within a box bounded by AI=93 to 100 and CCPI=50 to 100. Some sericite-chlorite-quartz-altered samples also plot within this domain (Figs. 2C and 2G).
- Hydrothermally-altered samples within the Highway-Reward alteration envelope fall along a trend between chlorite and albite on the box plot. Samples contain little carbonate.
- Diagenetically-altered albite-rich rocks and hydrothermally-altered hematite-rich rocks also trend in a zone between chlorite and albite on the box plot.
- Feldspar-chlorite-sericite±carbonate-altered samples typically have AI < 65 and CCPI < 55.
- Hematite-altered samples trend in a zone between AI= 12 to 97 and CCPI= 26 to 71. Most samples have AI <48 and CCPI <55.

PIMA spectral characteristics of muscovite

Detailed descriptions and interpretations of PIMA spectral characteristics of the Highway-Reward alteration zones are presented in Herrmann et al. (this volume) and summarised here.

- PIMA analyses suggest that alteration assemblages mapped as sericitic comprise muscovite and phengite. Chlorite has an intermediate Fe-Mg composition.

- The Highway-Reward alteration envelope corresponds to a zone with AlOH wavelengths in the range 2195 to 2212 (average=2200, Fig. 3). Samples from the footwall and hanging wall to the orebodies display similar trends (Fig. 3B).

- AlOH wavelength values for the hydrothermal alteration envelope are anomalously low in comparison with the 2202 to 2222 range (average = 2211) of background sericite-chlorite ± feldspar ± hematite±quartz-altered lithofacies which occur greater than 50 to 200 m from the orebodies. Muscovite in these samples trends towards phengitic compositions.

- The sericite-quartz±pyrite alteration zones are characterised by AlOH wavelengths in the range 2195-2204 (average=2199) and AI values typically >90. The exceptions are domains of moderate intensity sericite-quartz±pyrite alteration at the margins of the alteration zones and peripheral to the main Highway-Reward alteration envelope.

- Flanking sericite-chlorite-quartz and sericite-chlorite zones are characterised by AlOH wavelengths in the range 2198-2212 (average 2201).

- Down hole profiles show a relatively smooth trend of decreasing AlOH wavelength values (less phengitic compositions) passing from background sericite-chlorite±feldspar±hematite±quartz-altered lithofacies, through the sericite-chlorite±quartz zones, into the footwall and hanging wall sericite-chlorite±quartz zones (Fig. 4).

Exploration model and vectors to ore

Effective exploration for Highway-Reward type VHMS deposits requires a multidiciplinary approach incorporating volcanic facies mapping, alteration mapping, geochemical studies and geophysics. Figure 5 combines these critical features in an exploration and vector model for Highway-Reward.

Genetic considerations

Detailed discussions on the genesis of the Highway-Reward deposit were presented by Doyle (1997a,b) and are briefly reviewed below.

- The available evidence is consistent with syngenetic accumulation of the pyrite-chalcopyrite pipes and sphalerite-rich mineralisation.

- Doyle (1997b) critically assessed the evidence for sub-seafloor replacement versus exhalation in the genesis of VHMS deposits. Most of the massive sulfide ores at Highway-Reward formed by sub-seafloor replacement of rhyolite to dacite and volcaniclastic units because: (1) the mineralisation is hosted by intrusive or mass-flow emplaced units; (2) discordant and strata-bound ores contain relic patches of coherent facies or precursor volcanic particles; (3) peperite and massive sulfides are not mixed, implying sulfide deposition postdated emplacement of the enclosing succession; (4) pyrite pipes are discordant to bedding; (5) there are replacement fronts passing from strata-bound sphalerite-rich ores into discordant pyrite-pipes; (6) zones of strong quartz-sericite-alteration and pyrite veining extend into the hanging wall without any abrupt break in intensity.

- The distance below the seafloor at which infiltration and replacement took place is difficult to interpret, but was probably at least 60 m.

- At Highway-Reward, deformation, disruption of bedding, resedimentation, dewatering and low-grade metamorphism of the host succession accompanied emplacement of the intrusions. The resulting patterns of permeability and porosity

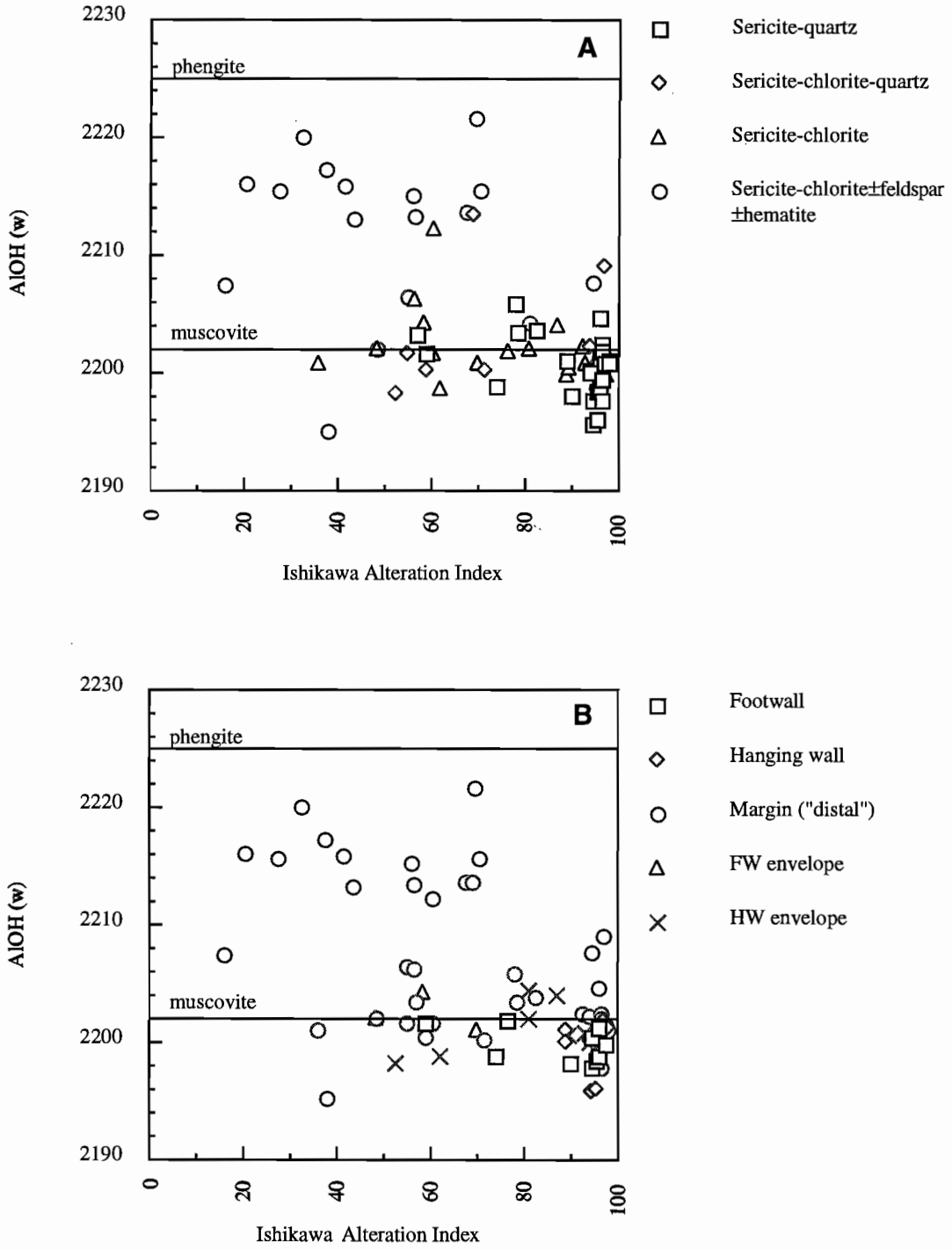

Figure 3. Variation in AlOH wavelength and Ishikawa Alteration Index as a function of alteration mineralogy and distribution.

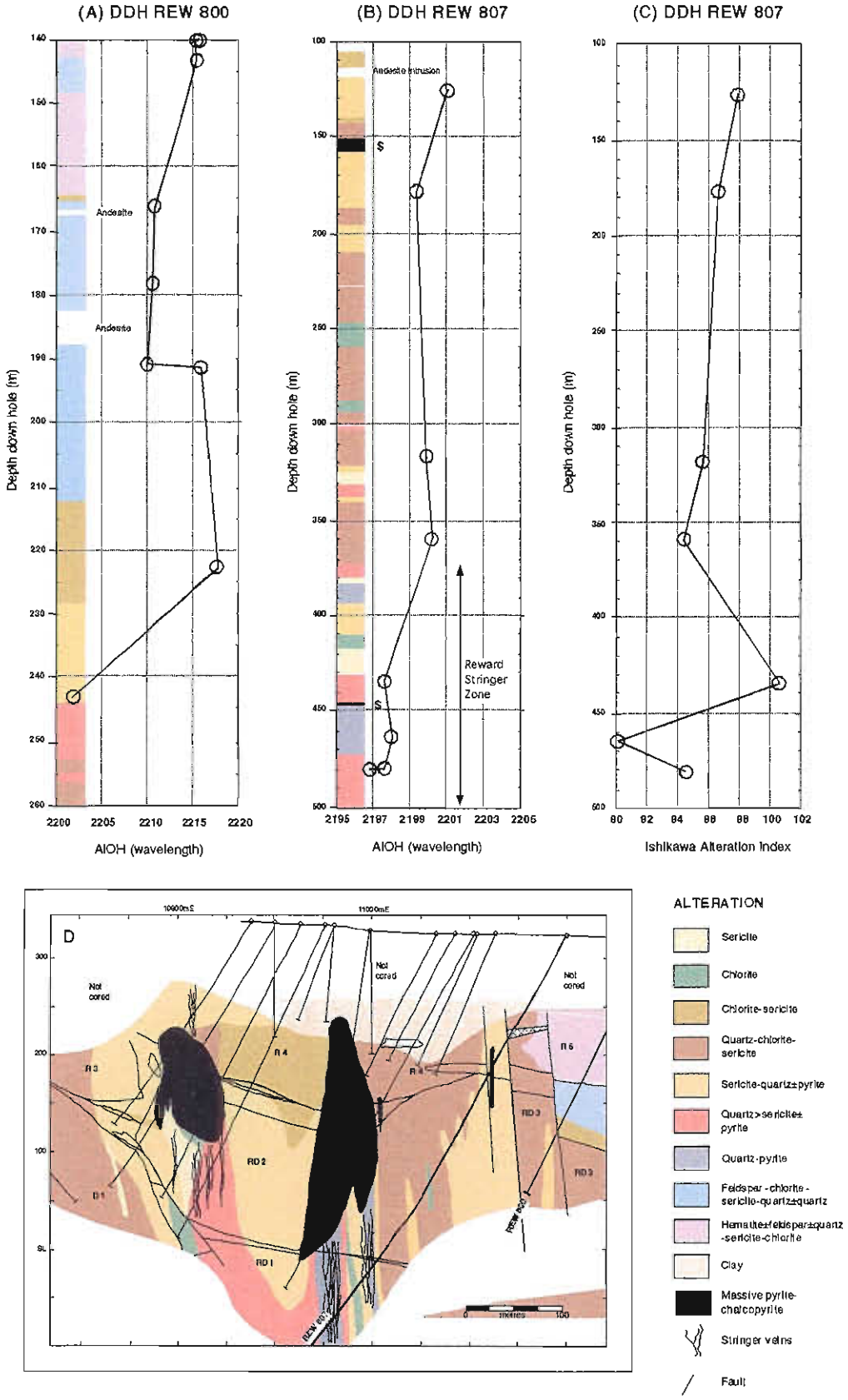

Figure 4. (A-B) Down hole AlOH wavelength variations in muscovite-bearing samples from DDH REW 800 and DDH REW 807. The distribution of alteration assemblages is also illustrated. (C) Down hole variation in Ishikawa Alteration Index values in DDH REW 807. (D) Simplified cross section showing the positions of DDH REW 800 and DDH REW 807 on section 10150N. Dacite D1, rhyodacites RD1-RD3 and rhyolites R2-4 and R6 are intersected on section 10150N (after Doyle, 1997b).

Fig. 5: Exploration model: Highway-Reward type Cu-Au-rich pipes and Pb-Zn lenses

- Known grades: 3.5-5.5% Cu, 6.5-13 g/t Au, 1 g/t Ag in primary ores
- Known tonnage: 1.9 m.t.
- Target tonnage: 5-20 m.t.
- Modern analogue: ?Manus Basin

Geological exploration criteria

- calc-alkaline felsic-intermediate volcanic succession
- hosted in the proximal facies association of non-explosive submarine (bswb) volcanic centre dominated by syn-sedimentary intrusions or lavas
- fluids focussed along fractured glassy margins of coalescing intrusions/lavas
- ponding of fluids beneath barrier (e.g. crystalline lava)
- structural control on magmatism and ?fluid flow
- syn-genetic sub-seafloor replacement of intrusions, lavas and volcaniclastic units
- stacked system
- halo of Pb-Zn-Ba mineralisation surrounds Cu-Au pipes
- potential for Pb-Zn lenses distal to pipes
- strong sericite-quartz±pyrite alteration in footwall and hanging wall
- alteration halo extends 10's m into hanging wall
- late structures focussed along alteration system

Geochemical exploration criteria

- footwall and hanging wall alteration halo
  - depletion Na_2O, CaO, MgO ± MnO
  - enrichment S, Bi, S/Na_2O, Rb/Sr ± Fe_2O_3, K_2O, MnO
  - low Sr/Ba (<0.1)
  - high Ishikawa alteration index (>93)
  - Rb/Sr generally higher (4-8) in HW alteration than FW (1.1-4.5). Values anomalous relative to background (<0.9)
  - AlOH wavelength 2195-2212 (generally <2200)
- anomalous Cu±Pb, Zn, Au, Ag, As and Mo
- $\delta^{34}S$ values in sulfides (pyrite±chalcopyrite; sphalerite) 5.0-8.7
- $^{208}Pb/^{204}Pb$ ratio in ore around 18.073 (±0.026)

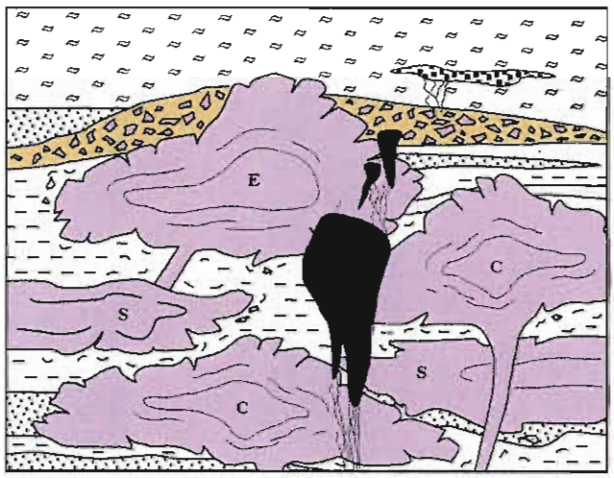

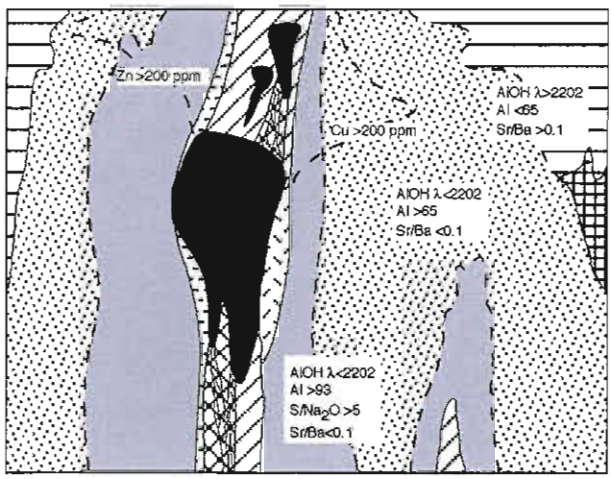

- Pb-Zn-rich massive sulfide
- Pyrite-chalcopyrite
- Resedimented hyaloclastite
- Pumice breccia
- Siltstone-sandstone
- S Syn-sedimentary sill
- C Cryptodome
- E Partly-extrusive cryptodome
- Sericite
- Chlorite
- Chlorite-sericite±quartz
- Sericite>quartz±pyrite
- Quartz>sericite±pyrite
- Quartz-pyrite
- Chlorite-sericite-feldspar±quartz
- Hematite±quartz-sericite-chlorite-feldspar
- Alteration zone boundary
- Geochemical vector boundary

Geophysical exploration criteria

- ground EM, IP and down hole EM will define targets
- ground EM response strong for Cu-rich massive sulfides
- pyrite pipes give good gravity response
- pyrite in FW and HW alteration zone may give significant IP response
- gravity and magnetics useful in mapping andesites

Ore fluid conditions

- pyrite-chalcopyrite pipes
  - high temperature (>300 °C)
  - low pH (2 to 4.5)
  - high fO_2
- shalerite-galena-rich mineralisation
  - low temperature (<300 °C)
  - slightly more alkaline
  - oxidised

Data from Large (1991), Dean and Carr (1992), Huston (1992), Doyle (1997a,b,c) and the present study

are interpreted to have focussed hydrothermal fluid flow within the fractured glassy margins of the cryptodomes. An advancing pyrite-chalcopyrite front progressively replaced the rhyolite to dacite intrusions, peperite and sediment (Fig. 6). A partly extrusive cryptodome formed a barrier to ascending hydrothermal fluids, promoting sub-seafloor ponding of the fluids and replacement within and below its peperitic base (Fig. 6C). Lower temperature fluids that diffused from the margins of the pyrite-chalcopyrite pipes deposited a broad halo of sphalerite-galena-barite mineralisation (Fig. 6D). Strata-bound ores formed by replacement of a porous and permeable pumice breccia bed above the main Reward pipe.

- Pipe-shaped massive sulfide deposits are likely to form in relatively impermeable lava- or intrusion-dominated volcanic centres as ascending hydrothermal fluids will be focussed in the fractured glassy margins of the lavas/intrusions, local autoclastic breccia units and syn-volcanic faults.

- This analysis suggests that the principal controls on the genesis of Highway-Reward-type VHMS deposits are: (1) a progressively evolving submarine intrusion- and/or lava-dominated volcanic centre; (2) an impermeable barrier to promote sub-seafloor ponding of hydrothermal fluids and replacement; (3) a hydrothermal system which remains active during continued volcanism, dewatering of the sediment pile by syn-sedimentary intrusions and sedimentation.

References

Beams S.D. and Dronseika E.V., 1995. The exploration history, geology and geochemistry of the polymetallic Reward and Highway deposits, Mt Windsor Subprovince. 17th International Geochemical Exploration Symposium. Mineral deposits of northeast Queensland: Geology and geophysics, Townsville, Queensland, Abstracts, 137-153.

Berry R.F., Huston D.L., Stolz A.J., Hill A.P., Beams S.D., Kuronen U. and Taube A., 1992. Stratigraphy, structure, and volcanic-hosted mineralisation of the Mount Windsor Subprovince, north Queensland, Australia. Econ. Geol., 87: 739-763.

Brooks E.R., 1995. Palaeozoic fluidisation, folding, and peperite formation, northern Sierra Nevada, California. Can. J. Earth Sci., 32: 314-324.

Busby-Spera C.J. and White J.D.L., 1987. Variation in peperite textures associated with differing host-sediment properties. Bull. Volc., 49: 765-775.

Dean J.A. and Carr G.R., 1992. Final report to Aberfoyle Resources Limited on the Pb isotopic compositions of mineralisation from Highway/Reward, Mt Windsor Joint Venture Project, NE Queensland. CSIRO Australia. Sirotope report SR22.

Dimroth E., Cousineau P., Leduc M. and Sanschagrin Y., 1978. Structure and organisation of Archean basalt flows, Rouyn-Noranda area, Quebec, Canada. Can. J. Earth Sci., 15: 902-918.

Doyle M.G., 1996. Volcanic influences in the formation of iron oxide-silica deposits in a volcanogenic-massive sulfide terrain, Mount Windsor Volcanic belt, Queensland. Australian Mineral Industries Research Association Limited - P439. 87-142.

Doyle MG, 1997a. Alteration associated with sub-seafloor replacement style massive sulfide deposits: evidence from the Cambro-Ordovician Highway-Reward deposit, Mount Windsor Subprovince. AMIRA - P439, Studies of VHMS-related alteration: geochemical and mineralogical vectors to ore. Report 4: 231-257.

Doyle MG, 1997b. A Cambro-Ordovician volcanic succession hosting massive sulfide mineralisation: Mount Windsor Subprovince, Queensland. [unpub. Ph.D thesis]. University of Tasmania, 264 pp.

Doyle MG, 1997c. Alteration geochemistry of the sub-seafloor replacement style Highway-Reward deposit, Mount Windsor Subprovince. AMIRA - P439, Studies of VHMS-related alteration: geochemical and mineralogical vectors to ore. Report 5: 201-219.

Henderson R.A., 1986. Geology of the Mt Windsor Subprovince-a Lower Proterozoic volcano-sedimentary terrane in the northern Tasman Orogenic Zone. Aust. J. Earth Sci., 33: 343-364.

Huston D.L., 1992. Geological and geochemical controls on mineralisation at the Reward deposit: detailed studies of the Highway pipe. [unpub.] CODES, University of Tasmania. 31 pp.

Large R.R., 1991. Ore deposit models and exploration criteria for VMS deposits in the Mt Windsor Volcanics. In: Pongratz, J. P. and Large, R. R. (eds.) Geological controls on VMS mineralisation in the Mt Windsor Volcanic Belt-research report No. 2 [unpub.], 181-198.

Stolz A.J., 1995. Geochemistry of the Mount Windsor Volcanics: Implications for the Tectonic setting of the Cambro-Ordovician volcanic-hosted massive sulfide mineralisation in Northeastern Australia. Econ. Geol., 90: 1080-1097.

Sigurdsson H., 1977. Chemistry of the crater lake during the 1971-72 Soufriére eruption. J. Volcanol. Geotherm. Res., 2: 165-186.

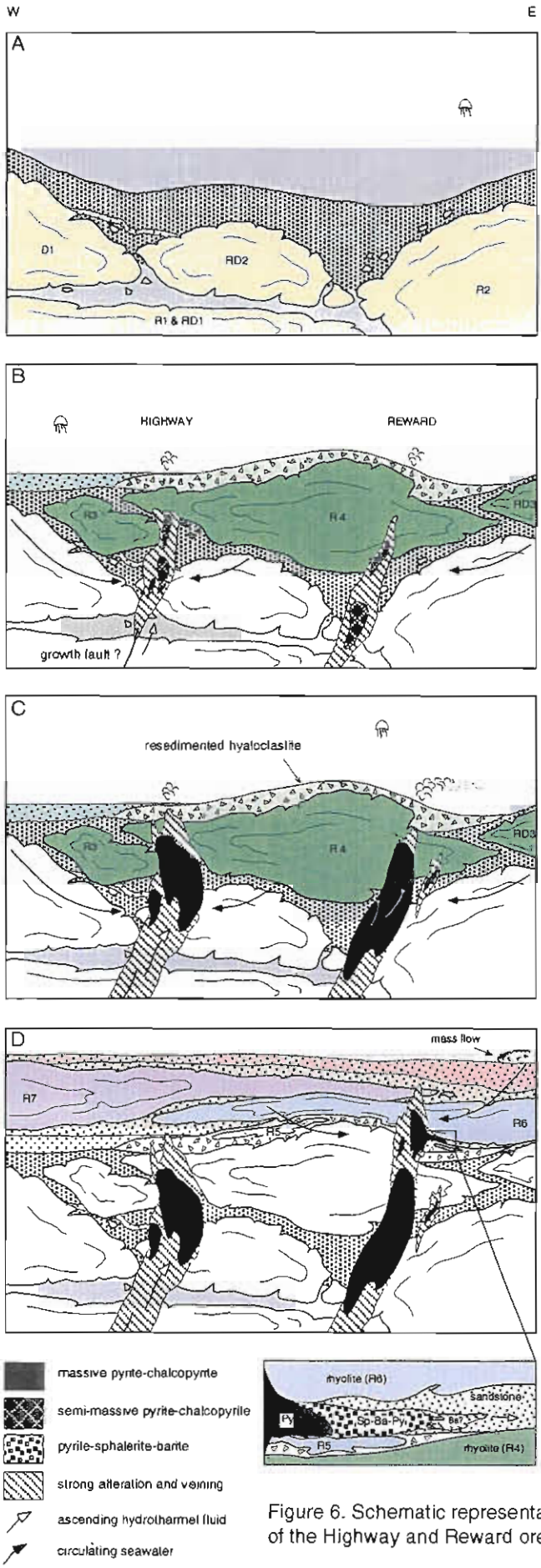

Subaqueous emplacement of feldspar±quartz-bearing pumiceous mass-flow deposits and overlying siltstone. Intrusion of rhyolitic to dacitic syn-sedimentary sills (R1, RD1) and cryptodomes (D1, RD2, R2). The intrusions influenced seafloor topography and partially dewatered the host succession.

Intrusion of a rhyolitic cryptodome (R3) and partial extrusion of a rhyolitic cryptodome (R4) through the seafloor. Onset of significant hydrothermal activity. Hydrothermal fluids ascend growth faults and are focussed along the margins of the overlying cryptodomes. Fluids mix with seawater circulating through the glassy, porous and permeable margins of the cryptodomes and volcaniclastic deposits. Sulfides replace the enclosing strata within a strongly altered and veined zone.

Intensification of the hydrothermal system to a maximum of >300°C. An advancing pyrite-chalcopyrite replacement front moves through the host strata overprinting earlier sulfide minerals. Ponding of hydrothermal fluids beneath rhyolite 4 promotes sulfide deposition. Hydrothermal fluids were locally expelled in the water column.

Intrusion of syn-sedimentary sills (R5-R7) into resedimented hyaloclastite of rhyolite 4, and the overlying deposits. At Reward, the pyrite pipe eventually penetrated rhyolite 4. Continued hydrothermal activity deposits pipe- and vein-style mineralisation above the main pipes. Hydrothermal fluids moving out from the margins of the pipes. Minor stratiform Pb-Zn-Ba-rich lenses deposited by sub-seafloor replacement of permeable volcaniclastic deposits.

An advancing pyrite-chalcopyrite front progressively replaces earlier low-temperature (<300°C) sphalerite (Sp)- and barite (Ba)-rich mineralisation.

Figure 6. Schematic representation of successive stages in the genesis of the Highway and Reward orebodies (Doyle, 1997b).

Sample No.	**REW 800/140.4m**
Location	Highway-Reward
Alteration zone	Margin; Hematite-feldspar-chlorite-sericite
Formation	Trooper Creek Formation

Description Patchy hematite-feldspar-sericite-chlorite-altered rhyolite. Diffuse boundaries between alteration domains

Facies Interp Massive coherent facies of a rhyolitic sill (rhyolite 6).

Alteration Intensity	none	weak	(moderate)	strong	intense	Py
Alteration Style	(patchy)	pervasive	veined		cleavage control	
Alteration Mineralogy	Groundmass	hematite-feldspar-sericite-chlorite				
	Feldspars	unaltered feldspar				
	Mafics	-				
Interpretation	diagenetic	metamorphic	syntectonic	(hydrothermal)		
Relict Mineralogy	quartz and feldspar phenocrysts					

Geochemistry

SiO_2	TiO_2	Al_2O_3	Fe_2O_3	MnO	MgO	CaO	Na_2O	K_2O	P_2O_5	S	LOI	Al	CCPI	Ti/Zr
73.08	0.30	13.09	2.22	0.05	2.02	2.97	5.15	1.04	0.06	<0.01	3.37	27.40	39.36	12.5

Rb	Sr	Ba	Cu	Pb	Zn	Sb	Tl	Zr	Nb	Y	$\delta^{18}O_{wr}$	AlOH λ
31	102	237	<2	2	34	0.7	<0.5	143	8	19		2215.4

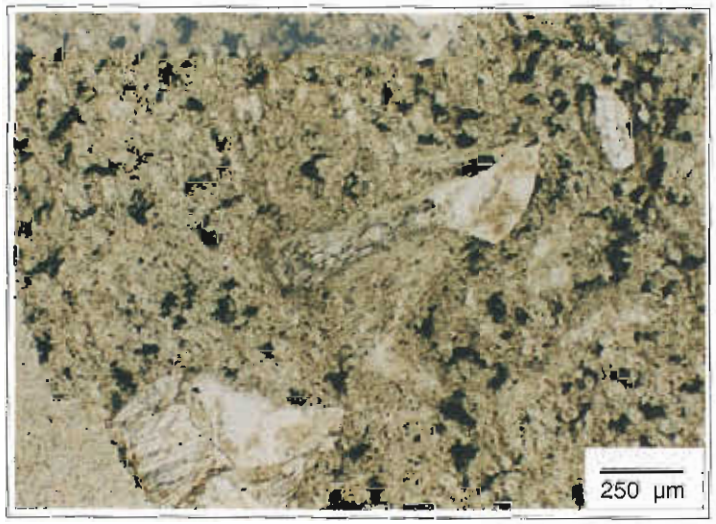

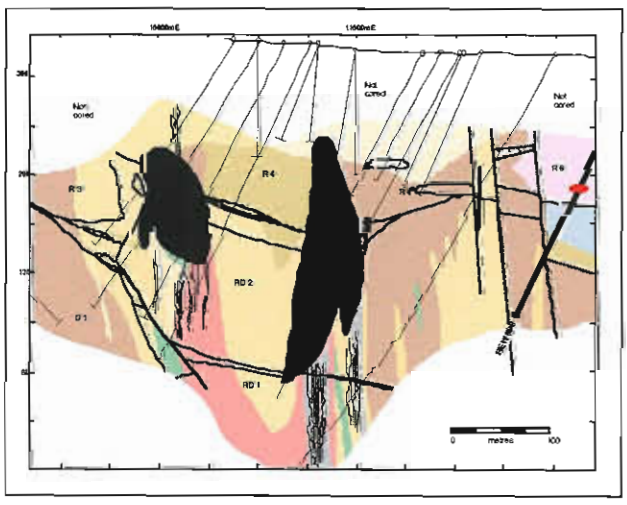

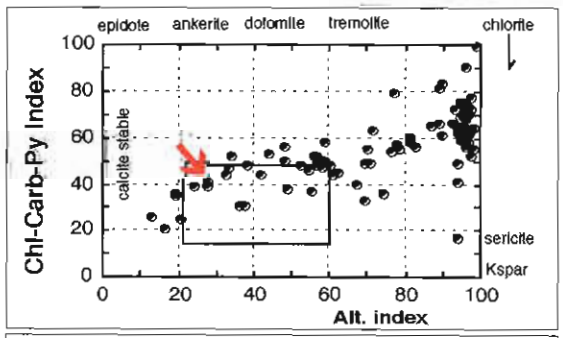

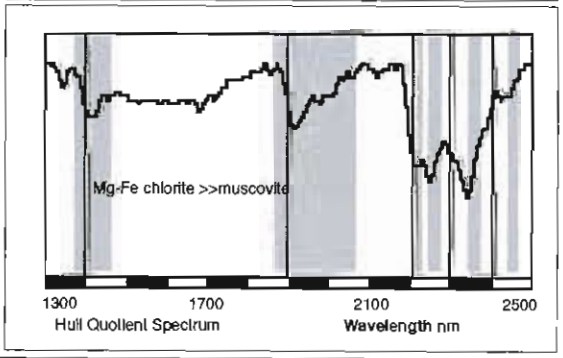

Sample No.	**REM 560/316.3m**
Location	Highway-Reward
Alteration zone	Margin; Chlorite-sericite
Formation	Trooper Creek Formation

Description Dark green pervasively chlorite-sericite-altered dacite.

Facies Interp Massive coherent dacite from the margin of a cryptodome (dacite 1).

Alteration Intensity	none	(weak)	moderate	strong	intense	Py
Alteration Style	patchy	(pervasive)	veined		cleavage control	
Alteration Mineralogy	Groundmass	chlorite-sericite				
	Feldspars	chlorite				
	Mafics	-				
Interpretation	diagenetic	metamorphic	syntectonic	(hydrothermal)		
Relict Mineralogy	chloritised feldspar phenocrysts					

Geochemistry

SiO_2	TiO_2	Al_2O_3	Fe_2O_3	MnO	MgO	CaO	Na_2O	K_2O	P_2O_5	S	LOI	Al	CCPI	Ti/Zr
68.49	0.56	17.07	4.41	0.18	2.55	0.19	4.52	1.86	0.1	<0.01	2.42	48.36	50.54	20.8

Rb	Sr	Ba	Cu	Pb	Zn	Sb	Tl	Zr	Nb	Y	$\delta^{18}O_{wr}$	AlOH λ
44.1	68	515	1	2	162	0.3	<0.5	161	9	25		2201.9

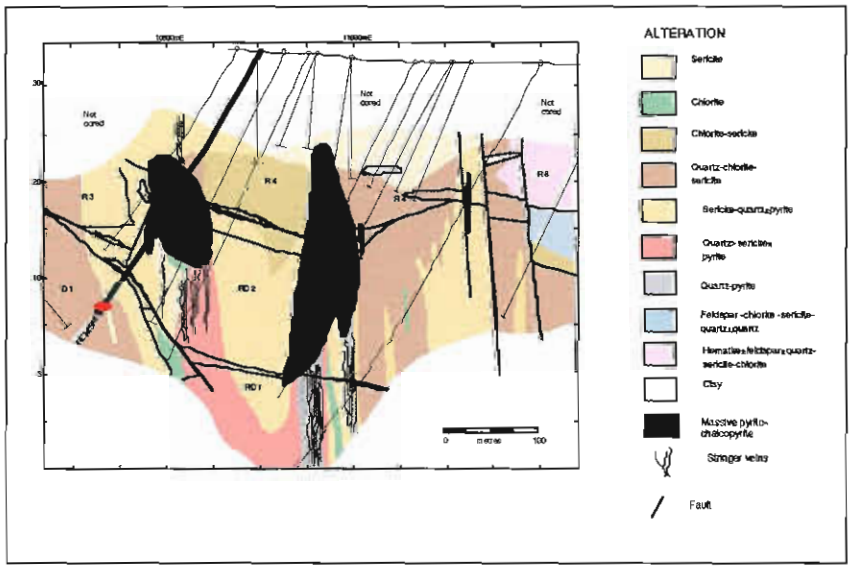

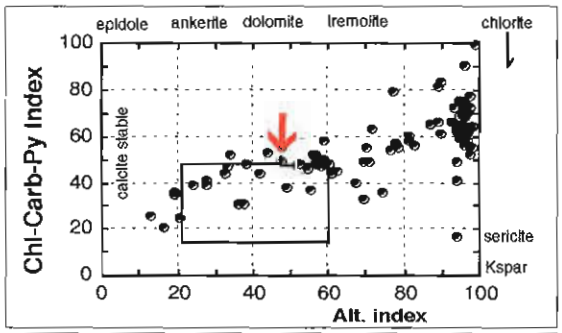

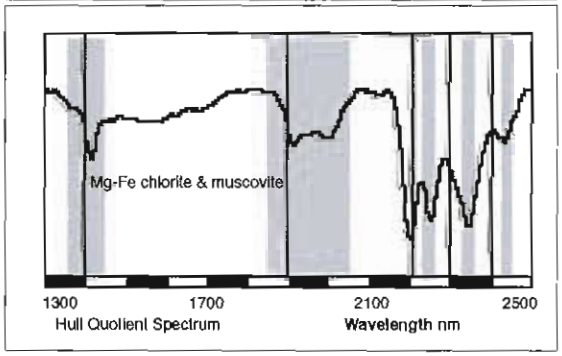

Sample No. REW 800/143.4m
Location Highway-Reward
Alteration zone Margin; Feldspar- sericite

Formation Trooper Creek Formation

Description Patchy and mottled feldspar-sericite alteration. Sericitie filled perlitic fractures enclosing formerly glassy kernals.

Facies Interp Massive perlicically fractured facies of a rhyolitic sill (rhyolite 6).

Alteration Intensity none (weak) moderate strong intense Py
Alteration Style (patchy) pervasive veined cleavage control
Alteration Mineralogy
Groundmass hematite-feldspar-sericite-chlorite
Feldspars unaltered feldspar
Mafics -
Interpretation (diagenetic) metamorphic syntectonic hydrothermal
Relict Mineralogy quartz and feldspar phenocrysts

Geochemistry

SiO_2	TiO_2	Al_2O_3	Fe_2O_3	MnO	MgO	CaO	Na_2O	K_2O	P_2O_5	S	LOI	Al	CCPI	Ti/Zr
62.7	0.51	20.4	3.64	0.05	4.25	0.39	3.32	4.60	0.09	<0.01	3.64	70.43	48.75	12.5

Rb	Sr	Ba	Cu	Pb	Zn	Sb	Tl	Zr	Nb	Y	$\delta^{18}O_{wr}$	AlOH λ
127	49	984	<2	4	70	1.6	1	242	12	33		2215.4

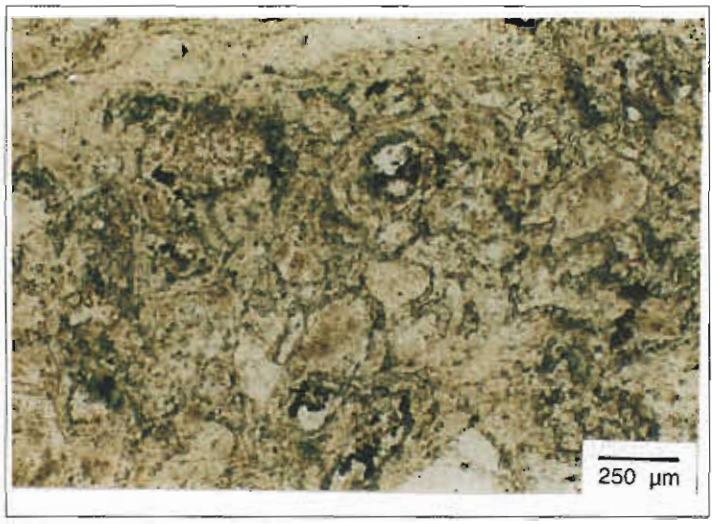

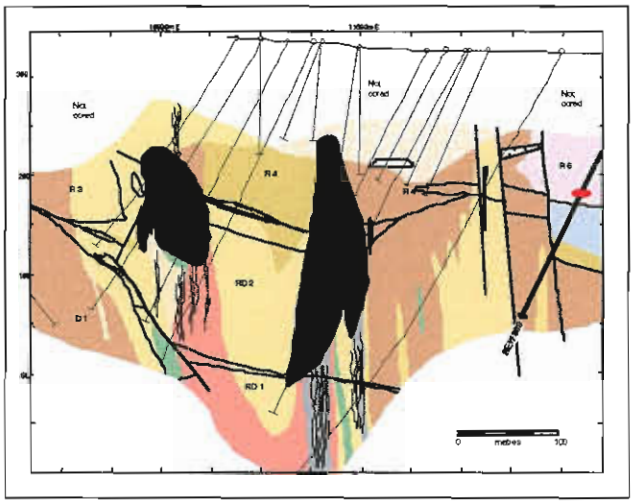

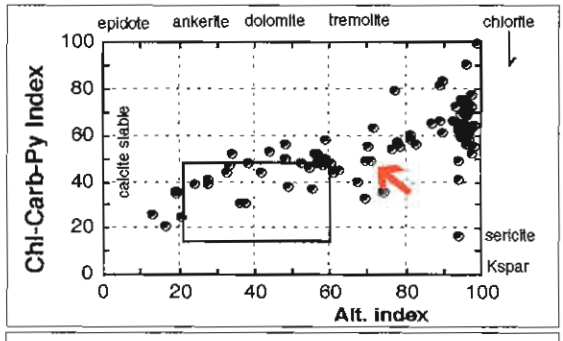

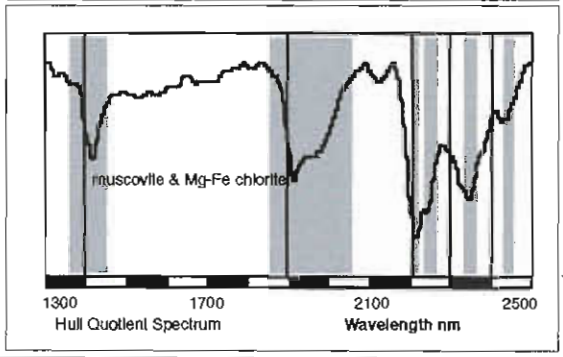

Sample No. REW 154/170.2m
Location Highway-Reward
Alteration zone Margin; sericite-chlorite

Formation Trooper Creek Formation

Description Patchy sericite-chlorite alteration of evenly quartz- and feldspar-phyric rhyolite. Patches have sharp to diffuse margins.

Facies Interp Coherent facies of a rhyolitic partly extrusive cryptodome (rhyolite 4).

Alteration Intensity	none	weak	(moderate)	strong	intense	Py
Alteration Style	(patchy)	pervasive	veined		cleavage control	
Alteration Mineralogy	Groundmass	sericite-chlorite				
	Feldspars	sericite-chlorite				
	Mafics	-				
Interpretation	diagenetic	metamorphic	syntectonic	(hydrothermal)		
Relict Mineralogy	quartz and feldspar phenocrysts, recrystallised					

Geochemistry

SiO_2	TiO_2	Al_2O_3	Fe_2O_3	MnO	MgO	CaO	Na_2O	K_2O	P_2O_5	S	LOI	Al	CCPI	Ti/Zr
73.72	0.31	14.58	3.52	0.16	3.71	0.40	0.17	3.38	0.05	0.01	3.61	92.56	65.97	11.3

Rb	Sr	Ba	Cu	Pb	Zn	Sb	Tl	Zr	Nb	Y	$\delta^{18}O_{wr}$	AlOH λ
70	21	1791	6	7	120	0.8	1.5	165	9	23		2202.2

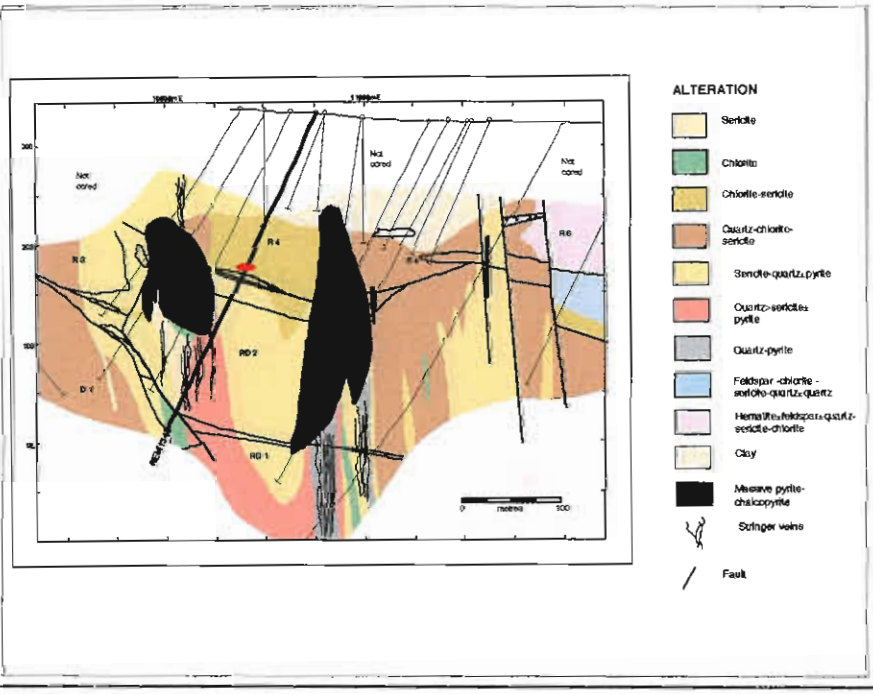

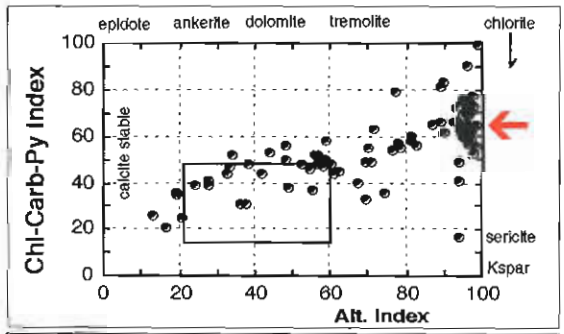

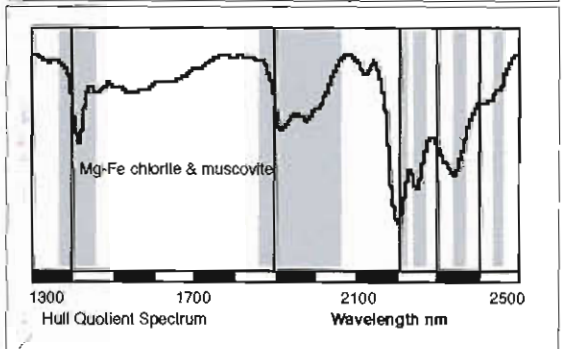

Sample No. REM 113/178.9 m.
Location Highway-Reward
Alteration zone Margin; sericite-chlorite-quartz

Formation Trooper Creek Formation

Description Sericite-chlorite-altered apparent clasts are separated by a sericite-quartz apparent matrix

Facies Interp Coherent facies of a rhyolitic p cryptodome (rhyolite 3); peperitic upper margin

Alteration Intensity none weak (moderate) strong intense Py
Alteration Style (patchy) pervasive veined cleavage control
Alteration Mineralogy
Groundmass sericite-chlorite-quartz
Feldspars chlorite
Mafics -

Interpretation diagenetic metamorphic syntectonic (hydrothermal)
Relict Mineralogy quartz and feldspar phenocrysts, recrystallised

Geochemistry

SiO_2	TiO_2	Al_2O_3	Fe_2O_3	MnO	MgO	CaO	Na_2O	K_2O	P_2O_5	S	LOI	Al	CCPI	Ti/Zr
76.23	0.3	13.03	4.0	0.23	3.02	0.17	0.12	2.86	0.05	0.35	3.13	95.32	68.93	11.8

Rb	Sr	Ba	Cu	Pb	Zn	Sb	Tl	Zr	Nb	Y	$\delta^{18}O_{wr}$	AlOH λ
71	19	939	48	280	1654	1.2	0.8	151	8	19		2200.8

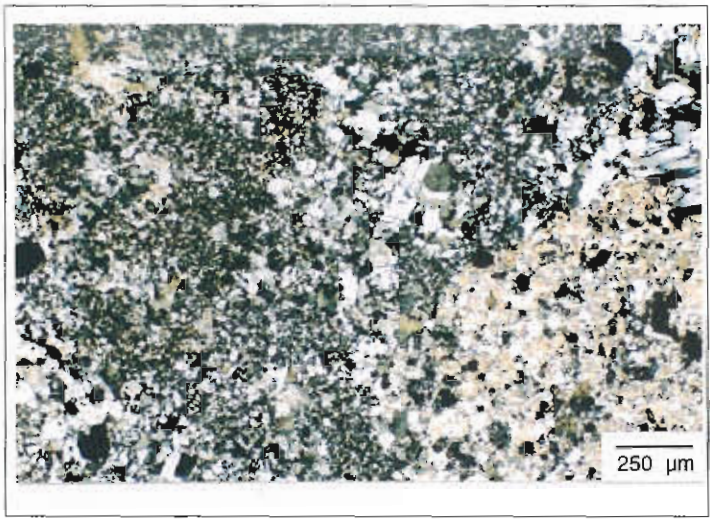

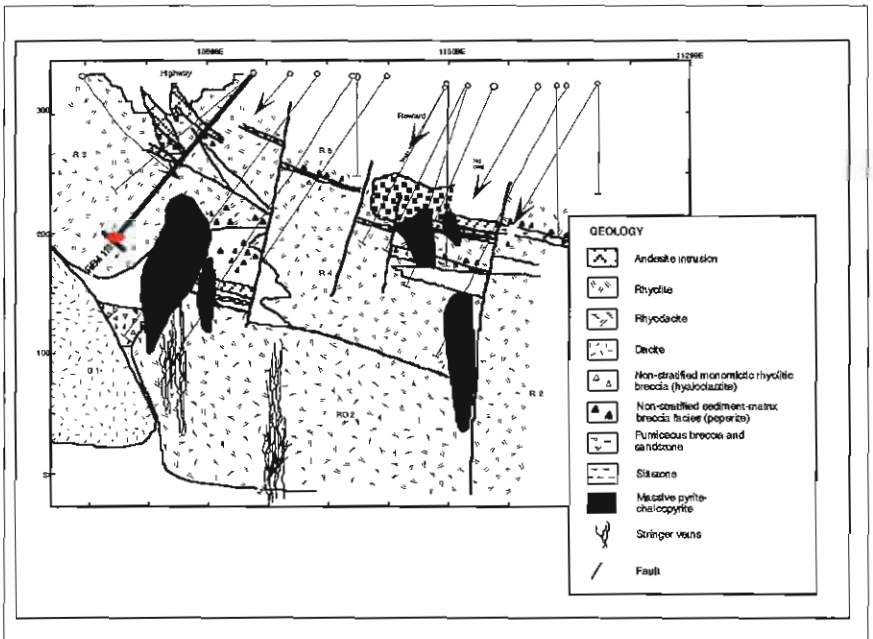

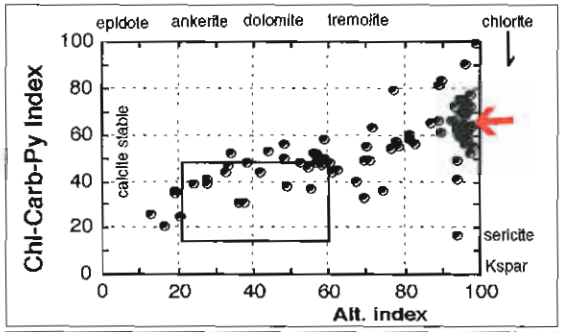

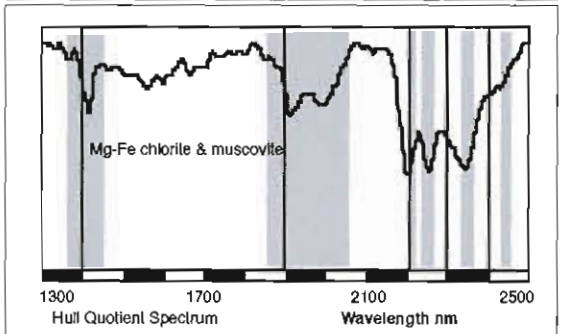

Sample No. REM 113/77.3m
Location Highway-Reward
Alteration zone Hanging wall quartz-sericite

Formation Trooper Creek Formation

Description Intensely quartz-sericite-pyrite altered, quartz phyric rhyolite; Py disseminated and in veinlets.

Facies Interp Coherent facies of a rhyolitic partly extrusive cryptodome (rhyolite 4); resedimented hyaloclastite at margins.

Alteration Intensity	none	weak	moderate	strong	(intense)	Py
Alteration Style	(patchy)	pervasive	veined		cleavage control	
Alteration Mineralogy	Groundmass	quartz-sericite-pyrite				
	Feldspars	sericite				
	Mafics	-				
Interpretation	diagenetic	metamorphic	syntectonic	(hydrothermal)		
Relict Mineralogy	quartz and feldspar phenocrysts, recrystallised					

Geochemistry

SiO_2	TiO_2	Al_2O_3	Fe_2O_3	MnO	MgO	CaO	Na_2O	K_2O	P_2O_5	S	LOI	Al	CCPI	Ti/Zr
71.53	0.31	12.63	11.33	<0.01	0.36	0.01	0.15	3.64	0.04	8.03	7.12	96.06	73.56	14

Rb	Sr	Ba	Cu	Pb	Zn	Sb	Tl	Zr	Nb	Y	$\delta^{18}O_{wr}$	AlOH λ
64	35	1444	71	5	80	1.1	3.4	80	6	20		2198.7

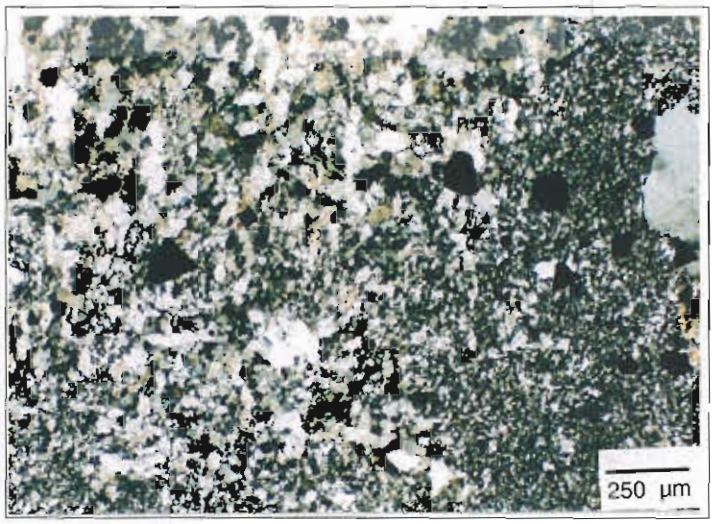

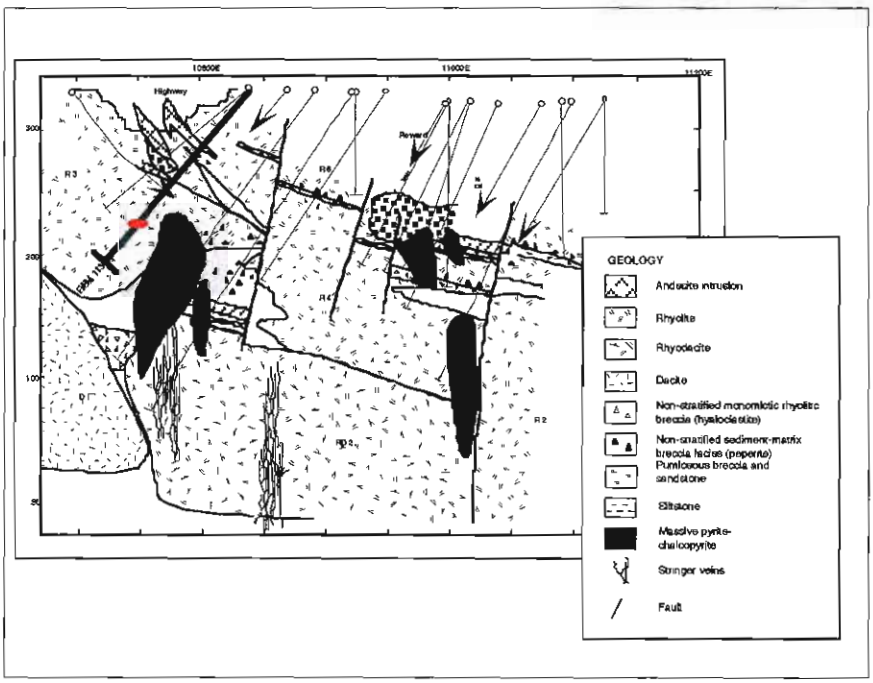

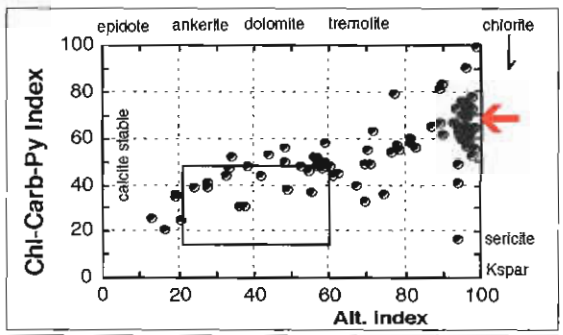

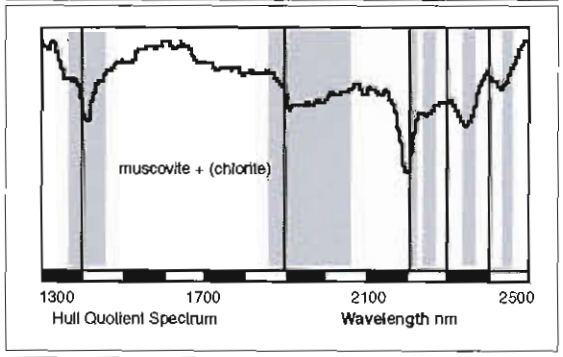

Sample No.	**REW 807/178.3m**
Location	Highway-Reward
Alteration zone	Margin; Sericite-quartz
Formation	Trooper Creek Formation

Description Weakly mottled sericite-quartz alteration of coherent rhyolite

Facies Interp Massive coherent rhyolite cryptodome (rhyolite 2). Siltstone matrix rhyolite breccia (peperite) along upper margin.

Alteration Intensity	none	weak	(moderate)	strong	intense	Py
Alteration Style	(patchy)	pervasive	veined		cleavage control	
Alteration Mineralogy	Groundmass	sericite-quartz				
	Feldspars	chlorite				
	Mafics	-				
Interpretation	diagenetic	metamorphic	syntectonic	(hydrothermal)		
Relict Mineralogy	feldspar and quartz phenocrysts					

Geochemistry

SiO_2	TiO_2	Al_2O_3	Fe_2O_3	MnO	MgO	CaO	Na_2O	K_2O	P_2O_5	S	LOI	Al	CCPI	Ti/Zr
63.23	0.55	20.45	7.70	0.05	1.68	0.04	0.23	6.04	0.03	5.16	6.04	96.63	57.87	20.4

Rb	Sr	Ba	Cu	Pb	Zn	Sb	Tl	Zr	Nb	Y	$\delta^{18}O_{wr}$	AlOH λ
123	33	2779	274	13	96	0.8	2.1	161	7	20		2199.3

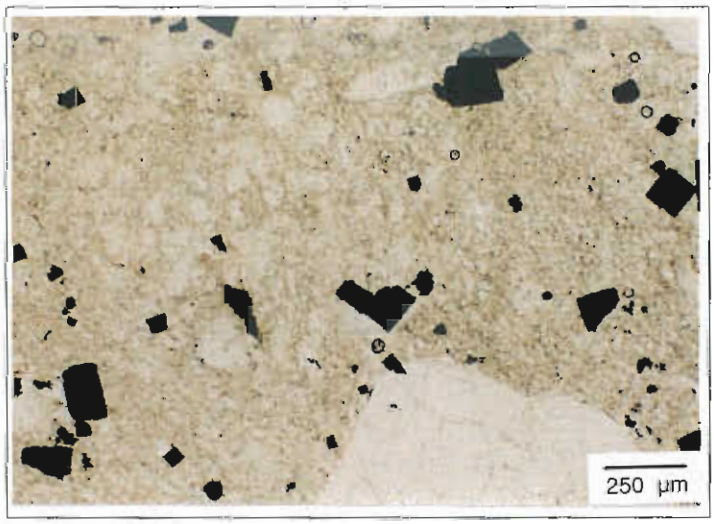

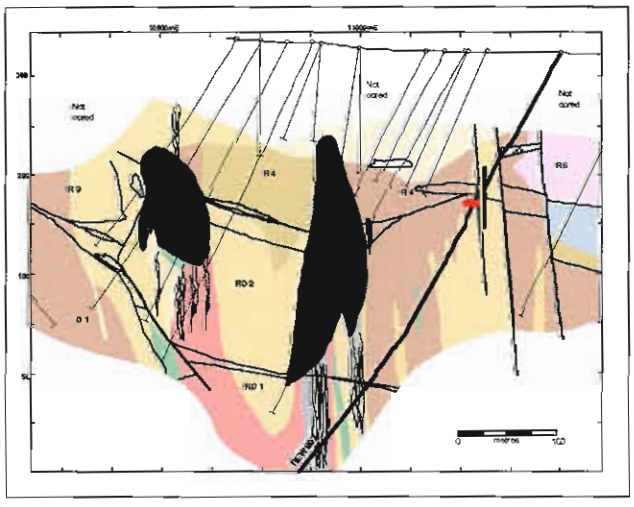

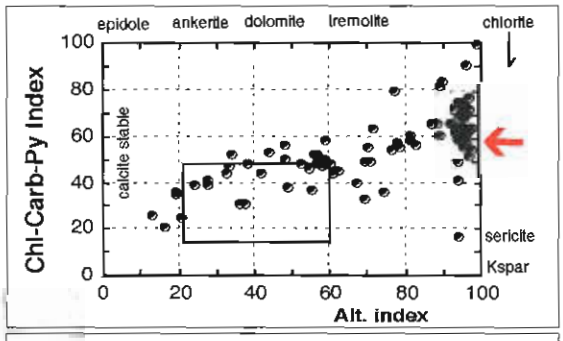

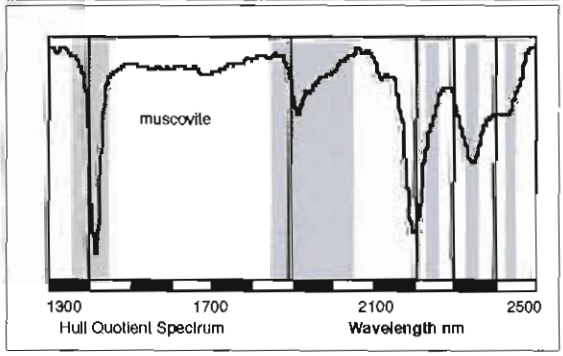

Sample No.	**REW 807/434.7m**
Location	Highway-Reward
Alteration zone	Footwall quartz-sericite
Formation	Trooper Creek Formation

Description Intense pervasive quartz-sericite alteration of rhyodacite. Sericite veinlets.

Facies Interp Margin of a rhyodacitic syn-sedimentary sill (rhyodacite 1). The sill occurs in the footwall to the Highway-Reward deposit.

Alteration Intensity	none	weak	moderate	strong	(intense)	Py 5%
Alteration Style	patchy	(pervasive)	veined		cleavage control	
Alteration Mineralogy	Groundmass	quartz-sericite				
	Feldspars	sericite				
	Mafics	-				
Interpretation	diagenetic	metamorphic	syntectonic	(hydrothermal)		
Relict Mineralogy	feldspar and rare quartz phenocrysts					

Geochemistry

SiO_2	TiO_2	Al_2O_3	Fe_2O_3	MnO	MgO	CaO	Na_2O	K_2O	P_2O_5	S	LOI	Al	CCPI	Ti/Zr
84.5	0.15	4.7	8.94	0.01	0.19	<0.01	<0.01	1.41	0.01	6.52	4.74	100.6	85.3	21.9

Rb	Sr	Ba	Cu	Pb	Zn	Sb	Tl	Zr	Nb	Y	$\delta^{18}O_{wr}$	AlOH λ
22	8	628	10	3	12	1.2	1.2	52	3	8		2197.6

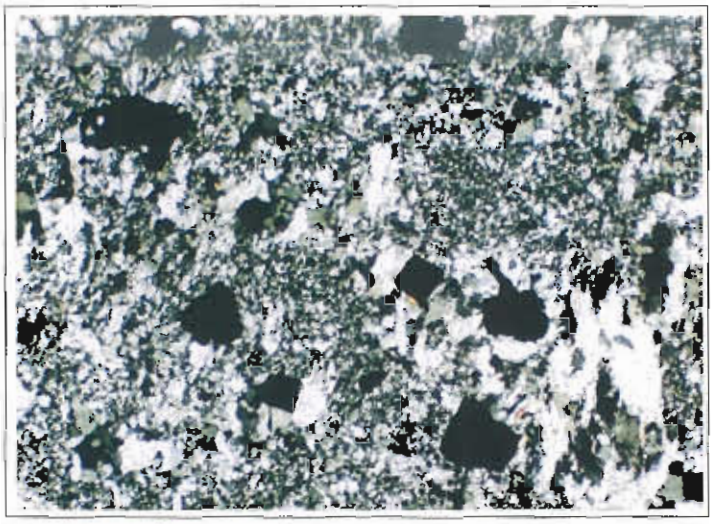

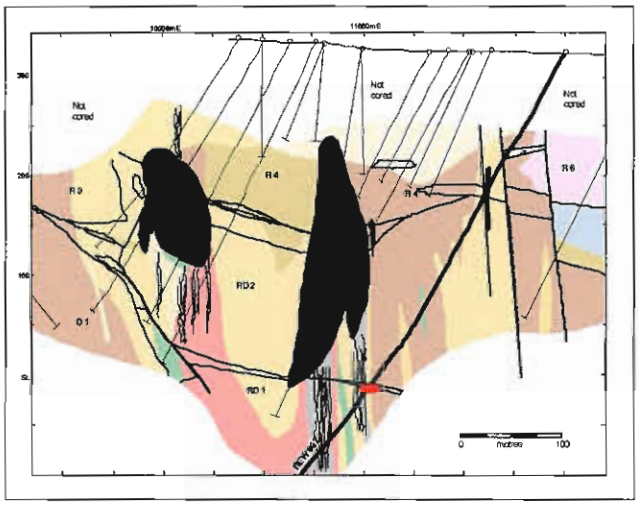

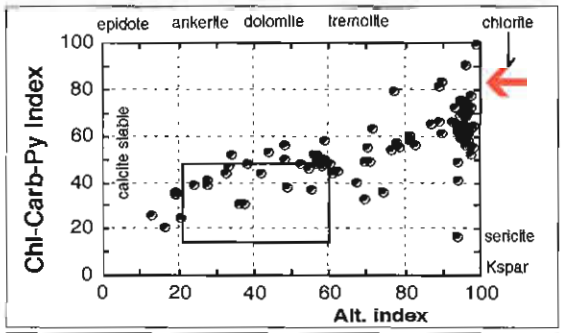

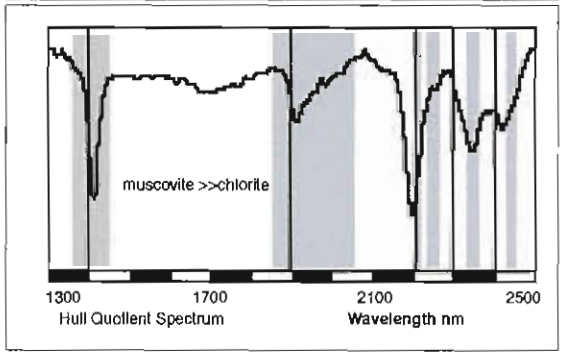

Alteration case study of the Gossan Hill VHMS deposit

Robina Sharpe and Bruce Gemmell
Centre for Ore Deposit Research

Summary

The AMIRA P439 Gossan Hill case study aimed to identify geological and geochemical vectors to VHMS mineralisation at Gossan Hill. The Gossan Hill Cu-Zn VHMS deposit is hosted by a succession of felsic tuffaceous volcaniclastics. These volcaniclastics form part of the Golden Grove Formation (GGF) that was deposited via successive subaqueous mass flows, which are thickest proximal to sulphide mineralisation. Coherent volcanics are absent from the GGF, but are the main rock type in the hangingwall Scuddles Formation. A massive dacite dome of the Scuddles Formation intrudes the Golden Grove Formation and overlies its feeder zone. This feeder zone represents a former synvolcanic structure along which, mineralising fluids were focussed.

Within the Golden Grove Formation host sequence, massive sulphide mineralisation forms two stratigraphically separate zones; a lower Cu-rich and upper Zn-rich zone, both of which are connected by stringer mineralisation. Massive magnetite also occurs, but is only associated with the lower Cu-rich zone and formed prior to massive sulphide mineralisation. The asymmetry of massive sulphide, massive magnetite and alteration zones at the Gossan Hill deposit indicate synvolcanic structural control.

Hydrothermal alteration at Gossan Hill is ubiquitous throughout the GGF. At least two types of hydrothermal alteration are identified: (1) **regional quartz±chlorite (±clay/zeolite?) alteration** of the tuffaceous GGF and (2) **localised siliceous, chlorite and ankerite-siderite alteration** enveloping and hosting mineralisation. Remarkable textural preservation of pumiceous and shard fragments within the GGF indicates that the regional alteration pre-dated the localised hydrothermal alteration and that this regional alteration was syndepositional and/or diagenetic. This early regional alteration event effectively sealed the tuffaceous host and footwall succession from subsequent modification by hydrothermal activity and metamorphism. Localised alteration (metre scale) occurs proximal to massive sulphides, massive magnetite and stringer mineralisation. This localised alteration varies from chlorite-carbonate alteration associated with Cu-rich sulphides and massive magnetite, to quartz alteration associated with Zn-rich sulphides. Within the localised chlorite-carbonate alteration, minor alteration minerals include talc, apatite, muscovite, chloritoid and andalusite, whilst near massive magnetite the main alteration minerals are carbonate, talc, chlorite and quartz. Comparatively, the hangingwall massive volcanics are characterised by pervasive ankerite-calcite and muscovite alteration.

As a result of regional silicification (±chlorite), whole rock geochemistry of the GGF reflects an intense alkali depletion and a strong SiO_2 and FeO enrichment. Towards the Cu-rich massive sulphide there is enrichment in FeO and MgO because of intense chlorite alteration. Towards massive magnetite there is enrichment in CaO and FeO because of carbonate and magnetite alteration, whilst towards Zn-rich sulphide, there is enrichment in SiO_2 resultant from siliceous alteration. Within the Golden Grove Formation at Gossan Hill, the Ishikawa, Chlorite and Mn-Carbonate alteration indices are not applicable because of this alkali depletion and intense SiO_2 (quartz) and FeO (chlorite) enrichment. However, alteration in the hangingwall is characterised by Na_2O depletion and by CaO and K_2O enrichment.

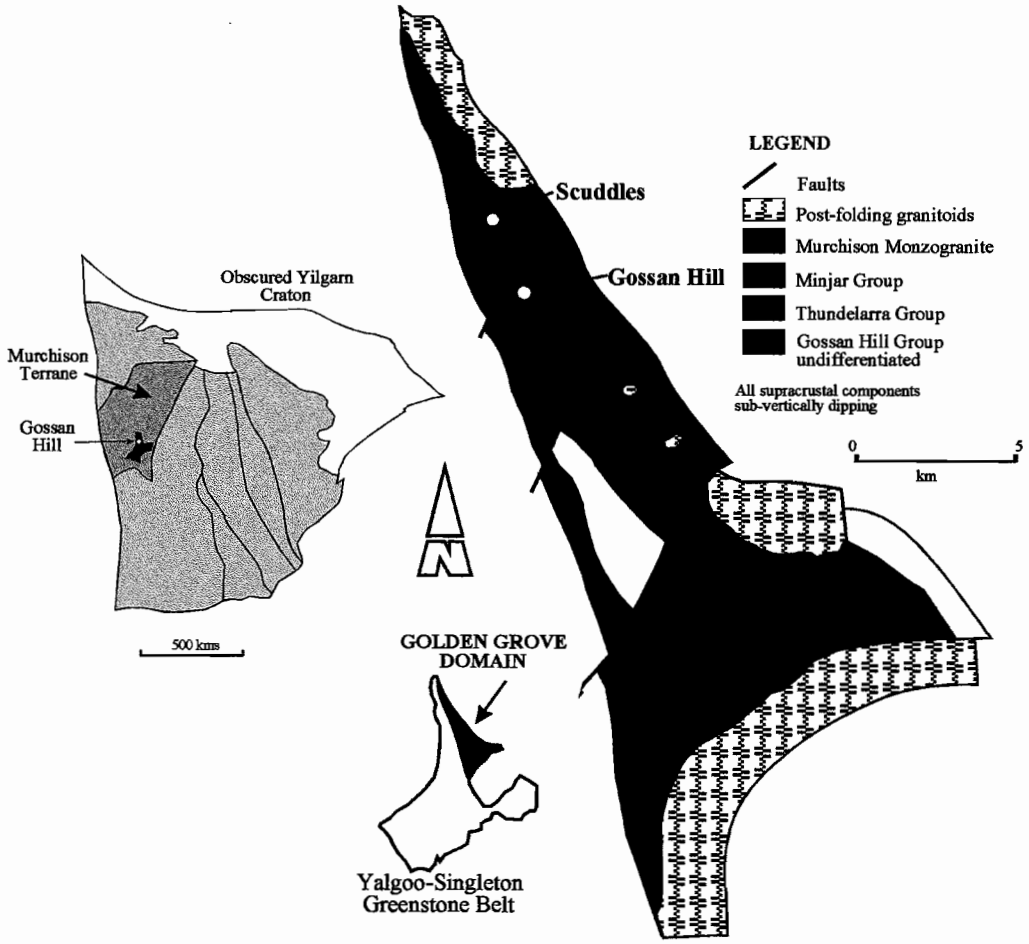

Figure 1: Location of the Gossan Hill VHMS deposit in the Yilgarn Craton of Western Australia. The Gossan Hill and Scuddles deposits occur within the Yalgoo-Singleton greenstone belt and are hosted within the Gossan Hill Group (modified from Myers, 1990).

Table 1: Results from the Murchison Zinc Company 1994-1997 feasibility study at Gossan Hill giving the estimated resource of the primary massive sulphide and oxide-supergene Au and Cu mineralisation zones.

	Tonnes (Mt.)	Zn (%)	Cu (%)	Pb (%)	Ag (g/t)	Au (g/t)
Zn-rich sulphide	2.2	11.4	0.3	1.1	103	1.5
Cu-rich sulphide	7.0	0.3	3.4	-	16	0.4
Cu-supergene	5.27	-	1.5	-	-	-
Au-oxide	2.01	-	-	-	86	2.2

At Gossan Hill, geochemical and mineralogical vectors to ore are only defined within metres of the sulphide mineralisation. However, the SiO_2 and FeO enrichment trends in the localised hydrothermal alteration are not significantly different from regional alteration trends. Therefore, geological vectors are more definitive than geochemical vectors, and include facies thickness variations, the M1 Marker hydrothermal chert horizons and discordant synvolcanic intrusions.

Introduction

The Archean Gossan Hill volcanic-hosted massive sulphide (VHMS) deposit is situated in the Yilgarn Craton, Western Australia. The Gossan Hill deposit is located approximately 500 km NNE of Perth in the Yalgoo–Singleton greenstone belt of the Murchison Province granite-greenstone terrane (Fig. 1). The age of this deposit is estimated between 2.7 to 2.9 Ga. (Pidgeon et al., 1994; Vaasjoki, 1984).

The research in this report is a summary of the primary mineralisation at the Gossan Hill deposit and was funded by an APRA-Industry postgraduate award with financial and logistical support from the Normandy Group. The financial contribution by the AMIRA P439 project has been through funding of ICP-MS trace element analyses and microprobe analyses. This final report incorporates results and conclusions of previous AMIRA P439 investigations on Gossan Hill, which are:

- Sharpe R., 1996 . Gossan Hill alteration: styles and distributions. AMIRA P439, Report2, May 1996, p. 155–170.
- Sharpe, R., 1997. Gossan Hill: the relationship between mineralogy, alteration and geochemistry. AMIRA P439 Report 4, May 1997, p. 97–183.

A total of 88 samples were analysed from unweathered drill core selected from specific stratigraphic members or zones of alteration. Limitations from the orientation and placement of drill holes, together with the stratigraphic separation of Zn- and Cu-rich mineralisation in a steeply dipping terrain, precluded investigation on any single section. As a result three intersections through mineralisation were investigated. All samples were analysed for major elements by XRF and for trace elements by XRF or ICP-MS according to the following scheme:

XRF	As, Ba, Ce, Cr, Cu, La, Nd, Ni, Pb, Rb, S, Sc, Sr, Th, V ,Y, Zn, Zr;
ICP-MS	Ag, As, Bi, Cd, Cs, Mo, Sb, Tl, U.

Tonnes/grades

The Gossan Hill deposit is a Cu-Zn VHMS that consists of weathered oxidised mineralisation overlying primary sulphide mineralisation, with metal grades and tonnage as listed in Table 1. Cu- and Zn-rich massive sulphides form stratigraphically separate zones, with Cu-rich sulphides below Zn-rich sulphides. Additionally, an estimated 12 Mt. of massive magnetite occurs at Gossan Hill, which is juxtaposed against Cu-rich mineralisation. These characteristics make Gossan Hill an atypical VHMS in the classification of Australian polymetallic VHMS deposits as given by Large (1992) . However, although these features are unusual in Australian VHMS deposits, similar attributes are documented in many Canadian Archean VHMS deposits (e.g., Franklin et al., 1975; Galley, et al., 1995 ; Zaleski and Peterson, 1995; Roberts, 1975).

Ore mineralogy

Three primary ore types are identified at Gossan Hill: (1) massive sphalerite, (2) massive pyrite and (3) massive magnetite. The mineralogy of each of these ore types is listed in Table 2. Massive sulphides are dominantly characterised by sphalerite, pyrite, chalcopyrite, magnetite, pyrrhotite and galena. Sphalerite however, only occurs in the upper Zn-rich sulphide zone. Other minor minerals in the Zn-rich massive sulphide zone include tetrahedrite, cobaltite, arsenopyrite, bornite, cassiterite, electrum and native silver. Comparatively, the ore mineralogy of the lower Cu-rich massive sulphide zone is simple (Table 2). The effects of recrystallisation and remobilisation, associated with penetrative deformation and greenschist facies metamorphism are strongly developed at Gossan Hill and thus, primary ore textures and their paragenetic associations are overprinted.

Gangue mineralogy

The major gangue minerals in massive sulphide and massive magnetite are listed in Table 2. Quartz and chlorite are the major gangue phases in massive sulphides and stringer veins, with chlorite the dominant gangue in the lower sulphide zone. Although carbonate is also a common gangue in massive sulphide, it is the main gangue mineral in massive magnetite.

Form of the Gossan Hill orebodies

The Gossan Hill deposit consists of a lower Cu-rich massive sulphide zone associated with massive magnetite and a upper Zn-rich zone (Fig. 2). The two sulphide zones contain and are connected by abundant stringer mineralisation. The formation of massive sulphide and massive magnetite is interpreted to represent at least two hydrothermal events. Each of these zones is briefly discussed below.

Upper Zn-rich massive sulphide zone

The upper Zn-rich massive sulphide zone is hosted by a bedded sandstone-siltstone and pebble breccia sequence (GGF M6), and consists of massive sphalerite, massive pyrite and stringer mineralisation. Massive sphalerite is laterally continuous (630 m strike) and forms a broadly stratabound sheet-like zone. From south to north, the thickness of massive sulphide increases, as does the underlying stringer mineralisation. Massive sulphides attain their greatest thickness at C zone in the north (Figs 2, 3a), which lies against the southern margin of a discordant dacite body (DAC3). At this locality (C zone), a core of massive pyrite underlies massive sphalerite, and both massive pyrite and stringer mineralisation are discordant. Thus, although the morphology of massive sphalerite is sheet-like, the occurrence of massive pyrite at C zone is mound-like and discordant, representing the transition from semi-conformable to discordant mineralisation with proximity to a feeder zone. On the northern side of the dacite (DAC3) is D zone, which represents a discontinuous narrow zone of stringer mineralisation and minor massive sulphide (Fig. 2). The change in thickness of massive sulphides across the dacite (DAC3) is interpreted as synvolcanic structural control to mineralisation, with the synvolcanic fault now occupied by dacite.

Sulphide vein mineralisation underlies, overlies and occurs within the massive sulphide zone. Therefore, massive sulphides have veined gradational upper contacts against the bedded epiclastics (GGF M6), which contain hydrothermal M1 Marker beds. Stringer vein mineralisation is best developed below massive sulphide where it forms an anastomosing stockwork. The form, occurrence and distribution patterns of sulphide veins indicate strong fracture

Table 2: Mineralogical constituents of massive sphalerite, massive pyrite and massive magnetite, listing the major, minor and accessory, gangue and supergene mineral associations for each. Supergene minerals occur within a 100 metre zone of weathering that overlies the primary mineralisation zones.

	Major	Minor	Accessory	Gangue	Supergene
massive sphalerite	sphalerite, pyrite, pyrrhotite	galena, magnetite arsenopyrite, tetrahedrite-tennantite, chalcopyrite, bismuthanite	electrum, native silver, cassiterite	quartz, chlorite, carbonate, muscovite, talc, rutile, ilmenite, epidote	marcasite, pyrrhotite, pyrite, goethite, chalcocite, Fe-oxides, electrum
massive pyrite	pyrite, chalcopyrite, pyrrhotite	magnetite, marcasite	sphalerite	chlorite, quartz, carbonate, talc, muscovite, ilmenite, rutile	marcasite, chalcocite, malachite, cuprite covellite, Fe-oxides, goethite, pyrrhotite
massive magnetite	magnetite	pyrite, pyrrhotite, chalcopyrite, marcasite	-	carbonate, talc, chlorite, quartz, muscovite, ilmenite, rutile	maghmeite, hematite

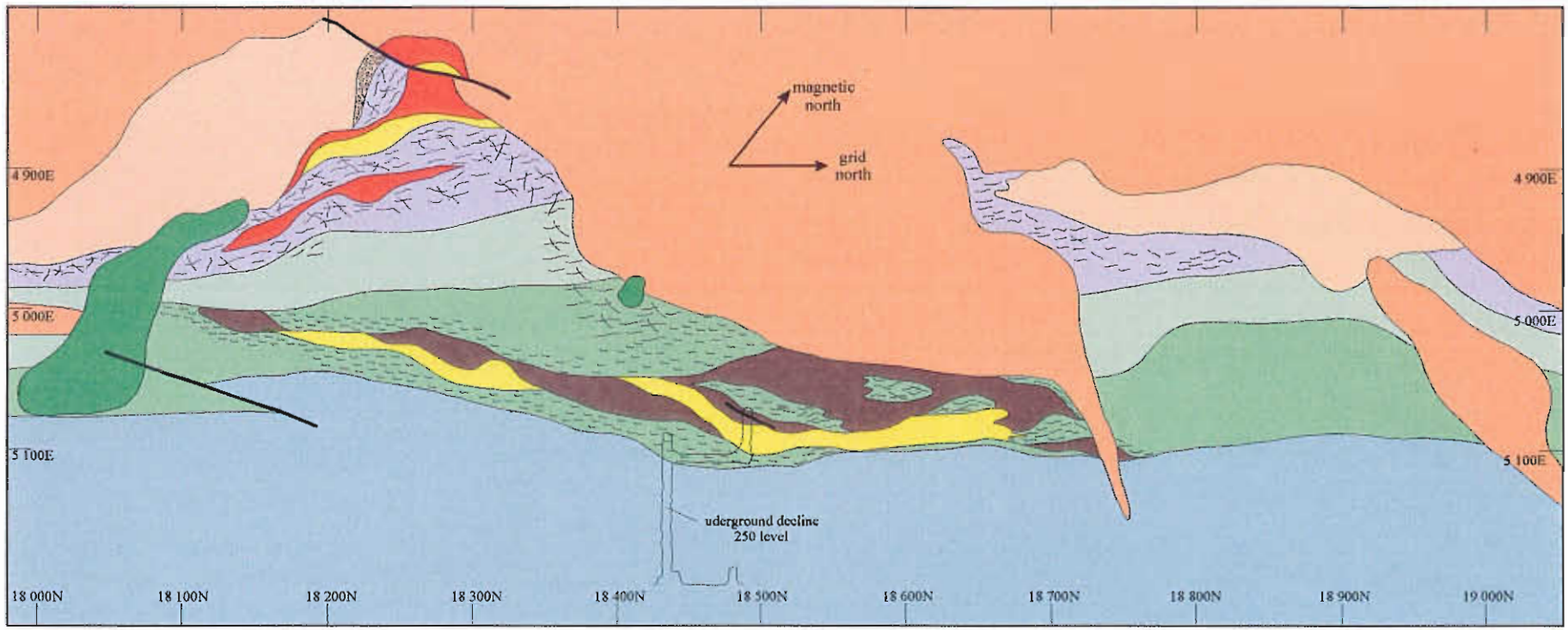

Figure 5.9 : Level plan 10150 R.L (200 metres below surface) of the central and northern area of mineralisation at Gossan Hill. Massive pyrite, massive magnetite and stringer mineralisation occur in GGF M4, with massive sulphide and massive magnetite thinning to the south and lensing out to stringer mineralisation. Massive sulphides in GGF M6, are massive sphalerite, massive pyrite and stringer veins. Massive sulphide is enveloped by stringer mineralisation that forms a semi-conformable zone, whichthins to the south as massive sulphide and GGF M6 thins. Upper and lower mineralisation is connected by a discordant stringer zone through GGF M5 which is poorly defined due to drilling limitations. The stringer zone is however, best developed adjacent to the massive DAC3 dacite which cuts the Golden Grove Formation Members 1 to 6 and the hangingwall rhyodacite (RD2). Outline of the 250 level development through the central parts of mineralisation is indicated. Refer to Figure 3 for legend.

and bedding control on this mineralisation. The abundance of veins and common chert clasts within massive sulphide indicates that the dominant mechanism of sulphide deposition was by veining and replacement. A replacement model is therefore proposed for the upper sulphide zone, invoking sub-seafloor deposition of sulphides. Stringer veins overlying and intercalated with massive sulphide could however, reflect synchronous volcaniclastic sedimentation during the interval of sulphide accumulation near the seafloor. The presence of multiple hydrothermally precipitated M1 Marker chert-lithic intervals supports a scenario with multiple seafloor horizons and due to burial by ongoing sedimentation, sulphide formation was associated with a migrating seafloor.

Massive magnetite

Massive magnetite forms two sheet-like bodies that are semi-conformable to discordant within tuffaceous sandstone (GGF M4). These two massive magnetite lenses are semi-continuous over 650 m , occur at two stratigraphic levels within the tuffaceous host, and do not coincide with the stratigraphic contacts of the enclosing strata (Fig. 3b). From south to north massive magnetite thickens, attaining a maximum thickness of 40 m against the southern margin of a dacite (DAC3). In this locality, the upper and lower magnetite lenses coalesce (Fig. 3b) and this area is interpreted to represent a hydrothermal focal area for hydrothermal fluids responsible for magnetite formation.

Massive magnetite is enveloped by zones of sub-massive, disseminated and vein magnetite, which represent gradational upper and lower contacts. Massive magnetite contains common bedded, quartz-rich sandstone intervals that are intensely altered to chlorite-quartz, but may contain relict volcanic textures or volcanic quartz. These associations indicate massive magnetite formed by replacement of the wall rock.

The separation between the upper and lower massive magnetite zones could represent multiple periods (at least two) of ironstone deposition at or near the seafloor. Interrupted ironstone formation by ongoing sedimentation of tuffaceous strata would result in the migration of the seafloor concurrent to magnetite deposition. Alternatively, magnetite deposition may have formed completely by replacement of GGF M4 strata with control on the distribution of massive magnetite due to permeability contrasts, resulting in lateral fluid migration in more permeable strata. Both mechanisms support the gradational contacts and the interfingering association between massive magnetite and wall rock.

Lower Cu-rich massive sulphide zone

Massive pyrite in the lower sulphide zone is hosted within the same tuffaceous strata that hosts massive magnetite (GGF M4). Pyrite bodies are podiform, discontinuous and interfinger with sulphide stringer and massive magnetite. This zone of sulphide is subvertical in dip and broadly conformable in strike, however massive pyrite may be locally discordant. Two massive pyrite zones occur within the lower 40 m of the tuffaceous host and are not as laterally extensive or continuous as massive magnetite. Massive pyrite has a maximum thickness of 25 m in the north (18,450 N to 18,650 N; Fig. 2) that coincides with the thickest development of massive magnetite. Massive pyrite exists in disconformable contact against and below the thickest development of the lower massive magnetite lens. Massive pyrite is only discordant where massive pyrite and ironstone are thickest. Both the northern and southern limits of massive pyrite are gradational to sulphide stringer mineralisation and elsewhere, the upper and lower contacts of massive pyrite are gradational to sulphide-rich veining which forms a stringer envelope.

Sulphide veins are abundant within ironstones and within the wall rock (GGF M4) and because of their enveloping distribution, appear to have formed synchronously with massive pyrite. Thus massive pyrite post-dates both massive magnetite and the tuffaceous wall rock (GGF M4) due to gradational and veined contacts against each, originating by replacement. Ruxton (1986) described the occurrence of the massive pyrite and sulphide stringer at Gossan Hill as a large Cu-rich stockwork zone. The cross cutting relations indicate massive pyrite and its associated stringer formed predominantly after massive magnetite. The juxtaposition of massive magnetite and massive pyrite and stringer, indicate that mineralising fluids used the same feeder. The relative duration of sulphide formation is never-the-less uncertain, as evidence supports the formation of

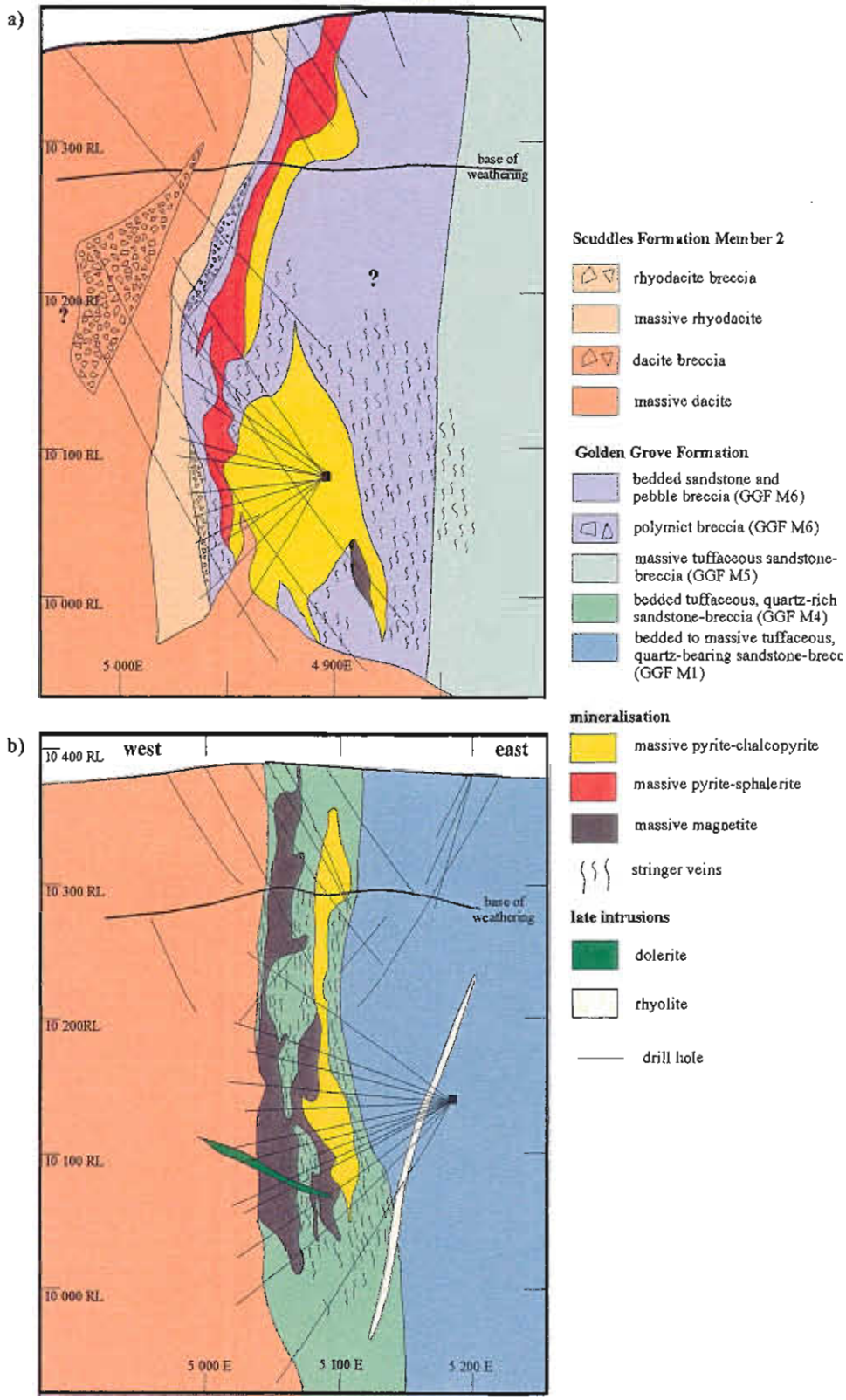

Figure 3a) transform section through C zone (underground drilling from Cuddy 27x, 10 metre window) highlighting the distribution of massive sphalerite, massive pyrite and stringer mineralisation in GGF M6. **b)**east west section 18 560N (25 m window) through the central massive pyrite-massive magnetite zone in GGF M4. The upper and lower massive magnetite zones coalesce with magnetite attaining its thiekest development. Massive pyrite forms a continuous zone below and discordant to massive magnetite.Stringer sulphide mineralisation envelops both massive magnetite and pyrite. Mine grid in metres.

some massive pyrite prior to the onset of magnetite formation.

Relationship between the upper and lower sulphide zones

Tuffaceous sandstone of GGF M5 separates the upper and lower massive sulphide zones and lacks massive sulphide. Nonetheless, this strata hosts sulphide-rich stringer mineralisation adjacent to the discordant DAC3 dacite (Fig. 2 at ~18,350 N). In places where these sulphide-rich veins occur, the wall rock is intensely silicified. Therefore a discordant stockwork connects the upper and lower sulphide zones. The morphology of this stringer zone has a broad asymmetric shape against massive dacite with stringer veins only developed on the southern side of the dacite underlying massive sulphide at C zone.

In summary, the asymmetric form of the massive sulphides and massive magnetite zones suggests a strong control and localisation of hydrothermal fluids by synvolcanic faults. The massive DAC3 dacite of the hangingwall Scuddles Formation, post-dates massive sulphide and massive magnetite formation and occupies the site of a former synvolcanic structure. The thickest development of the upper and lower massive sulphide zones, massive magnetite and discordant stringer, lie adjacent to a discordant massive dacite. Southwards away from the dacite, the thickness of mineralisation decreases, suggesting increased distance from the hydrothermal feeder. North of the dacite intrusion, mineralisation is weakly and sporadically developed in the form of stringer mineralisation. Thus hydrothermal fluid circulation must have been restricted to the southern side of the inferred feeder structure, now occupied by the dacite, possibly representing a structural low.

Volcanic facies architecture

The architecture of the volcanic facies at the Gossan Hill deposit is illustrated in Figure 4. The Golden Grove Formation (GGF) forms the footwall and host rocks to massive sulphide mineralisation, whilst the Scuddles Formation (SCF) forms the hangingwall. The GGF is a regionally extensive (~25 km strike; Clifford, 1992), layered sequence of felsic volcaniclastics that have a sub-vertical dip and north–south strike. The GGF forms part of the Gossan Hill Group volcano-sedimentary succession and massive coherent volcanics are absent from this formation at Gossan Hill. Massive volcanics are however, the main rock type in the hangingwall Scuddles Formation, where they occur as lavas, intrusions and related breccia facies that may be locally interbedded with volcaniclastics.

The volcano-sedimentary environment of deposition for the Gossan Hill Group is a deep subaqueous setting (Clifford, 1992), which is supported by the sedimentary characteristics of this sequence, including stratification and grading. Deposition of the GGF occurred by large volume and laterally extensive mass flow "Clifford, 1992" depositional events. A cold state of emplacement is also indicated by the absence of welded textures and gas pipe structures throughout the sequence. The absence of mudstone facies within the GGF sequence reflects successive sedimentation of strata, which lacked quiescent periods necessary for mudstone facies to accumulate.

Host-rock facies

Golden Grove Formation (GGF)

The GGF consists of six stratigraphic Members (GGF M1 to M6) that are dominantly tuffaceous, but which also include epiclastic facies (GGF M6)(Fig. 4). Massive sulphide and massive magnetite span the stratigraphic interval between Members GGF M4 to GGF M6, with massive magnetite and Cu-rich massive sulphides hosted by GGF M4 and Zn-rich massive sulphides within GGF M6 (Fig. 4).

GGF M1 forms the footwall to Cu-rich mineralisation and is a tuffaceous sequence of bedded to massive, pumiceous and shard-rich, pebble breccia and sandstone. The well preserved morphologies of lithic and fine-grained shard-rich fractions within breccia and sandstone of GGF M1, indicate little evidence of internal reworking. GGF M1 is interpreted to have been sourced from explosive felsic volcanism outside of the current Golden Grove Domain exposure (Clifford, 1992"Clifford, 1992").

GGF M2 and M3 either form a narrow interbedded zone between GGF M1 and M4 or are absent. GGF M2 consists of bedded fine-grained, epiclastics, whilst

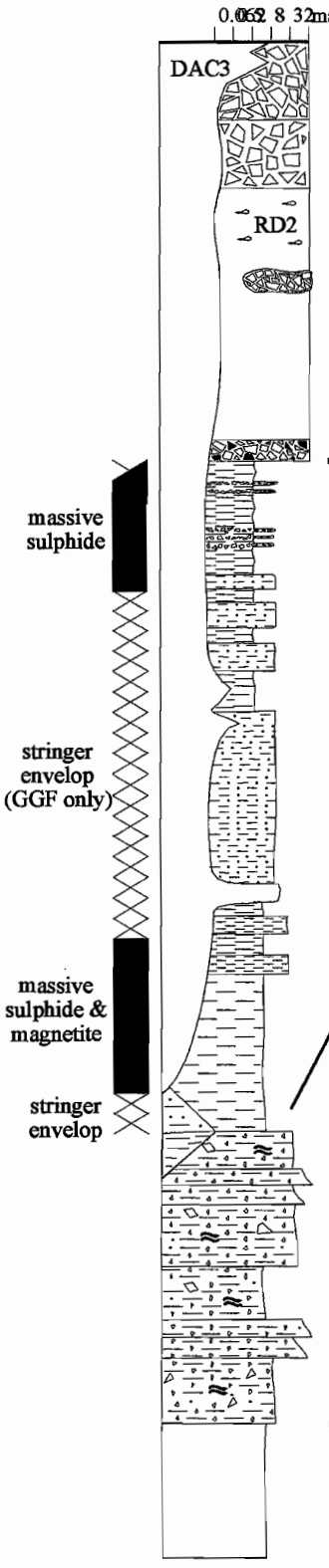

Scuddles Formation

Dacite (DAC3): Massive feldspar-quartz-phyric lava/intrusion and associated breccia facies. Intrudes GG4 to GG6 and rhyodacite and may form sills parallel to the GG5-GG4 contact or be discordant within Member GG5 (thickness 0 to 330 metres).

Rhyodacite (RD2): Massive quartz-feldspar-phyric lava and associated breccia facies. Large 5-8mm quartz phenocrysts, fractured and embayed are distinctive. Upper parts may be amygdaloidal. Lower and upper breccia facies are poorly sorted clast supported. Clasts include rhyodacite, bedded volcaniclastics and rare massive sulphide (thickness 0 to 330 metres).

Golden Grove Formation Member 6 (GGF M6)

Thinly to thickly bedded siltstone, sandstone and polymict pebble breccia. Sandstone and pebble breccia units may be tuffaceous. Normal grading, scoured basal contact, syndepositional faulting and mantling common. Lower part interbedded with Member GGF M5. GGF M6 includes exhalative chert horizons (M1 Marker) associated with massive sulphide (thickness 0 to 180 metres).

Golden Grove Formation Member 5 (GGF M5)

Massive, clast supported, lithic-rich pebble to granule breccia to sandstone with minor volcanic quartz (<1-2%). Lithics include <4 mm, pumiceous and formerly glassy detritus including tube and vesicular pumice, bubble wall fragments and shards (thickness 0 to 120 metres).

Golden Grove Formation Member 4 (GGF M4)

Quartz-rich, clast supported granule to pebble breccia to bedded sandstone-siltstone. Volcanic quartz forms 5 to 15%, up to 1-2 mm angular fragments. Formerly pumiceous-glassy lithics include relict tube pumice, vesicular glassy clasts and shards and pumiceous shreds (thickness 50 to 140 metres).

Golden Grove Formation Members 2 and 3 (GGF M2 and GGF M3)

Bedded silstone-sandstone and pebble breccia, some of which are tuffaceous (thickness 0 to 190 metres).

Golden Grove Formation Member 1 (GGF M1)

Massive, clast supported, poorly sorted pumiceous granule to pebble breccia interbedded with sandstone. A monomict lithic population of tube pumice with fragments up to 100 mm, but generally <10-20 mm. Blocky and angular volcanic quartz forms between 2-10%. Thinly bedded zones have normal and reverse grading and scoured basal contacts. Fine grained fractions of pebble breccia include pumice shreds and shards (thickness 100 to 170 metes).

Gossan Valley Formation

Massive quartz-rich sandstone to clast supported, polymict conglomerate-breccia. Quartz is 2-3 mm and forms 5-8% (thickness 50 to 660 metes).

Figure 4: Facies variation diagram of the stratigraphy of the Golden Grove Formation proximal to the Gossan Hill VHMS deposit. The Members GGF M4 and GGF M6 host Zn-rich and Cu-rich massive sulphide mineralisation respectively. The Golden Grove Formation is a thick sequence of felsic volcaniclastics that are overlain and intruded by coherent felsic volcanics of the Scuddles Formation. Stratigraphic subdivision and nomenclature from Clifford (1992).

GGF M3 consists of tuffaceous bedded sandstone and pebble breccia. Members GG2 and GG3 represent a quiescent period of ambient sedimentation (Clifford, 1992"Clifford, 1992") and their distribution reflects the local paleo-seafloor topography during deposition.

GGF M4 consists of bedded tuffaceous sandstone and siltstone in the basal parts and of bedded sandstone to granule lithic-rich breccias in the upper parts. Bedded strata with common normal grading within GGF M4 reflects deposition by suspension settling and density sorting or by high density turbidity currents. The abundance of quartz in some beds is suggestive of crystal enrichment by epiclastic processes.

GGF M5 is a massive sandstone to granule breccia with minor volcanic quartz (<1%) and infrequent visible lithics. A closed framework is indicated by the closely packed, clast supported, moderately sorted array of formerly glassy, shard and pumiceous lithics, with no evidence for diagenetic compaction, flattening or welding in the strata. Massive dacite (DAC3) also intrudes GGF M5 and forms discordant sills.

Epiclastic sandstone and siltstone dominate GGF M6 (Fig. 4). The M1 Marker at Gossan Hill occurs in the upper thinly bedded parts of GGF M6. Chert beds are thinly bedded within fine-grained green chlorite-rich siltstone and quartz-chlorite altered sandstone-siltstone sequences. Planar, laminated chert bands are translucent and between 1mm to 6 cm wide, laterally discontinuous to lensoidal. Lithic sandstone-siltstone beds are also thinly bedded, and may include poorly sorted, clast supported pebble breccias that contain abundant chert fragments. Chert-bearing pebble breccias may also contain chlorite-rich and chert clasts that are angular, with jigsaw fit textures. Although volumetrically insignificant, these mixed chert-lithic horizons precipitated from direct hydrothermal contribution. Their importance is therefore as a stratigraphic correlation tool in identifying stratigraphic time equivalent to massive sulphide formation.

Scuddles Formation (SCF)

The Scuddles Formation Member SC2 overlies the GGF at Gossan Hill and consists of two massive felsic volcanics that form the hangingwall to mineralisation (Fig. 4); rhyodacite (RD2) which is overlain and intruded by dacite (DAC3). Massive rhyodacite has an erosional basal contact, but is broadly conformable to the GGF. The continuity of rhyodacite is however, interrupted (18,200 N and 18,500 N) where it is intruded by dacite (Fig. 2). Rhyodacite has its thickest development against the southern margin of the dacite, overlying massive sulphide in GGF M6. The upper contact of massive rhyodacite is sharp to either a rhyodacite breccia facies or to massive dacite. Rhyodacite breccia is monomict, clast supported and characterised by quartz, feldspar-phyric rhyodacite clasts in a quartz, feldspar matrix. Massive rhyodacite is interpreted as an extrusive lava having an upper breccia facies.

Massive dacite (DAC3) overlies massive rhyodacite and the rhyodacite breccia facies (Fig. 4). Massive dacite also intrudes RD2 rhyodacite and GGF M1 to M6 inclusive, having a high angle to bedding in the GGF and discordant, sharp chilled margins. In the central mineralised area of Gossan Hill (18,300 N to 18,750 N), the DAC3 dacite intrusion forms a "V" shaped wedge that disrupts continuity of the GGF and RD2 strata from north to south across it (Fig. 2). Massive dacite (DAC3) at Gossan Hill is a dome-like body that overlies its discordant feeder zone. Thickness changes in the GGF (M2, M3, M4, M5 and M6) as well as in the rhyodacite occur across this dacite and thus it is interpreted to have intruded a synvolcanic structural site.

Chemostratigraphy

At Gossan Hill, the immobility of the elements Nb, Zr and Y is demonstrated by constant Y/Nb and Nb/Zr ratios (Sharpe, 1997; Whitford and Ashley, 1992). Based on these elements, the hangingwall rhyodacite (RD2) and dacite (DAC3) are geochemically distinct with DAC3 being transitional from dacite to andesite. The tuffaceous members of the GGF have a primary rhyodacitic composition with similar Nb/Y ratios. The compoistional clustering of tuffaceous members in the GGF indicates a relatively homogeneous source. A wide variation in immobile elements for epiclastics in GGF M4 and M6, reflect the compositional variation from andesite to rhyolite due to polymict sources.

Although Al and Ti are considered immobile (Whitford et al., 1989), in zones of extreme hydrothermal alteration proximal to sulphide mineralisation these elements may have limited mobility (Larson, 1984 ; Wynne and Strong, 1984). At Gossan Hill, local mobility of Al and Ti is due to hydrothermal alteration (Sharpe, 1997) and is supported petrographically by the presence of accessory chloritoid, andalusite, ilmenite and rutile. Thus at Gossan Hill, an initially constant TiO_2/Al_2O_3 ratio has been modified by the local mobility of Al and Ti under extreme hydrothermal alteration near the sites of massive sulphide mineralisation. This is illustrated in Figure 5, in terms of Ti/Zr ratio variation with stratigraphy. Elevated Ti/Zr ratios (up to 70) in GGF M6 occur near zones of massive sulphide, likely associated with local remobilisation of TiO_2. Elsewhere in the GGF variations in the Ti/Zr ratio are small, although coherent rhyodacite and dacite units of the Scuddles Formation have relatively constant Ti/Zr ratio of approximately10 and 20 respectively (Fig. 5).

Alteration mineral assemblages and paragenesis

Four dominant alteration mineral assemblages are identified at Gossan Hill and are (1) siliceous, (2) chlorite, (3) carbonate and (4) muscovite alteration. These alteration types form the main alteration zones at the Gossan Hill deposit and reflect the abundance of quartz, chlorite, carbonate and muscovite. Minor alteration minerals include talc, apatite and chloritoid, and exist as disseminations in chlorite alteration zones. Strong litho-stratigraphic control is observed between the distribution of alteration minerals, massive sulphide and lithofacies. These associations are listed in Table 3. The occurrence of alteration minerals within the GGF and SCF strata reflects stratabound alteration zonation within and locally adjacent to mineralisation.

Table 3: Alteration mineralogy of the stratigraphic Members within the GGF and SCF near mineralisation at Gossan Hill. The major alteration minerals in the GGF are quartz and chlorite. Proportion variations of quartz and chlorite with other minor alteration minerals are only observed adjacent to or within massive sulphide and massive magnetite, reflecting broadly stratabound alteration.

Stratigraphic Member	major minerals	minor minerals	associated mineralisation
SC2 (dacite)	muscovite, carbonate, quartz	chlorite	disseminated pyrite
SC2 (rhyodacite)	muscovite, quartz, carbonate	chlorite	disseminated pyrite
M1 Marker-chert	quartz, carbonate	chlorite	pyrite, magnetite
M1 Marker-lithic	chlorite, carbonate	ilmenite	pyrite, magnetite
GGF M6	quartz	chlorite, carbonate, ilmenite	massive sphalerite
GGF M5	quartz	chlorite, ilmenite, muscovite	none
	quartz, carbonate	chlorite, ilmenite	stringer veins
	quartz	chlorite, ilmenite	stringer veins
GGF M4	quartz, chlorite	carbonate, muscovite	disseminated pyrite stringer veins
	carbonate	talc, chlorite, quartz	ironstone
	chlorite, carbonate, magnetite, talc	muscovite, rutile, ilmenite, apatite	ironstone and massive sulphides
	chlorite	chloritoid, andalusite, rutile, ilmenite	ironstone and massive sulphides
GGF M1	quartz, chlorite	rutile, muscovite	none

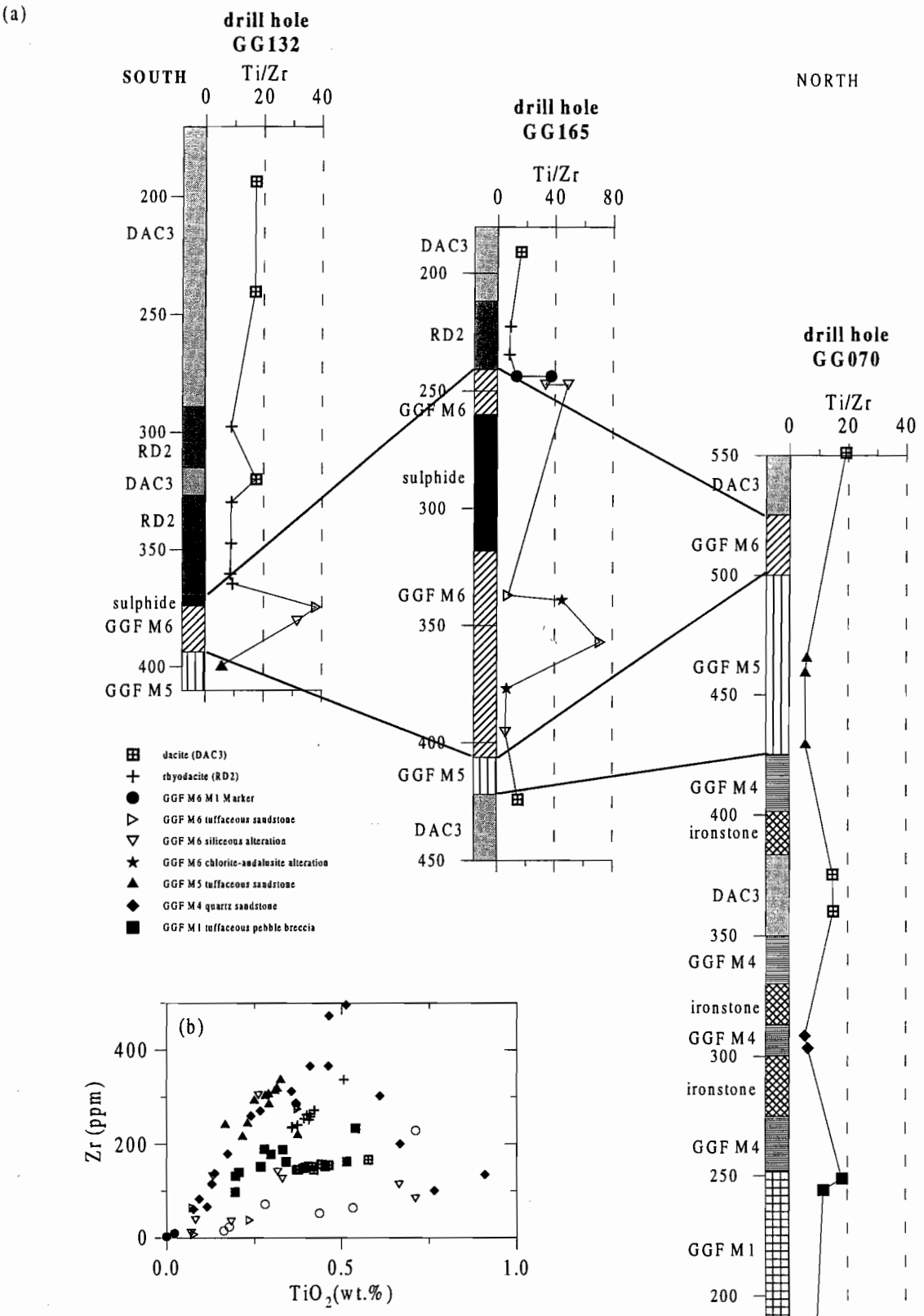

Figure 5: (a) Variation in the Ti/Zr ratio with stratigraphy. The three drill holes used are GG132 at the southern end of massive sulphide mineralisation, GG165 through C zone and GG070 at the north end of Gossan Hill through massive ironstone and Cu-rich mineralisation. Because of the steeply dipping strata, the three holes provide a complete stratigraphic transect. The highest Ti/Zr ratios are associated with GGF M6 below or adjacent to massive sulphide, where alteration is intense. Geology is given for each drill hole and distance down hole is in metres. Note differing horizontal scales of Ti/Zr axes. (b) TiO2 vs Zr has a broad linear distribution of data points. Variation in GGF M6 and GGF M4 is attributed to local mobility in Ti as evdienced by the presence of ilmenite and rutile in this strata.

Siliceous alteration

Silicification is the most widespread alteration at Gossan Hill and is the dominant alteration type within the GGF. Clifford (1992) reports this alteration to be a regional phenomenon throughout the GGF. Despite intense silicification, excellent textural preservation of tuffaceous constituents is observed, except near massive sulphide mineralisation in GGF M6 where silicification has obliterated most textures and converted the wall rock to chert. Thus two types of silicification are interpreted: (1) a regionally pervasive, texturally non-destructive silicification and (2) a localised texturally destructive hydrothermal silicification adjacent to massive sulphide. These two types of quartz alteration are texturally indistinct and consist of interlocking mosaics of megaquartz and microcrystalline quartz.

Regional siliceous alteration

Regional silicification in the GGF resulted in the transformation of an originally glassy felsic sequence to predominantly quartz and minor chlorite (after clay and zeolite?). Textural preservation of the tuffaceous strata (GGF M1, M4 and M5) indicates the uncompacted, non-welded state of pumiceous breccia and sandstone sequences. Alteration textures resulting from this silicification differ between lithofacies and are described in Sharpe (1997). Pebble breccia facies generally contain a domainal quartz-chlorite alteration, whilst sandstone have a more homogeneous silicification. Textural preservation supports regional silicification during or soon after deposition of the GGF, but prior to diagenetic compaction and hydrothermal alteration associated with massive sulphide formation. Thus regional silicification is an *en masse* silicification event that may have been synchronous with deposition of the GGF. By inference, the relative timing of this regional silicification was likely synchronous to ironstone formation and occurred pre- to syn-massive sulphide deposition, depending on the duration of this silicification event.

As stated above, the homogeneity of silicification varies between lithofacies. Therefore, the effects of silicification are also texturally different between Members and lithofacies in the GGF. A nodular siliceous alteration texture developed in GGF M4 and M5 is described in Sharpe (1997). Due to preserved uncompacted pumiceous and shard textures within these nodules, this alteration texture is interpreted to have formed during the early regional silicification event. These nodules are interpreted to have formed by accretion of silica around pumiceous and glassy debris, with quartz replacing glass and in fill of porosity within the nodular zones. The rounded shape of the nodules is interpreted as a natural habit for nucleating of silica in a porous environment (Knauth, 1994). The occurrence of siliceous nodules within massive sulphide and zones of intense chlorite alteration indicate the overprint of silicified wall rock by later chlorite alteration and sulphide mineralisation. In these occurrences, siliceous nodular zones were sealed to successive events of pervading alteration and mineralisation.

Feldspar does not occur in the GGF and sparse relict feldspathic textures reflect its general absence. Thus, the GGF is interpreted to have been largely glassy at the onset of silicification. The abundance of uncompacted tube pumice within the GGF indicates that the succession had an initially high porosity and permeability, ideal for alteration by migrating fluids. The effect of the early silicification reduced this permeability by the induration which resulted from quartz (and clay/zeolite?) deposition, effectively sealing the strata from later alteration by hydrothermal fluids. This is exemplified by intense silicification within GGF M1 and M5 and their relatively simple quartz and chlorite alteration mineralogy, where induration prevented more complex paragenetic mineral assemblages that typically characterise hydrothermal alteration and greenschist metamorphism. Additionally, GGF M1 forms the footwall to massive sulphides, whilst GGF M5 occurs between the upper and lower sulphide zones, and yet these strata do not host massive sulphides. Thus these units must have been sealed and impermeable to hydrothermal-mineralising fluids. Impermeable strata likely contributed to the focussing of the hydrothermal fluids to synvolcanic feeder sites and fracture induced permeability structures.

The interpreted early regional silicification of the GGF is consistent with an Archean environment. Widespread, large volume replacement cherts resultant from regional silicification are characteristic

of volcaniclastic sequences within Archean greenstone terranes (Lowe & Knauth 1977; DiMarco & Lowe, 1989). Knauth (1994) reports large-scale silica precipitation occurred in the Archean and was commonly associated with the precipitation of iron oxides and siderite. Explanations for the widespread silicification in the Archean environment include warmer climatic temperatures and silica saturated oceans (Knauth, 1994; Garrels, 1987). Archean silicification has previously been interpreted as the result of circulating seawater through originally permeable rocks in shallow hydrothermal systems during low temperature rock-water interactions (DeWitt et al., 1982; Gibson et al., 1983; Spooner & Fyfe, 1973; Barley, 1984). Irrespective of their formation, the nature of these original Archean silica precipitates is unknown, with Archean sediments silicified to a degree unknown in younger rocks (Knauth 1994).

Local siliceous alteration

Intense silicification adjacent to and hosting massive sulphide occurs in GGF M6 and M4, but has a minor occurrence in GGF M5 cross cutting stockwork mineralisation. This silicification is characterised by bleached, grey wall rock, with the only sedimentary features preserved being a banding relict of bedding. The resultant products of this alteration are replacement cherts that envelop and host massive sulphide and stringer stockwork. Variation in the alteration of thinly bedded sandstone in the GGF M6 sequence is observed on a bed scale, due to differential chlorite and quartz alteration. Massive chert in GGF M5 likely reflects the massive nature of granule breccias in GGF M5. The contact between regional background silicification to grey massive chert is gradational and transitional with proximity to mineralisation. Local silicification in GGF M4 has textures similar to the thinly bedded sequence of GGF M6, with intense local silicification only developed in the thinly bedded parts strata near the base of GGF M4. This silicification zone has conformable upper and lower contacts within GGF M4 and hosts stockwork mineralisation that underlies massive sulphide in GGF M4.

Local intense silicification envelopes and hosts massive sulphide and stockwork mineralisation at Gossan Hill. This association highlights the genetic link between sulphide, stringer mineralisation and the origin of silicified cherty wall rock. Localised silicification is attributed to formation by proximal hydrothermal alteration of the wall rock synchronous to sulphide stringer vein propagation and massive sulphide deposition. The localisation of this quartz alteration near mineralisation likely reflects the general impermeability of the strata due to previous silicification events. Localised intense silicification is a common alteration product in footwall and host rocks proximal to sulphide mineralisation (e.g., Gemmell & Large, 1992; Lentz & Goodfellow, 1996; Gibson et al., 1983; Skirrow & Franklin, 1994). In general, this silicification is associated with high temperature fluids depositing volcanogenic mineralisation, forming in the hottest parts of the VHMS system, reflecting high silica enrichment in the feeder zone.

Chlorite alteration

Chlorite is a major alteration mineral at Gossan Hill that occurs as disseminations and forms an alteration zone that envelopes ironstone, massive sulphide and stringer veins of GGF M4 (Sharpe, 1997). In this alteration, the wall rock consists of interlocking meshworks of chlorite (<10 mm grains) that contains relict volcanic quartz or subordinate disseminations of carbonate, sulphide and magnetite, apatite and chloritoid. Elsewhere away from mineralisation, chlorite forms disseminations through silicified pumiceous breccia and sandstone, where it is generally abundant in finer-grained ash to sand-sized fractions of the matrix. In GGF M1, preferential alteration of some lithics to chlorite results in a domainal chlorite alteration (Sharpe, 1997). Within GGF M6, the distribution of chlorite is erratic and may form disseminations in the silicified wall rock or occur as preferential chlorite alteration of beds within sandstone. Within the hangingwall, massive dacite and rhyodacite contain minor disseminated chlorite that generally occurs in altered feldspar phenocrysts.

Carbonate alteration

At Gossan Hill, carbonate is a major mineral that generally has a disseminated occurrence in massive sulphide and ironstone. Within the wall rock, the occurrences of carbonate are; (1) a disseminated

alteration of intensely chlorite altered zones in GGF M4 that envelopes massive pyrite, ironstone and stringer veins, (2) a minor to major constituent of stringer veins, (3) a nodular alteration in GGF M5, (4) an alteration in sandstone overlying massive sulphides in GGF M6 and (5) a pervasive disseminated alteration phase of dacite and rhyodacite in the Scuddles Formation.

Disseminated carbonate is common where chlorite alteration envelopes massive sulphide, ironstone and stringer mineralisation in GGF M4. Nodular carbonate textures described in Sharpe (1996) only occur in GGF M5, below the southern-most limit of massive sulphide in GGF M6. Notably, carbonate alteration is minor in GGF M6 and occurs in bedded sediments overlying massive sulphide generally associated with the M1 Marker as an alteration of tuffaceous beds. Pervasive disseminated carbonate alteration in dacite (DAC3) and rhyodacite (RD2) forms a strong alteration in the hangingwall volcanics and occurs throughout the groundmass and as an alteration of feldspar phenocrysts.

Muscovite alteration

Muscovite is a minor to accessory mineral within the GGF, forming disseminated grains through quartz and/or chlorite alteration zones. Where present, it is fine-grained (<20 mm) and acicular, with alignment that delineates regional penetrative cleavage. Within chlorite alteration of GGF M4, scattered disseminated muscovite may also delineate cleavage. Within massive sulphide, fibrous muscovite may have decussate forms, with grains less than 200 mm and which cross cut cleavage. In the SCF hangingwall, muscovite is a major alteration mineral forming in excess of 20% modal. In this occurrence, muscovite is fine-grained (<50 mm) and aligned to cleavage or coarser-grained (<100 mm) in altered relict feldspar phenocrysts.

Paragenesis

At Gossan Hill, the alteration mineralogy is simple and is classified into both regional and localised alteration zones associated with massive sulphide formation. The relative timing of alteration events is given in Table 4. The earliest alteration mineralogy identified is quartz with lesser chlorite (after clay and zeolite?). This alteration is associated with the regional pervasive mass silicification of the GGF. The duration of this hydrothermal alteration is not clear and may have been ongoing with depositional events up to the onset of hydrothermal alteration associated with massive sulphide deposition at Gossan Hill. This mass silicification effected the entire GGF in the Golden Grove Domain and resulted in the mass replacement of glassy tuffaceous strata by quartz and clay/zeolite. The latter was converted to chlorite either during successive hydrothermal alteration or during greenschist metamorphism. All other alteration minerals and alteration zones overprint this early silicification.

Mass silicification of the GGF is interpreted to have been a ground preparation event that indurated and reduced the permeability and porosity of the succession. Thus, subsequent hydrothermal fluid migration was focussed along a synvolcanic feeder at the site of the DAC3 intrusion and through proximal fracture induced permeability structures. Localised silicification of the wall rock occurred adjacent to these fracture sites and zones of massive sulphide mineralisation as a result of modification of the wall rock by hot silica saturated mineralising fluids. This localised silicification is semiconformable around massive sulphide lenses and discordant in stringer stockwork zones.

Based on the textural associations between quartz and chlorite in the GGF, the disseminated chlorite alteration within tuffaceous strata away from sulphide and ironstone, formed synchronously with the early regional silicification of these units. Clay and zeolite are common alteration products of glass (Iijima, 1974; Quantin et al., 1988) and chlorite is invoked to have a clay or zeolite precursor, which was transformed to chlorite either during hydrothermal alteration or during greenschist metamorphism.

Intense chlorite alteration enveloping massive sulphide, ironstone and stringer veins in GGF M4 overprint previous silicification of the GGF strata. Textural support for this timing relationship is indicated by the occurrence of siliceous nodules within massive chlorite and the occurrence of equivalent silicified strata away from massive sulphide and ironstone. Thus, chlorite alteration formed synchronously with massive sulphide and stringer veins in GGF M4. Chloritisation in Member

GG4 therefore overprints silicification and represents hydrothermal alteration associated with the deeper, Cu-enriched parts of mineralisation at Gossan Hill.

Carbonate alteration has a spatial and genetic association to both ironstone and massive sulphide where it occurs as a major mineral. Carbonate has a disseminated occurrence within the chlorite alteration zone enveloping the lower sulphide-ironstone mineralisation in GGF M4. This localised occurrence of carbonate indicates formation during both ironstone and massive sulphide deposition as a localised disseminated alteration of the wall rock. Comparatively, in GGF M5 carbonate has a nodular form and occurs below massive sulphide at the southern end of Gossan Hill. This occurrence is interpreted to represent a more distal alteration. Carbonate within GGF M6 generally overlies massive sulphide and forms bed-specific alteration of breccia and sandstone. The association of carbonate alteration to the hydrothermally derived M1 Marker, suggest a near sea floor alteration associated with lower temperatures. Carbonate alteration in the hanging-wall dacite and rhyodacite is ubiquitous, pervasive and represents alteration during burial and waning of the Gossan Hill hydrothermal system. Recrystall-isation and localised redistribution of carbonate occurred during greenschist metamorphism and deformation.

Decussate to aligned muscovite grains are late metamorphic minerals in the GGF and massive sulphide zones. The minor occurrence of these minerals in the GGF indicates that muscovite formation was minor and probably related to the general absence of K_2O in these strata. In the hangingwall volcanics however, muscovite is a major mineral and the intensity of muscovite alteration is

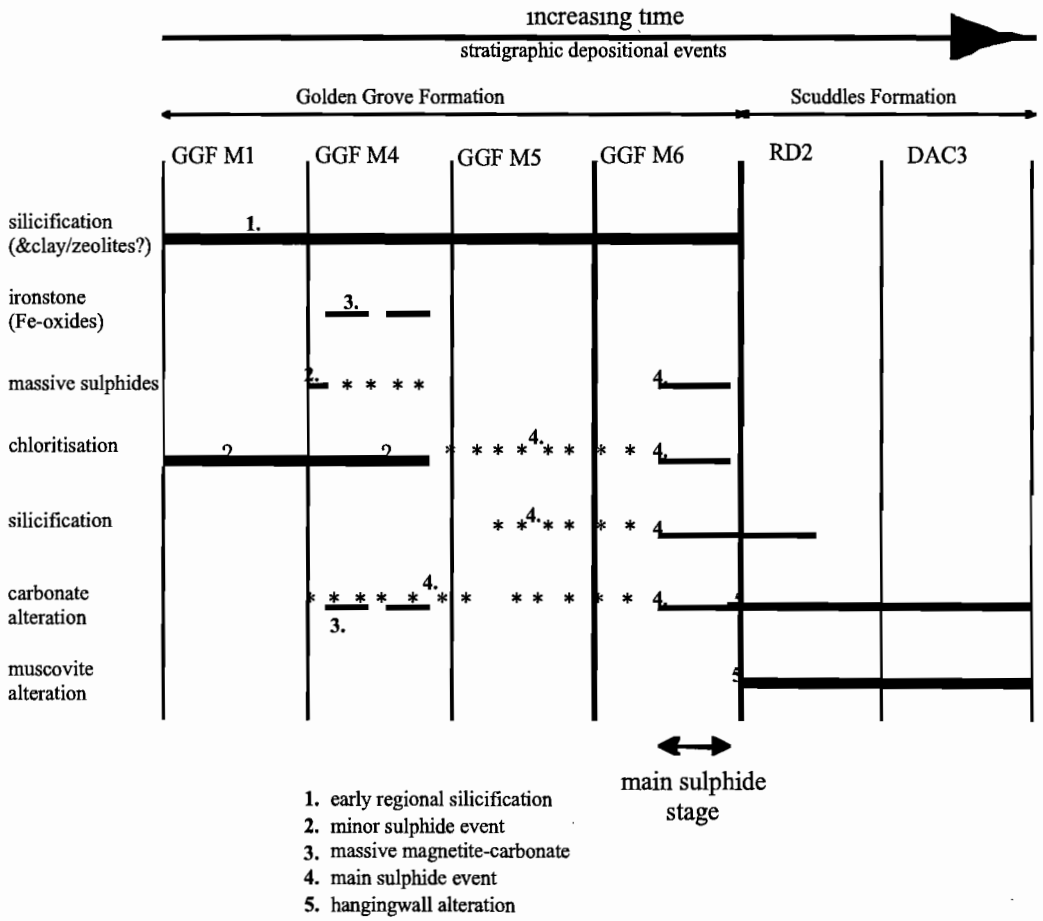

Table 4: Relative timing of the alteration events at Gossan Hill with respect to the deposition of stratigraphic members that host massive sulphide and massive magnetite. Solid lines indicate contemporaneous alteration with deposition of that Member and * indicates later alteration of stratigraphy by hydrothermal alteration associated with ore formation in GGF M6.Contemporaneous hydrothermal alteration associated with massive sulphide formation occurred during deposition of GGF M6 and overprints an early silicification event.

ubiquitous in rhyodacite, but within the dacite decreases in intensity away from mineralisation. Thus muscovite is interpreted to form a hangingwall alteration zone in the massive volcanics overlying mineralisation, possibly associated with effusion/intrusion of these volcanics over an active hydrothermal site. This alteration is attributed to burial of massive sulphides and the waning of the hydrothermal system, resulting in a carbonate-muscovite alteration of the hangingwall.

Alteration mineral zonation

Many authors suggest that a fragmental host rock to VHMS mineralisation results in a more expansive and diffuse hydrothermal alteration, resulting commonly in semi-conformable alteration zones (e.g., Morton & Franklin, 1987; Franklin et al., 1981). These expansive hydrothermal alteration patterns also relate to the variations in lithofacies and lithological control on the alteration distribution. At Gossan Hill, the host rock has abundant pumice within the breccia and sandstone sequences. Unaltered pumice has high intra-grain permeability that imparts a high permeability to pumice-rich lithofacies. However at Gossan Hill, the GGF experienced an early regional silicification that sealed this fragmental succession and resulted in the formation of a tightly constrained hydrothermal alteration peripheral to volcanogenic mineralisation. Early silicification of the tuffaceous GGF led to the formation of a simple alteration mineralogy, which was not significantly modified by successive hydrothermal alteration or metamorphism. The contrasts between alteration textures result from this silicification and reflect proportional variation between quartz and subordinate chlorite (after clay/zeolite?) between the lithofacies. Localised silicification occurs adjacent to massive sulphide mineralisation and stockwork mineralisation, has a semiconformable to discordant occurrence in GGF M6 and M5 respectively (Figs 6, 7a), and envelops stringer stockwork adjacent to the synvolcanic feeder site.

Intense chlorite alteration is an alteration envelope to massive sulphide and stringer vein mineralisation in GGF M4. The juxtaposition of massive magnetite and massive sulphide/stringer mineralisation means that chlorite also envelopes magnetite. The chlorite alteration zone is semiconformable and stratabound within GGF M4 and hosts stringer mineralisation (Fig. 7b). Thus although chlorite alteration is laterally continuous over the strike of mineralisation in GGF M4, its has the same lateral distribution as stringer mineralisation. It is likely that chlorite alteration was locally controlled by the distribution of sulphide veins through the silicified protolith, forming around sulphide vein conduits. This restricted occurrence of the chlorite alteration zone reflects the impermeability of the wall rock away from the central conduit or feeder of massive sulphide mineralisation.

Carbonate alteration is a disseminated alteration within chlorite in GGF M4, enveloping massive sulphide and magnetite. Nodular carbonate alteration in GGF M5 is a localised alteration to the southern end of the mineralised zone at Gossan Hill, whilst carbonate alteration in GGF M6 overlies massive sulphide and is discontinuous. Both rhyodacite and dacite have pervasive and strong carbonate alteration at Gossan Hill. However, this carbonate alteration is most intense in the dacite feeder that cuts the mineralised zone and decreases in intensity into the hangingwall (Figs 6, 7a). Muscovite alteration is ubiquitous in the hangingwall rhyodacite and dacite. This muscovite alteration zone extends at least 200–300 m in to the hangingwall but its limit is not well constrained (limit of sampling).

Alteration mineral chemistry

Chlorite

The composition of chlorite from alteration zones at Gossan Hill is described in Sharpe (1997). A summary of the range in chlorite compositions is given in Table 5. Chlorite at Gossan Hill is generally Fe-rich however, footwall chlorite (GGF M1) has a higher Mg/(Mg+Fe) ratio (0.47) compared to chlorites of GGF M6, which have a Mg/(Mg+Fe) ratio of 0.28. This change in chlorite composition represents Fe-enrichment from the footwall, through the host sequence towards zones of massive sulphide in GGF M6, with the most Fe-rich end member occurring in and overlying Zn-rich massive sulphides.

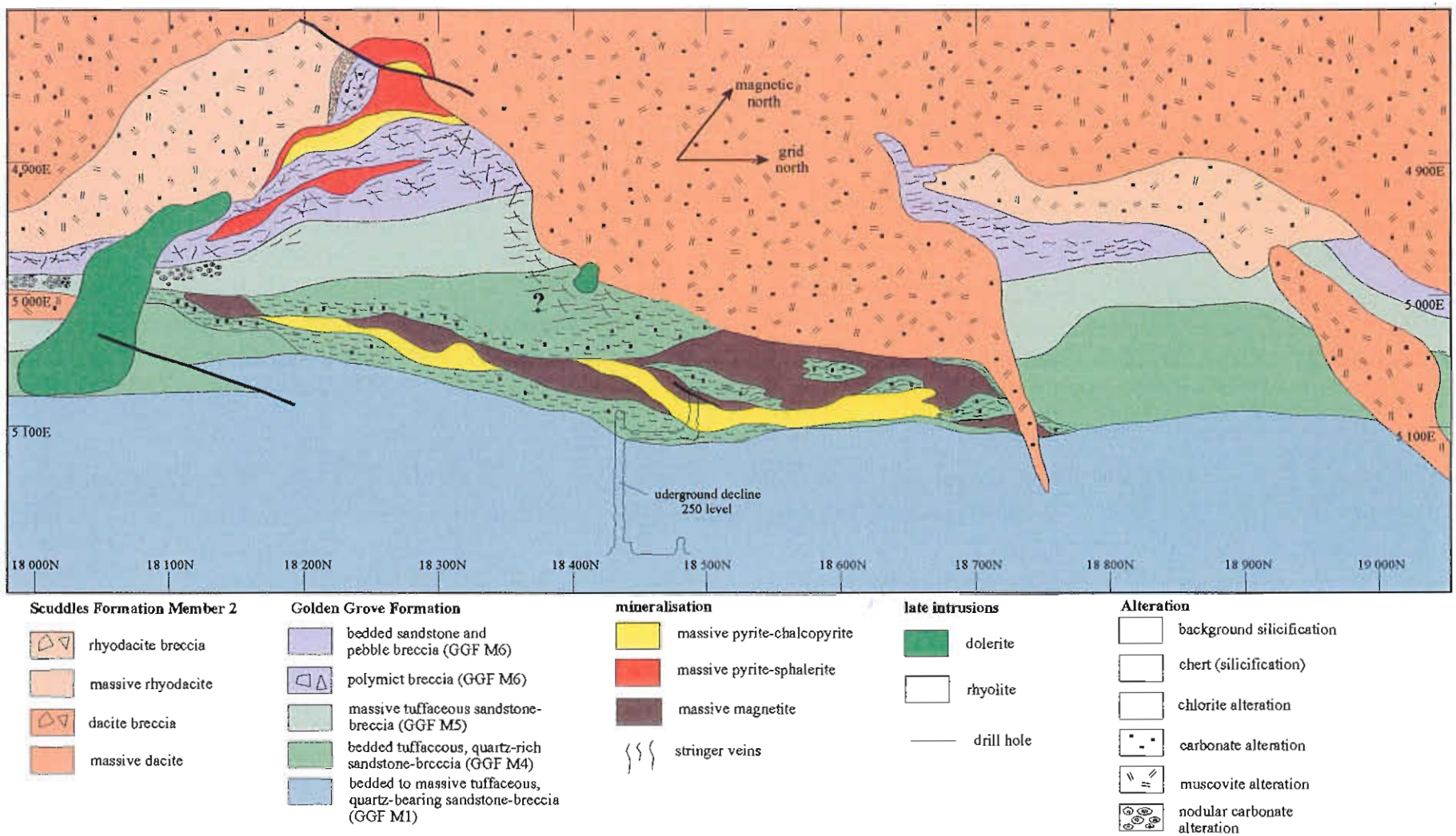

Figure 6 : Level plan 10150 R.L (200 metres below surface) of the central and northern area of mineralisation at Gossan Hill showing the distribution of alteration zones. Outline of the 250 level development through the central parts of mineralisation is indicated.

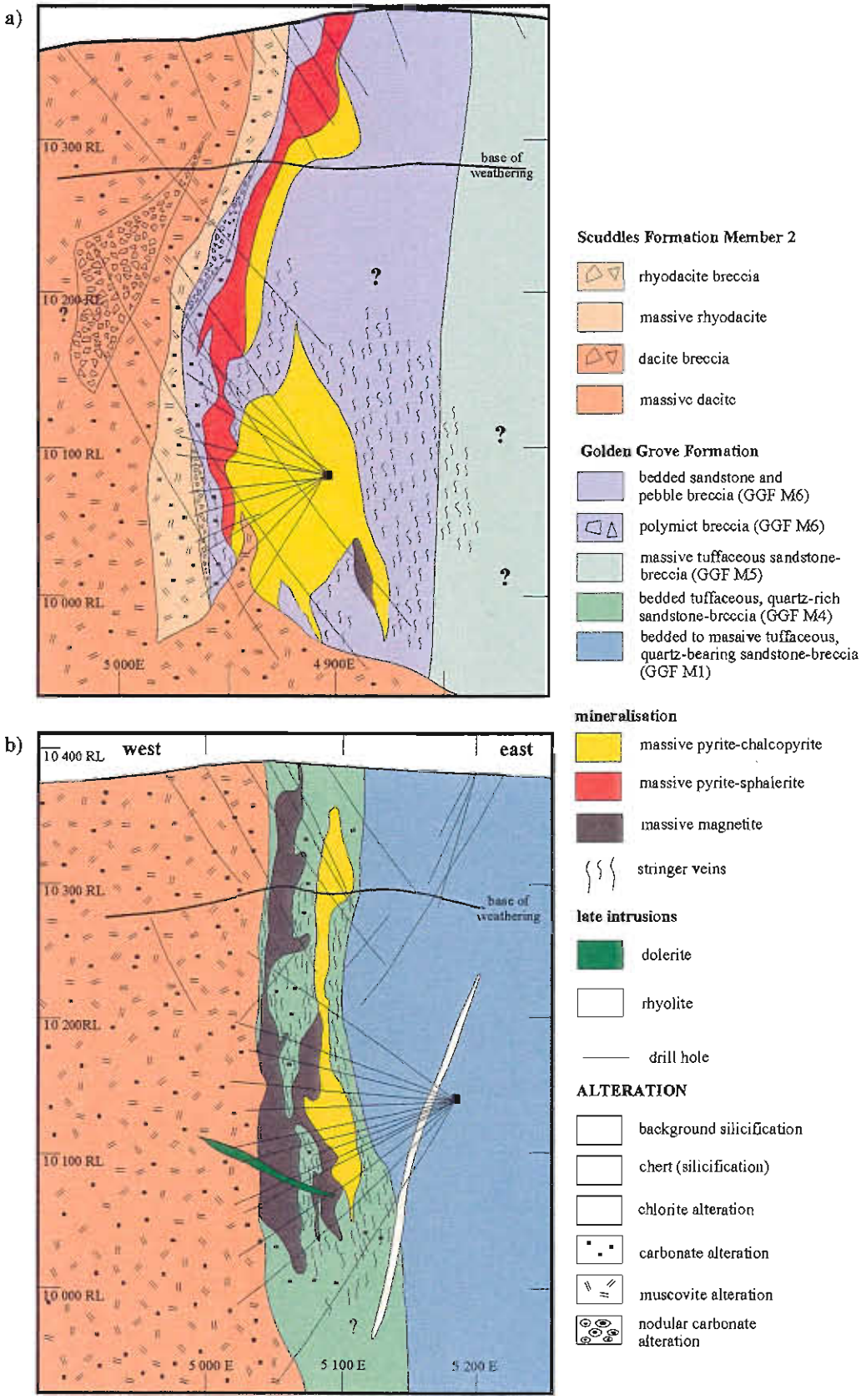

Figure 7a) transform section through C zone (underground drilling from Cuddy 27x) highlighting the distribution of alteration relative to massive sulphide in GGF M6 and M5 and hangingwall alteration in RD2 and DAC3.**b)**east west section 18,560 N with the alteration zonation in GGF M1 and around massive pyrite and magnetite in GGF M4. Massive dacite is ubiquitously altered in this location. Mine grid in metres.

Table 5: Average chlorite compositions from alteration and mineralisation at Gossan Hill

Stratigraphic Member	No. of analyses	SiO_2 wt.%	Al_2O_3 wt.%	MgO wt.%	CaO wt.%	MnO wt.%	FeO* wt.%	H_2O wt.%	Mg#
GGF M6									
sphalerite-chlorite	12	22.40	23.56	7.75	0.01	0.24	35.04	10.96	0.28
sulphide veins	22	23.07	23.58	12.38	0.02	0.25	28.67	11.17	0.43
chlorite-andalusite-chloritoid	12	22.27	22.28	6.06	0.02	0.24	37.62	10.68	0.22
GGF M5									
carbonate nodular alteration	3	28.47	21.87	22.26	0.04	0.05	16.22	12.16	0.71
GGF M4									
intense chlorite alteration	22	24.81	19.71	14.30	0.01	0.07	28.47	11.03	0.47
quartz sandstone	19	24.54	20.24	14.13	0.02	0.06	28.37	11.03	0.47
siliceous nodular alteration	3	25.35	18.73	13.68	0.01	0.02	30.22	11.06	0.45
chlorite-apatite alteration	16	23.34	20.91	9.18	0.02	0.15	33.98	10.78	0.32
GGF M1									
pumiceous breccia	9	24.01	23.17	13.09	0.02	0.09	27.83	11.27	0.46
OVERALL	118	24.72	22.57	12.07	0.02	0.16	32.11	11.48	0.41

** FeO* = total iron, Mg# = $Mg/(Mg+Fe_{(total)})$

Table 6: Average carbonate compositions from alteration and mineralisation at Gossan Hill

Strigraphic Member	No of analyses	$MgCO_3$ wt.%	$CaCO_3$ wt.%	$MnCO_3$ wt.%	$FeCO_3$ wt.%
GGF M6					
M1 marker chert bands	18	19.84	50.44	3.75	25.24
sandstone and breccia	29	19.12	54.23	3.11	23.45
GGF M5					
carbonate nodular alteration	37	33.02	52.92	1.61	13.07
GGF M4					
disseminated carbonate in chlorit	49	26.19	23.04	2.79	49.90
GGF M4 massive magnetite					
massive magnetite	27	29.21	41.04	0.58	30.58
GGF M4, M5 and M6: stringer veins					
sulphide-magnetite-carbonate vei	11	21.34	31.74	16.06	31.61
chlorite-magnetite-carbonate vein	8	21.96	23.05	1.47	55.58
carbonate-sulphide vein	20	24.58	51.27	0.86	23.62
pyrite-chlorite-carbonate vein	6	20.59	48.98	3.16	28.81
GGF M4 and M6: massive sulphide					
massive sphlaerite-pyrite GGF M	12	12.68	28.95	16.47	44.31
massive pyrite GGF M4	8	27.23	0.73	6.71	67.34

Carbonate

Carbonate at Gossan Hill range in composition from ankerite to siderite as illustrated in Figure 8 and summarised in Table 6. Massive sulphide (GGF M4 and M6), ironstone and stringer veins contain both siderite and ankerite compositions. Comparatively, nodular carbonate alteration (GGF M5) and carbonate in the M1 Marker and GGF M6 sandstone, are also ankerite but have less Fe enrichment, tending toward the more Ca-Mg-enriched, dolomitic end member. Mn-rich carbonate, up to 16.5 wt.% $MnCO_3$ (Table 6), is identified within massive sulphide and sulphide veins indicating some Mn enrichment associated with massive Zn-rich sulphides. However, no systematic compositional trends are identified within carbonate alteration, with most samples analysed containing both siderite and ankerite.

Alteration indices

Many alteration geochemistry studies of VHMS deposits implement alteration indices to characterise the intensity and style of alteration. Examples of these alteration indices include the Ishikawa Index (AI) (Ishikawa et al., 1976), the chlorite index (CCPI) (Large et al., 1996) and the Mn-carbonate index (Large et al., 1996). Alteration indices use oxide element ratios to highlight relative depletion and enrichment of elements within hydrothermal alteration. The indices listed specifically use Na_2O and K_2O, as alteration zones in many VHMS systems contain significant proportions of feldspar and sericite. Alteration indices thus implement the relative enrichment or depletion of Na_2O and K_2O to characterise plagioclase destruction and sericite alteration, which results in depletion of Na_2O and enrichment of K_2O respectively.

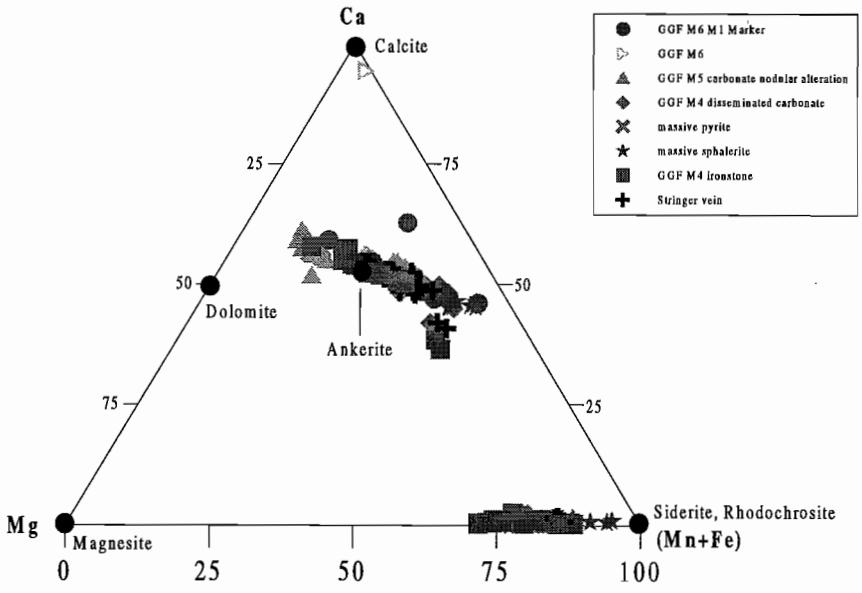

Figure 8: Microprobe analysis of carbonate from selected carbonate alteration zones at Gossan Hill. Carbonate compositions are ankerite and siderite, with both carbonate phases occurring in all samples analysed at Gossan Hill. The majority of carbonate from Gossan Hill are however ankerite.

At Gossan Hill, feldspar is absent in both the GGF host and footwall sequence, whilst muscovite alteration in the GGF is sporadic and minor (refer Table 3). Both feldspar and muscovite are however major minerals in the Scuddles Formation. Thus alteration of the GGF has resulted in complete depletion of Na_2O and K_2O, rendering use of the Ishikawa, Chlorite and Mn-carbonate indices inappropriate to characterise alteration at Gossan Hill. These alteration indices (Figs 9a, b) do however, highlight alteration in the hangingwall Scuddles Formation.

An index has been devised to define alteration trends at Gossan Hill, which does not use Na_2O and K_2O in the discriminant, but instead uses elements that occur within the main alteration minerals, chlorite and carbonate. The index is defined as:

chlorite-carbonate index (CCI) =

$$\frac{100*(0.5*FeO+MgO)}{(0.5*FeO+MgO+2*CaO+2*MnO)}$$

SiO_2 vs CCI plotted in Figure 9c differentiates between the hangingwall alteration and chlorite-carbonate alteration in the GGF at Gossan Hill. Carbonate alteration is represented by intermediate CCI ratios (20–80), whilst chlorite alteration is represented by high CCI ratios (>80). The compositions of chlorite and carbonate from Gossan Hill are also shown (Fig. 9c). In the hangingwall, alteration is less intense in dacite than in rhyodacite due to the spread of data from rhyodacite (Fig. 9c). However, although this CCI index uses the entire sample suite at Gossan Hill, this ratio has difficulty in discriminating wall rock alteration in the GGF, due to intense SiO_2 and FeO* enrichment that dominated the geochemistry of the GGF succession.

Lithogeochemical halos

Alteration trends in the GGF at Gossan Hill are typically characterised by intense enrichment in FeO*, MgO and SiO_2 due to silica flooding and chlorite alteration. Down hole variation and inter-element correlation of major and trace elements are previously outlined in Sharpe (1997) and summarised in Table 7. Critical geochemical halo patterns are:

Na distribution: complete depletion in the GGF (generally below detection) reflect background alteration in the GGF. Hangingwall units have a gradual depletion <200 m.

K distribution: complete depletion in the GGF reflects background alteration. Weak enrichment in rhyodacite as ore position is approached.

Fe, Mg distribution: strong to intense enrichment in the GGF (reflects intensity of chlorite alteration), with FeO* > 20% in chlorite alteration in GGF M4 adjacent to massive sulphide and hosting stringer mineralisation. Positive inter-element correlation between SiO_2, FeO*, MgO reflect proportional abundance of chlorite and quartz.

Thallium distribution: complete depletion (below detection) throughout the host and footwall (GGF), whilst thallium is present in the hangingwall rhyodacite (<2 ppm) and dacite (<0.5 ppm).

Zn and Pb distribution: sporadic enrichment in GGF M6 commonly associated with elevated levels of Cd, As, Zn, Fe, Ag, Bi, Sb and Sn in silicified wall rock. No systematic variation away from mineralisation.

Vectors to ore

Alteration of the host and footwall rocks to mineralisation at Gossan Hill is intense and has resulted in strong geochemical modification of this fragmental tuffaceous succession. Thus geochemistry reflects the proportional variation of a simple alteration mineralogy and has not been instructive in defining geochemical vectors to mineralisation in the Golden Grove Formation. The reasons for this are two fold:

1. Early regional silicification resulted in extensive metasomatism and effectively sealed the GGF to later modification by hydrothermal or metamorphic events. The alteration mineralogy resulting from this silicification (quartz and chlorite) are similar to the main alteration minerals associated with hydrothermal alteration;
2. As a result of impermeable wall rocks, hydrothermal alteration associated with mineralisation at Gossan Hill is tightly constrained to the immediate ore-depositional environment over-

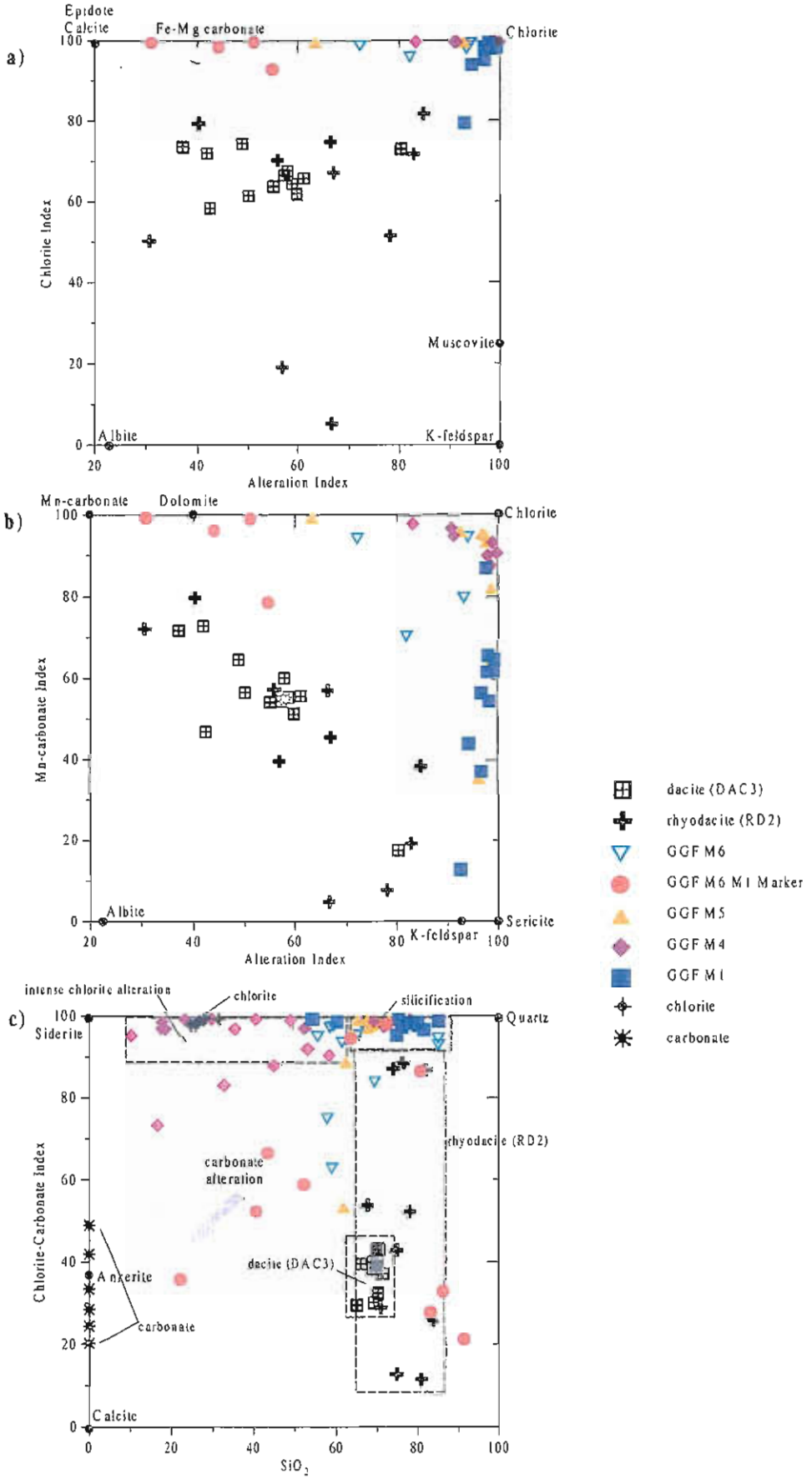

Figure 9: Chlorite index (a) and Mn-carbonate index (b) vs. alteration index of samples from Gossan Hill. Note samples with values of Na_2O and K_2O below detection are not plotted. Thus the alteration index, chlorite index and Mn-carbonate index do not illustrate geochemical alteration patterns in the Golden Grove Formation. These indices do however, highlight the alteration variation in the hangingwall lavas. (c) chlorite-carbonate index (CCI) = 100*(0.5*FeO*+MgO)/(0.5*FeO*+MgO+2*CaO+2*MnO) vs. SiO_2, which uses all geochemical data points to define alteration trends at Gossan Hill. Silicification and chloritisation in the GGF have high CCI indices (>90) and SiO_2 contents that are >60 and <60 respectively. Carbonate alteration in the GGF and the hangingwall volcanics have a range in CCI values between 10 to 90, however hangingwall volcanics have higher SiO_2 contents than carbonate altered GGF. Dacite (DAC3) has a tightly constrained field in both CCI and SiO_2, whilst rhyodacite (RD2) has a wider variation in the CCI indicating the relatively more intense alteration of the rhyodacite comparative to dacite.

Table 7: Summary of alteration characteristics of the stratigraphic sequence at Gossan Hill.

HANGINGWALL ALTERATION (SC2)			
Unaltered lithotype:	dacite	feldspar, quartz	
	rhyodacite	quartz, feldspar	
Alteration mineralogy:	carbonate, sericite, quartz, ± chlorite, ± pyrite, ± sphalerite		
Geochemistry:	Depletion	strong, ubiquitous	Na_2O,
	Depletion	<200m from GGF contact	Sr, Ba, (Rb), Cs, SiO_2
	Enrichment	<100 m from GGF contact	FeO, MgO, MnO, As, Sb, CaO, K_2O, Ag
HOST SEQUENCE (Member GG6)			
Unaltered lithotype:	siltstone-sandstone-breccia		
	pumiceous units consisting of quartz, pumice-glassy debris		
Alteration mineralogy:	quartz, ± chlorite, ± carbonate, ± sphalerite, ± pyrite, ± magnetite, ± ilmenite		
Geochemistry:	Depletion	strong and ubiquitous	Na_2O, K_2O
	Enrichment	sporadic distribution	Cd, As, Pb, Fe, Zn, Ag, Bi, Sb, Sn
	Enrichment	strong to intense	SiO_2, (±FeO, MgO, CaO, MnO)
HOST SEQUENCE (Member GG5)			
Unaltered lithotype:	sandstone consisting of quartz, pumice and shards		
		lithic pebble breccia consisting of quartz, pumice and shards	
Alteration mineralogy:	quartz, chlorite, ± carbonate, ± pyrite, ± ilmenite, ± rutile		
Geochemistry:	Depletion	strong and ubiquitous	Na_2O, K_2O
	Depletion	strong	CaO
	Enrichment	weak anomalism	Pb, Zn, ±Rb, ±Sr, ±Cs, ±Sb
	Enrichment	pervasive strong	SiO_2, FeO, MgO, MnO
	Enrichment	sporadic	CaO
HOST SEQUENCE (Member GG4)			
Unaltered lithotype:	sandstone to pebble breccia consisting of quartz, pumice and shards		
	breccia consisting of mixed provenance sandstone and quartz		
Alteration mineralogy:	quartz, chlorite, ± carbonate, ± pyrite, ± magnetite ± chloritoid, ± apatite, ±andalusite, ± pyrrhotite, ± talc, ± rutile, ± ilmenite		
Geochemistry:	Depletion	strong and ubiquitous	Na_2O, K_2O
	Depletion	strong	CaO
	Enrichment	weak anomalism	TiO_2, MnO ,Al_2O_3, ±Zn, ±Pb, Mo, ±Bi, ±Sb
	Enrichment	pervasive strong to intense	SiO_2, FeO, MgO, ±CaO, Cu
		Enrichment	pervasive intense FeO
FOOTWALL ALTERATION (Member GG1)			
Unaltered lithotype:	pumiceous pebble breccia consisting of quartz, pumice and shards		
Alteration mineralogy:	quartz, chlorite, ± pyrite, ± rutile		
Geochemistry:	Depletion	strong and ubiquitous	Na_2O, K_2O, CaO
	Enrichment	weak anomalism	TiO_2, MnO , Mo, Cs
	Enrichment	pervasive strong to intense	SiO_2, FeO, MgO

lying its structural feeder, and thus hydrothermal alteration coincides with mineralisation.

Hangingwall alteration is characterised by Na_2O depletion and local FeO, MgO, CaO and K_2O enrichment within 200 m of the upper ore horizon (GGF M6). Distal geochemical vectors have not been identified due to the localisation of the primary mineralisation to its synvolcanic feeder site and constrained rock-hydrothermal fluid interaction by a silicified sealed wall rock.

Geological vectors to mineralisation at Gossan Hill relate to its strong synvolcanic structural control on the localisation of massive sulphides and massive magnetite as well as post-mineralisation intrusion of the hangingwall volcanics. These geological vectors are:

1. Discontinuity of the Golden Grove Formation caused by discordant synvolcanic intrusions of the Scuddles Formation.
2. Thickness variations in the Golden Grove Formation across discordant synvolcanic intrusions, with mineralisation correlated to thickening of the volcaniclastic strata.
3. M1 Marker chert bands in bedded sandstone.
4. Magnetic anomalies.

References

Barley, M. E., 1994. Volcanism and hydrothermal alteration, Warrawoona Group, East Pilbara, *In* Muhling, J. R., Groves, D. I., and Blake, T. S., (Eds.), Archaean and Proterozoic basins of the Pilbara, Western Australia: Evolution and mineralization potential, Geology Department and University Extension, University of Western Australia, p. 23–36.

Clifford, B. A., 1992. Facies and palaeoenvironment analysis of the Archean volcanic-sedimentary succession hosting the Golden Grove Cu-Zn massive sulphide deposits, Western Australia: Unpub. Doctor of Philosophy thesis, Department of Earth Sciences, Monash University.

DeWit, M. J., Hart, R., Martin, A. and Abbott, P., 1982. Archean abiogenic and probably biogenic structures associated with mineralized hydrothermal vent systems and regional metasomatism, with implications for greenstone belt structures: Economic Geology, v. 77, p. 1783–1802.

DiMarco, M. J. and Lowe, D. R., 1989. Petrography and provenance of silicified early Archaean volcaniclastic sandstones, eastern Pilbara Block, Western Australia: Sedimentology, v. 36, p. 821–836.

Franklin, J. M., Kasarda, J. and Poulsen, K. H., 1975. Petrology and chemistry of the alteration zone of the Mattabi massive sulfide deposit: Economic Geology, v. 70, p. 63–73.

Franklin, J. M., Lydon, J. W. and Sangster, D. F., 1981. Volcanic-associated massive sulfide deposits: Economic Geology, v. 75th Anninversay, p. 485–627.

Galley, A. G., Watkinson, D. H., Jonasson, I. R. and Riverin, G., 1995. The subsea-floor formation of volcani-hosted massive sulfide: evidence from the Ansil Deposit, Rouyn-Noranda, Canada: Economic Geology, v. 90, p. 2006–2017.

Garrels, R. M., 1987. A model for the deposition of microbanded Precambrian iron-formations: American Journal of Science, v. 287, p. 91–106.

Gemmell, J. B. and Large, R. R., 1992. Stringer system and alteration zones underlying the Hellyer Volcanic-Hosted massive sulfide deposit, Tasmania, Australia: Economic Geology, v. 87, p. 620–649.

Gibson, H. L., Watkinson, D. H. and Comba, C. D. A., 1983. Silicification: hydrothermal alteration in an Archean geothermal system within the Amulet Rhyolite Formation, Noranda, Quebec: Economic Geology, v. 78, p. 954–971.

Iijima, A., 1974. Clay and zeolitic alteration zones surrounding Kuroko deposits in the Hokuroku district, Northern Akita, as submarine hydrothermal-diagenetic alteration products: Mining geology special issue, v. 6, p. 267–289.

Ishikawa, Y., Sawaguchi, T., Iwaya, S. and Horiachi, M., 1976. Delineation of prospecting targets for Kuroko deposits based on modes of volcanism underlying dacite and alteration halos: Mining Geology, v. 26, p. 105–117 (in Japanese with English abstract).

Knauth, L. P., 1994. Petrogenesis of chert, *In* In P.J. Heaney, (Ed.), Reviews in mineralogy. Silica: Physical behaviour, geochemistry and materials applications; Mineralogical Society of America, v. 29, p. 233–258.

Large, R. R., 1992. Australian volcanic-hosted massive sulfide deposits: Features, styles, and genetic models: Economic Geology, v. 87, p. 471–510.

Large, R. R., Stolz, A. J. and Duhig, N., 1996. Preliminary assessment of MRV geochemical database in terms of possible vectors: AMIIRA Project P439, May 1996, p. 197–209.

Larson, P. B., 1984. Geochemistry of the alteration pipe at the Bruce Cu-Zn volcanogenic massive sulphide deposit, Arizona: Economic Geology, v. 79, p. 1880–1896.

Lentz, D. R. and Goodfellow, W. D., 1996. Intense silicification of footwall sedimentary rocks in the stockwork alteration zone beneath the Brunswick No. 12 massive sulphide deposit, Bathurst, New Brunswick: Canadian Journal of Earth Science, v. 33, p. 284–302.

Lowe, D. R. and Knauth, L. P., 1977. Sedimentology of the Onverwacht Group (3.4 Billion Years), Transvaal, South Africa, and its bearing on the characteristics and evolution of the early earth: Journal of Geology, v. 85, p. 699–723.

Morton, R. L. and Franklin, J. M., 1987. Two fold classification of Archean volcanic associated massive sulfide deposits: Economic Geology, v. 82, p. 1057–1063.

Myers, J. S., 1990. Precambrian tectonic evolution of part of Gondwana, SW Australia: Geology, v. 18, p. 537–540.

Pidgeon, R. T., Furfaro, D. and Clifford, B. A., 1994. Investigation of the age and rate of deposition of part of the Gossan Hill Group, Golden Grove using conventional single grain zircon U-Pb geochronolgy: Geoscience Australia 1994 and beyond, 12th AGC, Perth, 1994, p. 346.

Quantin, P., Gautheyrou, J. and Lorenzoni, P., 1988. Halloysite formation through in situ weathering of volcanic glass from trachytic pumices, Vico's Volcano, Italy: Clay Minerals, v. 23, p. 423–437.

Roberts, R. G., 1975. The geological setting of the Mattagami Lake Mine, Quebec: A volcanogenic massive sulfide deposit: Economic Geology, v. 70, p. 115–129.

Ruxton, P., 1986. Controls of Au and Ag grades in volcanogenic sulphide deposits : Teutonic Bore: AMIRA Final Report, University of Tasmania, v. 84/P2, p. 72–83.

Sharpe, R., 1996. Gossan Hill: alteration styles and distributions: AMIRA P439, v. Report 2, p. 155–170.

Sharpe, R., 1997. Gossan Hill: the relationship between alteration,

mineralogy and geochemistry: AMIRA P439, v. Report 4, p. 97–183.

Skirrow, R. G. and Franklin, J. M., 1994. Silicification and metal leaching in semiconformable alteration beneath the Chisel Lake massive sulfide deposit, Snow Lake, Manitoba: Economic Geology, v. 89, p. 31–50.

Spooner, E. T. C. and Fyfe, W. S., 1973. Sub sea-floor metamorphism, heat and mass transfer: Contributions to Mineralogy and Petrology, v. 42, p. 287–304.

Vaasjoki, M., 1984. Geochronological and genetic implication of lead isotopic data from the Archean massive sulphide deposits at Golden Grove, Teutonic Bore and Salt Creek, Western Australia: Geoscience in the development of natural resources, 7th AGC, Geological Society of Australia, Abstract, v. 12, p. 522.

Whitford, D. J., McPherson, W. P. A. and Wallace, D. B., 1989. Geochemistry of the host rocks of the volcanogenic massive sulfide deposit at Que River, Tasmania: Economic Geology, v. 84, p. 1–21.

Whitford, D. J. and Ashley, P. M., 1992. The Scuddles volcanic-hosted massive sulfide deposit, Western Australia: geochemistry of the host rocks and evaluation of lithogeochemistry for exploration: Economic Geology, v. 87, p. 873–888.

Wynne, P. J. and Strong, D. F., 1984. The Strickland prospect of southwestern Newfoundland: A lithogeochemical study of metamorphosed and deformed volcanogenic massive sulphides: Economic Geology, v. 79, p. 1620–1642.

Zaleski, E. and Peterson, V. L., 1995. Depositional setting and deformation of massive sulfide deposits, iron-formation and associated alteration in the Manitouwadge Greenstone Belt, Superior Province, Canada: Economic Geology, v. 90, p. 2244–2261.

Sample No. 760357
Location Gossan Hill
Alteration zone Intense chlorite alteration zone in enveloping stringer mineralisation
Formation Golden Grove Formation Member 4

Description Quartz-rich sandstone with angular to sub-rounded volcanic quartz in a pervasive intense fine-grained chlorite matrix
Facies Interp Bedded sandstone-siltstone sequence deposited by mass flow processes

Alteration Intensity none weak moderate strong (intense) **PY** 2%
Alteration Style patchy (pervasive) veined cleavage control
Alteration Mineralogy Groundmass chlorite with disseminated ilmenite and pyrite
Feldspars none

Interpretation diagenetic metamorphic syntectonic (hydrothermal)
Relict Mineralogy Volcanic quartz forms up to 15% modal, having angular shapes

Geochemistry

SiO_2	TiO_2	Al_2O_3	Fe_2O_3	MnO	MgO	CaO	Na_2O	K_2O	P_2O_5	S	LOI	Al	CCPI	Ti/Zr
38.2	0.43	16.93	31.85	0.06	5.52	<0.01	<0.05	<0.01	0.01	<0.01	5.36	--	--	7.0

Rb	Ba	Cu	Pb	Zn	Sb	Tl	Zr	Nb	Y	Sr	PIMA: AlOH I	CCI
<1	9.5	11	2	73	1.6	<0.05	365.7	11.8	64	2.3	--	99.4

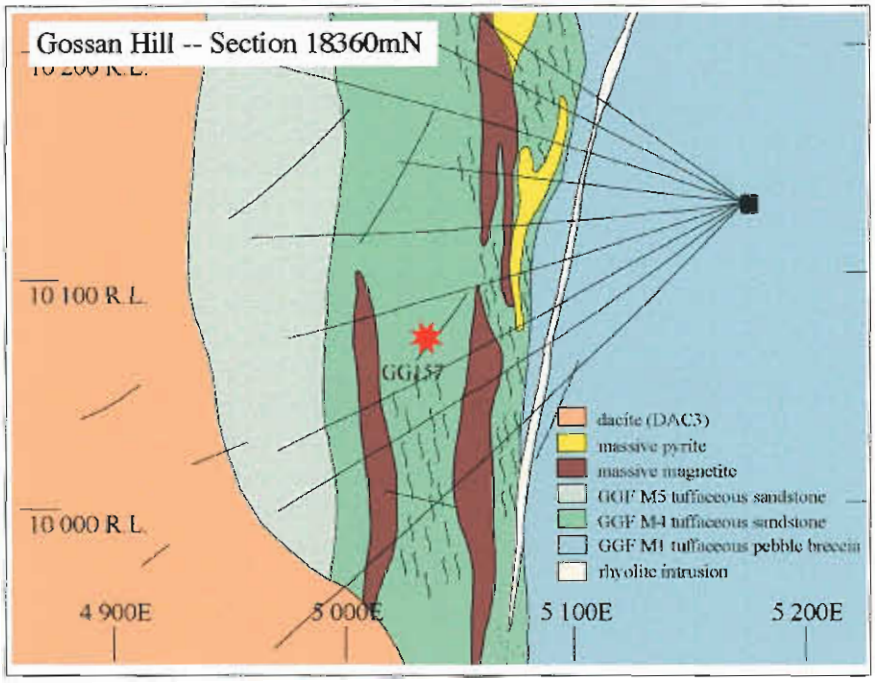

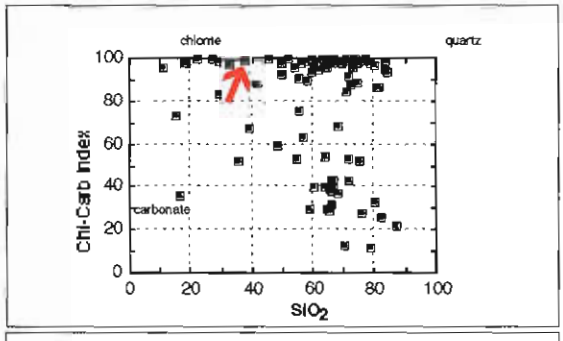

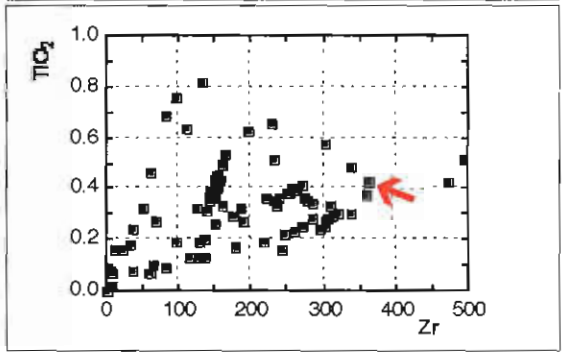

Sample No. 760364
Location Gossan Hill
Alteration zone Host horizon to massive Zn-rich sulphides and stringer mineralisation
Formation Golden Grove Formation Member 6

Description Polymict pebble breccia containing lithics of chert and quartz altered sandstone in a fine-grained lithic-rich matrix.
Facies Interp Clast supported, poorly sorted breccia, with locally scoured basal contacts and conformable upper contacts.

Alteration Intensity	none	weak	moderate	strong	(intense)	**PY** 4%
Alteration Style	patchy	(pervasive)	veined		cleavage control	
Alteration Mineralogy	Groundmass	quartz-chlorite				
	Feldspars	none				
	Clasts	microcrystalline quartz, chlorite, pyrite, sphalerite				
Interpretation	(diagenetic)	metamorphic	syntectonic	(hydrothermal)		
Relict Mineralogy	none, quartz-chlorite alteration ubiquitous through clasts and groundmass					

Geochemistry

SiO_2	TiO_2	Al_2O_3	Fe_2O_3	MnO	MgO	CaO	Na_2O	K_2O	P_2O_5	S	LOI	Al	CCPI	Ti/Zr
64.36	0.31	9.22	16.96	0.11	3.78	0.17	<0.05	<0.01	0.05	2.48	4.71	--	--	13.2

Rb	Ba	Cu	Pb	Zn	Sb	Tl	Zr	Nb	Y	Sr	PIMA: AlOH I	CCI
<1	7	925	213	445	4	<0.05	140.6	4.9	25	4	--	95.6

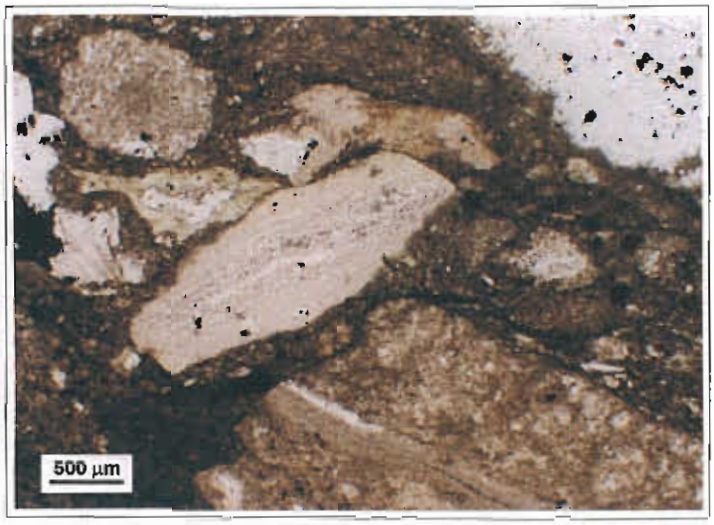

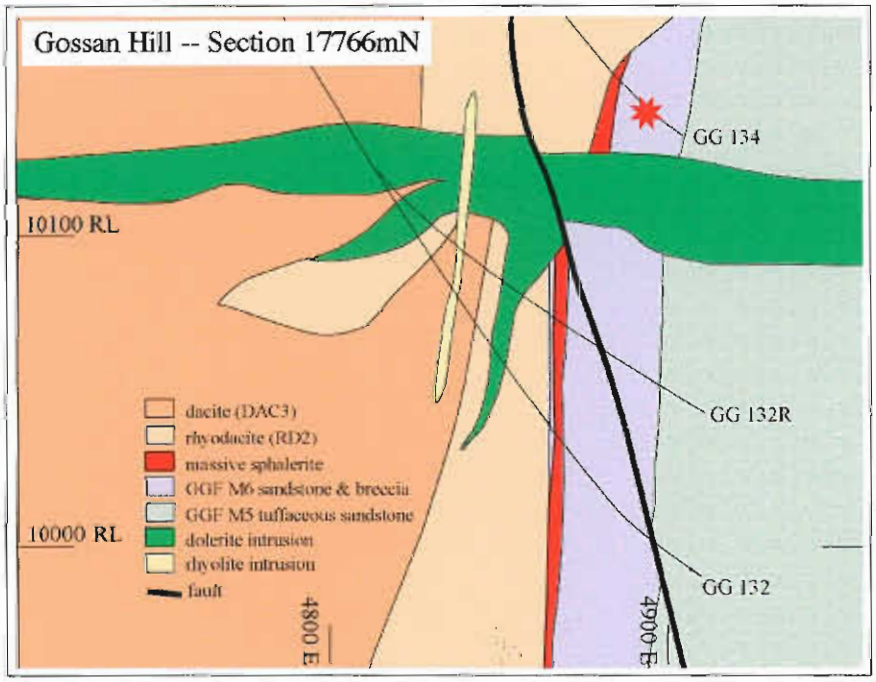

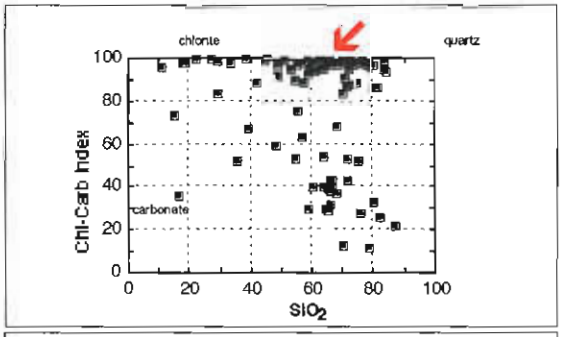

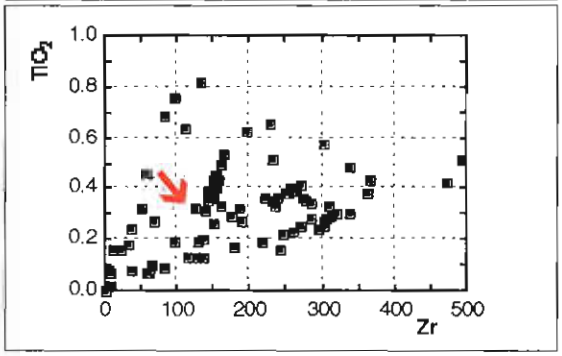

Sample No. 760490
Location Gossan Hill
Alteration zone M1 Marker chert-chlorite-carbonate beds
Formation Golden Grove Formation Member 6 overlying massive sulphide

Description Bedded to brecciated microcrystalline chert-carbonate bands interbedded with chlorite-carbonate bands
Facies Interp Hydrothermal chert horizons interbedded with lithic beds, which also have hydrothermal contribution

Alteration Intensity none weak moderate strong (intense) **PY** 5%
Alteration Style patchy (pervasive) veined cleavage control
Alteration Mineralogy
Chert bands quartz-carbonate-pyrite-magnetite
Lithic bands chlorite-carbonate-pyrite-magnetite

Interpretation diagenetic metamorphic syntectonic (hydrothermal)
Relict Mineralogy chert bands consist of microcrystalline quartz

Geochemistry

SiO_2	TiO_2	Al_2O_3	Fe_2O_3	MnO	MgO	CaO	Na_2O	K_2O	P_2O_5	S	LOI	Al	CCPI	Ti/Zr
76.09	0.02	0.35	5.86	0.32	1.88	5.86	<0.03	<0.01	0.01	0.26	8.84	--	--	13.2
Rb	Ba	Cu	Pb	Zn	Sb	Tl	Zr	Nb	Y	Sr		PIMA: AlOH I		CCI
<1	2.8	176	4	39	1.1	<0.05	9.1	<1	6	7.1		--		28.0

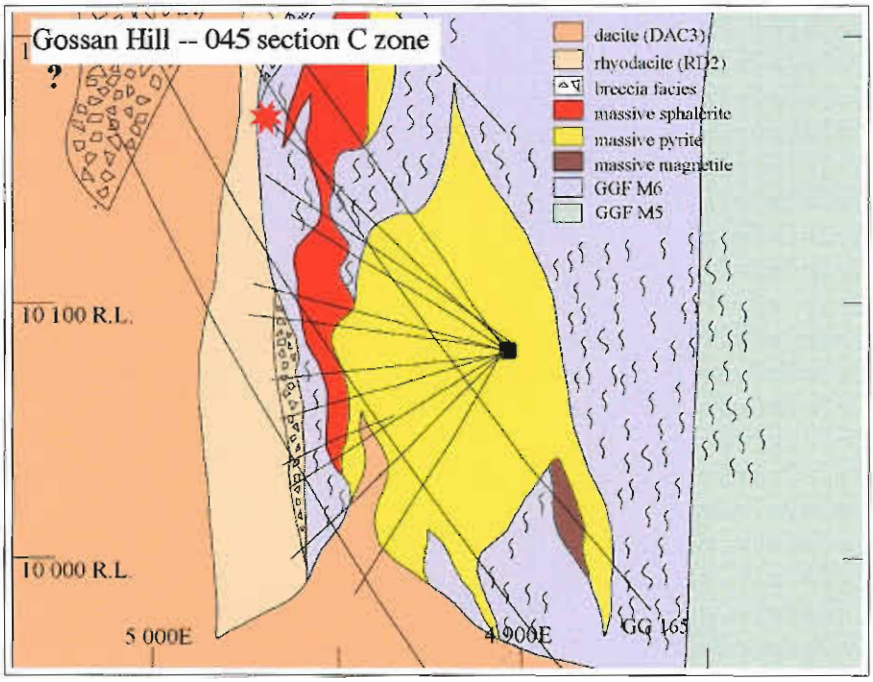

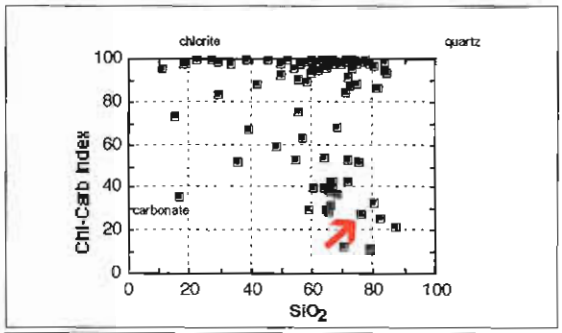

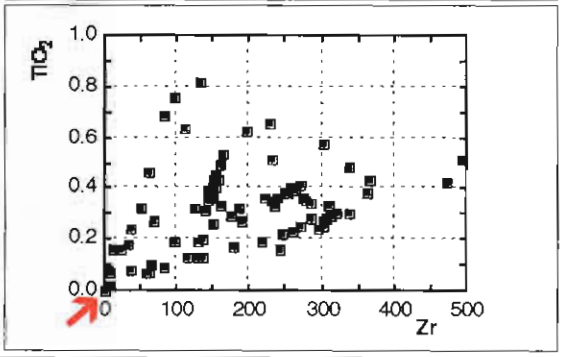

Sample No. 760207
Location Gossan Hill
Alteration zone Hangingwall carbonate-muscovite alteration zone
Formation Suddles Formation Member 2 (DAC3)

Description Massive feldspar, quartz phyric dacite with altered feldspar and <2% quartz phenocrysts

Facies Interp Coherent, discordant dacite dome with an upper breccia facies. Intrudes the GGF and RD2 along a synvolcanic fault

Alteration Intensity none weak moderate strong (intense) **PY** 1%
Alteration Style patchy (pervasive) veined cleavage control
Alteration Mineralogy Groundmass muscovite-carbonate-quartz
Feldspars carbonate-muscovite-chlorite

Interpretation diagenetic (metamorphic) syntectonic (hydrothermal)
Relict Mineralogy quartz phenocrysts, feldspar are completely altered to alteration minerals

Geochemistry

SiO_2	TiO_2	Al_2O_3	Fe_2O_3	MnO	MgO	CaO	Na_2O	K_2O	P_2O_5	S	LOI	Al	CCPI	Ti/Zr
68.0	0.43	13.93	3.87	0.07	1.92	3.19	0.59	2.71	0.1	0.18	4.74	55.1	63.7	17.0

Rb	Ba	Cu	Pb	Zn	Sb	Tl	Zr	Nb	Y	Sr	PIMA: AlOH I	CCI
74	578.2	13	7	45	1.1	<0.05	151.8	5.7	13	77.9	--	37.2

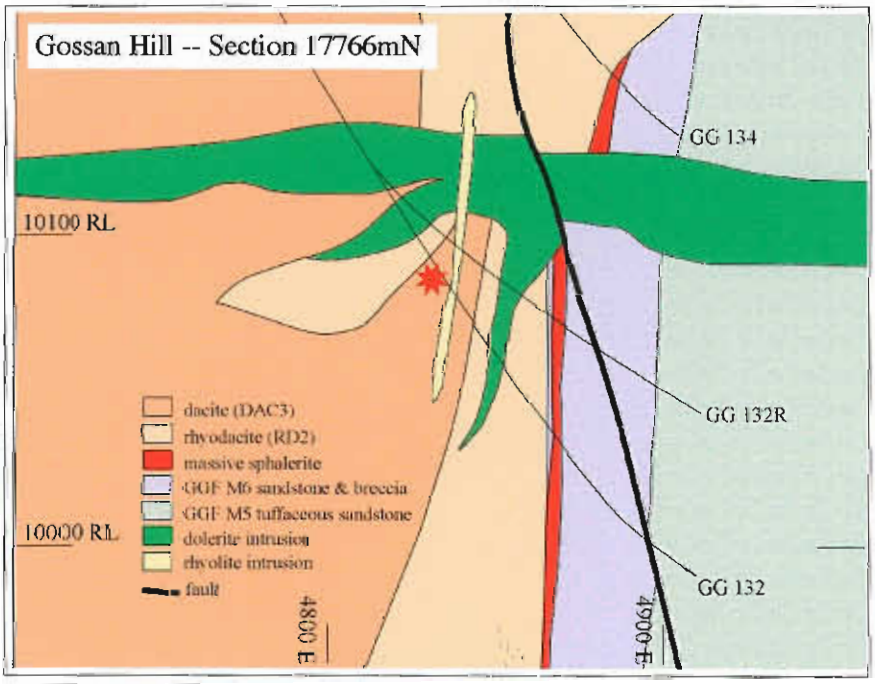

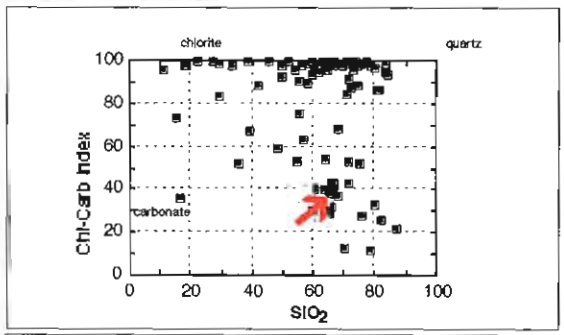

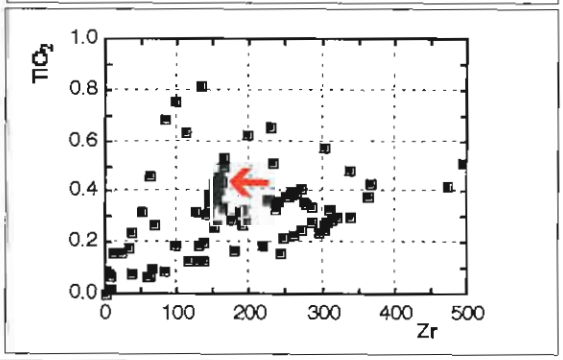

Sample No. 760218
Location Gossan Hill
Alteration zone Hangingwall carbonate-muscovite alteration zone
Formation Suddles Formation Member 2 (RD2)

Description Massive quartz, feldspar phyric rhyodacite with large quartz phenocrysts (up to 8mm).

Facies Interp Coherent, conformable rhyodacite lava with upper breccia facies and a locally disconformable basal contact to the GGF

Alteration Intensity none weak moderate strong (intense) **PY** 2%
Alteration Style patchy (pervasive) veined cleavage control
Alteration Mineralogy Groundmass quartz-muscovite-carbonate
Feldspars carboante-muscovite-chlorite

Interpretation diagenetic (metamorphic) syntectonic (hydrothermal)
Relict Mineralogy quartz phenocrysts, fractured, embayed with quartz overgrowths

Geochemistry

SiO_2	TiO_2	Al_2O_3	Fe_2O_3	MnO	MgO	CaO	Na_2O	K_2O	P_2O_5	S	LOI	Al	CCPI	Ti/Zr
64.1	0.48	15.38	6.4	0.17	2.6	2.33	0.37	2.68	0.11	0.19	5.16	66.2	74.7	8.5

Rb	Ba	Cu	Pb	Zn	Sb	Tl	Zr	Nb	Y	Sr	PIMA: AlOH I	CCI
66	252.4	19	128	250	3.2	2.5	336.6	13.9	107	26.3	--	53.7

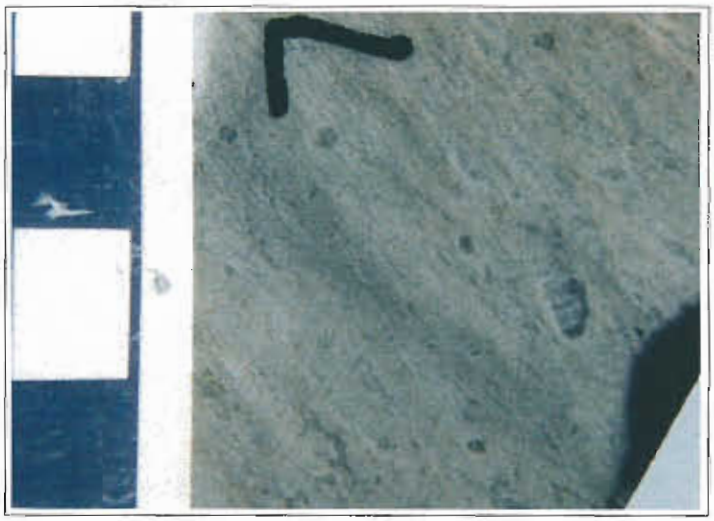

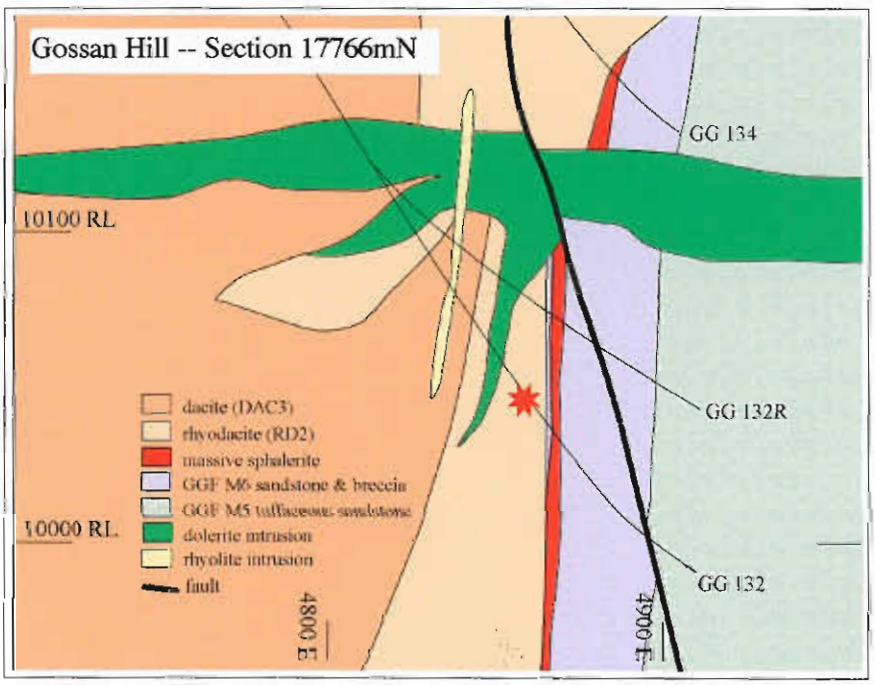

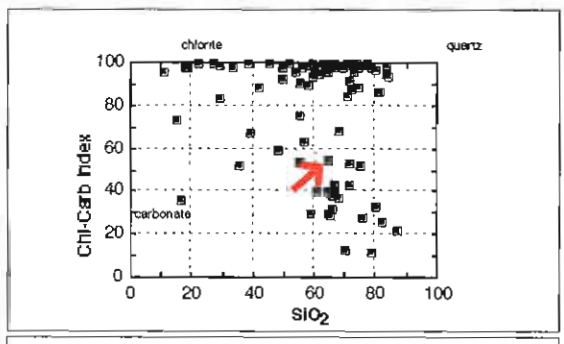

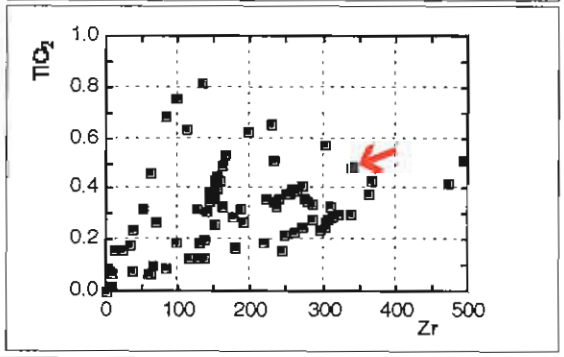

Sample No. 760411
Location Gossan Hill
Alteration zone Carbonate-quartz nodular alteration

Formation Golden Grove Formation Member 5

Description Massive sandstone with pervasive quartz-chlorite alteration and carbonate-microcrystalline quartz nodular alteration.
Facies Interp Tuffaceous sandstone of a homogeneous provenance deposited by mass flow processes

Alteration Intensity none weak moderate strong (intense) **PY** trace
Alteration Style (patchy) pervasive veined cleavage control
Alteration Mineralogy Groundmass ubiqutous quartz-chlorite and nodular carbonate-quartz
Feldspars none

Interpretation (diagenetic) metamorphic syntectonic (hydrothermal)
Relict Mineralogy no relict mineralogy; shard and pumice shred outlines may be preserved

Geochemistry

SiO_2	TiO_2	Al_2O_3	Fe_2O_3	MnO	MgO	CaO	Na_2O	K_2O	P_2O_5	S	LOI	Al	CCPI	Ti/Zr
54.7	0.19	7.25	7.67	0.13	11.13	6.37	0.04	0.00	0.03	0.23	10.9	63.5	99.8	5.2

Rb	Ba	Cu	Pb	Zn	Sb	Tl	Zr	Nb	Y	Sr	PIMA: AlOH I	CCI
<1	2.6	32	8	161	1.2	<0.05	217.4	8.2	60	50.4	--	55.5

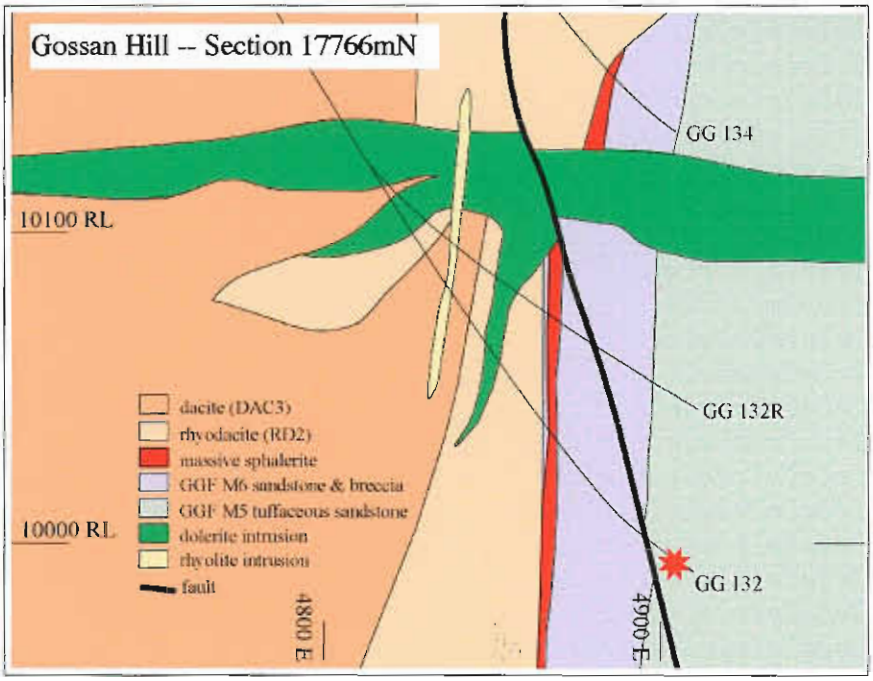

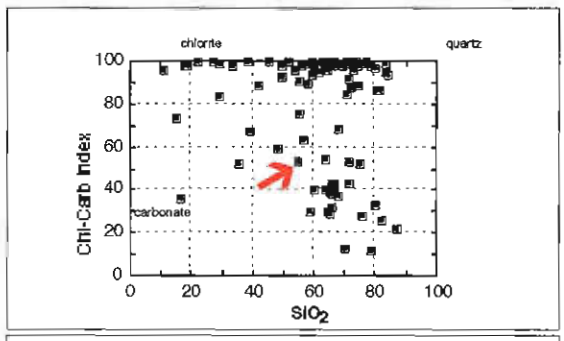

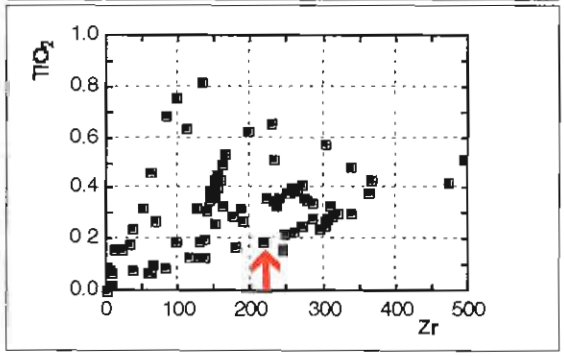

Sample No. 760231
Location Gossan Hill
Alteration zone Host to massive sulphides and stringer mineralisation
Formation Golden Grove Formation Member 6

Description Thinly bedded to laminated, fine grained sandstone, now consisting of microcrystalline quartz and disseminated chlorite
Facies Interp Epiclastic sandstone and silstone with intense silicification. Background sedimentation during sulphide formation.

Alteration Intensity none weak moderate strong (intense) **PY** <1%
Alteration Style patchy (pervasive) veined cleavage control
Alteration Mineralogy Groundmass quartz with disseminated chlorite that defines bedding
Feldspars none

Interpretation (diagenetic) metamorphic syntectonic (hydrothermal)
Relict Mineralogy no relict mineralogy, however bedding is preserved through the siliceous alteration

Geochemistry

SiO_2	TiO_2	Al_2O_3	Fe_2O_3	MnO	MgO	CaO	Na_2O	K_2O	P_2O_5	S	LOI	Al	CCPI	Ti/Zr
83.84	0.18	4.85	7.19	0.06	1.44	0.08	<0.03	0.14	0.02	0.06	1.74	93.5	98.1	31.5

Rb	Ba	Cu	Pb	Zn	Sb	Tl	Zr	Nb	Y	Sr	PIMA: AlOH I	CCI
4	8.1	10	8	730	0.7	<0.05	34.3	1.4	7	1.8	--	94.7

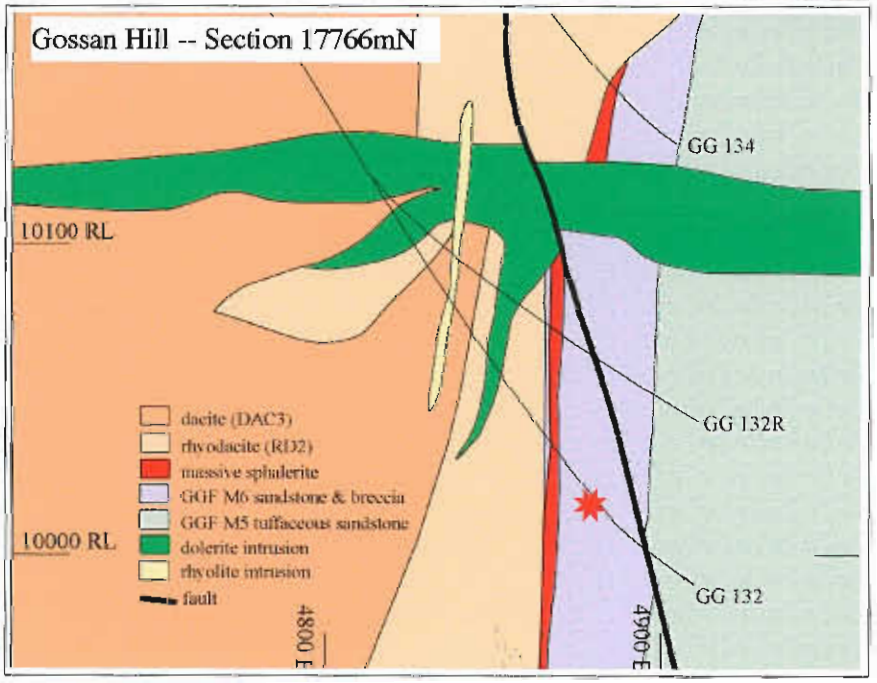

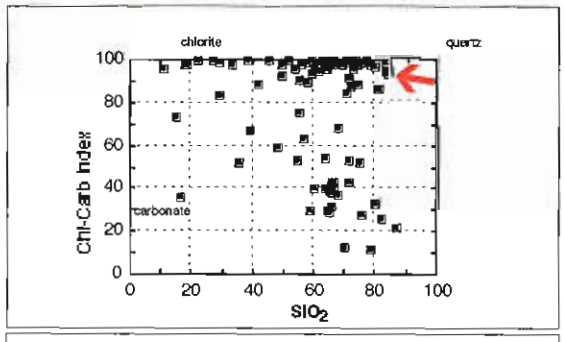

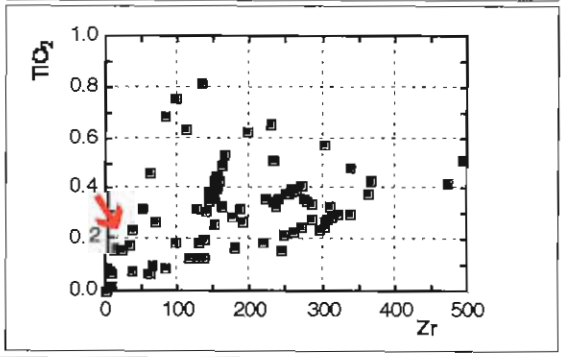

Sample No. 769325
Location Gossan Hill
Alteration zone Footwall quartz-chlorite alteration
Regional silicification
Formation Golden Grove Formation Member 1

Description Massive clast supported pebble breccia with abundant pumice clasts which have a domainal quartz-chlorite alteration.
Facies Interp Pebble breccia facies deposited by mass flow processes with little internal reworking and a homogeneous provenance

Alteration Intensity none weak moderate strong (intense) **PY** 1%
Alteration Style (patchy) (pervasive) veined cleavage control
Alteration Mineralogy Groundmass quartz-chlorite
Lithics quartz-chlorite

Interpretation (diagenetic) metamorphic syntectonic (hydrothermal)
Relict Mineralogy Volcanic quartz forms up to 5% occurring in matrix and in lithic clasts

Geochemistry

SiO_2	TiO_2	Al_2O_3	Fe_2O_3	MnO	MgO	CaO	Na_2O	K_2O	P_2O_5	S	LOI	Al	CCPI	Ti/Zr
73.1	0.32	9.76	9.21	0.05	3.52	0.14	0.11	0.7	0.01	0.04	2.87	94.4	94.0	10.2
Rb	Ba	Cu	Pb	Zn	Sb	Tl	Zr	Nb	Y	Sr		PIMA: AlOH I		CCI
15	136.1	4	3	31	0.3	<0.05	188.4	6.4	39	5.1		--		95.5

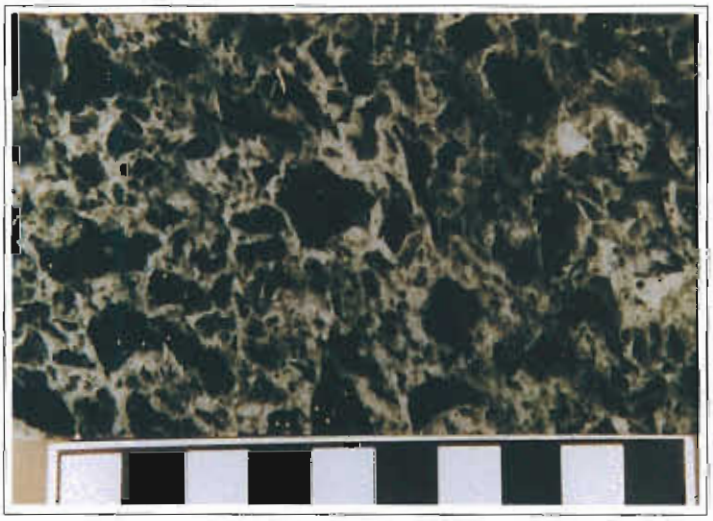

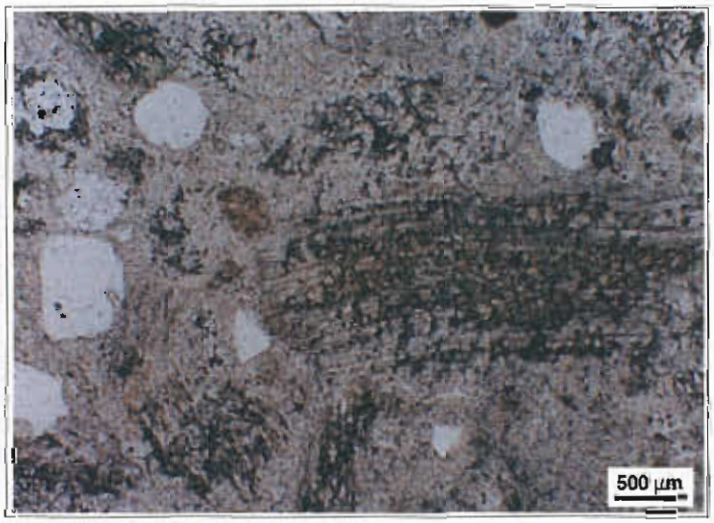

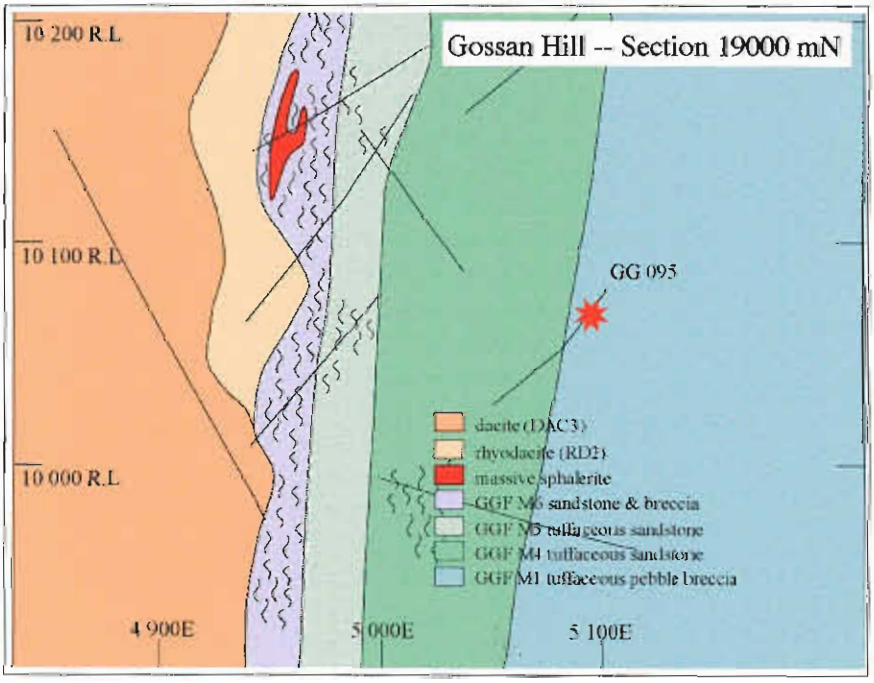

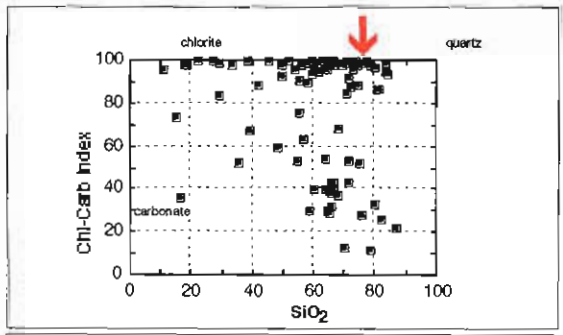

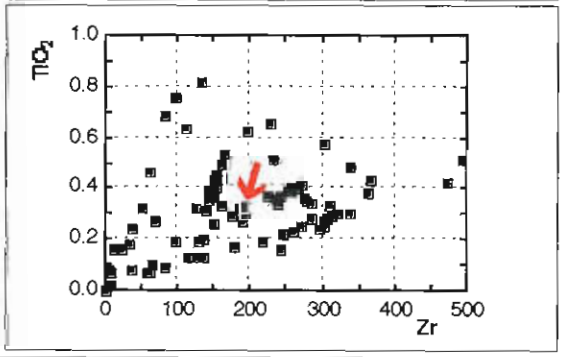

Sample No. 760376
Location Gossan Hill
Alteration zone Siliceous alteration of the host between massive sulphide zones
Formation Golden Grove Formation Member 5

Description Sandstone consisting of tube pumice and shards altered to microcrystalline quartz in a fine-grained (ash-sized) matrix.
Facies Interp Tuffaceous sandstone of a homogeneous provenance deposited by mass flow processes

Alteration Intensity none weak moderate strong (intense) **PY** trace
Alteration Style patchy (pervasive) veined cleavage control
Alteration Mineralogy Groundmass quartz-chlorite
Feldspars none

Interpretation (diagenetic) metamorphic syntectonic (hydrothermal)
Relict Mineralogy minor volcanic quartz less than 2%, pumice and shard outlines preserved

Geochemistry

SiO_2	TiO_2	Al_2O_3	Fe_2O_3	MnO	MgO	CaO	Na_2O	K_2O	P_2O_5	S	LOI	Al	CCPI	Ti/Zr
68.2	0.36	9.96	13.54	0.05	5.46	0.09	0.03	0.01	0.08	<0.01	3.72	97.9	99.8	9.8

Rb	Ba	Cu	Pb	Zn	Sb	Tl	Zr	Nb	Y	Sr	PIMA: AlOH l	CCI
<1	5.5	4	4	133	0.6	<0.05	221.3	7.5	48	2.1	--	97.8

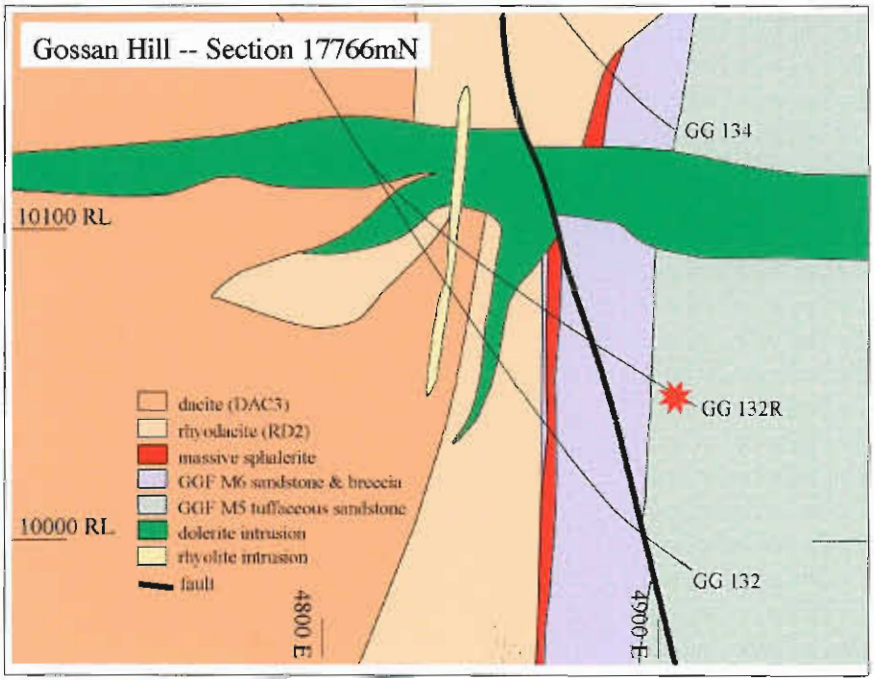

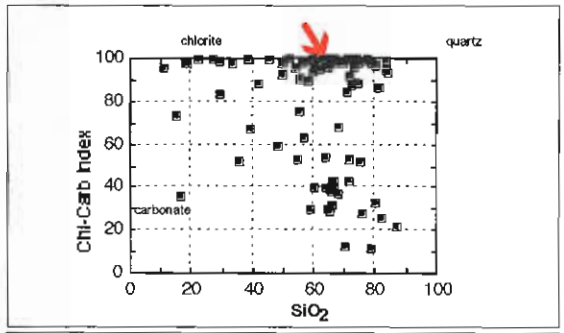

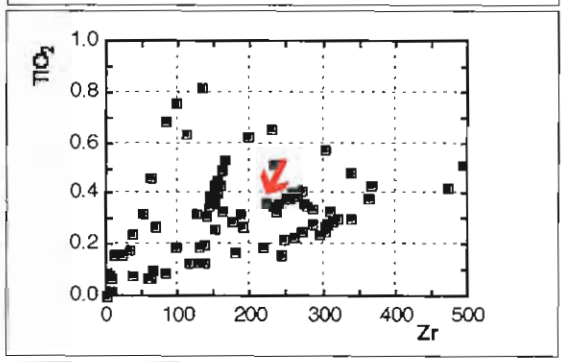

A molar element ratio analysis of lithogeochemical samples from the footwall andesite, Hellyer VHMS district, Tasmania, Australia

Clifford R. Stanley and J. Bruce Gemmell
MDRU, The University of British Columbia, and Centre for Ore Deposit Research

Introduction

Hydrothermal alteration zones about volcanic hosted massive sulphide (VHMS) deposits have historically been used as intermediate exploration targets because they are larger than the mineral deposits they surround. Muscovite- and chlorite-dominated alteration zones occur in the footwalls of many VHMS deposits (Sangster 1972; Goodfellow 1975; Sangster & Scott 1976; Franklin et al. 1981; Hutchinson et al. 1982; Lydon 1988), and commonly exhibit alkali (Na, Ca) depletion (Goodfellow 1975; Franklin et al. 1981; Hutchinson et al. 1982; Lydon 1988). However, efforts to quantitatively describe the extent of alteration using lithogeochemistry have met with less than overwhelming success in exploration. Compositional variations extant in the volcanic host rocks, largely due to differential sorting of phenocrysts, serve to introduce substantial noise, and limit resolution of the geochemical expression of alteration. Consequently, mass balance methods that do not account for this primary, underlying source of compositional variability (Akella 1966; Gresens 1967; Babcock 1973; Grant 1986; MacLean 1990; MacLean & Barrett 1992) can produce false anomalies unrelated to hydrothermal alteration.

In order to circumvent this problem, Stanley & Madeisky (1993) utilized Pearce element ratio diagrams (Pearce 1968) to develop linear models describing the compositional variability in fresh volcanic rocks that is attributable to phenocryst sorting. Hydrothermally altered rocks that exhibit deviations (residuals) from these associated fresh rock linear models thus describe the effects and extent of the alteration. By employing this approach, one can eliminate the primary igneous compositional variations so that only those variations caused by hydrothermal alteration are evident. This provides an alteration signature with a higher level of resolution that affords an opportunity to discriminate between different types of hydrothermal alteration, accurately quantify the extent of the alteration, and rigorously investigate the hydrothermal alteration processes. As a result, this methodology provides substantial advantage in both mineral exploration and mineral deposits research.

Successful applications of this methodology applied to exploration for and research of felsic VHMS deposits include Stanley & Madeisky (1993, 1994), Madeisky & Stanley (1993), Robinson et al. (1995) and Duncan (1996). However, fewer applications of this methodology exist applied to mafic VHMS alteration zones, and only one (Robinson et al. 1995) describes the PER approach in intermediate (andesite) VHMS deposit alteration zones. Consequently, application of PER analysis to lithogeochemical data from the footwall andesite in the Hellyer VHMS district, Tasmania, will provide further insight into how to employ this approach to VHMS exploration in intermediate volcanic rocks, improve the specific hydrothermal alteration model for the Hellyer deposit, and possibly identify new exploration targets within the camp.

MDRU Lithogeochemical Exploration Research
Contribution # 25

Pearce element ratio analysis

PERs rely on several inherent numerical characteristics to avoid the spurious compositional variations that overprint the hydrothermal alteration variations, so that only compositional variations related to hydrothermal alteration are considered. First, PERs are ratios, and thus avoid closure, the mathematical characteristic that prevents the manifestation of material transfer from directly mimicking its action (Chayes 1960; Pearce 1968; Nicholls 1988; Russell & Stanley 1990A, 1990B; Pearce & Stanley 1991; Stanley & Madeisky 1994). For example, if SiO_2 is added to a rock (say in a quartz vein; ***the action***), the Al_2O_3 concentration decreases (***the manifestation***), even though no Al_2O_3 was removed from the rock. Closure occurs because all compositions must sum to 100%. Creating ratios circumvents this problem.

Second, PERs use a conserved element in the denominator of the ratio (Pearce 1968). A conserved element does not participate in the material transfer processes that produce compositional variation in rocks. The conserved element in the denominator effectively acts as a standardizing variable. As a result, variations in the ratios are directly proportional to the material transfer variations that occur in the numerator element only (Russell & Stanley 1990A; Stanley & Madeisky 1993, 1994). This direct and linear relationship facilitates recognition of the material transfer process that took place.

Third, PERs are molar ratios, and thus directly relate to mineral formulae and the coefficients in balanced chemical reactions of import (Russell & Stanley 1990A, 1990B; Pearce & Stanley 1991; Stanley & Madeisky 1993, 1994; Stanley 1996). Fourth, linear combinations of PERs may be used to collapse the variability that mineral solid solutions may have on rock compositional variations [e.g. (Fe+Mg)/Z, where Z is any conserved element, would accommodate variations in composition of ferro-magnesian minerals; Stanley & Russell 1989; Nicholls & Gordon 1994; Stanley & Madeisky 1993, 1994; Stanley 1997]. These linear combinations can also be used to produce specific projections of PER space that resolve specific types of compositional variations, while avoiding other potentilly interfering variations. These linear combinations of PERs are commonly defined using matrix algebra (Stanley & Russell 1989; Nicholls & Gordon 1994; Stanley 1997).

Finally, PERs are typically plotted against each other on PER diagrams so that covariations of the numerator elements in the ratios of each axis can be used as fingerprints of specific material transfer processes. For example, if a rhyolite melt undergoes albite phenocryst sorting during ascent and eruption, some of the melt will have lost albite and some will have gained albite. For every mole of albite lost, one mole of Al and one mole of Na will be lost. As a result, on a PER diagram with numerators of Al and Na (both divided by a conserved element, an element that does not occur in albite), loss of albite will displace rock compositions down to the left along a line with unit slope (because of the proportional relationship described in point two, above). This slope of unity is thus a fingerprint of albite fractionation on an Al/Z *versus* Na/Z PER diagram.

Objective

In the following report, results of a PER analysis of lithogeochemical data from the footwall andesite to the Hellyer VHMS deposit, Tasmania, Australia, are described. These results illustrate the manner in which PER analysis may be used to develop a model for the background compositional variations that existed in the Hellyer host andesite before hydrothermal alteration, as well as the manner in which PER analysis may be used to identify, quantify and understand the effects of hydrothermal alteration about the deposit. In the process, specific effort has also been made to identify lithogeochemical parameters that will be effective in exploration for other VHMS deposits in the Hellyer area, and in andesites in general.

Geology and mineralization

The Hellyer VHMS deposit is a 17 Mt high grade (13.0% Zn, 6.8% Pb, 0.3% Cu, 160 g/t Ag and 2.3 g/t Au) ore deposit hosted within the Cambrian Mount Read volcanic belt of western Tasmania (McArthur 1986, 1989; Jack 1989; McArthur & Dronseika 1990; Gemmell & Large 1992). This volcanic belt contains numerous other VHMS deposits and potential for additional undiscovered deposits is high (Whitford et al. 1989; Gemmell & Large 1992; Offler & Whitford

1992; Corbett 1992). The Hellyer deposit is underlain by a massive and fragmental feldspar-phyric (and sparsely clinopyroxene-phyric) andesite that exhibits autobrecciated, quench fragmented and hyaloclastic textures. This andesite is up to 500 m thick and is overlain by an up to 40 m thick polymict, epiclastic mass flow unit containing abundant andesite but also dacite and basalt clasts. This unit represents the ore horizon in the Hellyer area. Immediately above this debris flow deposit occurs a 80 to 250 m thick massive and pillowed basalt, that is in turn overlain by 100 m of carbonaceous Que River shale and 500 m of interbedded rhyolite tuff volcaniclastics, shales and graywackes of the Upper Rhyolite Sequence.

The Hellyer massive sulphide deposit is 800 m (NS) by 200 m (EW) size in plan, and has an average thickness of approximately 45 m. It is cut by the Jack Fault, which has displaced rock upward to the east and north about 130 and 30 m, respectively. Mineralization consists of over 50% pyrite, 20% sphalerite, 8% galena, 2% arsenopyrite, 1% chalcopyrite and minor tetrahedrite. The approximately 15% gangue consists of quartz, barite, calcite, chlorite, sericite and siderite. The deposit also exhibits a classic vertical zoning pattern, with Cu–Fe sulphide below and Pb, Zn, Ag, As and Au-bearing sulphides above and lateral to the core. Middle Devonian deformation resulted in gentle folds and later wrench faulting (represented by the Jack fault) and prehnite-pumpellyite metamorphic grades dominate about the Hellyer deposit.

Underneath the Hellyer deposit is a well-developed hydrothermal alteration zone that is bounded by a stringer vein system. Footwall alteration is centred underneath the deposit, but stretches up to 1500 m north–south and 350 m east–west. This alteration is zoned, with a texturally preserved marginal stringer envelop zone consisting of incompletely altered muscovite plus quartz, a texturally destructive muscovite alteration zone, a chlorite alteration zone with chlorite–dolomite alteration zone near its top immediately below the massive sulphides, and finally a siliceous zone at its core (Fig. 1; Gemmell & Large 1992). Pyrite is ubiquitous in each alteration zone. Contacts are generally sharp (McArthur 1986).

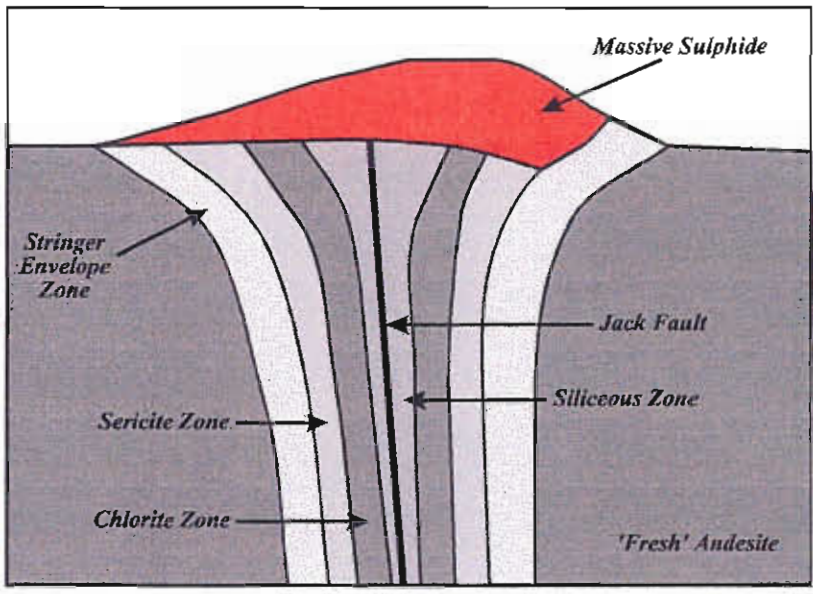

Figure 1 - Schematic alteration zoning relationships in the footwall andesite of the Hellyer volcanic hosted massive sulphide deposit (after Gemmell and Large 1992). The chlorite-carbonate zone has been omitted because it is not represented in the suite of samples under examination. See text for further discussion.

Sampling and geochemical analysis

Lithogeochemical data from 201 samples of Hellyer andesite footwall underwent a thorough numerical evaluation as part of this study. These data came from three sources : an M.Sc. thesis by Jack (1989; 27 samples), research by Gemmell & Large (1992; 153 samples), and the current study (21 samples). Samples from Jack (1989) and Gemmell & Large (1992) are largely from the hydrothermal alteration zone beneath the deposit, whereas those collected as part of the present study are largely from outside the alteration zone (as far south as the Que River deposit and a substantial distance to the west), and thus are relatively fresh. Although 106 samples of the footwall andesite were included in Jack's (1989) M.Sc. thesis, 79 of these were analyzed for additional elements by Gemmell & Large (1992), and thus are included in this later dataset.

Seventy four samples from Gemmell & Large (1992) and those collected in the present study were approximately 1 kg in mass, composed of sawed half portions of predominantly NQ core of 25 to 50 cm length. The remaining 79 samples from Gemmell & Large (1992) and samples from Jack (1989) were approximately 1/2 kg core grinds from up to 25 m of core (although most were from less than 10 m of core). In all data subsets, efforts were made to collect relatively homogeneous material representative of the local 5 m of core, and to avoid late calcite veins and other anomalous characteristics of the rock (weathered material fault, shear zones, etc.).

Samples acquired from Jack's M.Sc. thesis (1989), including the 79 samples included in Gemmell & Large's data subset, were prepared and analyzed by a variety of laboratories, including : the University of Tasmania (61 samples), the Tasmania Mines Department (5 samples), Launceston and AMDEL (45 samples). The remaining 74 samples from Gemmell & Large's (1992) dataset and all of the samples collected for the present study were analyzed at the University of Tasmania.

Samples analyzed at the University of Tasmania and at the Tasmanian Mines Department were prepared using W carbide pulverizing equipment and analyzed for major and trace elements by X-ray fluorescence after Li-metaborate fusion. Samples sent to AMDEL were analyzed by a similar X-ray fluorescence methodology for major oxides, and by atomic absorption spectrometry and inductively coupled plasma spectrometry for trace elements, after aqua regia digestion.

Although no samples were submitted to more than one laboratory to assess whether any bias exists between the various laboratory analyses, statistical analysis of the data from these disparate sources does not suggest that any significant difference in the mean or variance of each data subset exists. However, because of both the extensive fractionation and metasomatism that affected the andesite, variation in each data subset is substantial, and thus would probably mask any systematic inter-laboratory bias that might exist.

All samples were analyzed for major oxides (SiO_2, TiO_2, Al_2O_3, Fe_2O_3, MnO, MgO, CaO, Na_2O, K_2O, P_2O_5 and 'loss on ignition'), and most samples were analyzed for at least some trace elements (Cu, Pb, Zn, Ag, As, Rb, Sr, Ba, Y, Zr, Nb, Ni, Cr, V, Sc and La). In addition, all of Jack's (1989) samples were analyzed for S by LECO correlation spectrometry. Samples collected as part of the present study, and samples from Gemmell & Large's (1992) and Jack's (1989) studies whose pulps were retained by Aberfoyle Resources Ltd. were further analyzed for S, C and H (by Carlo Erba elemental analyzer) and H_2O^+ (structural water; by a litharge adsorption step heating process). Because a significant number of missing analyses exist for several trace elements, only a small number of element determinations were available for some elements. These elements, La and Sc, were not considered in the following analysis.

Lithogeochemical data treatment

Lithogeochemical data from the Hellyer footwall andesite were examined using PER analysis, a molar element ratio technique that avoids closure, relates directly to mineral compositions and chemical reactions, and can be used to model and remove interfering sources of variability in a dataset, so that the variation of interest can be understood and quantified. In the Hellyer footwall andesites, both igneous fractionation and hydrothermal alteration variations are probably extant in the dataset, and understanding and quantifying the later is the primary goal of this study.

Conserved element identification

In order to conduct any PER analysis, two requirements must be verified in the data. First, the samples must be cogenetic (derived from a single parent composition that was at one time homogeneous; Stanley & Madeisky 1993). Geological mapping, drill core logging and subsequent stratigraphic analysis reveals that the samples under investigation were all collected from a coherent feldspar-phyric andesite unit that occurs in the immediate footwall of the Hellyer and Que River VHMS deposits (Jack 1989; Gemmell & Large 1992; Waters & Wallace 1992). As a result, it is likely that these samples were all derived from the same parent melt, and thus are cogenetic.

The second requirement is that a conserved element, one that did not participate in any material transfer process (in this case, igneous fractionation and hydrothermal alteration) exists in the data set. This element is used as the standardizing denominator of the PERs that are evaluated in the subsequent analysis.

In order to identify a conserved element, two potentially conserved elements are plotted against each other on a scatterplot. If the data, given measurement error, plot on a single line that passes through the origin, then the two elements are likely conserved (Stanley & Madeisky 1993), and the rocks are likely cogenetic. If the samples plot, given measurement error, on a line with positive slope and non-zero intercept, then one element is likely more conserved than the other (positive ordinate intercept = abscissa element more conserved; positive abscissa intercept = ordinate element more conserved; Stanley & Madeisky 1993).

Consequently, a large number of scatterplots of potentially conserved elements (ones that are both relatively incompatible and immobile; Winchester & Floyd 1977; Floyd & Winchester 1978; Finlow-Bates & Stumpfl 1981; DePangher 1988; Stanley & Madeisky 1993) were examined. Five of these are presented in Figures 2 through 6. On the first three, TiO_2 is plotted against Y, Zr, and Nb, respectively. On each plot some outlying samples exist; however, the overall trends of the data on these plots have positive slopes and intercepts. This indicates that Y, Zr and Nb are likely more conserved than TiO_2. In contrast, scatterplots of Zr versus Y and Nb (Figs 5 and 6) have data that exhibit trends with positive slopes that pass through the origin. As a result, it is likely that Zr, Y and Nb are all equally conserved. Logical combination of the conclusions resulting from Figures 2 through 6 allow formulation of a statement describing the level of conservation of the elements examined :

$$Zr = Y = Nb > TiO_2 ,$$

where "=" means 'equally conserved' and ">" means 'more conserved'. This relative order of conserved element is sensible because TiO_2 is known to partition in minor amounts into clinopyroxene (Hyndman 1972) and thus if sorting (fractionation) of clinopyroxene phenocrysts occurred within the footwall andesite, TiO_2 would have moved, and thus would not be as conserved as Zr, Y or Nb.

As a result, either Zr, Y or Nb could be used as the denominator element in PER analysis of the Hellyer footwall andesites. However, because the concentrations of both Y and Nb are low, and are thus close to their detection limits (both 1 ppm), these data probably exhibit large relative measurement errors. As a result, because Zr concentrations are far higher and thus well above the Zr detection limit of 1 ppm, Zr is probably the best conserved element denominator because its relative measurement error is lowest (a feature that ensures that the PERs will provide the highest resolution to detect and accurately quantify the material transfer of other elements; Stanley & Madeisky 1993).

Zr is incompatible in most mafic and intermediate melts, and does not occur in either plagioclase or clinopyroxene, the two phenocrysts observed in the Hellyer footwall andesite (Jack 1989; Gemmell & Large 1992; Waters & Wallace 1992). Furthermore, Zr has low solubility in most hydrothermal solutions. As a result, Zr has been used as the conserved element denominator in all subsequent PER diagrams.

Controls on compositional variation

Compositional controls on the major element abundances in the Hellyer footwall andesite are likely exerted by two processes (igneous fractionation and hydrothermal alteration) and the minerals involved in them (plagioclase and clinopyroxene; muscovite, chlorite, quartz, pyrite, calcite, dolomite, etc.). As a result, these compositional controls were investigated by (i) examining those samples that are least altered

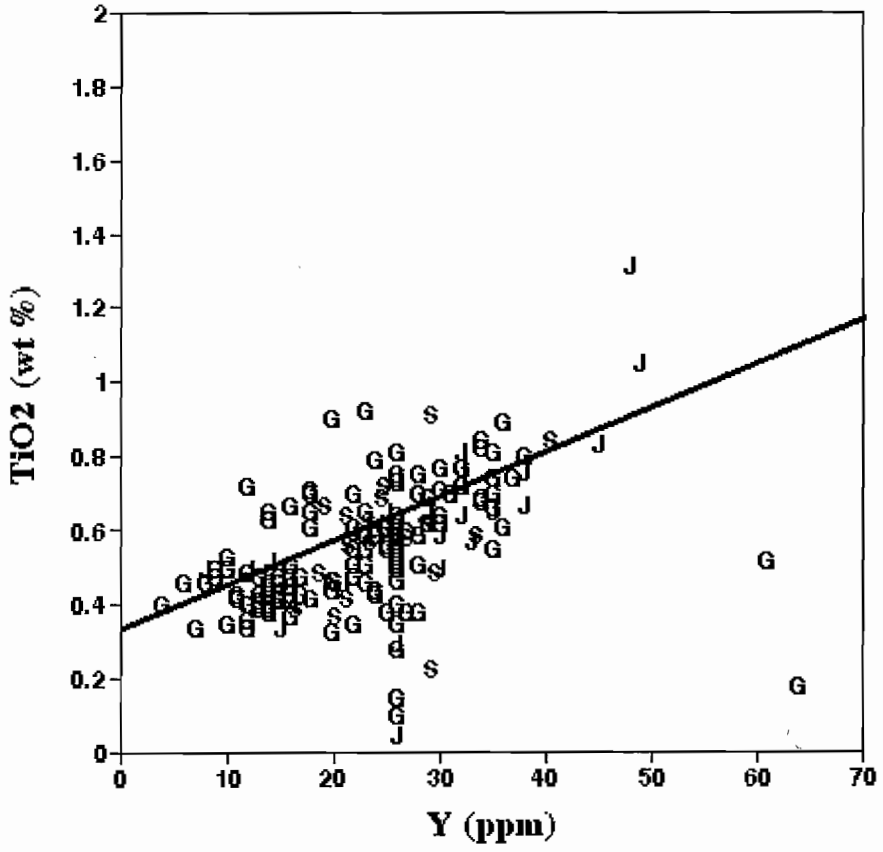

Figure 2 - Hellyer andesite footwall samples are plotted on a Y (ppm) *versus* TiO_2 (wt. %) scatterplot. Samples have been coded as to their origin : "G" = Gemmell and Large (1992), "J" = Jack (1989), "S" = Stanley and Gemmell (this report). Samples that exhibit Y concentrations of 25 ppm across a range of TiO_2 concentrations were analyzed by a less sensitive analytical method with a detection limit of 50 ppm. These data have been halved to distinguish 'at detection' concentrations from 'below detection' concentrations. The overall trend of the data is along a line with positive slope and intercept. This indicates that Y is probably more conserved than TiO_2, based on inequality analysis of the functional controls of slope and intercepts on scatterplots (Stanley and Madeisky 1993). See text for further discussion.

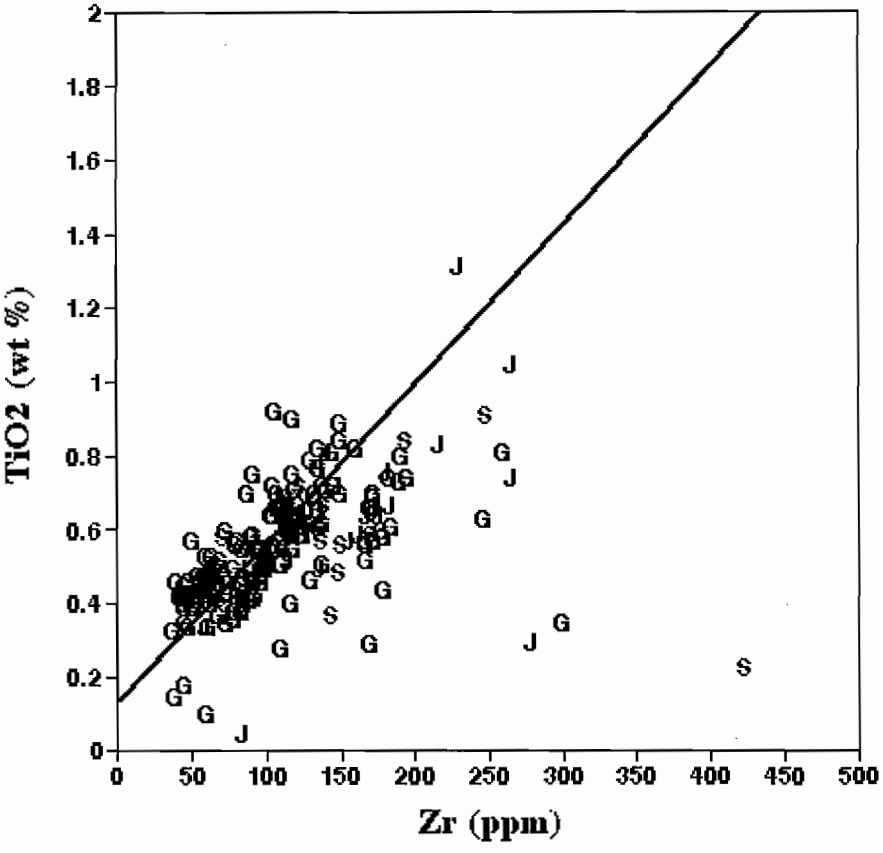

Figure 3 - Hellyer andesite footwall samples are plotted on a Zr (ppm) *versus* TiO_2 (wt. %) scatterplot. Samples have been coded as to their origin : "G" = Gemmell and Large (1992), "J" = Jack (1989), "S" = Stanley and Gemmell (this report). The overall trend of the data is along a line with positive slope and intercept. This indicates that Zr is probably more conserved than TiO_2, based on inequality analysis of the functional controls of slope and intercepts on scatterplots (Stanley and Madeisky 1993). See text for further discussion.

to determine the importance and nature of igneous fractionation, and then (ii) examining those samples that were significantly hydrothermally altered to understand and quantify the hydrothermal alteration processes that took place in the Hellyer footwall andesite. After the controls on compositional variability of the samples were determined using chemographic diagrams, parameters describing the extent and nature of hydrothermal alteration were plotted on geographic diagrams to determine the spatial extent and zoning of the various alteration assemblages.

Igneous Fractionation

Andesite samples were plotted on an Al/Zr *versus* (2Ca+Na)/Zr PER assemblage test diagram to determine whether the igneous fractionation of plagioclase and/or clinopyroxene, the minerals observed as phenocrysts in the footwall andesite at Hellyer andesite (Jack 1989; Waters & Wallace 1992; Sinclair 1994), are responsible for at least part of the compositional variation observed in these rocks (Fig. 7). The addition of plagioclase and clinopyroxene of any composition will displace rock compositions up and to the right on this diagram along lines with slopes of unity and infinity, respectively. The data plot generally beneath a line with slope of approximately 5/2. This indicates that some combination of plagioclase and clinopyroxene fractionation is likely responsible for the observed compositional variation. Samples that plot on (close to) or above the plagioclase control line (m = 1; with (2Ca+Na)/Al values > 2/3) have been labeled with an "F" symbol on Figure 7 to designate their relatively fresh (least altered) compositions.

Nevertheless, it is likely that these samples did undergo some exchange with seawater (spilitization; low temperature exchange of Na and Ca between seawater and the rocks), but the magnitude of the compositional changes resulting from this process was likely small compared to that of igneous fractionation.

Some of the samples plotting above the plagioclase control line might be spilitized or slightly hydrothermally altered, obtaining their compositions from joint plagioclase and clinopyroxene fractionation to produce compositions that plot along a line with slope of 5/2 on Figure 7, followed by undergoing minor hydrothermal alteration, which displaced these rock compositions a small distance downward such that their compositions still plot above the plagioclase control line. Alternatively, these samples may be significantly hydrothermally altered, causing their compositions to plot below the plagioclase control line, but were subsequently cut by veins containing abundant Ca-bearing carbonate minerals, which displace the rock compositions back above the plagioclase control line.

In order to evaluate which of these hypotheses is supported by the data, the andesite samples were plotted on a CO_2/Zr *versus* Ca/Zr PER assemblage test diagram (Fig. 8) to determine whether significant amounts of Ca-bearing carbonate minerals exist in these rocks. The addition of calcite, dolomite, siderite, anorthite and clinopyroxene will displace rock compositions up and to the right along lines with slopes of unity, one half, zero, infinity and infinity, respectively. Unfortunately, only about half of the samples (99 of 201) were analyzed for CO_2, so a full assessment of the importance of carbonate minerals in controlling the compositional diversity in the footwall andesites is not possible. Nevertheless, only three samples contain significant amounts of CO_2 (with values greater than 0.12), and thus the impact of Ca-bearing carbonate minerals on Figure 7 (and all subsequent PER diagrams) is minimal. As a result, because most andesite samples do not exhibit significant carbonate abundances, it is likely that the fresh andesites at Hellyer, as defined above, exhibit at most relatively small amounts of spilitization or hydrothermal alteration.

Most of the fresh samples exhibiting elevated CO_2 abundances plot close to the calcite control line (m = 1), indicating that it is the primary carbonate mineral in these rocks. The remaining fresh samples plot above the calcite control line, indicating that their Ca budgets are largely controlled by plagioclase and clinopyroxene fractionation.

Samples that plot significantly below the plagioclase control line on Figure 7 (labeled by the "." symbols) likely underwent significant hydrolysis (addition of H) during hydrothermal alteration associated with massive sulphide genesis at Hellyer. This metasomatism probably involved the loss of both Ca and Na, rather than the addition of Al. This is because the samples considered to be relatively

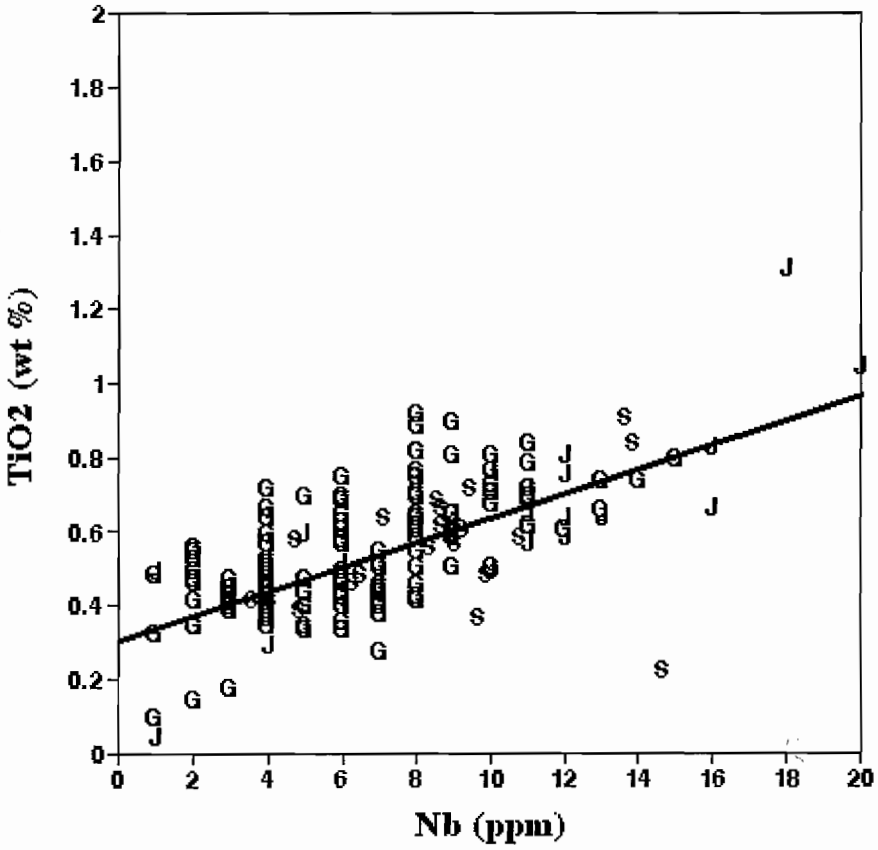

Figure 4 - Hellyer andesite footwall samples are plotted on a Nb (ppm) *versus* TiO_2 (wt. %) scatterplot. Samples have been coded as to their origin : "G" = Gemmell and Large (1992), "J" = Jack (1989), "S" = Stanley and Gemmell (this report). The overall trend of the data is along a line with positive slope and intercept. This indicates that Nb is probably more conserved than TiO_2, based on inequality analysis of the functional controls of slope and intercepts on scatterplots (Stanley and Madeisky 1993). See text for further discussion.

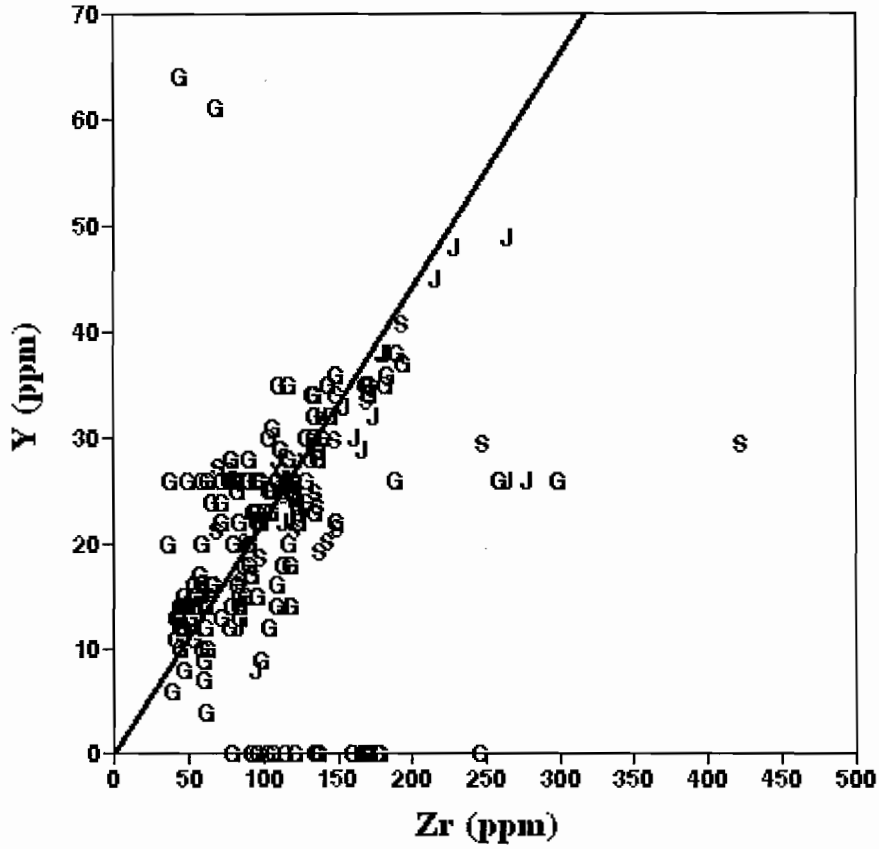

Figure 5 - Hellyer andesite footwall samples are plotted on a Zr (ppm) *versus* Y (ppm) scatterplot. Samples have been coded as to their origin : "G" = Gemmell and Large (1992), "J" = Jack (1989), "S" = Stanley and Gemmell (this report). Samples that exhibit Y concentrations of 25 ppm across a range of Zr concentrations were analyzed by a less sensitive analytical method with a detection limit of 50 ppm. These concentrations have been halved to distinguish 'at detection' concentrations from 'below detection' concentrations. Samples exhibiting Y concentrations of zero are missing data. The overall trend of the data is along a line with positive slope and zero intercept. This indicates that Zr and Y exhibit equal levels of conservation (Stanley and Madeisky 1993), and given their incompatible character in melts and relatively immobile behavior in most hydrothermal solutions, are probably both conserved. See text for further discussion.

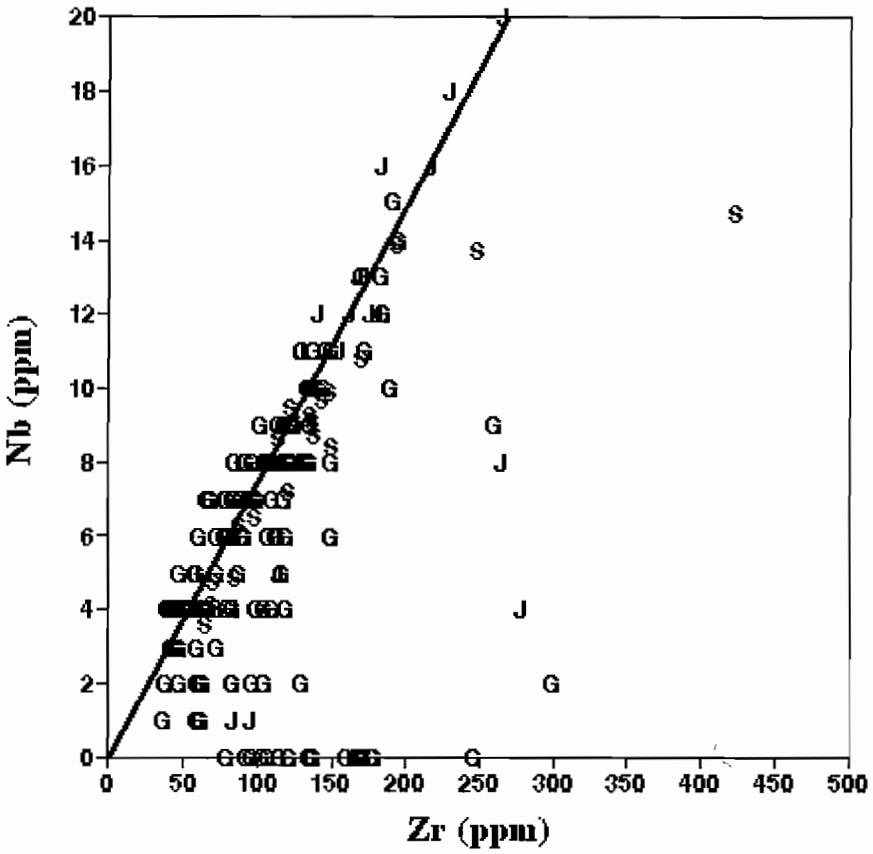

Figure 6 - Hellyer andesite footwall samples are plotted on a Zr (ppm) *versus* Nb (ppm) scatterplot. Samples have been coded as to their origin : "G" = Gemmell and Large (1992), "J" = Jack (1989), "S" = Stanley and Gemmell (this report). The overall trend of the data is along a line with positive slope and zero intercept. This indicates that Zr and Nb exhibit equal levels of conservation (Stanley and Madeisky 1993), and given their incompatible character in melts and relatively immobile behavior in most hydrothermal solutions, are probably both conserved. See text for further discussion.

fresh have an Al/Zr range that is similar to the Al/Zr range in samples that are considered to be hydrothermally altered. The analogous ranges for (2Ca+Na)/Zr values in fresh and hydrothermally altered andesites are not similar. Consequently, it is likely that Ca and Na, rather than Al, were involved in hydrothermal alteration. Furthermore, Al generally has a low solubility in most hydrothermal fluids (Garrells & Christ 1965; Drever 1982; Nordstrom & Munoz 1986), and thus would not likely be added in significant amounts during hydrothermal alteration. The location of samples exhibiting evidence of hydrolysis close to the muscovite and chlorite control lines (the abscissa) on this diagram is consistent with the mineral assemblages observed in the hydrothermally altered rocks adjacent to the Hellyer deposit.

As a result, (2Ca+Na)/Al, the slope of the line between a sample point and the origin, represents a quantitative measure of the degree of hydrolysis that occurred in these rocks. It may thus be used in exploration to describe the degree of alteration and to vector toward more intense hydrothermal alteration. This measure is independent of fractionation effects, and thus is specific to hydrothermal alteration.

Some of the hydrothermally altered samples that plot below the plagioclase control line in Figure 7 also plot along or just below the dolomite and ankerite control line on Figure 8. As a result, these samples may contain, in addition to muscovite and/or chlorite, significant amounts of dolomite.

Further corroboration of the control that igneous fractionation processes have on these rocks is presented in Figures 9 and 10. These confirm the importance of anorthite, albite and clinopyroxene fractionation as controls on the compositional variation observed in fresh andesite rocks from the Hellyer footwall. On Figure 9, an (Al-2Ca)/Zr *versus* Na/Zr PER assemblage test diagram, samples have been plotted using the same symbols as Figure 7. On this diagram, addition of albite displaces rock compositions up and to the right along a line with unit slope, but the addition of anorthite has no effect. As a result, this diagram is a projection from anorthite. The strongly correlated data trend along the albite

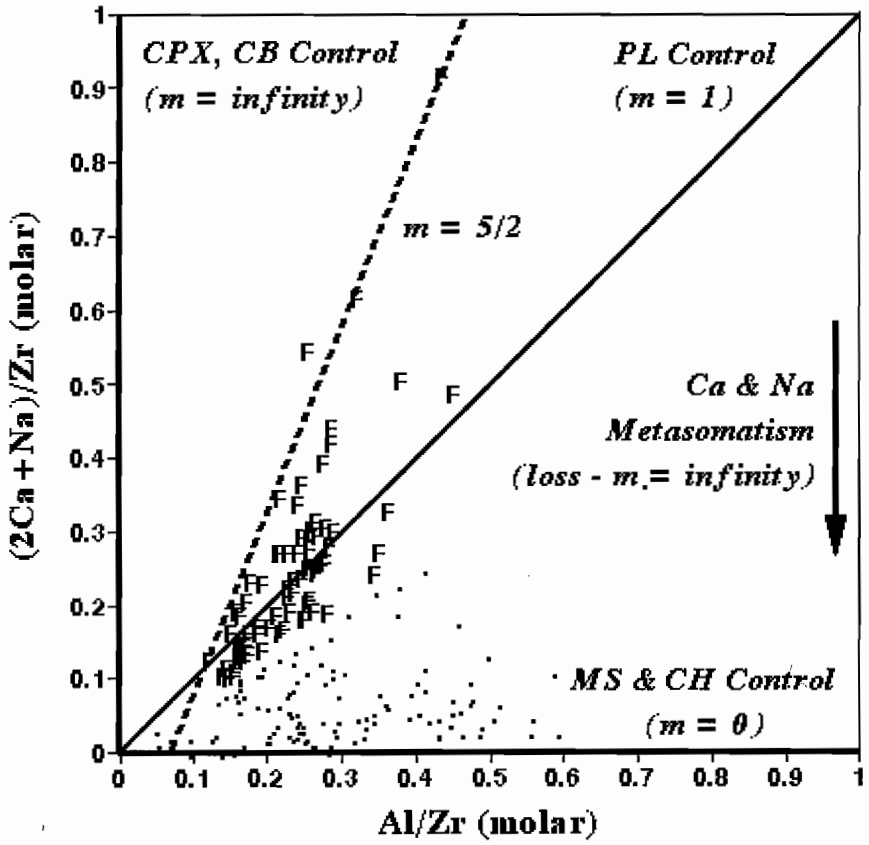

Figure 7 - Hellyer andesite footwall samples are plotted on an Al/Zr *versus* (2Ca+Na)/Zr PER assemblage test diagram. Addition of plagioclase (PL) and clinopyroxene (CPX) will displace rock compositions up and to the right along lines with slopes of unity and infinity, respectively. Furthermore, the addition of Ca-bearing carbonate veins (CB - calcite and dolomite) will displace rock compositions up along a line with infinite slope, and any Ca and Na metasomatic loss from these rocks will displace their compositions down along a line with infinite slope. Samples plotting along or significantly above the plagioclase control line (m = 1) have been labeled with "F" to denote their relatively fresh compositions. All other samples have been labeled with "." and are interpreted to be hydrothermally altered. These samples plot close to the control lines for muscovite (MS) and chlorite (CH; m = 0), the two significant alteration minerals observed in the Hellyer footwall andesites. See text for further discussion.

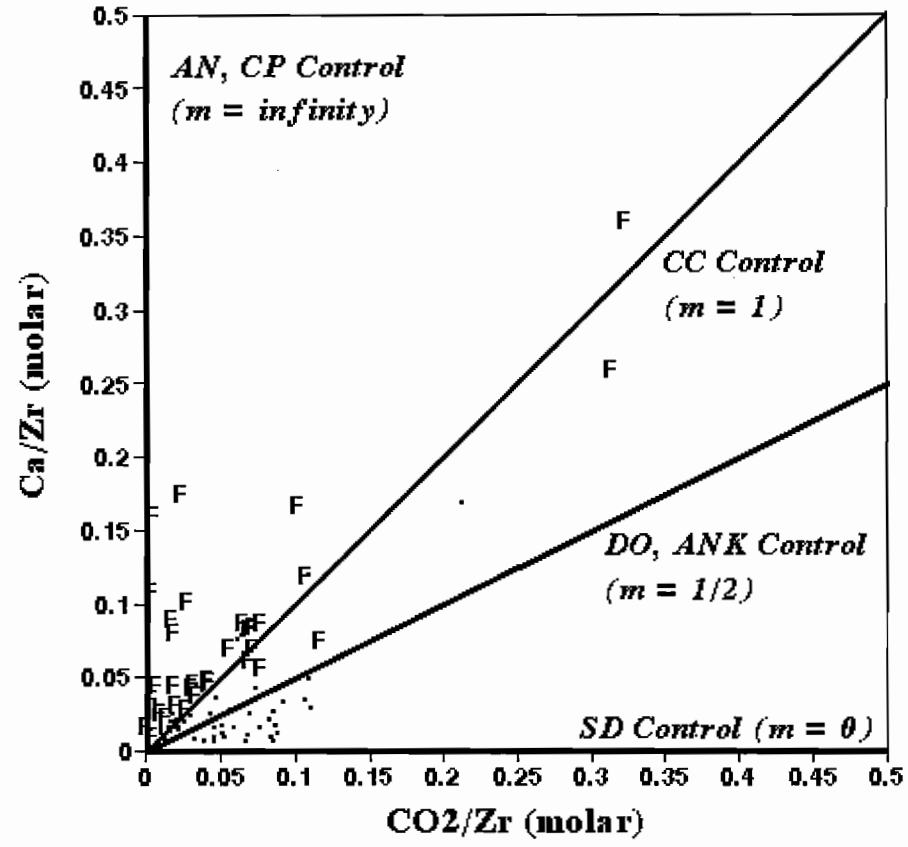

Figure 8 - Hellyer andesite footwall samples are plotted on an (Fe-S/2)/Zr *versus* Mg/Zr PER phase discrimination diagram. Addition of diopside (DI) and hedenbergite (HD) will displace rock compositions up and to the right along lines with slopes of infinity and zero, respectively. Furthermore, the addition of pyrite has no effect on this diagram because the molar subtraction of S/2 in the abscissa numerator negates the Fe contributed through pyrite addition. Finally, the addition of dolomite displaces rock compositions vertically upward. Fresh samples plot largely along a line with slope of 5/4, indicating that fractionation of clinopyroxene with an intermediate composition is likely responsible for the observed compositional variation observed in fresh andesites. Hydrothermally altered samples plot ubiquitously across the plot, indicating that they have undergone variable amounts of Fe and Mg metasomatism. See text for further discussion.

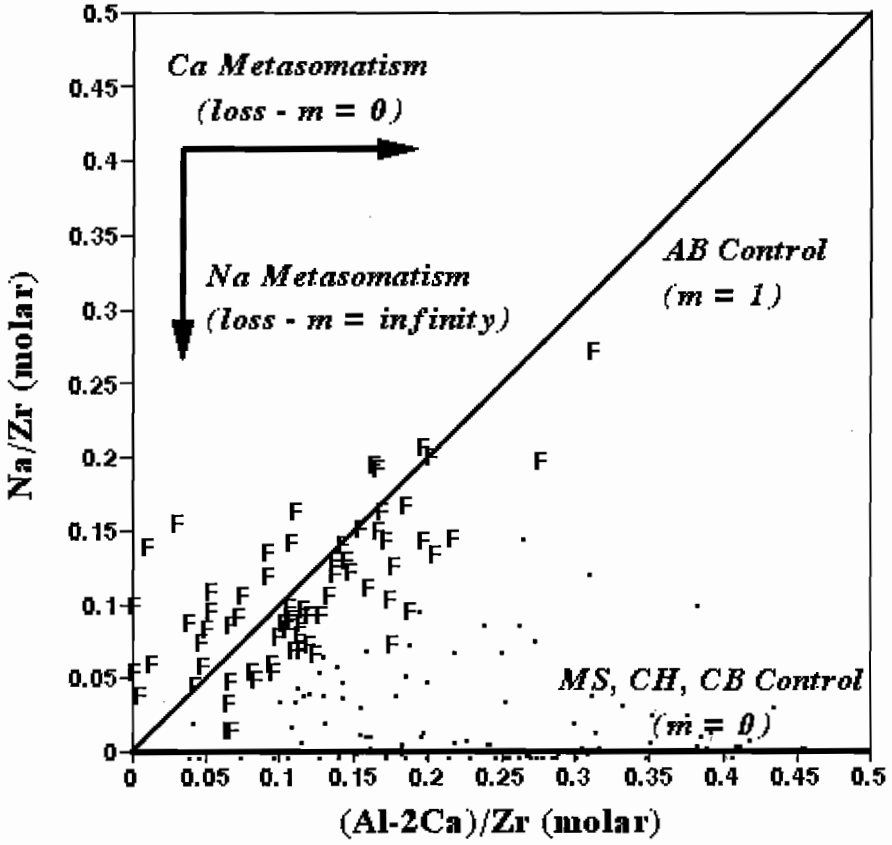

Figure 9 - Hellyer andesite footwall samples are plotted on an (Al-2Ca)/Zr *versus* Na/Zr PER assemblage test diagram. Addition of albite (AB) will displace rock compositions up and to the right along a line with unit slope. Furthermore, the addition of muscovite (MS) and chlorite (CH), and Ca-bearing carbonate veins (CB - calcite and dolomite) will displace rock compositions to the right and left along a line with zero slope, respectively. Finally, any Ca and Na metasomatic loss from these rocks will displace their compositions to the right or up along lines with slopes of zero and infinity, respectively. Fresh samples plot largely along the albite control line, confirming the control that plagioclase fractionation has on the compositional diversity of these andesites. Hydrothermally altered samples plot to the left of the albite control line along the muscovite and chlorite control lines (m = 0). Samples plotting to the right of the albite control line (m = 1) probably contain significant amounts of Ca-bearing carbonate vein material. See text for further discussion.

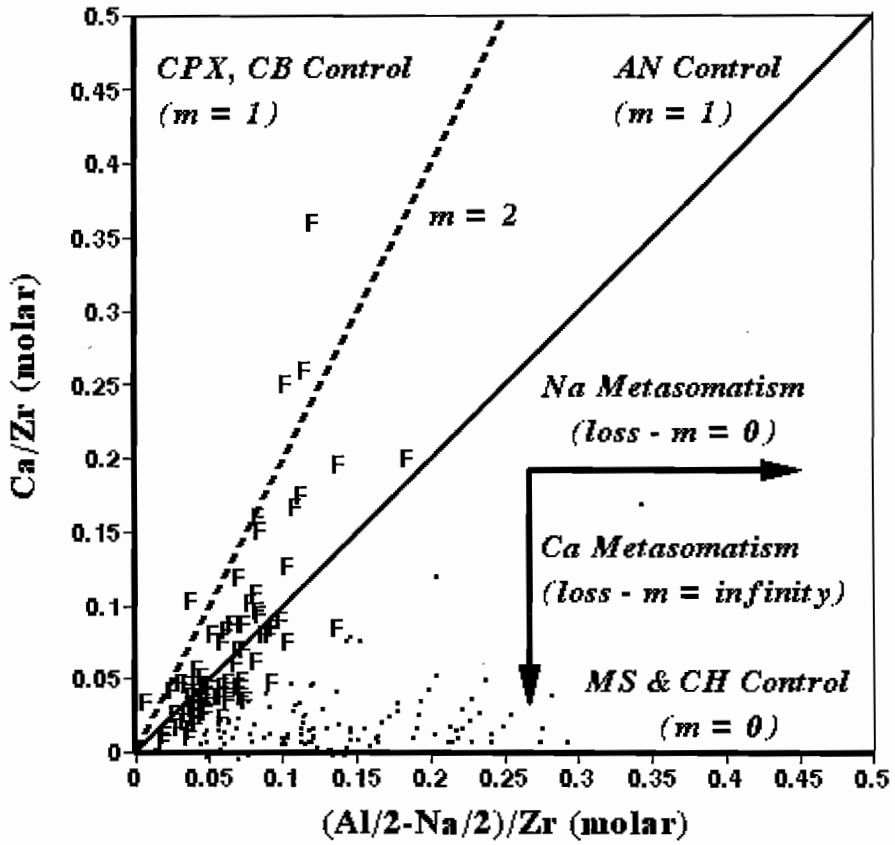

Figure 10 - Hellyer andesite footwall samples are plotted on an (Al/2-Na/2)/Zr *versus* Ca/Zr PER assemblage test diagram. Addition of anorthite (AN) will displace rock compositions up and to the right along a line with unit slope. Furthermore, the addition of muscovite (MS) and chlorite (CH), and Ca-bearing carbonate veins (CB - calcite and dolomite) will displace rock compositions up and to the right along lines with slopes of zero and infinity, respectively. Finally, any Ca and Na metasomatic loss from these rocks will displace their compositions down and to the right along lines with slopes of infinity and zero, respectively. Fresh samples plot largely along a line that is steeper than the anorthite control line, confirming the control that both plagioclase and clinopyroxene fractionation have on the compositional diversity of these andesites. Hydrothermally altered samples plot to the left of the anorthite control line along the muscovite and chlorite control lines (m = 0). See text for further discussion.

control line with unit slope reveals that albite fractionation exerts an important control on the compositional variability observed in fresh samples. Fresh samples plotting to the left of the albite control line may have undergone clinopyroxene fractionation; however, most hydrothermally altered samples plot to the right of the albite control line, indicating that they have metasomatically lost Ca and/or Na during hydrolysis. These samples contain significant amounts of muscovite and/or chlorite, and they plot along the control line for these minerals.

Fresh samples have also been plotted on the analogous PER assemblage test diagram of Figure 10, with axes of (Al/2-Na/2)/Zr *versus* Ca/Zr. On this diagram, addition of anorthite displaces rock compositions up and to the right along a line with unit slope, but the addition of albite has no effect. As a result, this diagram is a projection from albite. The fresh samples also exhibit a strongly correlated trend; however, this trend has a slope greater than unity (equal to approximately two), suggesting that clinopyroxene fractionation, along with anorthite fractionation, is also important in controlling the observed compositional variation observed in these rocks. Fresh samples plotting significantly to the left of the anorthite control line probably have undergone significant clinopyroxene fractionation. However, because many fresh samples plot directly on the anorthite control line whereas others plot significantly above it, it is possible that some andesites underwent plagioclase fractionation only, whereas other andesites underwent both plagioclase and clinopyroxene fractionation. Hydrothermally altered samples plot to the right of the anorthite control line, along the muscovite and chlorite control lines, indicating that they have likely undergone metasomatic loss of Ca and/or Na.

Other PER diagrams may be examined to determine the composition of the plagioclase and clinopyroxene involved in fractionation, and the plagioclase/clinopyroxene fractionation ratio. Specifically, Figure 11 presents a Na/Zr *versus* (Al/2-Na/2)/Zr PER phase discrimination diagram that is unaffected by (a projection from) clinopyroxene fractionation effects. On this diagram, the addition of albite and anorthite will displace rock compositions

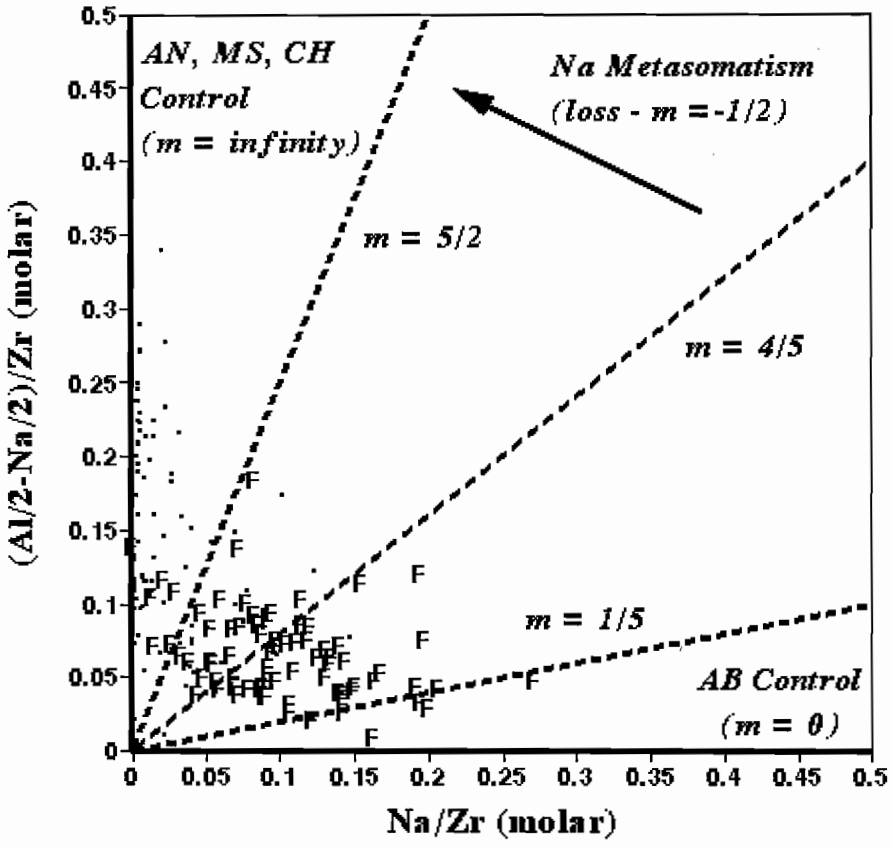

Figure 11 - Hellyer andesite footwall samples are plotted on a Na/Zr *versus* (Al/2-Na/2)/Zr PER phase discrimination diagram. Addition of anorthite (AN) and albite (AB) will displace rock compositions up and to the right along lines with slopes of infinity and zero respectively. Consequently, the addition of plagioclase of intermediate composition will displace rock compositions up and to the right along a line with slope that defines the composition of the plagioclase. The addition of muscovite (MS) and chlorite (CH) will displace rock compositions vertically upward. Finally, any Na metasomatic loss from these rocks will displace their compositions up to the left along a line with slope of -1/2. Fresh samples plot in a field bounded by lines with slopes of 1/5 and 5/2. They also exhibit a mode along a line with slope of approximately 4/5. Hydrothermally altered samples plot above and to the left of these fresh samples, indicating that they have likely lost significant Na. See text for further discussion.

up to the right along lines with slopes of zero and infinity, respectively. The addition of plagioclase of an intermediate composition will displace rock compositions up to the right along a line with positive slope, and the slope of this line can be used to determine the composition of the fractionating plagioclase by the formula :

$$X_{AN} = \frac{m}{m+1},$$

where m is the observed slope. Additionally, on this diagram, the simple metasomatic loss of Na will displace rock compositions up to the left along a line with slope of –1/2.

The fresh samples plot furthest to the right on Figure 11, indicating that they have undergone the least amount of Na loss. The field occupied by these fresh samples is bounded on its left-most edge by a line with slope of 1/5, on the right-most edge by a line with slope of 5/2, and the data exhibit a mode along a line with slope of approximately 4/5. As a result, using the formula above, the composition of plagioclase involved in fractionation in the Hellyer footwall andesite ranges from approximately X_{AN} = 0.17 (1/6) to X_{AN} = 0.71 (5/7) and exhibits a mode of approximately X_{AN} = 0.44 (4/9). Only the most sodic compositional estimate is consistent with petrographic determinations of plagioclase (albite) phenocrysts within the footwall andesite (Jack 1989; Waters & Wallace 1992; Sinclair 1994); however, this composition is not typical of plagioclase phenocrysts that occur in andesite melts (these generally have compositions ranging from X_{AN} = 0.40 to X_{AN} = 0.70). Thus, it is likely that this albitic plagioclase composition resulted from crystallization of a more calcic plagioclase that underwent fractionation, followed by Na addition during seafloor metasomatism (spilitization). This spilitization likely involved addition of Na from, and loss of Ca to, seawater as anorthite was converted into albite. These exchanges were probably balanced by Si^{+4}, provided by devitrifying volcanic glass, and Al^{+3} consumed by chlorite formation during devitrification by the reaction:

$$CaAl_2Si_2O_8 + Na^+_{(aqueous)} + Si^{+4}_{(glass)} \rightarrow NaAlSi_3O_8 + Ca^{+2}_{(aqueous)} + Al^{+3}_{(chlorite)}, \quad (-5\%)$$

where charge balance in the glass is probably accommodated through hydrolytic addition of H^+.

This reaction involves a net molar volume loss of approximately 5% (as indicated), and thus would produce voids in the plagioclase that were filled by calcite precipitated due to the Ca^{+2} liberated from anorthite (Waters & Wallace 1992). The effect of this reaction on Figure 11 is identical to that of simple Na metasomatism because the exchange of Si and Al between plagioclase and devitrifying glass would not modify the rock composition. Consequently, spilitization and Na metasomatism cannot be distinguished, but would have the opposite effect, on this diagram. Note also that the effect of this reaction on Figure 7 is to displace the rock compositions straight downward, possibly explaining why fresh samples exhibit a significantly large range in (2Ca+Na)/Al ratios.

Because a large range of (Al/2–Na/2)/Na ratios exist among the fresh samples, and because only albitic plagioclase compositions have been observed in the footwall andesite at Hellyer, it is likely that fresh samples exhibit a consistent degree of spilitization but a range in the minor intensity of hydrothermal alteration. Consequently, it is impossible to deduce the fractionating plagioclase composition because of the overprinting and ubiquitous spilitization effects. Nevertheless, the freshest rock compositions observed in the Hellyer footwall andesite define plagioclase compositions that are observed as spilitization products within these rocks.

Analogously, the (Fe–S/2)/Zr *versus* Mg/Zr PER phase discrimination diagram of Figure 12 can be used to determine the composition of clinopyroxene involved in fractionation. The addition of hedenbergite and diopside will displace rock compositions up or to the right on this diagram along lines with slopes of infinity and zero, respectively. Furthermore, the –S/2 term in the abscissa numerator of this diagram negates the Fe contributed by any pyrite in these samples. As a result, this diagram is a projection from pyrite. Relatively fresh samples (labeled "F") plot along a line with slope of approximately 5/4, which, using the above formula, indicates that the composition of clinopyroxene involved in fractionation is approximately X_{DI} = 5/9 (= 0.55). This composition is slightly more Fe-rich than that

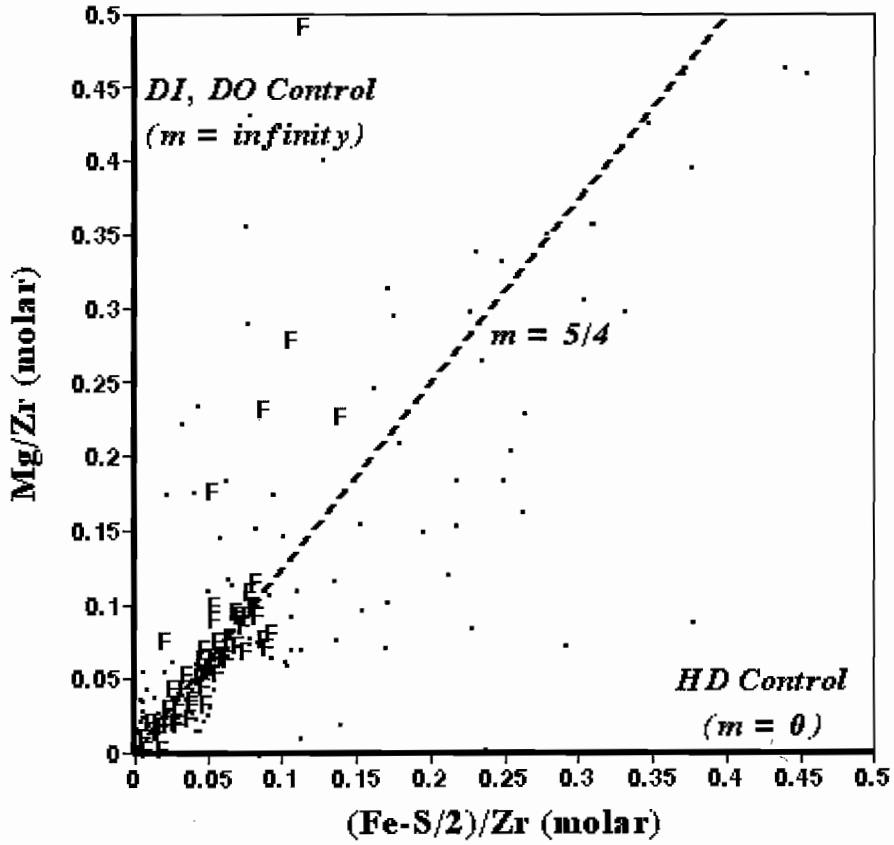

Figure 12 - Hellyer andesite footwall samples are plotted on an (Fe-S/2)/Zr *versus* Mg/Zr PER phase discrimination diagram. Addition of diopside (DI) and hedenbergite (HD) will displace rock compositions up and to the right along lines with slopes of infinity and zero, respectively. Furthermore, the addition of pyrite has no effect on this diagram because the molar subtraction of S/2 in the abscissa numerator negates the Fe contributed through pyrite addition. Finally, the addition of dolomite displaces rock compositions vertically upward. Fresh samples plot largely along a line with slope of 5/4, indicating that fractionation of clinopyroxene with an intermediate composition is likely responsible for the observed compositional variation observed in fresh andesites. Hydrothermally altered samples plot ubiquitously across the plot, indicating that they have undergone variable amounts of Fe and Mg metasomatism. See text for further discussion.

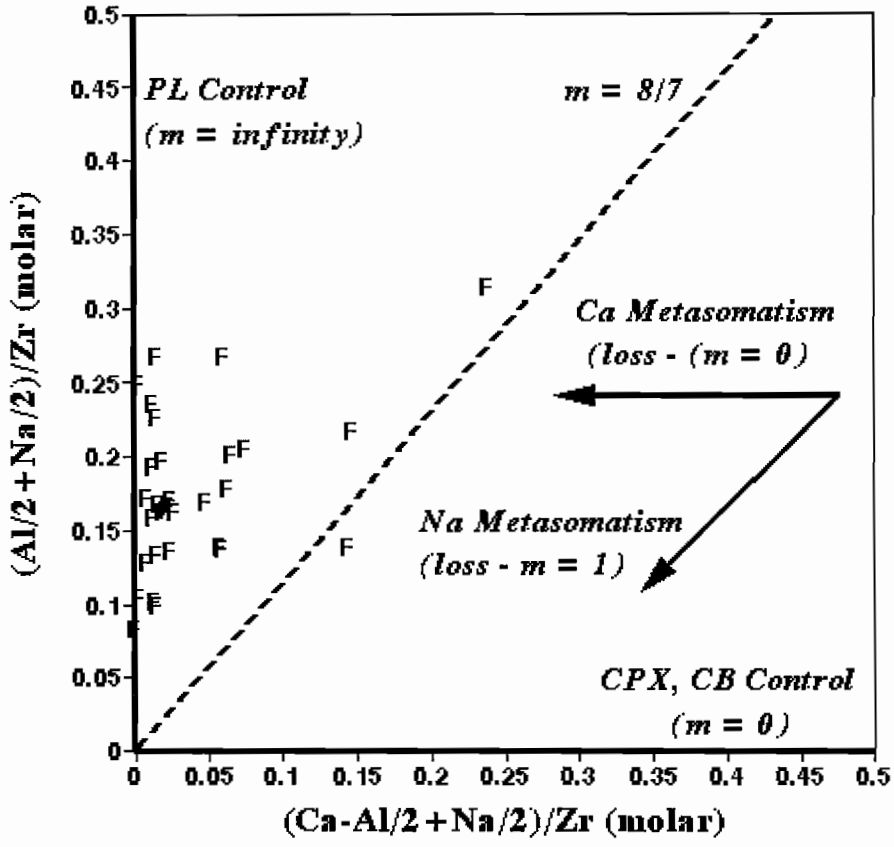

Figure 13 - Hellyer andesite footwall samples are plotted on a (Ca-Al/2+Na/2)/Zr *versus* (Al/2+Na/2)/Zr PER phase discrimination diagram. Addition of plagioclase (PL) and clinopyroxene (CPX) will displace rock compositions up and to the right on this diagram along lines with slopes of infinity and zero, respectively. Furthermore, Na metasomatic loss from these rocks will displace their compositions down to the left along a unit line. Fresh samples plot in a field bounded by a line with slope of 8/7 and the ordinate. This indicates that andesites exhibit compositional variations that can be attributed to fractionation of both plagioclase and clinopyroxene and fractionation of plagioclase only. Hydrothermally altered samples exhibit negative abscissa values, and thus do not plot on this diagram. See text for further discussion.

typically observed in the augite phenocrysts that do occur sparsely in the Hellyer footwall andesite (X_{DI} = 0.73 to 0.90; Jack 1989; Waters & Wallace 1992; Sinclair 1994). This discrepancy remains unexplained.

Some fresh samples so plot significantly above the line with slope of 5/4 defining a fractionating clinopyroxene composition, possibly corresponding to more consistent Mg-rich clinopyroxene compositions. However, these rocks contain large concentrations of CO_2, and thus likely contain significant amounts of dolomite.

Finally, the plagioclase/hedenbergite fractionation ratio can be determined by plotting the fresh samples (labeled "F") on a (Ca–Al/2+Na/2)/Zr *versus* (Al/2–Na/2)/Zr PER phase discrimination diagram (Fig. 13). On this diagram, the addition of plagioclase and clinopyroxene displace rock compositions up or to the right equal distances along lines with slopes of infinity and zero, respectively. As a result, the formula above can be used to determine the mole fraction of plagioclase and clinopyroxene involved in fractionation. Fresh samples plot in a field that is bounded on the right by a line with slope of approximately 8/7 and on the left by the ordinate. These lines define the molar plagioclase/clinopyroxene fractionation ratios suggested by the compositional variations observed in fresh andesite, which range from sub-equal plagioclase and clinopyroxene fractionation to plagioclase fractionation alone. Some fresh samples exhibit negative abscissa values, and these probably have undergone more metasomatic Ca and/or Na loss than most fresh andesites. Most hydrothermally altered samples also plot with negative abscissa values, and thus do not appear on this diagram.

Note that the sub-equal plagioclase/clinopyroxene fractionation ratio is a molar ratio, and corresponds to a 33/20 volume ratio, calculated using the molar volumes of X_{AN} = 1/6 and X_{DI} = 5/9. As a result, volume-based textural evidence indicating abundant plagioclase and occasional subordinate clinopyroxene phenocrysts that could have undergone fractionation (Jack 1989; Waters & Wallace 1992; Sinclair 1994) is consistent with the above fractionation parameter estimates.

The plagioclase/clinopyroxene fractionation ratio of 8/7, coupled with the spilitized plagioclase composition of X_{AN} = 1/6, can be used, along with vector algebra, to determine the limit of the precise effect of plagioclase and clinopyroxene fractionation on Figure 7. Addition of eight moles of anorthite, forty moles of albite, and thirty five moles of clinopyroxene (the proportions corresponding to the estimated fractionation parameters, above) will displace rock compositions up and to the right along a line with slope of 5/2 on Figure 7. This is exactly the slope of the line that bounds the field of fresh rock compositions on this plot. Thus, the spatial patterns of relatively fresh samples on Figures 7 through 13 are internally consistent, and provide consistent fractionation parameter estimates (plagioclase and clinopyroxene compositions and plagioclase/clinopyroxene fractionation ratio).

With knowledge of the compositional controls on the fresh (background) footwall andesite in the Hellyer area, recognition of the effects and quantification of the extent of hydrothermal alteration becomes far easier and more accurate. In the following section, the compositional controls in hydrothermally altered andesite are investigated, after accommodating the effects of fractionation, so that specific metrics defining the extent of the various types of alteration observed can be developed.

Hydrothermal Alteration

Alteration about many hydrothermal mineral deposits commonly involves hydrolysis. These reactions convert anhydrous minerals into phyllosilicates (*e.g.* smectites, illite, muscovite, chlorite) through the addition of H^+ and concomitant loss of alkali and alkali earth elements (*e.g.* - Ca^{+2}, Na^+, K^+). Most volcanic hosted massive sulphide deposits have footwall alteration assemblages that contain significant amounts of muscovite and chlorite. These alteration assemblages may be zoned, with muscovite on outside lateral to the deposit, and chlorite on the inside immediately beneath the deposit. As a result, both muscovite and chlorite alteration are important guides to mineralization, and identifying and quantifying their intensities may facilitate discovery of massive sulphide mineralization.

The formation of muscovite from an andesite must involve the addition of K^+. This is because fresh andesite melts do not commonly contain significant amounts of K_2O. Because muscovite alteration zones are typically mineralogically simple, consisting of

quartz, sericite and pyrite (QSP) ± Fe-bearing carbonate (ankerite or siderite), only one mineral, muscovite, commonly contains all of the K and Al in the rocks. As a result, Hellyer footwall andesite samples have been plotted on an Al/Zr *versus* K/Zr PER assemblage test diagram (Fig. 8). The addition of plagioclase and chlorite will displace rocks to the right along a line with zero slope, whereas the addition of muscovite will displace rock compositions up and to the right along a line with slope of 1/3. All samples plot generally below this muscovite control line. Most fresh samples plot close to the abscissa, indicating that their Al budgets are largely controlled by plagioclase. However, a significant number of hydrothermally altered samples also plot close to the abscissa. These samples likely contain significant amounts of chlorite. Finally, a large number of hydrothermally altered samples plot along the muscovite control line (m = 1/3). The Al and K budgets in these samples are likely controlled by muscovite, and thus these samples have been coded with an "M" symbol on this and all future diagrams. As a result, the K/Al ratio represents an accurate measure of how muscovite altered the rocks are, and may thus be used as an exploration parameter to describe degree of muscovite alteration.

Because muscovite altered rocks in volcanic hosted massive sulphide camps commonly also contains quartz, Hellyer footwall andesite samples were plotted on a Si/Zr *versus* (2Ca+3Na+K)/Zr PER assemblage test diagram (Fig. 15). On this diagram, the addition of plagioclase and clinopyroxene displace rock compositions up and to the right along a line with unit slope. As a result, Figure 15 provides a better model for primary, fractionation-related compositional variations in these rocks than Figure 7, because the effects of fractionation of both primary phenocrysts (plagioclase and clinopyroxene) in the Hellyer footwall andesite are colinear. Additionally, the inclusion of K in the ordinate numerator causes the addition of muscovite to have a different effect (up to the right along a line with slope of 1/3) than chlorite addition (to the right along a line with zero slope).

Hydrolysis will displace rock compositions downward along a line with infinite slope on this diagram. However, silicification (Si addition) will displace rock compositions to the right along a line with zero slope. As a result, muscovite and chlorite alteration and silicification serve to displace fresh rock compositions below the plagioclase and clinopyroxene fractionation line, and thus these three alteration effects, along with spilitization and carbonatization) cannot routinely be discriminated on this diagram. Because the abscissa numerator of Figure 7 is Al, which is largely immobile in most hydrothermal solutions, hydrolysis, spilitization and carbonate addition are the only alteration processes that affect Figure 7. As a result, although Figure 7 exhibits more complicated fractionation effects, it represents a better PER diagram for investigating and quantifying hydrolysis.

Most fresh andesite samples from Hellyer generally plot along or just below the plagioclase and clinopyroxene control line on Figure 15. In contrast, muscovite altered samples plot along or below the muscovite control line on Figure 15. Almost all of the remaining hydrothermally altered samples plot along the abscissa. These samples have probably undergone significant hydrolysis, and contain significant chlorite. However, some muscovite altered samples also plot along or close to the abscissa. Rather than having undergone more extensive hydrolysis through replacement of muscovite by chlorite (and the subsequent loss of K), these samples have probably been displaced below the muscovite control line (m = 1/3) by silicification.

Samples plotting close to the abscissa and exhibiting Si/Zr values greater than approximately 1.0 on Figure 15 contain significantly more Si than all but a small number of fresh samples. As a result, these samples may have undergone significant silicification. In order to evaluate the effects of this silicification, samples plotting significantly below the muscovite control line not classified as muscovite altered ("M") on Figure 14 that contain high Si/Zr values have been labeled with a "Q" (indicating that they have been silicified — they probably contain significant quartz), whereas samples plotting significantly below the muscovite control line that contain high Si/Zr values and are muscovite altered have been re-labeled with an "S" (indicating that they have been affected by sericitization and silicification). All of these samples also probably contain at least some chlorite.

Because the effect of silicification and hydrolysis

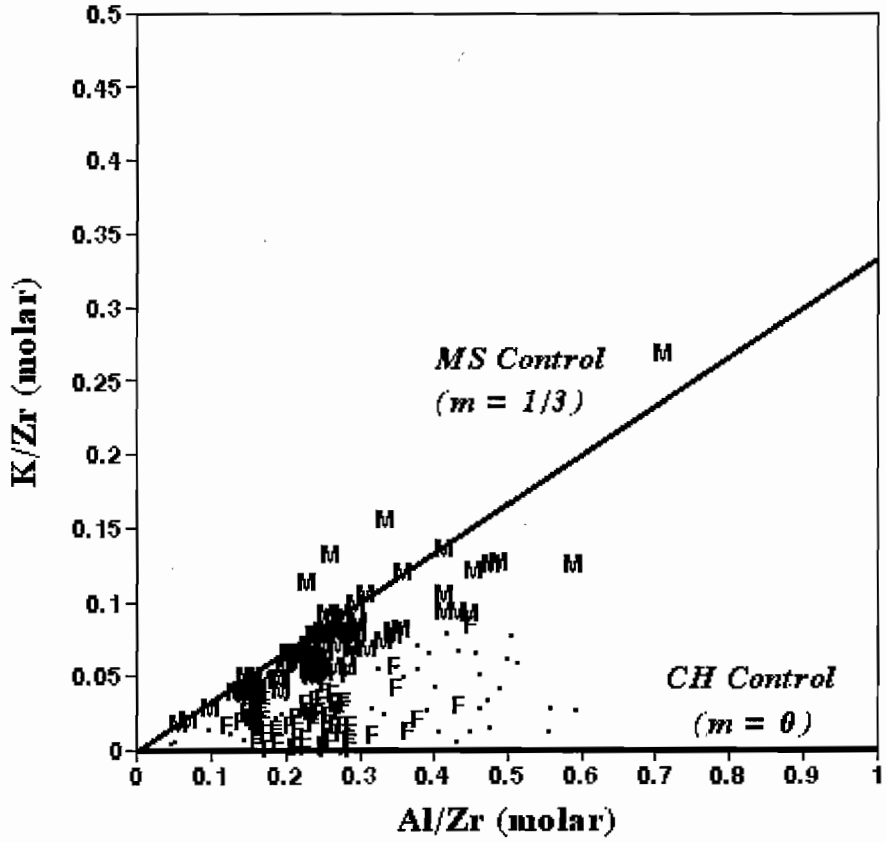

Figure 14 - Hellyer andesite footwall samples are plotted on an Al/Zr *versus* K/Zr PER assemblage test diagram. Addition of chlorite (CH), as well as plagioclase and clinopyroxene, will displace rock compositions to the right along a line with slope of zero, whereas addition of muscovite will displace rock compositions up and to the right along a line with slope of 1/3. Samples labeled "F" are identical to those presented in Figure 7, whereas samples labeled "M" plot close to the muscovite control line (M = 1/3; K/Al value > 0.20), indicating that they have undergone significant muscovite alteration. All other samples have been labeled with "." and are interpreted to be hydrothermally altered but not muscovite altered. See text for further discussion.

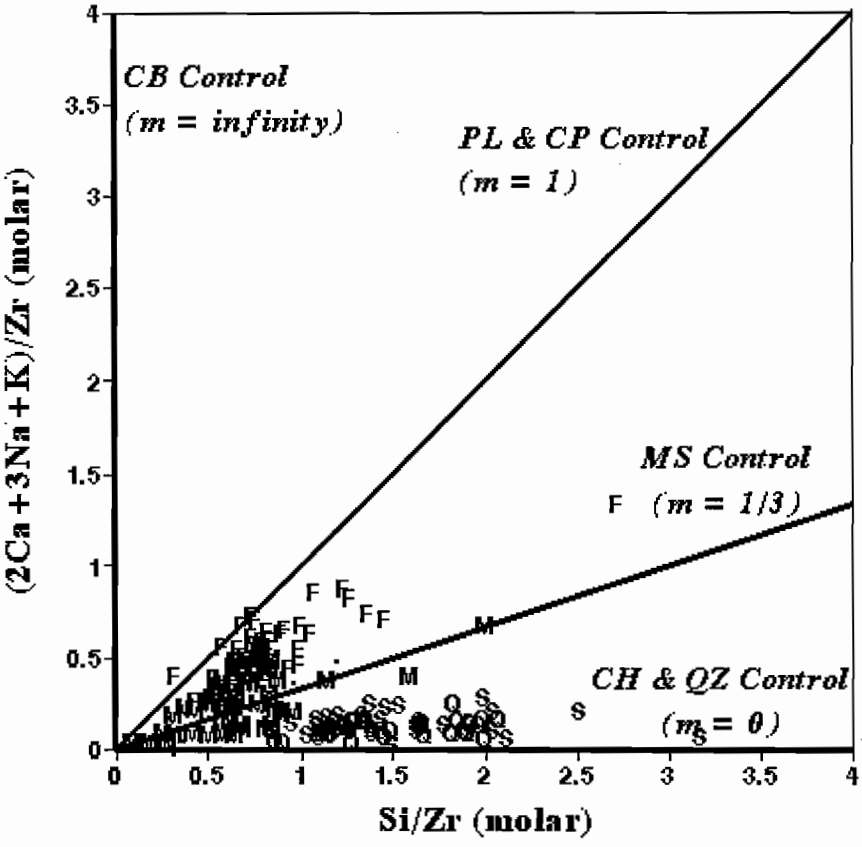

Figure 15 - Hellyer andesite footwall samples are plotted on a Si/Zr *versus* (2Ca+Na+K)/Zr PER assemblage test diagram. Addition of plagioclase (PL) and clinopyroxene (CPX) will displace rock compositions up to the right along a line with unit slope, whereas addition of muscovite (MS), chlorite (CH), Ca-bearing carbonate (CB) and quartz (QZ) will displace rock compositions up and to the right along lines with slopes of 1/3, zero, infinity and zero, respectively. Samples plotting significantly below the muscovite control line [(Si/Zr -1/2)/3 > (2Ca+3Na+K)/Zr] are either chlorite or quartz altered, and are labeled "S" (quartz ± chlorite + muscovite) and "Q" (quartz ± chlorite) depending on whether or not they contain muscovite, as defined in Figure 14. See text for further discussion.

both displace rock compositions away from the plagioclase and clinopyroxene control line on Figure 15, (2Ca+3Na+K)/Si also represents a possible metric for describing the combined hydrothermally generated effects of hydrolysis and silicification. Thus, it can also be used as an exploration parameter.

In order to further investigate any possible chloritization in these rocks, the effect of pyrite on the compositional variations observed in Hellyer footwall andesite must be assessed. As a result, samples were plotted on an Fe/Zr versus S/Zr PER assemblage test diagram (Fig. 16). On this diagram, the addition of pyrite, pyrrhotite, chlorite and clinopyroxene will displace rock compositions up and to the right along lines with slopes of two, unity, zero and zero, respectively. Most samples exhibiting significant S/Zr values plot just below the pyrite control line (m = 2), and are either classified as muscovite altered or sericitized and silicified ("M" or "S"). In contrast, most samples classified as only silicified ("Q") plot below the pyrrhotite control line (m = 1), indicating that they contain significant amounts of chlorite or other Fe-bearing mineral (ankerite, siderite or magnetite). As a result, the presence of chlorite in these silicified samples ("Q") is confirmed.

Because some samples exhibit significant S/Zr values (> 0.5), all andesite samples were plotted on an (Fe–S/2)/Zr *versus* Mg/Zr PER assemblage test diagram (Fig. 17). This diagram is a projection from pyrite, and on this diagram, addition of dolomite and magnetite will displace rock compositions vertically upward and horizontally to the right, respectively. In contrast, the addition of clinopyroxene, chlorite, ankerite and siderite will displace rock compositions up and to the right along lines with slopes defined by the Mg number [Mg# = Mg/(Fe+Mg) – molar] of these respective ferro-magnesian minerals.

Samples plot along two trends, one with a slope of approximately 10/9 and one with a slope of approximately 4. Samples plotting along the line with slope of 10/9 consist of those classified as chlorite + quartz-bearing ("Q"), muscovite-bearing ("M") and fresh ("F"). In contrast, samples yet to be classified because they do not appear to have undergone significant silicification or sericitization (".") plot along the line with slope of 4. These later samples are likely only chloritized, and it would appear that this chlorite exhibits a higher Mg number [Mg# = Mg/(Fe+Mg) – molar]. Finally, samples classified as having undergone both sericitization and silicification ("S") do not exhibit any trend on Figure 16.

Hellyer footwall andesite samples have also been plotted on an Al/Zr versus (2Ca+Na+K)/Zr PER assemblage test diagram (Fig. 18). This diagram is almost identical to that of Figure 7, except that the K in the ordinate numerator causes the effect of muscovite addition to displace rock compositions up and to the right along a line with slope of 1/3, instead of zero. Samples with the present classification define specific regions on this diagram, with fresh samples ("F") plotting highest on the diagram, muscovite altered ("M") and sericitized and silicified ("S") samples plotting along the muscovite control line, and silicified and chloritized ("Q") and chloritized (".") samples plotting along the abscissa. Because the locations of these regions differ by their ordinate values, this diagram is an effective measure of degree of hydrolysis. It readily distinguishes relatively fresh samples from muscovite altered samples from chlorite altered samples on the basis of the (2Ca+Na+K)/Al ratio (the slope of the line from each sample point to the origin). As a result, this metric [(2Ca+Na+K)/Al] represents the most robust and valuable alteration parameter for use in the Hellyer footwall andesite to quantify the degree of hydrolytic alteration.

Similarly, Hellyer footwall andesite samples have also been plotted on an (Al+2Fe+2Mg–S)/Zr versus (2Ca+Na+K)/Zr PER assemblage test diagram (Fig. 19). This diagram is almost identical to that of Figure 18, except that the abscissa numerator also contains 2Fe+2Mg–S. This ensures that the diagram is a projection from pyrite, and causes the effect of both plagioclase and clinopyroxene fractionation to be colinear, thus providing, like Figure 14 and 15, a unique representation of primary compositional variations. Samples with the present classification define specific regions on this diagram, although in contrast to Figure 18, the locations of these samples are not entirely consistent with their related control line on this diagram (they are lower), probably because of minor Fe and Mg metasomatism. Nevertheless, because the locations of these regions differ largely by their ordinate values, this diagram

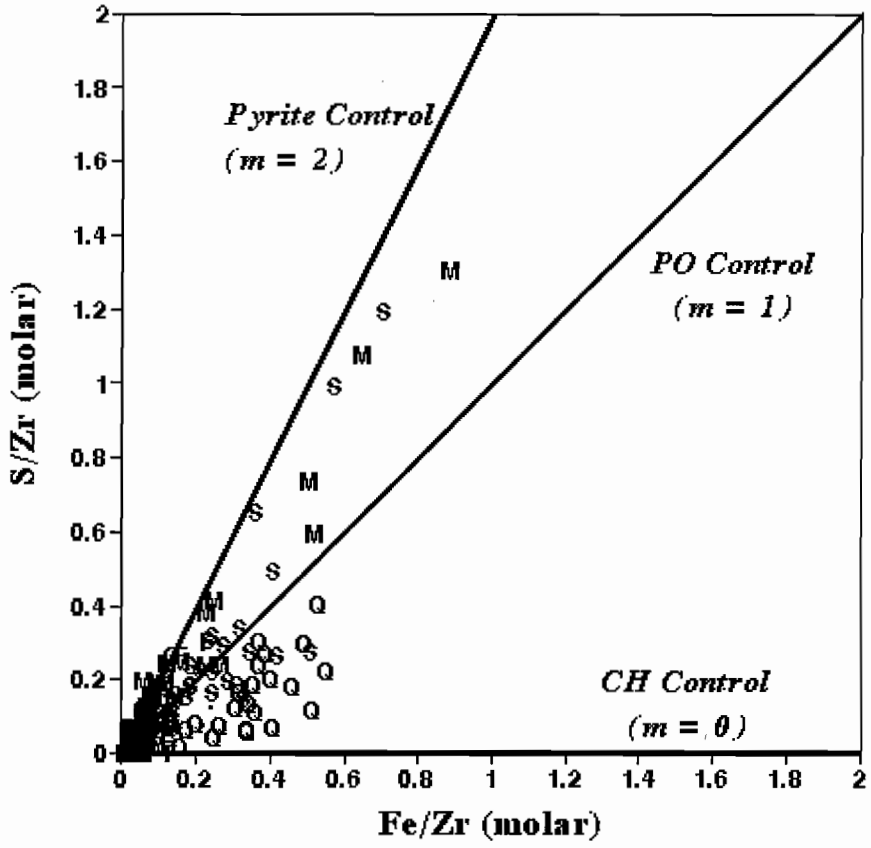

Figure 16 - Hellyer andesite footwall samples are plotted on an Fe/Zr *versus* S/Zr PER assemblage test diagram. Addition of chlorite (CH), pyrrhotite (PO) and pyrite (PY) will displace rock compositions up and to the right along lines with slopes of zero, one and two, respectively. Only samples exhibiting muscovite ("M") or sericitization and silicification ("S") exhibit significant amounts of S. Fresh samples plot largely close to the origin, indicating that they contain virtually no pyrite. Samples exhibiting silicification ('Q") plot to the right of the pyrrhotite control line, indicating that they also contain significant amounts of chlorite. See text for further discussion.

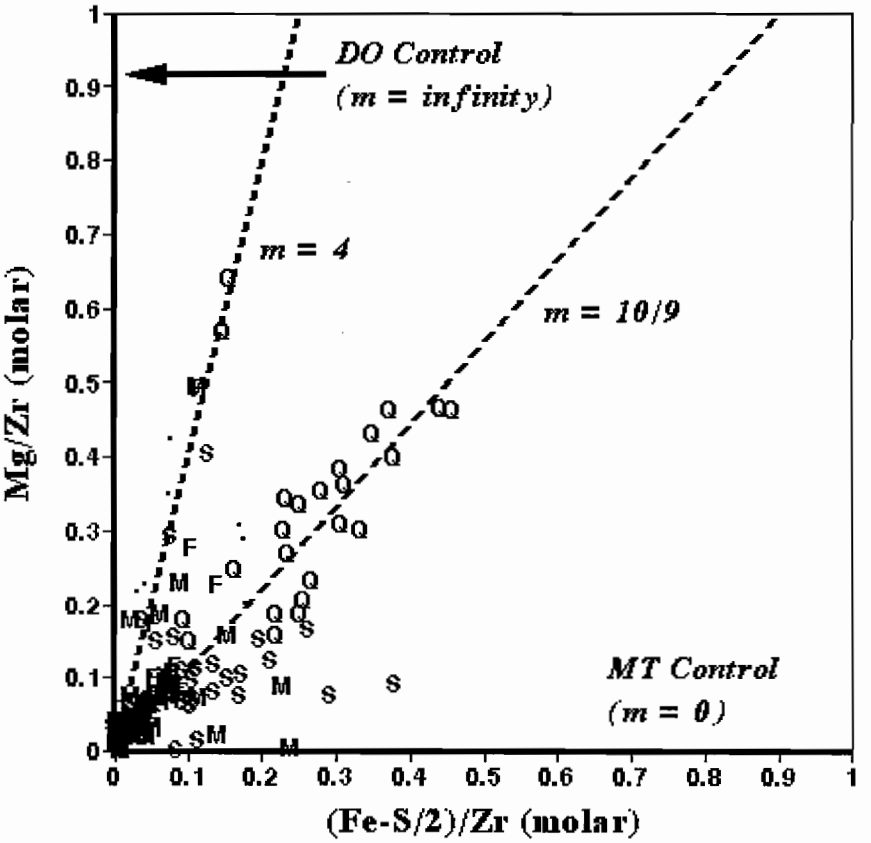

Figure 17 - Hellyer andesite footwall samples are plotted on an (Fe-S/2)/Zr *versus* Mg/Zr PER assemblage test diagram. On this diagram, the addition of dolomite (DO) and magnetite (MT) will displace rock compositions up and to the right along lines with slopes of infinity and zero, respectively. Additionally, the addition of clinopyroxene, chlorite, ankerite and siderite will displace rock compositions up and to the right along lines with slopes corresponding to the Mg number (Mg# = Mg/(Fe+Mg) - molar) of the respective ferro-magnesian mineral. Samples plotting along a line with slope of 8/7 are either silicified ("Q"), muscovite altered ("M") or fresh ("F"), whereas many samples that are altered but have yet to be classified (".") plot along a line with slope of four. These later samples are interpreted to be chloritized only and probably contain a Mg-rich chlorite. See text for further discussion.

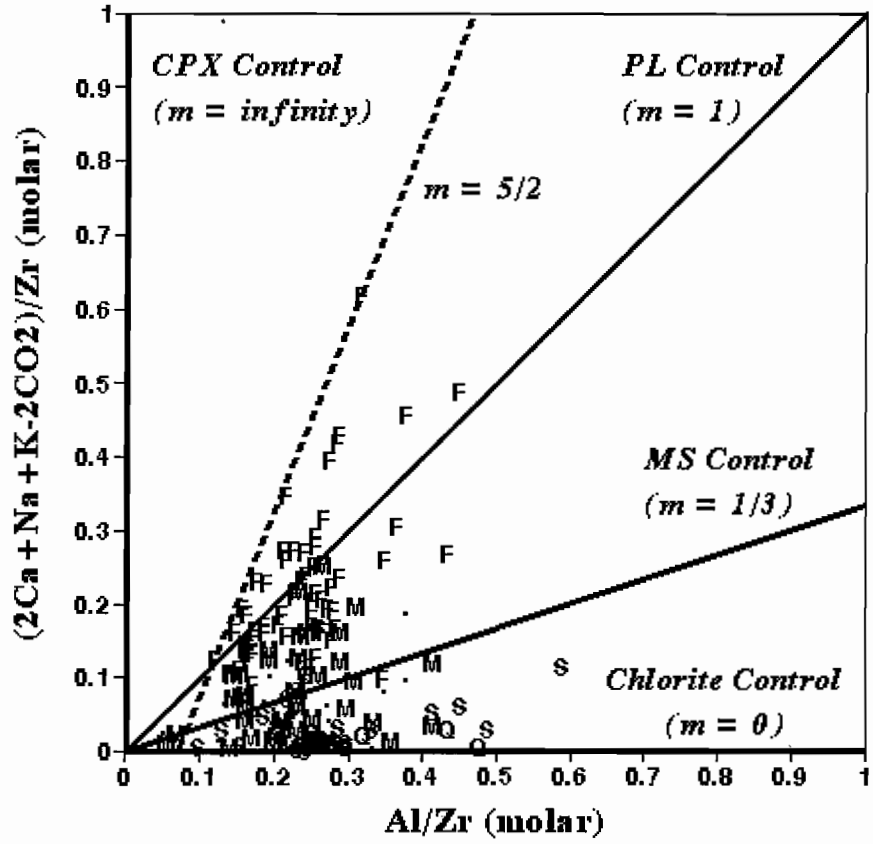

Figure 18 - Hellyer andesite footwall samples are plotted on a (2Ca+Na+K)/Zr *versus* Al/Zr PER assemblage test diagram. This diagram is identical to that of Figure 7, except that the K in the ordinate numerator causes the addition of muscovite to displace rock compositions up and to the right along a line with slope of 1/3. Fresh, muscovite altered and chlorite altered samples for a vertical array on this diagram, and because this array represents the alteration sequence commonly observed in volcanic hosted massive sulphide deposit footwall alteration zone, the slope of a line through each data point and the origin [= (2Ca+Na+K)/Al] can be used to quantify the amount of hydrolytic alteration (via two reactions - muscovite alteration of plagioclase, and chlorite alteration of muscovite). See text for further discussion.

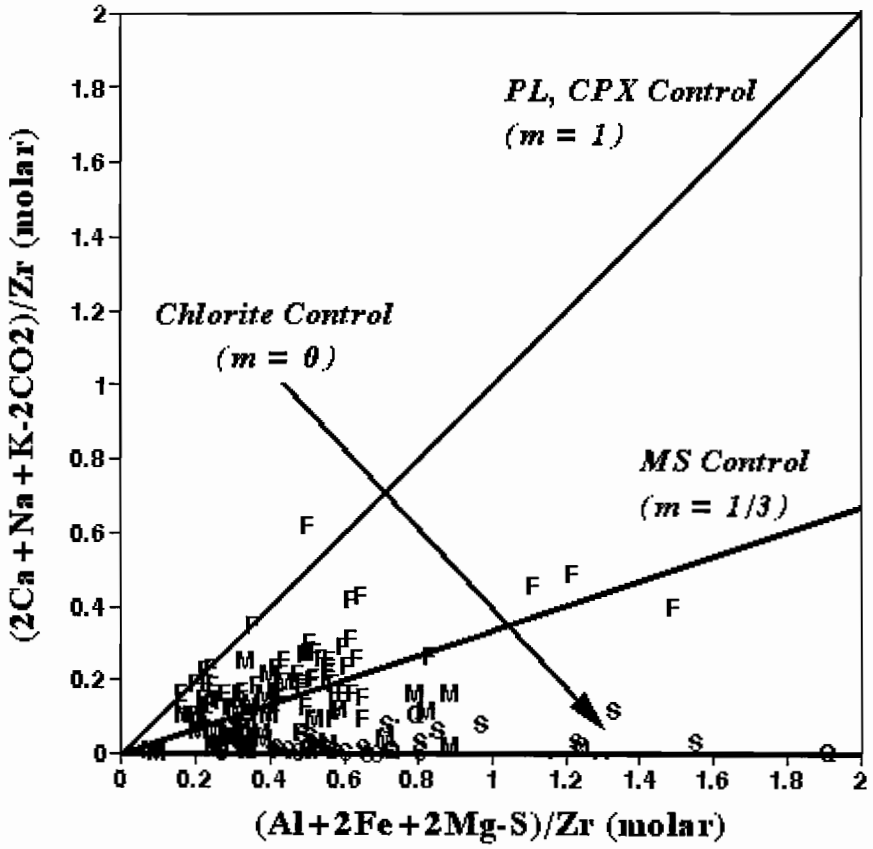

Figure 19 - Hellyer andesite footwall samples are plotted on a (2Ca+Na+K)/Zr *versus* (Al+2Fe+2Mg-S)/Zr PER assemblage test diagram. This diagram is identical to that of Figure 18, except that the 2Fe+2Mg-S has been added to the abscissa numerator. This causes the fractionation of both plagioclase and clinopyroxene to have colinear effects on the diagram (m = 1), and also ensure that the diagram is a projection from pyrite. Fresh, muscovite altered and chlorite altered samples for a vertical array on this diagram, and because this array represents the alteration sequence commonly observed in volcanic hosted massive sulphide deposit footwall alteration zone, the slope of a line through each data point and the origin [= (2Ca+Na+K)/(Al+2Fe+2Mg-S)] can be used to quantify the amount of hydrolytic alteration (via two reactions - muscovite alteration of plagioclase, and chlorite alteration of muscovite). See text for further discussion.

is also an effective measure of degree of hydrolysis. It does distinguish relatively fresh samples from muscovite altered samples from chlorite altered samples on the basis of the (2Ca+Na+K)/(Al+2Fe+2Mg–S) ratio (the slope of the line from each sample point to the origin). As a result, this metric [(2Ca+Na+K)/(Al+2Fe+2Mg–S)] represents another potential alteration parameter for use in the Hellyer footwall andesite to quantify the degree of hydrolytic alteration.

Hydrothermal Alteration Processes

A thorough investigation of the nature of hydrolytic alteration in the Hellyer footwall andesites can be undertaken by comparing the bulk measure of hydrolysis intensity [(2Ca+Na+K)/Al; the 'best' alteration metric and exploration parameter] with the additions and losses of individual elements (the simple PERs with Zr as the denominator). This has been done in Figures 20 through 24. On each of these diagrams, fresh rocks will exhibit abscissa values of unity or greater, whereas muscovite altered and chlorite altered rocks will exhibit abscissa values of approximately 1/3 and zero, respectively. Because the hydrothermal alteration zonation observed in the Hellyer footwall exhibits this mineral assemblage sequence, changes in the amount of each element during each reaction (feldspar → muscovite and muscovite → chlorite) will provide constraints that will facilitate determination and confirmation of the actual balanced alteration reaction(s) taking place.

Several distinct and consistent material transfer patterns are observed in geochemically and mineralogically related elements on Figures 20 through 24. Specifically, as fresh rocks were altered to muscovite, Na, Ca, and Sr were lost (Fig. 20), probably as a result of the destruction of plagioclase. In contrast, K, Rb and Ba were added as muscovite formed (Fig. 21). Al and Si do not appear to have been added or removed (Figs 13 and 14), so the use of Al to balance the anorthite-to-muscovite and albite-to-muscovite reactions, above is justified. Furthermore, the use of quartz, rather than a soluble Si-species, to capture the Si produced by the albite-to-muscovite reaction is also justified. Consequently, the net hydrolysis reactions :

$$3\ CaAl_2Si_2O_8 + 2\ K^+ + 4\ H^+ \rightarrow 2\ KAl_3Si_3O_{10}(OH)_2 + 3\ Ca^{+2}, \quad (-7\%)$$

and:

$$3\ NaAlSi_3O_8 + K^+ + 2\ H^+ \rightarrow KAl_3Si_3O_{10}(OH)_2 + 6\ SiO_2 + 3\ Na^+, \quad (-7\%)$$

were probably responsible for the formation of muscovite in these rocks. Note that these reactions are both volume loss reactions, thus providing open spaces that could have been filled by disseminated pyrite. Furthermore, the albite-to-muscovite reaction produces quartz, along with muscovite. As a result, these reactions, along with a direct pyrite precipitation reaction, may be responsible for the quartz-sericite-pyrite (QSP) alteration observed in the Hellyer footwall andesites.

In addition, Mg, Fe not contained in pyrite, OH, Al and Si, and minor amounts of Mn, V, Cr and Ni, were added to rocks that became chloritized (Figs 21, 22 and 24). The later four elements probably occur as trace constituents in chlorite, and thus their additions were controlled by how much chlorite formed.

The addition of Si and Al does not occur in many chloritic VHMS alteration zones (Stanley & Madeisky 1994; Madeisky & Stanley 1993; Robinson et al. 1995), especially given the fact that an aluminosilicate mineral, muscovite, was destroyed and could have provide the required Al and Si. If these elements were not added at Hellyer, the expected muscovite-to-chlorite reaction, balanced on Al and by quartz, would be :

$$4\ KAl_3Si_3O_{10}(OH)_2 + 6\ SiO_2 + 30\ (Fe,Mg)^{+2} + 48\ H_2O \rightarrow 3\ (Fe,Mg)_{10}Al_4Si_6O_{20}(OH)_{16} + 4\ K^+ + 56\ H^+ . \quad (+52\ /\ +94\%)$$

This reaction involves a substantial volume increase of 52 to 94%, depending on the Mg# [Mg/(Fe+Mg)] of the chlorite produced. However, given that both Al and Si were added during chlorite formation, it is likely that the above rection proceeded to completion, and then additional chlorite formed by direct precipitation from the hydrothermal fluid by the reaction :

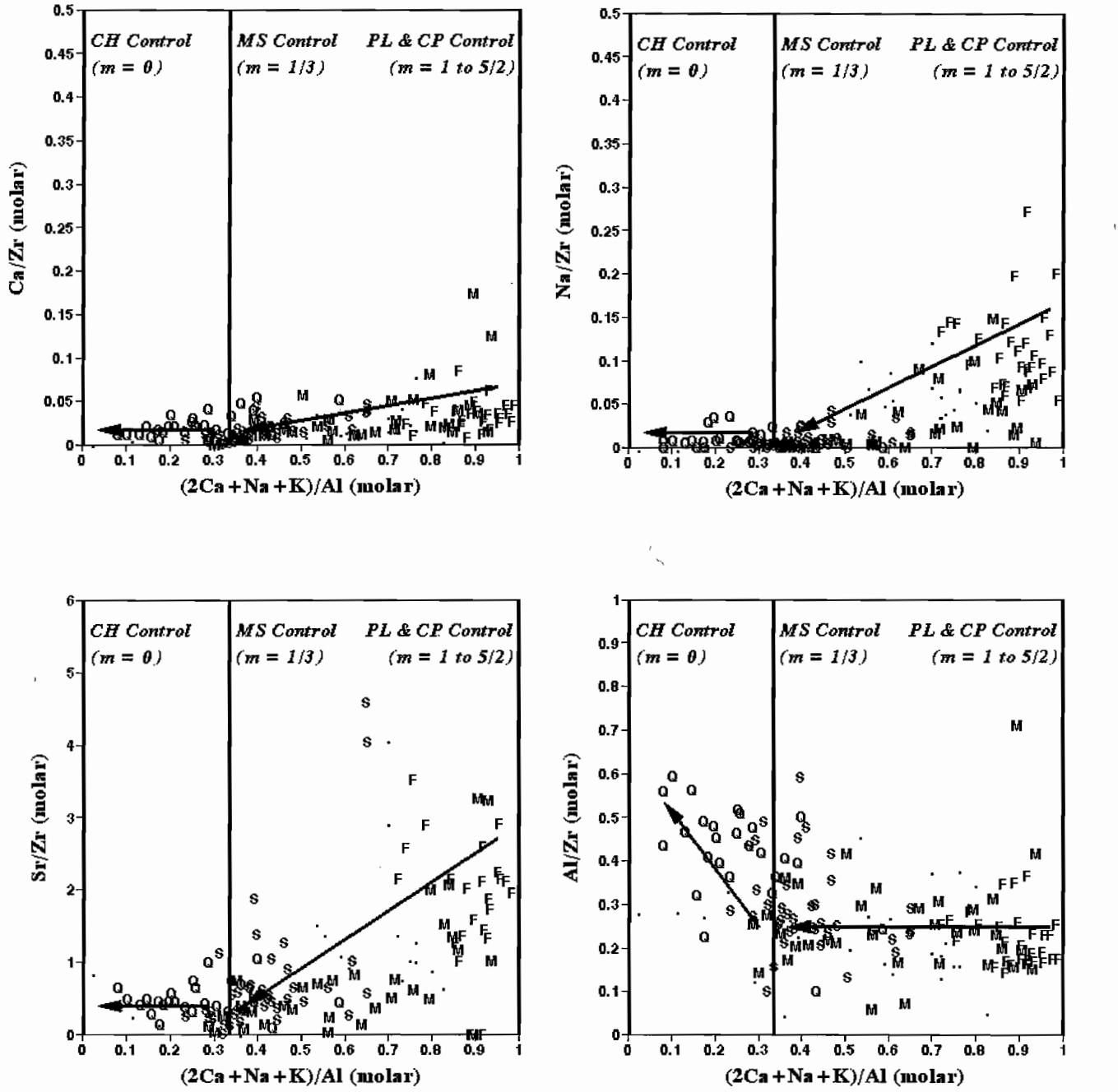

Figure 20 - Hellyer andesite footwall samples are plotted on four PER diagrams with (2Ca+Na+K)/Al on the abscissa and Ca/Zr (A), Na/Zr (B), Sr/Zr (C) and Al/Zr (D) on the ordinates. Symbols are those used in Figure 18. These diagrams compare the additions and losses of the ordinate numerator elements with the degree of hydrolysis, as defined by the slope of lines through samples and the origin on Figure 18. Fresh samples plot close to abscissa values of unity, whereas muscovite altered and chlorite altered samples plot close to abscissa values of 1/3 and zero, respectively. These plots demonstrate that Na and subordinate Ca are lost as the rocks altered to muscovite, and that they are completely absent from the rocks during chlorite alteration. Sr exhibits a similar pattern, probably because it resided predominantly in plagioclase and was lost during plagioclase destruction. Al was neither added nor lost during muscovite alteration; however, some Al addition appears to have occurred during subsequent chloritization. See text for further discussion.

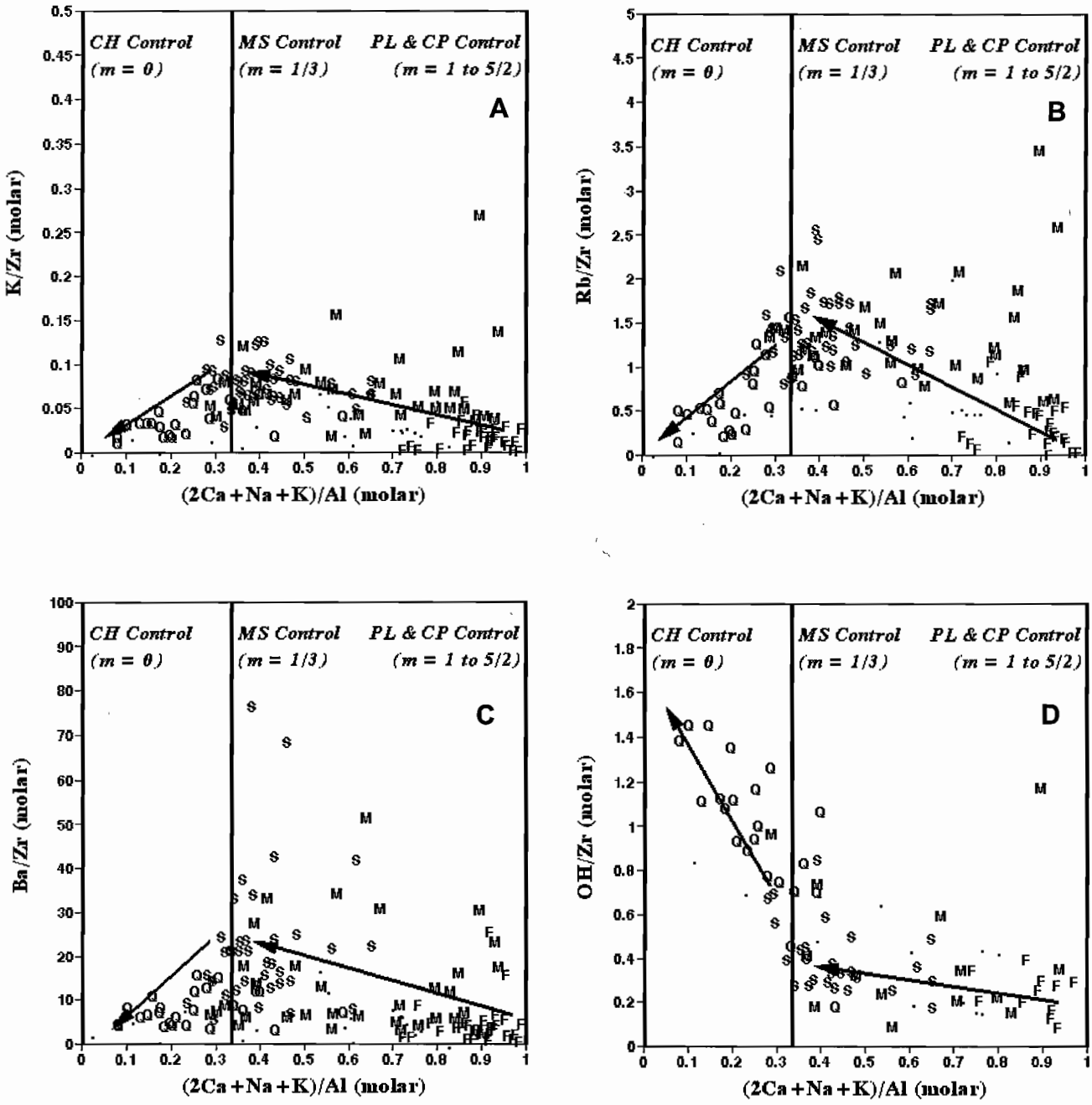

Figure 21 - Hellyer andesite footwall samples are plotted on four PER diagrams with (2Ca+Na+K)/Al on the abscissa and K/Zr (A), Rb/Zr (B), Ba/Zr (C) and OH/Zr (D) on the ordinates. Symbols are those used in Figure 18. These diagrams compare the additions and losses of the ordinate numerator elements with the degree of hydrolysis, as defined by the slope of lines through samples and the origin on Figure 18. Fresh samples plot close to abscissa values of unity, whereas muscovite altered and chlorite altered samples plot close to abscissa values of 1/3 and zero, respectively. These plots demonstrate that K was added during muscovite alteration and subsequently lost during chlorite alteration. Similar patterns for Rb and Ba also exist, as these probably resided in muscovite, and thus their abundances were controlled by the amount of muscovite present. Moderate OH was added during muscovite alteration, and substantial OH was added during chloritization. See text for further discussion.

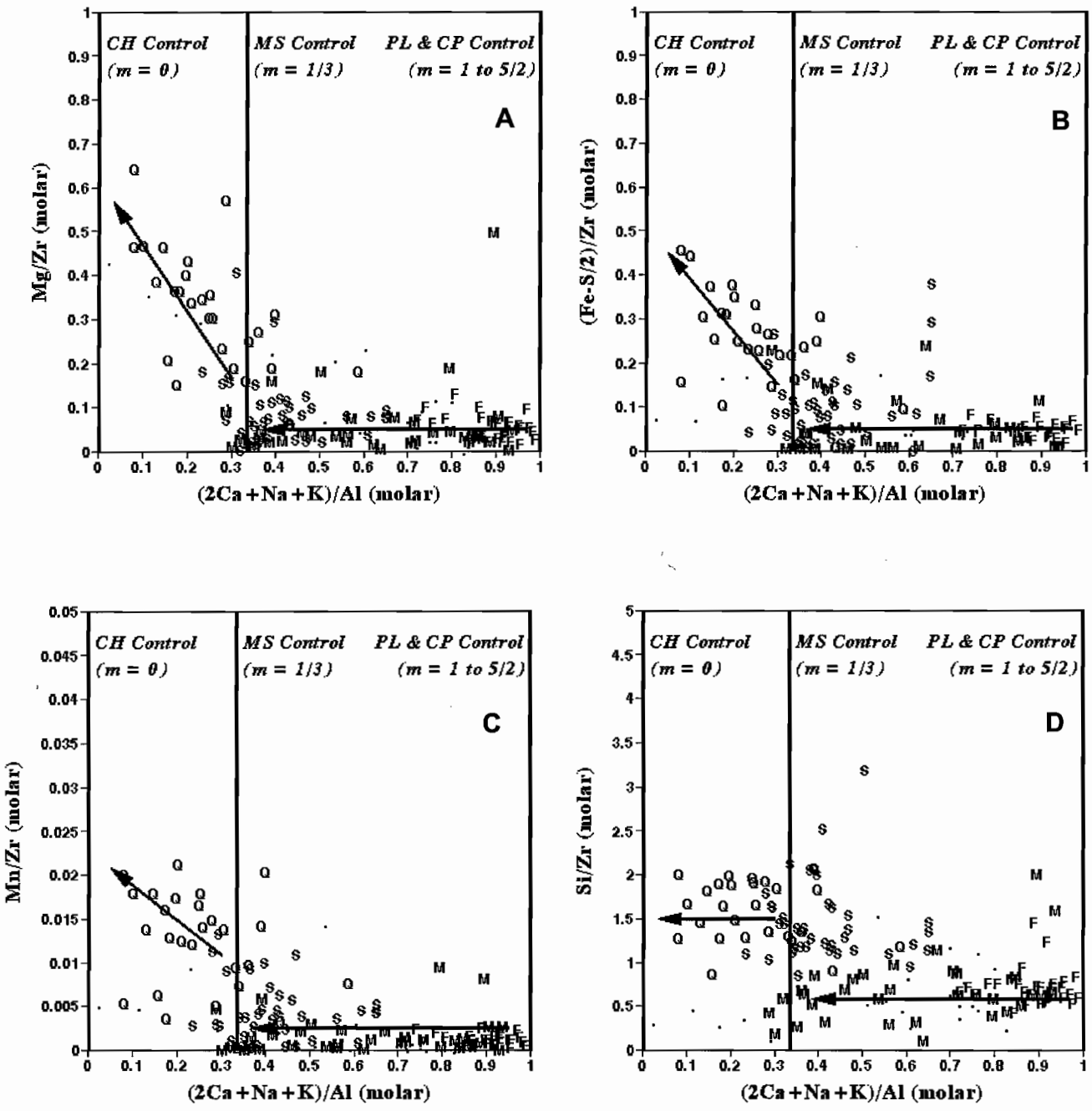

Figure 22 - Hellyer andesite footwall samples are plotted on four PER diagrams with (2Ca+Na+K)/Al on the abscissa and Mg/Zr (A), (Fe-S/2)/Zr (B), Mn/Zr (C) and Si/Zr (D) on the ordinates. Symbols are those used in Figure 18. These diagrams compare the additions and losses of the ordinate numerator elements with the degree of hydrolysis, as defined by the slope of lines through samples and the origin on Figure 18. Fresh samples plot close to abscissa values of unity, whereas muscovite altered and chlorite altered samples plot close to abscissa values of 1/3 and zero, respectively. These plots demonstrate that Mg, Fe-S/2 (the Fe not in pyrite) and Mn were substantially added only during chlorite alteration. The addition of significant Si occurred during this chloritization (probably as veins), and subtle Si addition occurred during muscovite alteration. Note that the addition of Si does not mean that quartz formed. See text for further discussion.

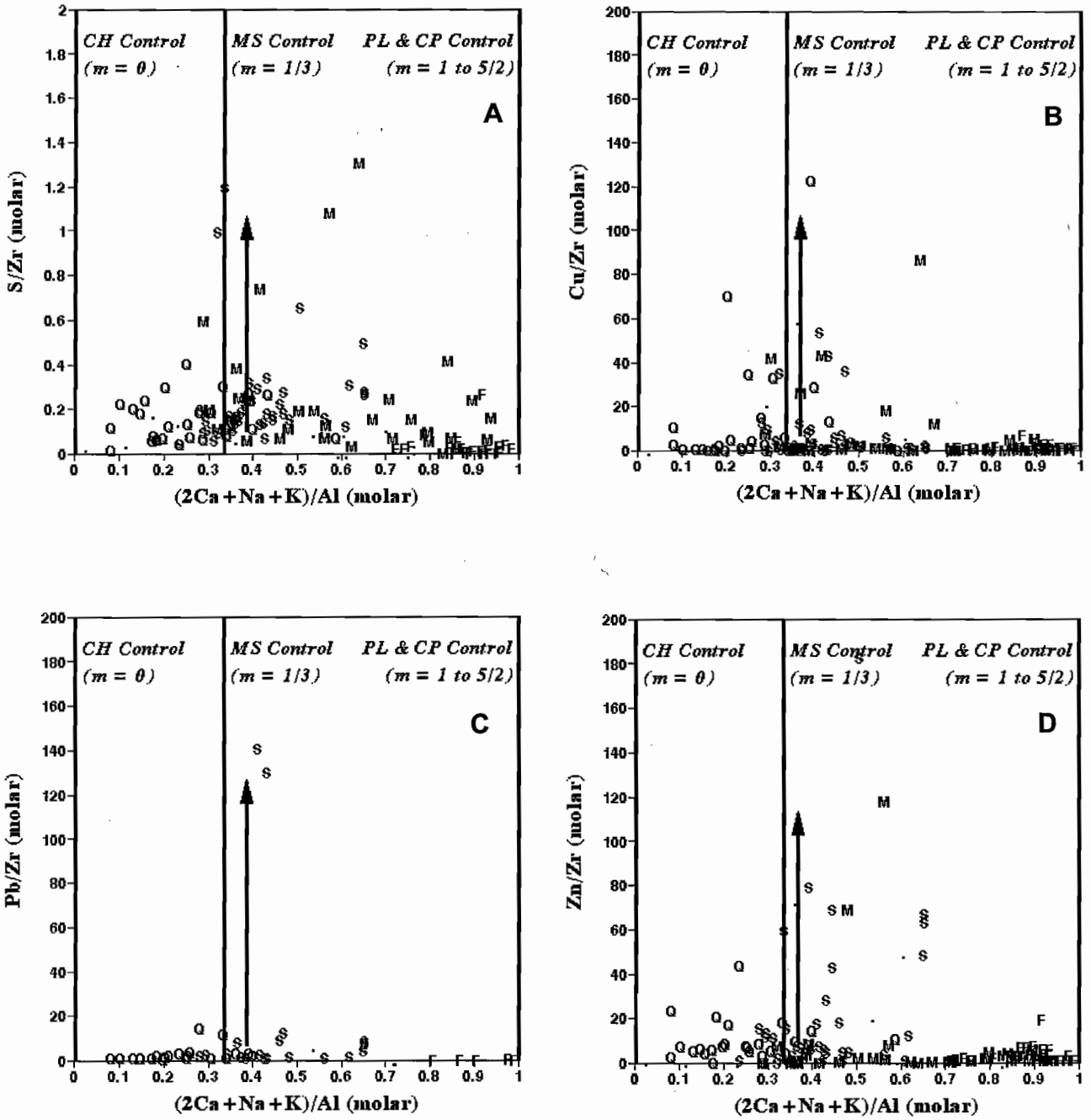

Figure 23 - Hellyer andesite footwall samples are plotted on four PER diagrams with (2Ca+Na+K)/Al on the abscissa and S/Zr (A), Cu/Zr (B), Pb/Zr (C) and Zn/Zr (D) on the ordinates. Symbols are those used in Figure 18. These diagrams compare the additions and losses of the ordinate numerator elements with the degree of hydrolysis, as defined by the slope of lines through samples and the origin on Figure 18. Fresh samples plot close to abscissa values of unity, whereas muscovite altered and chlorite altered samples plot close to abscissa values of 1/3 and zero, respectively. These plots demonstrate that the addition of S, Cu, Pb and Zn is sporadic with respect to degree of hydrolysis, but does appear to be more prevalent in muscovite altered rocks. No gradational addition or loss of these elements is observed with degree of hydrolysis, in contrast to the other element material transfers presented above. See text for further discussion.

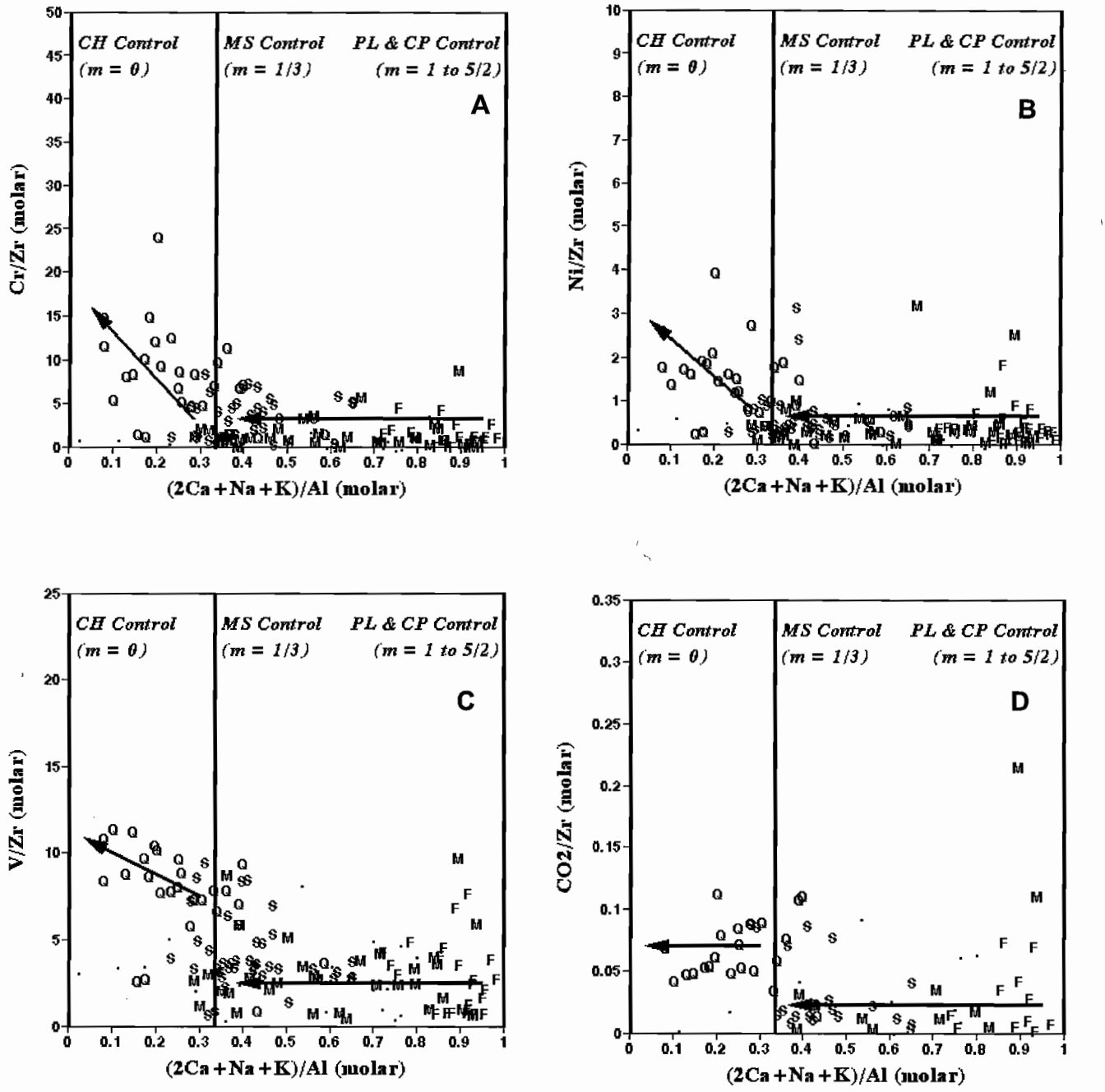

Figure 24 - Hellyer andesite footwall samples are plotted on four PER diagrams with (2Ca+Na+K)/Al on the abscissa and Cr/Zr (A), Ni/Zr (B), V/Zr (C) and CO_2/Zr (D) on the ordinates. Symbols are those used in Figure 18. These diagrams compare the additions and losses of the ordinate numerator elements with the degree of hydrolysis, as defined by the slope of lines through samples and the origin on Figure 18. Fresh samples plot close to abscissa values of unity, whereas muscovite altered and chlorite altered samples plot close to abscissa values of 1/3 and zero, respectively. These plots demonstrate that Cr, Ni and V are added to the rocks during chloritization, and that CO_2 is abundant only in fresh rocks, and in chloritized rocks. See text for further discussion.

$$4\ Al(OH)_2^+ + 6\ H_4SiO_4^\circ + 10\ (Fe,Mg)^{+2} + 4\ H_2O \rightarrow (Fe,Mg)_{10}Al_4Si_6O_{20}(OH)_{16} + 24\ H^+ .\quad (+\infty\%)$$

This reaction also requires a significant volume increase. Thus, these two chlorite-forming reactions could only have taken place where open space was made available, either through tectonic expansion or dissolution of other rock components. Unfortunately, no major element except K was lost during this reaction, and thus it is likely that tectonic expansion provided the open space to facilitate chlorite formation. This may explain why chlorite altered rocks occur proximal to the Jack fault at Hellyer. Tectonic forces causing dilation along this fault may have produced the open spaces, especially close to the seafloor, that were filled quartz, sulphide and carbonate veins, and by chlorite via the above reactions.

The substantial addition of OH during chloritization, relative to the moderate amount of OH added during muscovite alteration, is consistent with the stoichiometry of both the plagioclase-to-muscovite and these two hypothesized chlorite-forming reactions.

The addition of S, Cu, Pb and Zn (Fig. 23) appears to be unrelated to the degree of hydrolysis, but does occur most often in rocks that are muscovite altered. As a result, this chalcophile element association suggests that sulphide precipitation was largely restricted to muscovite-stable rocks. Muscovite altered rocks underwent moderate volume losses associated with their formation from plagioclase, so these sulphide minerals (pyrite, and possibly chalcopyrite, galena and sphalerite) probably filled the pores produced during these earlier reactions.

However, the core alteration zone at Hellyer consists of a siliceous pipe with muscovite alteration (rather than chlorite alteration). As a result, these base metal additions also occur in rocks that also underwent volume losses during formation. Consequently, sulphide precipitation within sericitized and silicified rocks ("S") probably took place in the voids produced as chlorite altered to muscovite.

Finally, CO_2 appears to have been added in both fresh and chloritized rocks. The carbonate in fresh rocks probably was introduced during the thermal event as calcite veins associated with regional Devonian granite intrusion. Hydrothermally altered rocks probably were not strong enough to fracture brittley to allow formation of these quartz veins, so CO_2 addition in hydrothermally altered rocks was probably restricted to those zones where carbonate minerals were part of the alteration assemblage, and do not occur in veins. Chloritized rocks exhibit CO_2 addition, probably because chlorite plus dolomite assemblages are common in upper part of the chlorite alteration zone (Gemmell & Large 1992).

Geographic distribution of hydrothermal alteration

The above set of net hydrothermal reactions are consistent with the individual element material transfers that occurred during hydrothermal alteration. As a result, predictable major oxide and trace element compositions exist in each alteration zone. The geographic distribution of these alteration zones is investigated in Figures 25 through 30. These distributions have been represented as bubbleplots of the simple PERs to provide some insight into where significant addition and loss of the various elements took place.

Results are entirely consistent with the alteration zoning observed by Gemmell & Large (1992) in the Hellyer footwall andesites. Figure 25 presents the spatial distribution of the samples, and the lithogeochemical classification developed from Figures 7, 14 and 15. Predominantly fresh rocks occur outside the visible alteration zone, whereas sericitized, chloritized and silicified rocks occur within it. Figures 26 through 30 present bubbleplots for the major and trace elements under consideration. Unfortunately, these do not resolve the fine-scale alteration zoning observed by Gemmell & Large (1992), largely because of the lack of detailed sampling geometries within the alteration zone. Nevertheless, all alteration styles are recognizable within the alteration pipe, in various locations, at Hellyer.

Several patterns not previously described are also evident in these plots. Specifically, anomalous amounts of calcite, as defined by Ca and CO_2 additions (Fig. 26A, D), occur exactly on the margin of the alteration pipe in both drill cores that cut this boundary. Additionally, V (Fig. 29D) appears to have been added throughout the alteration pipe, possibly because it resides in both chlorite and muscovite,

substituting for Al because of its V^{+3} valence state. Finally, enrichment of base metals (Fig. 30B, C, D) is highly sporadic within the alteration zone, and thus should probably not be relied on to indicate the presence of massive sulphide at the top of any newly discovered alteration pipe.

In the above investigation of hydrothermal alteration, several parameters were identified that represent potential exploration parameters. These are presented in Figure 31 through 35, and all respond in predictable ways to the observed presence of hydrothermal alteration. However, (2Ca+Na)/Al, (2Ca+Na+K)/Al and (2Ca+3Na+K)/Si all exhibit anomalous values outside the visible alteration zone near the contact between the footwall andesite and hangingwall basalt. These anomalies occur at the 'productive' horizon, and may reflect hydrothermal alteration near the seafloor after lateral migration of hydrothermal fluid out of the alteration zone. As a result, these exploration parameters define the location of the productive horizon, and may be indicative of proximal accumulations of VHMS mineralization.

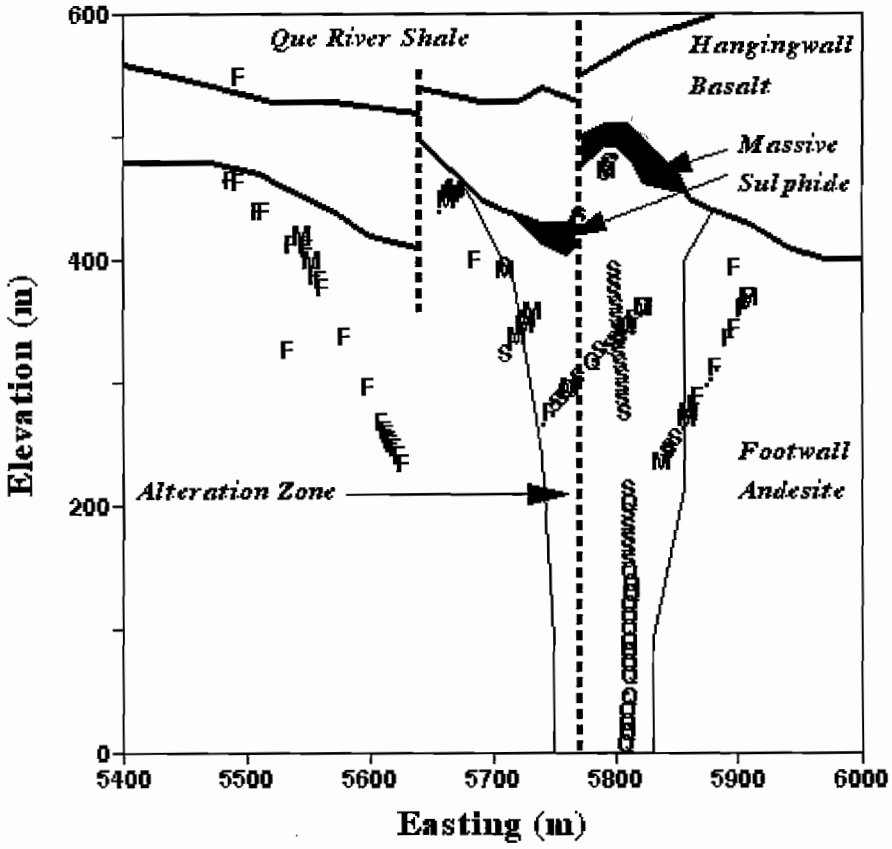

Figure 25 - Hellyer andesite footwall samples are plotted on an east-west cross-section at 10,750 m N to illustrate the distribution of element additions and losses that occurred during hydrothermal alteration. Symbols used are those of Figure 18. Geological contacts and alteration zone boundaries are based on Jack (1989) but have been modified to be consistent with the alteration zoning interpretation presented in the following figures. Results demonstrate a zoning sequence, from outside to inside, of fresh andesite ("F"), muscovite altered andesite ("M"), chloritized andesite ("Q"), and sericitized and silicified andesite ("S"). These correspond to the textural-mineralogical zoning sequence of Gemmell : fresh ("F"), stringer envelope zone ("M"), sericite zone ("M"), chlorite zone ("Q") and siliceous zone ("S"). See text for further discussion.

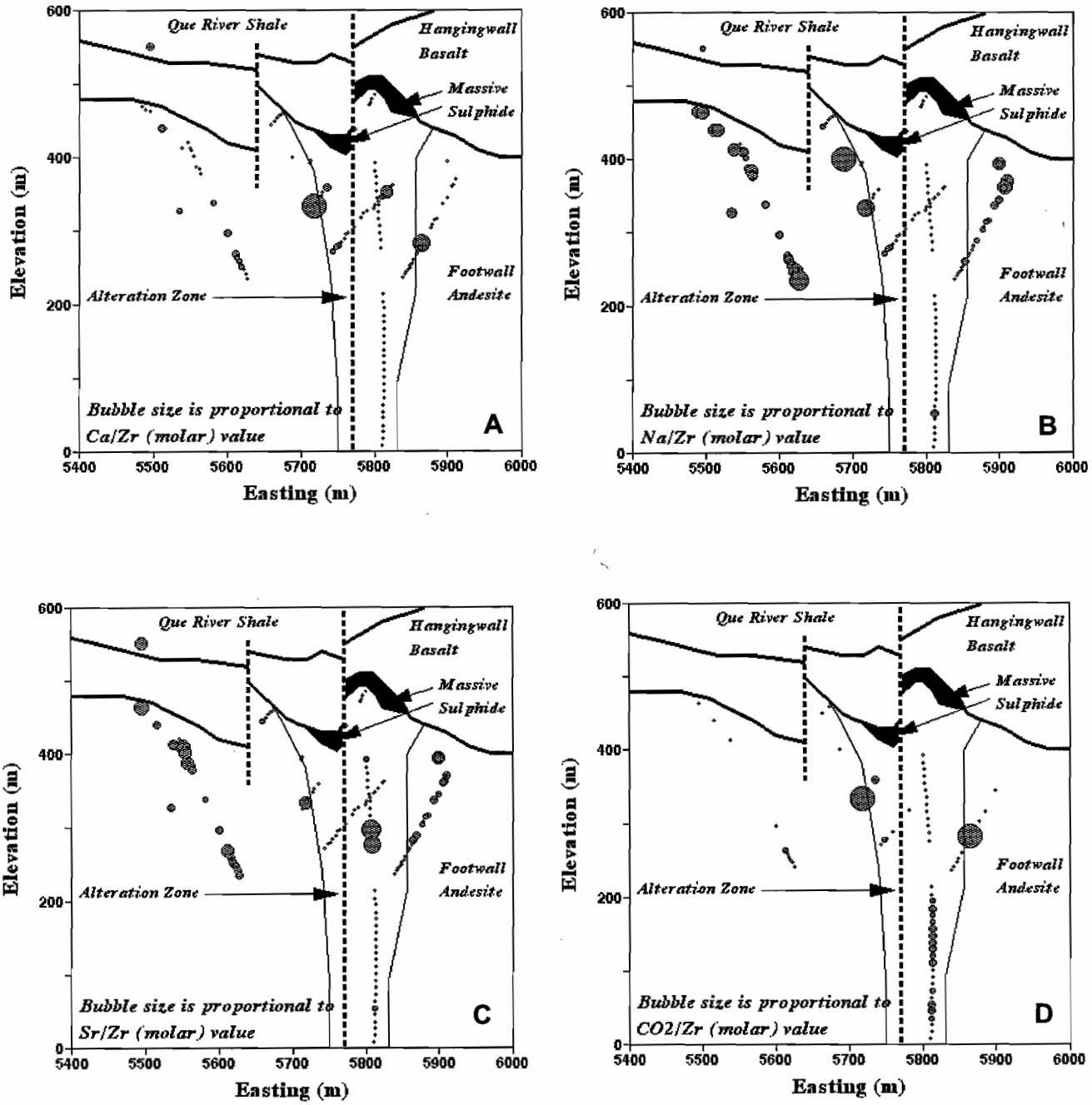

Figure 27 - Hellyer andesite footwall samples are plotted on an east-west cross-section at 10,750 m N to illustrate the distribution of element additions and losses that occurred during hydrothermal alteration. Bubble sizes are proportional to K/Zr (A), Rb/Zr (B), Ba/Zr (C) and Al/Zr (D). Geological contacts and alteration zone boundaries are based on Jack (1989) but have been modified to be consistent with the alteration zoning interpretation presented herein. K, Rb, and Ba were added to rocks at the margin of the alteration zone, but do not occur within chloritized rock closer to the core of the zone. Al is relatively constant in fresh rocks and the outer margins of the alteration zone, but has been added to rocks deep within the core of the alteration zone in regions that have been chloritically altered. See text for further discussion.

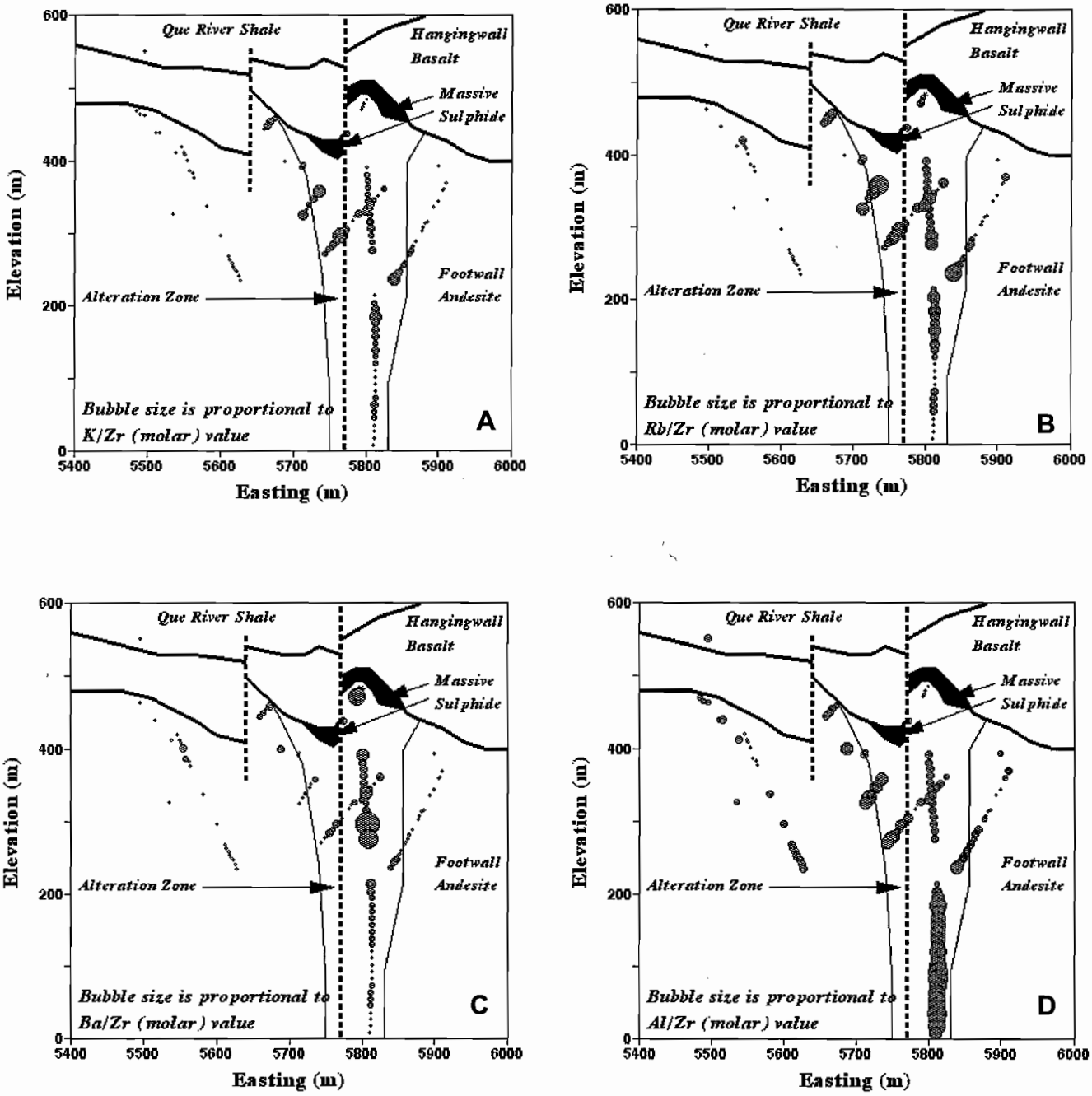

Figure 27 - Hellyer andesite footwall samples are plotted on an east-west cross-section at 10,750 m N to illustrate the distribution of element additions and losses that occurred during hydrothermal alteration. Bubble sizes are proportional to K/Zr (A), Rb/Zr (B), Ba/Zr (C) and Al/Zr (D). Geological contacts and alteration zone boundaries are based on Jack (1989) but have been modified to be consistent with the alteration zoning interpretation presented herein. K, Rb, and Ba were added to rocks at the margin of the alteration zone, but do not occur within chloritized rock closer to the core of the zone. Al is relatively constant in fresh rocks and the outer margins of the alteration zone, but has been added to rocks deep within the core of the alteration zone in regions that have been chloritically altered. See text for further discussion.

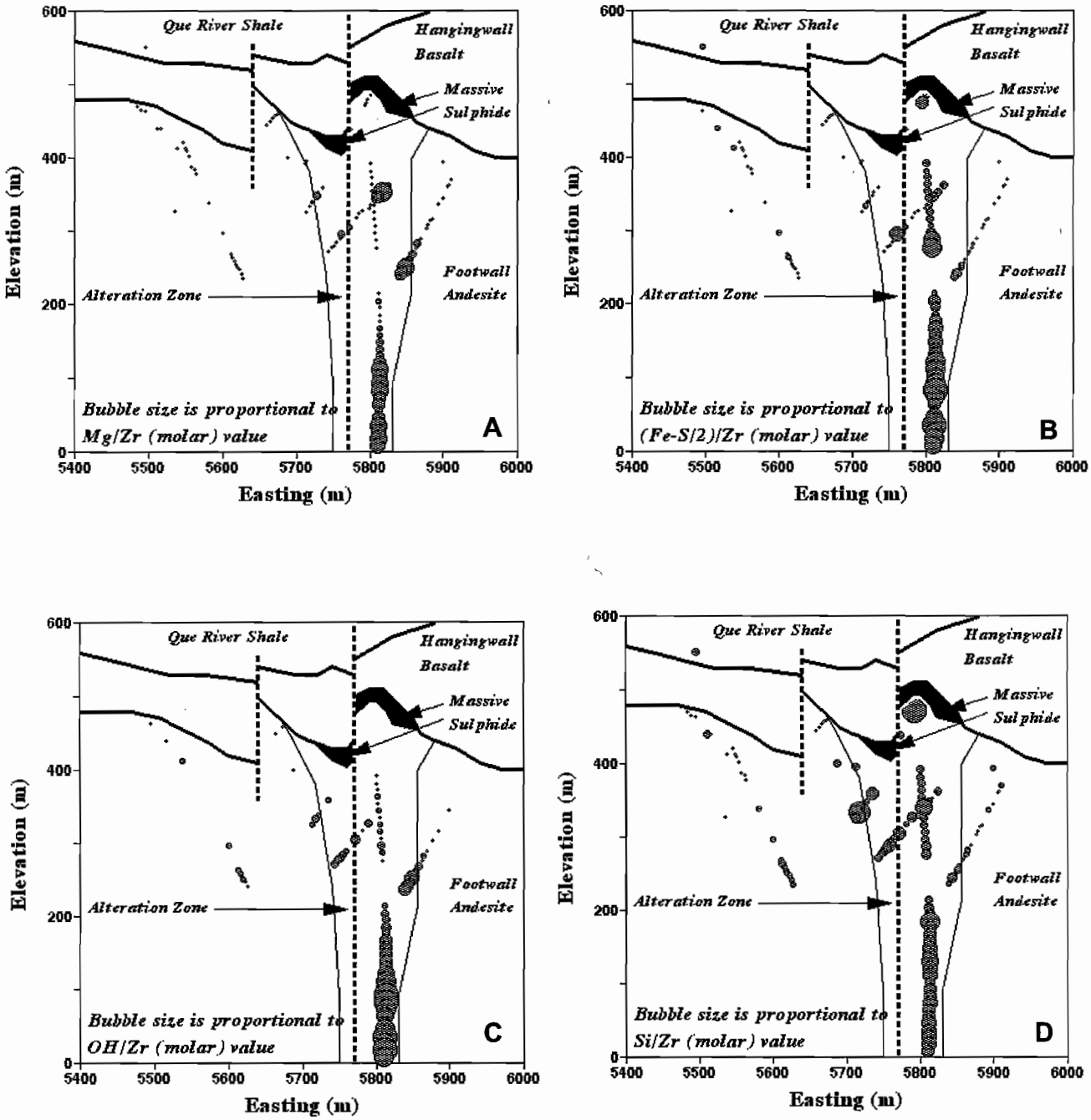

Figure 28 - Hellyer andesite footwall samples are plotted on an east-west cross-section at 10,750 m N to illustrate the distribution of element additions and losses that occurred during hydrothermal alteration. Bubble sizes are proportional to Mg/Zr (A), (Fe-S/2)/Zr (B), OH/Zr (C) and Si/Zr (D). Geological contacts and alteration zone boundaries are based on Jack (1989) but have been modified to be consistent with the alteration zoning interpretation presented herein. Mg, Fe not present in pyrite, OH and Si have been added to the core of the alteration zone, but more Mg addition and OH have been added to rocks deep within the alteration zone. See text for further discussion.

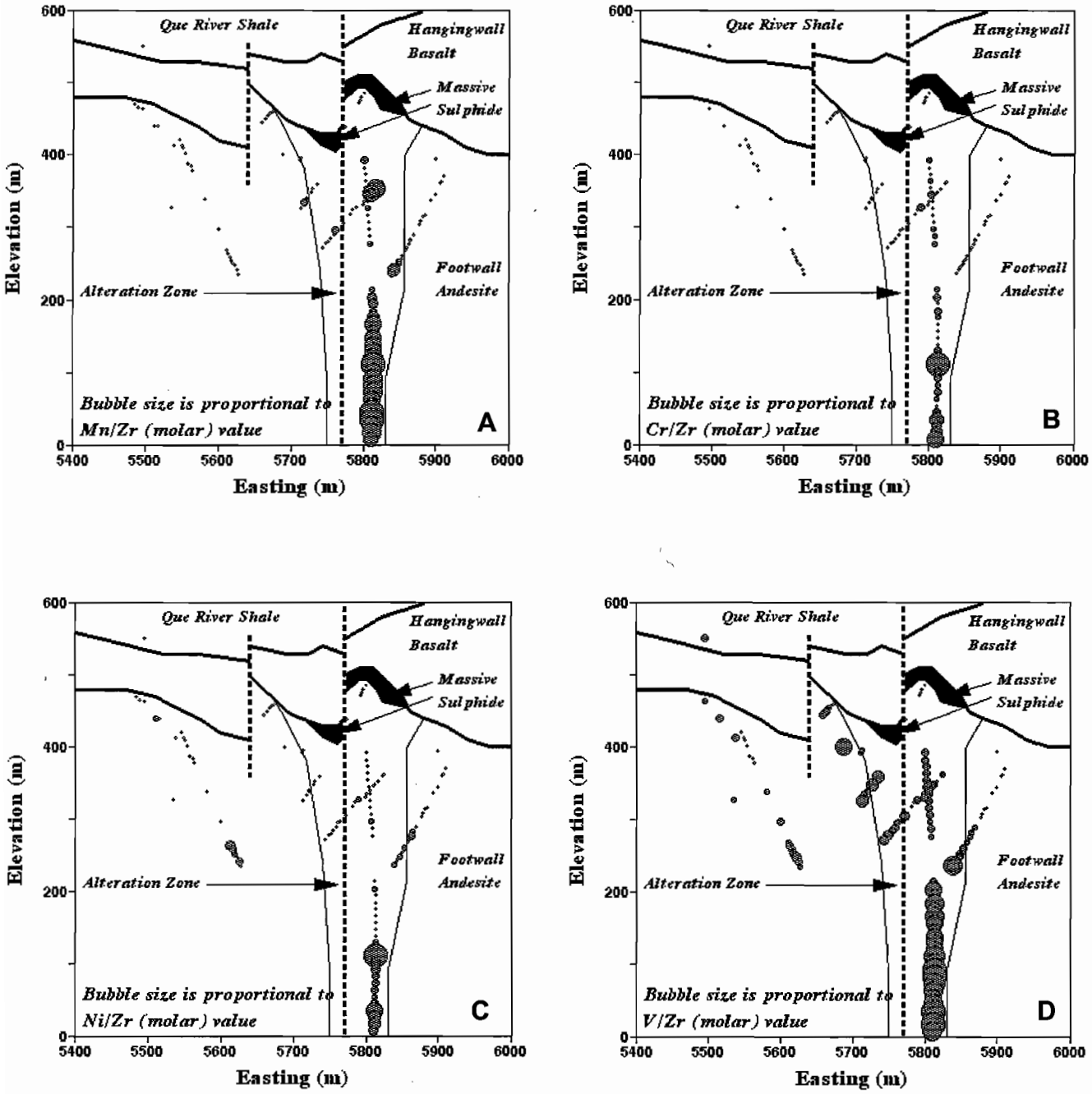

Figure 29 - Hellyer andesite footwall samples are plotted on an east-west cross-section at 10,750 m N to illustrate the distribution of element additions and losses that occurred during hydrothermal alteration. Bubble sizes are proportional to Mn/Zr (A), Cr/Zr (B), Ni/Zr (C) and V/Zr (D). Geological contacts and alteration zone boundaries are based on Jack (1989) but have been modified to be consistent with the alteration zoning interpretation presented herein. Mn, Cr and Ni have been added to rocks deep within the core of the alteration zone, but V appears to have been added to rocks located throughout the alteration zone. This may be because V has substituted for Al in both chlorite and muscovite. See text for further discussion.

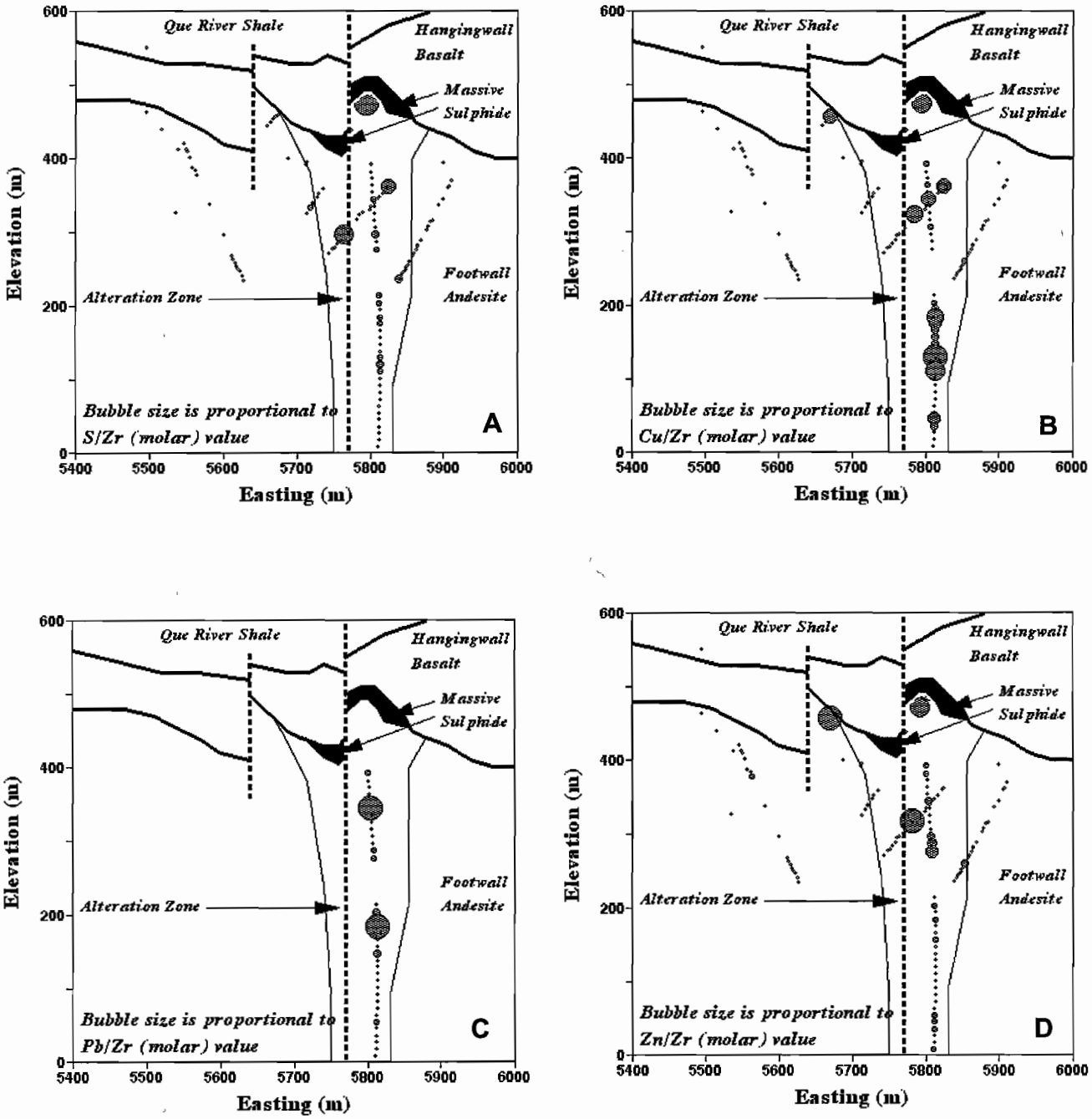

Figure 30 - Hellyer andesite footwall samples are plotted on an east-west cross-section at 10,750 m N to illustrate the distribution of element additions and losses that occurred during hydrothermal alteration. Bubble sizes are proportional to S/Zr (A), Cu/Zr (B), Pb/Zr (C) and Zn/Zr (D). Geological contacts and alteration zone boundaries are based on Jack (1989) but have been modified to be consistent with the alteration zoning interpretation presented herein. S, Cu, Pb and Zn have been added sporadically to rocks within the core of the alteration zone. See text for further discussion.

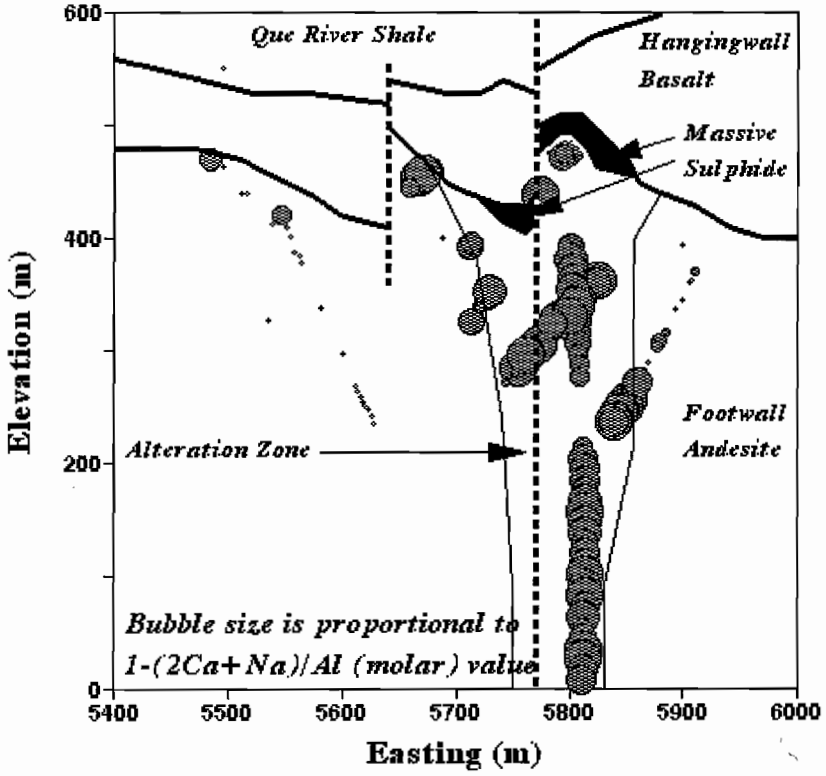

Figure 31 - Hellyer andesite footwall samples are plotted in bubbleplot form on an east-west cross-section at 10,750 m N. Bubble sizes re proportional to 1-(2Ca+Na)/Al, one of the metrics identified as a possible exploration parameter (the ratio is subtracted from unity to ensure that large bubble sizes correspond to samples that are strongly altered). This metric does not distinguish the type of alteration but does give a quantitative measure of hydrolysis. Anomalous samples occur within the recognized alteration zone, and outside the alteration zone near the contact between the footwall andesite and hangingwall basalt. See text for further discussion.

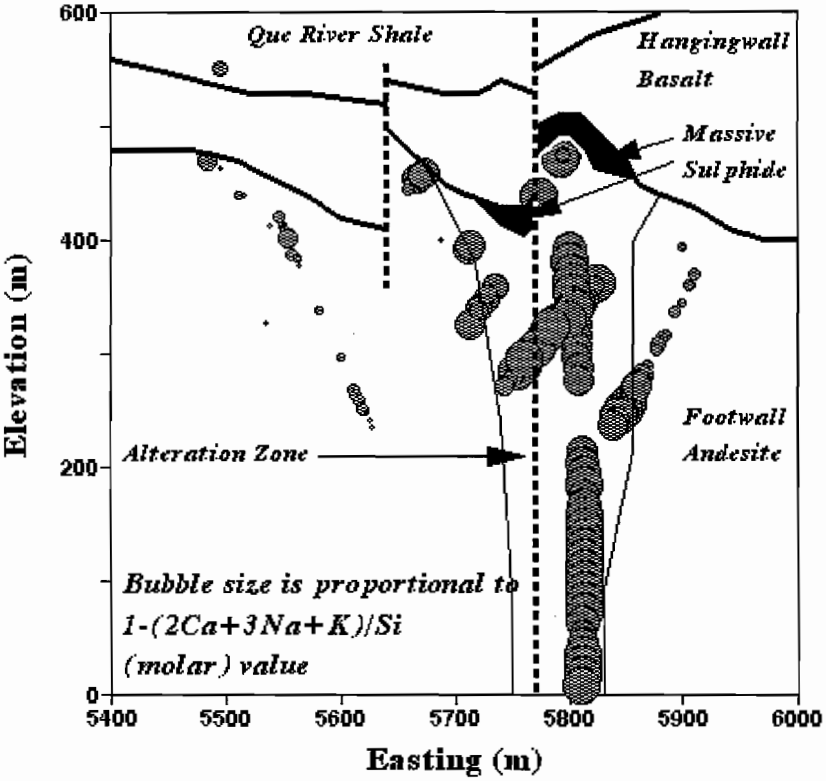

Figure 32 - Hellyer andesite footwall samples are plotted in bubbleplot form on an east-west cross-section at 10,750 m N. Bubble sizes re proportional to 1-(2Ca+3Na+K)/Si, one of the metrics identified as a possible exploration parameter (the ratio is subtracted from unity to ensure that large bubble sizes correspond to samples that are strongly altered). This metric distinguishes muscovite from chlorite alteration, and also responds to silicification. Anomalous samples occur exclusively within the recognized alteration zone. See text for further discussion.

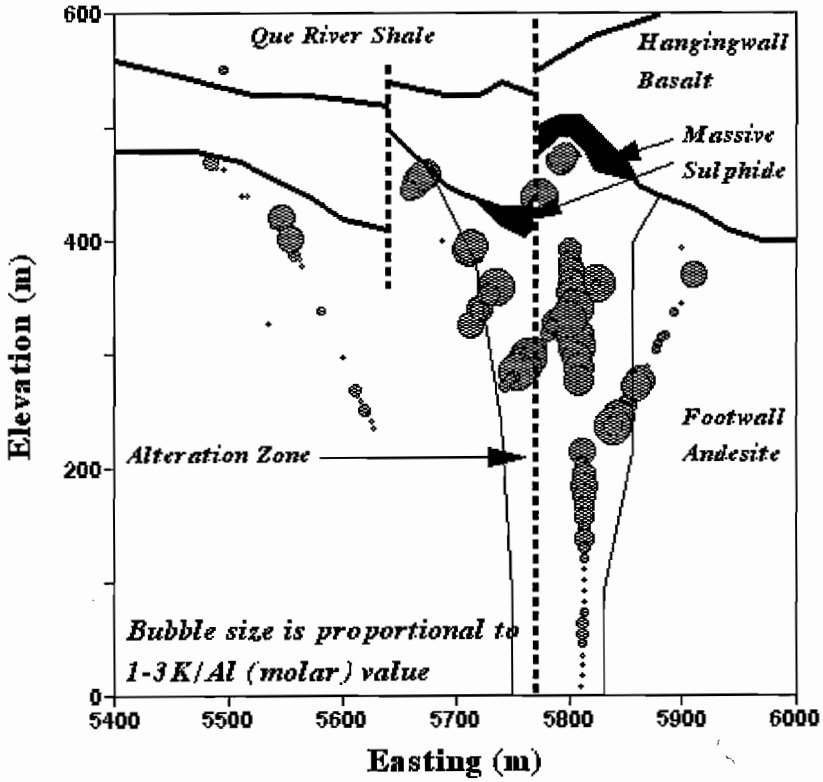

Figure 33 - Hellyer andesite footwall samples are plotted in bubbleplot form on an east-west cross-section at 10,750 m N. Bubble sizes re proportional to 1-3K/Al, one of the metrics identified as a possible exploration parameter (the ratio is subtracted from unity and multiplied by 3 to ensure that large bubble sizes correspond to samples that are strongly altered). This metric only responds to muscovite alteration, and cannot distinguish between fresh and chlorite altered rocks. Anomalous samples occur sporadically within the recognized alteration zone, and outside the alteration zone near the contact between the footwall andesite and hangingwall basalt. See text for further discussion.

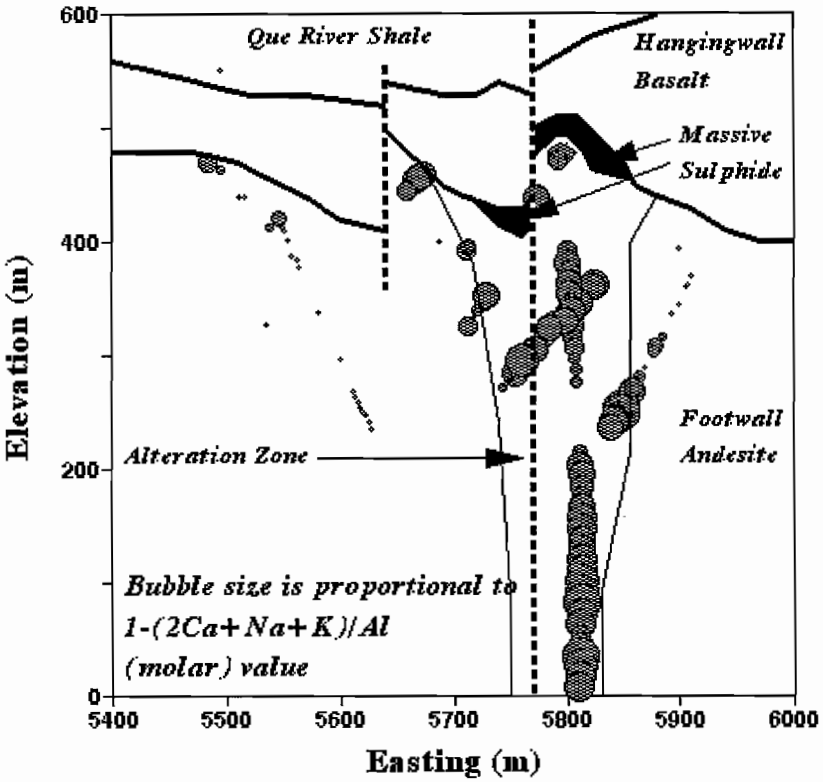

Figure 34 - Hellyer andesite footwall samples are plotted in bubbleplot form on an east-west cross-section at 10,750 m N. Bubble sizes re proportional to 1-(2Ca+Na+K)/Al, one of the metrics identified as a possible exploration parameter (the ratio is subtracted from unity to ensure that large bubble sizes correspond to samples that are strongly altered). This metric distinguishes between muscovite and chlorite alteration, giving a quantitative measure of hydrolysis. Anomalous samples occur within the recognized alteration zone, and outside the alteration zone near the contact between the footwall andesite and hangingwall basalt. See text for further discussion.

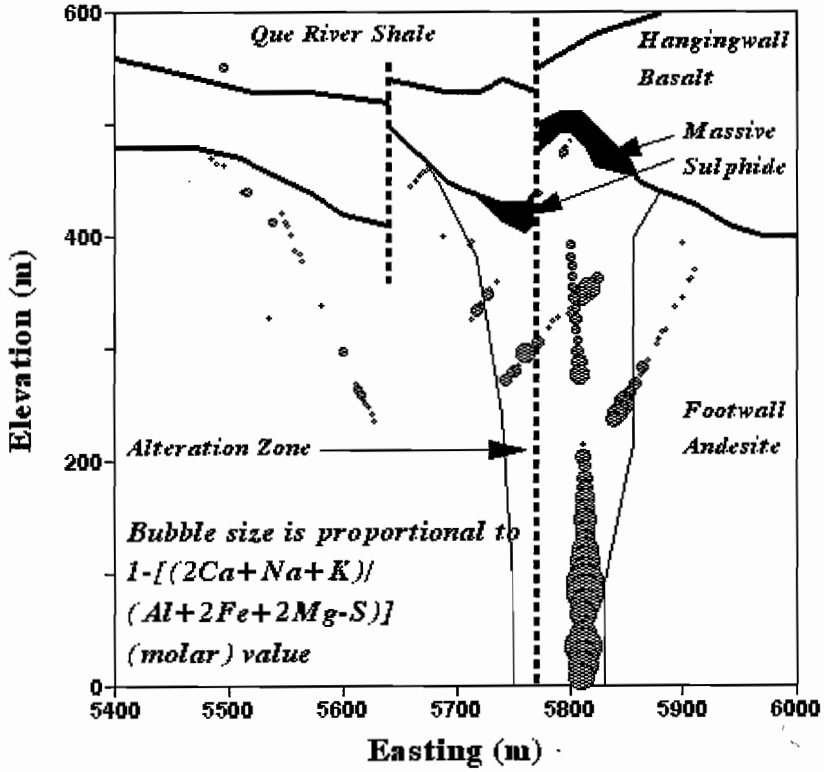

Figure 35 - Hellyer andesite footwall samples are plotted in bubbleplot form on an east-west cross-section at 10,750 m N. Bubble sizes re proportional to 1-(2Ca+Na+K)/(Al+2Fe+2Mg-S), one of the metrics identified as a possible exploration parameter (the ratio is subtracted from unity to ensure that large bubble sizes correspond to samples that are strongly altered). This metric distinguishes between muscovite and chlorite alteration, and responds to Fe and Mg metasomatism. Anomalous samples occur sporadically only within the recognized alteration zone. See text for further discussion.

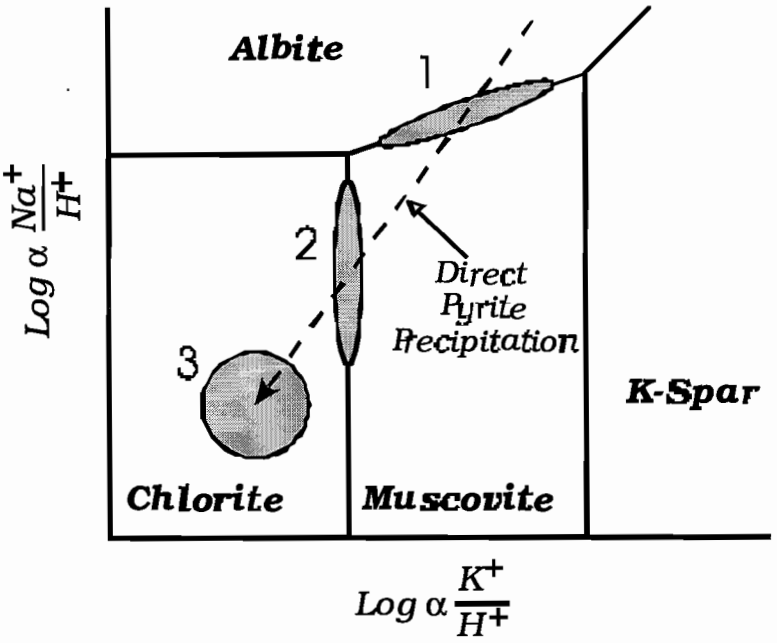

Figure 36 - A K-Na geochemical activity model describing the hydrothermal alteration reactions that occur within the Hellyer footwall andesite. This activity-activity diagram is topologically correct, but has been drawn without axis scales so that it is independent of temperature, a thermodynamic variable that is not constrained by the material transfers or alteration mineralogy observed. As such, this diagram traverses temperature space. Reactions between the hydrothermal fluid and the host andesite can be understood by considering the sequential titration of a small amount of hydrothermal fluid into the andesite and the waters that fill fractures within it. Addition of the hydrothermal fluid produces a mixed fluid composition that is displaced down to the left along the dashed arrow. True, metasomatic reactions occur as the mixed fluid composition passes into different mineral stability fields. First, the albite-to-muscovite reaction (#1) takes place, and then with more hydrothermal fluid introduction, the muscovite-to-chlorite reaction (#2) takes place. Finally, direct precipitation of chlorite from the hydrothermal fluid (#3) takes place, but this is not a consequence of the fluid entering a new stability field, and thus is not a true metasomatic reaction (the rock is not modified, it is only added to). Rather, it probably occurred due to conductive or adiabatic cooling, decompression, or mixing with another fluid, such as seawater drawn down into the volcanic pile by the upward flux streaming effect of the hydrothermal fluid. See text for further discussion.

Discussion

The above presentation identifies several hydrothermal alteration reactions that are probably responsible for the formation of the alteration pipe in the footwall of the Hellyer VHMS deposit. These reactions also provide insight into the geochemical controls on alteration and mineralization within the Hellyer region. Specifically, these reactions facilitate development of a thermally unconstrained activity model for alteration and mineralization at Hellyer. This model is presented in Figure 36, a K–Na activity diagram describing the hydrothermal alteration reactions that occur within the Hellyer footwall andesite. The diagram is topologically correct, but has been drawn without axis scales so that it is independent of temperature (and several other geochemical variables), a thermodynamic variable that is not precisely constrained by the material transfers or alteration mineralogy observed. As such, this diagram traverses temperature space.

The chemical reactions between the hydrothermal fluid and the host andesite can be understood by considering the sequential titration of a small amount of hydrothermal fluid into the andesite and the waters that fill fractures within it. This hydrothermal fluid was probably in equilibrium with chlorite. The added hydrothermal fluid mixes with the fluid in the rock fractures, producing a mixed fluid composition that has a composition displaced down to the left along the dashed arrow from the original fracture-filling fluid, which would be in equilibrium with albite. True metasomatic reactions occur as addition of hydrothermal fluid causes the mixed fluid composition to pass into different mineral stability fields. First, the albite-to-muscovite reaction (#1) takes place, and then with more hydrothermal fluid introduction, the muscovite-to-chlorite reaction (#2) takes place.

The occurrence of significant abundances of sulphide minerals only in rocks that are muscovite altered may provide some insight into the controls on sulphide precipitation within the alteration pipe. Specifically, when rocks are fully muscovite altered [and exhibit a (2Ca+Na+K)/Al ratio of 1/3], the fluids in equilibrium with the rocks reside within the muscovite stability field of Figure 36. As a result, no buffer exists to control the composition of the hydrothermal fluid. Each of these metasomatic reactions buffer the mixed fluid because they prevent the mixed fluid from migrating off the associated stability field boundary until all of the reactant minerals have been consumed. Consequently, the precipitation of sulphide minerals (largely pyrite) may not be impeded in fully muscovite altered rocks, and the pores produced by the albite-to-muscovite reaction, and fractures formed in association with movement along the Jack Fault, may have been the sites of sulphide precipitation.

Finally, direct precipitation of chlorite from the hydrothermal fluid (#3) takes place, but this is not a consequence of the fluid entering a new stability field, and thus is not a true metasomatic reaction (the rock is not modified, it is only added to). Rather, this reaction probably involved mixed fluid compositions that reside within the chlorite stability field, and thus is similar to the pyrite precipitation reaction described above because it too does not occur under buffered conditions.

This reaction is similar to one of the chloritization reactions interpreted to occur within the footwall alteration pipe of the United Verde felsic VHMS deposit, Arizona, USA (Stanley 1998). This structurally controlled alteration pipe consists of pure 'chloritite' (Vance & Condie 1987; Gustin 1988, 1990), and also exhibits Al addition, but no Si addition. The lack of Si addition at United Verde may be a consequence of the original volcanic composition (rhyolite), which probably contained significantly more Si than the Hellyer andesite, and thus acquired its Si from the rock rather than the hydrothermal fluid. At Hellyer, as at United Verde, this direct chlorite precipitation reaction probably was triggered by conductive or adiabatic cooling, decompression, or mixing with another fluid, such as seawater (not in equilibrium with the volcanics, altered or fresh) drawn down into the volcanic pile by the upward flux streaming effect of the hydrothermal fluid.

The alteration zoning observed within the Hellyer footwall andesite is consistent with the above model, except for the core siliceous zone. Although Si addition occurs within this zone, largely as quartz veins, the wall rocks exhibit evidence of resericitization. Pseudo-fragmental textures defined by sericite envelopes about fractures occur within the andesites, and clasts within the overlying polymict epiclastic mass flow unit exhibit sericite rims about

chloritic cores (Gemmell & Large 1992). As a result, in the very core alteration zone, muscovite appears to have been stable, and this is not consistent with the geochemical activity model described above. As a result, it is probable that at least this overprinting muscovite alteration represents the reaction products of alteration by a different hydrothermal fluid composition or at different pressure/temperature conditions.

Specifically, it is possible that this sericitization occurred during the waning stages of hydrothermal activity, perhaps after the deposition of the hangingwall basalts, and represents a period of different physico-chemical conditions underwhich muscovite became stable again. It is likely that the reaction through which this sericitization of chlorite took place is the opposite of that presented above for the chloritization of muscovite. This reaction would have produced a substantial volume loss, and voids produced may have been filled by significant amounts of quartz precipitated from solution. This could explain why two types of muscovite alteration are recognized at Hellyer, one involving Si addition (muscovite alteration of chlorite, forming the siliceous zone), and one without Si material transfer (muscovite alteration of plagioclase, forming the muscovite zone).

The volume changes associated with the hypothesized alteration reactions place certain constraints on the textural preservation of the original andesite. Clearly, the massive volume changes associated with chloritization of sericite, direct chlorite precipitation, and the re-sericitization of chlorite probably prevented textural preservation. However, minor sericitization of feldspar probably did not significantly destroy original textures, and only where significant does this later reaction, via its 7% volume loss, probably prevent textural preservation. As a result, the original discrimination of a stringer envelope zone and sericite zone (Gemmell & Large 1992), based largely on the percentage of sericite and the degree of textural destruction, may reflect alteration intensity rather than any fundamentally different hydrothermal alteration process.

Conclusions

The above PER analysis of rock compositions within the andesitic footwall to the Hellyer VHMS deposit, because of the superior resolution it offers, has revealed several new concepts regarding the hydrothermal alteration that occurred there. These include :

- Zr, Nb and Y are more conserved (more incompatible and immobile) than TiO_2;
- primary compositional variations within the andesite can be attributed to fractionation of plagioclase and clinopyroxene in an approximately 8/7 molar ratio, which corresponds to an 33/20 volume ratio — this ratio is crudely consistent with the phenocryst abundances observed within the andesite;
- late calcite veins do not appear to be significant contributors to the compositional variability within the andesites;
- the composition of fractionating clinopyroxene and plagioclase are estimated to be $X_{DI} = 5/9$ and $X_{AN} = 1/6$ — this clinopyroxene composition is Fe-rich relative to the clinopyroxene phenocrysts observed in the Hellyer andesites — this plagioclase composition is relatively albitic, and thus is not considered to be primary, but is likely a product of spilitic Na-Ca exchange between seawater and devitrifying andesite;
- metasomatism associated with muscovite alteration involved Na, Ca and Sr loss, K, OH, Rb and Ba addition, and did not involve significant Al or Si metasomatism — the alteration assemblage associated with muscovite alteration is muscovite plus quartz;
- pyrite (and trace chalcopyrite, galena and sphalerite) precipitation probably filled pore produced by this muscovite alteration, producing the classic QSP (quartz-sericite-pyrite) alteration assemblage observed in many VHMS camps — this reaction involved the addition of S, Fe, Cu, Pb and Zn;
- chlorite alteration of muscovite involved the loss of K, Rb and Ba, and the addition of Fe, Mg and OH - direct precipitation of chlorite from solution involved the addition of Fe, Mg, Si, Al and OH — both of these reactions involve significant volume increases, and so were restricted to proximal

locations about the Jack fault, where tectonically formed open space was available to facilitate reaction progress;
- re-sericitization of chlorite occurred in the core of the alteration zone, and involved a significant volume loss coupled with the addition of K and loss of Fe, Mg and OH — it also appears to be associated with Si addition (in contrast to simple muscovite alteration, above), accommodated via quartz precipitation within the pores produced — it also is associated with S, Cu, Pb and Zn addition, as sulphides also precipitated in the new pores;
- muscovite alteration of feldspar and chlorite alteration of muscovite represent simple metasomatic reactions which buffered the hydrothermal fluid via exchange of elements between fluid and rock — these reactions were likely driven by chemical/mineralogical dis-equilibrium between the host rocks and hydrothermal fluid; and
- direct chlorite and pyrite precipitation reactions represent non-metasomatic reactions, and these were likely triggered by changes in the physico-chemical state of the hydrothermal fluid — as such, these reactions were driven by physico-chemical dis-equilibrium between the hydrothermal fluid and its environment.

In addition, five exploration parameters have been identified that could be used to vector toward the most intense regions of hydrothermal alteration. These have different advantages and disadvantages, and include :
- (2Ca+Na)/Al, which describes the degree of hydrolysis, cannot discriminate between muscovite and chlorite alteration (> 1 = fresh; 0 = muscovite or chlorite altered) — it also suffers from a non-unique representation of the background compositional variation due to plagioclase and clinopyroxene fractionation;
- (2Ca+Na+K)/Al, which also describes the degree of hydrolysis, can discriminate between muscovite and chlorite alteration (> 1 = fresh; 1/3 = muscovite altered; 0 = chlorite altered) — it also suffers from a non-unique representation of the plagioclase and clinopyroxene fractionation;
- (2Ca+3Na+K)/Si, which also describes the degree of hydrolysis, is also affected by silicification — however, this parameter has the advantage of producing a unique fresh rock signature (1 = fresh; 1/3 = muscovite altered; 0 = chlorite altered; silicification decreases these values);
- (2Ca+Na+K)/(Al+2Fe+2Mg-S), which also describes the degree of hydrolysis, is also affected by Fe and Mg metasomatism — however, this metric also has the advantage of producing a unique fresh rock signature (1 = fresh; 1/3 = muscovite altered; 0 = chlorite altered; Fe and Mg metasomatic additions decrease these values); and
- K/Al, which describes the degree of muscovite alteration, cannot discriminate between fresh and chloritized andesite (0 = fresh or chloritized; 1/3 = muscovite altered) — it also has a unique fresh rock signature.

Although each of these five exploration parameters responds to hydrothermal alteration effects within the visible alteration zone, three [(2Ca+Na)/Al, (2Ca+Na+K)/Al and (2Ca+3Na+K)/Si] identify anomalies outside the alteration zone just below the contact between the footwall andesite and hanging-wall basalt. As such, they do define any cryptic alteration halo that may be indicative of proximal accumulations of VHMS mineralization. These parameters are also more quantitative measures of hydrothermal alteration than previously available. Furthermore, used in concert, they allow recognition and discrimination of different styles of hydrothermal alteration, and thus may provide substantial benefit where complex alteration zoning exists.

Future Work

An analogous Pearce element ratio analysis of the controls of compositional variation in the hanging-wall basalt and Que River shale at Hellyer will also be undertaken. Samples have been collected and analyzed, and the resulting data has been examined using scatterplots and PER diagrams.

Acknowledgments

CS and JBG are grateful to Gary McArthur, Andrew McNeil, Steve Richardson and David Wallace of Aberfoyle Resources who made the core library and

core logs at Hellyer available for this research. We also thank them for many stimulating discussions on the geology surrounding Hellyer. Phil Robinson and Nilar Hlaing are thanked for the geochemical analyses and June Pongratz and Darren Turner are thanked for manipulating email files from overseas and making good science look even better!

This research is supported by a collaborative agreement between the MDRU Lithogeochemical Exploration Research Project (sponsored by Inco Ltd., Inmet Mining Co., Placer Dome Inc., Hudson Bay Exploration and Development Co. Ltd., Orvana Minerals Ltd., BHP Minerals Canada Ltd., Aberfoyle Resources Ltd., Bondar Clegg Laboratories Ltd., Chemex Laboratories Ltd., X-ray Assay Laboratories Ltd., the Science Council of British Columbia, the Natural Sciences and Engineering Research Council of Canada, and the University of British Columbia) and CODES AMIRA/ARC P439 (sponsored by Aberfoyle Resources, CRA Exploration, Denehurst Limited, Pasminco Exploration, Normandy, Queensland Metals Corporation and RGC Exploration).

References

Akella, J. (1966): Calculation of Material Transport in Some Metasomatic Processes: Neues Jahrbuch für Mineralogische Abhandlungen, Vol. 104, pp. 316 -329.

Babcock, R.S. (1973): Computational Models of Metasomatic Processes. Lithos, Vol. 6, pp. 279-290.

Chayes, F. (1960): On Correlation Between Variables of Constant Sum. Journal of Geophysical Research, Vol. 65, No. 12, pp. 4185-4193.

Corbett, K.D. (1992): Stratigraphic-Volcanic Setting of Massive Sulphide Deposits in the Cambrian Mount Read Volcanics, Tasmania. Economic Geology, Vol. 87, pp. 564-586.

DePangher, M. (1988): Quantitative Assessment of Composition-Volume Changes During Metasomatism: New Techniques for Identifying Protoliths and Conserved Elements. Unpublished Ph.D. Thesis, University of Utah, Salt Lake City, Utah, 50 p.

Drever, J.I. (1982): The Geochemistry of Natural Waters. Prentice-Hall Inc. Englewood Cliffs, N.J, 388 p.

Duncan, R. (1996): Investigation of the Hydrothermal Alteration of the Baker-Patton Felsic Volcanic Complex. Unpublished B.Sc. Thesis, 122 p.

Finlow-Bates, T. and Stumpfl, E.E. (1981): The Behavior of So-Called Immobile Elements in Hydrothermally Altered Rocks Associated with Volcanogenic Submarine-Exhalative Ore Deposits. Mineralium Deposita, Vol. 16, pp. 319-328.

Floyd, P.A. and Winchester, J.A. (1978): Identification and Discrimination of Altered and Metamorphosed Volcanic Rocks Using Immobile Elements. Chemical Geology, Vol. 21, pp. 291-306.

Franklin, J.M., Sangster, D.M. and Lydon, J.W. (1981): Volcanic Associated Massive Sulphide Deposits. Economic geology, 75th Anniversary Volume, pp. 485-627.

Garrells, R.M. and Christ, C.L. (1965): Solutions, Minerals and Equilibria. Freeman, Cooper and Co., San Fransisco, 450 p.

Gemmell, J.B. and Large, R.R. (1992): Stringer System and Alteration Zones Underlying the Hellyer Volcanic-Hosted Massive Sulphide Deposit, Tasmania, Australia. Economic Geology, Vol. 87, pp. 620-649.

Goodfellow, W.D. (1975): Major and Minor Element Halos in Volcanic Rocks at Brunswick No. 12 Sulphide Deposit, New Brunswick, Canada. *in* 'Geochemical Exploration 1974'. *ed. by* Elliot, I.L. and Fletcher, W.K., Elsevier Scientific Publishing Co., Amsterdam, pp. 279-295.

Grant, J.A. (1986): The Isocon Diagram - A Simple Solution to Gresens' Equation for Metasomatic Alteration. Economic Geology, Vol. 81, pp. 1976-1982.

Gresens, R.L. (1967): Composition-Volume Relationships in Metasomatism. Chemical Geology, Vol. 2, pp. 47-55.

Gustin, M.S. (1988): A Petrographic, Geochemical and Stable Isotope Study of the United Verde Orebody and Its Associated Alteration, Jerome, Arizona; Unpublished Ph.D. Dissertation, University of Arizona, Tucson, Arizona, 261 pp.

Gustin, M.S. (1990): Stratigraphy and Alteration of the Host Rocks, United Verde Massive Sulfide Deposit, Jerome, Arizona; Economic Geology, Vol. 85, pp. 29-49.

Hutchinson, R.W., Spence, C.D. and Franklin, J.M. (1982): Precambrian Sulphide Deposits. Geological Association of Canada, Special Paper No. 25, 791 p.

Hyndman, D. (1972): Petrology of Igneous and Metamorphic Rocks. McGraw-Hill Book Co., New York, 533 p.

Jack, D.J. (1989): Hellyer Host Rock Alteration. Unpublished M.Sc. Thesis, University of Tasmania, Hobart, Tasmania, Australia, 181 p.

Lydon, J.K. (1988): Ore Deposit Models # 14, Volcanogenic Massive Sulphide Deposits, Part 2: Genetic Models. Geoscience Canada, Vol. 15, No. 1, pp. 43-65.

MacLean, W.H. (1990): Mass Change Calculations in Altered Rock Series. Mineralium Deposita, Vol. 25, pp. 44-49.

MacLean, W.H. and Barrett, T.J. (1992): Host Rock Alteration Associated with Noranda-Type Massive Sulphides: General Information. *in* 'New Developments in Lithogeochemistry'. MDRU Short-Course Notes SC-8, Mineral Deposits Research Unit, University of British Columbia, Vancouver, British Columbia, Feb. 20-21, 1992.

Madeisky, H.E. and Stanley, C.R. (1993): Lithogeochemical Exploration for Metasomatic Zones Associated with Volcanic-Hosted Massive Sulphide Deposits Using Pearce Element Ratio Analysis. International Geological Reviews, Vol. 35, pp. 1121-1148.

McArthur, G.J. (1986): The Hellyer Massive Sulphide Deposit. *in* 'The Mount Read Volcanics and Associated Ore Deposits'. *ed. by* Large, R.R., Geological Society of Australia, Tasmanian Division, Burnie, pp. 11-19.

McArthur, G.J. (1989): Hellyer. Geological Society of Australia, Special Publication No. 15, pp. 144-148.

McArthur, G.J. and Dronseika, E.V. (1990): Que River and Hellyer Zinc-Lead Deposits. Australian Institute of Mining and Metallurgy, Monograph No. 14, pp. 1331-1339.

Nicholls, J. (1988): The Statistics of Pearce Element Diagrams and the Chayes Closure Problem. Contributions to Mineralogy and Petrology, Vol. 99, pp. 1031-1057.

Nicholls, J. and Gordon, T.M. (1994): Procedures for the Calculation of Axial Ratios on Pearce Element Ratio Diagrams. Canadian Mineralogist, Vol. 32, pp. 969-977.

Nordstrom, D.K. and Munoz, J.L. (1986): Geochemical Thermodynamics. Blackwell Scientific Publications, Palo Alto, California, 477 p.

Offler, R. and Whitford, D.J. (1992): Wall-Rock Alteration and Metamorphism of a Volcanic Hosted Massive Sulphide Deposit at Que River, Tasmania: Petrology and Mineralogy. Economic Geology, Vol. 87, pp. 686-705.

Pearce, T.H. (1968): A Contribution to the Theory of Variation Diagrams. Contributions to Mineralogy and Petrology, Vol. 19, pp. 142-157.

Pearce, T.H. and Stanley, C.R. (1991): The Validity of Pearce Element Ratio Analysis in Petrology: An Example from the Uwekahuna Laccolith, Hawaii. Contributions to Mineralogy and Petrology, Vol. 108, pp. 212-218.

Robinson, M., Godwin, C.I. and Stanley, C.R. (1995): Geology, Lithogeochemistry and Alteration of the Battle Massive Sulphide Zone, Buttle Lake Mining Camp, Vancouver Island, British Columbia. Economic Geology, Vol. 91, pp. 527-548.

Russell, J.K. and Stanley, C.R. (1990A): A Theoretical Basis for the Development and Use of Chemical Variation Diagrams. Geochimica et Cosmochimica Acta, Vol. 54, No. 9, pp. 2419-2431.

Russell, J.K. and Stanley, C.R. *eds.* (1990B): Theory and Application of Pearce Element Ratios to Geochemical Data Analysis. Geological Association of Canada Short Course Notes, No. 8, 315 pp.

Sangster, D.F. (1972): Pre-Cambrian Volcanogenic Massive Sulphide Deposits in Canada: A Review. Geological Society of Canada, Special Paper No. 72-22, 43 p.

Sangster, D.F. and Scott, S.D. (1976): Precambrian Stratabound Massive Cu-Zn-Pb Sulphide Ores of North America. *in* 'Handbook of Stratabound and Stratiform Ore Deposits', *ed. by* Wolf, K.H. Elsevier Scientific Publishing Co., Amsterdam, pp. 129-222.

Solomon, M., Eastoe, C.J., Walshe, J.L. and Green G.R. (1988): Mineral Deposits and Sulfur Isotope Abundances in the Mount Read Volcanic Between Que River and Mt. Darwin, Tasmania. Economic Geology, Vol. 83, pp. 1307-1328.

Stanley, C.R. and Russell, J.K. (1989): Petrologic Hypothesis Testing with Pearce Element Ratio Analysis: Derivation of Diagram Axes. Contributions to Mineralogy and Petrology, Vol. 103, pp. 78-89.

Stanley, C.R. and Madeisky, H.E. (1993): Pearce Element Ratio Analysis : Applications in Lithogeochemical Exploration. Mineral Deposit Research Unit, Dept. of Geological Sciences, Univ. of British Columbia, Short Course No. 8, Vancouver, B.C., 540 p.

Stanley, C.R. and Madeisky, H.E. (1994): Lithogeochemical Exploration for Hydrothermal Ore Deposits Using Pearce Element Ratio Analysis. *in* 'Alteration and Alteration Processes Associated with Ore Forming Systems'. *ed. by* Lentz, D.R., Geological Association of Canada, Short Course Notes, Vol. 11, pp. 193-211.

Stanley, C.R. and Madeisky, H.E. (1995): Lithogeochemical Exploration for Metasomatic Zones Associated with Hydrothermal Mineral Deposits Using Pearce Element Ratio Analysis. Short Course Notes, 11th International Geochemical Exploration Symposium, Townsville, Australia, 98 p.

Stanley, C.R. (1996): Graphical Investigation of Lithogeochemical Variations Using Molar Element Ratio Diagrams : Theoretical Foundation. Mineral Deposit Research Unit Lithogeochemical Exploration Research Project, Annual Report, Year 1, Chapter 3, 40 p.

Stanley, C.R. (1997): Molar Element Ratio Diagram Design : Creating Powerful Projections of Multivariate Lithogeochemical Space to Investigate Compositional Variability in Rocks. Mineral Deposit Research Unit Lithogeochemical Exploration Research Project, Annual Report, Year 2, Chapter 16, 58 p.

Stanley, C.R. (1998): Lithogeochemical Exploration for Metasomatic Zones Associated with Hydrothermal Mineral Deposits Using Molar Element Ratio Analysis : Advanced Topics. Mineral Deposit Research Unit Lithogeochemical Exploration Research Project, Annual Report, Year 3, Chapter 26, 62 p.

Vance, R.K. and Condie, K.C. (1987): Geochemistry of Footwall Alteration Associated with the Early Proterozoic United Verde Sulphide Deposit, Jerome, Arizona. Economic Geology, Vol. 571-586.

Waters, J.C. and Wallace D.B. (1992): Volcanology and Sedimentology of the Host Succession to the Hellyer and Que River Volcanic-Hosted Massive Sulphide Deposits, Tasmania. Economic Geology, Vol. 87, pp. 650-666.

Winchester, T.A. and Floyd, P.A. (1977): Geochemical Discrimination of Different Magma Series and Their Differentiation Products Using Immobile Elements. Chemical Geology, Vol. 20, pp. 325-347.

Whitford, D.J., McPherson, W.P.A and Wallace, D.P. (1989): Geochemistry of the Host Rocks of the Volcanogenic Massive Sulphide Deposit at Que River, Tasmania. Economic Geology, Vol. 84, pp. 1-21.

Carbonate alteration at the Rosebery mine: The relationships between alteration texture, paragenesis, chemistry of carbonate minerals, and distance to ore

Rodney L. Allen, Michael Blake and Ross R. Large
Centre for Ore Deposit Research

Introduction

Carbonate alteration is an integral part of the hydrothermal alteration system at the Rosebery and Hercules massive sulphide deposits in Tasmania, and at several other important deposits (e.g. Skellefte district, Sweden, Allen et al., 1996). Brathwaite (1974), Dixon (1980) and Khin Zaw (1991) reported on the textures and compositional range of carbonate minerals at Rosebery and Hercules. However in general, carbonate alteration in VHMS systems is poorly understood and there have been few systematic studies of the variations in texture and composition of carbonate alteration relative to distance to ore, stratigraphic position, and paragenesis. A major focus of the Rosebery alteration study has been to systematically document and understand carbonate alteration at the Rosebery deposit.

The distribution of carbonate-bearing alteration zones and their relationship to other alteration types at the north end of the Rosebery deposit is provided in section 2.1 of this report. A summary of carbonate mineral chemistry and its use as a vector to ore is provided in Large et al. (1998a). That section provides an overview of the chemical and mineralogical variations that can be observed without regard to the particular type of carbonate alteration or the paragenesis of the carbonates that were sampled. Here we take the studies a step further and document the range of carbonate alteration textures at Rosebery, and the relationships between the different carbonate textures and carbonate mineral composition, stratigraphic position, distance to ore and time of formation (paragenesis relative to other hydrothermal and diagenetic alteration types, ore formation and tectonic deformations). Aims of this work were to establish what variations exist, and how these variations may be relevant to mineral exploration in the Rosebery area.

Data for this study comes from three main sources:

(1) the graphic geological logging of textural features, distribution and overprinting relationships of carbonate alteration in nine drill cores from the northern A-B and K lens area (e.g. drill logs 120R and R4452 reported in Allen, Duhig and Large, 1996),
(2) detailed petrographic study of 69 samples from a proximal drill hole through K lens (120R) and a distal drill hole 500 m north of K and A-B lenses (109R),
(3) microprobe analysis of carbonate mineral chemistry at 240 points in these samples, representing the various textural types and paragenetic stages of carbonates alteration.

Previous AMIRA reports

Previous reports concerning carbonate alteration at Rosebery include a preliminary description of carbonate alteration textures and paragenesis (Allen and Large, 1996), a study of carbonate textures using petrography and cathodoluminescence (Hill and Orth, 1995), carbonate mineral chemistry in drill hole 120R (Large, Allen and Blake, 1997), and the relation of carbonate alteration to regional diagenetic alteration (Allen, 1997).

Carbonate alteration types at Rosebery

In this study 12 different carbonate textural types were recognised at the north end of the Rosebery deposit (Table 1). These comprise 9 types of carbonate alteration texture spatially related to the ore deposit (1–9 in Table 1), calcite impregnations that are more widespread but could also be related to the ore deposit, several types and paragenetic stages of veining, of which only one type is specifically spatially related to the ore deposit, and finally calcitic limestone clasts which form a minor component of the lithic rich base of the second main mass flow unit of the hangingwall volcaniclastic sequence.

A selection of these carbonate textural types are shown in Plate 1. The nodular or spotty carbonate alteration types are a particularly distinctive feature of the Rosebery and Hercules ore deposits, and most of these types (1–5 in Table 1) only occur adjacent to ore: within 20 m of the stratigraphic level of an ore lens and within 100 m lateral distance from the edge of an ore lens. Consequently, these spotty carbonate types are an excellent guide to ore. The spotty carbonates can be further subdivided according to their degree of close packing or intergrowth, and according to the fineness and sharpness, or lack of, internal concentric layering (Table 1, Plate 1). All known occurrences of spotty carbonate types 1–5 are from pumice breccia, pumice sandstone and pumice siltstone (pumiceous rocks of breccia, sand and silt grain size) of the Rosebery–Hercules Footwall Volcanics stratigraphic unit of Allen (1991, 1994a, 1994b). Remarkably well preserved pseudomorphs of pumice clasts and glass shards are preserved within the faintly to non-concentric layered carbonate spots (Plate 1), and it is interesting that the best preserved delicate glass shard textures recorded anywhere in the Rosebery–Hercules region come from these carbonate spots directly adjacent to massive sulphide. The stratigraphic position of spotty carbonate types 1–5 and the relict textures within the carbonate spots, indicate that the spots formed by replacement of massive pumice breccia and sand- to silt-grade beds composed entirely of glass shards. In general, the carbonate spots that formed in pumice breccia and coarse shard-rich sandstone have either faint or no internal concentric layering. The most finely and distinctly layered carbonate spots appear to have grown in very fine grained beds composed of vitric dust (fine glass shard fragments).

Spotty carbonate types 1–5 and the platey and massive carbonates (7 and 9 in Table 1) have a matrix of sericite, or less commonly chlorite, and grade outwards away from ore into sericite–carbonate alteration that consists of pervasive sericite with abundant scattered carbonate blebs and/or carbonate–sericite pseudomorphs after feldspar phenocrysts (types 8 and 6 in Table 1).

Impregnation carbonate comprises rocks with abundant white calcitic carbonate in the matrix (Table 1). Textural gradations to unaltered patches indicate that the carbonate has replaced originally glassy grains and infilled any porosity in the rocks. In contrast, feldspar crystals and lithic clasts are commonly only weakly to moderately replaced by carbonate (Plate 1). Impregnation carbonate occupies volumes of rock 1–20 m thick and tens to hundreds of metres in lateral extent, mainly in the TSV (Transitional Stratified Volcaniclastics, uppermost member of the Footwall Volcanics of Allen, 1991, 1994) and Hangingwall Volcaniclastics (Alteration cross section in section 2.1 of this report).

Thin carbonate veins and carbonate–quartz veins occur throughout the Rosebery area. However, veins are not especially abundant near the ore lenses. In fact veins tend to increase in abundance deep in the footwall toward the Rosebery Fault, and in the hangingwall in the main black shale unit and toward the Mount Black Fault (Allen, 1991, 1994; alteration cross section in Large et al., 1998b). The one vein type that only occurs near ore, consists of cream to pink manganiferous carbonate veins that cut across spotty carbonates and have sub-spheroidal and irregular curving grains that in thin section show a spectacular "tins of worms" extinction pattern (Plate 1). Other vein sets have more typical massive to banded internal structure.

Table 1. Carbonate textures in the Rosebery-Hercules area

Texture		Variations	Internal structure	Composition	Example
1-6. Nodular or spotty					
1. Large nodules	(1 cm - 2 m diameter nodules)	- Dispersed - Intergrown	- Massive granular, or - Coarse concentric layering	not analysed	Hercules 4-level road
2. Spheroidal	(0.2 mm - 1 cm diameter spheroids of anhedral grains)	- Dispersed, distinct spheroids - Close-packed, intergrown	- Distinct fine concentric layering - Faint concentric layering - No visible concentric layering	$Ca_2Mg(Fe,Mn)(CO_3)_4$ $Ca(Mn>Fe,Mg)(CO_3)_2$ $(Mn»Fe)CO_3$	Rosebery 120R 1361m Rosebery 120R 1357m Rosebery 120R 1364B
3. Spheroidal-rhombic	(0.5 mm - 1 cm diameter spheroids composed entirely of, or with rim of radiating rhombs)	as above	- No concentric layering - coarse concentric layering	not analysed	Hercules South Dunnes shaft
4. Rhombic	(0.2 mm - 1 cm rhombs)	- Dispersed - Random intergrowth	- Concentric layering - No concentric layering	not analysed	Rosebery 120R 1364B
5. Lozenge	(0.2 mm - 1 cm lozenge-shaped grains)	- Dispersed - Close-packed, intergrown	- Concentric layering	$(Mn»Fe)CO_3$	Rosebery 120R 1364B
6. Feldspar pseudomorph	(replacement of 0.5-4 mm feldspar phenocrysts)	- Porphyritic distribution	Patchy-irregular to massive	$Ca(Mn>Fe=Mg)(CO_3)_2$ $(Ca»Mn)CO_3$	Rosebery 120R 1399m Rosebery 120R 1147m
7. Platey (rare)	(5 mm - 3 cm tabular laths or plates ?after anhydrite, gypsum)	- Dispersed - Interlocking network	Massive	not analysed	Hercules H1176, 106m
8. Blebby	(≤ 10 cm irregular patches)	- Dispersed - Interconnected	Massive, no distinct spheroidal texture or layering	$(Mn>Fe>Mg)CO_3$ $Ca(Mn>Fe,Mg)(CO_3)_2$ $(Fe>Mn)CO_3$	Rosebery 120R 1366m Rosebery 120R 1399m Rosebery 109R 709m
9. Massive	(irregular compact granular masses 5 cm - 2 m)	- Anhedral grains - Close-packed rhombs - Close-packed spheroids with carbonate-filled interstices	- Concentric layered grains - No layering in grains	$Ca(Mn>Mg>Fe)(CO_3)_2$	Rosebery 120R 1365m
10. Impregnation	(filling or replacement of matrix within non-carbonate rock)	- Irregular patches - Pervasive	Anhedral, non-layered grains	$CaCO_3$ $(Ca»Mn)CO_3$	Rosebery 120R 1237m Rosebery 120R 1169m
11. Veins	(carbonate ± quartz veins and their alteration haloes)	- early pre-S2 cleavage - pre- to syn-S2 cleavage - syn-S2 - post-S2	- subspheroidal - massive to banded - massive to banded - massive	$Ca(Mn>Fe=Mg)(CO_3)_2$ As above $CaCO_3$ $(Mn,Fe)CO_3$, $CaCO_3$	Rosebery 120R 1361m Rosebery 120R 1365m Rosebery 120R 1256m 120R 1436m, 109R 424m
12. Limestone	(fine grained, compact, calcitic carbonate)	- Layer, bed - Clasts in mass flow beds	- Massive to foliated - Fossiliferous (trilobites)	$CaCO_3$	Rosebery 109R 552m Rosebery 120R 1100m

Relationship between carbonate alteration type, paragenesis and mineral composition

The relative timing or paragenesis of alteration types at Rosebery was determined by documenting overprinting relationships between each alteration textural type and the S1 and S2 regional foliations, and between the different alteration types themselves. This was carried out routinely during drill core logging and petrographic study. Twenty main stages of alteration, including nine stages with a major carbonate component were recorded, and are listed in Table 1 of Large et al. (1998b).

In each rock sample studied, the different carbonate textural types and paragenetic generations were analysed by microprobe. The main carbonate mineral compositions for the various carbonate textural types are listed in Table 1. As shown in section 2.4 of this report these compositions can be classified as calcite with minor substitution of Mn, Fe and Mg, a spectrum of compositions between rhodochrosite [$MnCO_3$] and ferroan rhodochrosite [$MnFe(CO_3)_2$], locally extending to manganoan siderite [$(Fe>Mn)CO_3$], and a spectrum of compositions between ankerite [$Ca_2FeMg(CO_3)_4$] and kutnahorite [$CaMn(CO_3)_2$].

Table 2 is a synthesis of the main results of this study. It lists representative samples and representative analyses of the various carbonate textural types and parageneses. This data is arranged according to proximal or distal position relative to ore (120R and 109R data respectively) and according to stratigraphic level. This arrangement allows the reader to see almost all the variations and trends in the data set. The main important and interesting features are discussed briefly below.

Early parageneses (pre-S2 cleavage)

Carbonate alteration of definite early paragenesis consists of spotty, massive, blebby and platey carbonates and sub-spheroidal veins restricted to the Footwall Volcanics, in the spotty carbonate and sericite–carbonate alteration zones spatially associated with massive sulphide mineralisation (Allen, 1997; Table 2). Carbonate alteration of probable early paragenesis comprises matrix impregnations that are common in the TSV and lower units of the hangingwall volcaniclastic mass flow sequence, and that occur locally in the footwall and base of the hangingwall sill. These impregnations were recrystallised and remobilised during S2 development, but were probably first introduced into the rocks early because they have strong stratigraphic control and are locally overprinted by S1 foliation. Alteration within feldspar phenocrysts in the footwall, TSV and hangingwall probably formed at various stages, including early.

The spotty, massive and blebby carbonates and sub-spheroidal veins spatially associated with mineralisation are all manganiferous, at least to several tens of metres distance from massive suphide (Table 2). In contrast, the carbonate impregnations and alteration of feldspar phenocrysts are all calcitic with less than 4 mole% MnCO3 regardless of stratigraphic position, except in the base of the hangingwall sill directly above ore where values reach 8.1 mole% MnCO3.

Three analyses from different layers within the same finely and strongly concentrically layered carbonate spheroid returned three different compositions ranging from rhodochrosite to manganoan ankerite (Plate 1, Table 2 sample 1361.A2). This indicates there were fluctuations in fluid chemistry and/or environmental conditions during early concretionary growth of the carbonate spots. In contrast, the more faintly layered spots have a smaller range in chemical composition, but include the minerals rhodochrosite, kutnahorite and manganoan ankerite. These faintly layered spots include ones that were originally faintly layered, and others that were well layered but have been partially recrystallised. The sub-spheroidal veins cut the spotty carbonates and are therefore interpreted to be younger than most of the spotty carbonate. These early veins show an even smaller variation in chemical composition in the data set of this study and all comprise kutnahorite. This data suggests that Mn-bearing carbonate compositions were initially highly variable and became less varied or more homogenised with time during the early alteration stages.

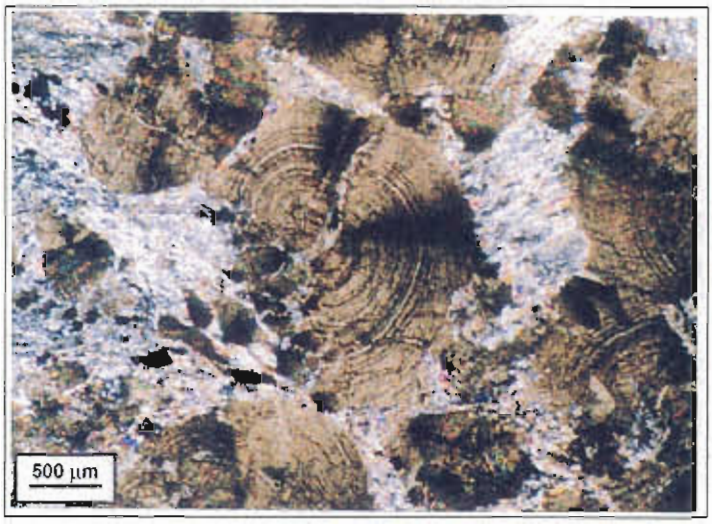

a)Photomicrograph (crossed nicols) of finely and strongly concentrically layered, spheroidal, manganiferous carbonate spots in sericite matrix. Matrix is strongly foliated and carbonate spots are partially dismembered by tectonic deformation. Sample 120R - 13161.4B

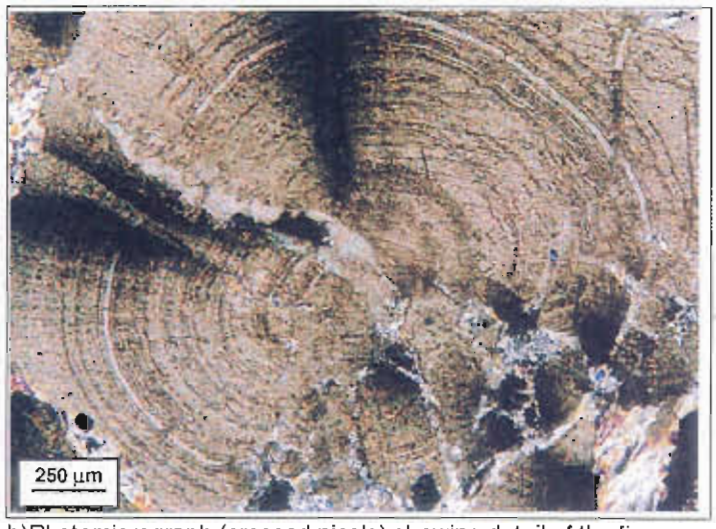

b)Photomicrograph (crossed nicols) showing detail of the fine concentric layering in the manganiferous carbonate spheroid in the cantre of photograph (a). Sample 120R - 1361.4B

c)Photomicrograph (crossed nicols) of a diffusely concentrically layered, spheroidal, manganiferous carbonate spot. Sample 120R - 1364.4A

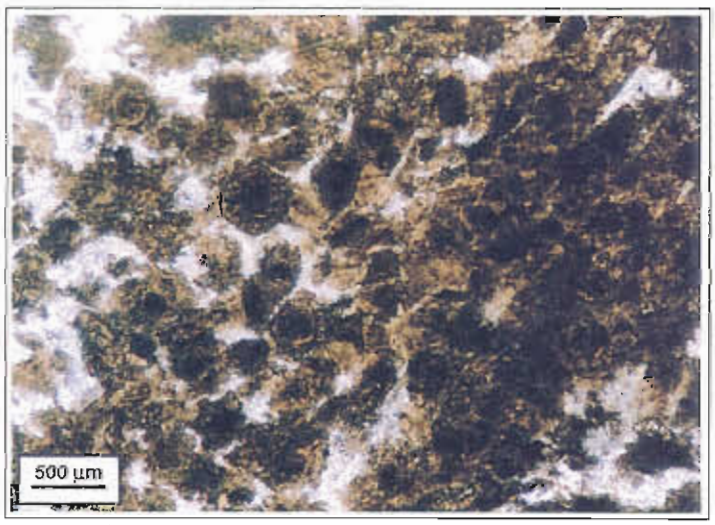

d)Photomicrograph (crossed nicols) of fine, spheroidal close - packed, spotty manganiferous carbonate (left side) grading to massive - granular manganiferous carbonate (right side). Most spots and granules are diffusely concentrically zoned and matrix is foliated sericite. Sample TS 120R 1361.4B

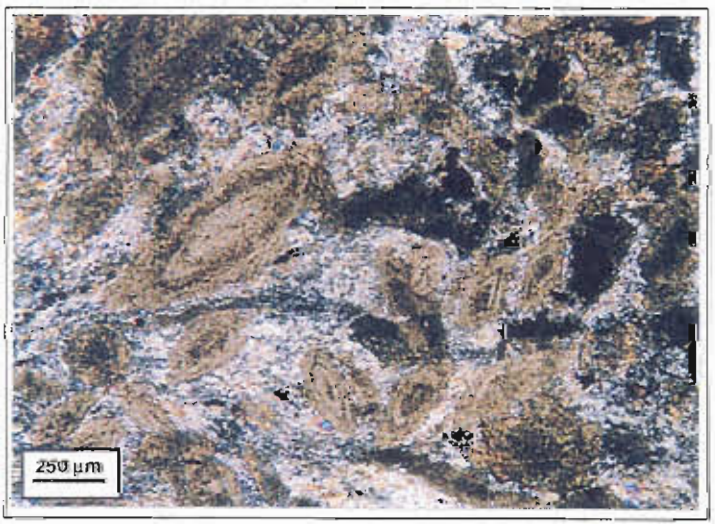

e)Photomicrograph (crossed nicols) of concentrically zoned, lozenge shaped, manganiferous carbonate spots in foliated sericite marix. Sample 120R - 1364.4B

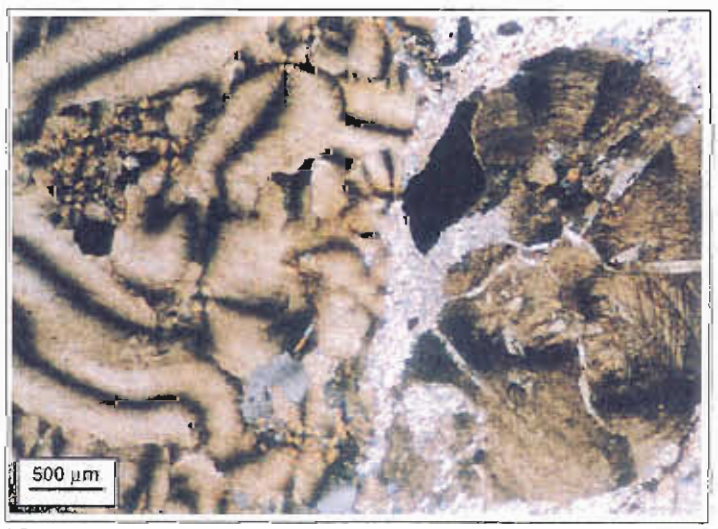

f)Photomicrograph (crossed nicols) of spotty manganiferous carbonate in sericite matrix (right side) cut by early manganiferous carboante vein (left side) with complex spherulitic to curvi - radial extinction. Sample 120R - 1361.4A

Parageneses related to the main tectonic deformation (syn-S2 cleavage)

Carbonate generations that formed during the main S2 cleavage deformation comprise carbonate veins, carbonate–quartz veins and minor carbonate–chlorite veins that cut S1 foliation and are strongly folded and/or foliated by S2. These veins occur in all stratigraphic units, and show no preferred spatial relationship to the massive sulphide lenses. The veins are especially abundant in the main hangingwall black shale where they form up to 20% of the rock. Some alteration within feldspar phenocrysts probably also occurred during tectonic deformation. Areas of earlier carbonate alteration that were recrystallised and locally remobilised during S2 deformation are classified as pre- to syn-cleavage alteration parageneses in Table 2.

The syn-cleavage veins, alteration of feldspar phenocrysts, and earlier carbonates that were recrystallised during deformation, are all calcitic in composition with less than 4 mole% $MnCO_3$ and 2 mole% $FeCO_3$, except where they occur in the spotty carbonate and sericite–carbonate alteration zones close to massive sulphide. These latter syn-cleavage carbonates that are close to ore and/or overprint earlier MnFe-bearing carbonate alteration, are generally similar in chemical and mineralogical composition to the precursor carbonates. For example, in the spotty carbonate alteration zone, the syn-tectonic carbonate veins are mainly kutnahorite, similar in composition to earlier sub-spheroidal veins. However, locally there is a trend to more Fe-rich carbonate compositions in the syn-cleavage veins, and Fe-rich compositions over 12 mole% $FeCO_3$ are restricted to syn-cleavage and post-cleavage alteration parageneses. The only possible exception consists of ferroan rhodochrosite blebs with 25–30 mole% $FeCO_3$ that are clasts (wall rock inclusions) within tectonically mechanically remobilised massive sulphide in K-lens (sample 1366.A3, Table 2). These blebs could be clasts of pre-cleavage spotty carbonate. However, they were strongly deformed and recrystallised during deformation and consequently their composition could have been modified during deformation.

The syn-cleavage veins within the spotty carbonate alteration zone, like the sub-spheroidal veins discussed above, also show less chemical variation than the early spotty to massive carbonates that they cut.

Late parageneses (late-S2 to post-S2 cleavage)

Late carbonate alteration parageneses comprise veins and their alteration haloes that have S2 foliation but are much less deformed than their host rocks (parageneses 17 and 19 in Table 1 of Large et al. (1998b)), or that cut S2 and are undeformed (parageneses 19 and 20). Veins of parageneses 19 and 20 are widespread, show no preferred spatial association with the massive sulphide ore, and are generally most abundant in the hangingwall volcaniclastics mass flow sequence, and deep in the footwall. Veins of paragenesis 17 are uncommon. Veins of parageneses 17 and 19 can be distinguished by their different overprinting relationship with the distinctive chlorite vein network of paragenesis 18 (Table 1 and Rosebery data sheet 113RD1-865 in section 2.1).

These late- to post-S2 veins include calcitic carbonate veins (paragenesis 19) identical in composition to the syn-cleavage veins discussed above. However, unlike the earlier generations of carbonate alteration discussed above, they also include Fe±Mn-rich compositions even in areas with no evidence of previous FeMn-bearing alteration. The paragenesis 19 veins that are not calcitic are pale brown weathering, weakly manganiferous ankerites. These veins typically occur in vein clusters with associated distinctive 1–5 m wide bleached sericite > carbonate alteration haloes. These occur in both the hangingwall and footwall, and proximal and distal to massive sulphide (see alteration cross section, Large et al. (1998b)). The paragenesis 17 veins have Fe>Mn manganoan siderite together with arsenopyrite, and the paragenesis 20 veins contain either Fe>Mn manganoan siderite or Mn>Fe ferroan rhodochrosite together with arsenopyrite, fluorite, tourmaline and chlorite. The paragenesis 20 veins are interpreted as medial to distal veins from the nearby mineralised Devonian granites that lie southwest and probably underneath Rosebery. Paragenesis 17 veins are similar in appearance and composition to the paragenesis 20 veins and could be the earliest members of the granite-related veining. If so they indicate that the granite-related mineralisation commenced before the end of S2 cleavage

Photomicrograph (crossed nicols) of intergrown, spheroidal, manganiferous carbonate spots enclosing abundant sericite altered glass shards. The glass shards are well preserved and undeformed wheras the sericite matrix enclosing the carbonate spots has no relict primary textures and is strongly deformed.

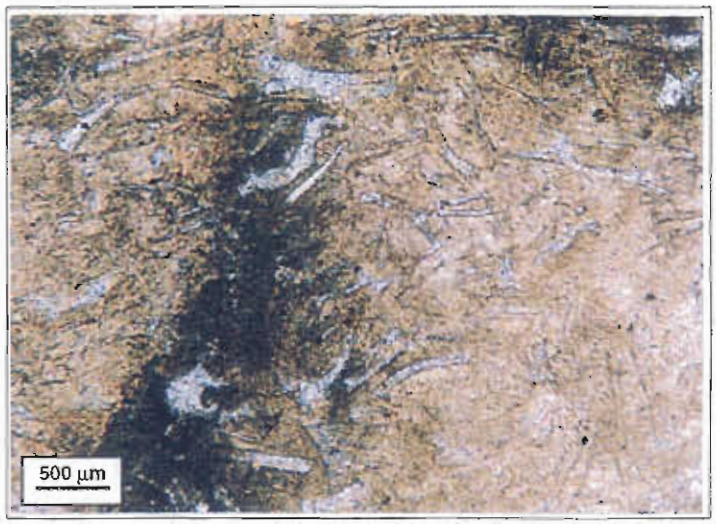

Photomicrograph (crossed nicols) showing detail of the relict glass shards in photograph (g). The glass shards are superbly preserved, undeformed, and replaced by very fine grained sericite and locally by carbonate. The space between the distinct sericite altered glass shards has faint stick like textures interpreted as small glass shard fragments (vitric dust) replaced by carbonate and sericite. sample 120R - 1364.4l

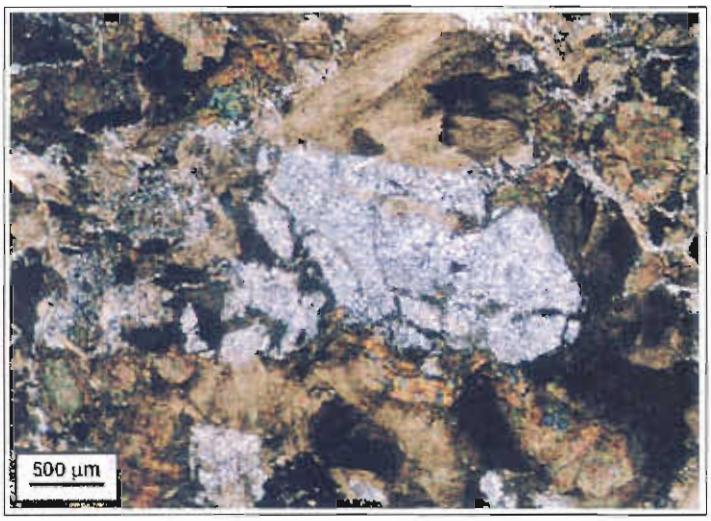

Photomicrograph (crossed nicols) of a feldspar phenocryst completely replaced by fine grained sericite and enclosed by a very diffusely concentrically layered, manganiferous carbonate spheroid. Sample 120R-1364.4B.

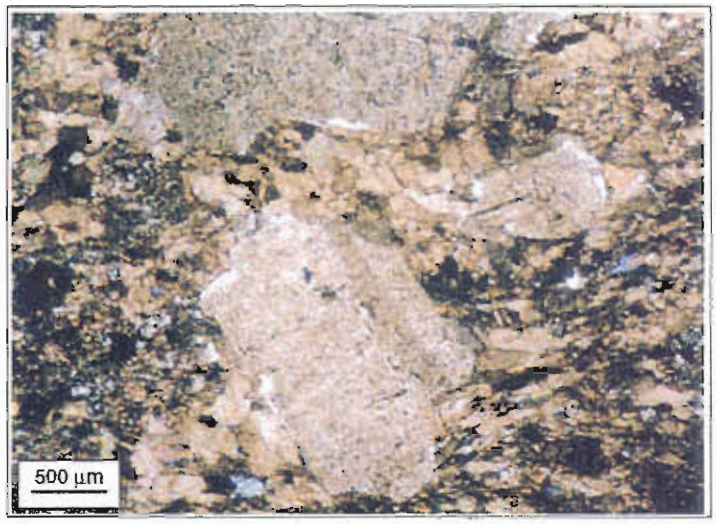

Photomicrograph (crossed nicols) of matrix calcite impregnation in the feldspar crystal rich lower part of a mass flow unit of the hangingwall volcaniclastics. The calcite locally has almost completely replaced the matrix and is strongy foliated. Sample 120R-1100.3.

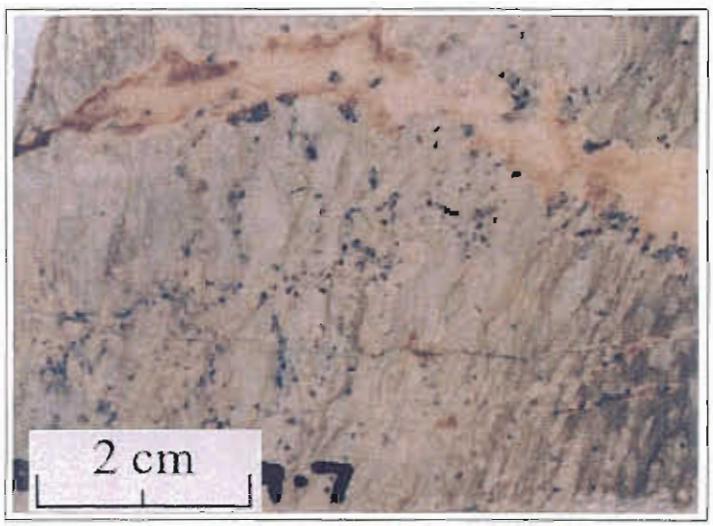

A moderately foliated manganiferous carbonate vein cutting strongly foliated, stongly sericite - carbonate altered, feldapar - phyric pumice breccia of the footwall volcanics. Tiny dark spots are disseminated sulphide. Sample 109R-709.7.

development, or at least before reactivation of S2 cleavage.

The Fe-rich, manganoan siderite compositions in paragenesis 17 and 20 veins were not recorded from any other carbonate generation. However, it is interesting that the Mn-rich ferroan rhodochrosite compositions in the paragenetically last set of veins are similar to ferroan rhodochrosites in the massive sulphide of K lens. This clearly demonstrates that carbonate composition is not specific to particular generations of carbonate alteration. A possible explanation, and a feature important to exploration, is that in our data set all the strongly manganiferous carbonates with mole% Mn>Fe occur in the footwall to massive sulphide in the proximal drill hole (120R). In contrast, all carbonates in the distal drill hole (109R), including the strongly manganiferous carbonates, have mole% Fe>Mn (Table 2). Although our data set is not large enough to be absolutely certain, the data suggests that the early chemical anomalies set up around the Rosebery orebody influenced the chemical and mineralogical composition of subsequent generations of alteration right through to the last (twentieth) major generation.

Mineral chemistry was not obtained from the Mount Black Fault, which marks the top of the Hangingwall Volcaniclastics unit. However, drill core logging and petrography indicate the fault zone contains cream to buff coloured, FeMn-bearing carbonates associated with late syn-tectonic to post-tectonic veins (generations 17, 19, 20 in Table 1 of Large et al. (1998b)). Whole rock chemistry (Large and Allen, 1997) indicates MnO values up to 2.5wt% (e.g. 120R) and these are attributed to manganiferous carbonates.

Conclusions

(1) There are many textural types, paragenetic generations, and chemical compositions of carbonate alteration at Rosebery.

(2) The earliest generations of carbonate comprise most of the types of spotty carbonates, and the massive and platey carbonate types. These formed soon after deposition of the host pumice breccia and vitric sandstone–siltstone facies and were spatially and temporally associated with massive sulphide mineralisation. They occur only near massive sulphide mineralisation, in the spotty carbonate and sericite–carbonate alteration zones, within 20 m of the stratigraphic level of an ore lens and within 100 m lateral distance from the edge of an ore lens. These spotty carbonate types are distinctive in drill core and consequently are an excellent guide to ore. Subsequent, syn-, late- and post-cleavage generations of carbonates do not show a prefered spatial association with the massive sulphide lenses.

(3) In the spotty carbonate alteration zone, the earliest generation of carbonate spheroids are manganiferous but very variable in composition, even within individual spheroids. Subsequent generations of spheroids and early veins have less variation in composition. This indicates that fluctuations in fluid chemistry and/or environmental conditions during early concretionary carbonate growth, resulted in great chemical and mineralogical complexity right down to the grain and hand specimen scales. This initial complexity is interpreted to have been partially homogenised by subsequent generations of carbonate growth.

(4) Within 10–50 m of massive sulphide mineralisation, and especially in the footwall, where Mn–Fe anomalies were set up in early generations of alteration, subsequent overprinting generations perpetuate the anomalous Mn-rich character, but as noted above the compositions tend to be more homogenised. Thus although the early generations of carbonate alteration are most diagnostic of proximity to ore, sampling of most later generations of carbonates in the same rocks would return a similar chemical signature, i.e. recognition of the textural type and paragenetic generation of carbonate is desirable, but does not preclude the use of carbonate mineral chemistry as an exploration guide.

(5) Where early alteration was not anomalous in Mn and Fe, subsequent generations of carbonate alteration were mainly calcitic. Important exceptions are the late generations of veins

Table 2: Rosebery carbonate alteration: Relationships between carbonate mineral composition and alteration texture, paragenesis, stratigraphic position and proximal versus distal position. Data from drill holes 120R and 109R.

Stratigraphic position	Texture	Paragenesis (1-20)	Sample numbers	MnCO3 mole%	FeCO3 mole%	MgCO3 mole%	CaCO3 mole%	Total
PROXIMAL STRATIGRAPHIC TRANSECT INCLUDING ORE LENS (120R)								
Hangingwall	Veins	syn-cleav (16)	1083.A3.2	3.3	0.9	0	97.5	101.7
			1094.A4.1	1.9	0.4	0	100.0	102.4
			1100.A1.2	1.7	0.4	0	101.5	103.6
	Matrix impregnation	pre- to syn-cleavage (10-16)	1083.A2.1	2.2	0.7	0	98.6	101.4
			1100.A4.2	1.3	0.4	0	100.3	101.9
			1169.A3.4	2.1	1.6	0.4	98.4	102.5
	Alteration within feldspar phenocryst	pre- to syn-cleav (7-16)	1147.A1.1	3.0	1.3	0	96.4	100.7
			1169.A1.2	2.4	1.6	0	98.0	102.0
Black shale	Veins	syn-cleav (16)	1184.A2.1	1.3	1.8	1.2	96.9	101.2
			1229.A1.2	0.7	1.4	1.4	95.9	99.5
			1256.A1.1	0.9	0.4	0.5	98.2	100.1
TSV	Veins	syn-cleav (16)	1237.R4.1	0.5	0.5	0.9	96.2	98.1
			1241.A1.2	0.7	1.7	0.8	95.1	98.3
			1265.A2.1	0.7	0.6	0.3	103.0	104.7
	Matrix impregnation	pre- to syn-cleav (10)	1237.A2.2	0.5	0	0	101.1	101.7
			1265.A1.3	0.5	0.4	0	101.2	102.1
	Alteration within feldspar phenocryst	pre- to syn-cleav (7-16)	1241.A3.1	0.5	0.8	0.5	95.7	97.9
Hangingwall sill: top	Alteration within feldspar phenocryst	pre- to syn-cleav (7-16)	1291.A2.1	0.9	0.4	0.5	98.0	99.8
	Veins	syn-cleav (16)	1315.A3.1	2.3	1.0	0	99.1	102.4
Hangingwall sill: base	Alteration within feldspar phenocryst	pre- to syn-cleav (7-16)	1353.A2.1	8.1	1.6	1.1	88.2	98.9
	Matrix impregnation	pre- to syn-cleav(10-15)	1353.A3.1	7.8	1.5	0.8	89.3	99.5
Carbonate alteration at top of ore zone	Late veins in spotty carbonate	pre- to syn-cleav (7-16)	1357.A1.1	34.0	7.7	6.7	47.9	96.2
			1361.A1.3	55.8	27.2	13.6	6.7	103.7
			1361.A1.6	36.6	10.4	8.3	46.1	101.4
			1365.A6.1	41.3	3.6	3.8	52.1	100.7
			1365.B5.2	36.8	9.7	7.8	45.9	100.2
	Early sub-spheroidal veins in spotty carbonate	early pre-cleav (6)	1357.A3.1	33.7	7.7	6.8	48.7	97.0
			1361.A1.1	39.0	5.7	5.5	46.6	96.8
			1364.B7.1	41.8	2.8	4.4	52.1	101.0
			1365.A2.1	44.8	4.0	4.7	47.2	100.7
	Massive	pre-cleav (6)	1365.B2.1	27.4	3.3	16.5	53.9	101.1
	Spotty-lozenge	pre-cleav (6)	1364.A6.1	91.2	5.1	3.8	1.7	101.8
	Spotty-spheroidal, faint concentric layering	pre-cleav (2-6)	1357.A2.1	34.2	7.0	7.3	48.3	96.9
			1364.A1.1	90.6	7.0	2.7	2.5	102.7
			1364.B8.1	89.9	1.4	1.6	6.7	99.5
	Spotty-spheroidal, strong fine concentric layering	pre-cleav (2)	1361.A2.2	87.1	7.4	1.5	2.3	98.3
			1361.A2.1	7.7	11.6	25.9	54.3	99.8
			1361.A2.4	16.3	9.0	22.3	50.6	98.2

Ore	Blebs in remobilized ore	pre- to syn-cleav (6-7)	1366.A3.1	71.2	25.7	4.0	1.1	101.9
			1366.A3.2	54.6	30.9	13.2	4.1	102.7
Footwall	Veins, and halo	post-cleav (20)	1436.A3.1	70.5	18.9	2.8	9.5	101.7
			1436.A4.2	60.8	32.5	4.5	4.6	102.4
	Blebs (replacing feldspar crystals)	pre- to syn-cleav (6-10	1399.A2.1	28.3	10.2	13.5	48.5	100.6
	Alteration within feldspar phenocryst	pre- to syn-cleav (7-16)	1421.A1.2	3.9	30.1	16.0	52.3	102.3
			1421.A5.2	3.0	20.5	24.3	53.8	101.6
			1440.A3.1	2.8	1.7	0.8	94.0	99.2
DISTAL TRANSECT 500 m FROM ORE (109R)								
Hangingwall	Veins	late- to post-cleav (19)	424.A4.2	0.8	0.3	0.1	98.9	100.0
			475.A1.1	3.5	30.2	13.0	53.4	100.0
			509.A1.2	0.7	0.4	0.3	98.6	100.0
	Veins, extensional fractures	syn-cleav (15-16)	450.A2.2	1.4	0.5	0.2	97.9	100.0
			481.A4.1	1.8	1.2	0.2	96.8	100.0
	Matrix impregnation	pre- to syn-cleav(10-16)	450.A3.1	0.8	1.2	0.2	97.8	100.0
	Alteration within feldspar phenocryst	pre- to syn-cleav (7-16)	373.A5.2	1.1	0.4	0.3	98.2	100.0
			424.A1.1	0.8	0.4	0.4	98.4	100.1
			434.A1.1	1.4	0.6	0.2	97.9	100.0
			509.A3.1	0.6	0.4	0.4	98.5	99.9
Black shale	Veins	syn-cleav (16)	553.A1.1	1.0	0.9	1.4	96.6	99.8
			553.A2.2	0.8	0.5	1.1	97.5	100.0
TSV	Matrix impregnation	pre- to syn-cleav (10)	561.A1.2	0.8	0.4	0.8	98.1	100.0
			561.A2.2	1.0	0.6	1.2	97.4	100.0
Footwall	Vein and bleached halo	post-cleav (20)	723.A1.1	43.6	51.2	4.2	1.1	100.0
	Vein	late-cleav (19)	590.A2.1	1.8	1.1	0.5	96.5	99.9
			698.A2.2	1.3	0.8	0.6	97.2	100.0
			709.A4.2	9.9	17.5	16.7	56.1	100.1
			709.A4.3	3.1	0.7	0.1	96.2	100.1
	Vein	syn-/late-cleav (17)	709.A3.1	30.8	60.8	6.2	2.1	99.9
	Blebs in bleached halo to above vein	syn-/late-cleav (17)	709.A8.2	32.7	58.7	5.5	3.1	100.0
			709.A1.2	44.3	49.9	4.3	1.6	100.1
	Veins, extensional fractures	syn-cleav (15-16)	573.A1.2	1.7	0.8	0.6	96.9	100.0
			590.A1.1	1.8	1.1	0.5	96.6	99.9
			670.A1.1	1.6	0.7	0.4	97.2	100.0
			707.A4.2	1.1	0.5	0.4	98.2	100.1
			726.A5.1	1.4	0.7	0.3	97.7	100.0
	Alteration within feldspar phenocryst	pre- to syn-cleav (7-16)	620.A3.1	2.2	1.1	0.4	96.0	99.7
	Matrix impregnation	pre-cleav (10)	701. A3.1	0.5	1.4	0.6	97.5	100.0

(paragenesis 17, 19 and 20), which include Fe ± Mn-rich compositions even in areas with no evidence of previous FeMn-bearing alteration. This emphasises that the presence of Mn–Fe carbonates does not alone indicate close proximity to massive sulphide. The presence of early, pre-cleavage generations of MnFe-bearing carbonates, and Mn>Fe composition, are additional criteria that characterise carbonates proximal to ore at Rosebery.

(6) The late generations of carbonate veins that are interpreted to be many millions of years later than massive sulphide mineralisation, appear to show a large scale zonation from both Mn>Fe and Fe>Mn compositions within 100 m of ore, to only Fe>Mn compositions distal to ore. The data set in this study is not large enough and the sampling was not extended sufficiently distal from ore to be certain of this large scale zonation, and whether the MnFe contents of these late paragenetic alterations reflect partial redistribution of the early formed MnFe anomaly associated with massive sulphide mineralisation, or whether they include the influx of new MnFe unrelated to the earlier mineralisation. This should be resolved to determine whether the Mn/Fe ratio of carbonates associated with isolated distal veins can be used as a regional exploration guide, and for mine scale exploration more than 100 m from known ore.

(7) Early carbonate alteration in the hangingwall more than 10–20 m stratigraphically above the level of massive sulphide mineralisation comprises calcitic impregnations with very low Mn and Fe contents. Apart from along the Mount Black Fault, the only FeMn-bearing carbonates recorded in these hangingwall rocks are a late- to post-cleavage generation (paragenesis 19) of weakly manganiferous ankerite veins with less than 4 mole% $MnCO_3$ and Fe>Mn. These veins typically occur in vein clusters with associated distinctive 1–5 m wide bleached sericite > carbonate alteration haloes. They occur in both the hangingwall and footwall, and proximal and distal to massive sulphide, and consequently do not appear to be related to the Rosebery deposit.

References

Allen, R. L., 1991, Stratigraphy, structure, volcanology and ore genesis of the Rosebery–Hercules Zn–Pb–Cu–Au massive sulphide district, Tasmania. Unpublished report to Pasminco Exploration, Melbourne Australia. 3 volumes.

Allen, R. L. 1994a. Volcanic facies analysis indicates large pyroclastic eruptions, sill complexes, synvolcanic grabens, and subtle thrusts in the Cambrian "Central Volcanic Complex" volcanic centre, western Tasmania. Contentious Issues in Tasmanian Geology Symposium, Geological Society Australia Tasmania Division, Hobart. Abstracts number 39, p. 3.

Large, R., Gemmell, J.B. and Herrmann, W., 1998a. Summary of geochemical and mineralogical vectors to ore, based on the seven case studies in P439. CODES AMIRA/ARC P439, Final report.

Large, R., Allen, R.L., Blake, M. and Herrmann, W., 1998b. Alteration halo model for the Rosebery VHMS deposit, western Tasmania. CODES AMIRA/ARC P439, Final report.

Chlorite alteration associated with syn-volcanic granites and Cu-Au mineralisation: A pilot study along the Jukes Road

Bill Wyman
Centre for Ore Deposit Research

Abstract

Hydrothermal alteration mineral assemblages containing chlorite form some of the most easily identified and mapped alteration mineral assemblages surrounding the granite related Cu-Au mineralisation at the Jukes Prospect. The Jukes Road forms an excellent cross-section through several of these chlorite bearing alteration mineral assemblages and it therefore offers an excellent opportunity to examine potential variations in chlorite mineral chemistry as a function of distance. Chlorite analyses were conducted using the Electron Microprobe at the University of Tasmania Central Science Laboratory (CSL). Five different habits of chlorite were probed as part of this study. The five habits are: (1) chlorite replacing biotite (?) phenocrysts (some could be amphiboles), (2) chlorite in chlorite-magnetite ± sulfide veins, (3) chlorite replacing feldspar phenocrysts, (4) interstitial (intergranular) chlorite between feldspar and quartz grains, and (5) chlorite in the matrices of mineralised hydrothermal breccias.

Microprobe data was examined in relation to distance from mineralisation and also in relation to each of the other five habits of chlorite. Chlorite alteration typically occurs with weak to moderate sericite alteration and occasionally with weak to intense K-feldspar alteration. Chlorite alteration is almost always accompanied by magnetite in amounts directly proportional to the degree of chlorite alteration. This study examined the mineral chemistry of chlorite within the various habits. A comparison is made between chlorites within a single relatively homogeneous feldspar-phyric rhyolite lava and chlorites within a cross-cutting quartz-feldspar ± biotite porphyry.

Data from the chlorite microprobe analysis indicate that for both the feldspar-phyric rhyolite lava and the quartz-feldspar ± biotite porphyry: (1) There is a large variability in Mg number (Mg# = $Mg_{(total)}$ / $Fe_{(total)}$ + $Mg_{(total)}$) within individual samples for a given chlorite type. (2) The range of Mg#'s from chlorite replacing feldspar phenocrysts, interstitial chlorite and chlorite in veins is the same and overlaps the range of Mg#'s from chlorite in the cores of the hydrothermal breccias. (3) There is a weakly defined decrease in the Mg# within the cores of the mineralised breccias that probably reflects an increase in iron associated with an increase in mineralisation. (4) Chlorites from within the quartz-feldspar ± biotite porphyry dykes overlap the same ranges in Mg# values as those within the feldspar-phyric rhyolite lava. (5) The Mg# of whole rocks corresponding to the probed samples, show the same range of Mg# values outside the mineralised zone. Near the boundaries of , and within the mineralised zone the Mg# of the host rocks is less than the Mg# of chlorite indicating increased iron. This supports the conclusion that magnesium in the mineralised zone is contained within chlorite and not within other mineral phases. (6) As a result of the overlap in the ranges of chlorite values within a given chlorite habit and the overlap in the ranges between various chlorite types, when plotted against distance, chlorite composition is not a useful vector toward mineralisation.

Based on the Al^{IV} content an attempt to calculate chlorite formation temperatures was made for each main type of chlorite. The determined range of average chlorite temperature values is relatively narrow (328-362°C) and the overall range is only slightly broader (312-386°C). Several distinct separations in the temperature data can be observed.

First, the average chlorite temperature data within the quartz-feldspar ± biotite porphyry dykes (356-358°C) is almost identical regardless of chlorite habit. Second, the average chlorite temperatures of the chlorite veins, interstitial chlorite and the breccia matrix chlorite within the rhyolite (360-362°C) are very close to the temperatures shown in the quartz-feldspar ± biotite porphyry dykes. Third, the chlorite temperatures in the chlorite that replaced both biotite and feldspar phenocrysts within the feldspar-phyric rhyolite are almost identical (328° and 331°C) and are significantly lower than the chlorite temperatures within the quartz-feldspar ± biotite porphyry dykes. The 320–360°C range would be consistent with temperatures expected from the later lower greenschist facies regional metamorphic event. However, equilibration of calculated chlorite temperatures and compositions would also be expected. Since two clear populations of temperature exist and the data shows scatter on a plot of chlorite Mg# vs whole rock Mg#, the calculated temperatures are interpreted to represent relict hydrothermal chlorite formation temperatures.

Introduction

Hydrothermal alteration mineral assemblages containing chlorite form some of the most easily identified and mapped alteration mineral assemblages surrounding granite related Cu-Au mineralisation at the Jukes Prospect. Jukes Road forms an excellent cross-section through several of these chlorite bearing alteration mineral assemblages as shown on the geologic plan (Figure 1). This cross-section, therefore offers an excellent opportunity to examine potential variations in chlorite mineral chemistry as a function of distance from the mineralised breccias at Jukes. Chlorite in the Central Volcanic Complex (CVC) is expressed in varying degrees throughout almost all facies mapped as part of this study. Chlorite typically occurs with weak to moderate sericite ± carbonate alteration and occasionally with moderate to intense K-feldspar alteration.

Chlorite alteration is well developed in all volcaniclastic and mass flow deposits along the western margin of the CVC where it is typically weak to moderate and is best developed in rocks with well developed regional cleavage. Shears and faults are typically associated with intense, texturally destructive chlorite development. Details of the regional geology and hydrothermal alteration along the Jukes Road are described in (Wyman, 1996) and (Wyman et al., 1996).

This report will focus on chlorite alteration within the feldspar-phyric columnar jointed rhyolite unit that is the host to the Jukes Cu-Au mineralisation. Comparisons will be made with chlorite alteration within several quartz-feldspar ± biotite porphyry dykes that cut through the rhyolite unit. Sample description sheets of each rock sampled are included for reference.

Chlorite alteration within the large feldspar-phyric columnar jointed rhyolite unit occurs in two fashions. Regional weak chlorite alteration is well developed in all rocks. Hydrothermal chlorite alteration is also well developed and is discussed in the next section. The regional chlorite alteration is associated with weak to moderate sericite alteration throughout the entire unit. This alteration is not texturally destructive, and is believed to be of metamorphic or diagenetic origin. Chlorite alteration is confined to the groundmass probably as a result of ferromagnesian mineral destruction. The intensity of chlorite alteration development in this type of alteration is controlled by fluid/rock ratios and by the original ferromagnesian mineral contents of the rocks.

Hydrothermal chlorite alteration

Studies of hydrothermal chlorite alteration have been conducted by several other workers in the Mt. Read Volcanics including Walshe (1981), Polya et al. (1986) and Hendry (1981). Polya et al. (1986), studied the Murchison River Gorge as a possible cross-section through a Cambrian massive sulfide system and included a detailed study of chlorite mineral chemistry. He recognised similar overall alteration mineral assemblages to those found in the Jukes-Darwin area in this study.

Hydrothermal chlorite development in the feldspar phyric rhyolite unit is associated with a corresponding increase in total iron and manganese in the rocks. Studies of chlorite textures and chemistry suggest six major habits of chlorite at the Jukes

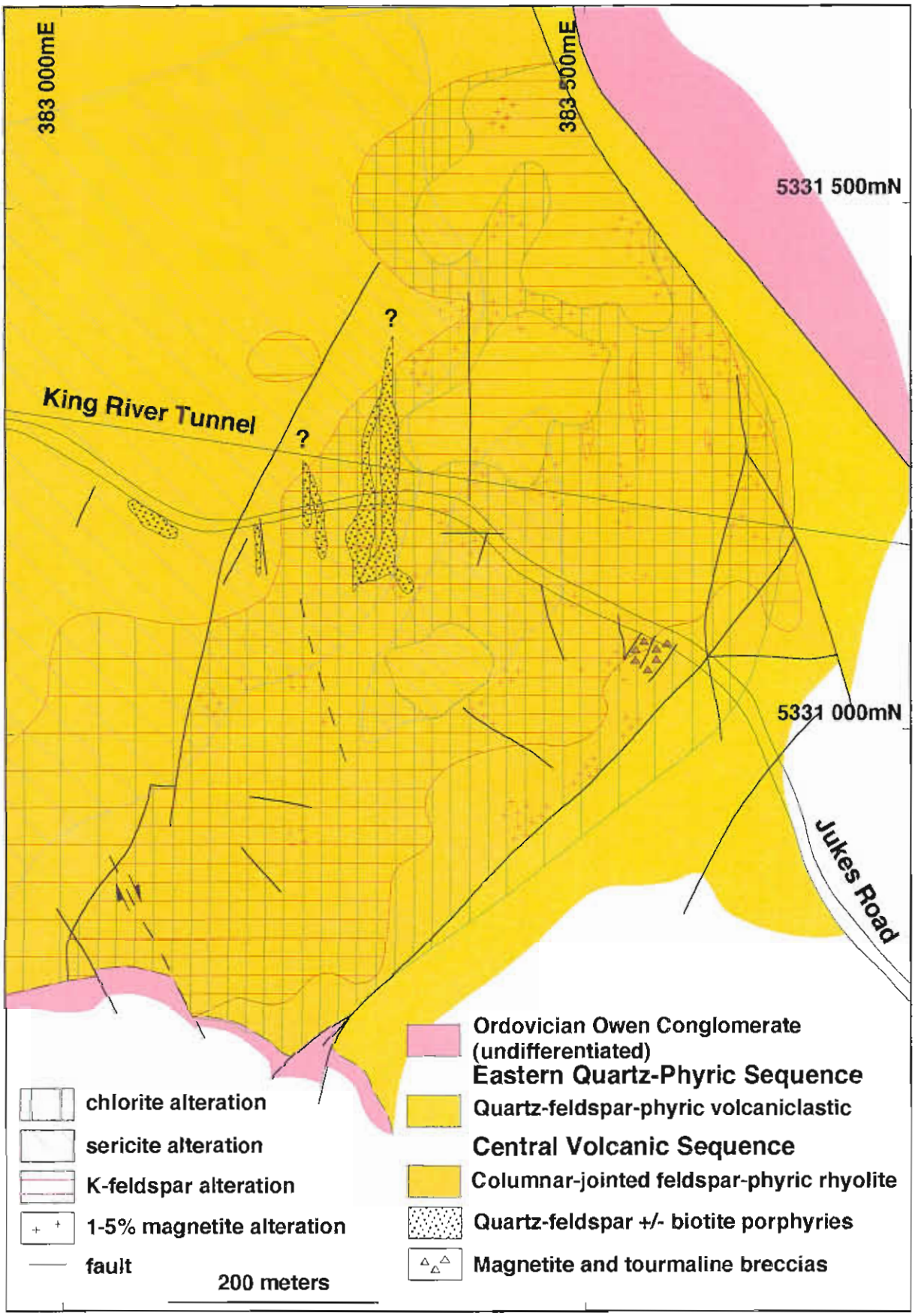

Figure 1: Geologic Plan of the Jukes Road and Jukes Prospect area.

prospect, including the coarse euhedral chlorite that occurs with quartz in cross-cutting veins of obvious post tectonic (Devonian?) age.

Studies of chlorite textures by Doyle (1990) identified two phases of chlorite alteration at the Jukes Pty. Prospect. The first phase of Doyle's chlorite alteration (pale green) is probably part of the regional pervasive alteration seen throughout the CVC, and is not part of the hydrothermal story. Doyle's second phase of chlorite alteration (dark green) is probably part of the Phase One chlorite alteration of hydrothermal origin as described by Wyman et al. (1996) and Wyman (1996). Wyman's phase One chlorite was described as pre K-feldspar alteration and generally associated with only one accessory mineral, magnetite. Phase One chlorite includes chlorite veins that have cut sericite/chlorite altered rhyolites and chlorite replacement of feldspars and the moderate occurrence with sericite in the groundmass of the feldspar phyric rhyolite. Phase Two chlorite alteration has two diagnostic features: (1) It post dates K-feldspar alteration. (2) It is associated with sulfides, magnetite and traces of tourmaline. Separating chlorite alteration into two phases is probably greatly oversimplifying the alteration story and should, therefore be revised. It is now believed that fluids capable of contributing to the formation of chlorite alteration probably existed off and on as pulses throughout the entire mineralisation history at Jukes.

Chlorite microprobe data and interpretation

Chlorites of five different types corresponding to Phase One and Phase Two chlorites of Wyman et al. (1996), were probed as part of this study. The sixth habit mentioned above, chlorite in Devonian(?) crosscutting veins was not sampled or analysed. The five sampled chlorite types are: (1) chlorite replacing biotite phenocrysts, (2) chlorite in chlorite-magnetite ± sulfide veins, (3) chlorite replacing feldspar phenocrysts, (4) interstitial (intergranular) chlorite between feldspar and quartz grains, and (5) chlorite in the matrices of mineralised hydrothermal breccias.

Chlorite alteration occurs in and around several quartz-feldspar ± biotite porphyry dykes that crosscut the feldspar-phyric rhyolite. Chlorite alteration within the dykes can be of moderate to strong intensities, and in dykes proximal to the Jukes prospect may be texturally destructive to all but the largest quartz phenocrysts. This phase of chlorite alteration is clearly syn or post-dyke emplacement. Chlorite occurs as feldspar and biotite replacement as well as in chlorite veins within the quartz-porphyry dykes. These chlorite habits were also examined in this study and results are compared to results from chlorite analyses from chlorites within the feldspar-phyric rhyolite.

Table 1 presents average microprobe chemical analyses from the five types of chlorite. The detailed chemical analyses of all of the reported samples are included in the AMIRA Project P439 database created by Blake, 1998, and discussed in another part of this report. Figure 2 is a plot of the Mg number ($Mg\# = Mg_{(total)} / Fe_{(total)} + Mg_{(total)}$) vs distance for the five habits of chlorite in both the feldspar-phyric rhyolite and the quartz-feldspar ± biotite porphyry.

Caution should be used in analysing the data using the Mg# in high iron chlorites as the FeO content in the chlorites is at least a half to a full order of magnitude greater than the MgO value. This results in a much greater influence in the chlorite chemistry as a result of the high FeO relative to MgO. In real terms, however an Fe# ($Fe\# = Fe_{(total)} / Fe_{(total)} + Mg_{(total)}$) is simply the inverse of the Mg# and does not give any more useful information in terms of chlorite mineralogy. In addition, the FeO content in the whole rocks is almost a full order of magnitude greater than the MgO value as well. The iron content of the whole rock is also effected by other iron sources such as minor iron in the feldspars, magnetite and pyrite. One possible effect of these other iron sources would be to add iron to the chlorite structure during hydrothermal and/or metamorphic alteration.

Bearing in mind the possible pitfalls of the use of the Mg# in chlorite, it is still possible to draw some useful information from the data. Data from the chlorite microprobe analysis indicate: (1) There is a large variability (range) in Mg number ($Mg\# = Mg_{(total)} / Fe_{(total)} + Mg_{(total)}$) within individual samples for a given chlorite type. The same large variability would occur in Fe#. (2) The range of Mg#'s from chlorite replacing feldspar phenocrysts, interstitial chlorite and chlorite veins is the same and overlaps the range of Mg#'s from chlorite in the matrix of the hydrothermal breccias. (3) There is a weakly defined decrease in the Mg# within the matrix of the

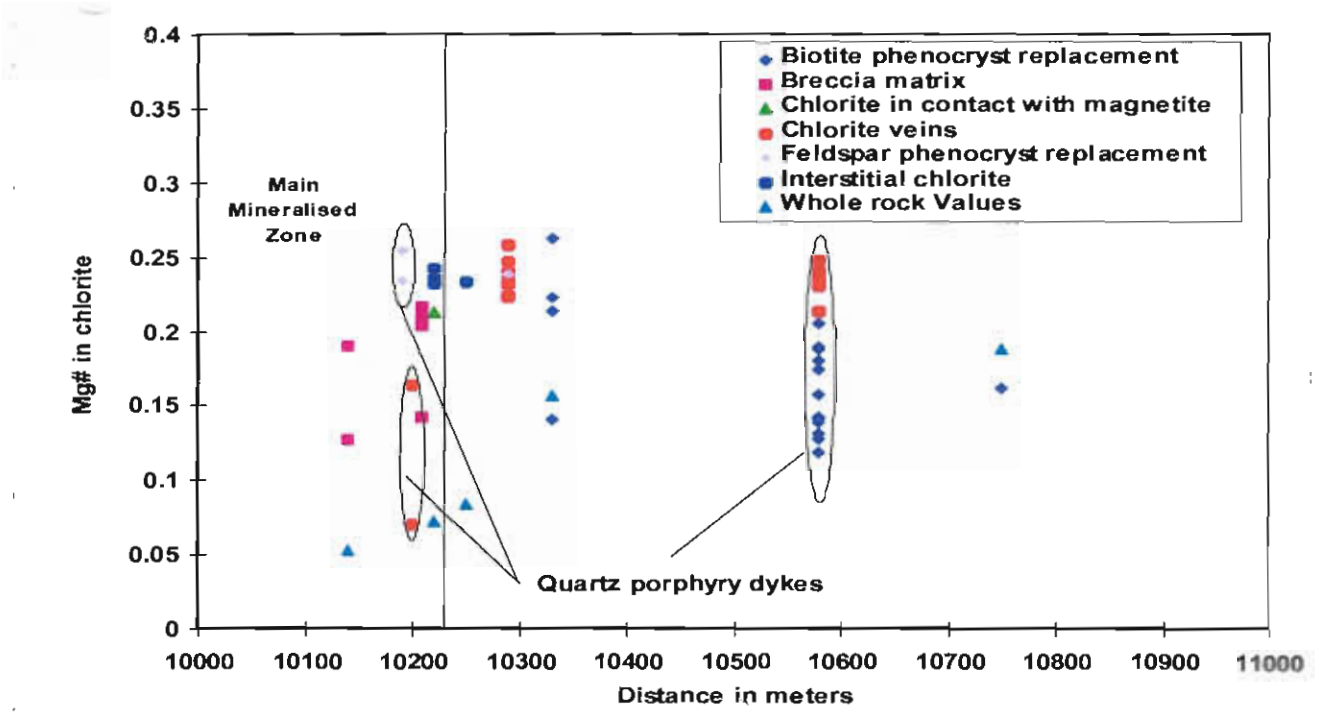

Figure 2: Plot of the Mg number (Mg# = $Mg_{(total)}$ / $Fe_{(total)}$ + $Mg_{(total)}$) vs distance for the five habits of chlorite in both the feldspar-phyric rhyolite and the quartz-feldspar +/- biotite porphyry.

mineralised breccias reflecting an increase in iron (from magnetite and pyrite) associated with an increase in mineralisation. (4) The three habits of chlorite within the quartz-feldspar ± biotite porphyry dykes overlap the same ranges in Mg# values as those within the feldspar-phyric rhyolite. (5) Outside the mineralised zone, the Mg#'s of the chlorites and the Mg#'s of the whole rocks that contain them have a similar range This supports the conclusion that magnesium in the more mineralised zone is contained within chlorite and not within other mineral phases. (6) As a result of the overlap in the ranges of chlorite values within a given chlorite habit and the overlap in the ranges between various chlorite types, when plotted against distance, the chlorite composition is not a useful vector toward mineralisation.

Chlorite geothermometry

Various models for calculating chlorite formation temperatures have been proposed by Walshe (1981, 1986a, 1986b), (Cathelineau (1985) and Kranidiotis (1987). Walshe (1981) represented the non-stoichiometry of chlorite by six end-members. Walshe (1986b) later refined this model claiming that temperature, and oxygen fugacity (fO_2) could be calculated where quartz and chlorite coexisted with an iron sulphide, and the H_2S content of the fluid could also be calculated. However, he noted that the model cannot be used to determine a temperature for chlorites with a total iron content between 32-40 wt% FeO. As shown in Table 1, all of the chlorites in this study have total FeO values within this range, therefore the model is not applicable.

Kranidiotis (1987) adapted the chlorite geothermometer of Cathelineau (1985) and proposed the following equation for the temperature of chlorite formation, based on corrected Al^{IV} concentrations where:

$$Al^{IV}_{corrected} = Al^{IV}_{uncorrected} + 0.7[Fe/(Fe + Mg)_{chl}]$$

$$\text{Temperature (T)} = 106Al^{IV}_{corrected} + 18$$

Table 2 summarises the temperature ranges calculated, based on the Al^{IV} chlorite geothermometer, for each main type of chlorite. While the range of

Table 1 Average microprobe chemical analyses from the five habits of chlorite probed as part of this study.

	Feldspar-phyric rhyolite					Quartz-feldspar ± biotite porphyry dykes		
Label	Biotite Pheno. Repl.	Feld. Pheno. Repl.	Chlotite vein	Interstitial	Breccia, Matrix	Biotite Pheno. Repl.	Feld. Pheno. Repl.	Chlotite vein
SiO2	25.28	24.67	23.67	23.44	23.65	23.68	23.49	23.66
TiO2	0.05	0.05	0.05	1.13	0.04	0.08	0.03	0.03
Al2O3	19.55	19.16	20.28	19.56	20.39	20.14	19.20	19.87
Cr2O3	0.02	0.01	0.01	0.01	0.00	0.02	0.00	0.01
FeO	36.67	39.26	38.40	38.03	39.57	37.10	40.70	37.86
MnO	0.36	0.32	0.53	0.21	0.38	0.25	0.16	0.24
MgO	6.42	3.70	5.33	5.28	4.51	6.65	4.73	6.14
CaO	0.01	0.05	0.03	0.02	0.03	0.05	0.03	0.06
Na2O	0.04	0.13	0.05	0.03	0.03	0.02	0.02	0.03
K2O	0.22	0.30	0.14	0.31	0.09	0.04	0.12	0.06
ZnO	0.19	0.16	0.14	0.12	0.09	0.06	0.05	0.06
NiO	0.00	0.01	0.01	0.01	0.01	0.01	0.00	0.02
H2O(c)	10.80	10.48	10.63	10.57	10.60	10.66	10.48	10.60
Sum Ox%	99.58	98.27	99.26	98.72	99.39	98.77	99.01	98.64
Cations								
Si	5.61	5.64	5.34	5.32	5.35	5.33	5.38	5.35
Ti	0.01	0.01	0.01	0.19	0.01	0.01	0.01	0.01
Al/Al IV	2.39	2.36	2.66	2.68	2.65	2.67	2.62	2.65
Al VI	2.73	2.81	2.73	2.56	2.79	2.67	2.55	2.65
Cr	0.00	0.00	0.00	0.00	0.00	0.00	0.00	0.00
Fe2+	6.81	7.51	7.26	7.23	7.49	6.98	7.79	7.17
Mn2+	0.07	0.06	0.10	0.04	0.07	0.05	0.03	0.05
Mg	2.12	1.26	1.79	1.78	1.52	2.23	1.61	2.07
Ca	0.00	0.01	0.01	0.01	0.01	0.01	0.01	0.01
Na	0.02	0.06	0.02	0.01	0.01	0.01	0.01	0.01
K	0.06	0.09	0.04	0.09	0.02	0.01	0.04	0.02
Zn	0.03	0.03	0.02	0.02	0.02	0.01	0.01	0.01
Ni	0.00	0.00	0.00	0.00	0.00	0.00	0.00	0.00
OH	16.00	16.00	16.00	16.00	16.00	16.00	16.00	16.00
Sum Cat#	35.86	35.84	35.99	35.92	35.94	36.00	36.05	36.00
XMg	0.24	0.14	0.20	0.20	0.17	0.24	0.17	0.22
Uncorrected Al IV	2.39	2.36	2.66	2.68	2.65	2.67	2.62	2.65
Fe/(Fe+Mg)	0.76	0.86	0.80	0.80	0.83	0.76	0.83	0.78
Corrected Al IV	2.92	2.96	3.22	3.24	3.23	3.20	3.20	3.19
Chlorite Temp oC	328	331	360	362	360	357	358	356

average chlorite temperature values is relatively narrow (328°–362°C), the overall range is slightly broader (312°–386°C). Several distinct separations in the temperature data can be observed. First, the average chlorite temperature data within the quartz-feldspar ± biotite porphyry dykes (356°–358°C) is almost identical regardless of chlorite habit. Second, the average chlorite temperatures of the chlorite veins, interstitial chlorite and the breccia matrix chlorite (360°–362°C) are very close to the temperatures shown in the quartz-feldspar ± biotite porphyry dykes. Is there a possible relationship? Third, the chlorite temperatures in the chlorite that replaced both biotite and feldspar phenocrysts within the feldspar-phyric rhyolite are almost identical (328° and 331°C) and are significantly lower than the chlorite temperatures within the quartz-feldspar ± biotite porphyry dykes.

Two possible explanations for this relatively restricted range of chlorite temperatures are: First, the temperature data is real and reflects different alteration fluid temperatures related to the mineralisation at Jukes. The 320°–360°C range would be consistent with the expected mineralisation temperature and temperatures obtained by Doyle (1990). Second, the temperature data of the chlorite has been reset by the later lower greenschist facies regional metamorphic event. The 320°–360°C range would be

Table 2.

Chlorite type	Feldspar-phyric rhyolite					Quartz-feldspar +/- biotite porphyry dykes		
	Biotite Pheno. Repl.	Feld. Pheno. Repl.	Chlotite vein	Interstitial	Breccia, Matrix	Biotite Pheno. Repl.	Feld. Pheno. Repl.	Chlotite vein
Number of analyses	4	2	8	4	6	17	2	9
Temperature range	312-341	329-334	330-386	342-378	338-371	313-380	349-366	343-370
Average temp. oC	328	331	360	362	360	357	358	356

also be consistent with this temperature. If the chlorite iron and magnesium values (and Mg#) equilibrated with the whole rock iron and magnesium values (Mg#) a linear relationship between the two would be expected.

To test this possibility the Mg# of the various chlorite habits was plotted against the Mg# of the whole rock samples. Results are presented as Figure 3. As can be seen in Figure 3, the relationship is not linear. Possible explanations include: First, the scatter is a result of chlorite formation from multiple fluids. or: Second the scatter simply reflects a difference in the iron and magnesium in the original mineral. In either case, it appears that real differences in the Mg#'s do still exist and were not equilibrated during the regional greenschist facies metamorphic event. The higher ratios in the chlorites suggest that the that magnesium in the rocks in more mineralised zones is contained within chlorite and not within other mineral phases. It is interesting to note that the different chlorite habits plot as separate groups on this plot. These differences will be investigated as part of the on going research.

Conclusions

The Jukes Road cross-section cuts through several chlorite bearing alteration mineral assemblages and therefore offers an excellent opportunity to examine

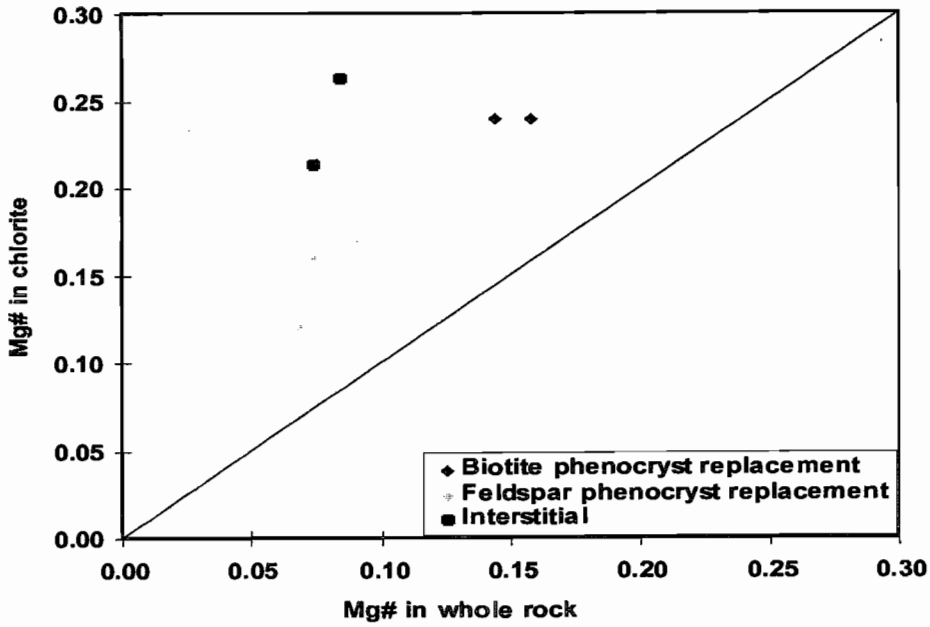

Figure 3 Plot of the Mg# of the various chlorite habits vs. the Mg# of the whole rock sample. Chlorite in veins and breccias were not plotted as they were excluded from the whole rock analysis

potential variations in chlorite mineral chemistry as a function of distance. Five different habits of chlorite were probed as part of this study. The five habits are (1) chlorite replacing biotite (?) phenocrysts (some could be amphiboles), (2) chlorite in chlorite-magnetite ± sulfide veins, (3) chlorite replacing feldspar phenocrysts, (4) interstitial (intergranular) chlorite between feldspar and quartz grains, and (5) chlorite in the matrices of mineralised hydrothermal breccias.

Results of the study to date indicate that for both the feldspar-phyric rhyolite lava and the quartz-feldspar ± biotite porphyry: (1) There is a large variability in Mg number (Mg# = $Mg_{(total)}$ / $Fe_{(total)}$ + $Mg_{(total)}$) within individual samples for a given chlorite type. (2) The range of Mg#'s from chlorite replacing feldspar phenocrysts, interstitial chlorite and chlorite in veins is the same and overlaps the range of Mg#'s from chlorite in the cores of the hydrothermal breccias. (3) There is a weakly defined decrease in the Mg# within the cores of the mineralised breccias that probably reflects an increase in iron associated with an increase in mineralisation. (4) Chlorites from within the quartz-feldspar ± biotite porphyry dykes overlap the same ranges in Mg# values as those within the feldspar-phyric rhyolite lava. (5) The Mg# of whole rocks corresponding to the probed samples, show the same range of Mg# values outside the mineralised zone. Near the boundaries of , and within the mineralised zone the Mg# of the host rocks is less than the Mg# of chlorite. This supports the conclusion that magnesium in the more mineralised zone is contained within chlorite and not within other mineral phases. (6) As a result of the overlap in the ranges of chlorite values within a given chlorite habit and the overlap in the ranges between various chlorite types, when plotted against distance, chlorite composition is not a useful vector toward mineralisation.

Based on the Al^{IV} content an attempt to calculate chlorite formation temperatures was made for each main type of chlorite. The determined range of average chlorite temperature values is relatively narrow (328°–362°C) and the overall range is only slightly broader (312°–386°C). Several distinct separations in the temperature data can be observed. First, the average chlorite temperature data within the quartz-feldspar ± biotite porphyry dykes (356°–358°C) is almost identical regardless of chlorite habit. Second, the average chlorite temperatures of the chlorite veins, interstitial chlorite and the breccia matrix chlorite (360°–362°C) are very close to the temperatures shown in the quartz-feldspar ± biotite porphyry dykes. Third, the chlorite temperatures in the chlorite that replaced both biotite and feldspar phenocrysts within the feldspar-phyric rhyolite are almost identical (328° and 331°C) and are significantly lower than the chlorite temperatures within the quartz-feldspar ± biotite porphyry dykes. The 320°–360°C range would be consistent with the expected mineralisation temperature and/or temperatures expected from the later lower greenschist facies regional metamorphic event.

References

Cathelineau, I. H. a. N., D., 1985. A chlorite solid solution geothermometer: the Los Azufres (Mexico) geothermal system. Contributions to Mineralogy and Petrology, 91: 235-244., 1985, A chlorite solid solution geothermometer: the Los Azufres (Mexico) geothermal system.: Contributions to Mineralogy and Petrology, v. 91, p. 235-244.

Doyle, M. G., 1990, The geology of the Jukes Proprietary prospect, Mt. Read Volcanics: Unpub. B.Sc.(Honours) thesis, University of Tasmania, 114 p.

Hendry, D. A. F., 1981, Chlorites, Phengites, and siderites from the Prince Lyell Ore deposit, Tasmania, and the Origin of the Deposit: Economic Geology, v. 76, p. 285-303.

Kranidiotis, P. a. M., W.H., 1987, Systematics of chlorite alteration at the Phelps Dodge massive sulfide deposit, Matagami, Quebec.: Economic Geology, v. 82, p. 1898-1911.

Polya, D. A., Solomon, M., Eastoe, C. J., and Walshe, J. L., 1986, The Murchison Gorge, Tasmania - a possible Cross-Section through a Cambrian Massive Sulphide System: Economic Geology, v. 81, p. 1341-1355.

Walshe, J. L., Hedges, M.M. and Harrold, B.P., 1986a, Evaluating the conditions of chlorite formation in hydrothermal and geothermal systems., Fifth annual symposium on Water-Rock interaction, 605-607: Extended abstracts. Orkustofnum, Reykjauik:.

Walshe, J. L., 1986b, A six-component solid solution model and the conditions of chlorite formation in hydrothermal and geothermal systems.: Economic Geology, v. 81, p. 681-703.

Walshe, J. L. a. S., M., 1981, An Investigation into the Environment of Formation of the Volcanic-Hosted Mt. Lyell Copper Deposits Using Geology, Mineralogy, Stable Isotopes, and a Six-Component Chlorite Solid Solution Model: Economic Geology, v. 76, p. 246-281.

Wyman, B., 1996, Road log of the Jukes Road and the Jukes Cu-Au Prospect with emphasis on petrology, alteration assemblages and preliminary geochemistry, Studies of VHMS-related alteration: geochemical and mineralogical vectors to ore: CODES Centre for Ore Deposit Studies, AMIRA/ARC project P439, p. 235-290.

Wyman, B., Allen, R., and Duhig, N., 1996, Jukes Road: Preliminary volcanic facies analysis and alteration petrography, Studies of VHMS-related alteration: geochemical and mineralogical vectors to ore: CODES Centre for Ore Deposit Studies, AMIRA/ARC project P439, p. 29-54.

Jukes Road Alteration Data Sheet

Sample No.	**10750**
Location	Jukes Road
Alteration zone	Distal chlorite-sericite +/- carbonate zone
Formation	Mt Read Volcanics, Central Volcanic Complex

Description Micropoikilitic groundmass weakly altered by sericite/chlorite. Phenocrysts replaced by sericite (20-50%) with lesser chlorite and carbonate.

Facies Interp Coherent columnar jointed feldspar-phyric rhyolite sill.

Alteration Intensity	none	(weak)	moderate	strong	intense	Py	
Alteration Style	(phenocryst replacement)		chlorite-magnetite veins	patchy	(interstitial)		
	pervasive	veined cleavage control					
Alteration Mineralogy	Groundmass	sericite-chlorite-carbonate					
	Feldspars	sericite-chlorite-carbonate					
	Mafics						
Interpretation	diagenetic	metamorphic	syntectonic	(hydrothermal)			

Relict Mineralogy Micropoikilitic quartz and K-feldspar in groundmass, phenocrysts of K-feldspar

Geochemistry

SiO_2	TiO_2	Al_2O_3	Fe_2O_3	MnO	MgO	CaO	Na_2O	K_2O	P_2O_5	LOI	Al	CCPI	MI	Ti/Zr
74.2	0.29	13.47	3.08	0.01	0.72	0.03	1.44	4.06	0.04	2.66	76.48	38.94	2.31	6.14

Rb	Sr	Ba	Cu	Pb	Zn	Sb	Tl	Zr	Nb	Y	$\delta^{18}O_{wr}$
145	18	882	6	26	57			291	14	38	

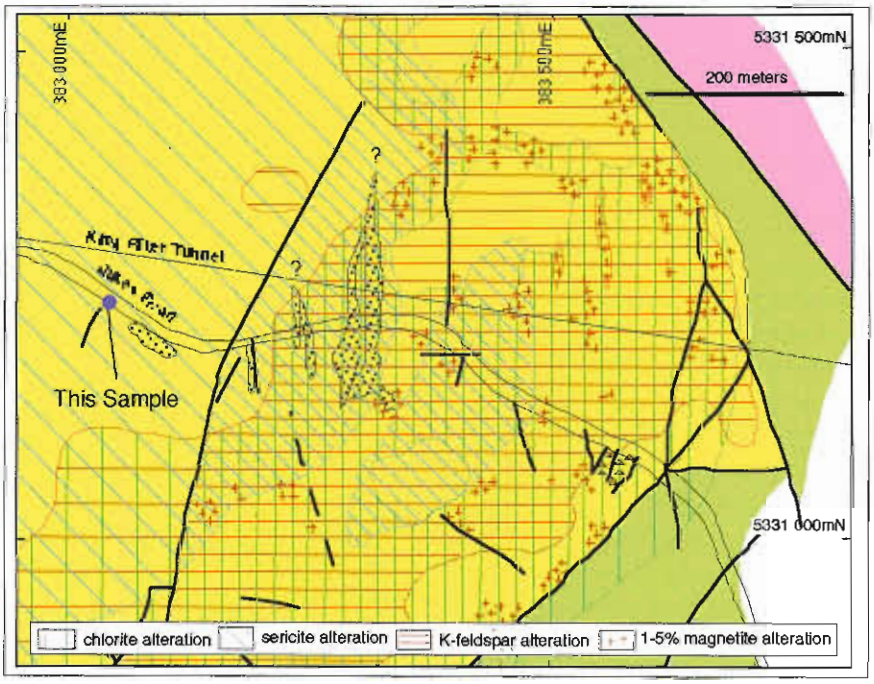

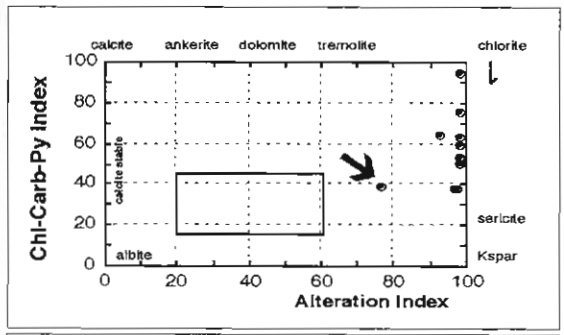

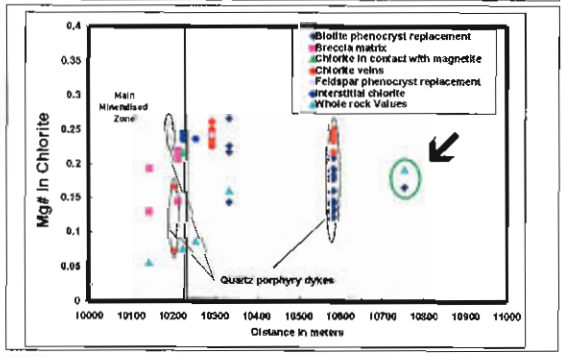

Jukes Road Alteration Data Sheet

Sample No. **10580**
Location Jukes Road
Alteration zone Distal chlorite-sericite +/- carbonate zone
Formation Mt Read Volcanics, Central Volcanic Complex

Description Groundmass weakly altered by sericite/chlorite. Feld. phenocrysts replaced by sericite (20-50%) with lesser chlorite. Biotite phenocrysts replaced by chlorite. Carbonate less than 10750 and is

Facies Interp Quartz-feldspar-biotite porphyry Dyke.

Alteration Intensity none weak moderate strong (intense) Py
Alteration Style (phenocryst replacement) (chlorite-magnetite veins) patchy interstitial
pervasive veined cleavage control Sericite-chlorite-carbonate
Alteration Mineralogy Groundmass
Feldspars
Mafics
Interpretation diagenetic metamorphic syntectonic (hydrothermal)
Relict Mineralogy Quartz and K-feldspar in groundmass, phenocrysts of Quartz, K-feldspar and biotite

Geochemistry

SiO_2	TiO_2	Al_2O_3	Fe_2O_3	MnO	MgO	CaO	Na_2O	K_2O	P_2O_5	LOI	Al	CCPI	MI	Ti/Zr
67.96	0.54	13.29	8.71	0.08	1.46	0.15	0.33	4.98	0.11	2.41	93.06	63.76	15.18	10.62

Rb	Sr	Ba	Cu	Pb	Zn	Sb	Tl	Zr	Nb	Y	$\delta^{18}O_{wr}$
178	24	996	74	3	82		312				

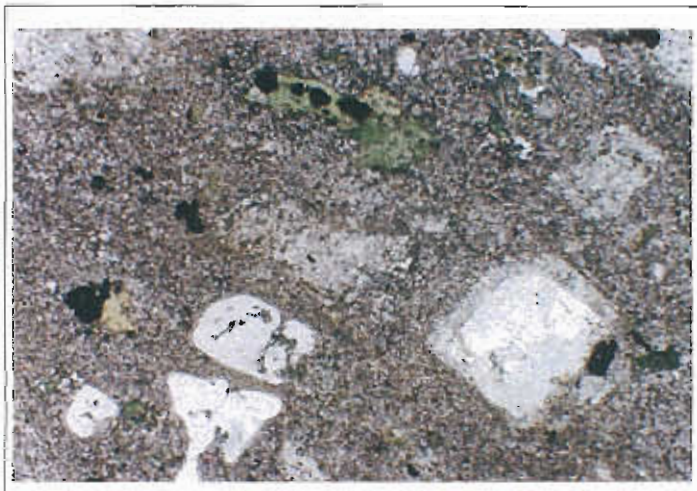

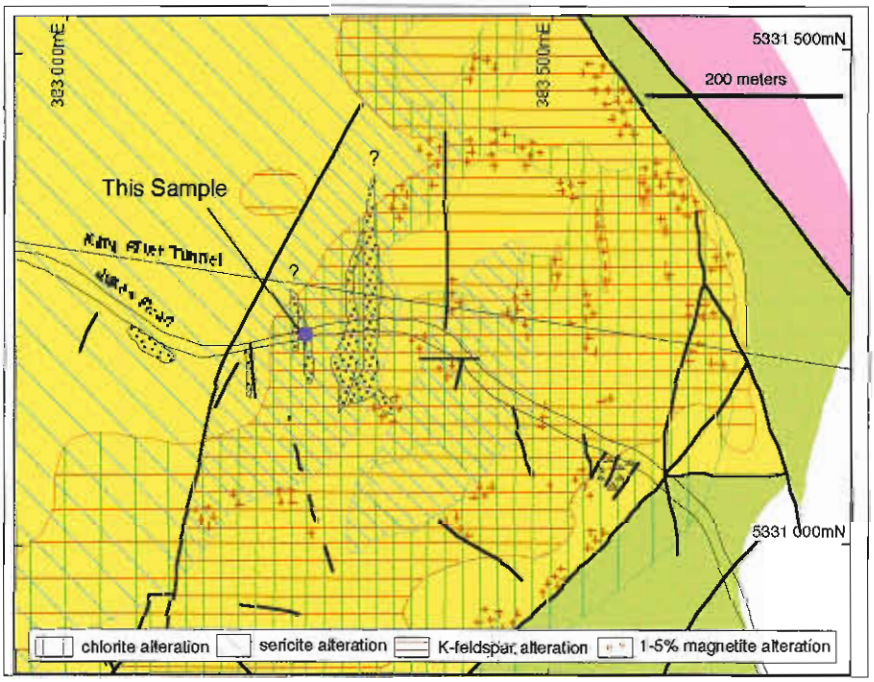

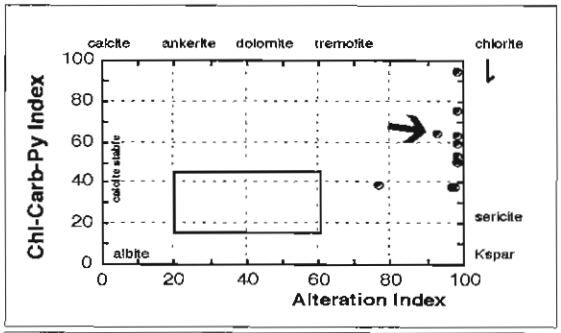

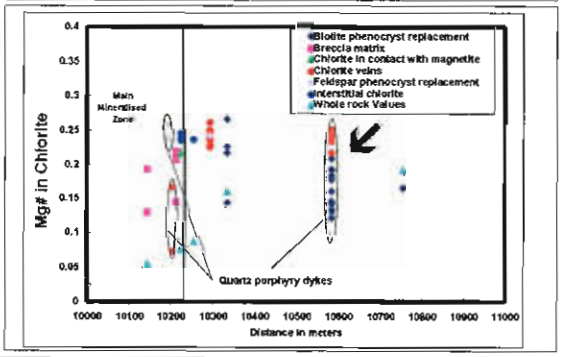

Jukes Road Alteration Data Sheet

Sample No. **10330**
Location Jukes Road
Alteration zone Sericite-chlorite

Formation Mt Read Volcanics, Central Volcanic Complex

Description Micropoikilitic groundmass is intensely altered by sericite. Phenocrysts replaced by sericite (20-50%) with lesser chlorite. Chlorite occurs as replacement to feld. phenocrysts, interstitial and biotite phenocryst replacement.

Facies Interp Coherent columnar jointed feldspar-phyric rhyolite sill.

Alteration Intensity none weak moderate strong (intense) Py

Alteration Style (phenocryst replacement) chlorite-magnetite veins patchy interstitial (pervasive) veined cleavage control

Alteration Mineralogy
Groundmass sericite-chlorite
Feldspars sericite-chlorite
Mafics chlorite

Interpretation diagenetic metamorphic syntectonic (hydrothermal)

Relict Mineralogy Micropoikilitic quartz and K-feldspar in groundmass, phenocrysts of K-feldspar

Geochemistry

SiO_2	TiO_2	Al_2O_3	Fe_2O_3	MnO	MgO	CaO	Na_2O	K_2O	P_2O_5	LOI	Al	CCPI	MI	Ti/Zr
71.08	0.3	13.22	5.55	0.03	1.04	0.02	0.11	5.99	0.03	2.45	98.18	49.85	4.98	6.66

Rb	Sr	Ba	Cu	Pb	Zn	Sb	Tl	Zr	Nb	Y	$\delta^{18}O_{wr}$
176	30	1961	469	11	94			276	12	36	

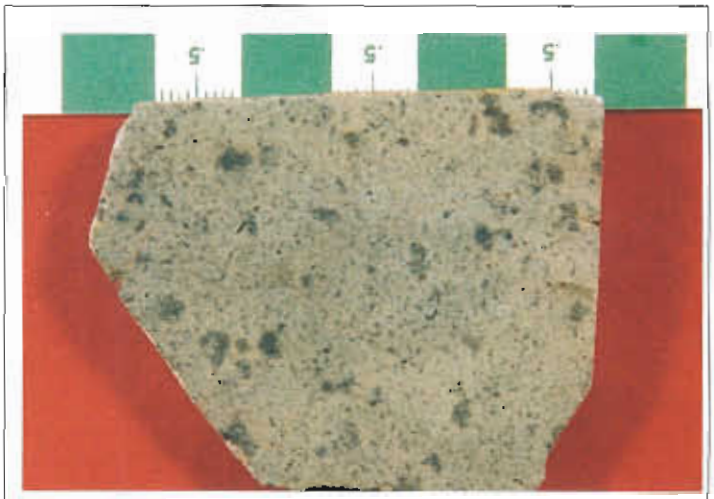

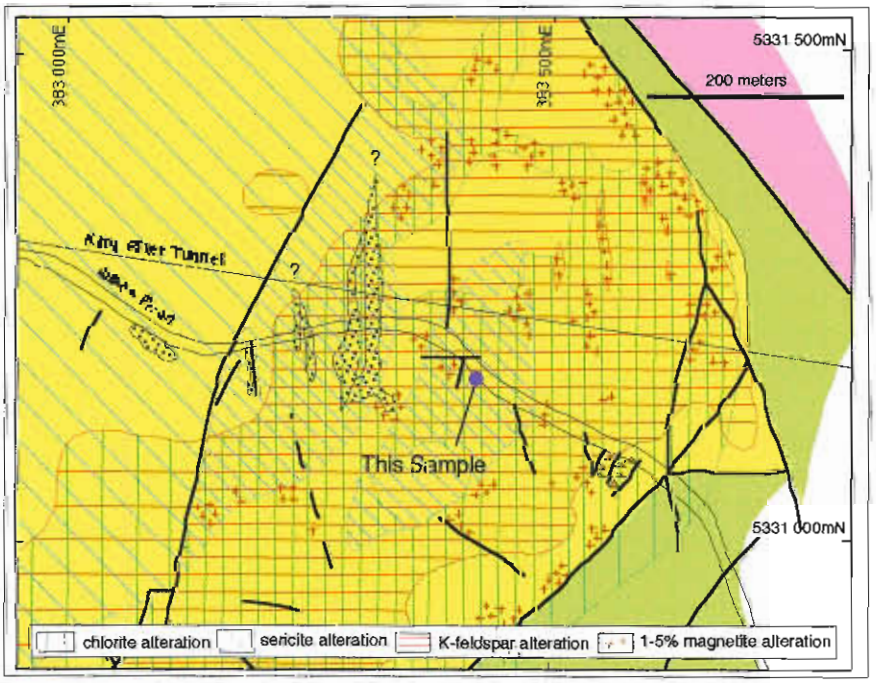

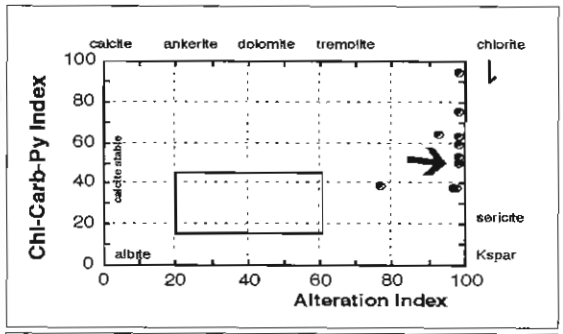

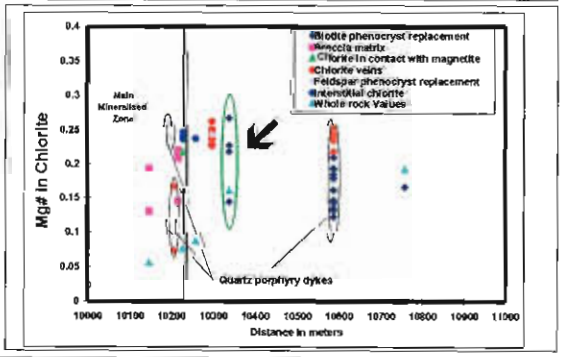

Jukes Road Alteration Data Sheet

Sample No. **10220**
Location Jukes Road
Alteration zone K-feldspar-sericite

Formation Mt Read Volcanics, Central Volcanic Complex

Description The groundmass is mostly K-feld. and sericite altered. Chlorite and sericite occur as: small masses in the groundmass, replacement of K-

Facies Interp Coherent columnar jointed feldspar-phyric rhyolite sill.

Alteration Intensity none weak moderate strong (intense) Py 5%
Alteration Style (phenocryst replacement) (chlorite-magnetite veins) patchy interstitial
pervasive veined cleavage control
Alteration Mineralogy Groundmass K-feldspar-sericite-chlorite
Feldspars sericite-chlorite
Mafics chlorite
Interpretation diagenetic metamorphic syntectonic (hydrothermal)
Relict Mineralogy Micropoikilitic quartz and K-feldspar in groundmass

Geochemistry

SiO_2	TiO_2	Al_2O_3	Fe_2O_3	MnO	MgO	CaO	Na_2O	K_2O	P_2O_5	LOI	Al	CCPI	MI	Ti/Zr
69.00	0.28	11.99	8.07	0.06	0.64	0.02	0.10	6.79	0.04	2.15	98.41	53.55	8.26	8.75

Rb	Sr	Ba	Cu	Pb	Zn	Sb	Tl	Zr	Nb	Y	$\delta^{18}O_{wr}$
158	44	2088	1200	44	98			245			

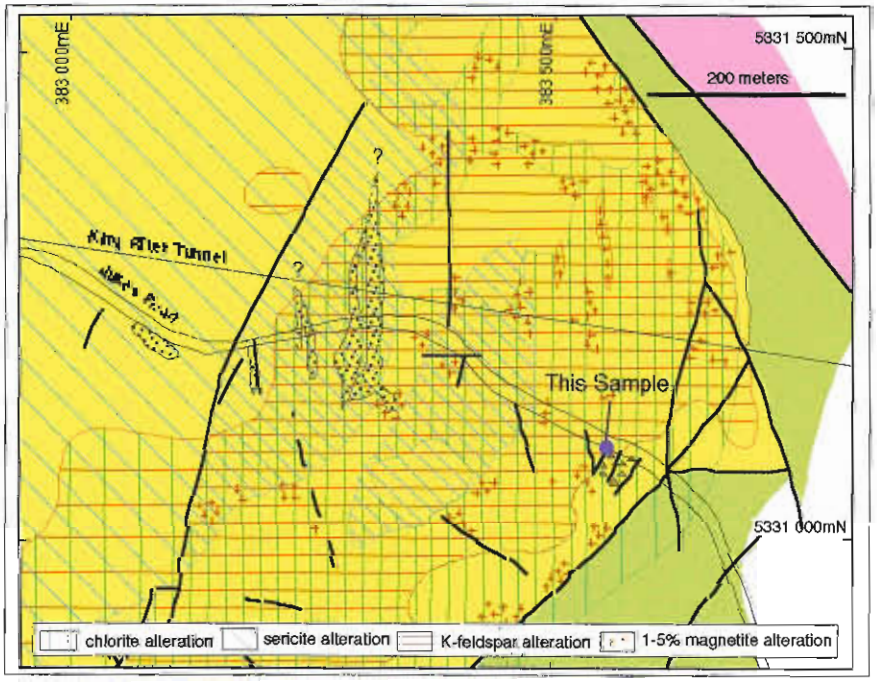

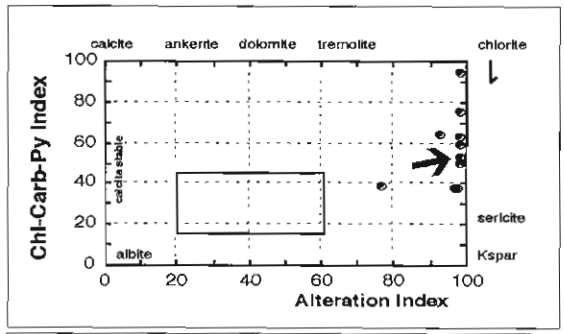

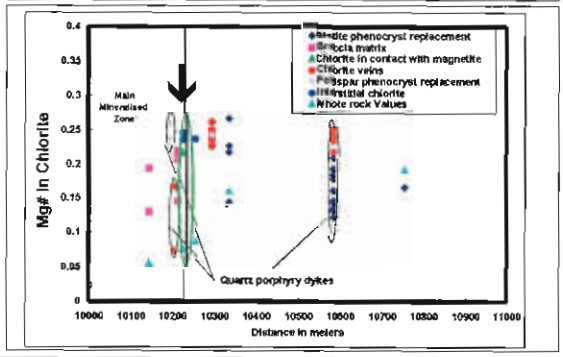

Jukes Road Alteration Data Sheet

Sample No. **10290**
Location Jukes Road
Alteration zone K-feldspar-chlorite-sericite

Formation Mt Read Volcanics, Central Volcanic Complex

Description Feld. laths and cores of micropoikilitic quartz show complete transition in alteration from very weak sericite alteration to complete chlorite alteration in a K-feld. altered rock. Sericite +/- chlorite forms cores in some feld. phenocrysts.

Facies Interp Coherent columnar jointed feldspar-phyric rhyolite sill

Alteration Intensity none weak moderate strong (intense) Py

Alteration Style (phenocryst replacement) chlorite-magnetite veins patchy interstitial (pervasive) veined cleavage control

Alteration Mineralogy Groundmass K-feldspar-sericite +/- chlorite.
Feldspars sericite-chlorite
Mafics

Interpretation diagenetic metamorphic syntectonic (hydrothermal)

Relict Mineralogy Micropoikilitic quartz in groundmass

Geochemistry

SiO_2	TiO_2	Al_2O_3	Fe_2O_3	MnO	MgO	CaO	Na_2O	K_2O	P_2O_5	LOI	Al	CCPI	MI	Ti/Zr
66.97	0.29	12.72	9.66	0.04	0.71	0.01	0.11	6.34	0.06	2.95	98.33	59.44	5.98	6.66

Rb	Sr	Ba	Cu	Pb	Zn	Sb	Tl	Zr	Nb	Y	$\delta^{18}O_{wr}$
162	32	2101	1400	71	78			259	15	96	

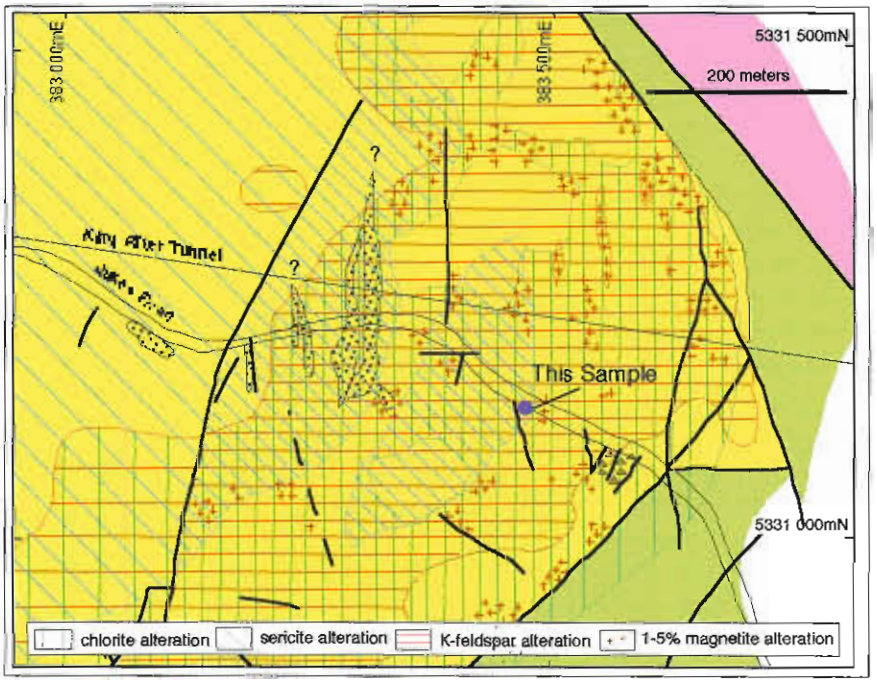

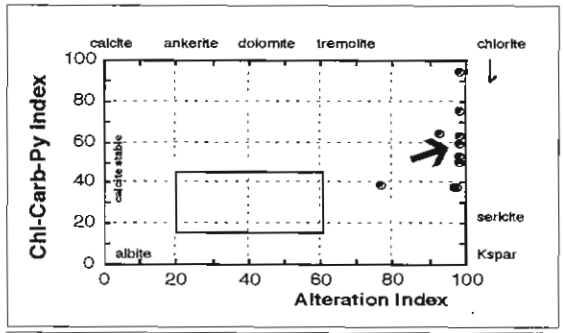

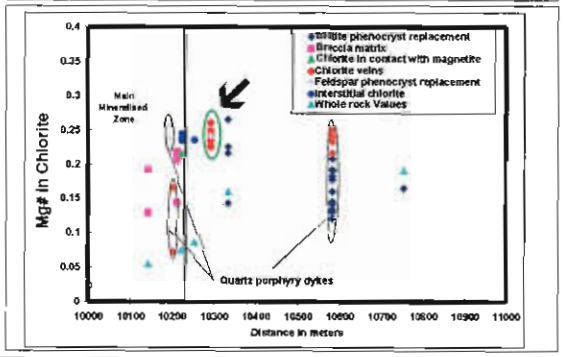

Jukes Road Alteration Data Sheet

Sample No. **10210 (10212)**
Location Jukes Road
Alteration zone K-feldspar-chlorite-sericite

Formation Mt Read Volcanics, Central Volcanic Complex

Description Mineralised breccia. The groundmass is mostly K-feld. and chlorite altered. Chlorite occurs as: replacement of K-feld. laths, phenocrysts and in magnetite-pyrite and chalcopyrite veins.
Facies Interp Brecciated, Coherent columnar jointed feldspar-phyric rhyolite sill.

Alteration Intensity none weak moderate strong (intense) Py
Alteration Style (phenocryst replacement) (chlorite-magnetite veins) patchy interstitial
(pervasive) veined cleavage control
Alteration Mineralogy Groundmass K-feldspar-chlorite-sericite
Feldspars sericite-chlorite
Mafics
Interpretation diagenetic metamorphic syntectonic (hydrothermal)
Relict Mineralogy Micropoikilitic quartz

Geochemistry

SiO_2	TiO_2	Al_2O_3	Fe_2O_3	MnO	MgO	CaO	Na_2O	K_2O	P_2O_5	LOI	Al	CCPI	MI	Ti/Zr
54.61	0.24	10.51	24.90	0.09	1.27	0.01	0.04	1.45	0.03	6.43	98.19	94.11	37.92	7.83

Rb	Sr	Ba	Cu	Pb	Zn	Sb	Tl	Zr	Nb	Y	$\delta^{18}O_{wr}$
59	6	190	491	137	307			197			

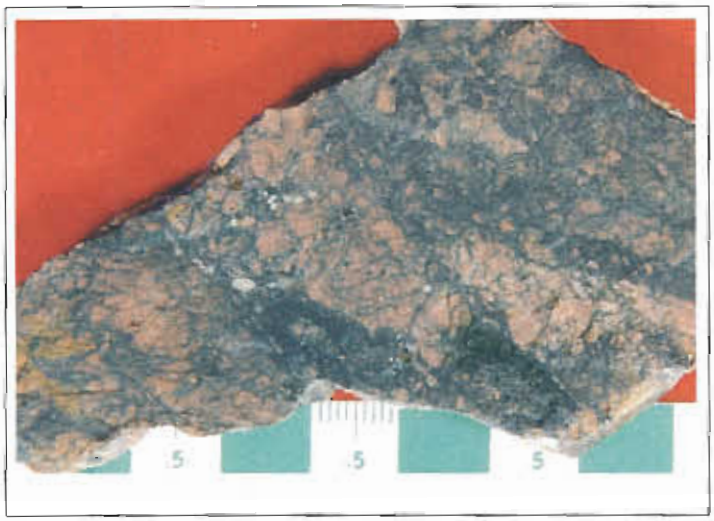

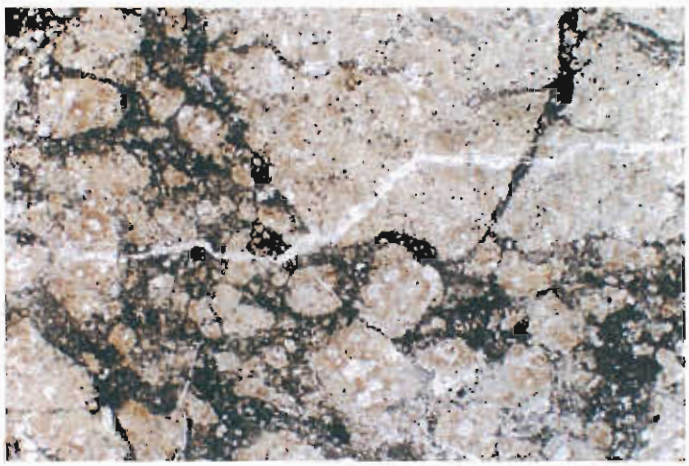

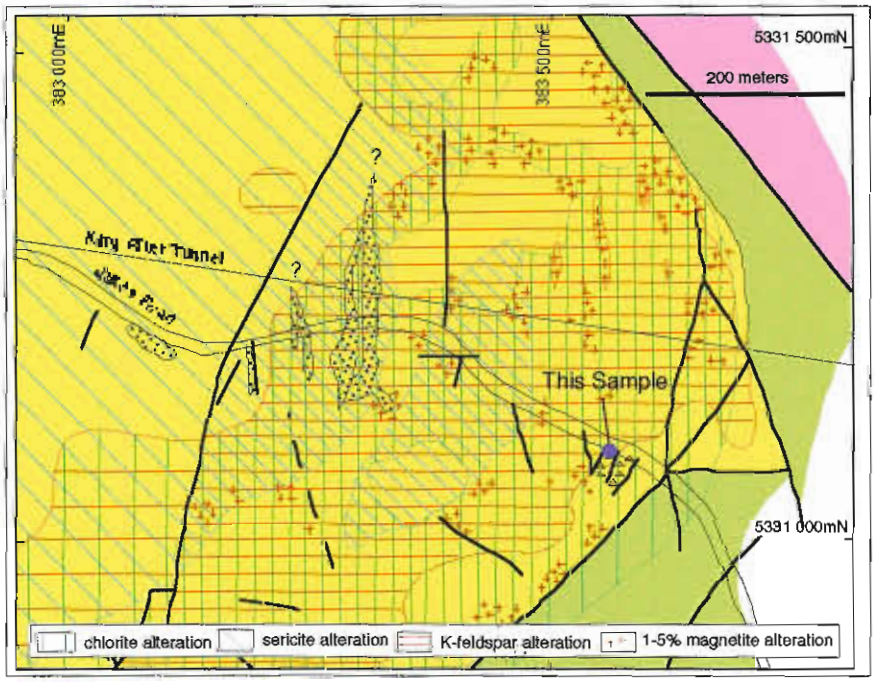

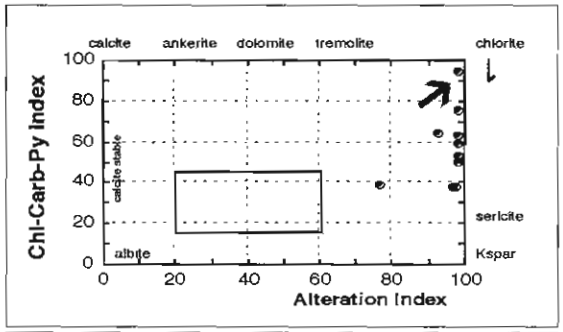

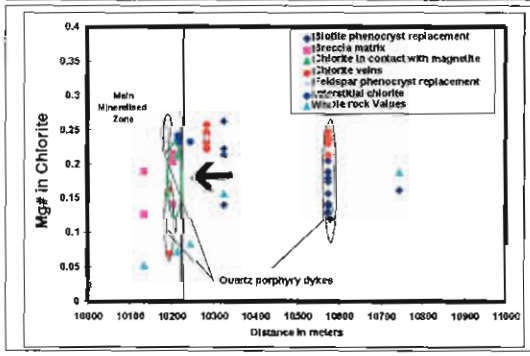

Jukes Road Alteration Data Sheet

Sample No.	**10200**
Location	Jukes Road
Alteration zone	K-feldspar-chlorite-sericite
Formation	Mt Read Volcanics, Central Volcanic Complex

Description Quartz-feldspar phyric dike cutting hydrothermal breccia.. Chlorite veins contain minor sulfides.

Facies Interp Quartz-feldspar-biotite porphyry Dyke.

Alteration Intensity	none weak moderate strong (intense) Py 5%
Alteration Style	(phenocryst replacement) (chlorite-magnetite veins) patchy interstitial (pervasive) veined cleavage control
Alteration Mineralogy	Groundmass chlorite-sericite Feldspars sericite-chlorite Mafics chlorite
Interpretation	diagenetic metamorphic syntectonic (hydrothermal)
Relict Mineralogy	Micropoikilitic quartz

Geochemistry

SiO_2	TiO_2	Al_2O_3	Fe_2O_3	MnO	MgO	CaO	Na_2O	K_2O	P_2O_5	LOI	Al	CCPI	MI	Ti/Zr
69.42	0.36	12.28	9.06	0.06	0.68	0.02	0.06	5.01	0.06	2.82	98.61	63.65	10.90	7.55

Rb	Sr	Ba	Cu	Pb	Zn	Sb	Tl	Zr	Nb	Y	$\delta^{18}O_{wr}$
59	6	190	491	137	307			197			

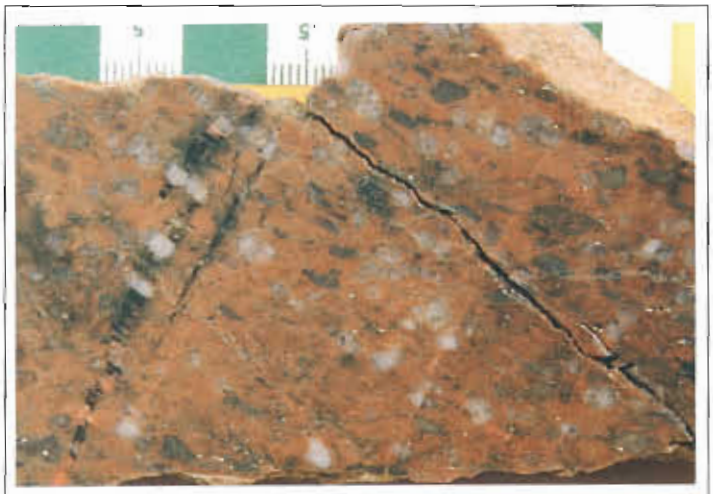

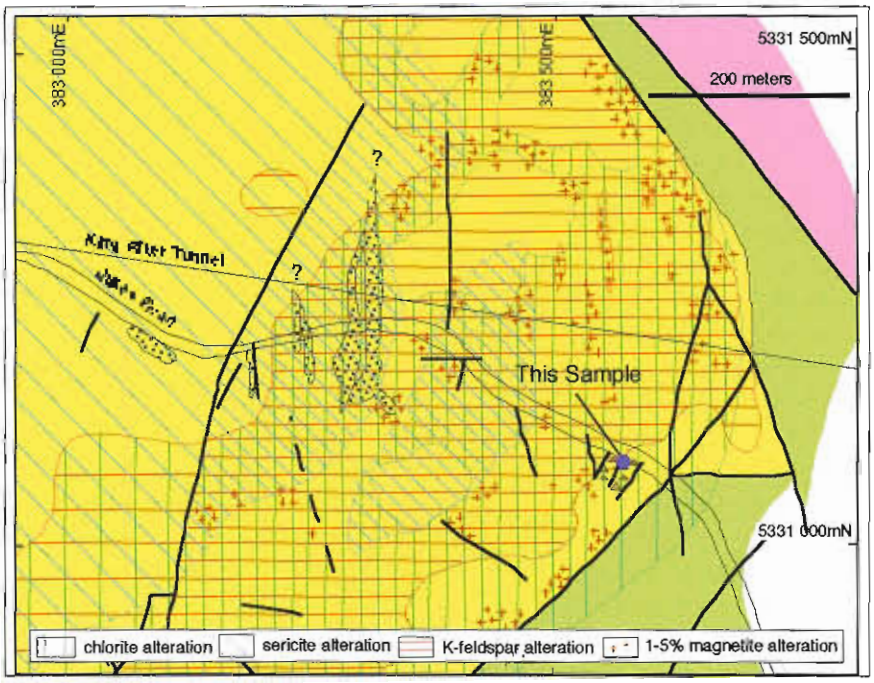

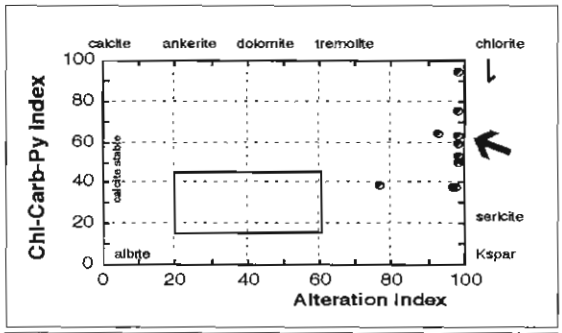

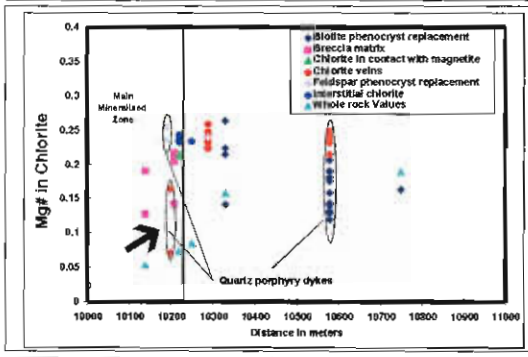

Jukes Road Alteration Data Sheet

Sample No. **10250**
Location Jukes Road
Alteration zone K-feldspar-sericite-chlorite

Formation Mt Read Volcanics, Central Volcanic Complex

Description K-feldspar and sericite occur in approximately equal amounts with lesser chlorite in the groundmass. Disseminated pyrite and magnetite are common. Sericite is 20-90% of feld. phenocrysts with lesser chlorite.

Facies Interp Coherent columnar jointed feldspar-phyric rhyolite sill.

Alteration Intensity none weak moderate strong (intense) Py 5%

Alteration Style (phenocryst replacement) chlorite-magnetite veins patchy interstitial
(pervasive) veined cleavage control

Alteration Mineralogy

Groundmass	K-feld.-sericite	
Feldspars	sericite-chlorite	
Mafics		

Interpretation diagenetic metamorphic syntectonic (hydrothermal)

Relict Mineralogy Micropoikilitic quartz and K-feldspar in groundmass, phenocrysts of K-feldspar

Geochemistry

SiO_2	TiO_2	Al_2O_3	Fe_2O_3	MnO	MgO	CaO	Na_2O	K_2O	P_2O_5	LOI	Al	CCPI	MI	Ti/Zr
72.47	0.29	12.46	4.92	0.02	0.45	0.01	0.19	7.88	0.04	1.52	97.66	37.79	2.54	7.21

Rb	Sr	Ba	Cu	Pb	Zn	Sb	Tl	Zr	Nb	Y	$\delta^{18}O_{wr}$
17	55	2689	430	11	56			260			

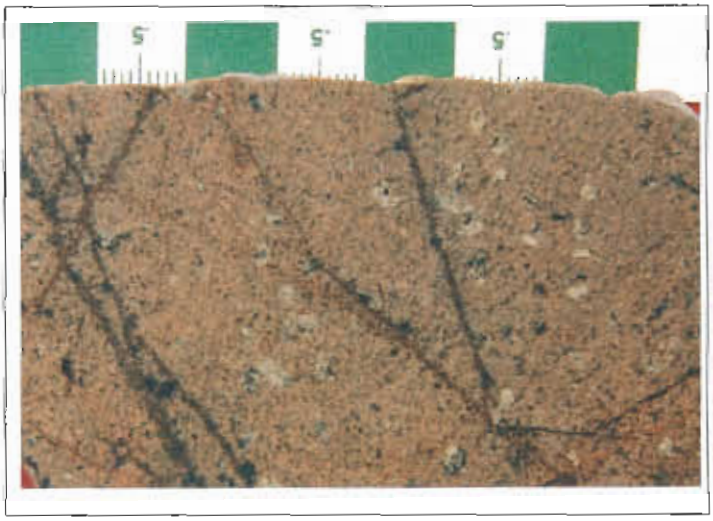

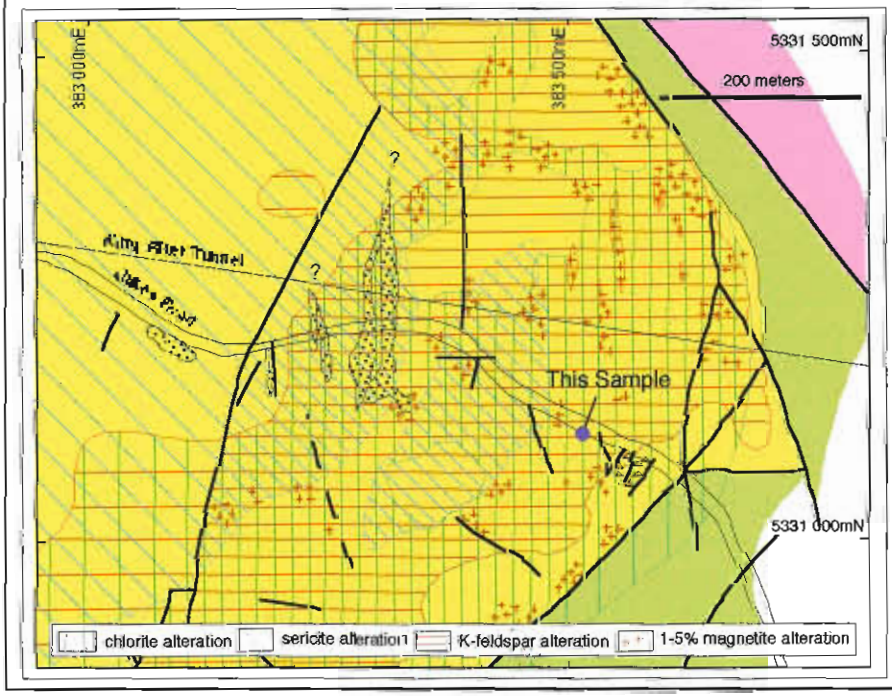

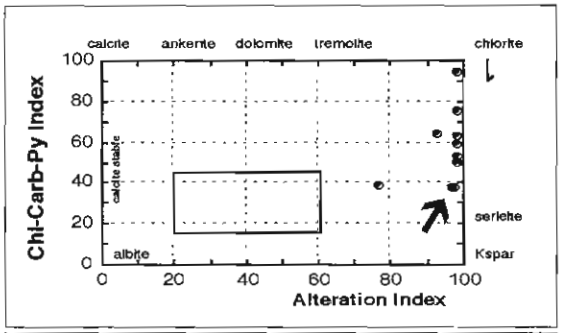

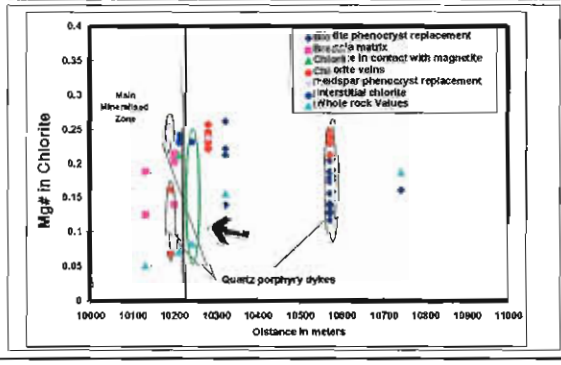

Jukes Road Alteration Data Sheet

Sample No. **10140**
Location Jukes Road
Alteration zone K-feldspar-chlorite

Formation Mt Read Volcanics, Central Volcanic Complex

Description Weakly mineralised breccia. The groundmass is mostly K-feld. and chlorite altered. Chlorite occurs as: replacement of K-feld. laths, phenocrysts and in pyrite and chalcopyrite veins.

Facies Interp Brecciated, Coherent columnar jointed feldspar-phyric rhyolite sill.

Alteration Intensity none weak moderate strong (intense) Py 2-3 %

Alteration Style (phenocryst replacement) (chlorite-magnetite veins) patchy interstitial (pervasive) veined cleavage control

Alteration Mineralogy
Groundmass K-feldspar-chlorite
Feldspars sericite-chlorite
Mafics chlorite

Interpretation diagenetic metamorphic syntectonic (hydrothermal)

Relict Mineralogy Micropoikilitic quartz and K-feldspar in groundmass, phenocrysts of K-feldspar

Geochemistry

SiO_2	TiO_2	Al_2O_3	Fe_2O_3	MnO	MgO	CaO	Na_2O	K_2O	P_2O_5	LOI	Al	CCPI	MI	Ti/Zr
66.13	0.14	11.06	13.77	0.12	0.78	0.01	0.08	4.33	0.04	3.23	98.27	75.02	21.53	6.72

Rb	Sr	Ba	Cu	Pb	Zn	Sb	Tl	Zr	Nb	Y	$\delta^{18}O_{wr}$
100	27	1161	1500	13	156			129			

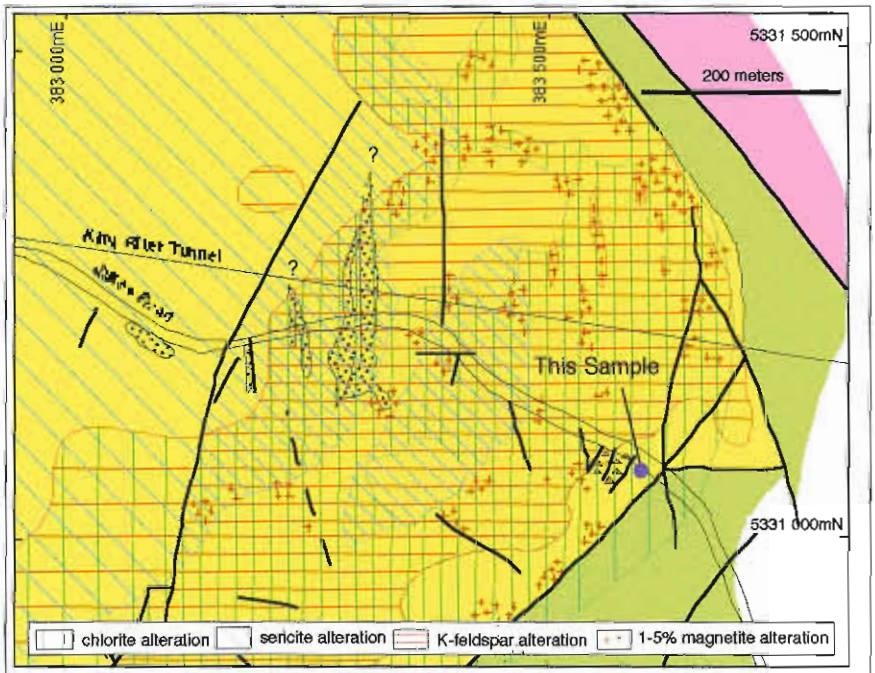

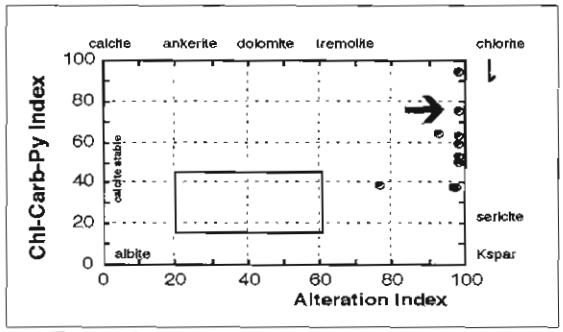

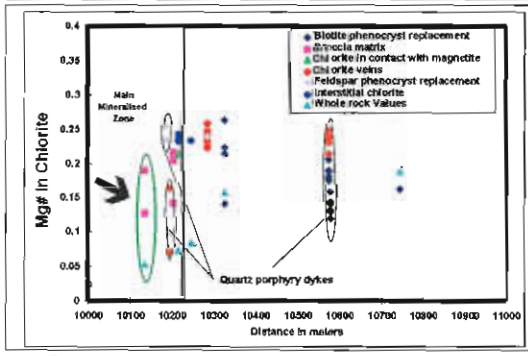

Jukes Road Alteration Data Sheet

Sample No. **10190 (MJ 96-4)**
Location Jukes Road
Alteration zone K-feldspar-chlorite-sericite

Formation Mt Read Volcanics, Central Volcanic Complex

Description Quartz-feldspar phyric dike cutting hydrothermal breccia. Breccia matrix is magnetite-tourmaline and chlorite. Veins contain minor sulfides.

Facies Interp Quartz-feldspar-biotite porphyry Dyke.

Alteration Intensity none weak moderate strong (intense) Py 2-3 %
Alteration Style (phenocryst replacement) (chlorite-magnetite veins) patchy interstitial
pervasive veined cleavage control
Alteration Mineralogy Groundmass chlorite-sericite
Feldspars sericite-chlorite
Mafics chlorite
Interpretation diagenetic metamorphic syntectonic (hydrothermal)
Relict Mineralogy Micropoikilitic quartz and K-feldspar in groundmass, phenocrysts of K-feldspar

Geochemistry

SiO_2	TiO_2	Al_2O_3	Fe_2O_3	MnO	MgO	CaO	Na_2O	K_2O	P_2O_5	LOI	Al	CCPI	MI	Ti/Zr
70.42	0.34	12.09	5.10	0.22	0.50	0.07	0.17	8.18	0.06	2.31	97.31	37.99	21.37	7.10

Rb	Sr	Ba	Cu	Pb	Zn	Sb	Tl	Zr	Nb	Y	$\delta^{18}O_{wr}$
158	111	2987	48	11	39	1.5	1	295	17.4	35